Copy Available

GEOCHEMISTRY AND MINERALOGY OF SELECTED ATLANTIC OCEAN BASALTS

by

A.P. LE ROEX

Department of Geochemistry,
University of Cape Town.

February, 1980

Thesis submitted in fulfilment of the requirements
for the degree of Ph.D. at the
University of Cape Town.

ABSTRACT

Bulk rock compositional variations in lavas from four localities in the Atlantic Ocean are evaluated quantitatively in terms of fractional crystallisation and partial melting models. Samples studied are from the Mid-Atlantic Ridge at $36^{o}49'N$ (FAMOUS), from the Islas Orcadas fracture zone on the Southwest Indian Ocean Ridge, from the Conrad fracture zone on the America-Antarctica Ridge and from Bouvet Island, situated at the southernmost tip of the Mid-Atlantic Ridge and in the vicinity of both the fracture zones mentioned above.

Bulk rock major and trace element variations in selected basalts from the FAMOUS area, in conjunction with a detailed study of the chemistry of phenocryst minerals and associated melt inclusions are used to place constraints on the genetic relationships between the various lava types. The distribution of NiO in olivine and Cr-spinel phenocrysts distinguishes the picritic basalts, plagioclase phyric basalts and plagioclase-pyroxene basalts from the olivine basalts. The NiO content of these phenocrysts in the former three basalt types is low, for a given $Mg/Mg+Fe^{2+}$ atomic ratio of the mineral, relative to the phenocrysts in the olivine basalts. Consideration of the Zr/Nb ratio of the lavas similarly distinguishes the olivine basalts from the plagioclase phyric and plagioclase-pyroxene basalts but, in addition, distinguishes the picritic basalts from the former three basalt types.

Consideration of Fe-Mg partitioning between olivine and host rock suggests that the picrites represent olivine (±Cr-spinel) enriched magmas, derived from a less MgO rich parental magma. The

partitioning of Fe and Mg between Cr-spinel and coexisting glass is evaluated in terms of the equilibrium constant $K_D^{Fe-Mg}=(X^{FeO}/X^{MgO})^{sp}/(X^{FeO}/X^{MgO})^{gl}$. The value of this K_D is shown to be close to unity in the olivine basalts and picrites, which implies that the FeO/MgO ratio of melt inclusions trapped within Cr-spinel phenocrysts closely reflects the FeO/MgO ratio of the magma at the time of melt entrapment. This factor is used to predict a primary magma composition parental to the picrites, which is characterised by relatively high MgO (12.3%) and CaO (12.6%) and low FeO^* (7.96%) and TiO_2 (0.63%).

Least squares calculations indicate that the plagioclase phyric basalts are related to the plagioclase-pyroxene basalts by plagioclase and minor clinopyroxene and olivine accumulation. The compositional variations within the olivine basalts can be accounted for by fractionation of plagioclase, clinopyroxene and olivine in an open system, steady state, magma chamber in the average proportions 45 : 32 : 23. It is suggested that the most primitive olivine basalts can be derived from a pristine mantle composition by approximately 17% equilibrium partial melting. Although distinguished by its Zr/Nb ratio and NiO content of phenocryst phases, the parental magma to the picrites can be derived from a similar source composition by approximately 27% equilibrium partial melting. It is suggested that the parental magma to the plagioclase-pyroxene and plagioclase phyric basalts is derived from greater depth resulting in the fractionation of the Zr/Nb ratio by equilibration against residual garnet.

The Islas Orcadas and Conrad fracture zone basalts are

characterised by their evolved compositions and large compositional variation. The Islas Orcadas fracture zone basalts are further characterised by a transitional to mildly alkaline chemistry while the Conrad fracture zone basalts are more similar to 'normal' or depleted mid-ocean ridge basalt. The major and trace element variations in the Islas Orcadas fracture zone basalts can be accounted for by up to 40% fractional crystallisation of dominantly plagioclase and clinopyroxene with minor olivine. The lavas dredged from the south-eastern wall of the Islas Orcadas fracture zone can be distinguished on the basis of their lower Zr/Nb and Y/Nb ratios and higher Zr/Y ratio from those dredged from the northwestern wall. These differences can be accounted for by varied degrees of partial melting of a garnet bearing source. The basalts have a similar bulk chemistry to other samples dredged from the Southwest Indian Ocean Ridge, and are characterised by low Zr/Nb and Y/Nb ratios and LREE enrichment. It is suggested that the chemical features of these lavas reflect the influence of a mantle plume situated near Bouvet Island.

Both extrusive and intrusive rocks were recovered from the Conrad fracture zone. The samples generally show a significant degree of alteration and K-and Na-feldspar replacement of plagioclase is common. Systematic variations in immobile major and trace elements indicate that most of the samples are genetically related, a feature borne out by quantitative geochemical modelling. Extensive fractionation (up to 66 to 76%) of plagioclase, clinopyroxene and minor opaque oxides is required to account for the compositions of

the evolved ferrobasalts (13-16% FeO^*, 2.5 - 3.5% TiO_2).

Bouvet Island is characterised by lavas ranging in composition from hawaiite through mugearite and benmoreite to rhyolite. Major and trace element modelling indicates that the compositional variation can be described by extensive differentiation of a parental hawaiite. Following this scheme an hawaiite parent magma experienced 44% fractional crystallisation of plagioclase + clinopyroxene + olivine + opaque oxides and minor apatite to give rise to the mugearite magma, which in turn experienced a further 69% fractional crystallisation of the same phase assemblage (though with more evolved compositions) to give rise to the Bouvet Island rhyolite. Extensive fractional crystallisation (64%), possibly separated in time, of the parental hawaiite gave rise to the benmoreite magma. The fractionating phases are similar in composition and proportion to those crystallising in the passage from hawaiite to mugearite.

It has been demonstrated that it is possible to account for much of the chemical variation encountered in the ridge, fracture zone and island basalts investigated in this study by fractional crystallisation processes. It has, in most instances, not been necessary to invoke a process such as magma mixing to account for the variations, although it is recognised that such a process is probably more realistic than 'closed system' fractionation.

The common occurrence of highly differentiated basalts in fracture zones, even when transecting slow spreading ridges, is regarded as reflecting a lower magma supply rate than at the ridge axis. Magma would therefore reside in crustal chambers for a sufficient

length of time to experience substantial 'closed-system' fractional crystallisation without mixing with new batches of 'primary' magma. This results in the extrusion of a higher proportion of differentiated basalts at fracture zones relative to mid-ocean ridges.

Chemical variations not accounted for by fractional crystallisation can to a first approximation be attributed to equilibrium partial melting. Knowledge of mantle mineralogies and distribution coefficients under melting conditions for the elements considered in this study are such that melting models are less tightly constrained. It is possible to account for observed variations by simple equilibrium partial melting, and it was found to be unnecessary to consider more complex, though probably more realistic, models such as dynamic melting. Instead, on the basis of imcompatible inter-element ratios, persistent chemical differences are attributed to source area characteristics. In this regard, there appears to be no distinctive differences with respect to tectonic location, and the differences are best ascribed to deep mantle plumes.

CONTENTS

ACKNOWLEDGEMENTS

In presenting this thesis I owe much to many people. Firstly, it is impossible to express adequately my appreciation to those who have suffered most during this work, my wife Sue, and children Craig and Tanya, who for the past few years have not received the attention they deserved. Without Sue's selfless understanding and willing sacrifice this work would not have been possible.

I am sincerely grateful to Profs. A.J. Erlank and A.M. Reid for acting as my supervisors, and for providing me with the opportunity to undertake this study and to use the vast facilities of the Geochemistry and Geology Departments. Their continual encouragement, advice and penetrating criticism throughout this study are gratefully acknowledged.

Without the analytical expertise of Drs. J.P. Willis and A.R. Duncan the analytical work in this thesis would not have been of such high quality and my knowledge of X-ray fluorescence would still be negligible. Mr. Dick Rickard provided additional assistance with the operation of the electron microprobe. My thanks go also to the many other members of the Geochemistry Department who at various stages gave up their valuable time in discussions and advice. The efforts of, amongst others, Drs. A.R. Duncan and J.P. Willis in teaching me the rudiments of FORTRAN programming are also gratefully acknowledged. I would like to give special thanks to Paula Cardoso for sacrificing many hours of her free time helping me with the menial task of hand-picking the mineral separates analysed in this study and for drafting most of the diagrams. I would also like to

thank my wife, Sue, for the help she gave with drafting.

The study was made possible through the kind donation of samples, to Prof. A.J. Erlank, by Dr. H.D. Needham (Centre Océanologique de Bretagne, Brest), Dr. H.J.B. Dick (Woods Hole Oceanographic Institution) and Prof. W.J. Verwoerd (Stellenbosch University). Financial support was received through a S.A.N.C.O.R. research grant to Prof. A.M. Reid and from a University of Cape Town research associateship, which are gratefully acknowledged.

Finally, I would like to thank Marianne Reichardt and Mrs. G. Verblun for typing the text and tables and especially my wife, Sue, for the many, many hours she spent in performing the essential task of proof-reading.

CHAPTER 1

INTRODUCTION

1. GENERAL

Interest in basalts extruded from the ocean floor (commonly referred to as ocean floor basalts) has been concomitant with the development of the theory of plate tectonics. The inter-connecting 65,000 km mid-ocean ridge system, which forms the constructive margins of the spreading lithosphere plates, marks the site of eruption of the vast majority of these ocean floor basalts; the most voluminous eruptive rocks on earth. Extensive sampling over the last one and a half decades has shown that these basaltic lavas are a major component of the upper oceanic crust, and their eruption and emplacement is the principle mechanism for the generation of new oceanic crust.

Early studies of ocean floor basalts (e.g. Engel et al., 1965; Gast, 1965; Tatsumoto et al., 1965; Kay et al., 1970) emphasised their rather consistent and unique chemical composition; e.g. low large ion lithophile element abundances, light rare earth element depletion, high K/Rb, Na/K, and K/Ba ratios, and constant silica values. The close compositional similarities between ocean floor basalts and Ca-rich achondrites was taken as evidence of their 'primitive' nature (Engel et al., 1965) and consequently ocean floor basalts were regarded as providing a 'window' to the upper mantle, unaffected by the possible contamination by sialic continental crust.

More recent studies, aided by detailed sampling by means of drilling and use of submersibles, have however shown that despite broad

2. SCOPE OF STUDY

This thesis involves the quantitative investigation of the compositional variation in lava suites from four widely separated areas within the Atlantic Ocean: the Mid-Atlantic Ridge at $36^{\circ}49'N$, the Islas Orcadas fracture zone on the Southwest Indian Ocean Ridge, the Conrad fracture zone on the America-Anarctica Ridge, and Bouvet Island situated at the southernmost extremity of the Mid-Atlantic Ridge. The basalts from these areas range in composition from the most primitive (e.g. basalts from $36^{\circ}49'N$ on the Mid-Atlantic Ridge) to the most evolved ever recovered from the ocean basins (e.g. ferrobasalts from the Conrad fracture zone). The main aims of the study include:

(i) To establish the extent of compositional variation within the individual lava suites.

(ii) To augment bulk rock chemical data with a detailed investigation of the chemistry of phenocryst and matrix mineral phases.

(iii) To quantitatively evaluate possible petrogenetic models to explain the observed petrographic and geochemical variation within the individual lava suites.

(iv) To evaluate criteria for the recognition of potential 'primary' magmas and to discuss source area characteristics in the light of estimated 'primary' magma compositions.

Petrogenetic models involving fractional crystallisation and crystal accumulation have been evaluated quantitatively by means of least squares calculations (e.g. Bryan et al., 1969). Further evaluation of these models has been carried out using trace elements and by applying recently developed ideas of trace element distribution (e.g. Gast, 1968; Shaw, 1970). Geochemical modelling has been taken to the extreme and postulated petrogenetic models have been assessed according

to rigid criteria in an attempt to rigorously evaluate the extent to which the observed compositional variations can be attributed solely to the above-mentioned processes, rather than to a combination of processes. The success achieved in most instances supports the contention that much of the compositional variation observed in different oceanic environments can be attributed to a simple process of phenocryst redistribution which, given precise geochemical data, can be accurately modelled.

The data from the four study areas are finally compared in an attempt to provide answers to some important questions in terms of the relationship between rock type and tectonic setting:

(i) Do rock types from ridge systems and fracture zones show consistent differences?

(ii) Do the differences in igneous rock suites (e.g. ridge-axis basalts and fracture zone basalts) reflect source area differences or differences introduced by differentiation processes, and how do these relate to the tectonic setting?

(iii) To what extent can systematic geochemical differences be attributed to the action of mantle plumes?

This thesis falls naturally into five main sections: a discussion of computer-simulated models and the determination of trace element distribution coefficients; a study of the basalts from the Mid-Atlantic Ridge at $36^{\circ}49'N$; a study of the basalts from the Islas Orcadas and Conrad fracture zones; a study of the Bouvet Island lavas; and finally a general evaluation in terms of tectonic setting. The chapters related to the study of the four oceanic areas are each preceded by a more specific introduction.

CHAPTER II

ANALYTICAL TECHNIQUES, SOURCES AND PRESENTATION OF DATA, AND PETROLOGIC MODELLING

1. ANALYTICAL TECHNIQUES

All bulk rock major and trace element analyses have been obtained using X-ray fluorescence techniques (XRF). The specific methods used are those currently applied in the Geochemistry Department, University of Cape Town. They have been described by Willis et al. (1971, 1972) and are briefly summarised in the appendix. Analytical errors and detection limits for individual major and trace elements are also given in the appendix. Mineral compositions (except in the case of mineral separates which were analysed by XRF) have been determined with the use of a Cambridge Microscan 5 microanalyser (electron microprobe). The analytical data were reduced using the method of Bence and Albee (1968) with the alpha factors of Albee and Ray (1970). Operating conditions, standards used, and analytical errors are given in the appendix. In selected cases minerals have been analysed for Sr (as a trace element) by electron microprobe. The analytical technique developed has been described by Rickard and le Roex (1977) and is outlined in the appendix.

2. PRESENTATION OF ANALYTICAL DATA

2.1 Bulk Rock Analyses

Individual bulk rock major and trace element analyses, CIPW norms and selected interelement ratios are presented in tables throughout the text. Since the Fe_2O_3 content of basaltic rocks commonly reflects post consolidation oxidation, FeO was not specifically analysed for in most

samples (by wet chemistry), and an Fe_2O_3/FeO ratio of 0.15 has been assumed throughout. This value has been selected in accord with the suggestion of Brooks (1976). Only in selected instances were H_2O^+ and CO_2 determined by gas chromatograph. For all other analyses, loss on ignition at 1000°C (LOI) was determined and is arbitrarily expressed as H_2O^+ in the tables of analyses. Since much of the volatile content of the basalts studied can probably be attributed to post consolidation alteration and is therefore not a primary compositional feature, all data have been normalised to 100% on a volatile-free basis before use in calculations and diagrams.

2.2 Mineral Analyses

The number of mineral analyses made in the course of this study is rather large and only selected analyses are presented in tables within the text. All individual analyses are given in microfiche tables as appendices to the thesis and table numbers are listed in the appendix. For silicate minerals all Fe has been expressed as FeO and no attempt has been made to calculate Fe_2O_3 for pyroxenes or amphiboles. Consideration of charge balance in certain pyroxenes indicates that it is probable that a significant proportion of Fe_2O_3 is present, but owing to the large errors inherent in the estimation of ferric iron in silicates (e.g. Papike et al., 1974), Fe_2O_3 has not been calculated.

Ferric iron in Fe-Ti oxides and Cr-spinels has been estimated from the microprobe data (total Fe as FeO) by assuming stoichiometry and charge balance. The method used is based on the same principles as discussed by Neumann (1976) and expresses ferric iron as equivalent to the difference between the ideal charge based on stoichiometry and the calculated charge. The proportion of ferric iron has then been used to

calculate end-member components of titanomagnetite (ulvospinel and magnetite) and ilmenite (ilmenite, geikelite and hematite). In calculating these end-members, minor components have been excluded and only the pure end-member cations have been used to calculate the end-member molecules. For ilmenite, end-member compositions have been calculated as follows:

$$\text{Il (mol \%)} = \frac{\text{Ti} - \text{Mg}}{\frac{1}{2}\text{Fe}^{3+} + \text{Ti}} * 100$$

$$\text{Gk (mol \%)} = \frac{\text{Mg}}{\frac{1}{2}\text{Fe}^{3+} + \text{Ti}} * 100$$

$$\text{Hm (mol \%)} = \frac{\frac{1}{2}\text{Fe}^{3+}}{\frac{1}{2}\text{Fe}^{3+} + \text{Ti}} * 100$$

Titanomagnetite end-members were calculated as follows:

$$\text{Us (mol \%)} = \frac{\text{Ti}}{\frac{1}{2}\text{Fe}^{3+} + \text{Ti}} * 100$$

$$\text{Mt (mol \%)} = \frac{\frac{1}{2}\text{Fe}^{3+}}{\frac{1}{2}\text{Fe}^{3+} + \text{Ti}} * 100$$

These are simplified molecular formulae and titanomagnetite end-members such as hercynite ($FeAl_2O_4$), magnesioferrite ($MgFe_2O_4$) and jacobsite ($MnFe_2O_4$), which are present in only very minor amounts (<1 mol %), have been ignored. The ratios Cr/Cr+Al, Mg/Mg+Fe^{2+} and Fe^{3+}/Fe^{3+}+Cr+Al have been calculated for Cr-spinels and are noted in the tables as Cr, Mg and Fe respectively.

3. PETROLOGIC MODELLING

3.1 Fractional Crystallisation

3.1.1 Major Elements:

One of the more important aims of this study is to investigate the role of fractional crystallisation as a mechanism for producing compositional variations observed in oceanic basalts from different tectonic environments, e.g. ridge systems, fracture zones and oceanic islands. In order to evaluate whether fractional crystallisation is responsible for the observed total major element variation, use has been made of a least squares approximation programme based on that of Bryan et al. (1969). The programme enables the solution of an overdetermined major element data matrix to test whether or not postulated 'parent' and 'daughter' compositions can be related by addition or subtraction of various minerals (vectors). The matrix may be weighted or unweighted, and the calculated solutions are unconstrained in terms of sign (i.e. may be positive or negative). For this study a simple unweighted data matrix has been used throughout. To maintain an overdetermined matrix, the maximum number of vectors (e.g. fractionating phases plus 'parent' and 'daughter' compositions) must be at least one less than the number of elements in the matrix. Mixing calculations (the terms 'least squares approximation', 'mixing calculation' and 'mix' will be used synonomously throughout this thesis) involving 'parent' and 'daughter' compositions can be approached as either fractional crystallisation (i.e. 'parent' - various minerals = 'daughter') or crystal accumulation (i.e. 'parent' + various minerals = 'daughter') problems. Since both are linear mass balance calculations, either can be performed in reverse. For example, fractional crystallisation can be regarded as

'daughter' + various minerals = 'parent'. This latter approach has the advantage of yielding the proportion of residual magma (F) and of fractionating minerals directly and is therefore adopted throughout this study.

Input data for the computer program used (written by A.R. Duncan of this Department) comprises 'parent' and 'daughter' compositions together with proposed fractionating mineral phases. All data were first normalised to 100% volatile free, with all Fe expressed as FeO. Any elements not desired in the calculations (e.g. K - due to alteration) were then excluded. For Fe-Ti oxides all Fe was expressed as FeO before normalising to 100%. The daughter composition and mineral phases are 'independent vectors' in the program which then calculates the 'dependent vector' (parent composition). Output from the program consists of the observed and calculated composition of the dependent 'vector' (i.e. the parent composition), the oxide residuals, the sum of squares of the oxide residuals and the calculated proportions of the independent 'vectors' (i.e. 'daughter' composition and fractionating mineral phases). Standard deviations on the proportions of the independent 'vectors' are also presented in the output. These data can then be evaluated to assess the consistency of the mixing calculation. In general, solutions were assumed to be potentially valid only if the sum of squares of residuals was <0.10 (e.g. Wright, 1974), with no major discrepancies occurring in any of the individual oxide residuals. This constraint is compatible with the precision and accuracy of the data used. For samples which were obviously altered (as shown by petrographic examination and chemical data such as LOI) the individual oxide residuals were evaluated in accordance with their known mobility during weathering;

such models were regarded as being provisionally acceptable if the residuals were less than the known uncertainty in the whole rock compositional data. Additional criteria that were evaluated before a mix was accepted were that the proportions of the independent 'vectors' should sum close to 100% and that the standard deviations on the individual vectors and on the total should be as small as possible. Large standard deviations imply that the mixing calculation is not tightly constrained. A most important criterion was that the calculated proportions of fractionating phases, and their compositions, should be realistic in terms of the modal proportions and the compositions observed in the 'parent' and 'daughter' rocks. Examples of what are regarded as an acceptable and an unacceptable least squares approximation are given in Tables 2-1 and 2-2 respectively.

The choice of suitable mineral compositions to use in the mixing calculations was based on the range of determined mineral compositions in the proposed 'parent' and 'daughter'. Where this range was extremely large (between parent and daughter), pure end-member compositions (e.g. Fo, Fa, An, Ab) were used for the initial mix. The relative proportions of the end-members, calculated by the program as best satisfying the known compositional variation, were then combined to give the appropriate mineral composition. This composition was then compared to the observed range in mineral composition and if realistic, the mixing calculation was repeated using the deduced mineral compositions.

3.1.2 Trace Elements:

Once an acceptable fractional crystallisation model had been obtained for the major elements, the trace element data were used to provide an independent check on the validity of the proposed model.

Table 2-1: An example of an acceptable major element least squares approximation relating two arbitrary magmas, 'PARENT' and 'DAUGHTER', via fractional crystallisation of olivine, plagioclase, clinopyroxene, ilmenite and titanomagnetite. Note the low sum of squares of residuals and the low standard deviations on the 'vectors'.

Input data

	PARENT	PLAG	OLIV	CPX	ILM	TiMGT	DAUGHTER
SiO_2	50.71	53.38	35.28	48.68	0.15	0.23	55.62
TiO_2	3.54	0.11	0.11	2.03	50.00	23.61	2.00
Al_2O_3	15.56	28.68	0.06	3.90	0.07	0.48	15.90
FeO*	12.11	0.67	36.25	10.69	47.02	74.44	11.21
MnO	0.19	0.01	0.51	0.17	0.53	0.51	0.21
MgO	4.35	0.13	27.29	13.54	2.04	0.22	2.22
CaO	8.82	12.18	0.31	20.51	0.18	0.51	6.12
Na_2O	3.40	4.77	0.01	0.47	0.01	0.01	4.42
K_2O	1.32	0.08	0.01	0.01	0.01	0.01	2.30

Least squares approximation

	PARENT			MIX		
	OBS.	CALC.	DIFF.	VECTOR	Wt.%	S.D.
SiO_2	50.71	50.70	-0.01	DAUGHTER	56.19	0.91
TiO_2	3.54	3.54	0.00	PLAG	21.17	0.74
Al_2O_3	15.56	15.55	-0.01	OLIV	4.28	0.45
FeO*	12.11	12.11	0.00	CPX	13.61	0.52
MnO	0.19	0.19	0.00	ILM	3.61	0.30
MgO	4.35	4.36	0.01	TiMGT	1.29	0.33
CaO	8.82	8.84	0.02			
Na_2O	3.40	3.56	0.16	TOTAL	100.16	1.43
K_2O	1.32	1.31	-0.01			

Sum of squares of residuals = 0.026

Table 2-2: An example of an unacceptable major element least squares approximation. The input data is the same as that in Table 2-1 with the exception that ilmenite is excluded as a fractionating phase. Note the high sum of squares of residuals, and the high standard deviations on the 'vectors'.

Input data

as in Table 2-1.

Least squares approximation

	PARENT				MIX	
	OBS.	CALC.	DIFF.	VECTOR	Wt.%	S.D.
SiO_2	50.71	50.68	-0.03	DAUGHTER	56.97	5.57
TiO_2	3.54	2.56	-0.98	PLAG	20.24	4.48
Al_2O_3	15.56	15.48	-0.08	OLIV	2.31	2.59
FeO*	12.11	12.42	0.31	CPX	15.12	3.12
MnO	0.19	0.18	-0.01	TiMGT	4.63	1.10
MgO	4.35	3.98	-0.37			
CaO	8.82	9.08	0.26	TOTAL	99.27	8.29
Na_2O	3.40	3.56	0.16			
K_2O	1.32	1.33	0.01			

Sum of squares of differences = 1.29

Only models that satisfy the trace element variations as well as the major element constraints are regarded as being internally consistent and potentially valid.

The partitioning of a trace element in a crystal-magma system can be described either in terms of surface equilibrium (i.e. Rayleigh Fractionation) or of total equilibrium (i.e. Nernst) crystallisation. Expressions describing the behaviour of a trace element during surface equilibrium have been proposed by Gast (1968) and Greenland (1970) and are reproduced below. Following Gast's formulation, the concentration of a trace element a in the residual magma is given by:

$$C_a^l / C_a^o = F^{\bar{D}_a - 1} \quad \ldots\ldots\ldots\ldots\ldots\ldots\ldots\ldots\ldots\ldots \quad (1)$$

where F = weight fraction of residual liquid (calc. in the major element model).

C_a^l = concentration of trace element a in the residual liquid.

C_a^o = concentration of trace element a in the initial liquid.

$\bar{D}_a$ = bulk distribution coefficient for element a.

The bulk distribution coefficient $\bar{D}$ is a function of all the phases crystallising from the initial liquid, such that

$$\bar{D}_a = \sum_i D_i^a \cdot X_i \quad \ldots\ldots\ldots\ldots\ldots\ldots\ldots\ldots\ldots\ldots \quad (2)$$

where D_i^a = the distribution coefficient for element a in mineral i.

X_i = weight fraction of mineral i (calculated in the major element model).

Equations (1) and (2) assume constant distribution coefficients. For linear variation of the distribution coefficient with crystallisation such that $D = D_a + dF$ (i.e. D changes from $D_o + d$ to D_o as F changes from 1 to 0), equation (1) can be rewritten as (Greenland, 1970):

$$\ln \frac{C^l}{C^o} = (D_o - 1)\ln F + d(F - 1) \quad \ldots\ldots\ldots\ldots\ldots\ldots (3)$$

The lack of specific knowledge on the variation of D with crystallisation limits the application of equation (3), and since the differences produced by using equation (3) rather than equation (1) are within the uncertainties of the known values for distribution coefficients, equation (1) has been used in preference.

The above equations allow quantitative modelling of trace element variations during fractional crystallisation. To model trace element variations during crystal accumulation, it is necessary to calculate first the average trace element content of the accumulating minerals. This was done by assuming surface equilibrium and using the formula proposed by Gast (1968), modified to allow for the simultaneous crystallisation of more than one phase (le Roex and Reid, 1978):

$$\bar{C}_a / C_a^o = \frac{1 - F^{\bar{D}_a}}{1 - F} \quad \ldots\ldots\ldots\ldots\ldots\ldots\ldots\ldots (4)$$

where $\bar{C}_a$ = average concentration of element a in a suite of perfectly zoned crystals.

Le Roex and Reid (1978) have noted that two assumptions are necessary before crystal accumulation can be modelled quantitatively:

(1) Phenocrysts were homogeneously distributed throughout the magma.

(2) At the instant when the weight fraction of residual liquid was equal to F, all the phenocrysts migrated to the cumulus-enriched magma.

These assumptions allow an estimate of the maximum value for F, using the following equation:

$$F = 1 - M \frac{V_1}{V_2} \quad \ldots\ldots\ldots\

X_i = weight fraction of the phenocryst assemblage added to the cumulus-enriched magma (calculated in the major element model).

Recently, O'Hara (1977) has formulated equations for quantitatively modelling more complex processes such as open-system fractional crystallisation. These formulations allow for the periodic replenishment of a magma chamber by new batches of unfractionated 'parental' magma from depth. Ignoring the added possibility of digestion of previously erupted basalt, O'Hara's equation for describing this process can be written as follows:

$$C_B^S/C_o = \frac{(X+Y)(1-X)^{D-1}}{1-(1-X-Y)(1-X)^{D-1}} \quad \ldots\ldots\ldots\ldots\ldots\ldots (7)$$

where C_B^S = concentration of an element in the residual liquid of the fractionation cycle, in the steady state.

C_o = initial concentration of an element in the parental liquid.

X = weight fraction of cumulate formed from the magma in each cycle.

Y = weight fraction of the original liquid before this fractionation, which is extracted as a lava flow at the end of each cycle.

D = bulk distribution coefficient.

O'Hara (1977) has suggested that such an open-system fractionation process provides the possibility of fractionating incompatible element ratios, rather than attributing them to source area heterogeneities. Quantitative application of this type of model, however, indicates that only a limited degree of incompatible element fractiona-

tion is achieved and is not a viable alternative in those cases where mantle heterogeneity has been invoked on the basis of trace element data (Pankhurst, 1977). Although the model of O'Hara (1977) may be geologically more reasonable than single closed-system fractionation and may provide a mechanism for explaining the commonly noted decoupling of compatible and incompatible elements in oceanic basalts, it is unlikely to result in large changes in diagnostic incompatible element ratios. O'Hara's equations have not been quantitatively applied in this study, but the qualitative effects of open-system fractionation are apparent in selected cases and are further discussed where relevant.

An alternative method for evaluating quantitatively the trace element variation within a suite of lavas is that introduced by Allègre et al. (1977) and discussed further by Minster et al. (1977). This method involves the calculation of bulk distribution coefficients for a range of elements from the slope of trace element variations on log-log plots involving a highly incompatible element as the abscissa. Combining these calculated bulk distribution coefficients with known mineral-liquid distribution coefficients in a matrix of equations enables one to solve for the weight fractions of individual minerals which are theoretically contributing to the fractionation sequence. At present mineral-liquid distribution coefficient data are insufficiently well known and consequently errors are propagated and amplified during solution of the relevant equations by matrix inversion. This can lead to results which are incompatible with known petrology and therefore this method is not used here.

Most of the lava suites studied are characterised by zoned phenocrysts and thus Rayleigh fractionation has been adopted for trace

element modelling. Equations for modelling equilibrium or Nernst crystallisation are the same as those applicable for equilibrium partial melting. The relevant equation as formulated by Shaw (1970) is given in the following section on partial melting (equation 9).

3.2 Partial Melting

3.2.1 Major Elements:

Quantitative modelling of partial melting processes has generally been limited to consideration of trace element variations. However, Hanson and Langmuir (1978) have recently developed a method for calculating the behaviour of major elements using an approach similar to that used for trace elements, and this will be briefly outlined below.

The behaviour of major elements can be modelled in a fashion similar to that used for evaluating trace element behaviour during partial melting, but with the additional constraints imposed by stoichiometric requirements. During equilibrium or batch partial melting, the distribution of an element between the melt and the residual solid must satisfy the mass balance:

$$C_o = FC_l + (1-F)C_s \quad \ldots\ldots\ldots\ldots\ldots\ldots\ldots\ldots\ldots\ldots (8)$$

where C_o = initial source concentration.

C_l = concentration in the liquid.

C_s = concentration in the residual source.

F = the fraction of melting.

This mass balance equation can be rewritten in the form of the equilibrium or batch melting equation of Schilling (1967) and Shaw (1970):

$$C_l/C_o = 1/(F+D(1-F)) \quad \ldots\ldots\ldots\ldots\ldots\ldots\ldots\ldots\ldots\ldots (9)$$

and

$$C_s = C_l \cdot D \quad \ldots\ldots\ldots\ldots\ldots\ldots\ldots\ldots\ldots\ldots\ldots\ldots (10)$$

where D = bulk distribution coefficient.

Hanson and Langmuir (1978) have shown that equations (9) and (10) can be used to model FeO and MgO variations during partial melting by utilising the known mineral-liquid K_d's, in conjunction with known stoichiometric constraints in mantle minerals. Their approach is briefly as follows:

The calculation of the concentration of MgO and FeO in a mantle-derived melt requires knowledge of the following parameters: (1) initial concentration (mol %) of MgO and FeO in the source (C_o); (2) the temperature of melting (T); (3) the degree of melting (F); and (4) the bulk distribution coefficients for MgO and FeO (D). It is necessary to assume values for the first three parameters, while the fourth can be calculated by indirect means. Although K_d's for all mantle minerals are not known, it is possible to model MgO and FeO accurately, providing residual olivine is present, because of the following relation for D:

$$D = \frac{C_s}{C_l} = \frac{C_s}{C_{ol}} \cdot \frac{C_{ol}}{C_l} = \frac{C_s}{C_{ol}} \cdot K_d^{ol/liq} \quad \ldots\ldots\ldots (11)$$

where C_{ol} = concentration of FeO or MgO in olivine.

The bulk distribution coefficient D for MgO and FeO can therefore be calculated with a knowledge of their concentration in the residual source, their concentration in the residual olivine and $K_d^{ol/liq}$. The $K_d^{ol/liq}$ for MgO and FeO is temperature dependent and over the range 1000-1300°C at 1 atm. is given by the expressions (Roeder & Emslie, 1970):

$$\log_{10} K_d^{MgO} = \frac{3740}{T(K)} - 1.85 \quad \ldots\ldots\ldots\ldots\ldots\ldots (12)$$

$$\log_{10} K_d^{FeO} = \frac{3911}{T(K)} - 2.50 \quad \ldots\ldots\ldots\ldots\ldots\ldots (13)$$

When only olivine is left in the residue, i.e. for the maximum degree of

melting, then $D = K_d^{ol/liq}$ (from equation 10) and the composition of the melt is controlled only by the temperature of melting and the composition of the residual olivine. For the minimum degree of melting ($F = 0$), D can be calculated from equation (11) with $C_s = C_o$. For intermediate degrees of melting between these two extremes, the value of D can be calculated via an iterative procedure involving equations (9), (10) and (11), the stoichiometric relationships relating the molar concentration of MgO and FeO in olivine:

$$MgO + FeO = 66.67 \quad \ldots\ldots\ldots\ldots\ldots\ldots\ldots\ldots \quad (14)$$

and the equilibrium constant K_D relating the FeO/MgO ratio of a liquid to the FeO/MgO ratio of an equilibrium olivine:

$$K_D^{FeO/MgO} = (FeO/MgO)^{ol}/(FeO/MgO)^{liq} \quad \ldots\ldots\ldots\ldots \quad (15)$$
$$= 0.30 \pm 0.03 \quad \text{(Roeder \& Emslie, 1970)}$$

The procedure involves estimating an initial D which lies between the maximum and minimum values (equation 11). This allows the calculation of an estimated C_1 for a given F and source composition. The estimated D_1^{FeO} and C_1^{MgO} enables the calculation of the equilibrium olivine composition (equations 15 and 14) and an estimate of the residual source composition (C_s) (equation 10). These data can then be combined to give a new improved estimate of D (equation 11). This is repeated until the iteration converges to give a final estimation of D and thereby the MgO and FeO content of the equilibrium melt. This normally occurs within three or four iterations. When K_d's for other major elements in mantle phases become available, their behaviour during partial melting will be able to be evaluated in a similar fashion.

3.2.2 Trace Elements:

Models describing trace element behaviour during partial melting have been extensively discussed by Schilling and Winchester (1967), Gast (1968), Shaw (1970), Hertogen & Gijbels (1976), Consolmagno & Drake (1976), Langmuir & Hanson (1977), and Langmuir et al. (1977). As in fractional crystallisation, melting can occur with total equilibrium (batch melting) or under surface equilibrium conditions (fractional melting). The simplest models and relevant equations describing the trace element distribution during partial melting are discussed below (formulations and definitions are taken from the above references).

(1) Equilibrium (or batch) melting - melting in which the liquid remains continually in equilibrium with the residual solids until the moment of removal when all the melt is removed:

$$C^l/C^o = \frac{1}{D_o + F(1-P)} \quad \ldots\ldots\ldots\ldots\ldots\ldots\ldots\ldots \quad (16)$$

where D_o = bulk distribution coefficient calculated from the initial source mineral assemblage.

P = bulk distribution coefficient calculated from the proportions of phases entering the melt.

This equation has been extended by Hertogen and Gijbels (1976) to allow for incongruent melting and for the disappearance of phases during melting. Consolmagno and Drake (1976) have noted that provided the residual mineral composition of the source is known, the complex equations of Hertogen and Gijbels (1976) simplify to the original Shaw (1970) type equation where D_o and P can be replaced by D, the bulk distribution coefficient based on the residual mineral assemblage.

(2) Fractional melting - melting in which infinitesimal fractions of melt are continuously and completely removed from the solid phases as melting proceeds.

$$C^l/C^o = \frac{1}{D_o}\left(1-\frac{PF}{D_o}\right)^{(1/P-1)} \quad \ldots\ldots\ldots\ldots\ldots\ldots\ldots (17)$$

(3) Fractional melting plus accumulation - melting occurs as in (2) above, but melt fractions accumulate and mix together.

$$C^l/C^o = \frac{1}{F}\left(1 - \left(1-\frac{PF}{D_o}\right)^{(1/P)}\right. \quad \ldots\ldots\ldots\ldots\ldots\ldots\ldots (18)$$

Models (2) and (3) involve only surface equilibria and the composition of the melt is influenced by all initial phases, i.e. even if a phase is exhausted during melting it will leave its imprint on the liquid. To allow for the possibility of a phase being exhausted during a given melting interval, Hertogen and Gijbels (1976) have extended equations (17) and (18) respectively as follows:

$$C^l/C^o = \frac{M_A}{(1-F_A)D_A}\left[1 - \frac{P_{II}(F-F_A)}{D_A(1-F_A)}\right]^{\left(1/P_{II} - 1\right)} \quad \ldots\ldots (19)$$

and

$$C^l/C^o = \frac{1}{F}\left\{1 - M_A\left[1 - \frac{P_{II}(F-F_A)}{D_A(1-F_A)}\right]^{1/P_{II}}\right\} \quad \ldots\ldots (20)$$

where $M_A = 1 - \frac{C_A^l}{C_o} F_A$

and F_A = degree of melting corresponding to the disappearance of a phase 'A'.

D_A = bulk distribution coefficient calculated at the point where phase 'A' is exhausted.

P_{II} = bulk distribution coefficient calculated from the proportions of minerals entering the melt after the disappearance of phase 'A'.

C_A^l = concentration in the liquid at the point where phase 'A' is exhausted.

(4) Continuous melting - melting in which fractions of the melt are continuously, but not completely, removed from the solid residue as melting proceeds. The first melt formed by this model is derived by simple batch melting (equation 16). The source for the second melt is calculated as the sum of the solid residue from the first melt plus the fraction of first melt left behind, i.e.

$$C^{BS} = X^l \cdot C^l + (1 - X^l)C^S \quad \ldots\ldots\ldots\ldots\ldots\ldots (21)$$

where C^{BS} = concentration in the bulk residue.

X^l = weight fraction of residual melt.

C^l = concentration in the residual melt.

C^S = concentration in the residual solid.

The concentration in the second melt is then calculated using this new source and equation (16), and so on.

The concept of continuous melting was introduced by Langmuir and Hanson (1977) and Langmuir et al. (1977) as representing a more realistic model of the partial melting process. The model is of a process gradational between batch melting and fractional melting and involves increments of melting occurring in a source consisting of both melt and solid residue. The melt increments may then either be erupted as separate magmas or alternatively may accumulate and mix elsewhere. Models developed by Sleep (1975) and experimental work and theoretical

considerations of Arndt (1977a) support models in which the melt remains in the residue until a certain degree of melting is reached. Beyond this point the melt becomes unstable and separation occurs, leaving some melt behind in the residue.

Evaluation of the role of partial melting in various sample suites studied in this project has involved the use of a computer program written so as to produce results for all four of the models given above, together also with the respective residual source concentrations. Results are calculated for any range of F-values and compared (in terms of sums of squares of differences) with the postulated primary magma. A typical input and output for an arbitrary F-value is shown in Tables 2-3 and 2-4. The data in Table 2-4 also serve to illustrate quantitatively some of the differences in the results obtained using the various models. In Tables 2-3 and 2-4 the term 'incremental equilibrium melting plus accumulation' is synonomous with the term 'continuous melting' in which melt increments accumulate and mix. All trace element data in Tables 2-3 and 2-4 are given in ppm, while the oxide data are given in weight percent. Most emphasis in this thesis has been placed on simple equilibrium melting rather than on the more complex models as the results were found to be consistent (within the uncertainty of the data) with the analytical data, and it was not necessary to appeal to more complex processes.

4. DISTRIBUTION COEFFICIENTS

Reliable values for trace element distribution coefficients are essential for the accurate quantitative geochemical evaluation of petrogenetic processes. Although there is a wealth of data on crystal/liquid distribution coefficients in the literature, and significant

TABLE 2-3: EXAMPLE OF A TYPICAL INPUT DATA-SET TO THE PARTIAL MELTING PROGRAM.

INPUT DATA
****

A) INITIAL SOURCE COMPOSITION
****

ELEMENT	CONCENTRATION
NI	1850.000
SC	17.000
ZR	9.000
NB	1.000
Y	5.200
RB	.570
BA	7.000
SR	20.000
GA	3.000
K20	.030
P205	.018
TI02	.180

MINERAL	INITIAL WT. FRACTION
OLIVINE	.580
OPX	.220
CPX	.140
GARNET	.060

B) MELTING PARAMETERS
****

MINERAL	WT. FRACTION ENTERING LIQUID (1)	(2)	(3)	(4)	INCONGRUENT MELTING PRODUCTS	WEIGHT FRACTIONS
OLIVINE	.100	.200				
OPX	.100	.200				
CPX	.400	.600				
GARNET	.400					

INITIAL DEGREE OF MELTING:	.0500
FINAL DEGREE OF MELTING:	.1900
MELTING INCREMENTED BY:	.0200
AMOUNT OF IRREMOVABLE MELT:	.0500

DEGREE OF BATCH MELTING PRECEEDING INCREMENTAL EQUILIBRIUM MELTING: .0500

(1) INITIAL WEIGHT FRACTIONS ENTERING LIQUID
(2)-(4) WEIGHT FRACTIONS ENTERING LIQUID AFTER DISAPPEARENCE OF SUCESSIVE PHASES

C) DISTRIBUTION COEFFICIENTS USED
****

ELEMENT	OLIVINE	OPX	CPx	GARNET
NI	9.350	4.000	1.500	.100
SC	.150	.400	2.000	10.000
ZR	.010	.010	.200	1.200
NB	.010	.010	.030	.010
Y	.100	.100	.500	3.000
RB	.010	.010	.011	.015
BA	.010	.010	.013	.023
SR	.010	.010	.100	.010
GA	.010	.010	.400	.010
K20	.010	.010	.011	.015
P205	.010	.010	.010	.100

TABLE 2-4: EXAMPLE OF A TYPICAL OUTPUT FROM THE PARTIAL MELTING PROGRAM.

F = .1700 NON-MODAL MELTING
****

ELEMENT	BULK D	INITIAL SOURCE	MAGMA	EQUILIBRIUM MELTING ********** MELT	EQUILIBRIUM MELTING ********** SOURCE	INCREMENTAL EQUIL. MELTING + ACCUM. ********** MELT (ACCUM.)	INCREMENTAL EQUIL. MELTING + ACCUM. ********** SOURCE	FRACTIONAL MELTING ********** MELT (ACCUM.)	FRACTIONAL MELTING ********** MELT	FRACTIONAL MELTING ********** SOURCE
NI	7.321	1.850+003	270.	293.	2.165+003	288.	2.054+003	268.	293.	2.170+003
SC	.384	17.0	35.4	36.1	13.2	30.0	15.3	26.3	41.7	15.1
ZR	.028	9.00	49.2	47.1	1.22	47.8	2.63	51.5	11.7	.299
NB	.012	1.00	6.10	5.57	6.499-002	3.79	7.224-002	5.88	2.628-005	3.058-007
Y	.138	5.20	19.0	18.6	2.48	18.5	3.37	18.2	19.1	2.53
RB	.010	.570	3.40	3.20	3.222-002	2.06	3.423-002	3.35	8.623-007	8.694-009
BA	.010	7.00	41.6	39.2	.402	25.7	.441	41.2	2.170-005	2.224-007
SR	.018	20.0	114.	108.	1.90	86.2	2.37	118.	.134	2.320-003
GA	.047	3.00	15.2	14.6	.625	14.6	.856	17.1	2.68	.112
K2O	.010	3.000-002	.170	.168	1.696-003	.108	1.802-003	.176	4.538-008	4.576-010
P2O5	.010	1.800-002	9.000-002	.101	1.010-003	6.998-002	1.350-003	.106	4.900-007	4.900-009
TIO2	.030	.180	.870	.932	2.640-002	.882	3.869-002	1.05	5.696-002	1.594-003
SUM OF SQUARES OF DIFFERENCES:				556.		1.408+003		415.	1.687+004	
SUM OF SQUARES OF % DIFFERENCES:				481.		7.170+003		1.681+003	8.169+004	

MINERAL PROPORTIONS IN RESIDUE:

MINERAL	PROPORTION
OLIVINE	.6742
OPX	.2420
CPX	.0838
GARNET	.0000

** NB ** F = .0500 BEFORE INCREMENTAL EQUILIBRIUM MELTING IS INITIATED(IF THERE IS 5.00% BATCH MELTING PRECEEDING REMOVAL).THEREAFTER THE MELT IS REMOVED IN 2.00% INCREMENTS,LEAVING 5.00% IRREMOVABLE MELT CONTRIBUTING TO THE SOURCE COMPOSITION.

experimental progress has been made in estimating distribution coefficients under controlled conditions, the choice of appropriate values for D for a given magma composition is still somewhat arbitrary. Experimental results clearly indicate that the magnitude of D is dependent on composition (e.g. Henderson, 1977; Hart and Davis, 1978; Glassley and Piper, 1978; Pierozynski and Henderson, 1978; Ryerson and Hess, 1978; Irving, 1978; Lindstrom, 1976; Irving and Frey, 1976, 1978; Watson, 1977; Takahashi, 1978), temperature (e.g. Leeman, 1974; Lindstrom, 1976; Leeman and Scheidegger, 1977; Leeman and Lindstrom, 1978; Arndt, 1977b; Drake and Weill, 1975; Long, 1978), and pressure (e.g. Mysen and Kushiro, 1979; Mysen, 1976a,b, 1978). In addition parameters such as fO_2 and pH_2O (e.g. Mysen and Kushiro, 1976; Mysen, 1978, 1979) and adsorption (e.g. Dowty, 1977) also affect trace element distribution. Ideally, D's should be determined on the specific lava suite of interest either by experimental measurements on the compositions in question or by phenocryst-matrix separation and analysis. This is rarely possible and one is generally forced to turn to the literature of published distribution coefficients and attempt to select 'realistic' values. The range in published values is however often large and the choice of 'inappropriate' values, especially for the more compatible elements, can lead to misleading conclusions. A compilation of published and unpublished (this work) mineral/liquid distribution coefficients for a large number of minerals and trace elements is given in Tables A2-1 to A2-13 in the appendix. This compilation includes experimentally determined values, data from phenocryst/matrix pairs and data from coexisting minerals in ultramafic rocks. Selected values from this compilation have been used in the quantitative modelling throughout the thesis; where necessary

the basis for the choice of specific values is discussed in the relevant sections.

4.1 Mineral Separates

Prior to the publications of McCallum and Charette (1978) and Pearce and Norry (1979), there was little quantitative information available on the distribution coefficients for Zr, Nb and Y in basaltic minerals. These three elements have generally been regarded as being incompatible during partial melting and fractional crystallisation processes. Since much importance will be attached to the quantitative variation of these elements during magma generation and subsequent fractionation, an attempt has been made to determine applicable D's specifically for these elements. Minerals have been separated from four porphyritic lavas and three kimberlite nodules to allow XRF and spark source mass spectroscopy analysis of coexisting phases for the selected trace elements. Mineral/liquid and mineral/mineral distribution coefficients have been combined to estimate mineral/liquid distribution coefficients for all of the separated minerals.

To ensure a high degree of purity in the mineral separates, all grains were hand picked under a binocular microscope from 20-40 mesh jaw crush material and then washed in HCl in an ultrasonic cleaner. This cleaned material was then crushed further and any foreign material and impure grains were removed by hand picking. This final separate was then finally washed again in HCl, dried and analysed for major and trace elements by XRF or for selected trace elements by spark source mass spectroscopy. Trace elements determined by XRF were analysed using a loose powder technique to ensure infinite thickness. Analytical errors are comparable to those given in Table A1-2 in the appendix for trace

elements which were determined on pressed briquettes.

4.1.1 Phenocryst-matrix Data:

(i) Olivine, plagioclase and clinopyroxene

Two porphyritic alkali-basalts from Gough Island (ALR51G and ALR52G) were selected for mineral separation to allow estimation of mineral/liquid distribution coefficients for, amongst other elements, Zr, Nb and Y in olivine, clinopyroxene and plagioclase. Clinopyroxene from an additional extremely porphyritic lava (ALR41G) was also separated and analysed. Whole rock analyses done by XRF for ALR51G and ALR52G, together with matrix and mineral separate analyses for these two samples and the clinopyroxene separate from ALR41G are given in Table 2-5. These data have been used to calculate mineral/liquid distribution coefficients for a Rayleigh fractionation model in the following manner:

Rearrangement of equation (4) as follows:

$$\bar{C}/C^{o} = \frac{1 - F^{\bar{D}}}{1 - F}$$

$$\longrightarrow \quad \bar{D} = \frac{1n(1-(\bar{C}/C^{o})(1-F))}{1n\ F} \qquad \ldots\ldots\ldots\ldots\ldots\ldots\ldots\ldots (22)$$

enables the bulk distribution coefficient ($\bar{D}$) to be expressed as a function of the average trace element concentration of a suite of zoned crystals, the initial liquid composition (C^{o}) and the amount of residual liquid (F). The individual mineral/liquid distribution coefficients can then in turn be derived from $\bar{D}$ by the following relationships:

$$\bar{D} = D^{a/l} \cdot X_a + D^{b/l} \cdot X_b + \text{-----} + D^{n/l} \cdot X_n \quad \ldots\ldots (23)$$

and

$$D^{a/l} = D^{a/b} \times D^{b/l} \qquad \ldots\ldots\ldots\ldots\ldots\ldots\ldots\ldots (24)$$

T A B L E 2-5

MAJOR & TRACE ELEMENT ANALYSES OF MINERAL SEPARATES FROM GOUGH ISLAND

	ALR 52G	52MAT	52OL	52PYX	52PLAG	ALR 51G	51MAT	51OL	51PYX	41PYX
SIO2	49.64	50.22	38.71	50.01	53.08	47.64	49.92	38.73	49.63	50.92
TIO2	3.09	3.51	.10	1.80	.18	2.74	3.34	.07	1.68	1.55
AL203	14.96	15.69	.20	4.44	29.21	11.98	15.02	.19	4.92	3.84
FE203	1.73	1.75	-	-	-	1.82	1.62	-	-	-
FEO	8.67	8.74	22.46	8.12	.80	9.10	8.10	20.21	7.05	7.48
MNO	.15	.15	.30	.16	.01	.16	.14	.27	.13	.15
MGO	6.14	4.54	38.59	14.78	.23	12.11	6.93	40.18	15.22	15.99
CAO	7.73	7.14	.31	20.59	12.15	9.11	9.55	.32	20.58	19.99
NA20	3.64	3.57	.04	.39	3.94	2.91	3.10	.03	.42	.37
K20	3.11	3.52	.03	.06	.73	1.80	2.36	.02	.02	.06
P205	.74	.83	.03	.08	.07	.44	.57	.03	.04	.03
H20+	.58	-	-	-	-	.30	-	-	-	-
H20-	.17	-	-	-	-	.10	-	-	-	-
CO2	-	-	-	-	-	-	-	-	-	-
TOTAL	100.35	99.66	100.77	100.43	100.40	100.21	100.65	100.05	99.69	100.38

* * * TRACE ELEMENTS * * *

ZR	355.	410.	9.5	84.4	10.5	240.	313.	7.1	71.1	56.5
NB	64.1	69.1	3.7	6.1	2.1	38.8	42.0	2.2	4.7	3.5
Y	33.4	34.2	4.5	24.2	6.7	25.7	28.8	3.6	19.7	19.9
RB	70.9	76.2	ND	ND	2.9	40.2	49.1	ND	ND	ND
BA	860.	935.	6.1	12.2	320.	591.	678.	3.0	14.1	8.9
SR	847.	847.	8.0	96.0	2094.	630.	759.	4.6	94.7	77.0
CO	38.3	36.3	191.	46.2	ND	64.4	47.2	194.	45.6	49.8
CR	142.	108.	78.3	1396.	6.5	414.	323.	108.	3010.	2942.
NI	111.	67.3	1359.	147.	6.4	351.	169.	1485.	254.	294.
V	174.	236.	19.0	299.	7.2	181.	239.	15.9	274.	360.
ZN	105.	112.	224.	49.9	5.1	101.	98.7	180.	39.5	47.2
CU	33.5	32.2	ND	8.2	15.5	45.6	49.1	ND	8.9	ND
SC	16.9	16.1	3.5	78.4	4.1	23.9	25.0	3.3	76.6	77.3
TH	-	-	-	-	-	-	-	-	-	-
PB	-	-	-	-	-	-	-	-	-	-
GA	23.7	23.3	ND	9.6	21.6	17.9	19.6	ND	7.2	8.1

** ND = NOT DETECTED **

where $D^{a/l}$ = mineral/liquid distribution coefficient for mineral a.

$D^{a/b}$ = mineral/mineral distribution coefficient for minerals a and b.

X_a = weight fraction of mineral a.

Comination of equations (23) and (24) leads to the following expression:

$$\overline{D} = D_a(X_a + D^{a/b} X_b + \text{-----} + D^{a/n} X_n) \quad \text{.....} \quad (25)$$

To calculate mineral/liquid distribution coefficients, knowledge is required of the following parameters: (1) F - the weight fraction of residual liquid (equivalent to the groundmass); (2) X_i - the weight fractions of individual mineral phases; (3) $\overline{C}$ - the average trace element content of these mineral phases; (4) C^o - the initial liquid composition (equivalent to the whole rock composition); and (5) $\overline{D}$ - the bulk distribution coefficient. The weight fractions of residual liquid (F) and mineral phases (X_a) have been calculated by least squares approximations using the major element data for the whole rock, the matrix (groundmass) and the individual minerals. The calculated chemical modes for ALR52G and ALR51G are as follows:

ALR52G		ALR51G	
COMP.	Wt.Fr.	COMP.	Wt.Fr.
Matrix	0.8732	Matrix	0.7811
Oliv.	0.0379	Oliv.	0.1398
Pyx.	0.0499	Pyx.	0.0791
Plag.	0.0389		

This data can then be combined with that in Table 2-5 to calculate the average trace element content of the phenocryst minerals which can then

be substituted into equation (22) together with F and the whole rock composition to give an estimate of $\bar{D}$. The weight fractions of the phenocryst minerals and the calculated mineral/mineral distribution coefficients can then be substituted into equation (25) in order to solve for D.

Implicit in the above calculations is the fact that the whole rock composition represents a liquid composition, i.e. is not phenocryst-enriched. Since both samples are porphyritic with large (1-4mm) phenocrysts of olivine and clinopyroxene set in a fine grained matrix, the possibility of phenocryst enrichment has been monitored by calculating olivine-whole rock K_D^{Fe-Mg}'s (see Chapter III, section 5.2.1 for definition and discussion) for each sample using, in each case, the most Mg-rich olivine analysed by electron microprobe. Results of these calculations suggest that ALR51G could well represent a liquid composition ($K_D = 0.32$), while ALR52G is highly unlikely to represent a liquid composition ($K_D = 0.60$). Mineral/liquid distribution coefficients have therefore only been calculated for ALR52G. The calculated Rayleigh distribution coefficients are given in Table 2-6, together with simple Nernst (equilibrium) distribution coefficients (i.e. the ratio of the concentration of an element in a mineral to the concentration of the element in the groundmass). The mineral/mineral distribution coefficients used in equation (24) have been determined from both ALR51G and ALR52G, and slight differences have led to slightly different calculated D's in Table 2-6. The values on the right have been derived using the mineral/mineral distribution coefficients from ALR51G. The low concentration of incompatible elements (e.g. Rb, Ba) in the mineral separates (less than 1% of their concentration in the matrix) attests to the

Table 2-6: Mineral-liquid distribution coefficients calculated assuming a Rayleigh crystallisation model for two Gough Island lavas. Values given in brackets have been calculated assuming an equilibrium (Nernst) crystallisation model. See text for further explanation.

	$D^{cpx/liq}$	$D^{ol/liq}$	$D^{plag/liq}$
Zr	0.22 - 0.23 (0.21)	0.03 - 0.02 (0.02)	0.03 (0.03)
Nb	0.09 - 0.10 (0.09)	0.05 (0.05)	0.03 (0.03)
Y	0.69 - 0.70 (0.71)	0.13 (0.13)	0.18 (0.20)
Rb	-	-	0.04 (0.04)
Ba	0.013 (0.013)	0.007 (0.007)	0.35 (0.34)
Sr	0.11 (0.11)	0.009 (0.009)	2.44 (2.47)
Co	1.30 - 1.27 (1.27)	5.36 - 5.40 (5.26)	-
Cr	12.89 -13.08 (12.93)	0.72 - 0.47 (0.73)	0.06 (0.06)
Ni	1.77 - 2.60 (2.18)	16.33 -15.23 (20.19)	0.08 (0.10)
V	1.68 - 1.69 (1.27)	0.11 - 0.10 (0.08)	0.04 (0.03)
Zn	0.47 - 0.46 (0.45)	2.11 (2.00)	0.05 (0.05)
Cu	0.23 (0.25)	-	0.44 (0.48)
Sc	4.98 - 4.99 (4.87)	0.22 (0.22)	0.26 (0.25)
Ga	0.39 (0.41)	-	0.88 (0.93)

purity of the separated fractions. In addition to olivine, clinopyroxene and plagioclase phenocrysts, ALR52G has sparse (<0.5%) phenocrysts of titano-magnetite which were not separated from the matrix. This could lead to very slight errors in the calculated distribution coefficients.

The data given in Table 2-6 compare favourably with available published values (Tables A2-1, A2-2, A2-5). The distribution coefficients for the immobile incompatible elements Zr, Nb and Y (e.g. Pearce and Cann, 1973; Erlank and Kable, 1976) indicate that Y is significantly less incompatible with respect to the major basaltic minerals (olivine, clinopyroxene and plagioclase) than either Zr or Nb, and that clinopyroxene favours Zr over Nb ($D^{Zr}_{cpx} = 0.22$, $D^{Nb}_{cpx} = 0.09$), a feature also noted by McCallum and Charette (1978). The high distribution coefficient for Y in clinopyroxene ($D^{Y}_{cpx} = 0.70$) is in good agreement with data from Ewart and Taylor (1969) and Pearce and Norry (1979), and with available data on the partitioning of the heavy rare earth elements into clinopyroxene (e.g. Arth, 1976). The less incompatible nature of Ba in plagioclase (An_{60}) relative to Rb is also evident from the data in Tables 2-5 and 2-6. A final point worth emphasising from Table 2-6 is the high distribution coefficients for Zn in olivine ($D^{Zn}_{ol} = 2.1$) and clinopyroxene ($D^{Zn}_{cpx} = 0.47$) which, if applicable at mantle depth and temperature, would account for the limited range of Zn in basaltic rocks since a bulk distribution coefficient for Zn would be close to unity. Choices of appropriate values for quantitative modelling are discussed more fully in the individual chapters.

(ii) Titanomagnetite

Due to the marked lack of published distribution coefficient data for Zr, Nb and Y between Fe-Ti oxides and liquid, an attempt has been

made to estimate these distribution coefficients. A porphyritic benmoreite (WJ10B) from Bouvet Island (see Chapter V) was selected as being the most suitable sample due to the relatively large size (0.5mm) and discrete habit of the titanomagnetite phenocrysts. Seventy milligrams were separated by using a magnet and then cleaned by hand picking; it was however not possible to obtain a completely pure separate. The final separate was then analysed for Zr, Nb, Y and Ba by spark source mass spectroscopy at the Australian National University, Canberra, by kind favour of A.R. Duncan.

Although Ba is excluded from titanomagnetite, analysis of the mineral separate showed the presence of significant Ba (216 ppm), indicating substantial 'matrix' contamination (Ba tends to be excluded from the other phenocryst phases). Assuming Rayleigh fractionation and using equation (1), it is possible to calculate the Ba concentration of the 'matrix' in WJ10B. The weight fractions of the phenocrysts in WJ10B have been recalculated from modal proportions (vol %), determined by point counting, using mineral densities from Deer, Howie and Zussman (1966), and are as follows: matrix 0.7437, plagioclase 0.1720, clinopyroxene 0.0365, olivine 0.0111, titanomagnetite 0.0367. Assuming $D^{Ba}_{plag} = 0.25$ (selected from Table A2-2) and that the distribution coefficients for the other phases all equal 0.01, then a Ba concentration of 754 ppm is obtained for the matrix. A value of 749 ppm is obtained assuming equilibrium crystallisation and using equation (9). Hereafter, values given in brackets are for equilibrium crystallisation. This implies 28.6% (28.8%) matrix contamination in the separate. The amount of Zr, Nb and Y in the 'matrix' portion of the separate can similarly be calculated using known D's for the phenocryst phases (Tables A2-1,

A2-2, A2-5) and initially assuming a $D_{mgt} = 0.01$ for the three elements. This enables one to remove the effect of matrix contamination for these elements and finally to calculate distribution coefficients. The whole calculation can then be repeated with these improved D's and so on until the iteration converges. In practice the bulk D's are found to be relatively small and so the calculation converges on the second iteration. Corrected and uncorrected concentrations in the titanomagnetite using this procedure and the concentrations in the whole rock are given below in ppm.

	Whole Rock	Uncorrected Ti-Mgt	Corrected Ti-Mgt
Ba	590	216	0 (0)
Zr	676	462	206 (205)
Nb	99	272	237 (237)
Y	63	37	14 (14)

Titanomagnetite/matrix distribution coefficients can now be calculated assuming either equilibrium (Nernst) crystallisation (equation 9) or fractional (Rayleigh) crystallisation (equation 4). For equilibrium crystallisation, equation (9) can be used in an iterative fashion to calculate a titanomagnetite/matrix distribution coefficient. This is done by initially assuming a D for titanomagnetite for a given trace element which then enables the calculation of an approximate bulk D using equation (2) and the distribution coefficients given below (source of data is Tables A2-1, A2-2 and A2-5).

	Plag.	Cpx	Olivine
Zr	0.01	0.21	0.01
Nb	0.01	0.09	0.01
Y	0.18	0.70	0.12

Equation (9) can now be used to calculate a first approximation to the concentration of the respective trace elements in the 'matrix' which can then be ratioed to the concentration in the titanomagnetite to obtain an initial distribution coefficient. This distribution coefficient can then be used to calculate a new bulk D which in turn enables the calculation of a better approximation of the respective trace element in the matrix and so eventually a better estimation of the titanomagnetite D. This is done until the calculated D's converge. Equilibrium distribution coefficients calculated in this fashion are as follows:

$$D^{Zr}_{Ti\text{-}Mgt} = 0.23, \qquad D^{Nb}_{Ti\text{-}Mgt} = 1.96, \qquad D^{Y}_{Ti\text{-}Mgt} = 0.18$$

Since the phenocrysts in WJ10B show evidence of zoning, D's calculated assuming Rayleigh fractionation might be more realistic. To enable use of equation (4) in this respect, it is however necessary to make one assumption. This assumption is that since the amount of titanomagnetite is small relative to the total phenocryst population, the trace element contents of the remaining phenocrysts are relatively unaffected by its presence. This assumption enables one to calculate the average trace element content of the remaining phenocryst phases using equations (2) and (4). The known trace element content of the titanomagnetite can then be added to that of the other phenocrysts (in the correct proportions) and then substituting this value ($\overline{C}$) into equation (4), $\overline{D}_a$ can be solved for. With a knowledge of $\overline{D}_a$, equation (2) enables the solution of D^a_{Mgt}. This method results in the following estimated D's for titanomagnetite:

$$D^{Zr}_{Ti\text{-}Mgt} = 0.24, \qquad D^{Nb}_{Ti\text{-}Mgt} = 2.16, \qquad D^{Y}_{Ti\text{-}Mgt} = 0.17$$

These data compare favourably with those values obtained assuming equilibrium crystallisation and will be used as estimates for titanomagnetite/liquid distribution coefficients for quantitative petrogenetic modelling throughout this thesis.

4.1.2 Mantle-nodule Data

Shimizu and Allègre (1978) have reported ion-microprobe data for, amongst other elements, Zr, Co, Sc and V in coexisting garnet and clinopyroxene from kimberlite nodules. Calculated garnet-cpx distribution coefficients for these elements using Shimizu and Allègre's data are given in Table 2-8B. The most interesting feature of these data is the strong preference of Zr for garnet relative to clinopyroxene. The ability for Zr to substitute readily into the garnet lattice is indicated by the production of synthetic Ca-Zr garnets (e.g. Ito and Frondel, 1967; Erlank et al., 1978b), and of the rare occurrence of natural zirconium-rich garnets (e.g. Platt and Mitchell, 1979). In order to investigate the partitioning of specifically Zr, Nb and Y among mantle phases, clinopyroxene, garnet and orthopyroxene were separated from a garnet websterite (JJG1424) from the Mothae kimberlite pipe, Lesotho (kindly provided by Dr. J.J. Gurney). Phlogopite and clinopyroxene, and phlogopite and ilmenite were separated from two phlogopite nodules (198) and AJE31) from the Bultfontein kimberlite pipe, Kimberley (kindly provided by Prof. A.J. Erlank).

Major and trace element analyses of these mineral separates by XRF are given in Table 2-7 and the major elements are compared to average microprobe analyses of individual grains in Table A1-4 in the appendix. It was not possible to make a fusion disc of the ilmenite separate for major element XRF analysis and so an average microprobe analysis of the major

Table 2-7: Major and trace element data for mineral separates from kimberlite nodules JJG1424, 198 and AJE31, determined by XRF. With the exception of ilmenite, all Fe is expressed as FeO.

	JJG1424			198		AJE31	
	GARNET	CPX	OPX	CPX	PHLOGO	PHLOGO	ILM††
SiO_2	42.78	54.57	57.18	53.59	43.26	42.26	ND
TiO_2	0.09	0.27	0.14	0.29	3.69	0.59	51.81
Al_2O_3	23.15	3.03	1.29	0.73	8.65	10.73	0.04
Cr_2O_3	1.06	0.80	0.19	0.13	0.07	0.18	2.67
Fe_2O_3	-	-	-	-	-	-	8.10
FeO	7.71	1.65	4.78	6.60	6.67	5.00	26.76
MnO	0.34	0.05	0.09	0.15	0.03	0.03	0.40
MgO	20.55	16.44	35.57	15.41	22.53	25.60	10.91
CaO	4.62	21.45	0.34	20.25	0.40	0.07	-
Na_2O	0.04	1.43	0.08	1.19	0.28	0.17	-
K_2O	ND	ND	ND	0.16	9.08	10.25	-
H_2O^+	-	-	-	0.17	-	-	-
CO_2	-	-	-	0.23	-	-	-
Zr	30.5	56.0	3.5	37.4	18.0	22.0	282
Nb	<1.5	<1.5	1.8	4.4	13.1	38.0	3520
Y	23.4	5.0	<1.5	9.6	2.5	3.4	7.4
Rb	<1.5	<1.5	<1.5	5.0	451	578	24.2
Ba	<2.0	4.2	10.6	2860	6676	388	311
Sr	<1.5	323	3.0	775	365	16.7	127
Co	42.9	175	56.5	33.3	95	74.3	195
Cr	6912	5025	1288	821	500	1241	-
Ni	30.1	281	587	165	652	1301	1458
V	155	496	71.8	388	179	51.9	825
Zn	7.6	7.0	30.9	28.5	57.0	42.1	126
Cu	7.2	7.7	9.5	17.4	29.2	<3.0	48.1
Sc	67.8	25.7	1.7	40.0	2.8	2.1	22.1

†† Major element composition determined by electron microprobe.

elements is given in Table 2-7. The excellent major element agreement between the XRF mineral separate data and the microprobe data from individual grains (Table A1-4) plus the low concentrations of elements such as Rb and Ba attest to the high purity of the garnet websterite separates. The high Rb and Ba contents of the clinopyroxene and ilmenite from the phlogopite nodules suggest that these separates are not as pure and may contain a significant amount of impurity. Less importance has therefore been attached to these data, but they do serve to give an approximate estimate of the distribution coefficients of some important trace elements such as Zr, Nb and Y. The temperature and pressure of equilibration of the phlogopite nodules is not known but following the methods of Ellis and Green (1979) and Wood (1974) the conditions of equilibration for the garnet websterite are 1180°C at 45 kbar. These data are in good agreement with the results of studies on similar nodules from the Lesotho area (J.J. Gurney, pers. comm.).

The trace element data given in Table 2-7 have been expressed in terms of mineral/mineral distribution coefficients in Table 2-8A. Combination of these data with published clinopyroxene/liquid distribution coefficients allow the estimation of mineral/liquid distribution coefficients via the relationship given in equation (24). Results of these calculations are given in Table 2-9. They were derived from the data in Table 2-8A and B in combination with the clinopyroxene/liquid distribution coefficients from Table 2-6 and the published values from Lindstrom (1976), Bougault and Hekinian (1974) and McCallum and Charette (1978). In the absence of experimental values, these data have been used in the quantitative evaluation of partial melting processes, bearing in mind however the effects of composition, temperature and pressure.

Table 2-8: Calculated mineral/mineral D's: - Kimberlite nodules.

A. This work:

	$D^{gt/cpx}$	$D^{cpx/opx}$	$D^{gt/opx}$	$D^{cpx/ph}$	$D^{Ilm/ph}$	$D^{cpx/Ilm}$
Zr	0.54	16.0	8.64	2.08	12.8	0.16
Nb	±1	-	-	0.34	93	.004
Y	4.68	-	-	3.84	2,18	1.76
Rb	-	-	-	-	-	-
Ba	-	0.40	-	-	-	-
Sr	-	-	-	-	-	-
Co	2.45	0.31	0.76	0.35	2.62	0.92
Ni	0.11	0.48	0.05	0.25	1.12	0.22
V	0.31	6.91	2.16	2.17	15.9	0.14
Zn	1.09	0.23	0.25	0.50	3.00	0.17
Cu	0.94	0.81	0.76	0.60	-	-
Sc	2.64	15.1	39.9	14.3	10.5	1.36

B. Shimizu and Allègre (1978)

	$D^{gt/cpx}$ (N=12)
Zr	4.99 ± 2.9 (0.75 - 11.0)
Co	1.62 ± 0.63 (0.80 - 3.0)
V	2.00 ± 0.84 (0.85 - 3.4)
Sc	5.66 ± 1.27 (3.11 - 7.38)

	$D^{gt/liq}$	$D^{opx/liq}$	$D^{Ilm/liq}$	$D^{phl/liq}$	$D^{cpx/liq}$
Zr	0.02 - 2.42	.003 - .014	0.19 - 1.38	0.01 - 0.11	0.04 - 0.22
Nb	0.03 - 0.09	0.04 - 0.11	7.5 - 22.5	0.09 - 0.26	0.03 - 0.09
Y	3.28	-	0.40	0.18	0.70
Sc	2.61 - 65	0.06 - 0.58	0.62 - 6.43	0.06 - 0.61	0.84 - 8.75
Co	0.40 - 6.0	1.61 - 6.45	1.46	3.83	0.50 - 2.0
Ni	0.17 - 0.96	3.15 - 18.1	6.86 - 39.5	6.04 - 34.8	1.51 - 8.69
V	0.01 - 2.64	0.01 - 1.23	0.29 - 61	0.77	0.04 - 8.50
Zn	0.51 - 0.55	2.04 - 2.17	2.76 - 2.94	0.94 - 1.00	0.47 - 0.50
Cu	0.17 - 0.22	0.22 - 0.28	-	0.30 - 0.38	0.18 - 0.23

Table 2-9: Calculated mineral/liquid distribution coefficients for garnet, orthopyroxene, ilmenite and phlogopite. Values were calculated by combining the mineral/cpx distribution coefficinets given in Table 2-8 with cpx/liquid distribution coefficients given above. The sources of cpx/liquid distribution coefficients were; this study (Table 2-6), McCallum and Charette (1978), Bougault and Hekinian (1974) and Lindstrom (1976).

CHAPTER III

MID-ATLANTIC RIDGE AT $36^{\circ}49'N$ - FAMOUS

1. INTRODUCTION

One of the most intensely investigated areas of the ocean floor is that situated in the central rift valley of the Mid-Atlantic Ridge (MAR) at $36^{\circ}50'N$ (Fig. 3-1). The area lies just to the south of the Azores and within the geochemical transition zone between the 'normal' large-ion lithophile (LIL) element-depleted, low Sr^{87}/Sr^{86}, mid-ocean ridge basalts (MORB) south of $33^{\circ}N$ and the LIL element-enriched, higher Sr^{87}/Sr^{86}, basalts to the north in the vicinity of the Azores Plateau (Schilling, 1975a; White and Schilling, 1978). Samples were collected during Project FAMOUS (French-American Mid-Ocean Undersea Study) which was initiated as a joint French-American undertaking and resulted in over 150 samples being recovered from an area of approximately 15 km^2 within the inner floor and adjacent walls of the rift valley. An important feature of the sampling in the FAMOUS area was the use of manned submersibles (Archimedes, Alvin and Cyana), in addition to more conventional dredging techniques. Many of the recovered rock samples could thus be precisely positioned to within 5 or 10 m relative to each other (Bryan and Moore, 1977).

Initial studies on the recovered rocks showed that with respect to major elements, the lavas from the FAMOUS area virtually span the compositional range of all basalts returned from the ocean floors. In addition some of the most primitive lavas and glasses (in terms of high MgO and Ni) reported from the ocean basins are to be found in the FAMOUS

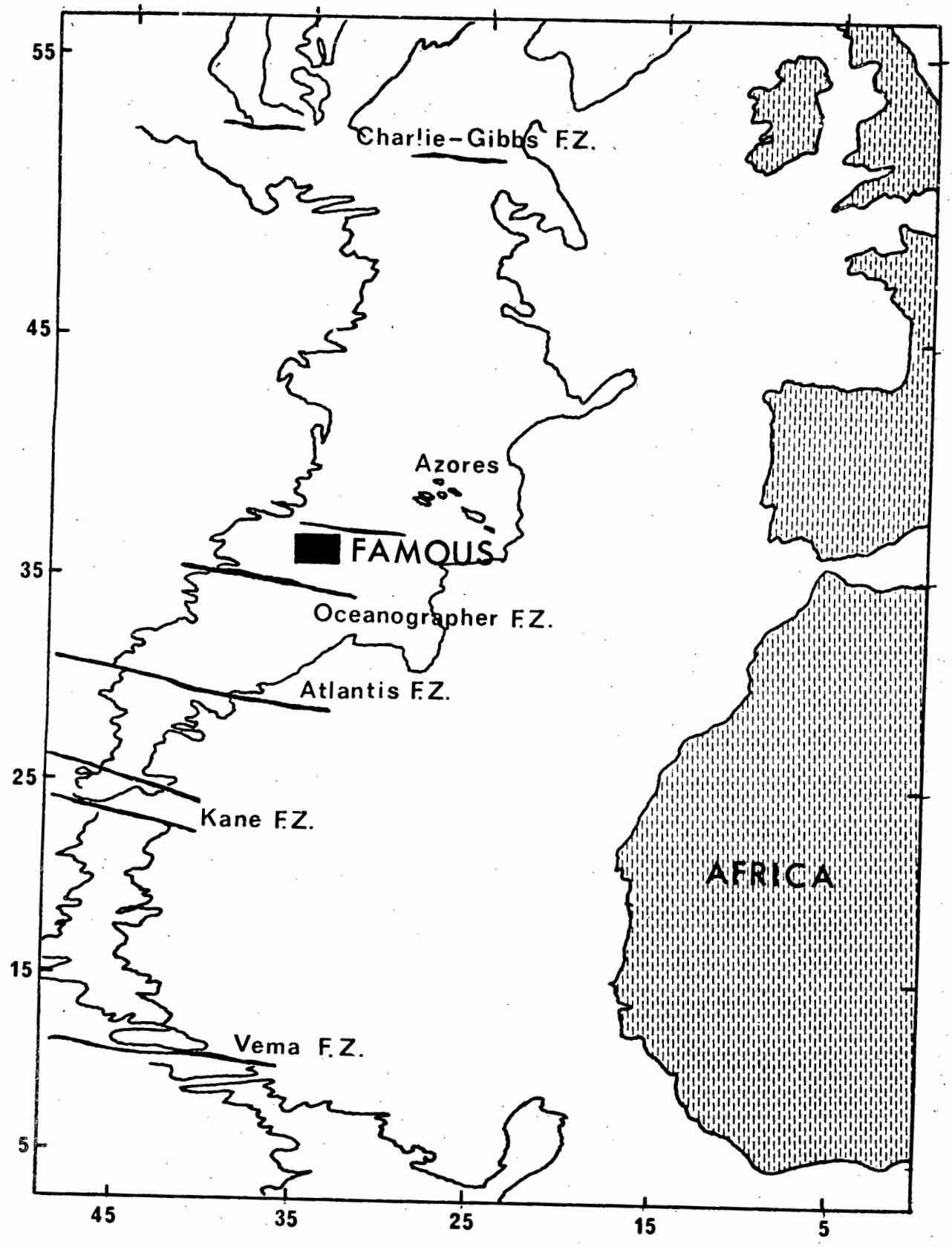

Fig. 3-1: Simplified bathymetric map of the North Atlantic Ocean (taken from Hekinian and Thompson, 1976) showing the location of the FAMOUS area.

area. The close spatial association of the samples, the known field relationships, and the diversity in major element composition provides therefore a unique opportunity to investigate the importance of low pressure crystal fractionation and/or partial melting processes as controlling factors in the evolution of ocean floor basalts.

Initial work on dredged samples was reported by Bougault and Hekinian (1974) and subsequently Arcyana (1977), Hekinian et al. (1976), Bryan and Moore (1977), White and Bryan (1977) and Langmuir et al. (1977) have reported on compositional variations primarily in basaltic glasses from the FAMOUS area. Various petrogenetic models have been proposed to account for the observed compositional variations. Bender et al. (1977) reported experimental work on primitive basalt glass from the FAMOUS area, and Nisbet and Fowler (1978) have reviewed the geochemical and geophysical data from the area and have attempted to derive a model that reconciles both sets of data.

This study was initially based on 6 samples (DR8, DR4, DR3-1, ARP74-11-18, ARP74-8-10 and CYP74-31-38) provided by Dr. H.D. Needham (Centre Océanologiqué de Bretagne, Brest). The samples were specifically chosen to span the compositional range shown by the FAMOUS collection to enable a detailed mineralogical and geochemical study of the relationship, if any, between the various rock types. On the basis of the preliminary findings from this suite of 6 samples, an additional 12 samples (ARP73-10-03C, DR1-122, DR4-303, DR4-329, DR9-308, DR9-322, DR9-323, DR3-131, DR2-174, DR2-301, DR10-101C, DR10-310) were selected, and kindly provided by Dr. Needham, in order to allow a more rigorous test to be made of the initial conclusions. Most of the findings presented in this chapter are based on the study of the initial 6 samples.

In addition to the analytical data determined by the writer, some data have been drawn from the literature, specifically the publications of Bougault and Hekinian (1974), Arcyana (1977) and Bougault et al. (1979).

In addition to the interest in the effect of low pressure fractionation as a controlling factor in the compositional diversity of the FAMOUS lavas, a major aim of the study is an attempt to elucidate the enigma of the identification of possible high magnesium basalt precursors to typical ocean floor basalt. The recovery of abundant high-Mg basalts (picrites) from the FAMOUS area (Bougault and Hekinian, 1974) provides a unique opportunity for the study of the whole rock and mineral chemistry of these lavas in an attempt to place genetic constraints on their origin.

2. GEOLOGICAL SETTING

The MAR at $36^{\circ}50'N$ comprises a main rift valley 26-30 km wide with walls 1.2-1.5 km high, and an inner rift valley 1.5-3 km wide with its floor 2.5-2.9 km below sea level (Hekinian et al., 1976). The inner rift valley is bounded by scarps 100-400 m high and defines the actual boundary where the African and North American plates are diverging at a rate of approximately 2.2 cm/yr (Hekinian et al., op. cit.). Topographic highs occur within the inner rift valley in the form of volcanic hills (e.g. Mt de Venus and Mt Pluto) which rise 100-250 m above the floor and mark the sites of some of the most recent volcanism.

The basalts recovered from the FAMOUS area have been classified on the basis of petrography into six categories: picritic basalts, olivine basalts, plagioclase-olivine basalts, highly phyric plagioclase basalts (HPPB), moderately phyric plagioclase basalts (MPPB), and plagioclase-pyroxene basalts (Arcyana, 1977). These rock types show an

assymetrical distribution within the rift valley (Fig. 3-2). Picritic basalts (20 - >40% modal olivine) are restricted to the inner floor of the rift valley and occur mainly on the flanks of Mt de Venus. Picrite DR8 was dredged from the flanks of the central high (Bougault and Hekinian, 1976) and ARP73-10-03C was sampled near the foot of the eastern slope of Mt de Venus (Arcyana, 1977). Olivine basalts (2-6% modal olivine, Hekinian et al., 1976) are also confined to the rift valley axis and are associated with Mt de Venus and Mt Pluto (Fig. 3-2). The olivine basalts studied were dredged from the inner floor (DR4, DR4-303, DR4-329, DR1-122) and from the foot of the western (DR9-308, DR9-322, DR9-323) and eastern walls (DR2-174) (Bougault and Hekinian, 1976).

Plagioclase-olivine basalts occur on both sides of the rift valley axis (to 1.4 km east and 2.0 km west; Hekinian et al., 1976) and also between Mt de Venus and Mt Pluto (Fig. 3-2). Plagioclase-olivine basalt ARP74-8-10 was sampled from the prolongation of the Eastern Marginal High (Arcyana, 1977).

There is some contradiction in the classification of some of the less phyric samples with Hekinian et al. (1976) not recognising the sub-division plagioclase-pyroxene basalts (Arcyana, 1977). The former authors have a general category of plagioclase-olivine-pyroxene basalts, which incorporates both the plagioclase-pyroxene and plagioclase-olivine basalts of Arcyana (1977). They also have a category of aphyric basalts which include many of the plagioclase-olivine basalts of Arcyana (1977). The classification proposed by Arcyana (1977) has been adopted for this study.

Plagioclase-pyroxene basalt CYP74-31-38 is a sample of thick dyke exposed on the western scarp of the inner floor. Sample DR2-301 was

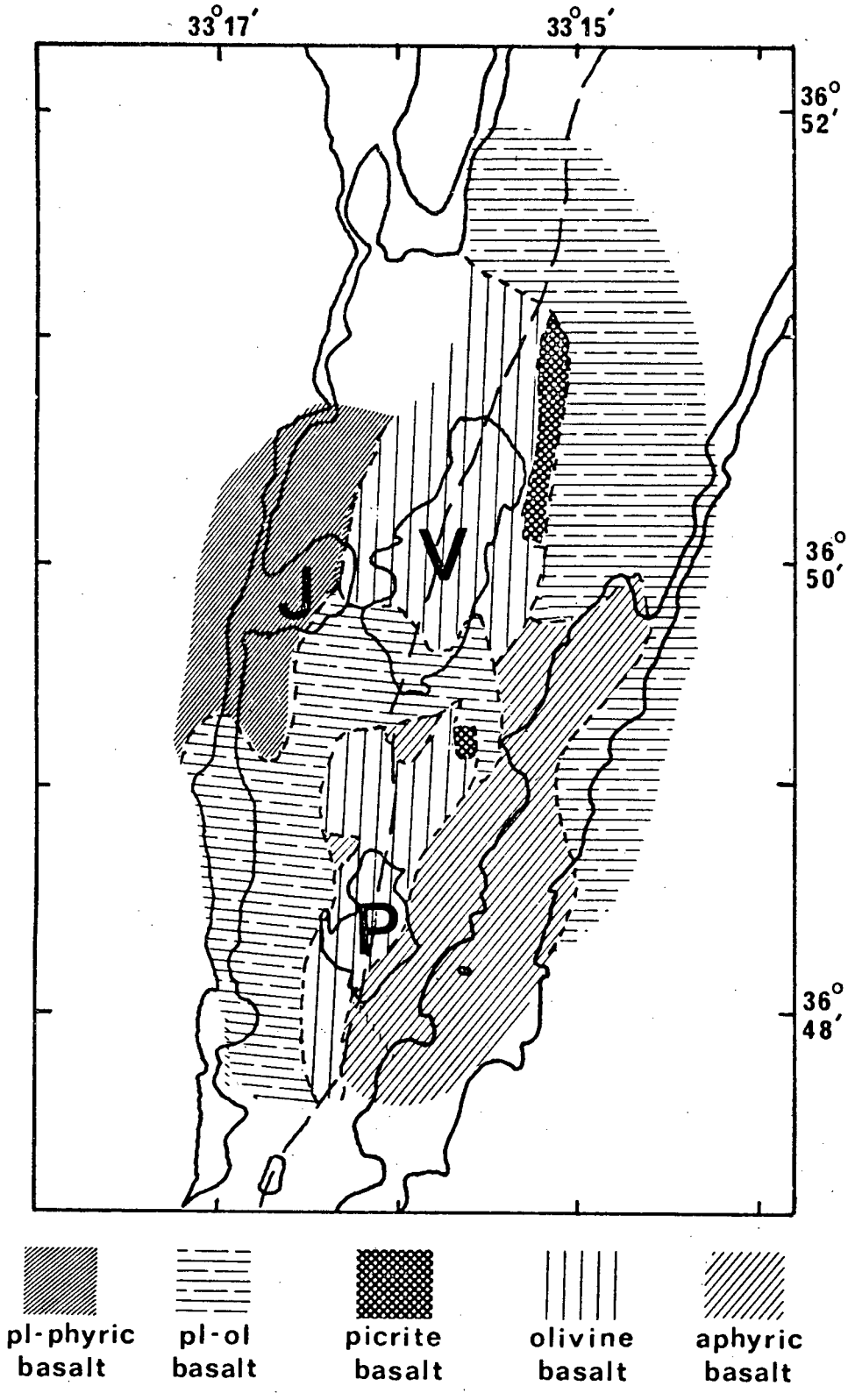

Fig. 3-2: Generalised distribution of five basalt types in the FAMOUS area, after Hekinian et al. 1976. Mt. Venus (V) and Mt. Pluto (P) are on the rift valley axis (longer dashed line). J, indicates Mt. Jupiter.

dredged from the eastern wall, while sample DR10-310 was dredged from the foot of the western wall.

Hekinian et al. (1976) have suggested that the plagioclase phyric basalts were restricted to the west rift valley wall (Fig. 3-2) which is the location of the HPPB DR10-101C. However, DR3-131 and DR3-1 are both HPPB's and were dredged from the eastern wall (Bougault and Hekinian, 1974). ARP74-11-18 has been classified as a MPPB by Arcyana (1977) and as a plagioclase-olivine-pyroxene basalt by Hekinian et al. (1976). Due to its extreme similarity to DR4 both in composition and texture, it will be classed in this work as an olivine basalt.

Samples studied in this thesis therefore include examples from each of the dominant petrographic categories and, in terms of spatial distribution, cover most of the sampled area. More detailed descriptions of sample locations are given in Arcyana (1977) and Bougault and Hekinian (1974).

3. PETROGRAPHY AND MINERAL ASSEMBLAGES

The petrography of the rocks recovered from the FAMOUS area has been extensively described by Bougault and Hekinian (1974), Arcyana (1977) and Hekinian et al. (1976) and only the more salient features pertinent to the rocks comprising this study will be described here.

3.1 Picritic basalts

The picritic basalts DR8 and ARP73-10-03C (10-03C) are highly porphyritic (Plate 3-1A) and are characterised by abundant (>20%) olivine phenocrysts (up to 4mm in diameter) portraying a variety of habits from euhedral to highly embayed (Plate 3-1B). Olivine phenocrysts show a very small compositional range (Fo_{91}-Fo_{89}) and are marked by a complete lack of zoning. Olivine microphenocrysts have a composition of Fo_{88}. Olivine

phenocrysts are also characterised by the presence of trapped melt inclusions which can reach sizes of up to 0.5 mm (Plate 3-1C). A feature of these Mg-rich olivines is their relatively high Cr_2O_3 contents. Average Cr_2O_3 concentrations range from 0.04 to 0.10% but can be as high as 0.19%. Representative olivine analyses are presented in Table 3-1 and individual analyses are given in microfiche Table F3-1. Plagioclase phenocrysts are relatively sparse in picrite DR8 and are absent in 10-03C, but plagioclase microlites are abundant. Plagioclase phenocrysts (1-2mm) in DR8 are generally rounded in habit and show compositional zoning covering nearly the full range in compositions observed, An_{91}-An_{81} (Fig. 3-3A, Table 3-1), while plagioclase microlites are slightly more sodic (An_{79}) (Fig. 3-3A, Table 3-1). Individual plagioclase analyses are presented in microfiche Table F3-2. Quench glass is present on the outer surface of DR8 and assuming this average glass to be in equilibrium with the plagioclase microlites present, a quench temperature of 1162°C is obtained using the Kudo-Weill plagioclase thermometer as modified by Mathez (1973).

Euhedral to subhedral 'Cr-spinel' phenocrysts (up to 1mm in diameter) occur as inclusions in, or attached to, olivine phenocrysts or as discrete crystals in the groundmass (Plates 3-1B, C and D). The spinels commonly contain trapped melt inclusions which occur either as a few large inclusions or as numerous small inclusions defining the dominant crystal faces (Plate 3-1D). Over 40 'Cr-spinels' have been analysed and two distinct populations were found. The dominant variety, comprising over 90% of the spinel phenocrysts, are red-brown in colour, show little zoning and in composition correspond to the magnesiochromites typical of basaltic lavas from the Mid-Atlantic Ridge

TABLE 3-1

FAMOUS AREA: SELECTED MINERAL ANALYSES. PICRITIC BASALTS

	1	2	3	4	5	6	7	8	9	10
SIO2	40.47	40.79	40.28	40.88	39.91	ND	-	-	.09	.15
TIO2	ND	.03	.02	-	.03	-	.29	.31	.17	.18
AL203	.07	.07	.07	-	.08	26.43	28.22	29.10	43.18	41.93
CR203	.04	.05	.08	-	.07	40.90	40.14	39.41	24.59	26.04
FE203	-	-	-	-	-	5.70	4.21	4.27	2.32	2.08
FEO	9.60	10.28	10.54	8.35	12.08	8.47	10.18	10.08	9.84	10.75
MNO	-	-	-	.12	-	-	-	-	-	-
MGO	49.13	48.60	47.96	50.06	47.05	17.90	17.44	17.69	18.90	18.31
CAO	.35	.40	.36	-	.34	-	.04	.04	.06	.06
NA20	-	-	-	-	-	-	-	-	-	-
K20	-	-	-	-	-	-	-	-	-	-
NIO	.28	.29	.26	.33	.22	.19	-	-	-	-
TOTAL	99.95	100.51	99.57	99.74	99.78	99.60	100.52	100.90	99.15	99.50

* * ATOMIC PROPORTIONS BASED ON SELECTED NO. OF OXYGENS * *

OXYGEN	4	4	4	4	4	4	4	4	4	4
SI	.993	.998	.996	.999	.992	-	-	-	.002	.004
AL	.002	.002	.002	-	.002	.919	.970	.992	1.404	1.370
TI	-	.001	.000	-	.001	-	.006	.007	.004	.004
CR	.001	.001	.002	-	.001	.954	.925	.901	.536	.571
FE3+	-	-	-	-	-	.127	.092	.093	.048	.043
FE2+	.197	.210	.218	.171	.251	.209	.248	.244	.227	.249
MN	-	-	-	.002	-	-	-	-	-	-
MG	1.797	1.772	1.768	1.823	1.744	.787	.758	.762	.777	.757
CA	.009	.010	.010	-	.009	-	.001	.001	.002	.002
NA	-	-	-	-	-	-	-	-	-	-
K	-	-	-	-	-	-	-	-	-	-
NI	.006	.006	.005	.006	.004	.005	-	-	-	-
SUM	3.005	3.000	3.001	3.001	3.005	3.000	3.000	3.000	3.000	3.000
	FO 90.12	FO 89.39	FO 89.02	FO 91.44	FO 87.41	CR .51	CR .49	CR .48	CR .28	CR .29
	FA 9.88	FA 10.61	FA 10.98	FA 8.56	FA 12.59	MG .79	MG .75	MG .76	MG .77	MG .75
						FE .06	FE .05	FE .05	FE .02	FE .02

* * * S A M P L E D I R E C T O R Y * * *

ANALYSIS NO.	DESCRIPTION
1	OLIVINE, PHENO (CORE, ADJ. TO CR-SPINEL)
2	OLIVINE, PHENO (AS ABOVE, RIM)
3	OLIVINE, PHENO (ADJ. TO GLASS INCL.)
4	OLIVINE, PHENO (LARGE, SUBHEDRAL)
5	OLIVINE, MICROPHENO
6	CR-SPINEL
7	CR-SPINEL (CORE, ADJ. TO OLIVINE)
8	CR-SPINEL (AS ABOVE, RIM)
9	CR-SPINEL (HIGH AL, INCL. IN OLIVINE)
10	CR-SPINEL (HIGH AL, MATRIX)

** ND = NOT DETECTED **

T A B L E 3-1 (CONTINUED)

FAMOUS AREA: SELECTED MINERAL ANALYSES. PICRITIC BASALTS

	11	12	13	14	15
SIO2	44.33	46.38	44.85	45.90	47.21
TIO2	.03	.04	.03	.04	.04
AL2O3	35.25	33.99	35.06	33.73	32.89
CR2O3	-	-	-	-	-
FEO	.33	.38	.33	.47	.55
MNO	-	-	-	-	-
MGO	.22	.29	.23	.16	.33
CAO	18.74	17.53	18.52	17.34	16.49
NA2O	1.03	2.06	1.39	1.94	2.41
K2O	ND	.03	.02	.02	.03
TOTAL	99.94	100.70	100.43	99.60	99.95

* * ATOMIC PROPORTIONS BASED ON SELECTED NO. OF OXYGENS * *

OXYGEN	8	8	8	8	8
SI	2.053	2.127	2.067	2.127	2.175
AL	1.924	1.837	1.905	1.843	1.786
TI	.001	.001	.001	.001	.001
CR	-	-	-	-	-
FE2+	.013	.015	.013	.018	.021
MN	-	-	-	-	-
MG	.015	.020	.016	.011	.023
CA	.930	.861	.915	.861	.814
NA	.093	.183	.124	.174	.215
K	-	.002	.001	.001	.002
SUM	5.030	5.046	5.042	5.038	5.038
	AN 90.90	AN 82.33	AN 87.94	AN 83.07	AN 78.95
	AB 9.04	AB 17.51	AB 11.94	AB 16.82	AB 20.88
	OR .06	OR .17	OR .11	OR .11	OR .17

* * * S A M P L E D I R E C T O R Y * * *

ANALYSIS NO.	DESCRIPTION
11	PLAG, PHENO (CORE)
12	PLAG, PHENO (RIM)
13	PLAG, PHENO
14	PLAG, PHENO (SMALL)
15	PLAG, MICROLITE

** ND = NOT DETECTED **

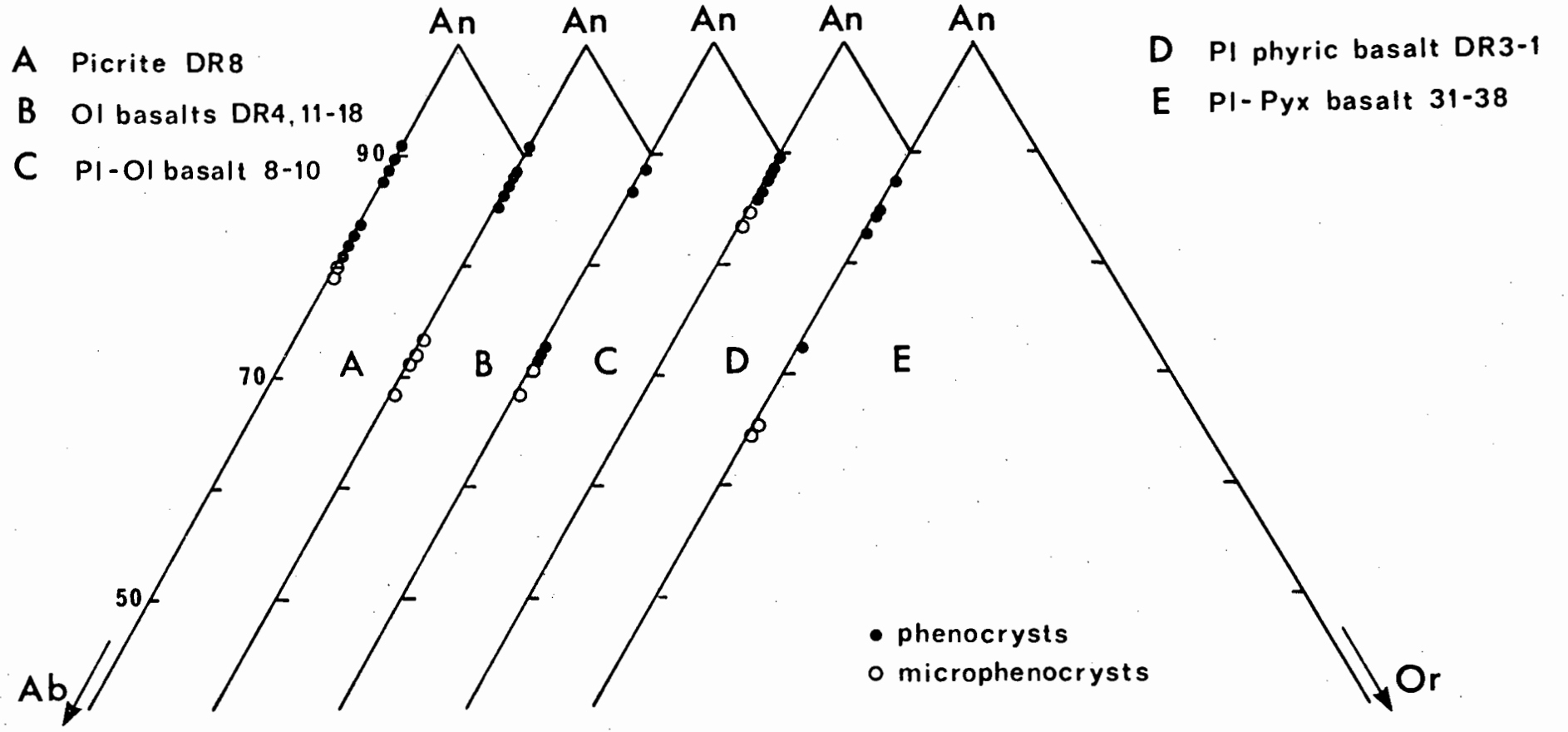

Fig. 3-3: Plagioclase end-member compositional variation in basalts from the FAMOUS area.

(Sigurdsson and Schilling, 1976), though they are slightly more magnesian (Fig. 3-4). Representative analyses are given in Table 3-1 (No's 6, 7 & 8), and individual analyses in microfiche Table F3-3. The second generation of spinel is yellow brown in colour and has a distinctly different composition (Table 3-1, No's 9 & 10, Fig. 3-4). These correspond to the chrome-spinels from high-alumina picrites from the Mid-Atlantic Ridge at 33°N (Sigurdsson and Schilling, 1976). Compositionally these spinels are richer in Al_2O_3 and MgO and poorer in Cr_2O_3 and Fe_2O_3 (Table 3-1) than the dominant variety of spinel and occur both included within olivine phenocrysts and in the matrix. Similar spinels have been found in ocean floor basalts by other workers (e.g. Bryan (1972); Frey et al. (1974); Dick (1976). Dick (pers. comm.) has found a complete range in spinel compositions from those rich in Al_2O_3 to more typical Cr-rich spinels in FAMOUS lavas.

Sigurdsson and Schilling (1976) and Sigurdsson (1977) have shown that a correlation exists between the Al_2O_3 content of the magma and the coexisting spinel. Experimental works suggest also that formation of high-Al spinel is favoured by high pressure, consistent with the significantly smaller partial molar volume of the Al-rich spinel end-members (Robie and Waldbaum, 1968). The origin of the high-Al spinels at 33°N has been attributed to high pressure crystallisation by Sigurdsson and Schilling (1976).

The occurrence of the aluminous spinels in DR8 could be explained by one of the following hypotheses:

(1) They could represent early spinel which crystallised at significantly greater depth (i.e. higher pressure) than the dominant variety. Subsequent rapid transport to the surface and quenching

preserved some of these Al-rich spinels.

(2) They could represent xenocrystic spinel derived from disaggregated mantle material brought up by the rising magma. Spinels found in lherzolite inclusions in alkali basalt, for example, have very similar compositions with respect to Cr and Al (Best, 1974; Frey and Green, 1974). Simkin and Smith (1970) have shown that slowly crystallised mantle-derived olivine and olivine crystallised from basaltic magma can be distinguished on the basis of their CaO content. Mantle olivine typically contains <.10% CaO, while volcanic olivine commonly has 0.20-0.40% CaO. The higher and uniform CaO content (± 0.33%) of DR8 olivine, including those containing inclusions of Al-rich spinel, argues against some of the olivines and Al-rich spinels representing disaggregated mantle material. Olivines containing Al-rich spinel inclusions also have significantly lower NiO content (± 0.29%) than that typically found in mantle olivine (± 0.40%, Sato, 1977).

3.2 Olivine Basalts

The olivine basalts are characteristically sparsely phyric to aphyric with olivine and plagioclase microphenocrysts (and in some cases euhedral to subhedral phenocrysts (1-2mm) of both plagioclase and olivine) set in a hyalocrystalline matrix (Plates 3-1E & F). The term 'aphyric' is not used in the strictest sense but will be used for rocks which are essentially aphyric (i.e. < 2% phenocrysts). The relative proportions of plagioclase and olivine vary considerably within the olivine basalts. Samples DR4-303 and DR1-122 have dominantly olivine microphenocrysts (showing typical hopper morphologies; Donaldson, 1976) with

PLATE 3-1

A: Photomicrograph of picrite DR8 showing abundant olivine phenocrysts and plagioclase microphenocrysts.

B: Large embayed olivine phenocryst in picrite DR8 containing numerous Cr-spinel inclusions.

C: Euhedral olivine phenocryst in picrite DR8 containing trapped melt inclusions and poikilitically enclosing Cr-spinel microphenocrysts.

D: Equant Cr-spinel microphenocrysts set in the matrix of picrite DR8 and containing abundant trapped melt inclusions. Note the distribution of the inclusions subparallel to the dominant crystal faces.

E: Photomicrograph of sparsely phyric olivine basalt DR4-303.

F: Photomicrograph of olivine basalt DR4-329 showing large plagioclase phenocryst and smaller clinopyroxene and olivine phenocrysts. Note the quench glass in the lower right hand corner. Crossed polars.

G: Photomicrograph of highly plagioclase phyric basalt DR3-1. Note the abundant trapped melt inclusions in one large phenocryst. A single large clinopyroxene phenocryst is shown in upper right hand corner. Crossed polars.

H: Photomicrograph showing large Cr-rich diopsidic clinopyroxene phenocrysts in plagioclase phyric basalt DR10-101C.

PLATE 3-1

A

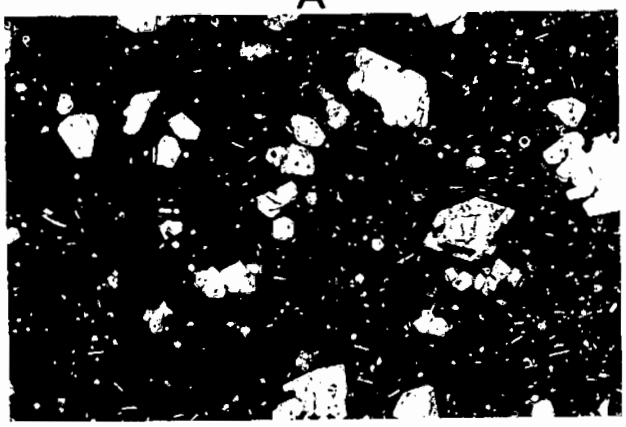

6mm

B

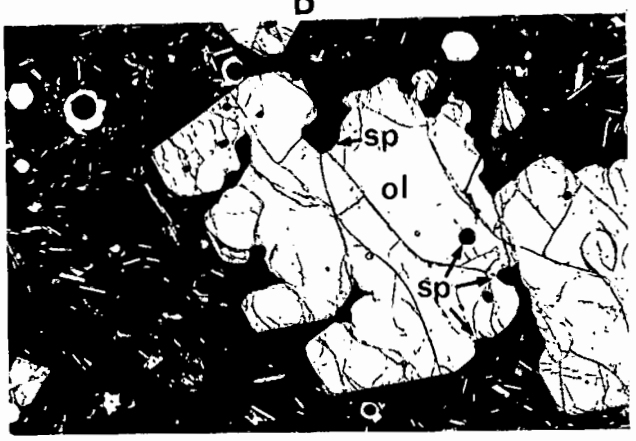

2mm

C

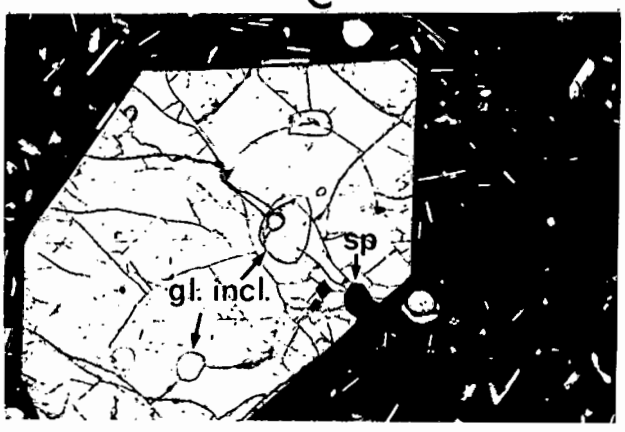

0·9mm

D

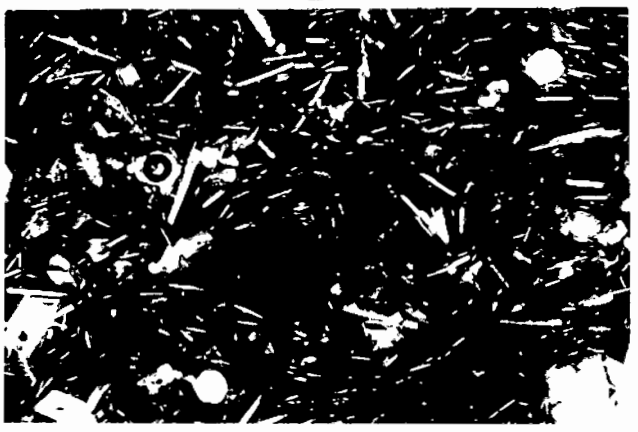

1mm

E

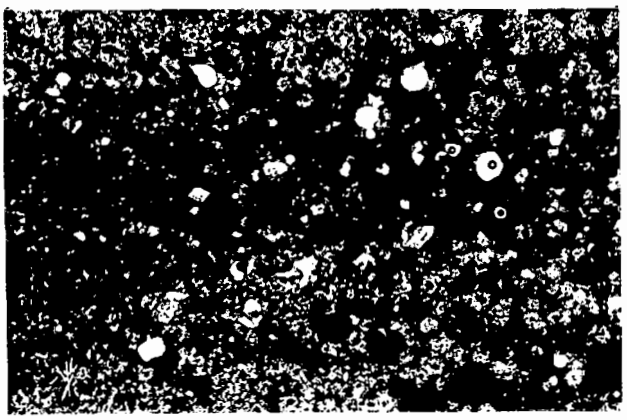

4mm

F

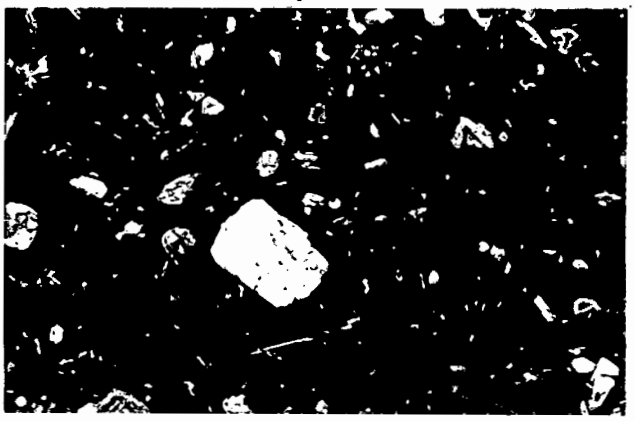

5mm

G

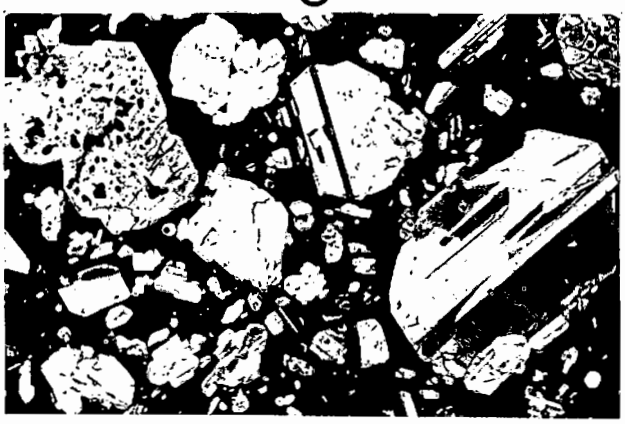

6mm

H

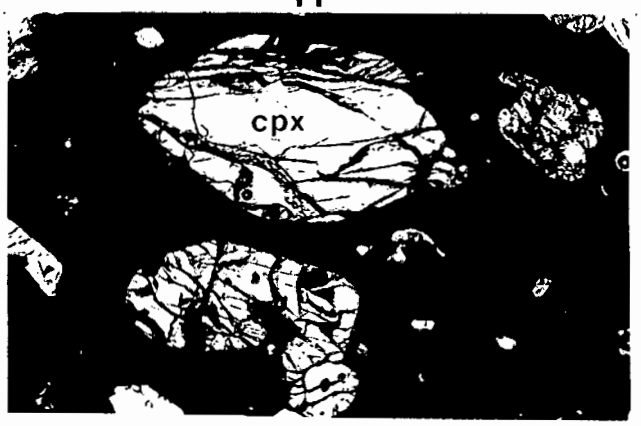

2mm

very minor plagioclase, while DR4, DR4-329, and 11-18 have significantly more plagioclase phenocrysts than olivine (Plate 3-1F). Clinopyroxene is also a phenocryst phase in the latter three. A chemical mode of DR4 indicates the following modal proportions of phenocrysts (wt %): 5% plagioclase, 3.5% olivine, and 1.2% clinopyroxene. The majority of the olivine basalts studied show the presence of sparse Cr-spinel (magnesiochromites) microphenocrysts occurring as inclusions in olivine or as isolated grains in the matrix.

Olivine phenocrysts range in composition from Fo_{90} to Fo_{80} (Table 3-2) and are typically zoned, e.g. Fo_{88} (core) to Fo_{83} (rim). Olivine phenocrysts in DR4 and 11-18 span the full compositional range observed for the olivine basalts. An interesting feature of the olivines analysed is their relatively high Cr_2O_3 content (0.04-0.10%). Individual analyses are given in microfiche Table F3-4.

A number of authors have shown that the distribution of Mn between olivine and coexisting melt is a relatively sensitive indicator of temperature of crystallisation (Roeder, 1974; Duke, 1976; Leeman and Schreidegger, 1977). Watson (1977) has found that $D_{Mn}^{ol\text{-}liq}$ is also a function of liquid composition, and that the temperature and compositional effects can be separated by comparing melts of similar Si/O ratio. Following these methods, initial olivine crystallisation temperatures have been calculated using the whole rock MnO content and the MnO content of the most MgO-rich olivines. Calculated temperatures for the olivine basalts, plagioclase-olivine basalts and plagioclase-pyroxene basalts which approximate liquid compositions (in terms of the Fe-Mg distribution in olivine and whole rock, see section 5.2) are given in Table 3-3. Quench temperatures for DR4 and 11-18 from

T A B L E 3-2

FAMOUS AREA: SELECTED MINERAL ANALYSES. OLIVINE BASALTS

	1	2	3	4	5	6	7	8	9	10
SIO2	40.19	40.33	40.25	39.42	39.63	46.46	50.33	45.76	45.09	50.93
TIO2	-	-	.04	.04	-	.02	.06	.05	.05	.07
AL203	-	-	.05	.06	-	34.35	31.31	34.22	35.24	30.95
CR203	-	-	.04	-	-	-	-	-	-	-
FEO	10.47	11.71	11.91	16.43	16.47	.37	.54	.58	.35	.57
MNO	.16	.18	-	-	.24	-	-	-	-	-
MGO	47.98	47.23	47.20	43.47	42.84	.17	.31	.48	.20	.28
CAO	-	-	.34	.33	-	17.64	15.09	18.15	18.66	14.14
NA20	-	-	-	-	-	1.50	3.14	1.48	1.02	3.55
K20	-	-	-	-	-	.02	.04	ND	ND	.05
NIO	.35	.31	-	-	.18	-	-	-	-	-
TOTAL	99.15	99.76	99.83	99.75	99.36	100.53	100.82	100.73	100.62	100.54

* * ATOMIC PROPORTIONS BASED ON SELECTED NO. OF OXYGENS * *

OXYGEN	4	4	4	4	4	8	8	8	8	8
SI	.998	1.000	.998	.999	1.008	2.129	2.284	2.102	2.071	2.312
AL	-	-	.001	.002	-	1.855	1.675	1.852	1.908	1.656
TI	-	-	.001	.001	-	.001	.002	.002	.002	.002
CR	-	-	.001	-	-	-	-	-	-	-
FE2+	.217	.243	.247	.348	.350	.014	.020	.022	.013	.022
MN	.003	.004	-	-	.005	-	-	-	-	-
MG	1.776	1.746	1.744	1.641	1.624	.012	.021	.033	.014	.019
CA	-	-	.009	.009	-	.866	.734	.893	.919	.688
NA	-	-	-	-	-	.133	.276	.132	.091	.313
K	-	-	-	-	-	.001	.002	-	-	.003
NI	.007	.006	-	-	.004	-	-	-	-	-
SUM	3.002	3.000	3.000	3.000	2.992	5.010	5.015	5.037	5.018	5.015
	FO 89.09	FO 87.79	FO 87.60	FO 82.50	FO 82.25	AN 86.56	AN 72.48	AN 87.09	AN 90.95	AN 68.56
	FA 10.91	FA 12.21	FA 12.40	FA 17.50	FA 17.75	AB 13.32	AB 27.29	AB 12.85	AB 9.00	AB 31.15
						OR .12	OR .23	OR .06	OR .06	OR .29

* * * S A M P L E D I R E C T O R Y * * *

ANALYSIS NO.	DESCRIPTION
1	OLIVINE, PHENO (DR4-303)
2	OLIVINE, PHENO (DR1-122)
3	OLIVINE, PHENO (CORE, DR4)
4	OLIVINE, PHENO (AS ABOVE, RIM)
5	OLIVINE, MICROPHENO (DR4)
6	PLAG, PHENO (CORE, DR4)
7	PLAG, PHENO (AS ABOVE, RIM)
8	PLAG, PHENO (CORE, 11-18)
9	PLAG, PHENO (AS ABOVE, RIM)
10	PLAG, MICROPHENO

** ND = NOT DETECTED **

T A B L E 3-2 (CONTINUED)

FAMOUS AREA: SELECTED MINERAL ANALYSES. OLIVINE BASALTS

	11	12	13	14	15	16	17	18	19	20
SIO2	52.53	52.73	53.27	52.45	52.18	.14	.05	.08	.08	.11
TIO2	.25	.24	.21	.20	.31	.51	.33	.36	.38	-
AL203	3.36	3.28	3.20	4.08	2.97	26.50	30.14	28.84	29.13	24.06
CR203	.99	.93	.95	1.32	.40	36.86	38.14	39.42	38.59	41.21
FE203	-	-	-	-	-	6.02	2.97	3.17	3.04	6.96
FEO	3.59	3.67	3.24	3.07	4.44	15.22	12.38	11.76	12.84	11.38
MNO	.08	.10	.09	.08	.10	-	-	-	-	-
MGO	18.35	18.25	18.49	17.81	18.55	13.89	16.27	16.52	15.78	15.87
CAO	21.29	21.63	21.13	21.66	19.94	.06	.06	ND	.03	-
NA20	.21	.17	.16	.18	.21	-	-	-	-	-
K20	ND	ND	ND	ND	ND	-	-	-	-	-
NIO	-	-	-	-	-	-	-	-	-	.18
TOTAL	100.66	101.01	100.75	100.86	99.11	99.20	100.34	100.16	99.87	99.77

* * ATOMIC PROPORTIONS BASED ON SELECTED NO. OF OXYGENS * *

OXYGEN	6	6	6	6	6	4	4	4	4	4
SI	1.899	1.901	1.916	1.890	1.914	.004	.001	.002	.002	.003
ALIV	.101	.099	.084	.110	.086	.947	1.036	.996	1.012	.854
ALVI	.042	.040	.052	.063	.042	-	-	-	-	-
TI	.007	.007	.006	.005	.009	.012	.007	.008	.008	-
CR	.028	.027	.027	.038	.012	.884	.880	.913	.899	.981
FE3+	-	-	-	-	-	.137	.065	.070	.067	.158
FE2+	.109	.111	.097	.092	.136	.386	.302	.288	.316	.287
MN	.002	.003	.003	.002	.003	-	-	-	-	-
MG	.989	.981	.991	.956	1.014	.628	.707	.722	.693	.712
CA	.825	.836	.814	.836	.784	.002	.002	-	.001	-
NA	.015	.012	.011	.013	.015	-	-	-	-	-
K	-	-	-	-	-	-	-	-	-	-
NI	-	-	-	-	-	-	-	-	-	.004
SUM	4.016	4.016	4.002	4.006	4.015	3.000	3.001	3.000	3.000	3.000
	WO 42.91	WO 43.37	WO 42.79	WO 44.36	WO 40.52	CR .48	CR .46	CR .48	CR .47	CR .53
	EN 51.44	EN 50.89	EN 52.08	EN 50.73	EN 52.43	MG .62	MG .70	MG .71	MG .69	MG .71
	FS 5.65	FS 5.74	FS 5.12	FS 4.91	FS 7.04	FE .07	FE .03	FE .04	FE .03	FE .08

* * * S A M P L E D I R E C T O R Y * * *

ANALYSIS NO.	DESCRIPTION
11	CPX, PHENO (CORE, DR4)
12	CPX, PHENO (AS ABOVE, RIM)
13	CPX, PHENO (CORE, 11-18)
14	CPX, PHENO (AS ABOVE, RIM)
15	CPX, PHENO (DR4)
16	CR-SPINEL, PHENO (DR4)
17	CR-SPINEL, PHENO (DR4)
18	CR-SPINEL, PHENO (CORE, 11-18)
19	CR-SPINEL, PHENO (AS ABOVE, RIM)
20	CR-SPINEL, PHENO (DR4-303)

Table 3-3: Olivine crystallisation temperatures (^{o}C) calculated using the distribution of Mn between olivine and liquid (K_D^{Mn} ol-liq).

	A	B	C
1) Olivine basalts			
DR4-303 (liquidus olivine)	1258	1274	1213
DR1-122	1245	1273	1198
DR9-322	1216	1223	1160
DR9-323	1210	1210	1152
DR4-329	1227	1246	1174
*11-18 (quench olivine)	1201	1198	1141
*DR4 (quench olivine)	1172	1142	1105
DR2-174 (liquidus olivine)	1197	1186	1136
2) Plagioclase-olivine basalt			
8-10 (liquidus olivine)	1218	1224	1162
3) Plagioclase-pyroxene basalt			
**DR2-301 (liquidus olivine)	(1199)	(1199)	(1154)
31-38 (liquidus olivine)	1246	1273	1199
DR10-310 (liquidus olivine)	1201	1198	1142

A: $T(K) = \frac{12184}{\ln D + 7.96}$ Leeman (1977) (wt. ratio)

B: $T(^{o}C) = \frac{4.02 - \ln D}{0.00329}$ Watson (1977) (mol. ratio)

C: $T(K) = \frac{3850}{\log D + 2.59}$ Roeder (1974) (wt. ratio)

* These samples have possibly experienced redistribution of phenocrysts (see section 5.2) so liquidus temperatures were not calculated.

** Only one olivine was analysed from DR2-301, and had a very low total (Table 3-6).

coexisting olivine microphenocryst-quench glass pairs are also given. The calibration from Watson (1977) (Table 3-3, col. B) was taken for a melt with Si/O = 0.30, corresponding to the average Si/O ratio of most basalts. The calculated temperatures following Leeman and Schreidegger (1977) and Watson (1977) are in good agreement, while that calculated following Roeder (1974) is consistently lower. All three methods indicate decreasing olivine crystallisation temperatures with decreasing whole rock MgO content with the exception of DR4-329. The calculated liquidus temperatures (following Watson, 1977) of the two most primitive samples (DR4-303 and DR1-122) of 1274 and 1273°C (Table 3-3) are in good agreement with the experimentally determined liquidus temperature of 1268°C on a high-MgO glass from the FAMOUS area (Bender et al., 1978).

Plagioclase phenocrysts in DR4 and 11-18 show a restricted range in composition (An_{91}-An_{85}) (Table 3-2, Fig. 3-3). Reverse zoning (An_{87} (core) to An_{91} (rim)) is present in some phenocrysts in sample 11-18 (Table 3-2). Plagioclase microphenocrysts are significantly more sodic with compositions of An_{68} to An_{73} (Table 3-2, Fig. 3-3). Individual plagioclase analyses are presented in microfiche Table F3-5. Plagioclase microphenocryst-quench glass pairs in DR4 and 11-18 indicate a quench temperature of 1118-1149°C (Mathez, 1973) in good agreement with olivine quench temperatures (Table 3-3). Assuming the core of the most calcic-plagioclase to be in equilibrium with the whole rock, an initial plagioclase crystallisation temperature of 1232-1261°C can be calculated for DR4 and 11-18 respectively (Mathez, 1973).

Fifteen Cr-spinels have been analysed from olivine basalts DR4, 11-18, DR4-303, DR1-122 and DR9-322. Individual analyses are presented in microfiche Table F3-6 and representative spinel analyses are presented

in Table 3-2. Compositionally the spinels fall within the field of Mid-Atlantic Ridge magnesio-chromites (Fig. 3-4) and tend to be slightly more iron-rich than the spinels from the picrites DR8 and 10-03C.

Clinopyroxene phenocrysts in DR4 and 11-18 are relatively constant in composition (Fig. 3-5A, Table 3-2) and range from $Wo_{44}En_{51}Fs_5$ to $Wo_{40}En_{51}Fs_9$. A characteristic feature of these clinopyroxenes is their high Cr_2O_3 contents (0.30-1.32% Cr_2O_3). Individual analyses are presented in microfiche Table F3-7. Donaldson and Brown (1977) have suggested that such refractory chromian diopside 'megacrysts' observed in oceanic tholeiites have multiple origins and could represent:

(1) cognate or accidental mantle fragments;

(2) relict fragments from fractional crystallisation of parental liquids considerably more primitive than oceanic tholeiitic; and, most commonly,

(3) the fractional crystallisation product of such liquids mixed with oceanic tholeiitic magma.

The reverse zoning in plagioclase from 11-18 and the rounded morphology of many of the larger phenocrysts in DR4 are in accord with those lavas possibly having a hybrid origin.

3.3 Plagioclase-olivine Basalts

Sample 8-10 is an aphanitic, holocrystalline plagioclase-olivine basalt. The matrix consists of an intergrowth of plagioclase, pyroxene and olivine microlites, with very rare phenocrysts of plagioclase being present.

A wide range in plagioclase composition is observed in sample 8-10, with sparse large phenocrysts being relatively calcic (An_{88}) and commonly having a thin rim of relatively more sodic composition (An_{72}).

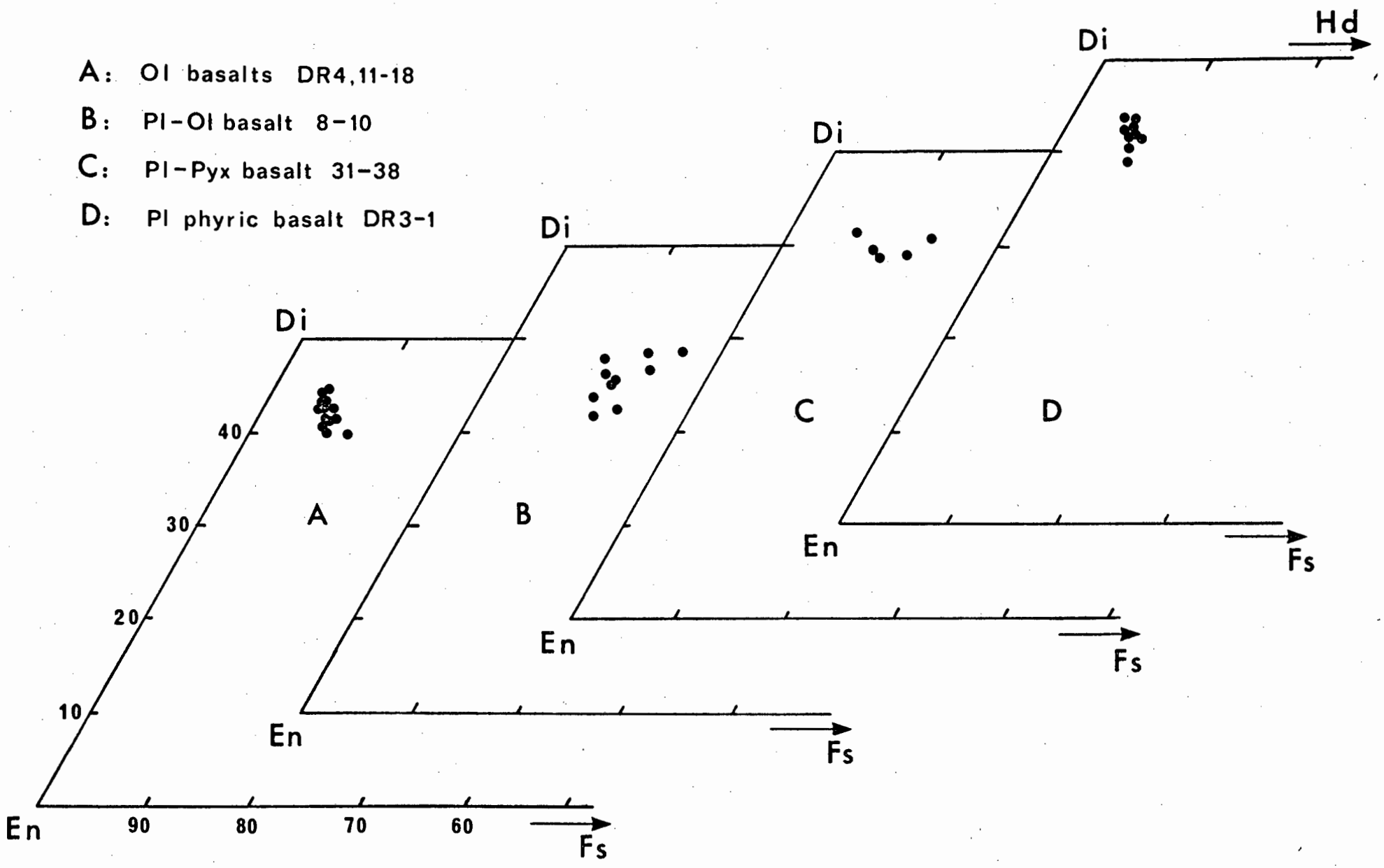

Fig. 3-5: Pyroxene end-member compositional variation in basalts from the FAMOUS area.

The rims correspond closely to the composition of the groundmass plagioclase (An_{68}-An_{71}) (Fig. 3-3C). Application of the Kudo-Weill plagioclase thermometer as modified by Mathez (1973) for basaltic rocks yields temperatures of first crystallisation of plagioclase of 1238°C. Clinopyroxene ranges in composition from $Wo_{38}En_{52}Fs_{10}$ to $Wo_{38}En_{45}Fs_{17}$ (Fig. 3-5B) with zoning spanning the full compositional range. Relative to pyroxenes from the other basalt types, those in 8-10 are characterised by their sub-calcic nature (Fig. 3-5B). Olivines are small in size and range in composition from Fo_{84} to Fo_{81}. The distribution of Mn between the most Mg-rich olivines and the whole rock indicates a temperature of 1162-1224°C for the start of olivine crystallisation (Table 3-3). The predicted liquidus temperatures, using plagioclase phenocrysts (Mathez, 1973) and olivine (Watson, 1977), of 1238°C and 1224°C respectively are in remarkably good agreement. Representative mineral analyses are presented in Table 3-4 and individual analyses are given in microfiche Table F3-8.

3.4 Highly Plagioclase Phyric Basalts (HPPB)

The plagioclase phyric basalts studied are characterised by abundant (10-50%) large plagioclase phenocrysts (1-10mm) and glomercrysts, and subordinate ($< 3\%$) green chromian diopside (1-3mm) and olivine (0.5-1.5mm) (Plate 3-1G and H). The matrix is fine grained with sheaves of plagioclase and pyroxene in an aborescent texture (DR3-1, DR3-131) or is hyalocrystalline (DR10-101C).

Plagioclase phenocrysts in DR3-1 range in composition from $An_{89.5}$ to An_{86} (Fig. 3-3D). There is a marked lack of zoning, though an increase in albite component is sometimes observed along the extreme rims. Plagioclase microphenocrysts have an average composition of $An_{84.6}$.

T A B L E 3-4

FAMOUS AREA: SELECTED MINERAL ANALYSES. PLAGIOCLASE - OLIVINE BASALTS

	1	2	3	4	5	6	7	8	9
SIO2	39.01	38.72	38.73	45.24	51.14	51.17	51.57	52.50	50.44
TIO2	.04	.05	.06	.02	.05	.06	.49	.44	.69
AL203	.04	.04	.04	34.21	30.06	30.15	3.87	2.20	4.19
CR203	.05	.02	.03	-	-	-	.64	.08	.08
FEO	15.87	17.12	17.78	.31	.60	.93	6.53	8.81	9.01
MNO	.21	.24	.23	-	-	-	.16	.21	.18
MGO	44.34	42.77	42.83	.23	.33	.36	18.80	19.68	17.35
CAO	.32	.35	.38	18.28	14.16	14.36	17.73	16.35	18.14
NA20	-	-	-	1.25	3.04	3.65	.21	.19	.18
K20	-	-	-	.05	.05	.09	ND	ND	.02
TOTAL	99.88	99.31	100.08	99.59	99.43	100.77	100.01	100.47	100.28

* * ATOMIC PROPORTIONS BASED ON SELECTED NO. OF OXYGENS * *

OXYGEN	4	4	4	8	8	8	6	6	6
SI	.987	.991	.987	2.099	2.343	2.325	1.883	1.918	1.861
ALIV	.001	.001	.001	1.871	1.623	1.615	.117	.082	.139
ALVI	-	-	-	-	-	-	.050	.013	.044
TI	.001	.001	.001	.001	.002	.002	.013	.012	.019
CR	.001	.000	.001	-	-	-	.018	.002	.002
FE2+	.336	.367	.379	.012	.023	.035	.199	.269	.278
MN	.005	.005	.005	-	-	-	.005	.006	.006
MG	1.672	1.632	1.627	.016	.023	.024	1.023	1.072	.954
CA	.009	.010	.010	.909	.695	.699	.694	.640	.717
NA	-	-	-	.112	.270	.322	.015	.013	.013
K	-	-	-	.003	.003	.005	-	-	.001
SUM	3.011	3.007	3.011	5.023	4.981	5.028	4.018	4.028	4.034
	FO 83.27	FO 81.66	FO 81.11	AN 88.73	AN 71.80	AN 68.15	WO 36.20	WO 32.31	WO 36.79
	FA 16.73	FA 18.34	FA 18.89	AB 10.98	AB 27.90	AB 31.34	EN 53.39	EN 54.10	EN 48.94
				OR .29	OR .30	OR .51	FS 10.41	FS 13.59	FS 14.26

* * * S A M P L E D I R E C T O R Y * * *

ANALYSIS NO.	DESCRIPTION
1	OLIVINE, PHENO (CORE)
2	OLIVINE, PHENO (RIM)
3	OLIVINE, MICROPHENO
4	PLAG, PHENO (CORE)
5	PLAG, PHENO (RIM)
6	PLAG, MICROPHENO
7	CPX, MICROPHENO (CORE)
8	CPX, MICROPHENO (RIM)
9	CPX, MICROLITE

** ND = NOT DETECTED **

Representative analyses are presented in Table 3-5 and individual analyses in microfiche Table F3-9.

Clinopyroxene compositions similarly show a restricted range (Fig. 3-5D) varying from $Wo_{43}En_{52}Fs_5$ to $Wo_{38}En_{54}Fs_8$ (Table 3-5). The Cr_2O_3 content of the clinopyroxenes is high; many of the euhedral green clinopyroxene phenocrysts can be classed as chromian-diopside. Cr_2O_3 contents vary from 0.26% to 1.43% with marked zoning of Cr_2O_3 being evident (Table 3-5). Individual analyses are presented in microfiche Table F3-10. Olivine occurs mainly as phenocrysts and varies in composition from Fo_{90} to Fo_{86} (Table 3-5). Olivine phenocrysts in DR3-1 are on the whole extremely uniform in composition (Fo_{86}); individual olivine analyses are presented in microfiche Table F3-11.

Cr-spinel has been analysed from DR3-1 and DR3-131. It is generally very scarce and shows a restricted compositional range in terms of Cr/Cr+Al ratio but with variable $Mg/Mg+Fe^{2+}$ ratios and ferric iron content (Table 3-5). Compositionally the spinels are similar to those observed in the picrites (red-brown Cr-spinels, Table 3-1), and olivine basalts (Table 3-2) and fall within the range of MAR magnesio-chromites (Fig. 3-4) found by Sigurdsson and Schilling (1976). Individual analyses are presented in microfiche Table F3-12.

3.5 Plagioclase-pyroxene Basalts

Three plagioclase-pyroxene basalts (DR2-301, 31-38, DR10-310) have been studied, though only in sample 31-38 have all the mineral phases been analysed. These basalts are aphyric with a holocrystalline matrix comprising interlocking laths of plagioclase, pyroxene and olivine microlites suggesting cotectic crystallisation of all three phases. Though aphyric in texture, in thin section it is possible to

T A B L E 3-5

FAMOUS AREA: SELECTED MINERAL ANALYSES. PLAGIOCLASE - PHYRIC BASALTS

	1	2	3	4	5	6	7	8	9	10
SIO2	44.75	44.62	44.97	45.64	46.28	40.09	40.06	40.43	41.12	39.80
TIO2	.02	.04	.03	.03	.05	.04	.04	-	-	-
AL2O3	35.12	35.06	35.12	34.46	33.86	.04	.03	-	-	-
CR2O3	-	-	-	-	-	.03	.06	-	-	-
FEO	.33	.37	.36	.42	.43	13.37	12.98	10.97	9.13	13.33
MNO	-	-	-	-	-	.18	.17	.17	.16	.22
MGO	.25	.22	.20	.24	.23	46.33	46.21	48.12	49.74	45.72
CAO	18.62	18.38	18.15	17.68	17.28	.31	.35	-	-	-
NA2O	1.19	1.30	1.47	1.59	1.82	-	-	-	-	-
K2O	ND	.03	.02	.02	.03	-	-	-	-	-
NIO	-	-	-	-	-	.15	.15	.19	.28	.16
TOTAL	100.29	100.02	100.32	100.08	99.98	100.54	100.05	99.88	100.43	99.23

* * ATOMIC PROPORTIONS BASED ON SELECTED NO. OF OXYGENS * *

OXYGEN	8	8	8	8	8	4	4	4	4	4
SI	2.065	2.065	2.073	2.105	2.134	.995	.997	.998	1.001	1.000
AL	1.910	1.912	1.908	1.873	1.840	.001	.001	-	-	-
TI	.001	.001	.001	.001	.002	.001	.001	-	-	-
CR	-	-	-	-	-	.001	.001	-	-	-
FE2+	.013	.014	.014	.016	.017	.277	.270	.226	.186	.280
MN	-	-	-	-	-	.004	.004	.004	.003	.005
MG	.017	.015	.014	.016	.016	1.714	1.715	1.770	1.804	1.712
CA	.921	.911	.896	.874	.854	.008	.009	-	-	-
NA	.106	.117	.131	.142	.163	-	-	-	-	-
K	-	.002	.001	.001	.002	-	-	-	-	-
NI	-	-	-	-	-	.003	.003	.004	.005	.003
SUM	5.033	5.037	5.038	5.029	5.026	3.003	3.001	3.002	2.999	3.000
	AN 89.58	AN 88.50	AN 87.12	AN 85.90	AN 83.85	FO 86.06	FO 86.38	FO 88.66	FO 90.66	FO 85.94
	AB 10.36	AB 11.33	AB 12.77	AB 13.98	AB 15.98	FA 13.94	FA 13.62	FA 11.34	FA 9.34	FA 14.06
	OR .06	OR .17	OR .11	OR .12	OR .17					

* * * S A M P L E D I R E C T O R Y * * *

ANALYSIS NO.	DESCRIPTION
1	PLAG, PHENO (CORE, DR3-1)
2	PLAG, PHENO (AS ABOVE, RIM)
3	PLAG, PHENO (ADJ. TO SPINEL)
4	PLAG, PHENO (DR3-1)
5	PLAG, MICROLITE (DR3-1)
6	OLIVINE, PHENO (CORE, DR3-1)
7	OLIVINE, PHENO (AS ABOVE, RIM)
8	OLIVINE, PHENO (DR3-1)
9	OLIVINE, PHENO (DR3-131)
10	OLIVINE, PHENO (DR3-131)

** ND = NOT DETECTED **

TABLE 3-5 (CONTINUED)

FAMOUS AREA: SELECTED MINERAL ANALYSES. PLAGIOCLASE - PHYRIC BASALTS

	11	12	13	14	15	16	17	18	19
SIO2	40.78	51.88	52.09	51.45	51.97	.13	-	ND	.23
TIO2	-	.24	.30	.21	.28	.48	.41	-	-
AL203	-	2.72	3.14	3.90	2.93	25.72	25.72	26.55	27.41
CR203	-	1.23	.49	1.43	.47	39.08	36.13	39.90	36.98
FE203	-	-	-	-	-	5.13	9.50	6.11	6.80
FEO	9.85	3.89	4.45	3.29	4.02	14.99	11.28	10.55	12.20
MNO	.17	.10	.12	.09	.12	-	-	-	-
MGO	49.49	18.40	18.30	17.86	18.40	14.01	16.23	16.64	15.75
CAO	-	21.04	20.85	21.08	20.87	.09	-	-	-
NA20	-	.19	.19	.18	.17	-	-	-	-
K20	-	ND	ND	ND	ND	-	-	-	-
NIO	.26	.04	-	-	-	-	-	.14	.14
TOTAL	100.55	99.74	99.94	99.50	99.24	99.63	99.27	99.90	99.51

* * ATOMIC PROPORTIONS BASED ON SELECTED NO. OF OXYGENS * *

OXYGEN	4	6	6	6	6	4	4	4	4
SI	.995	1.899	1.901	1.882	1.907	.004	-	-	.007
ALIV	-	.101	.099	.118	.093	.918	.910	.928	.963
ALVI	-	.016	.036	.050	.034	-	-	-	-
TI	-	.007	.008	.006	.008	.011	.009	-	-
CR	-	.036	.014	.041	.014	.936	.857	.935	.871
FE3+	-	-	-	-	-	.117	.215	.136	.152
FE2+	.201	.119	.136	.101	.123	.380	.283	.262	.304
MN	.004	.003	.004	.003	.004	-	-	-	-
MG	1.800	1.004	.995	.974	1.006	.632	.726	.735	.699
CA	-	.825	.815	.826	.821	.003	-	-	-
NA	-	.013	.013	.013	.012	-	-	-	-
K	-	-	-	-	-	-	-	-	-
NI	.005	.001	-	-	-	-	-	.003	.003
SUM	3.005	4.025	4.023	4.014	4.021	3.000	3.000	3.000	3.000
	FO 89.95	WO 42.36	WO 41.89	WO 43.47	WO 42.08	CR .50	CR .49	CR .50	CR .48
	FA 10.05	EN 51.53	EN 51.13	EN 51.23	EN 51.60	MG .62	MG .72	MG .74	MG .70
		FS 6.11	FS 6.98	FS 5.30	FS 6.33	FE .06	FE .11	FE .07	FE .08

* * * S A M P L E D I R E C T O R Y * * *

ANALYSIS NO.	DESCRIPTION
11	OLIVINE, PHENO (DR10-101C)
12	CPX, PHENO (CORE, DR3-1)
13	CPX, PHENO (AS ABOVE, RIM)
14	CPX, PHENO (DR3-1)
15	CPX, PHENO (DR3-1)
16	CR-SPINEL (DR3-1)
17	CR-SPINEL (DR3-1)
18	CR-SPINEL (DR3-131)
19	CR-SPINEL (DR3-131)

distinguish larger plagioclase microphenocrysts and smaller groundmass laths. Plagioclase microphenocrysts range in composition (Fig. 3-3, Table 3-6) and are marked by extreme compositional zoning (An_{84}-An_{72}, Table 3-6). Groundmass plagioclase is significantly more sodic with average composition of $An_{64.5}$ (Table 3-6, Fig. 3-3). Individual analyses are presented in microfiche Table F3-13. Clinopyroxene compositions range from $Wo_{41}En_{52}Fs_7$ to $Wo_{41}En_{46}Fs_{13}$ (Fig. 3-5C, Table 3-6) and though similar to those in plagioclase-olivine basalt 8-10 in terms of ferrosilite component, they have significantly lower Cr_2O_3 and are not as subcalcic (Tables 3-4; 3-6). Individual analyses are presented in microfiche Table F3-14.

Olivine from DR2-301, 31-38 and DR10-310 shows a limited compositional range (Table 3-6, microfiche Table F3-15) of Fo_{82} to Fo_{88}. The distribution of the Mn between the most Mg-rich phenocrysts and whole rock indicates temperatures of initial olivine crystallisation of 1246-1200°C (Leeman and Schreidegger, 1977) and 1273-1200°C (Watson, 1977) (Table 3-3). The values for 31-38 (1246°C, Leeman and Schreidegger, 1977; 1273°C, Watson, 1977) compare favourably with the predicted liquidus temperature of 1237°C using the Kudo-Weill plagioclase thermometer as modified by Mathez (1973).

4. WHOLE ROCK CHEMISTRY

4.1 General Statement

The overall chemistry of the FAMOUS lavas has been extensively discussed by Bougault and Hekinian (1974) and Arcyana (1977), while that of the quench-glass compositions has been reported by Hekinian et al. (1976), Bryan and Moore (1977), White and Bryan (1977), Langmuir et al., (1977) and Bryan et al. (1979). This section is therefore limited to a general review of the whole rock chemistry, with a more detailed dis-

TABLE 3-6

FAMOUS AREA: SELECTED MINERAL ANALYSES. PLAGIOCLASE - PYROXENE BASALTS

	1	2	3	4	5	6	7	8	9
SIO2	39.74	38.97	40.25	46.40	46.82	50.11	52.02	51.82	50.49
TIO2	.04	.03	-	.04	.04	.07	.09	.32	1.03
AL2O3	.07	.05	-	34.40	33.94	31.40	29.52	2.80	3.37
CR2O3	.02	.02	-	-	-	-	-	.28	.02
FEO	13.42	16.89	14.84	.44	.41	.64	.81	4.34	8.65
MNO	.18	.22	.23	-	-	-	-	.09	.14
MGO	43.99	43.79	44.44	.24	.27	.31	.24	19.03	16.31
CAO	.40	.39	-	17.84	17.22	14.80	13.01	20.92	20.35
NA2O	-	-	-	1.46	1.77	3.12	3.90	.15	.39
K2O	-	-	-	ND	ND	.03	.08	ND	ND
NIO	.13	.12	.13	-	-	-	-	-	-
TOTAL	97.99	100.48	99.89	100.83	100.48	100.48	99.67	99.76	100.76

* * ATOMIC PROPORTIONS BASED ON SELECTED NO. OF OXYGENS * *

OXYGEN	4	4	4	8	8	8	8	6	6
SI	1.011	.985	1.010	2.122	2.145	2.281	2.376	1.895	1.866
ALIV	.002	.001	-	1.854	1.833	1.685	1.589	.105	.134
ALVI	-	-	-	-	-	-	-	.016	.013
TI	.001	.001	-	.001	.001	.002	.003	.009	.029
CR	.000	.000	-	-	-	-	-	.008	.001
FE2+	.286	.357	.311	.017	.016	.024	.031	.133	.267
MN	.004	.005	.005	-	-	-	-	.003	.004
MG	1.669	1.650	1.662	.016	.018	.021	.016	1.037	.898
CA	.011	.011	-	.874	.845	.722	.637	.820	.806
NA	-	-	-	.129	.157	.275	.345	.011	.028
K	-	-	-	-	-	.002	.005	-	-
NI	.003	.002	.003	-	-	-	-	-	-
SUM	2.987	3.013	2.990	5.015	5.016	5.013	5.002	4.037	4.046
	FO 85.38	FO 82.21	FO 84.22	AN 87.05	AN 84.27	AN 72.26	AN 64.52	WO 41.20	WO 40.87
	FA 14.62	FA 17.79	FA 15.78	AB 12.89	AB 15.67	AB 27.57	AB 35.00	EN 52.13	EN 45.56
				OR .06	OR .06	OR .17	OR .47	FS 6.67	FS 13.56

* * * S A M P L E D I R E C T O R Y * * *

ANALYSIS NO.	DESCRIPTION
1	OLIVINE, MICROPHENO (DR2-301)
2	OLIVINE, MICROPHENO (31-38)
3	OLIVINE, MICROPHENO (31-38)
4	PLAG, MICROPHENO (31-38)
5	PLAG, MICROPHENO (CORE, 31-38)
6	PLAG, MICROPHENO (AS ABOVE, RIM)
7	PLAG, MICROLITE (31-38)
8	CPX, MICROPHENO (31-38)
9	CPX, MICROPHENO (31-38)

** ND = NOT DETECTED **

cussion of a few salient points and of additional trace element data obtained during the present study. Major and trace elements, CIPW norms and selected element ratios of the samples analysed in this study are given in Table 3-7, together with the following differentiation indices: M.I. (mafic index = $FeO + Fe_2O_3/MgO + FeO + Fe_2O_3$), $Mg^{\#}$ (magnesium number = atomic $Mg/Mg + Fe^{2+}$) and D.I. (Thornton and Tuttle differentiation index, 1960).

4.2 Major Elements

With the exception of three samples (DR4-329, 8-10 and 31-38), the samples studied are all olivine normative tholeiites. With the exception of two picritic basalts (DR8 and 10-03C), all the samples fall within the field of typical MORB (from Dickey et al., 1977) in terms of total alkalis versus SiO_2 (Fig. 3-6). The compositional variation in terms of an AFM diagram, together with designated fields for Atlantic Rift Valley volcanics, Atlantic Fracture Zone volcanics and Aseismic Ridges (Hekinian and Thompson, 1976), is shown in Fig. 3-7.

The study of the FAMOUS lavas has revealed some diagnostic features:

(1) The large overall chemical diversity of lavas in this single well sampled area of the Mid-Atlantic Ridge. This variation is almost as large as that observed for all sea-floor basalts recovered from the three major ocean basins.

(2) The abundance of relatively primitive (in terms of high MgO contents, high Mg-number and low TiO_2) aphyric lavas and quench-glass crusts on pillow lavas.

(3) The apparent asymetric distribution of the lava types across the rift valley (Hekinian et al., 1976).

TABLE 3-7

FAMOUS AREA: WHOLE ROCK MAJOR & TRACE ELEMENT ANALYSES, CIPW NORMS & RATIOS

	DR4-303	DR1-122	DR9-322	DR9-308	DR9-323	11-18	DR 4	DR4-329	DR2-174	8-10
SIO2	50.23	50.16	50.21	50.17	50.25	50.10	50.71	50.35	50.71	50.89
TIO2	.86	.86	1.00	1.00	1.01	1.02	1.15	1.13	1.38	1.15
AL203	15.30	15.42	15.55	15.07	15.29	16.06	15.44	15.00	15.02	15.02
FE203	1.10	1.09	1.15	1.20	1.21	1.15	1.42	1.27	1.34	1.32
FEO	7.33	7.26	7.66	8.00	8.06	7.65	8.26	8.47	8.92	8.78
MNO	.15	.15	.16	.17	.17	.15	.16	.17	.18	.17
MGO	10.45	10.33	9.69	9.54	9.50	8.92	8.71	8.58	8.25	7.92
CAO	11.83	11.81	12.50	12.16	12.27	12.09	11.91	11.61	11.66	11.96
NA20	2.09	1.93	2.19	2.13	2.20	2.09	2.05	2.03	2.14	2.13
K20	.18	.17	.16	.14	.14	.16	.16	.18	.26	.21
P205	.09	.08	.10	.08	.08	.14	.12	.10	.14	.15
H20+	.39	.55	.44	.36	.44	.27	.41	.34	.53	.34
H20-	.08	.16	.10	.08	.12	.16	.12	.06	.10	.10
CO2	-	-	-	-	-	.05	-	-	-	.06
TOTAL	100.08	99.97	100.91	100.10	100.74	100.01	100.62	99.29	100.63	100.20
				* * * C.T.P.W. NORMS * * *						
Q	.00	.00	.00	.00	.00	.00	.00	.11	.00	.27
OR	1.06	1.00	.95	.83	.83	1.00	.95	1.06	1.54	1.24
AB	17.68	16.33	18.53	18.02	18.62	18.19	17.35	17.18	18.11	18.79
AN	31.83	32.91	32.13	31.15	31.43	34.27	32.43	31.28	30.61	30.40
DI	21.19	20.30	23.65	23.23	23.45	20.51	20.99	20.89	21.47	23.65
HY	17.08	20.36	13.10	16.68	14.78	18.51	23.60	24.15	23.37	20.65
OL	7.32	4.96	8.22	5.93	7.22	3.05	.17	.00	.02	.00
MT	1.59	1.58	1.67	1.74	1.75	2.22	2.06	1.84	1.94	2.54
IL	1.63	1.63	1.90	1.90	1.92	1.99	2.18	2.15	2.62	2.20
AP	.21	.19	.24	.19	.19	.26	.28	.24	.33	.28
				* * * TRACE ELEMENTS * * *						
ZR	48.8	49.0	57.6	54.8	55.4	56.8	64.8	64.2	81.0	59.3
NB	6.1	6.0	7.0	6.5	5.3	6.7	8.2	7.7	10.8	7.0
Y	18.2	19.5	22.3	23.8	24.0	22.8	23.5	23.4	27.2	24.9
RB	3.3	3.4	3.1	2.2	2.0	2.5	3.5	4.8	4.8	3.2
BA	41.4	41.4	34.1	28.1	29.9	36.0	39.4	37.3	58.9	44.0
SR	117.	111.	99.1	85.0	86.8	110.	114.	111.	113.	103.
CO	54.0	51.6	51.9	52.9	51.4	50.4	52.7	54.2	52.0	50.6
CR	573.	585.	486.	388.	373.	388.	353.	350.	253.	171.
NI	269.	267.	208.	182.	171.	174.	160.	156.	122.	85.0
V	193.	201.	231.	243.	240.	212.	235.	240.	276.	277.
ZN	68.2	69.1	67.9	71.8	73.2	73.4	90.5	83.7	88.9	81.1
CU	73.7	74.8	68.8	68.9	69.1	65.4	97.0	65.1	62.8	61.1
SC	35.2	34.8	38.7	40.2	39.5	34.4	39.1	39.4	41.1	39.9
TH	-	-	-	-	-	-	-	-	-	-
PB	-	-	-	-	-	-	-	-	-	-
GA	14.8	15.3	15.0	15.3	15.6	14.7	15.3	16.4	17.4	14.8

T A B L E 3-7 (CONTINUED)

FAMOUS AREA: WHOLE ROCK MAJOR & TRACE ELEMENT ANALYSES, CIPW NORMS & RATIOS

	10-03C	DR 8	DR3-131	DR 3-1	DR10-101	DR2-301	31-38	DR10-310
SIO2	45.44	47.72	49.09	49.20	50.40	49.31	49.95	50.25
TIO2	.41	.58	.69	.62	1.13	.99	.99	1.00
AL203	10.83	14.15	18.41	21.71	15.88	14.94	14.71	14.55
FE203	1.10	1.26	.91	1.38	1.15	1.14	1.18	1.24
FEO	7.36	7.28	6.07	4.50	7.66	7.57	7.89	8.24
MNO	.15	.16	.13	.11	.15	.16	.16	.17
MGO	24.22	16.41	8.28	6.46	8.10	8.23	8.54	7.97
CAO	8.49	11.33	13.86	15.03	12.52	13.15	12.75	12.41
NA20	1.16	1.42	1.96	1.75	2.22	2.17	2.45	2.52
K20	.06	.07	.16	.11	.32	.29	.18	.30
P205	.02	.05	.08	.08	.12	.10	.14	.10
H20+	.12	.45	.82	.04	.63	.77	.32	.69
H20-	.03	.08	.20	.10	.19	.24	.44	.14
CO2	-	-	-	-	-	-	.24	-
TOTAL	99.39	100.96	100.66	101.09	100.47	99.06	99.94	99.58

* * * C.T.P.W. NORMS * * *

Q	.00	.00	.00	.00	.00	.00	.61	.00
OR	.35	.41	.95	.65	1.89	1.71	1.47	1.77
AB	9.82	11.93	16.58	14.64	18.79	18.36	18.44	21.32
AN	24.17	31.91	40.96	50.60	32.42	30.17	28.98	27.50
DI	14.14	18.95	22.03	18.35	23.50	27.94	27.95	27.25
HY	4.95	9.73	8.01	10.09	15.49	4.80	14.21	10.67
OL	43.40	24.03	8.30	2.36	3.48	6.01	.00	6.31
MT	1.59	1.81	1.32	1.99	1.67	1.59	4.72	1.80
IL	.78	1.10	1.31	1.16	2.15	1.88	1.86	1.90
AP	.05	.12	.19	.17	.28	.24	.25	.24

* * * TRACE ELEMENTS * * *

ZR	22.1	30.2	40.7	34.5	68.1	56.9	52.5	55.4
NB	2.0	3.0	6.6	5.7	11.3	10.3	8.7	9.3
Y	11.8	16.4	16.1	14.0	23.6	20.5	21.6	22.2
RB	ND	1.7	1.8	1.9	5.0	5.6	4.4	4.6
BA	11.7	24.0	31.6	23.7	58.0	61.1	49.9	51.6
SR	48.0	69.0	119.	122.	121.	135.	106.	113.
CO	93.6	73.1	43.7	34.1	48.4	50.1	51.7	52.4
CR	2128.	1554.	392.	242.	411.	159.	86.1	85.6
NI	1127.	570.	152.	83.3	134.	98.8	73.4	74.0
V	133.	180.	184.	160.	249.	242.	246.	246.
ZN	52.5	59.8	51.9	43.2	71.7	28.7	65.6	70.9
CU	88.0	99.8	65.4	59.9	64.4	88.2	83.5	83.3
SC	28.1	37.1	32.7	30.5	39.3	42.3	38.1	39.9
TH	-	-	-	-	-	-	-	-
PB	-	-	-	-	-	-	-	-
GA	8.7	10.8	13.7	13.0	15.5	14.9	14.2	15.4

** ND = NOT DETECTED **

T A B L E 3-7 (CONTINUED)

FAMOUS AREA: WHOLE ROCK MAJOR & TRACE ELEMENT ANALYSES, CIPW NORMS & RATIOS

	10-03C	DR 8	DR3-131	DR 3-1	DR10-101	DR2-301	31-38	DR10-310
				* * * ELEMENT RATIOS * * *				
ZR/NB	11.1	10.1	6.12	6.05	6.03	5.55	6.02	5.97
ZR/BA	1.89	1.26	1.29	1.45	1.18	.931	1.05	1.08
ZR/Y	1.88	1.84	2.53	2.46	2.88	2.78	2.43	2.49
K/RB	-	342.	746.	481.	535.	426.	340.	541.
K/BA	42.6	24.2	42.1	38.5	45.8	39.4	29.9	48.3
K/ZR	22.5	19.3	32.6	26.5	39.0	42.3	28.5	44.9
Y/NB	5.89	5.46	2.42	2.46	2.09	2.00	2.48	2.40
CA/Y	5.147+003	4.944+003	6.149+003	7.673+003	3.788+003	4.587+003	4.211+003	3.986+003
TI/ZR	111.	115.	102.	108.	99.4	104.	113.	108.
TI/NB	1.229+003	1.159+003	622.	652.	600.	578.	681.	646.
TI/Y	208.	212.	257.	265.	287.	290.	274.	269.
TI/P	28.2	15.9	11.8	10.6	12.9	13.6	9.71	13.7
CR/V	16.0	8.64	2.13	1.52	1.65	.657	.350	.348
NI/CO	12.0	7.81	3.48	2.44	2.76	1.97	1.42	1.41
M.I.	25.9	34.2	45.7	47.6	52.1	51.4	51.5	54.3
MG#	.854	.798	.709	.695	.653	.659	.659	.633
D.I.	10.2	12.3	17.5	15.3	20.7	20.1	22.1	23.1

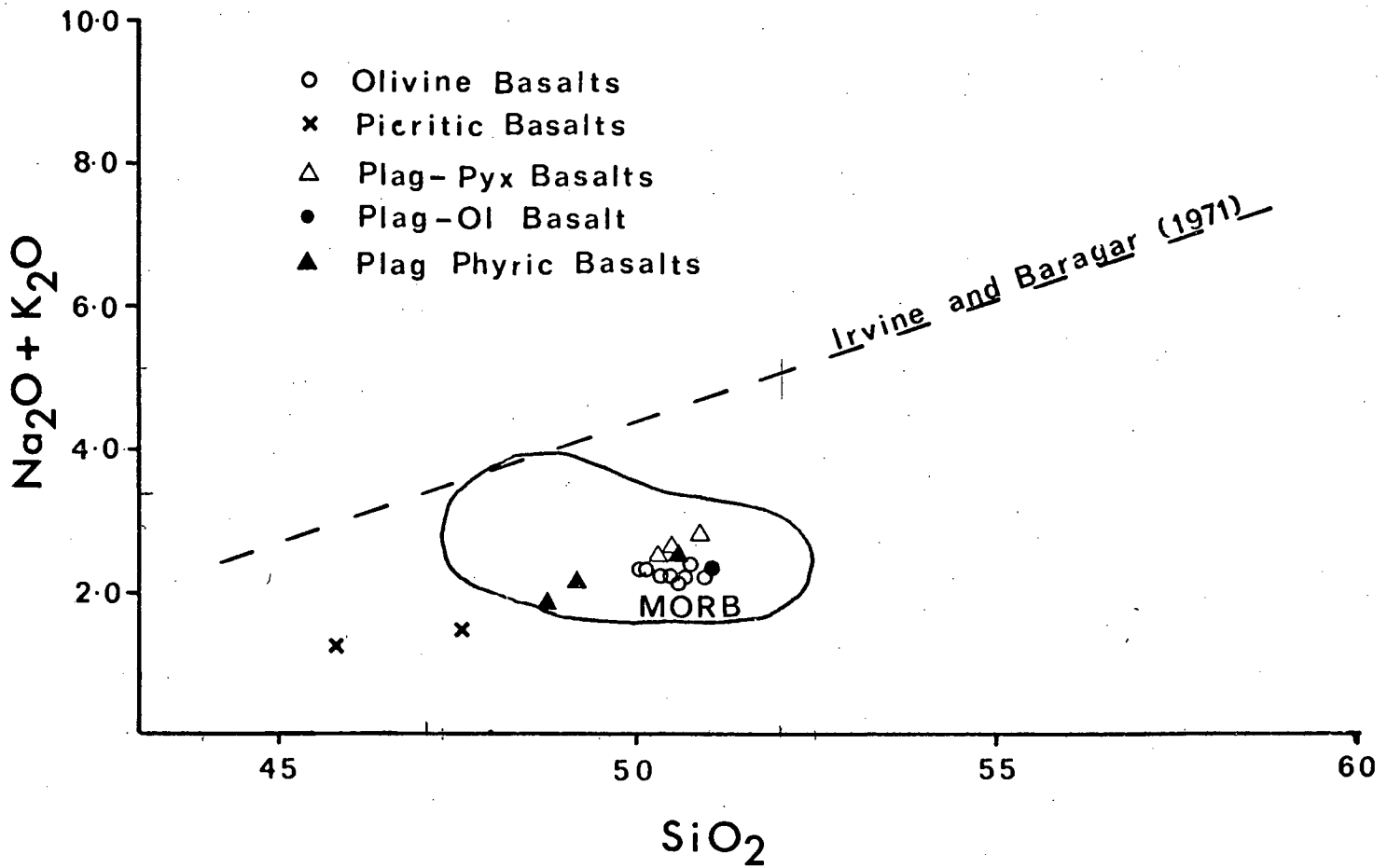

Fig. 3-6: Total alkalis - SiO_2 variation in FAMOUS basalts. The field of mid-ocean ridge basalt (MORB) is taken from Dickey et al. (1977).

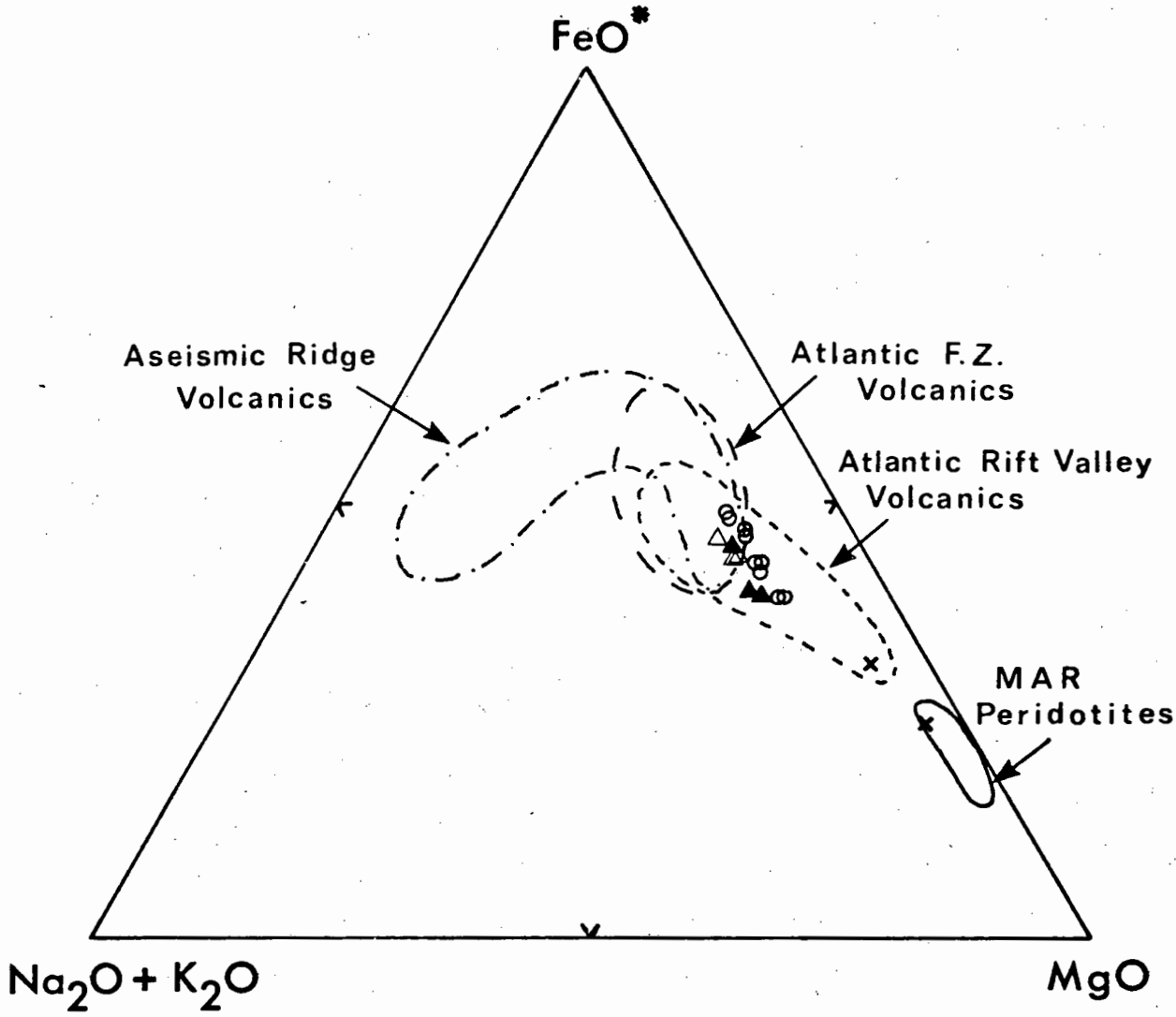

Fig. 3-7: A-F-M diagram showing the compositional variation of FAMOUS basalts. Fields for asiesmic ridge, Atlantic fracture zone and Atlantic rift valley volcanics and MAR peridotites are taken from Hekinian and Thompson (1976). Symbols as in Fig. 3-6.

(4) A remarkably systematic compositional change across the rift valley (Hekinian et al., 1976).

The chemical characteristics of the different rock types can be summarised as follows (Bougault and Hekinian, 1974; Arcyana, 1977):

(1) Picritic basalts: These lavas are characterised by high MgO content (>14%) and low K_2O (<0.11%), TiO_2 (<0.64%) and Al_2O_3 (<14.5%). Samples DR8 (16.3% MgO) and 10-03C (24.4% MgO) are therefore both classified as picritic basalts and 10-03C is in fact the most MgO-rich picrite sample recovered from the FAMOUS area.

(2) Olivine basalts: The olivine basalts have between 8.0 and 11.0% MgO, less than 0.2% K_2O and TiO_2 contents of between 0.8 and 1.5%. Al_2O_3 shows a very restricted range (14.8-15.5%). The nine olivine basalts analysed in this study span the full compositional range of all the olivine basalts and show uniformly increasing TiO_2 and P_2O_5 with decreasing MgO (Table 3-7). Samples DR4-303 and DR1-122 are the most primitive of the olivine basalts studied with $\pm$ 10.45% MgO, Mg-number 0.717 and have the lowest TiO_2 (0.86%) and P_2O_5 (0.08%) contents.

(3) Plagioclase-olivine basalts: These basalts are in general more evolved than the olivine basalts and are characterised by lower MgO (6-8%) and higher incompatible element contents (TiO_2, P_2O_5 and K_2O). Sample 8-10 (Table 3-7) is an example of the plagioclase-olivine basalts.

(4) Plagioclase-pyroxene basalts: The lower constant TiO_2 ($\pm$ 1.00%) and higher MgO (8-8.5%) contents distinguish these basalts from the plagioclase-olivine basalts. They are also characterised by

high CaO contents (12.6-13.7%) relative to the olivine basalts. The three plagioclase-pyroxene basalts analysed in the study (Table 3-7: DR2-301, DR10-310 and 31-38) span the compositional range observed for all FAMOUS plagioclase-pyroxene basalts.

(5) Plagioclase phyric basalts: These basalts are characterised by high Al_2O_3 (up to 21%) and CaO (14-15%) coupled with low TiO_2 (<1%). MgO contents vary from 6.4 to 8.3%. The three samples of this rock type analysed (Table 3-7: DR3-131, DR3-1 and DR10-101C) span the Al_2O_3 and CaO range shown by the plagioclase phyric basalts, and are relatively primitive in terms of Mg-number (0.65-0.71).

The overall chemical diversity of the FAMOUS lavas is clearly illustrated by two variation diagrams: Al_2O_3 versus MgO (Fig. 3-8) and CaO versus MgO (Fig. 3-9). In these plots the aphyric to sparsely phyric olivine basalts, plagioclase-olivine basalts and plagioclase-pyroxene basalts fall within a central field in terms of MgO (8-10.5%), Al_2O_3 (14.5-15.5%) and CaO (11.5-13.5%), while the plagioclase phyric basalts and picritic basalts lie, respectively, along well defined plagioclase (An_{89}) and olivine (Fo_{90}) control lines.

4.3 Trace Elements

The trace element variations (Bougault and Hekinian, 1974; White and Bryan, 1977; Langmuir et al., 1977; Bougault et al., 1979) and Sr isotope characteristics (White and Bryan, 1977) of the FAMOUS lavas show them to be transitional between the incompatible element-enriched high Sr^{87}/Sr^{86} basalts of the Azores Plateau and 'normal' ocean ridge basalts south of latitude 33°N. In general the basalts are characterised by

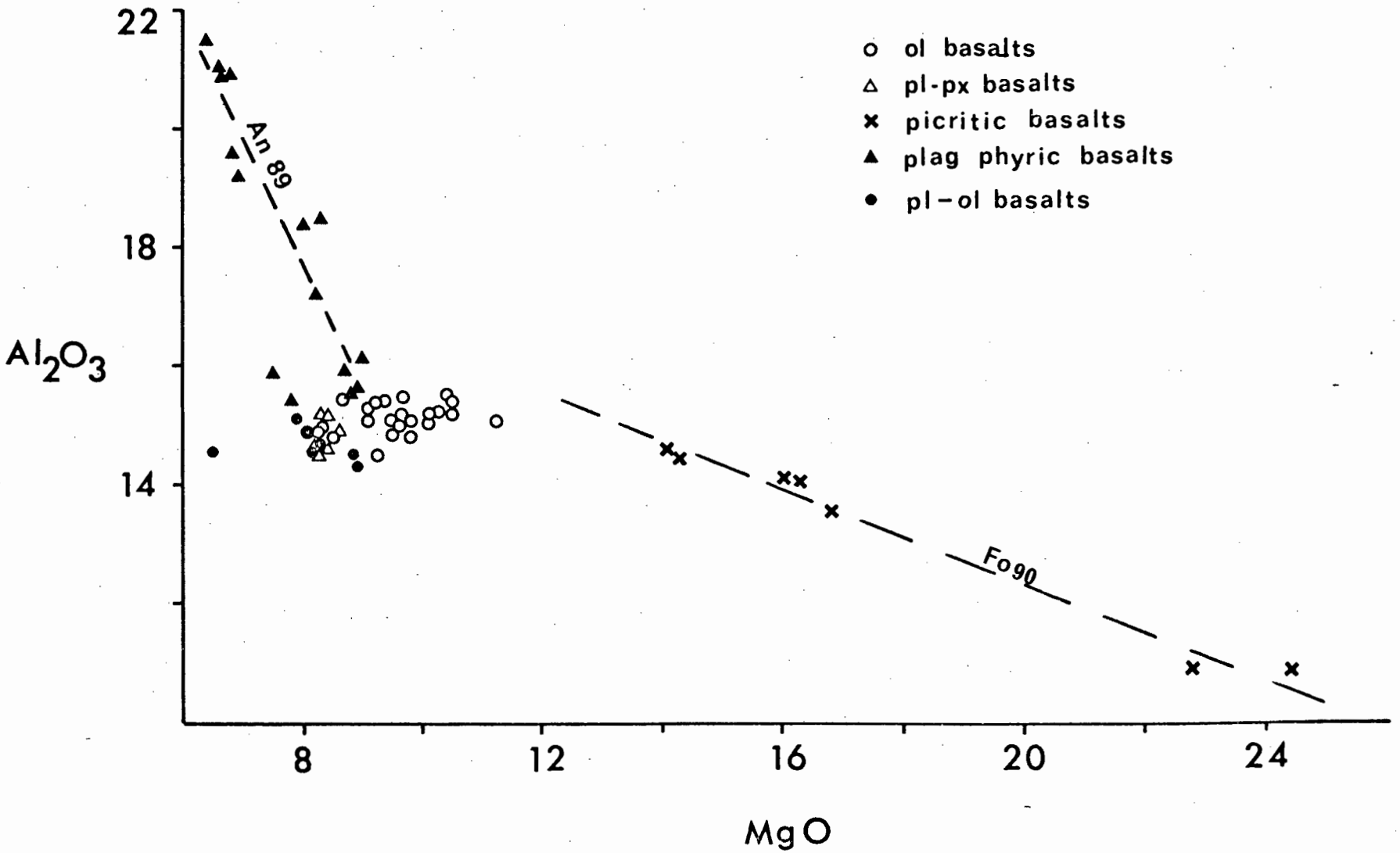

Fig. 3-8: Variation of Al_2O_3 with MgO in FAMOUS basalts. Plagioclase (An_{89}) and olivine (Fo_{90}) control lines are shown. Data from this study, Bougault and Hekinian (1974) and Arcyana (1977) are included.

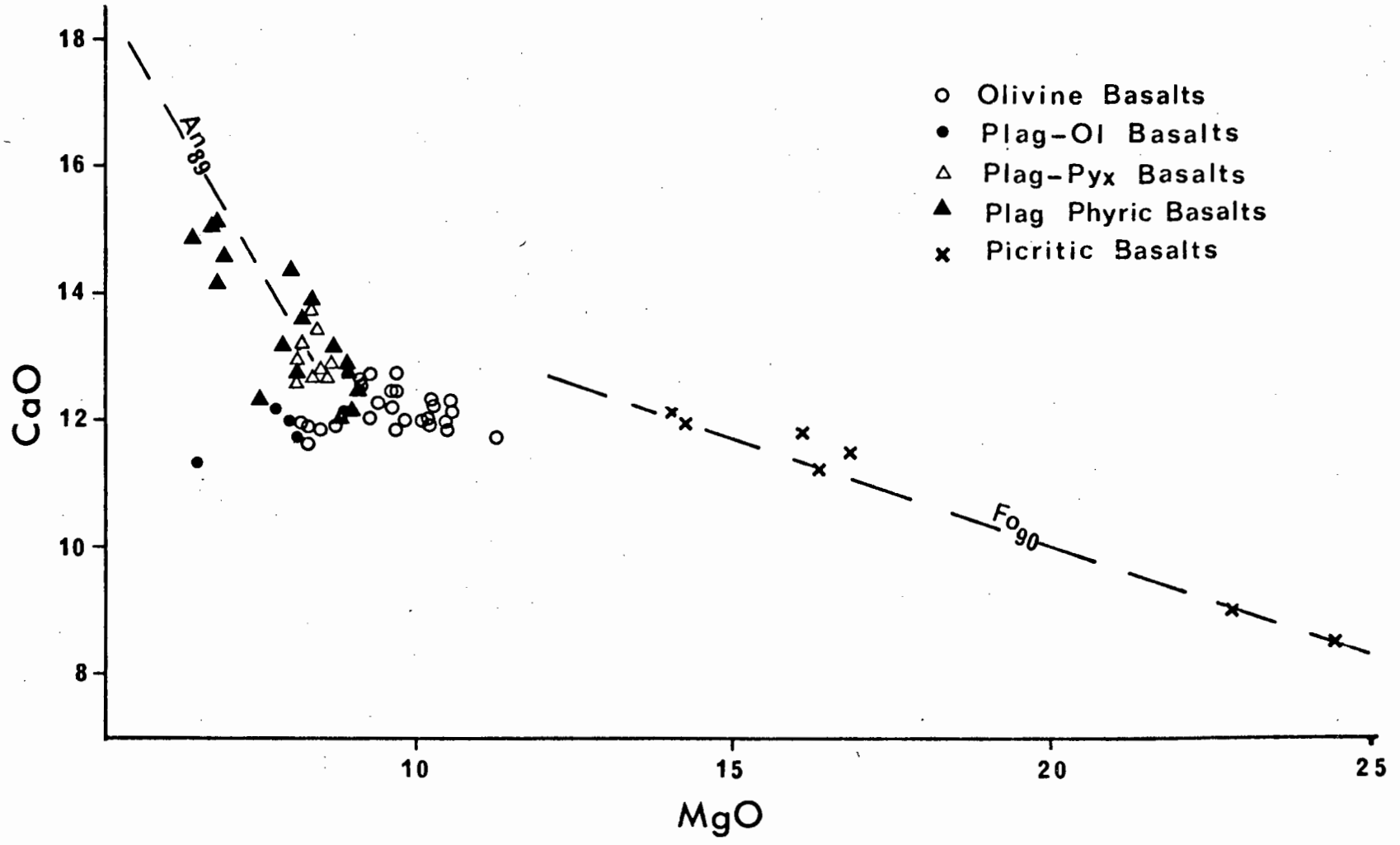

Fig. 3-9: Variation of CaO with MgO in FAMOUS basalts. Plagioclase (An_{89}) and olivine (Fo_{90}) control lines are shown. Data from this study, Bougault and Hekinian (1974) and Arcyana (1977) are included.

high concentrations of Ba (28-91 ppm), Rb (2.0-6.7 ppm) and Nb (5-11 ppm) and low concentrations of Sr (74-136 ppm) and Zr (31-80 ppm) relative to normal MORB (average MORB: Ba = 9.3 ppm, Rb = 1.3 ppm, Nb = 3.3 ppm, Sr = 137 ppm, and Zr = 122 ppm; Erlank and Kable, 1976). The enrichment in LIL (large ion-lithophile) elements is further emphasised by the generally flat to LREE-enriched patterns of the FAMOUS lavas (Langmuir et al., 1977), in contrast to the LREE depletion found in typical MORB (Frey et al., 1968; Schilling, 1971). Schilling (1975a) has noted a progressive change from LREE enrichment on the Azores Plateau to LREE depletion south of 33°N. This gradation across the FAMOUS area has also been observed for Sr-isotope ratios, LIL elements and LIL element ratios by White and Schilling (1978).

Sr^{87}/Sr^{86} ratios in ten selected FAMOUS lavas range from 0.70288 to 0.70307, implying an isotopically very homogeneous source (White and Bryan, 1977). Three of the basalts comprising the present study (DR-8, DR3-1 and DR4) were analysed for Sr^{87}/Sr^{86} by Dr. A.J. Erlank at Oxford University. The results, Sr^{87}/Sr^{86} = 0.70302±5 (DR3-1), 0.70299±5 (DR4) and 0.70302±5 (DR8), confirm that these lavas have been derived from an isotopically homogeneous source. All ratios have been normalised to a Sr^{86}/Sr^{88} ratio of 0.11940 and are reported relative to a value of 0.70800 for the Eimer and Amend standard.

The suite of eighteen samples included in this study have been analysed for 14 trace elements (Table 3-7) and selected elements are plotted against mafic-index (M.I. = $FeO + Fe_2O_3/MgO + FeO + Fe_2O_3$) as a measure of differentiation in Figs. 3-10A, B, C, D, 3-11 and 3-12. The following qualitative discussion of the trace element variations in the FAMOUS lavas is, except for Ni and Cr, limited to those samples analysed

Fig. 3-10: Trace element variation in FAMOUS basalts with respect to mafic index (M.I. = $FeO + Fe_2O_3/FeO + Fe_2O_3 + MgO$). Symbols are as follows:

- o Olivine basalts
- Δ Plagioclase-pyroxene basalts
- ● Plagioclase-olivine basalts
- ▲ Plagioclase phyric basalts
- ✖ Picritic basalts.

A

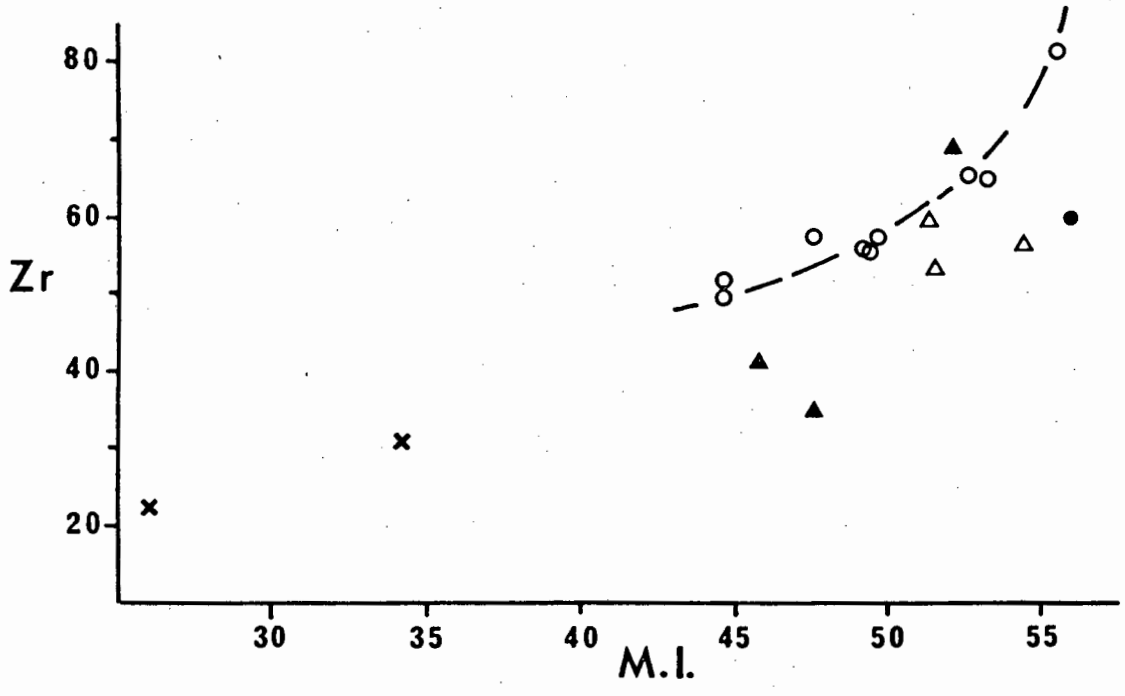
Zr
80
60
40
20
30
35
40
45
50
55
M.I.

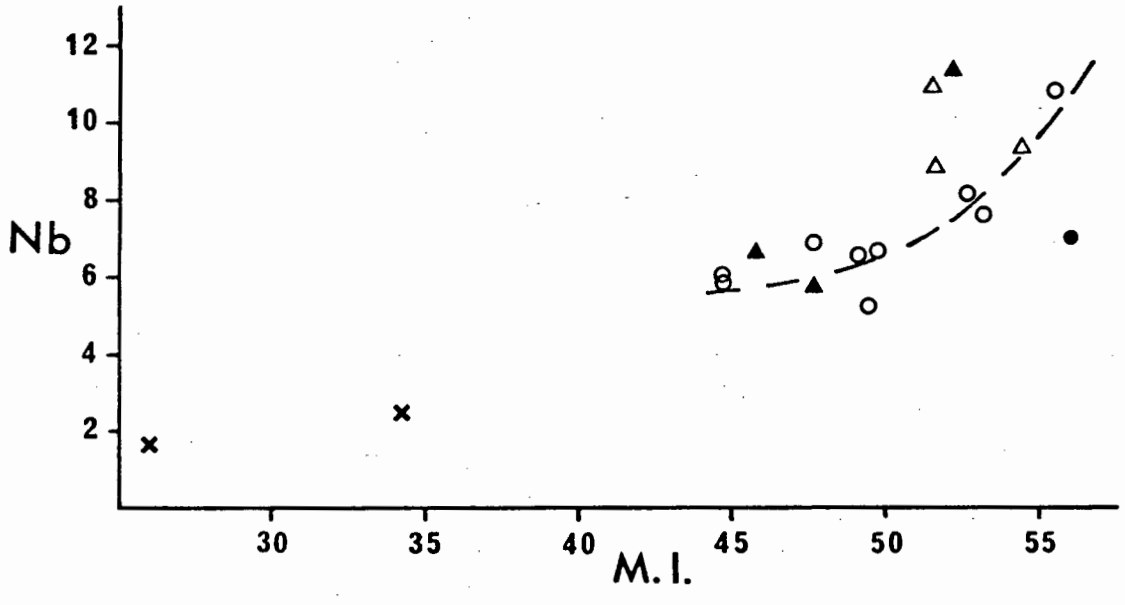
Nb
12
10
8
6
4
2
30
35
40
45
50
55
M.I.

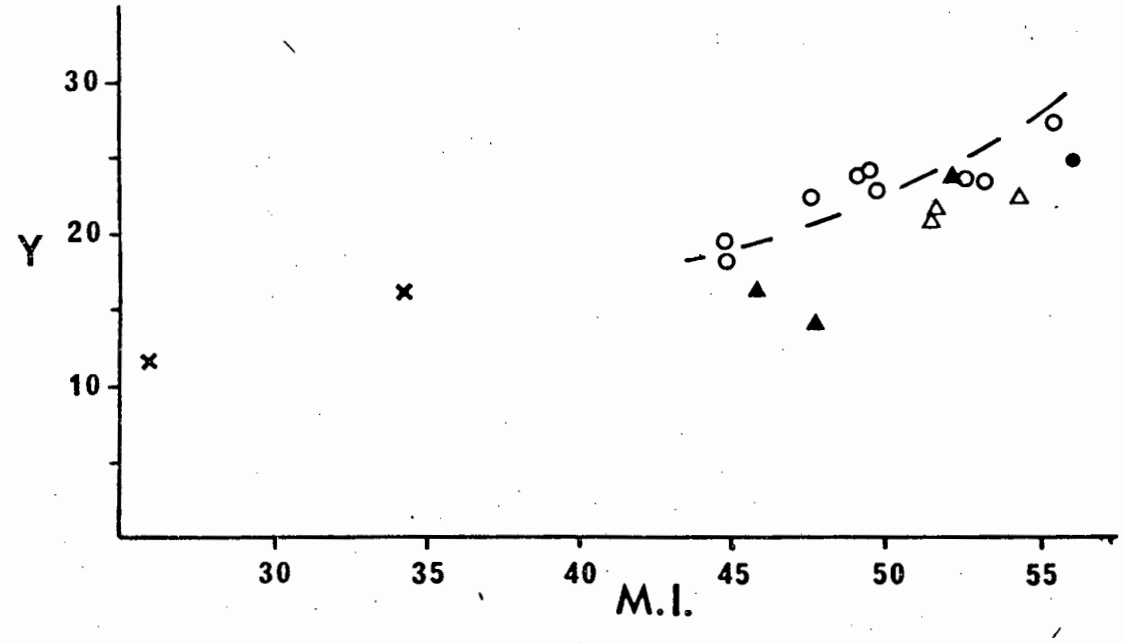
Y
30
20
10
30
35
40
45
50
55
M.I.

Fig. 3-10:

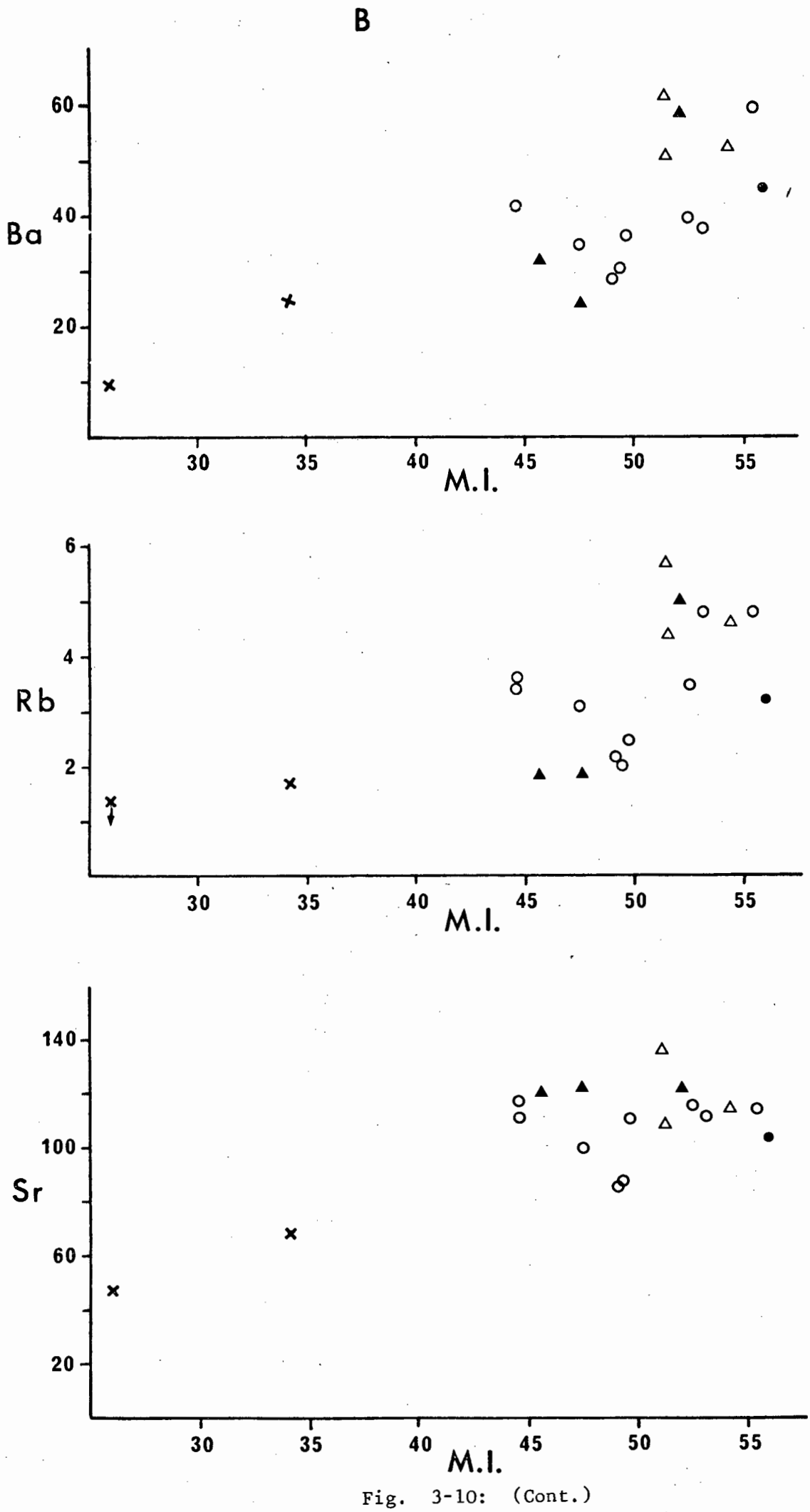
B
Ba
60
40
20
30
35
40
45
50
55
M.I.
Rb
6
4
2
30
35
40
45
50
55
M.I.
Sr
140
100
60
20
30
35
40
45
50
55
M.I.

Fig. 3-10: (Cont.)

C

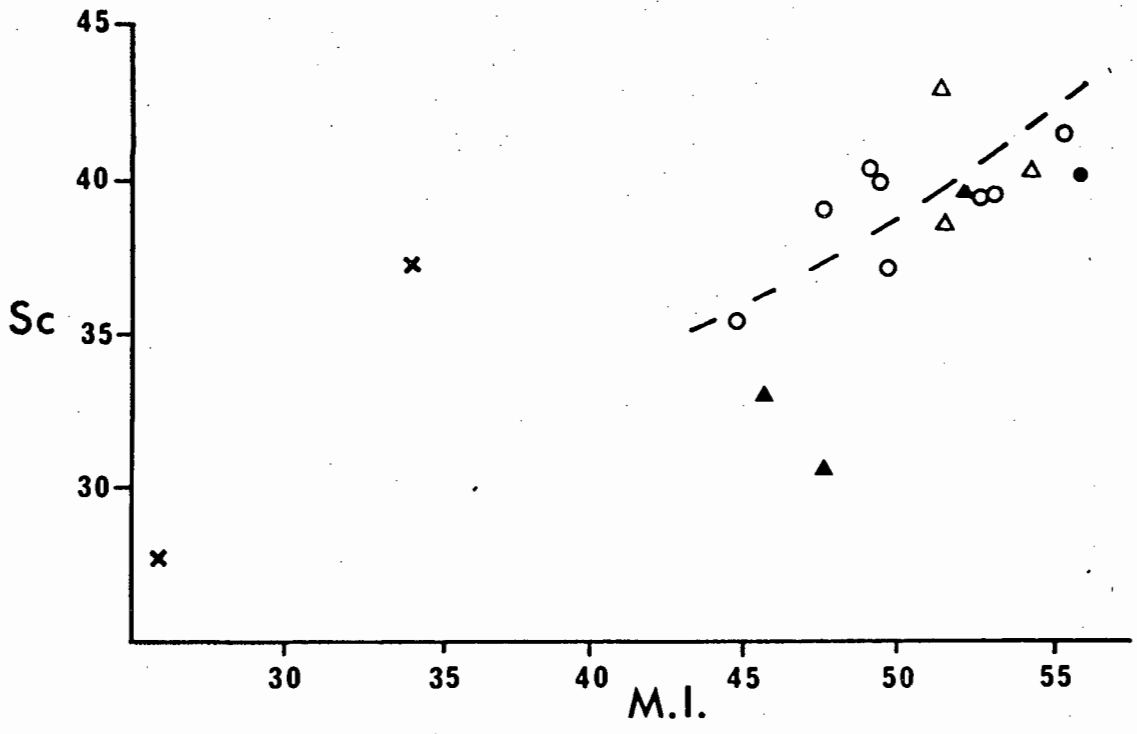

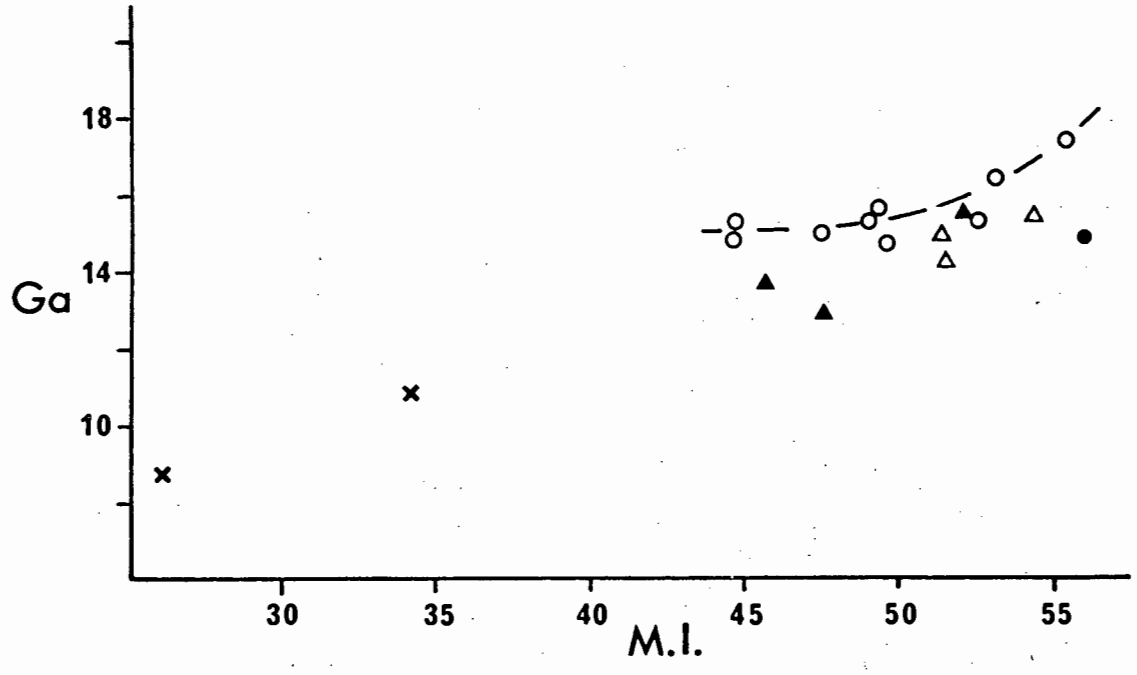

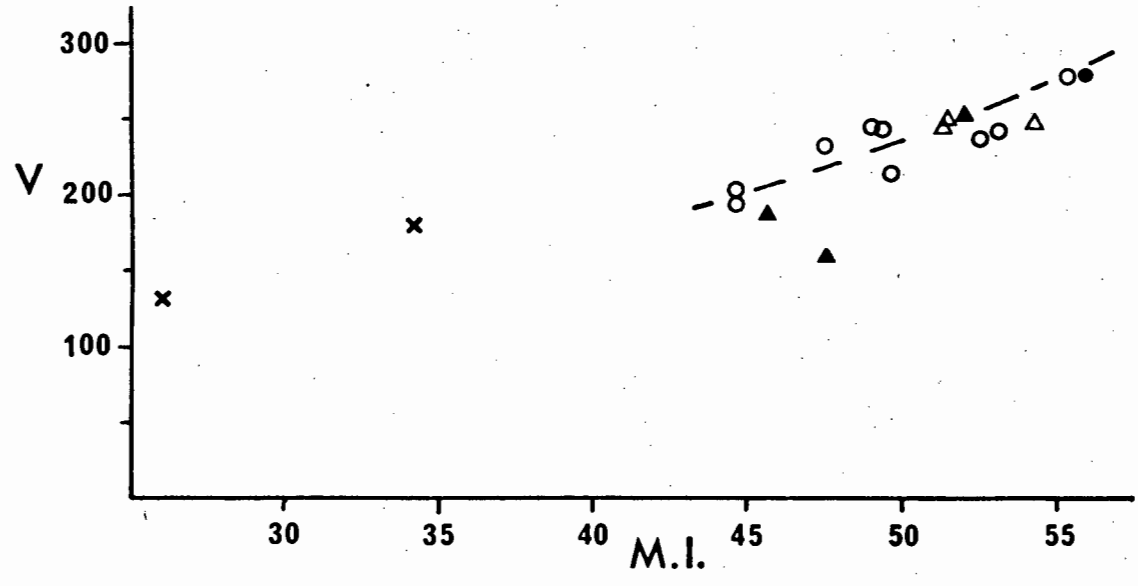

Fig. 3-10: (Cont.)

D

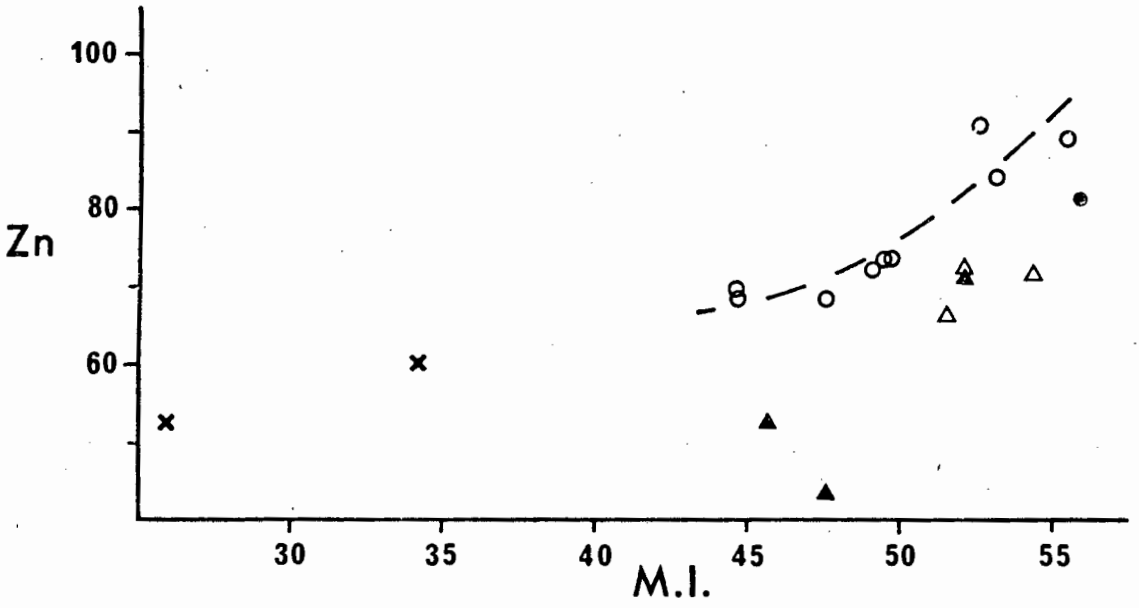

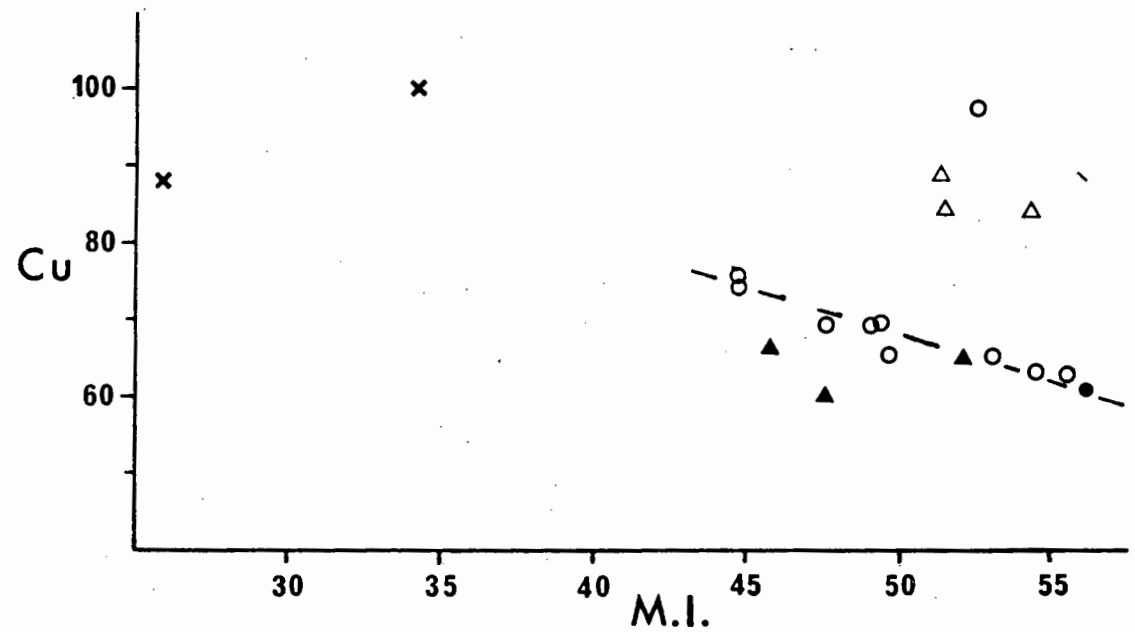

Fig. 3-10: (Cont.)

in this study, so as to exclude possible effects of interlaboratory bias.

The immobile incompatible elements (Zr, Nb and Y) show uniform enrichment in the olivine basalts with differentiation (Fig. 3-10A). Of these three elements, Nb is the most incompatible with respect to the observed phenocryst phases (Tables A2-1, A2-2, A2-5) and the approximate 2.4-fold enrichment in Nb implies that at least 60% crystallisation must occur if the observed trend is due solely to low pressure fractionation from a single magma. The plagioclase-olivine basalt (8-10) is depleted in Nb, Zr and to a lesser extent Y relative to the trend shown by the olivine basalts, while the plagioclase-pyroxene basalts show an enrichment in Nb and slight depletion in Zr and Y relative to the olivine basalt trend (Fig. 3-10A). Assuming that the plagioclase phyric basalts have experienced dominantly plagioclase enrichment, and so dilution of incompatible elements at constant M.I., the parent magma would appear to have been enriched in Nb relative to the olivine basalts prior to plagioclase accumulation (Fig. 3-10A).

Ba, Rb and Sr show significant scatter when plotted against M.I. (Fig. 3-10B). Since these elements are known to show varying degrees of mobility during sea-floor weathering (Hart et al., 1974; Humphris and Thompson, 1978b; Mottl and Holland, 1978), much of the observed scatter could be related to alteration effects and so little significance has been attached to variations observed in these elements.

The variations in Sc, Ga and V with M.I. are shown in Fig. 3-10C. Both Ga and V show well defined enrichment trends with increasing M.I. in the olivine basalts. The plagioclase-olivine and plagioclase-pyroxene basalts plot slightly below the trend defined by the olivine

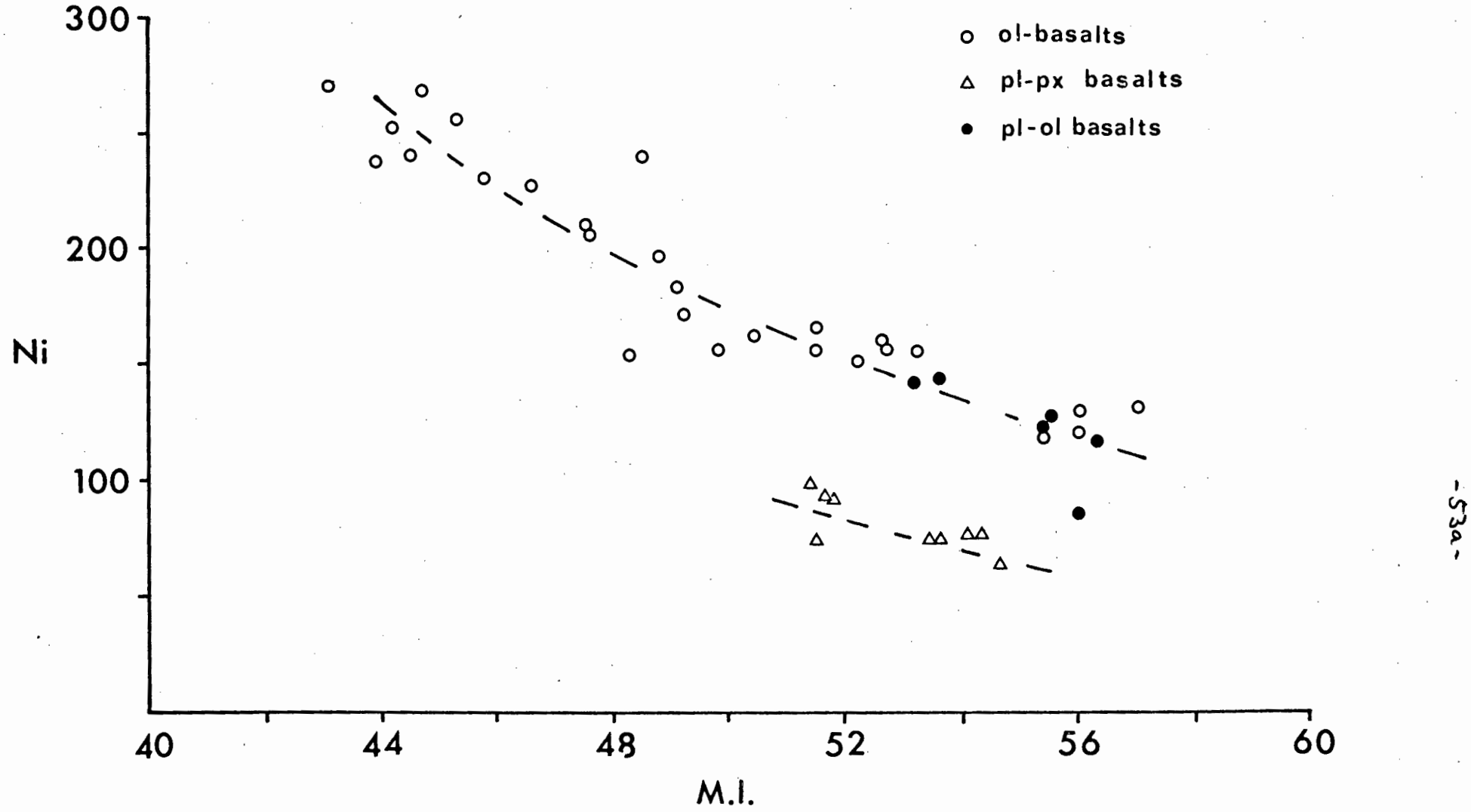

Fig. 3-11: Variation in Ni content of aphyric and sparsely phyric FAMOUS basalts with respect to M.I. Data from this study, from Bougault and Hekinian (1974) and from Arcyana (1977) are included.

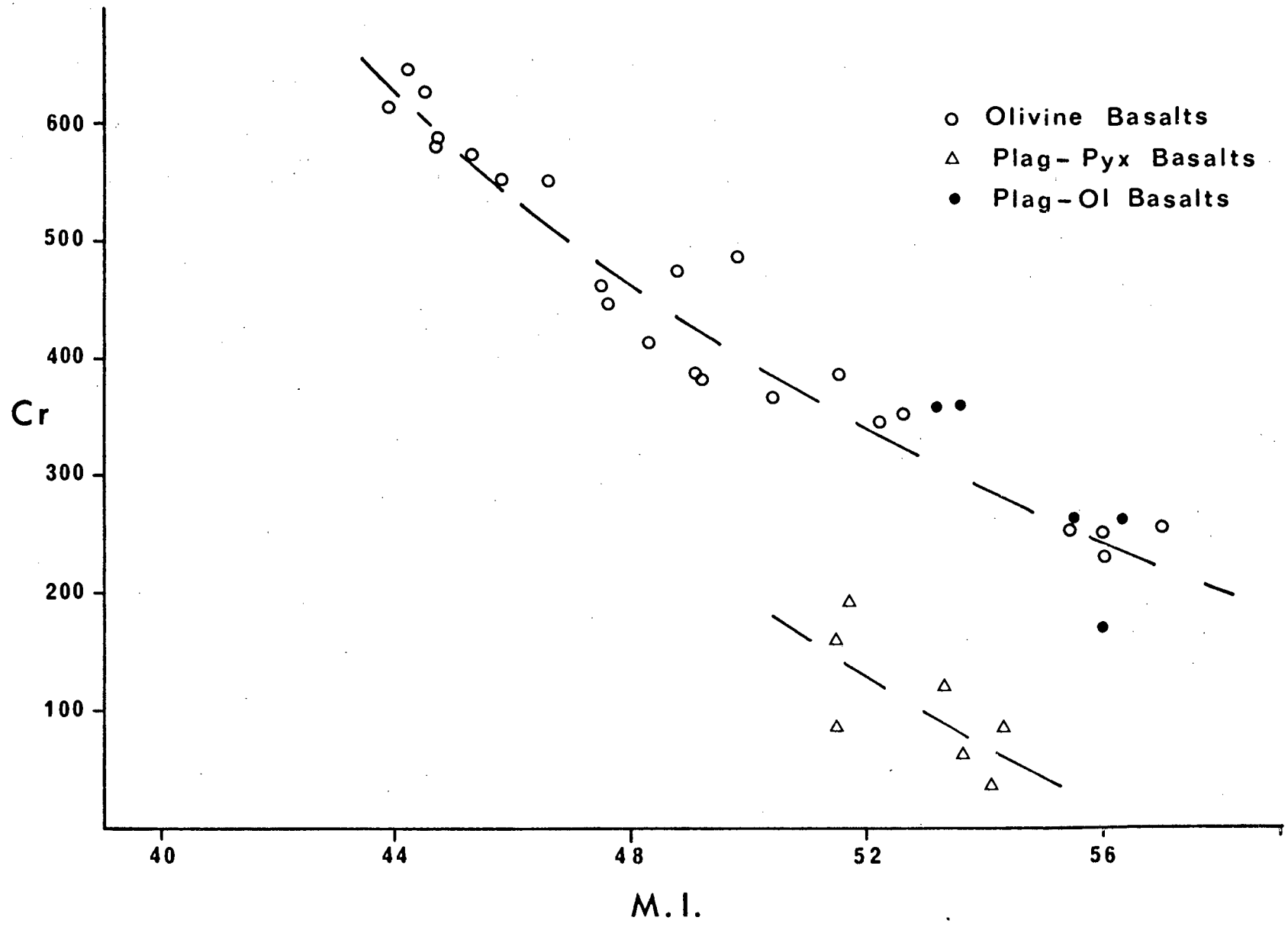

Fig. 3-12: Variation in Cr content of aphyric and sparsely phyric FAMOUS basalts with respect to M.I. Data from this study, from Bougault and Hekinian (1974) and from Arcyana (1977) are included.

sitions found in the FAMOUS area. Additional evidence for the distinction between the olivine basalts and plagioclase-pyroxene basalts is provided by the small scale variations of Zr and Nb. This is clearly illustrated in a plot of Nb versus Zr (Fig. 3-13) where two distinct trends are apparent; one corresponding to the olivine basalts (including the single plagioclase-olivine basalt), and one corresponding to the plagioclase-pyroxene basalts and plagioclase-phyric basalts. The picrites have extremely low Nb concentrations but appear to fall on the trend defined by the olivine basalts. Since both Nb and Zr can be regarded as incompatible elements with respect to basaltic minerals, the Zr/Nb ratio should be unaffected by fractional crystallisation and so reflect source area characteristics (Erlank and Kable, 1976). Reference to Fig. 3-13 and Table 3-7 shows that the plagioclase-pyroxene basalts and plagioclase-phyric basalts have similar Zr/Nb ratios (ave. 5.96; range 5.6-6.1), while the olivine basalts have slightly higher and more variable ratios (ave. 8.4; range 7.5-10.4). In contrast to the two distinct trends for Zr and Nb variations, all samples define a common trend with respect to the variation of Y and Zr (Fig. 3-14).

4.4 Residual Glass Composition

Quench glass rinds present in picrite DR8 and olivine basalts DR4 and 11-18 have been analysed for major elements by electron microprobe. The quench glass in DR8 (Table 3-8) is characterised by low TiO_2 (0.70-0.73%) and Na_2O (1.63-2.07%) and high Al_2O_3 (15.9-16.9%) and CaO (13.2-14.2%) contents. The glass has an MgO content of 8.5-9.5% and the high Mg-number (0.68-0.70) attests to its relatively primitive nature. The glass in DR4 and 11-18 (Table 3-9) is more evolved (MgO = 7.1-8.5%, Mg-number = 0.60-0.66) than that present in DR8 and is relatively

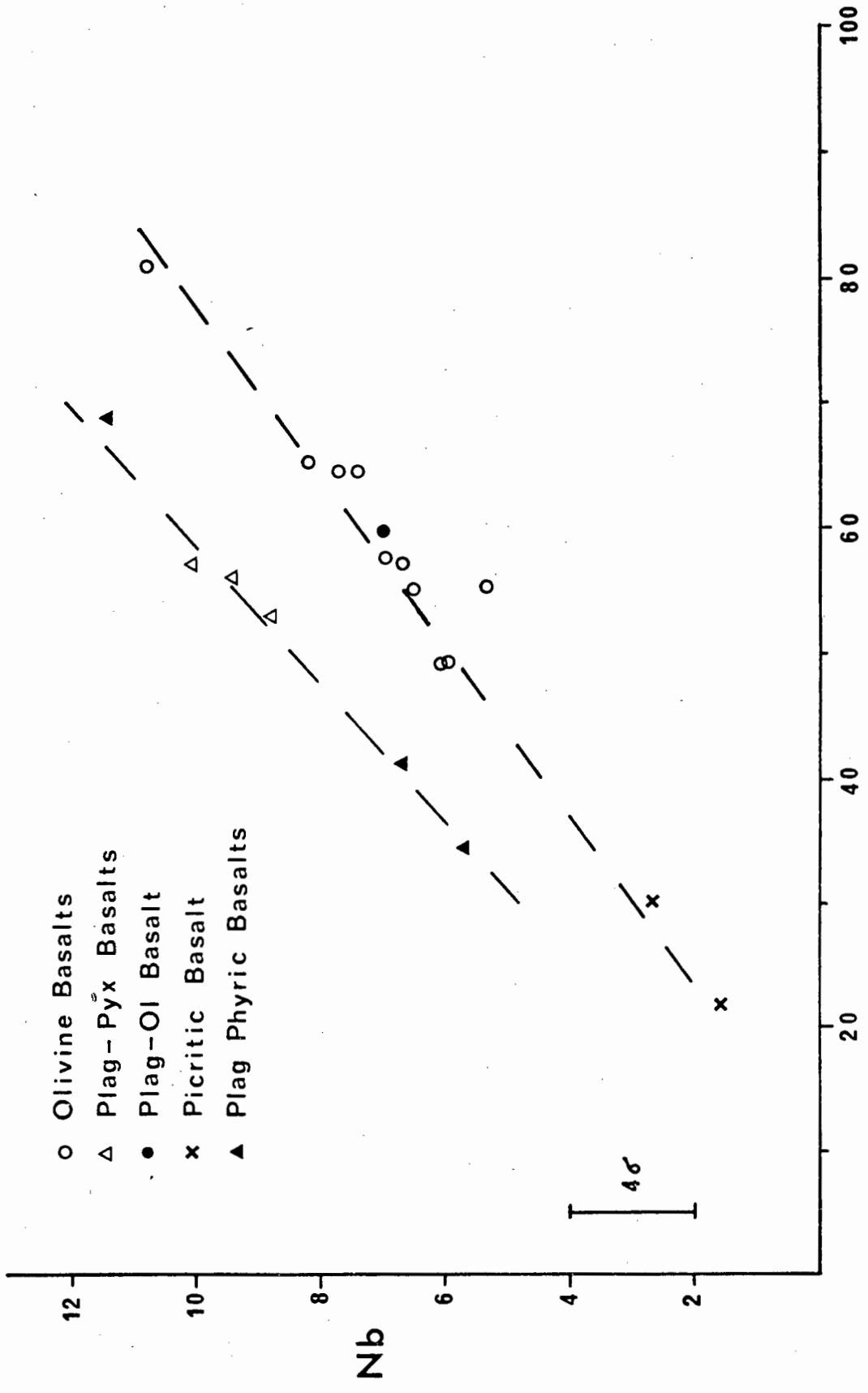

Fig. 3-13: Covariation of Nb and Zr in FAMOUS basalts. The error in Nb (4σ) based on counting statistics is shown.

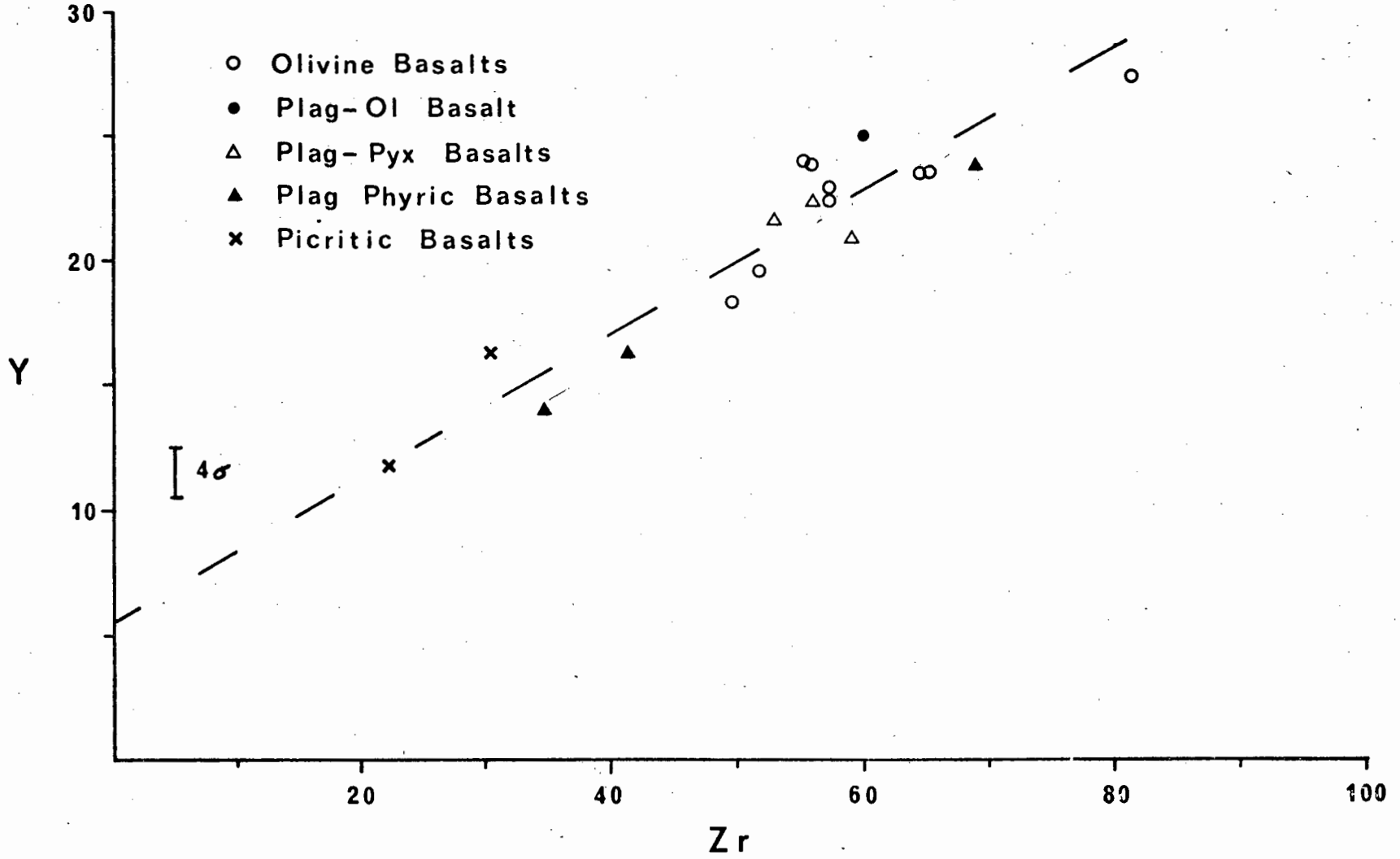

Fig. 3-14: Covariation of Y and Zr in FAMOUS basalts. The 4σ error on Y, based on counting statistics, is shown.

enriched in TiO_2 (1.0-1.2%), Na_2O (2.2-2.6%) and depleted in Al_2O_3 (14.9-15.6%) and CaO (11.5-12.8%). The TiO_2 and Na_2O contents of the quench glass in DR8 are significantly lower than those observed in even the most primitive olivine basalts (DR4-303, DR1-122; Table 3-7). Since the glass is residual (i.e. has lost olivine), these TiO_2 and Na_2O contents indicate that the parental magma had extremely low concentrations of these elements. It will be argued later that the differences in incompatible element contents (Na_2O and TiO_2) between the olivine basalts and the parent to the picritic basalts are real and reflect differing degrees of partial melting during generation of these magma types.

4.5 Discussion

Major and trace element variations in FAMOUS lavas indicate them to be compositionally diverse, with most of the variations being apparently related to olivine and plagioclase control (Figs. 3-8, 3-9, 3-11). Qualitatively the compositional variations within the olivine basalts (Figs. 3-10, 3-11, 3-13, 3-14) suggest that they comprise a consanguinous suite of lavas, related either by fractional crystallisation and/or partial melting. Variation of Ni, Cr, Cu and Zn with M.I. (Figs. 3-10D, 3-11, 3-12) suggests that the plagioclase-pyroxene basalts are unrelated to the olivine basalts, a fact which is supported by Zr/Nb ratios (Fig. 3-13). The similar Zr/Nb ratio of the plagioclase-phyric basalts and plagioclase-pyroxene basalts suggests that these lava types may be genetically related, so indicating the presence of at least two distinct magma types in the FAMOUS area. This possibility was previously suggested by Bougault and Hekinian (1974) who postulated the possibility of two magma types in the FAMOUS area, one giving rise to

T A B L E 3-8

FAMOUS AREA: QUENCH GLASS ANALYSES - PICRITE DR8.

	1	2	3	4	5
SIO2	50.33	50.04	50.01	49.25	49.41
TIO2	.71	.70	.72	.73	.70
AL2O3	16.04	16.14	15.86	16.23	16.94
CR2O3	.08	.07	.07	.08	.09
FE2O3	1.23	1.33	1.28	1.25	1.22
FEO	7.26	7.85	7.50	7.35	7.20
MNO	.15	.16	.15	-	-
MGO	8.52	9.24	8.84	9.51	8.65
CAO	13.75	13.17	13.83	14.03	14.15
NA2O	1.74	1.72	1.63	2.07	2.12
K2O	.13	.11	.12	.14	.14
NIO	.02	.02	.02	.02	.02
TOTAL	99.96	100.55	100.03	100.66	100.64

* * ATOMIC PROPORTIONS BASED ON SELECTED NO. OF OXYGENS * *

OXYGEN	20	20	20	20	20
SI	6.028	5.972	5.999	5.889	5.898
AL	2.264	2.270	2.242	2.287	2.384
TI	.064	.063	.065	.066	.063
CR	.008	.007	.007	.008	.008
FE3+	.111	.119	.116	.112	.110
FE2+	.727	.783	.752	.735	.719
MN	.015	.016	.015	-	-
MG	1.521	1.643	1.580	1.695	1.539
CA	1.765	1.684	1.778	1.798	1.810
NA	.404	.398	.379	.480	.491
K	.020	.017	.018	.021	.021
NI	.002	.002	.002	.002	.002
SUM	12.929	12.975	12.953	13.092	13.044

* * * S A M P L E D I R E C T O R Y * * *

ANALYSIS NO.	DESCRIPTION
1	QUENCH GLASS, 1
2	QUENCH GLASS, 2
3	QUENCH GLASS, 3
4	QUENCH GLASS, 4
5	QUENCH GLASS, 5

T A B L E 3-9

FAMOUS AREA: QUENCH GLASS ANALYSES - OLIVINE BASALTS DR4 & 11-18.

	1	2	3	4	5	6	7
SIO2	51.20	51.07	51.28	51.30	50.99	50.86	50.85
TIO2	1.15	1.15	1.20	1.17	1.05	1.08	1.07
AL2O3	14.86	15.03	14.94	15.00	15.57	15.47	15.47
CR2O3	.08	.08	.10	.09	.09	.07	.07
FE2O3	1.31	1.27	1.28	1.28	1.13	1.18	1.24
FEO	8.72	8.44	8.50	8.50	7.53	7.87	8.25
MNO	.15	.15	.14	.14	.13	.15	.14
MGO	7.72	7.73	7.75	7.12	8.48	8.35	8.05
CAO	11.55	11.46	11.59	12.14	12.75	12.32	12.25
NA2O	2.63	2.68	2.60	2.73	2.31	2.33	2.20
K2O	.18	.19	.19	.18	.09	.12	.11
NIO	.02	.02	.02	.02	-	-	-
TOTAL	99.56	99.26	99.58	99.66	100.12	99.80	99.70

* * ATOMIC PROPORTIONS BASED ON SELECTED NO. OF OXYGENS * *

OXYGEN	20	20	20	20	20	20	20
SI	6.170	6.165	6.171	6.179	6.089	6.098	6.109
AL	2.111	2.138	2.119	2.130	2.192	2.186	2.190
TI	.104	.104	.109	.106	.094	.097	.097
CR	.008	.008	.010	.009	.008	.007	.007
FE3+	.119	.115	.116	.116	.102	.106	.112
FE2+	.879	.852	.855	.856	.752	.789	.829
MN	.015	.015	.014	.014	.013	.015	.014
MG	1.387	1.391	1.390	1.278	1.509	1.492	1.441
CA	1.491	1.482	1.494	1.567	1.631	1.583	1.577
NA	.615	.627	.607	.638	.535	.542	.512
K	.028	.029	.029	.028	.014	.018	.017
NI	.001	.001	.001	.001	-	-	-
SUM	12.928	12.929	12.916	12.921	12.940	12.935	12.905

* * * S A M P L E D I R E C T O R Y * * *

ANALYSIS NO.	DESCRIPTION
1	QUENCH GLASS, 1 (DR4)
2	QUENCH GLASS, 2 (DR4)
3	QUENCH GLASS, 3 (DR4)
4	QUENCH GLASS, 4 (DR4)
5	QUENCH GLASS, 1 (11-18)
6	QUENCH GLASS, 2 (11-18)
7	QUENCH GLASS, 3 (11-18)

the olivine basalts and the other to the plagioclase basalts. This hypothesis is not in accord with the views of Bryan and Moore (1977) and Hekinian et al. (1976). The relationship of the picrites to the other basalt types will be discussed in a later section, but assuming simple olivine accumulation and so dilution of most trace elements, it can be seen from plots of, for example, Sc, V (Fig. 3-10C) and Cu (Fig. 3-10D) that the picrites are unlikely to be related by fractional crystallisation to the olivine basalts. Additional evidence and quantitative modelling of the relationships between the various basalt types is considered in later sections.

5. MINERAL CHEMISTRY

5.1 General Statement

A critical factor in the evaluation of partial melting and fractional crystallisation models is the extent to which postulated parental magmas truly represent liquid compositions. Fresh aphyric lavas and glass quenched on the outer surface of pillow basalts can in general be taken unequivocally to represent liquid compositions. Lavas with varying proportions of phenocrysts, however, pose more of a problem due to the possibility of phenocryst accumulation. Such lavas are especially problematical if one accepts the concept of compensated crystal settling (Cox and Bell, 1972; Krishnamurphy and Cox, 1977) which would allow a lava to become extremely porphyritic yet maintain its initial chemistry.

The possible occurrence of high-Mg basaltic precursors to the voluminous ocean floor basalts has long been a contentious issue (O'Hara, 1965, 1968; Green and Ringwood, 1967; Donaldson and Brown, 1977; Hart and Davis, 1978; Jakobsson et al., 1978; Dungan and Rhodes, 1979; Elthon, 1979; Maaløe, 1979). As yet no high-Mg (>10-11%) glasses have

ever been recovered from the ocean floors. Numerous porphyritic high-Mg picrites have however been found on the ocean floors and the possibility that such lavas may represent high-Mg liquids is of crucial importance to an understanding of ocean floor basalt petrogenesis. With this problem in mind, a detailed study of the mineral chemistry, and specifically the Fe-Mg-Ni distribution, of olivine and Cr-spinel has been conducted in order to assess the relationship between the picrites and the more evolved lavas of the FAMOUS region.

A consanguinous suite of lavas should, amongst other factors, show uniform variations in their mineral chemistry, especially with respect to minor elements. If the wide compositional variations in the FAMOUS lavas are purely a function of low pressure fractionation in a centrally situated magma chamber (Bryan and Moore, 1977; Hekinian et al., 1976), then liquidus mineral compositions should show systematic chemical variations. If one or more parental magmas are involved (Bougault and Hekinian, 1974; Nisbet and Fowler, 1978; Langmuir et al., 1977), then it is feasible to expect displaced or discontinuous mineral compositional variations. As will be shown below, Ni variations in both olivine and Cr-spinel unequivocally exclude the hypothesis that all the lavas are derived from a single magma chamber.

5.2 Olivine

Olivine is ubiquitous in the FAMOUS basalts and since it is probably the liquidus phase (or co-liquidus phase with Cr-spinel) at pressures less than 10 kbar (Bender et al., 1978), a study of the distributions of Fe, Mg and Ni in the olivines should reflect the nature of the liquids at the onset of crystallisation.

5.2.1 Fe-Mg Distributions

The distribution of magnesium and ferrous iron between olivine and coexisting liquid can be used to assess whether olivine phenocrysts are in equilibrium with the host rocks in which they occur. This distribution can be represented by the following equation:

$$\tfrac{1}{2}(Mg_2SiO_4)_{ol} + \tfrac{1}{2}(Fe_2SiO_4)_{liq} = \tfrac{1}{2}(Mg_2SiO_4)_{liq} + \tfrac{1}{2}(Fe_2SiO_4)_{ol} \quad .. \quad (1)$$

The distribution coefficient (K_D) for this reaction can be written as:

$$K_D = (X^{ol}_{FeO}/X^{ol}_{MgO})\ (X^{liq}_{MgO} / X^{liq}_{FeO}) \quad ..... \quad (2)$$

where X^{ol}_{FeO} is the mole fraction of FeO in olivine, etc.

Roeder and Emslie (1970) investigated the equilibrium represented in equation (1) for a variety of basaltic compositions over a range in temperature (1150-1300°C) and oxygen fugacities ($10^{-0.68}$ to 10^{-12} atm) at one atmosphere total pressure and found that the value of K_D (equation 2) was essentially constant (0.30 ± 0.03) and independent of temperature and oxygen fugacity. Subsequently experimental studies by Roeder (1974) and Longhi et al. (1978) have confirmed the value of $K_D = 0.30 \pm 0.03$ over a wide variety of compositions. Cawthorne et al. (1974), Thompson (1975) and O'Hara (1977) have predicted a slightly higher average K_D of 0.33. Roeder (1974) suggested that the K_D was also relatively insensitive to changes in the bulk composition of the liquid in that alkalis and Al_2O_3 affected the solubility of MgO and FeO in the liquid in the same direction. Longhi et al. (1978), however, found a small but significant compositional effect on the distribution of FeO and MgO which can best be ascribed to variations in silica concentration. In addition Longhi et al. (1978) found a noticeable pressure effect above

5 kbar. A systematic increase in K_D with pressure has also been reported from experimental studies on a FAMOUS glass (Bender et al., 1978). The findings of Bender et al. (1978) in this respect, however, may be open to question as no account appears to have been taken of possible Fe_2O_3 in the experimental charges. Mysen (1975) found a similar pressure effect on K_D' (all Fe expressed as FeO). For the purposes of this study K_D values of between 0.27 and 0.33 will be regarded as representing equilibrium conditions.

This relationship has been verified on those FAMOUS basalts that clearly represent liquids on the basis of texture (i.e. are aphyric) and also on microphenocryst glass pairs. Since the analysed olivines in the aphyric and sparsely phyric rocks all show nominal zoning, the assumption has been made that the core of the most-Mg olivine should represent the equilibrium composition that crystallised from a liquid with the FeO/MgO ratio of the host rock (the Fe_2O_3/FeO ratio of the whole rock is assumed to equal 0.15). Calculated Fe-Mg K_D's for the olivine basalts (excluding DR4 and 11-18), plagioclase-olivine basaltsand plagioclase-pyroxene basalts range from 0.31 to 0.33 (Table 3-10), indicating that the samples listed have probably not experienced phenocryst redistribution. If the assumed Fe_2O_3/FeO ratio is lowered to 0.10, then the K_D's range from 0.30 to 0.31. DR4 and 11-18 both give bulk rock K_D values that are too low (0.24 and 0.22 respectively) to indicate equilibrium and indicate that the most Mg-rich olivines are too fosteritic to have crystallised from a liquid with a composition equivalent to the whole rock. The low calculated K_D's in DR4 and 11-18 could be attributed to the Mg-rich olivines either: (1) being xenocrysts, i.e. the rocks are enriched in olivine, or (2) representing remnant olivines left after the

Table 3-10: Predicted liquidus temperatures of aphyric to sparsely phyric 'FAMOUS' lavas, based on Fe-Mg distributions. (Longhi et al., 1979).

	OBS. K_D	Predicted K_D	T(°C)
1) Olivine basalts			
DR4-303	0.311 (0.299)*	0.303	1268
DR1-122	0.325 (0.312)	0.304	1267
DR9-322	0.321 (0.308)	0.303	1249
DR9-308	- (-)	0.304	1250
DR9-323	0.322 (0.310)	0.303	1248
DR2-174	0.314 (0.302)	0.306	1224
2) Plag-olivine basalts			
8-10	0.313 (0.301)	0.307	1217
3) Plag-pyroxene basalts			
DR2-301	0.315 (0.302)	0.304	1219
31-38	0.316 (0.303)	0.304	1219
DR10-310	0.309 (0.296)	0.306	1215

* values in brackets calculated assuming $Fe_2O_3/FeO = 0.10$, others assuming $Fe_2O_3/FeO = 0.15$.

bulk of liquidus olivines have been lost by gravitational settling from a more primitive parental magma. Average microphenocryst-quench glass pairs in DR4 and 11-18 give Fe-Mg K_D values of 0.35 and 0.32 respectively. The high K_D in DR4 can be attributed to the slight but significant variations in glass compositions (Table 3-9) relative to the fairly uniform microphenocryst compositions. The most Mg-poor glass (Table 3-9, No. 4) gives a K_D of 0.32 against the average microphenocryst.

Roeder and Emslie (1970) and Longhi et al. (1978) have shown that it is possible to calculate the liquidus temperatures of olivine-saturated basaltic liquids given only the bulk composition. This requires the calculation of a predicted K_D by the following equation (Longhi et al., 1978):

$$K_D = 0.165 + 0.299\ X_L^{Si} \quad \ldots\ldots\ldots\ldots\ldots\ldots\ldots\ldots \quad (3)$$

where X_L^{Si} = Si/Σcations (mol. proportions).

This predicted K_D can then be combined with the bulk composition to give the Fe/Mg ratio of the coexisting olivine. From the simple stoichiometry of olivine, X_{ol}^{MgO} can then be calculated. From X_L^{MgO}, X_{ol}^{MgO} and X_L^{Si} one can then calculate the liquidus temperatures using the following expression (Longhi et al., 1978):

$$\log K^{Mg} = \frac{3469}{T(K)} - 1.512 \quad \ldots\ldots\ldots\ldots\ldots\ldots\ldots\ldots \quad (4)$$

$$\text{where } K^{Mg} = X_{ol}^{MgO} / (X_L^{MgO} \cdot (X_L^{Si})^{\frac{1}{2}}) \quad \ldots\ldots\ldots\ldots\ldots\ldots \quad (5)$$

Predicted K_D's and liquidus temperatures for the aphyric olivine basalts, plagioclase-olivine basalt and plagioclase-pyroxene basalts are given in Table 3-10. The predicted and observed K_D's are in good agreement

if a liquidus Fe_2O_3/FeO ratio of 0.10 is assumed (Table 3-10). The calculated liquidus temperatures show extremely good agreement with those predicted by the Mn distribution (Table 3-3) using the formulation of Watson (1977) or of Leeman and Schreidegger (1977). It is interesting to note that the liquidus temperature of DR4-303 and DR1-122 (the two most MgO-rich rocks: 10.5% MgO) are identical to that found experimentally for the MgO-rich glass 572-1-1 from the FAMOUS region by Bender et al. (1978). These authors found that the sequence of appearance of phases at one atmosphere was: olivine - 1268°C, plagioclase - 1235°C and clinopyroxene - 1135°C.

Similar calculations for the plagioclase phyric samples indicate that DR3-1 might have been enriched in only plagioclase as the olivine-whole rock K_D is 0.29, while DR10-101C (K_D = 0.21) and DR3-131 (K_D = 0.26) have probably experienced enrichment in Mg-rich olivine in addition to plagioclase.

Olivine microphenocrysts and quench glass in picrite DR8 have been analysed and give an average K_D of 0.32. The Fe_2O_3/FeO ratio of the quench glass in DR8 was calculated by a mass balance equation using the chemical mode and whole rock Fe_2O_3/FeO ratio, to compensate for the large proportion of FeO present in the olivine phenocrysts. The Fe_2O_3/FeO ratio of the whole rock is 0.13, while the calculated value for the matrix is 0.25.

The experimental studies of Roeder and Emslie (1970), Roeder (1974) and Longhi et al. (1978) were conducted on relatively low MgO liquids. In an attempt to verify the K_D at higher MgO levels (for comparison with DR8 and 10-03C whole rock compositions), the experimental data from Arndt (1977b) was investigated. Arndt (1977b) conducted melting experi-

ments on basaltic compositions ranging in MgO content from 25% to 10% at controlled temperatures and oxygen fugacities. Using the quoted temperatures and fO_2's, the amount of ferrous iron in the melt can be calculated from the following equation (Lindstrom, 1976):

$$\log Fe^{3+} / Fe^{2+} = \frac{-6300}{T(K)} + 3.01 - \tfrac{1}{4}\log fO_2$$

Using FeO contents determined by this method, calculated K_D's range from 0.31 to 0.33 for coexisting liquid-olivine compositions. This suggests that a K_D value of 0.30 ± 0.03 is applicable at MgO levels shown by the FAMOUS picrites (14-24%). Using the whole rock composition as representing a liquid, the K_D calculated for DR8 (16% MgO) is 0.38, while that for 10-03C (24% MgO) is 0.56, indicating that the observed most Mg-rich olivines (Fo_{91}) are too Fe-rich to have crystallised from the observed compositions for the respective whole rocks. However if, as suggested by the unzoned nature of the olivine phenocrysts, these rocks have experienced equilibrium crystallisation, then an erroneous (and apparently too high) K_D would be obtained since the cores would no longer represent liquidus compositions. Two factors, however, argue against closed system equilibrium crystallisation: (1) though zoning is absent, different phenocrysts show a range in composition (Fo_{91}-Fo_{89}), an unlikely situation for closed system equilibrium crystallisation, and (2) if equilibrium crystallisation occurred, then the phenocrysts should give a K_D of 0.30 when calculated against the groundmass. An average value for DR8 of 0.22 is however obtained. It is suggested then that at least DR8 and 10-03C and probably all the FAMOUS lavas with >14% MgO do not represent liquid compositions and are cumulus-enriched in olivine.

From this conclusion it is possible to postulate the composition

of the parental liquid. If one envisages the accumulation as taking place at the base of a temperature-zoned magma chamber, then the accumulating olivines would probably reflect a range in compositions in accord with their temperature of crystallisation. Assuming a melt-olivine K_D of 0.30, then it is necessary to accumulate 10% average olivine (Fo_{90}) into DR8 and 32% into 10-03C to give the observed compositions. Predicted parental melts would then have the following characteristics:

	DR8 (P)	10-03C (P)	Average
SiO_2	48.57	47.77	48.17
TiO_2	0.64	0.60	0.62
Al_2O_3	15.72	15.93	15.83
FeO*	8.30	7.85	8.08
MnO	0.16	0.15	0.15
MgO	12.76	12.42	12.59
CaO	12.59	12.49	12.54
Na_2O	1.58	1.71	1.65
K_2O	0.08	0.09	0.09
Totals	100.40	99.01	99.72
Mg-number	74.9	75.5	75.2
CaO/Al_2O_3	0.80	0.78	0.79
CaO/Na_2O	7.97	7.26	7.63

This average parental melt is obviously only a first approximation from the simplified accumulation model adopted. The accumulation of minor Cr-spinel will for example contribute to a very small extent towards the observed composition. Nevertheless this composition is in good agreement with other predicted parental melts (Table 3-11) and reflects some

Table 3-11: Possible parental magmas for ocean floor basalts. (Extracted from the literature).

	1	2	3	4	5	6
SiO_2	50.26	49.58	50.3	50.4	49.4	47.76
TiO_2	0.61	0.65	0.73	0.7	0.81	0.59
Al_2O_3	14.21	14.43	16.6	15.6	15.64	12.06
FeO*	6.82	8.19	7.99	7.1	7.44	8.96
MnO	0.10	-	0.12	0.2	0.15	0.12
MgO	11.89	11.64	10.2	9.1	10.01	17.78
CaO	13.46	12.89	13.2	13.6	12.93	11.20
Na_2O	1.42	1.70	2.00	2.0	1.95	1.31
K_2O	0.07	0.03	0.01	0.3	0.17	0.03
TOTAL	98.66	99.10	101.15	99.0	98.50	99.81
Mg-number	77.9	74.2	72.1	72.2	73.1	80.1
CaO/Al_2O_3	0.95	0.89	0.80	0.87	0.83	0.93
CaO/Na_2O	9.48	7.58	6.60	6.80	6.63	8.55

1. Donaldson and Brown (1977) - Melt inclusions in Cr-spinel.
2. Dungan and Rhodes (1978) - Reconstructed melt inclusion in olivine.
3. Frey et al. (1974) - South Atlantic. Quench glass 3-18-7-1.
4. Watson (1976) - Melt inclusion reconstruction, Bouvet Triple Junction.
5. Rhodes - 45°N MAR (from Dungan and Rhodes, 1978).
6. Elthon (1979) - Calculated from Tortuga ophiolite.

Table 3-12: Calculated Mg-Ni K_D's for aphyric basalts and microphenocryst-glass pairs from FAMOUS lavas.

	K_D^{Mg-Ni}
1) Olivine basalts	
DR4-303	2.24
DR1-122	2.21
DR9-322	2.10
DR9-323	2.33
DR2-174	2.27
*DR4-329	2.59
*DR4	2.56
2) Plagioclase-olivine basalts	
8-10	---
3) Plagioclase-pyroxene basalts	
DR2-301	2.06
31-38	2.58
DR10-310	2.63
4) Quench glass-microphenocryst	
DR4	2.33
DR8	2.31

* Slightly phyric samples which have possibly experienced slight phenocryst redistribution (see section 5.2).

Kushiro (1976) and Takahashi (1978) have similarly noted the compositional and, to a lesser extent, temperature effect on K_D^{Mg-Ni}. Experimental data of Takahashi (1978) indicate a variation in K_D from 1.4 to 3.5. This trend is graphically illustrated using the data from Hart and Davis (1978) in Fig. 3-15. With the exception of a few data points, an exponential decrease in K_D with increasing MgO is observed. K_D clearly only falls within the range 2.0-2.6 for lavas with between 6 and 12% MgO. The K_D values obtained for DR8 (1.50) and 10-03C (1.24) are well below that observed at even the highest MgO levels in Hart and Davis' (1978) experiments and, taken together with the Fe-Mg Data, lend support to the contention that these lavas are cumulus-enriched. However, the fact that the Mg-Ni K_D is clearly composition-dependent severely limits its applicability for determining liquid-crystal equilibrium at high MgO levels.

It has become more and more apparent in recent years that trace element distribution coefficients are strongly dependent on compositonal variations as well as being dependent on temperature and pressure (Lindstrom, 1976; Leeman and Schreidegger, 1977; Hart and Davis, 1978; Ryerson and Hess, 1978). The sensitivity of D_{ol}^{Ni} to compositional variation (Hart and Davis, 1978) and/or temperature (Arndt, 1977b; Leeman and Schreidegger, 1977) makes it important to be able to predict suitable values applicable to the composition of interest. The formulation of Hart and Davis (1978) relating D_{ol}^{Ni} to the composition of the magma is potentially useful to determine D_{ol}^{Ni} for a fractional crystallisation series as temperatures are not always easily determined. The relatively accurate Ni data from quench glass-microphenocryst pairs, and olivine microphenocryst-aphyric lava data have been used to calculate

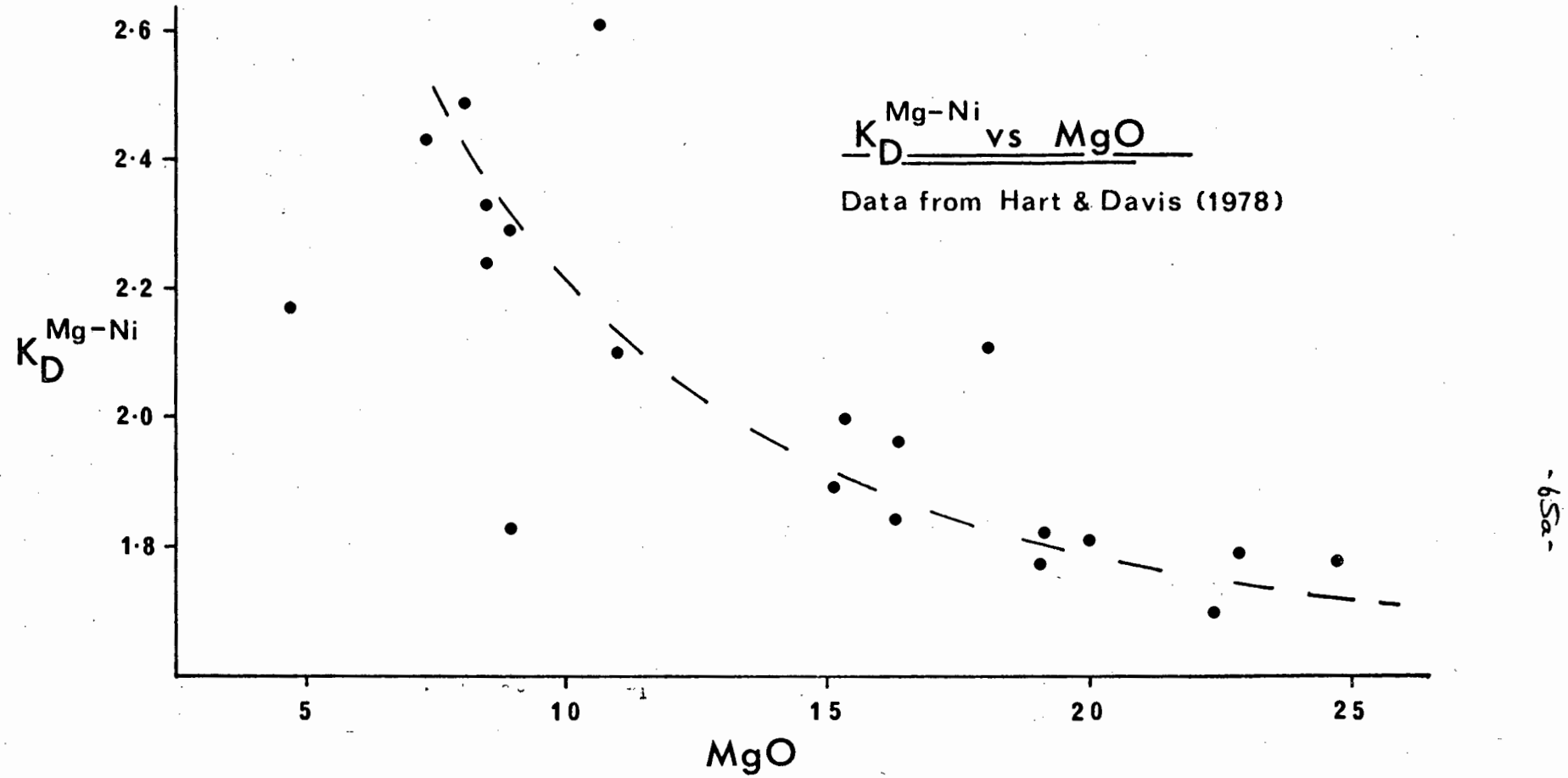

Fig. 3-15: Variation in the partitioning of Mg and Ni between olivine and coexisting liquid (K_D^{Mg-Ni}) with the MgO content of the liquid. Data are taken from Hart and Davis (1978).

$D^{Ni}_{ol\text{-}liq}$ and are compared with the Hart and Davis (1978) predicted values in Table 3-13. In general there is good agreement between the two sets of values. In subsequent quantitative modelling the Hart and Davis (1978) equation will be used to predict D^{Ni}_{ol} unless otherwise stated.

The minor (or trace) element content of early phenocryst minerals can be very diagnostic of the parental melt chemistry, especially when the distribution coefficient for a given element is significantly greater than unity. Ni is such a minor element in the olivines from the FAMOUS lavas. Since olivine is ubiquitous in the FAMOUS lavas, the distribution of Ni should closely reflect the chemistry of the parental melt(s) and/or the physico-chemical conditions of crystallisation. How Nickel has been determined in olivines from picrites DR8 and 10-03C, plagioclase-phyric lavas DR3-1, DR3-131 and DR10-101C, plagioclase-pyroxene basalts DR2-301, 31-38 and DR10-310, and olivine basalts DR4-303, DR1-122, DR9-323, DR9-322, DR4-329, DR4 and DR2-174. Individual analyses are presented in microfiche Tables F3-1, F3-4, F3-11 and F3-15. Variation in NiO content with fosterite content in the olivine is shown in Fig. 3-16 where two very distinct trends are defined. The upper trend comprises olivines from the olivine basalt series, which are clearly more Ni-rich, for a given fosterite content, than those from the picrites, plagioclase-phyric basalts and plagioclase-pyroxene basalts (lower trend). Another important feature of the two varieties of olivine is that those from the upper trend show significant compositional zoning, while those from the lower trend tend to be unzoned ($<0.01\%$ NiO, $<0.5\%$ Fo), though different grains within a thin section show different compositions (Fo_{91}-Fo_{89}). The variation shown in Fig. 3-16 negates a single magma chamber hypothesis

Table 3-13: Calculated $D^{Ni}_{ol\text{-}liq}$ for glass-olivine pairs and host rock-liquidus olivine pairs for aphyric FAMOUS lavas.

	D(obs)	D*(calc.)
Glass-olivine microphenocryst		
DR4	13.3	15.46
DR8	12.2	12.95
Glass inclusion-olivine host		
DR8	12.00	12.9
DR8	13.50	12.9
DR8	14.40	14.50
Olivine basalts		
DR4-303	10.81	10.98
DR1-122	10.30	11.10
DR9-322	10.20	11.90
DR9-323	11.50	12.15
DR2-174	12.2	14.13
Plagioclase-pyroxene basalts		
DR2-301	11.13	14.17
31-38	13.92	13.6
DR10-310	14.47	14.66

* $D = \frac{124}{MgO} - 0.90$ (Hart and Davis, 1978).

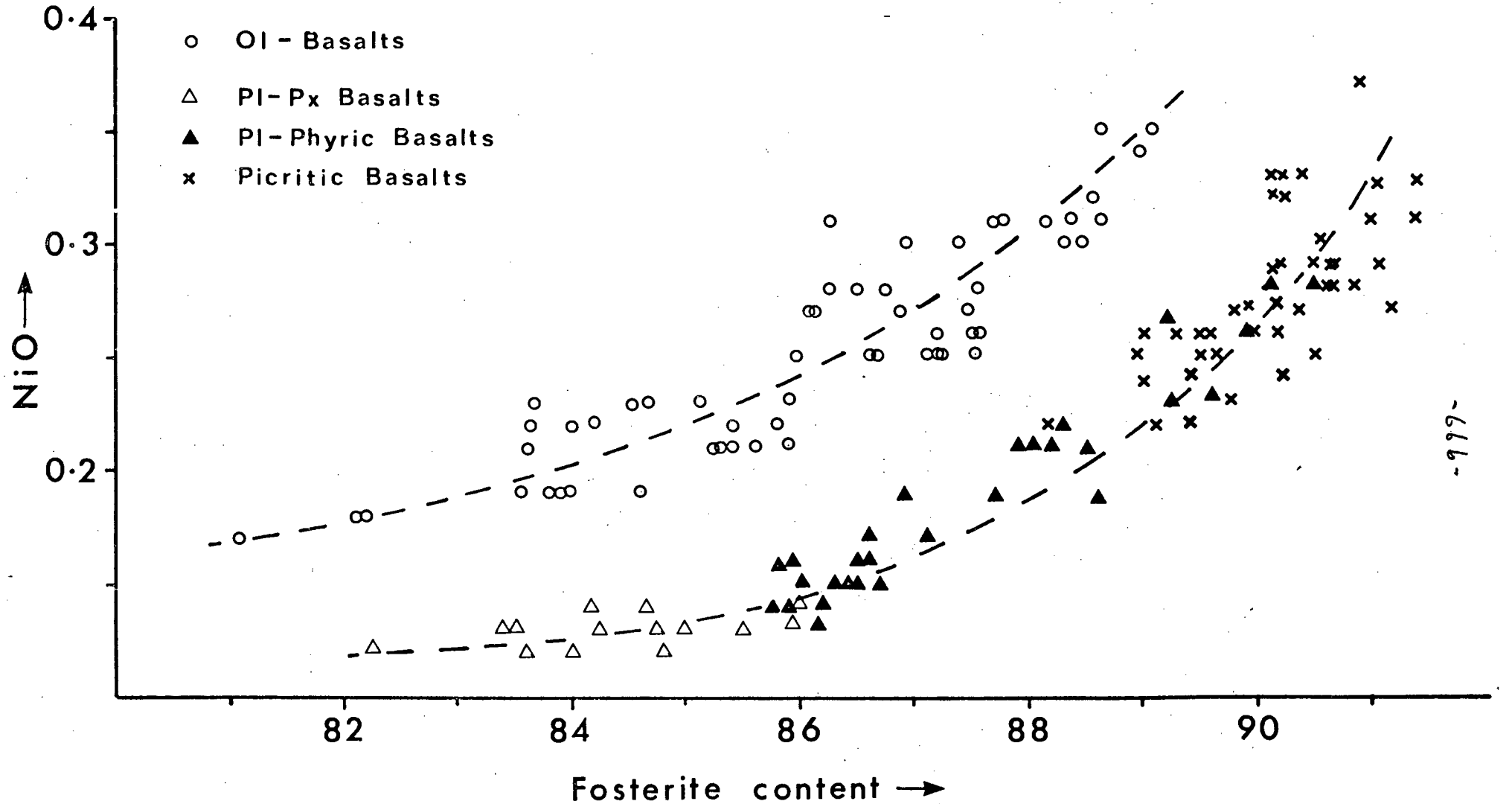

Fig. 3-16: Variation in NiO content of olivine phenocrysts and microphenocrysts with fosterite content, in FAMOUS basalts. Data are from 7 olivine basalts, 3 plagioclase-pyroxene basalts, 3 plagioclase phyric basalts and 2 picrite basalts.

(Bryan and Moore, 1977; Hekinian et al., 1976) and clearly distinguishes the voluminous olivine basalts from the subordinate picrites, plagioclase-pyroxene basalts and plagioclase-phyric basalts which would appear to be related to a single differentiating magma. This variation is also reflected in the whole rock chemistry of the lavas (Section 4, Fig. 3-11).

The significance of this distinction in olivine composition with respect to the petrogenetic relationships of the FAMOUS lavas will be discussed in Section 7.

5.3 Cr-spinel

Cr-spinel is a co-liquidus phase with olivine in the less evolved FAMOUS basalts and so can potentially provide additional constraints on the chemistry of possible parental magma(s). A discussion on the distribution of Fe-Mg and Ni in Cr-spinel is therefore of relevance.

5.3.1 Fe-Mg Distribution

The distribution of Fe and Mg between olivine and Cr-spinel was suggested to be a potentially useful geothermometer by Irvine (1967). Jackson (1969) discussed the olivine-spinel geothermometer which appeared to give realistic temperatures when applied to plutonic rocks. Subsequently, however, a number of workers (e.g. Evans and Wright, 1972; Evans and Frost, 1975) have found that Jackson's formulation gives excessively high temperatures, though the relative scale of temperatures appears to be correct (Evans and Frost, 1975; Wood and Fraser, 1976).

Fujii (1978) has similarly claibrated an olivine-spinel geothermometer from experimental data over a range of pressures, but calculated temperatures for volcanic rocks from Kilauea are still excessive (1600-2000°C). Recently Roeder et al. (1979) have re-evaluated the olivine-spinel geothermometer and used a different free energy value for $FeCr_2O_4$

in the formulation and found that more realistic temperatures could be obtained. The exchange reaction of interest is:

$$\tfrac{1}{2}Fe_2SiO_4 + Mg(Cr_\alpha Al_\beta Fe^{3+}_\gamma)_2O_4 = \tfrac{1}{2}Mg_2SiO_4 + Fe(Cr_\alpha Al_\beta Fe^{3+}_\gamma)_2O_4 \quad .. (1)$$

where α, β and γ are the atomic fractions of the respective trivalent cations. The equilibrium constant for this reaction,

$$K_D = (FeO/MgO)^{sp}/(FeO/MgO)^{ol}, \quad ..... (2)$$

is temperature-dependent, and the potential geothermometer as formulated by Jackson (1969) and modified by Roeder et al. (1979) is as follows:

$$T(K) = \frac{3480\alpha + 1018\beta - 1720\gamma + 2400}{2.23\alpha + 2.56\beta - 3.08\gamma - 1.47 + 1.9871\ln K_D} \quad ... (3)$$

where $\alpha = \dfrac{Cr}{Cr+Al+Fe^{3+}}$; $\beta = \dfrac{Al}{Cr+Al+Fe^{3+}}$; $\gamma = \dfrac{Fe^{3+}}{Cr+Al+Fe^{3+}}$

The formulation and the constraints are extensively discussed by Jackson (1969) and by Roeder et al. (1979) and will not be repeated here. The relationship in equation (3) has been used to calculate olivine-spinel equilibration temperatures in selected FAMOUS lavas.

With this object in mind, 8 olivines containing Cr-spinel inclusions from DR8 and one from 10-03C were analysed to determine the distribution of Fe and Mg between the two phases. Analyses on the olivines were carried out as close to the actual contact as possible. One of the olivines analysed from DR8 has two Cr-spinel inclusions of the high-Al variety. The (Fe/Mg) atomic ratios for coexisting pairs are plotted in Fig. 3-17, where an excellent correlation is clearly defined, giving an average $K_D = 2.828$. This is significantly lower than that observed for

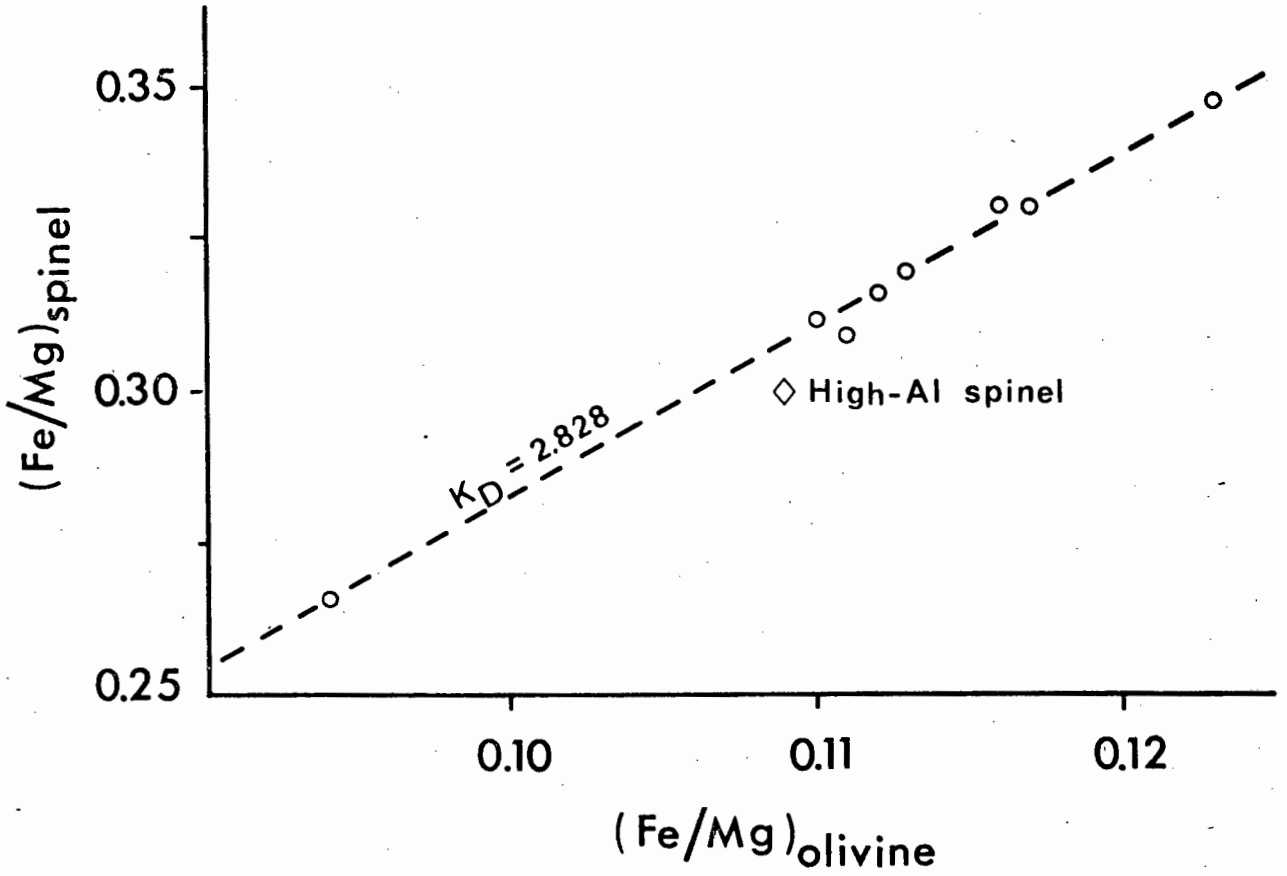

Fig. 3-17: Variation in the atomic Fe/Mg ratio of coexisting Cr-spinel and host olivine pairs in picrite basalts DR8 and 10-03C. The regression line giving the average K_D (i.e. $(Fe/Mg)^{sp}/(Fe/Mg)^{ol}$) was calculated excluding the single high-Al spinel.

olivine-spinel pairs from strataform intrusions (Jackson, 1969) and the Hawaiian lavas (Evans and Wright, 1972), but is similar to that observed in some lherzolite inclusions in alkali basalt (Aoki and Prinz, 1974; Littlejohn and Greenwood, 1974). The data from Sigurdsson and Schilling (1976) indicate an average $K_D = 3.11$ for spinel-olivine pairs from the MAR basalts. The average Al-rich spinels in DR8 give a $K_D = 2.62$, similar to that observed for spinels of similar composition from DSDP Leg 3 basalts ($K_D = 2.52$; Frey et al., 1974).

The average temperature of equilibration for the Cr-spinels from DR8 is 1365 $\pm$ 21°C (after Roeder et al., 1979) which would appear to be somewhat high relative to the liquidus temperature of 1268°C for a 10% MgO basaltic glass obtained experimentally by Bender et al. (1978). However, it is believed that the parental liquid to DR8 was more basic ($\pm$ 12.3-13.1% MgO, see Sections 5.2.1 and 6.3) than that used by Bender et al. (1978) and so a somewhat higher liquidus temperature might be expected. Roeder et al. (1979) have pointed out that temperatures calculated for high-Al spinels tend to be somewhat high, using any combination of available free energy data. The Al-spinels in DR8 indicate a temperature of 1165°C, significantly lower than that for the 'normal' spinels, a factor possibly indicating a xenocrystic origin for the subordinate high-Al spinels.

5.3.2 Ni Distribution

It has been shown that the olivines from the picrites, HPPB and plagioclase-pyroxene basalts can be dist inguished from those in the olivine basalt in terms of their NiO content. A similar separation is obtained for the Cr-spinels in these lavas (Fig. 3-18). Relatively few data are available, but there is a definite tendency for the Cr-spinels

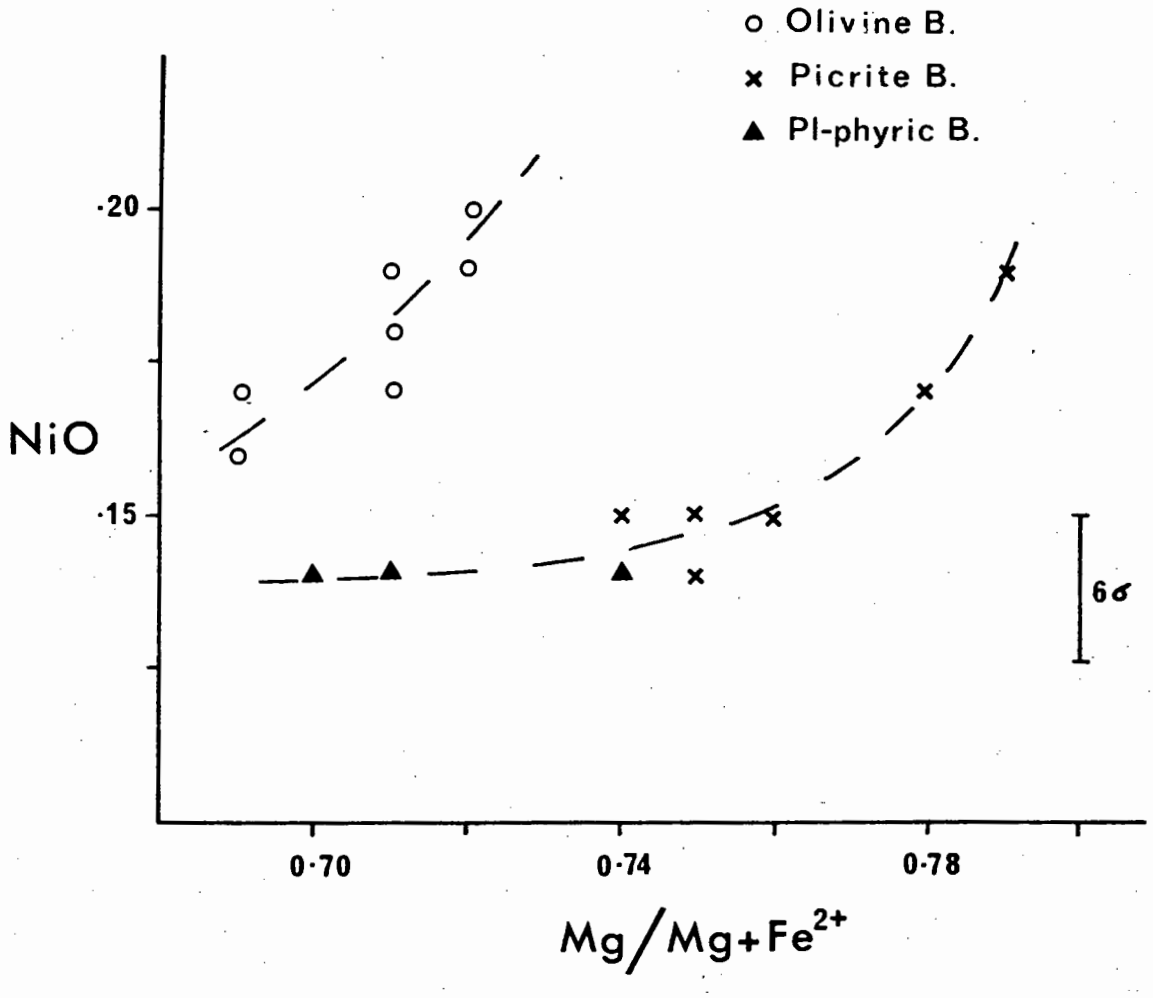

Fig. 3-18: Variation in NiO content of Cr-spinel from selected FAMOUS basalts. Data are from 3 olivine basalts, 2 picrite basalts and 1 plagioclase phyric basalt.

in olivine basalts (DR4-303, DR1-122 and DR9-322) to have higher NiO for a given Mg/Mg+Fe atomic ratio than the Cr-spinels in picrites DR8, 10-03C and HPPB DR3-131. It is suggested that this distribution reflects an inherent difference in the parental magmas for these two distinct suites of lavas.

6. MELT INCLUSION CHEMISTRY

6.1 General Statement

Recently it has been increasingly realised that the study of melt inclusions in liquidus mineral phases can provide important constraints on the composition of the magma at the time of melt entrapment (Anderson and Wright, 1972; Anderson, 1974, 1976; Watson, 1976; Donaldson and Brown, 1977; Dungan and Rhodes, 1978). The picritic basalts DR8 and 10-03C contain melt inclusions in both olivine and Cr-spinel. The study of these inclusions enables constraints to be placed on the composition of the magma from which they crystallised and will be used as independent evidence in postulating a parental magma composition.

6.2 Melt Inclusions in Olivine

Abundant, clear, rounded glass inclusions occur in the larger olivine phenocrysts present in DR8 (Plate 3-1C), a number of which have been analysed. Inclusion analyses and host olivine compositions are presented in Table 3-14. One or two inclusions per olivine grain are generally present and have subspherical morphologies. This tendency towards sphericity has been attributed by Watson (1976) to equilibration between the melt and host phase after incorporation. Calculated Fe-Mg K_D's for inclusion - host olivine pairs indicate an apparent marked lack of equilibrium between the inclusions and host olivines. Values of K_D (Table 3-15) vary from 0.22 to 0.29 ($Fe_2O_3/FeO = 0.15$), indicating that

T A B L E 3-14

FAMOUS AREA: MELT INCLUSION - HOST OLIVINE ANALYSES. PICRITE DR8

	1	2	3	4	5	6	7	8	9	10
SIO2	50.33	40.68	50.45	50.23	50.55	40.66	50.76	40.63	50.56	50.48
TIO2	.69	.02	.78	.76	.75	ND	.75	.03	.54	.56
AL203	16.11	.06	16.07	15.89	15.98	.05	16.03	.04	15.84	15.86
CR203	.10	.14	.09	.09	.11	.07	.08	.08	.05	.08
FE203	1.12	-	1.05	1.07	1.05	-	1.06	-	1.00	1.01
FEO	6.63	9.70	6.16	6.31	6.14	9.48	6.24	9.37	5.88	5.93
MNO	.14	-	.11	.13	.11	-	.12	-	.14	.12
MGO	8.70	49.41	8.79	8.67	8.74	48.91	8.32	48.73	8.92	8.49
CAO	14.34	.33	13.79	13.67	13.65	.35	13.71	.32	14.55	14.75
NA2O	1.68	-	1.87	1.82	1.86	-	1.91	-	1.48	1.38
K2O	.06	-	.07	.06	.05	-	.06	-	.06	.06
NIO	-	-	-	.02	.02	.24	-	-	.02	.02
TOTAL	99.90	100.34	99.23	98.72	99.01	99.77	99.04	99.20	99.04	98.74

* * ATOMIC PROPORTIONS BASED ON SELECTED NO. OF OXYGENS * *

OXYGEN	20	4	20	20	20	4	20	4	20	20
SI	6.019	.994	6.051	6.060	6.071	.998	6.094	1.002	6.072	6.082
AL	2.271	.002	2.272	2.259	2.262	.001	2.269	.001	2.242	2.252
TI	.062	.000	.070	.069	.068	-	.068	.001	.049	.051
CR	.009	.003	.009	.009	.010	.001	.008	.002	.005	.008
FE3+	.101	-	.095	.097	.095	-	.096	-	.090	.092
FE2+	.663	.198	.618	.637	.617	.195	.627	.193	.591	.598
MN	.014	-	.011	.013	.011	-	.012	-	.014	.012
MG	1.551	1.799	1.571	1.559	1.564	1.790	1.489	1.790	1.597	1.525
CA	1.838	.009	1.772	1.767	1.757	.009	1.764	.008	1.872	1.904
NA	.390	-	.435	.426	.433	-	.445	-	.345	.322
K	.009	-	.011	.009	.008	-	.009	-	.009	.009
NI	-	-	-	.002	.002	.005	-	-	.002	.002
SUM	12.927	3.004	12.914	12.906	12.898	3.000	12.879	2.997	12.887	12.857
		FO 90.08 FA 9.92				FO 90.19 FA 9.81		FO 90.26 FA 9.74		

* * * S A M P L E D I R E C T O R Y * * *

ANALYSIS NO.	DESCRIPTION
1	MELT INCL. 1 (EDGE) IN OLIVINE 4
2	OLIVINE 4
3	MELT INCL. 2 (CENTER) IN OLIVINE 7
4	MELT INCL. 2 (EDGE) IN OLIVINE 7
5	MELT INCL. 3 (CENTER) IN OLIVINE 7
6	OLIVINE 7
7	MELT INCL. 4 IN OLIVINE 8
8	OLIVINE 8
9	MELT INCL. 5 (CENTER) IN OLIVINE 10
10	MELT INCL. 5 (EDGE) IN OLIVINE 10

** ND = NOT DETECTED **

T A B L E 3-14 (CONTINUED)

FAMOUS AREA: MELT INCLUSION - HOST OLIVINE ANALYSES. PICRITE DR8

	11	12	13	14	15	16	17	18	19	20
SIO2	40.65	51.23	40.54	50.36	50.52	40.28	50.38	40.51	51.22	40.70
TIO2	.02	.73	.02	.58	.60	.02	.70	ND	.70	ND
AL203	.07	16.73	.04	16.17	16.26	.07	16.03	.06	17.03	.05
CR203	.11	.12	.08	.10	.10	.09	.08	.09	.11	.08
FE203	-	.98	-	1.14	1.13	-	1.05	-	.96	-
FEO	9.27	5.74	9.11	6.68	6.66	10.54	6.15	10.10	5.65	9.50
MNO	-	.12	-	.16	.13	-	.13	-	.11	-
MGO	48.87	7.00	49.27	7.57	7.19	47.96	8.64	48.61	6.84	49.37
CAO	.36	14.87	.33	14.79	14.88	.36	13.98	.34	14.25	.32
NA20	-	1.80	-	1.49	1.51	-	1.62	-	1.85	-
K20	-	.19	-	.11	.13	-	.10	-	.05	-
NIO	.27	.02	.28	.02	-	.26	-	-	-	-
TOTAL	99.62	99.52	99.67	99.17	99.11	99.58	98.86	99.72	98.77	100.03

* * ATOMIC PROPORTIONS BASED ON SELECTED NO. OF OXYGENS * *

OXYGEN	4	20	4	20	20	4	20	4	20	4
SI	.999	6.116	.995	6.069	6.088	.996	6.063	.997	6.137	.996
AL	.002	2.354	.001	2.297	2.310	.002	2.274	.002	2.405	.001
TI	.000	.066	.000	.053	.054	.000	.063	-	.063	-
CR	.002	.011	.002	.010	.010	.002	.008	.002	.010	.002
FE3+	-	.088	-	.103	.102	-	.095	-	.087	-
FE2+	.191	.573	.187	.673	.671	.218	.619	.208	.566	.194
MN	-	.012	-	.016	.013	-	.013	-	.011	-
MG	1.790	1.245	1.803	1.360	1.291	1.768	1.550	1.783	1.221	1.800
CA	.009	1.902	.009	1.910	1.921	.010	1.803	.009	1.829	.008
NA	-	.417	-	.348	.353	-	.378	-	.430	-
K	-	.029	-	.017	.020	-	.015	-	.008	-
NI	.005	.001	.006	.002	-	.005	-	-	-	-
SUM	2.999	12.815	3.003	12.857	12.833	3.001	12.882	3.001	12.768	3.002
	FO 90.38		FO 90.60			FO 89.02		FO 89.56		FO 90.25
	FA 9.62		FA 9.40			FA 10.98		FA 10.44		FA 9.75

* * * S A M P L E D I R E C T O R Y * * *

ANALYSIS NO.	DESCRIPTION
11	OLIVINE 10
12	MELT INCL. 6 IN OLIVINE 11
13	OLIVINE 11
14	MELT INCL. 7 (CENTER) IN OLIVINE 12
15	MELT INCL. 7 (EDGE) IN OLIVINE 12
16	OLIVINE 12
17	MELT INCL. 8 (EDGE) IN OLIVINE 13
18	OLIVINE 13
19	MELT INCL. 9 IN OLIVINE 14
20	OLIVINE 14

** ND = NOT DETECTED **

T A B L E 3-14 (CONTINUED)

FAMOUS AREA: MELT INCLUSION - HOST OLIVINE ANALYSES. PICRITE DR8

	21	22	23	24	25	26
SIO2	49.28	40.50	51.35	40.52	49.74	40.62
TIO2	.59	-	.43	-	.27	-
AL203	16.69	-	17.35	-	17.58	-
CR203	.07	-	.06	-	.07	-
FE203	1.21	-	1.05	-	1.03	-
FEO	7.14	9.42	6.18	9.23	6.04	9.07
MNO	-	.14	-	.15	-	.14
MGO	8.97	49.69	7.86	49.23	8.07	49.00
CAO	14.21	-	14.75	-	15.48	-
NA2O	1.99	-	1.97	-	2.02	-
K2O	.08	-	.07	-	.05	-
NIO	-	.33	-	.25	-	.29
TOTAL	100.23	100.08	101.07	99.38	100.35	99.12

* * ATOMIC PROPORTIONS BASED ON SELECTED NO. OF OXYGENS * *

OXYGEN	20	4	20	4	20	4
SI	5.904	.992	6.044	.998	5.926	1.002
AL	2.357	-	2.407	-	2.469	-
TI	.053	-	.038	-	.024	-
CR	.007	-	.006	-	.007	-
FE3+	.109	-	.093	-	.092	-
FE2+	.715	.193	.608	.190	.602	.187
MN	-	.003	-	.003	-	.003
MG	1.601	1.814	1.379	1.806	1.433	1.801
CA	1.824	-	1.860	-	1.976	-
NA	.462	-	.450	-	.467	-
K	.012	-	.011	-	.008	-
NI	-	.007	-	.005	-	.006
SUM	13.044	3.008	12.895	3.002	13.003	2.998
		FO 90.38 FA 9.62		FO 90.48 FA 9.52		FO 90.59 FA 9.41

* * * S A M P L E D I R E C T O R Y * * *

ANALYSIS NO.	DESCRIPTION
21	MELT INCL. 10 IN OLIVINE 21
22	OLIVINE 21
23	MELT INCL. 11 IN OLIVINE 27
24	OLIVINE 27
25	MELT INCL. 12 IN OLIVINE 28
26	OLIVINE 28

Table 3-15: Calculated Fe-Mg K_D's for melt inclusion-host olivine pairs in picrite DR8. (See Table 10 for analyses).

	K_D ($\frac{Fe_2O_3}{FeO} = 0.15$)	K_D ($\frac{Fe_2O_3}{FeO} = 0.25$)
Melt 1 (Edge) - Olivine 4	0.25	0.27
Melt 2 (Center) - Olivine 7	0.27	0.29
Melt 2 (Edge) - Olivine 7	0.26	0.28
Melt 3 (Center) - Olivine 7	0.27	0.29
Melt 4 (Center) - Olivine 8	0.25	0.27
Melt 5 (Center) - Olivine 10	0.28	0.31
Melt 5 (Edge) - Olivine 10	0.27	0.29
Melt 6 (Edge) - Olivine 11	0.22	0.24
Melt 7 (Center) - Olivine 12	0.25	0.26
Melt 7 (Edge) - Olivine 12	0.23	0.25
Melt 8 (Edge) - Olivine 13	0.29	0.31
Melt 9 - Olivine 14	0.23	0.25
Melt 10 - Olivine 21	0.23	0.25
Melt 11 - Olivine 27	0.23	0.25
Melt 12 - Olivine 28	0.24	0.26
	Av. 0.25 ± 0.02	0.27 ± 0.02

many of the inclusions have evolved in composition since the time of entrapment. A detailed study of the contact between the host olivines and melt inclusions (Fig. 3-19) shows an enrichment in Fe and depletion in Mg in olivine, and depletion in both Mg and Fe in the inclusion adjacent to the contact. The inclusions have apparently continued to crystallise out olivine after entrapment and no longer represent the initial melt composition. The approximate 8% relative increase in Fe in the olivine adjacent to the contact (Fig. 3-19) is sufficient to raise the average K_D from 0.25 to 0.29. Assuming an Fe_2O_3/FeO ratio slightly higher than 0.15 would also tend to increase the K_D, but to raise the K_D from 0.26 to 0.30 would require an Fe_2O_3/FeO ratio of 0.35, significantly higher than the observed ratios for these FAMOUS lavas.

These melt inclusions have clearly experienced differing degrees of olivine fractionation and their bulk compositions will therefore reflect decreases in FeO, MgO and increases in SiO_2. The remaining elements are all essentially incompatible and so will reflect absolute enrichment to varying degrees. Ratios between the latter elements should however be unaffected and will indicate the ratios in the parental magma. Of significance in this respect are the high CaO/Al_2O_3 (0.878 ± 0.03) and CaO/Na_2O (7.25 ± 3) ratios, a feature that has been suggested as characteristic of primitive ocean floor basalt (Dungan and Rhodes, 1978). There is a significant range in TiO_2 and K_2O contents of the melt inclusions (Table 3-14) which would appear to be too great to be attributed solely to post-entrapment crystallisation (up to $\pm30\%$ crystallisation would be required). Dungan and Rhodes (1978) found a similar phenomenon in melt inclusions in olivines from DSDP Legs 45 and 46 which, in conjunction with decreasing CaO/Al_2O_3 content with increasing TiO_2, led

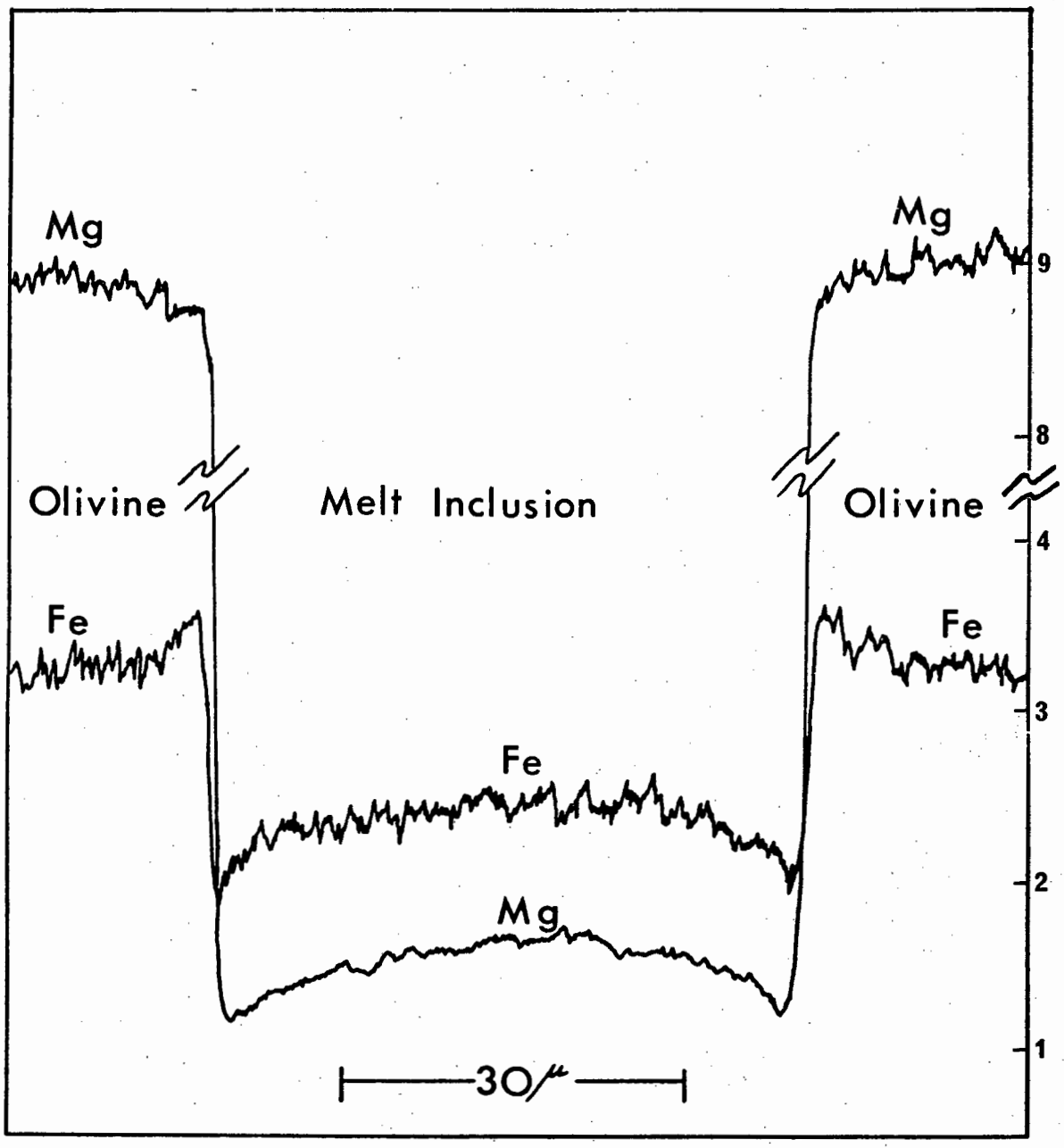

Fig. 3-19: Electron microprobe scan for Fe and Mg across a melt inclusion in an olivine from picrite DR8. Analytical conditions were: 15kV, 1500nA; scale range - $3x10^3$ cts/div. (Fe) and $1x10^4$ cts/div. (Mg); Scanning speed-beam 30 μm/min, chart 50 mm/min. Crystal-RAP (Mg), Qtz (Fe), flow proportional counters.

them to postulate magma mixing and clinopyroxene fractionation (to decrease CaO/Al_2O_3) in a magma chamber. A similar broad decrease in CaO/Al_2O_3 ratio with increasing TiO_2 is found in the melt inclusions in DR8 and might be ascribed to a similar process. However, an alternative mechanism that could result in a decreasing CaO/Al_2O_3 ratio with increasing TiO_2 is a combination of olivine fractionation within a magma chamber and injection of successive impulses of new magma formed by increasing degrees of partial melting of a source with residual clinopyroxene.

6.3 Melt Inclusions in Cr-spinel

Some of the larger Cr-spinel phenocrysts in the picritic basalts contain dark, rounded glass inclusions (Plate 3-1D). These generally occur three or four per grain and they are mostly too small for accurate analysis. Four of the larger inclusions have however been analysed and their compositions, together with host Cr-spinels, are presented in Table 3-16 (No's 13-19). A comparison of the overall chemistry of these inclusions with those from olivines (Table 3-14) indicates their more primitive nature. This is reflected in higher absolute MgO contents and lower TiO_2 and K_2O.

Donaldson and Brown (1977) have analysed melt inclusions in Cr-spinel from basalts from Leg 37, and postulate an average composition as representing primitive oceanic basalt magma. The characteristics of their magma composition are: high MgO (~12%), high CaO (~13.5%) and low Al_2O_3 (14.4%), coupled with low incompatibles: TiO_2 (0.6%) and Na_2O (1.4%). Inspection of Table 3-16 shows that the inclusions analysed show a range in composition, e.g. MgO 12.04% to 9.5%, but are similarly characterised by high CaO, Low TiO_2 and Na_2O. Al_2O_3 is somewhat higher

T A B L E 3-16

FAMOUS AREA: COMPOSITIONS OF COEXISTING CR-SPINEL - LIQUID PAIRS.

	1	2	3	4	5	6	7	8	9	10
SIO2	.11	50.23	ND	50.16	-	50.21	.11	.11	50.90	.24
TIO2	-	.86	-	.86	-	1.00	.47	.44	1.07	.58
AL203	24.06	15.30	25.37	15.42	25.31	15.55	27.52	27.00	15.50	27.55
CR203	41.21	-	41.11	-	41.83	-	38.16	37.09	.08	38.01
FE203	6.96	1.10	6.51	1.09	5.83	1.15	4.20	6.93	1.32	4.03
FEO	11.38	7.33	11.15	7.26	12.44	7.66	13.38	13.26	7.76	15.14
MNO	-	.15	-	.15	-	.16	-	-	.14	-
MGO	15.87	10.45	16.23	10.33	15.51	9.69	15.13	15.37	8.29	14.18
CAO	-	11.83	-	11.81	-	12.50	.06	.06	12.44	.31
NA20	-	2.09	-	1.93	-	2.19	-	-	2.27	-
K20	-	.18	-	.17	-	.16	-	-	.11	-
NIO	.18	-	.20	-	.16	-	-	-	-	-
TOTAL	99.77	99.52	100.58	99.18	101.08	100.27	99.03	100.26	99.88	100.04

* * ATOMIC PROPORTIONS BASED ON SELECTED NO. OF OXYGENS * *

OXYGEN	4	20	4	20	4	20	4	4	20	4
SI	.003	6.027	-	6.031	-	6.002	.003	.003	6.097	.007
AL	.854	2.164	.888	2.185	.887	2.191	.973	.947	2.188	.971
TI	-	.078	-	.078	-	.090	.011	.010	.096	.013
CR	.981	-	.966	-	.983	-	.905	.872	.008	.898
FE3+	.158	.099	.146	.099	.130	.103	.095	.155	.119	.091
FE2+	.287	.736	.277	.730	.309	.766	.336	.330	.777	.378
MN	-	.015	-	.015	-	.016	-	-	.014	-
MG	.712	1.869	.719	1.851	.687	1.726	.676	.681	1.480	.632
CA	-	1.521	-	1.522	-	1.601	.002	.002	1.597	.010
NA	-	.486	-	.450	-	.508	-	-	.527	-
K	-	.028	-	.026	-	.024	-	-	.017	-
NI	.004	-	.005	-	.004	-	-	-	-	-
SUM	3.000	13.021	3.000	12.987	3.000	13.027	3.000	3.000	12.921	3.000
	CR .53 MG .71 FE .08		CR .52 MG .72 FE .07		CR .53 MG .69 FE .07		CR .48 MG .67 FE .05	CR .48 MG .67 FE .08		CR .48 MG .63 FE .05

* * * S A M P L E D I R E C T O R Y * * *

ANALYSIS NO.	DESCRIPTION
1	CR-SPINEL DR4-303
2	DR4-303 - WHOLE ROCK
3	CR-SPINEL DR 1-122
4	DR1-122 - WHOLE ROCK
5	CR-SPINEL DR9-322
6	DR9-322 - WHOLE ROCK
7	CR-SPINEL 11-18
8	CR-SPINEL 11-18
9	AVERAGE QUENCH GLASS 11-18
10	CR-SPINEL DR 4

** ND = NOT DETECTED **

T A B L E 3-16 (CONTINUED)

FAMOUS AREA: COMPOSITIONS OF COEXISTING CR-SPINEL - LIQUID PAIRS.

	11	12	13	14	15	16	17	18	19
SIO2	.14	51.21	50.31	.12	50.05	50.57	-	49.38	.16
TIO2	.51	1.17	.50	.23	.55	.54	.28	.64	.31
AL2O3	26.50	14.96	15.22	28.33	15.06	15.39	26.56	15.71	29.56
CR2O3	36.86	.09	.61	38.98	.56	.86	41.91	.38	39.37
FE2O3	6.02	1.43	1.15	3.00	1.17	1.16	4.79	1.16	2.36
FEO	15.22	8.41	6.74	11.61	6.87	6.84	10.12	6.80	11.00
MNO	-	.15	.13	-	.14	.16	-	-	-
MGO	13.89	7.58	9.51	16.14	10.66	10.41	17.43	12.04	17.06
CAO	.06	11.69	13.25	.04	12.98	12.83	-	12.68	.06
NA2O	-	2.66	1.49	-	1.51	1.44	-	1.44	-
K2O	-	.19	.08	-	ND	.03	-	.08	-
TOTAL	99.20	99.54	98.99	98.45	99.56	100.23	101.09	100.31	99.88

* * ATOMIC PROPORTIONS BASED ON SELECTED NO. OF OXYGENS * *

OXYGEN	4	20	20	4	20	20	4	20	4
SI	.004	6.169	6.065	.004	6.006	6.019	-	5.881	.005
AL	.947	2.124	2.163	.996	2.130	2.159	.915	2.205	1.017
TI	.012	.106	.045	.005	.050	.048	.006	.057	.007
CR	.884	.009	.058	.919	.053	.081	.968	.036	.908
FE3+	.137	.130	.104	.067	.106	.104	.105	.104	.052
FE2+	.386	.847	.679	.290	.689	.681	.247	.677	.268
MN	-	.015	.013	-	.014	.016	-	-	-
MG	.628	1.361	1.708	.718	1.906	1.847	.759	2.137	.742
CA	.002	1.509	1.711	.001	1.669	1.636	-	1.618	.002
NA	-	.621	.348	-	.351	.332	-	.333	-
K	-	.029	.012	-	-	.005	-	.012	-
SUM	3.000	12.920	12.908	3.000	12.976	12.929	3.000	13.061	3.000
	CR .48 MG .62 FE .07			CR .48 MG .71 FE .03			CR .51 MG .75 FE .05		CR .47 MG .73 FE .03

* * * S A M P L E D I R E C T O R Y * * *

ANALYSIS NO.	DESCRIPTION
11	CR-SPINEL DR 4
12	AVERAGE QUENCH GLASS DR 4
13	MELT INCLUSION 1 IN CR-SPINEL 26 (DR8)
14	CR-SPINEL 26 (DR8)
15	MELT INCLUSION 2 IN CR-SPINEL 8 (DR8)
16	MELT INCLUSION 3 IN CR-SPINEL 8
17	CR-SPINEL 8 (DR8)
18	MELT INCLUSION 4 IN CR-SPINEL 40
19	CR-SPINEL 40 (DR8)

** ND = NOT DETECTED **

than that found by Donaldson and Brown (1977).

In an attempt to monitor the effect of post-entrapment crystallisation on the FeO/MgO ratio of the melt, the distribution of FeO and MgO between Cr-spinel and liquid has been investigated. The exchange reaction of interest can be expressed as follows:

$$Mg(Cr_\alpha Al_\beta Fe^{3+}_\gamma)_2O_4^{sp} + Fe(Cr_\alpha Al_\beta Fe^{3+}_\gamma)_2O_4^{liq} = Mg(Cr_\alpha Al_\beta Fe^{3+}_\gamma)_2O_4^{liq} + Fe(Cr_\alpha Al_\beta Fe^{3+}_\gamma)_2O_4^{sp} \quad \ldots\ldots (1)$$

where $\alpha + \beta + \gamma = 1$, and $\alpha = X^{Cr}$, $\beta = X^{Al}$ and $\gamma = X^{Fe^{3+}}$

In a manner analogous to that of Jackson (1969), it can be shown that:

$$K_D = (FeO/MgO)^{sp}/(FeO/MgO)^{liq} \quad \ldots\ldots\ldots\ldots\ldots\ldots\ldots (2)$$

This expression assumes ideality in equation (1) which, though not strictly true, may suffice as a first approximation (Jackson, 1969). It is likely that K_D will to a certain extent be temperature-dependent, while the pressure effect is likely to be small, a conclusion supported by partial molar volume data from Robie and Waldbaum (1968).

The magnitude of K_D (equation 2) has been investigated empirically using (1) Cr-spinel microphenocryst-whole rock pairs from three relatively aphyric olivine basalts, (2) quench glass-Fe-rich Cr-spinel pairs from DR4 and 11-18 (olivine basalt), and (3) glass inclusion-host spinel pairs in picrite DR8. The aphyric olivine basalts DR4-303, DR1-122 and DR9-322 have been shown to represent liquid compositions and the most Mg-rich Cr-spinels have been assumed to represent the liquidus Cr-spinel composition. These should reflect equilibrium partitioning of FeO and MgO with the liquid (whole rock). Calculated K_D values for the three occurrences are given in Table 3-17; they give an average value very close to

Table 3-17: Calculated Cr-spinel-liquid Fe-Mg K_D's for aphyric lavas and trapped melt inclusions in Cr-spinel from picrite DR8.

	K_D^{Fe-Mg}
Olivine basalts	
1) Whole rock - Av. spinel phenocryst (Fe_2O_3/FeO whole rock = 0.15)	
DR4-303	1.02
DR1-122	0.98
DR9-322	1.01
Average	1.00
2) Quench glass - Fe-rich spinel (Fe_2O_3/FeO glass = 0.17)	
DR4	0.96
DR4	0.99
11-18	0.94
11-18	0.92
Average	0.95
Picrite basalt	
Glass inclusion-host spinel	
DR8	1.01
DR8	1.14
DR8 (average of 2 incl. in 1 spinel)	0.90
Average	1.01

unity. It has not been possible to obtain any directly comparable data from the literature but, using an indirect method, i.e.

$$K_D^{sp\text{-}liq} = K_D^{sp\text{-}ol} \times K_D^{ol\text{-}liq}$$

it is possible to utilize the coexisting spinel-olivine data given by Sigurdsson and Schilling (1976). Assuming an olivine-liquid $K_D = 0.31$, an average spinel-liquid K_D of 0.96 is obtained, in excellent agreement with the measured values obtained in the present study.

Assuming that, at least over the temperature range of interest, the $K_D^{Fe\text{-}Mg}$ for spinel-liquid is close to unity, the FeO/MgO ratio of the trapped glass inclusion should then reflect that of the magma at the time of melt entrapment. Donaldson and Brown (1977) found no evidence for reaction between melt inclusion and spinel and noted that there was no zoning across the interface between spinel and glass. However, three of the four inclusions analysed in this study do show evidence of a narrow reaction rim surrounding the inclusions, and the opaque nature of the rim suggests it is probably an Fe-Ti oxide. Crystallisation of a Ti-bearing phase from the inclusion would account for the slightly lower TiO_2 contents of the three inclusions (No's. 13, 15 and 16, Table 3-16) which are surrounded by such rims. Since melt inclusion 4 (No. 18, Table 3-16) has the highest MgO and shows no evidence for post-entrapment crystallisation, this composition has been assumed as that most likely representative of the parental melt. This composition is given below and compares favourably with that calculated from the olivine phenocryst compositions (Section 5.2.1).

With the exception of the high MgO parent suggested by Elthon (1979), this predicted parental melt (P_1) shows marked compositional similarity to other postulated parental magmas for ocean floor basalt,

PREDICTED PARENTAL MELTS

	Cr-spinel Inclusion	From olivine data	Average (P_1)
SiO_2	49.38	48.17	48.78
TiO_2	0.64	0.62	0.63
Al_2O_3	15.71	15.83	15.77
FeO*	7.84	8.08	7.96
MnO	-	0.15	0.15
MgO	12.04	12.59	12.32
CaO	12.68	12.54	12.61
Na_2O	1.44	1.65	1.55
K_2O	0.08	0.09	0.09
Ni (ppm)	-	396	396
Mg-number	75.7	75.2	75.8
CaO/Al_2O_3	0.807	0.792	0.800
CaO/Na_2O	8.81	7.63	8.14

though with slightly higher MgO (cf. Table 3-11). Characteristic features of these magmas are: high CaO/Al_2O_3 and CaO/Na_2O ratios (Dungan and Rhodes, 1978), high absolute CaO (~12-13%) and MgO (10-12.3%) and low TiO_2 (0.63-0.82%). The chemical composition of this postulated primary magma is discussed further in Section 7. The overall mineralogical evidence suggests, therefore, that the picritic basalts in the FAMOUS area are derived from a relatively MgO-rich parental magma by olivine ($\pm$ Cr-spinel) accumulation and do not represent liquid compositions.

7. PETROGENESIS

7.1 General Statement

Knowledge of the field relationships of the large number of samples collected from the relatively small area of the Mid-Atlantic Ridge comprising the FAMOUS area has provided a unique opportunity for the detailed investigation of local heterogeneities in ocean floor basalts. Possible causes of such heterogeneities are: low pressure fractional crystallisation, different degrees of partial melting, source area heterogeneities, magma mixing or some or other combination of these processes. The initial study of samples dredged from the FAMOUS area was carried out by Bougault and Hekinian (1974). From their study of the transition elements, these authors recognised the possibility of the occurrence of at least two distinct magma types in the FAMOUS region; one giving rise to the olivine basalts and the other to the plagioclase basalts. They further suggested that the plagioclase-pyroxene basalts could be the product of fractional crystallisation of either the olivine basalts or of megacryst-free plagioclase basalts.

Subsequently, a study of the compositional variations of basaltic glasses from the FAMOUS area, led Hekinian et al. (1976), Bryan and Moore (1977) to postulate the presence of a single, shallow, magma chamber ($\pm$ 6 km wide) underlying the median valley and elongate parallel to it. They proposed that the chamber was compositionally zoned with the hotter axial zone giving rise to the primitive lavas (olivine basalts, picrites) comprising the central volcanic hills and with the flank lavas (plagioclase-phyric basalts, plagioclase-pyroxene basalts) deriving from the cooler, differentiated melt towards the margins of the chamber. Fractional crystallisation of olivine, plagioclase and clino-

pyroxene within this chamber then gave rise to the observed range of lava compositions. This single magma chamber hypothesis, however, fails to account for observed differences in incompatible element concentrations (K_2O, TiO_2 Ba, Rb, LREE, H_2O) between the centrally situated olivine basalts and the flank lavas (Bryan and Moore, 1977; White and Bryan, 1977; Bryan, 1979; Bryan et al., 1979). To compensate for these differences, the authors appealed to processes such as volatile transfer of alkali metals and other LIL elements from the 'hot' central zone of the magma chamber to the 'cooler' walls. The above-mentioned discrepancies led White and Bryan (1977), Bryan (1979) and Bryan et al. (1979) to suggest that the zonation in the central magma chamber might alternatively arise from injections of primary magma batches derived by successively greater degrees of partial melting of the same source, into the centre of the chamber. The zonation in the chamber could be established if each magma batch was incompletely mixed with the preceding batch.

A study of the REE distributions in the most primitive FAMOUS lavas led Langmuir et al. (1977) to reject the single magma chamber hypothesis as fractional crystallisation processes fail to account for crossing REE patterns observed for several pairs of FAMOUS lavas. In this respect they note that the seismic study of Fowler (1976) shows no evidence for a single magma chamber beneath the FAMOUS area. To account for the observed REE patterns, Langmuir et al. (1977) postulated a mechanism of dynamic melting, acting on a homogeneous mantle source, leaving varied amounts of clinopyroxene and lesser garnet in the residue. Postulated degrees of partial melting range from 8-25%, with 5% melt always being left in the residue. To explain the REE patterns

in some samples, the above authors suggest that in addition to dynamic melting, fractional crystallisation processes were also probably operative. The apparent decoupling of major and trace elements in the FAMOUS region, as observed by Bryan and Moore (1977) and White and Bryan (1977), may therefore be produced through dynamic melting (Langmuir et al., 1977). Experimental work by Bender et al. (1978) on a primitive FAMOUS glass led these authors to conclude that fractionation of olivine followed by olivine and plagioclase can account for much of the observed major element variations in FAMOUS basalt glasses. They note however that some of the variations in TiO_2 and Na_2O can only be explained by postulating different primary liquids.

Nisbet and Fowler (1978) have reviewed existing geophysical and petrographical evidence from 37°N. From thermal considerations they conclude that it is questionable whether a steady-state magma chamber can exist at slow spreading ridges with half-spreading rates of less than 1 cm/yr. It has been suggested that spreading in the FAMOUS area is asymmetric (0.7 and 1.5 cm/yr), Needham and Francheteau, 1974; 1.0 and 1.2 cm/yr, Greenwalt and Taylor, 1974), and Nisbet and Fowler (1978) calculate a maximum width of a possible magma chamber (assuming an average half-spreading rate of 1.1 cm/yr) of 1.2 km, which would be confined to depths equivalent to the lower part of layer 3. Nisbet and Fowler (1978) propose a model (the 'infinite leek') whereby melting is initiated at depths of $\pm$ 60 km with the melt then rising in equilibrium with the mantle until it segregates at depths of 15-25 km and then rises rapidly to form pools at the base of the crust. Lava is extruded from these pools by utilising cracks that propagate into the crust.

In summary then, there are two schools of thought with respect to

the petrogenesis of the FAMOUS lavas; the one favouring fractional crystallisation within a single low level magma chamber as being the process whereby the range in compositions is generated, the other favouring partial melting processes as being the prime mechanism for accounting for the compositional variations. Certain data obtained from the present study place additional constraints on any possible petrogenetic model for the FAMOUS lavas. As noted previously by Bougault and Hekinian (1974) and confirmed for additional samples in this study, the distribution of the ferromagnesian elements, and specifically Ni, Cr and Cu (Figs. 3-11, 3-12 and 3-10D), clearly indicates the presence of at least two distinct magma types; the one giving rise to the olivine basalts and the other to the plagioclase-pyroxene basalts (Figs. 3-11 and 3-12). This division into two magma types is supported by the NiO content of the olivine (Fig. 3-16) and Cr-spinel phenocrysts (Fig. 3-18) of the lavas. This observed distribution suggests that the picrites and plagioclase-phyric basalts may be genetically related to the plagioclase-pyroxene basalts, rather than to the olivine basalts. Variations in Zr and Nb (Fig. 3-13) similarly suggest the presence of at least two distinct magma types, one having an average Zr/Nb ratio of 8.41 ± 0.8, corresponding to that of the olivine basalts, and the other having an average ratio of 5.96 ± 0.2, corresponding to the plagioclase-pyroxene basalts and the plagioclase-phyric basalts. Since olivine of similar fosterite content but with significantly different NiO content will not crystallise from a single magma chamber with relatively constant fO_2, and since incompatible element ratios will not be fractionated by fractional crystallisation processes (e.g. Gast, 1968), it seems improbable that one parental magma could give rise to all the FAMOUS lavas. The

above observations therefore are inconsistent with the single magma chamber hypothesis and provide strong evidence for the presence of at least two distinct parental magmas in the FAMOUS region. The possibility of attributing the compositional variations within the postulated lava suites to low pressure fractional crystallisation will be quantitatively discussed below. The older plagioclase-pyroxene and highly plagioclase-phyric basalts (Arcyana, 1977) will be discussed first, followed by the younger olivine basalts and finally the possible relationship of the picrites to one or other of these two suites will be considered.

7.2 Plagioclase-pyroxene Basalts

The possibility that the aphyric plagioclase-pyroxene basalts comprise a consanguinous suite related by low pressure fractional crystallisation has been quantitatively investigated using the least squares approximation technique of Bryan et al. (1969) and utilising the compositions of observed microphenocryst phases. A least squares approximation relating one of the most primitive plagioclase-pyroxene basalts (31-38) to one of the most evolved (DR10-310) is presented, together with input data, in Table 3-18. With the exception of K_2O, the major element composition of DR10-310 can be explained by the removal of 1.3% olivine (Fo_{86}), 4.1% plagioclase (An_{84}) and 3.5% clinopyroxene ($Wo_{39}En_{52}Fs_9$) from 31-38. The plagioclase-pyroxene basalts show evidence for a certain degree of alteration, to which the slight discrepancy in K_2O can probably be attributed.

The adequacy of this model, based on the major elements, is attested to by the close agreement between the observed trace element content of DR10-310 and the predicted trace element content calculated

Table 3-18: Least squares approximation relating plagioclase-pyroxene basalts 31-38 and DR10-310.

Input data

	31-38	OLIVINE	PLAG	PYX	DR10-310
SiO_2	50.49	39.74	47.00	51.56	50.89
TiO_2	1.00	0.04	0.04	0.61	1.01
Al_2O_3	14.87	0.07	33.31	2.87	14.73
FeO*	9.04	13.42	0.40	5.75	9.47
MgO	8.63	45.99	0.27	18.99	8.07
CaO	12.89	0.40	17.18	20.07	12.57
Na_2O	2.48	0.01	1.78	0.14	2.55
K_2O	0.18	0.01	0.02	0.01	0.30
		Fo 85.93	An 84.08	Wo 39.37	
		Fa 14.07	Ab 15.81	En 51.82	
			Or 0.12	Fs 8.80	

Least squares approximation

	31-38			MIX		
	OBS.	CALC.	DIFF.	COMP.	Wt.%	S.D.
SiO_2	50.49	50.52	0.03	DR10-310	90.88	0.85
TiO_2	1.00	0.94	-0.06	OLIVINE	1.31	0.26
Al_2O_3	14.87	14.86	-0.01	PLAG	4.11	0.46
FeO*	9.04	9.00	-0.04	CPX	3.52	0.56
MgO	8.63	8.62	-0.01			
CaO	12.89	12.84	-0.05	TOTAL	99.83	1.14
Na_2O	2.48	2.40	-0.08			
K_2O	0.18	0.27	0.09			

Sum of squares of residuals = 0.023

using the above model (Table 3-19). The predicted trace element content of DR10-310 was calculated assuming Rayleigh fractionation (Equation (1), Chapter II). Distribution coefficients were taken from the compilation in the appendix and are given in Table 3-19. The value for D_{ol}^{Ni} was calculated from the expression of Hart and Davis (1978), $D_{ol}^{Ni} = \frac{124}{MgO} - 0.9$, using the average MgO content of DR10-310 and 31-38. D_{ol}^{Co} was calculated assuming an olivine crystallisation temperature of 1220°C (Table 3-10) and using the expression of Lindstrom and Schreidegger (1977):

$$\ln D_{ol}^{Co} = \frac{9676}{T(K)} - 5.23$$

Though samples 31-38 and DR10-310 span the compositional range of plagioclase-pyroxene basalts with respect to M.I. and can apparently be related by a simple process of fractional crystallisation, it appears that not all samples can be explained by this simple scheme. For example, DR2-301, though more primitive than DR10-310 in terms of higher MgO, Al_2O_3, CaO, Ni and Cr, has significantly higher concentrations of incompatible elements (Table 3-7) than DR10-310. It is therefore not possible to obtain a satisfactory major and trace element fit relating DR2-301 to either 31-38 or DR10-310 using observed microphenocryst phases. It is necessary to propose a more complex relationship which would allow for the decoupling of major and trace elements. The similar incompatible element ratios (e.g. Zr/Nb) of the plagioclase-pyroxene basalts suggest derivation from a homogeneous source area. Apparent decoupling of major and trace elements can be achieved to a certain extent by small variations in the degree of partial melting (e.g. Langmuir et al., 1977) or by fractional crystallisation within a magma chamber which is periodi-

Table 3-19: Predicted and observed trace element composition of DR10-310 using results of the least squares approximation given in Table 3-18: The source of distribution coefficients are Tables A2-1, A2-2, A2-5. The calculated Ni value given in brackets was derived using distribution coefficient given in brackets.

DISTRIBUTION COEFFICIENTS

	OLIVINE	PLAG	CPX
Zr	0.01	0.01	0.20
Nb	0.01	0.01	0.04
Y	0.13	0.18	0.70
Rb	.001	.001	.001
Ba	.001	.001	.001
Sr	.01	1.8	0.12
Sc	.01	.01	2.5
Ga	.01	.90	.30
Ni	13.95 (11.00)	.01	1.5
Co	3.5	.01	1.0

TRACE ELEMENT MATCH

	31 - 38	DR10-310	
	OBS.	CALC.	OBS.
Zr	53	58	56
Nb	8.8	9.7	9.4
Y	21.9	23.2	22.4
Rb	4.4	4.8	4.6
Ba	50	55	52
Sr	108	109	114
Sc	39	39	40
Ga	14.3	15.0	15.5
Ni	74	63 (66)	75
Co	52	52	53

cally refilled by new batches of magma from depth, which then mix with existing magma (e.g. O'Hara, 1977; Usselman and Hodge, 1978; Donaldson and Brown, 1977; Dungan and Rhodes, 1978). The small scale variations within the plagioclase-pyroxene basalts may be attributed to one, or a combination of such processes.

On the basis of similar Zr/Nb ratios and similar NiO content in olivine, it was postulated above that the plagioclase-phyric basalts might be genetically related to the plagioclase-pyroxene basalts rather than to the olivine basalts. Table 3-20 presents a least squares approximation relating HPPB DR3-1 to plagioclase-pyroxene basalt 31-38 by accumulation of 37.65% plagioclase (An_{88}), 1.25% olivine (Fo_{86}) and 4.84% clinopyroxene ($Wo_{42}En_{51}Fs_{7}$). The excellent major element agreement, realistic phenocryst proportions with respect to the modal mineralogy of DR3-1 and the low standard deviations of the components, attest to the consistency of the model. The model is further supported by the excellent agreement between predicted and observed trace element contents of DR3-1 shown in Table 3-21. An equally good agreement between predicted and observed major and trace element concentrations is obtained if one relates the other highly plagioclase-phyric sample DR3-131 to 31-38 by the accumulation of 23.52% plagioclase, 3.24% olivine and 4.54% clinopyroxene. Predicted trace element concentrations in these accumulation models were calculated using equations (4) and (5) (Chapter II) and assuming equal values for V_1 and V_2. Distribution coefficients are given in Table 3-19. It should be noted that although DR3-1 and DR3-131 have been related to aphyric plagioclase-pyroxene basalt 31-38, it is not suggested that 31-38 is the direct 'parent' liquid. The more evolved nature of the mineral phases in 31-38 relative to DR3-1 and DR3-131

Table 3-20: Least squares approximation relating plagioclase-pyroxene basalt 31-38 to HPPB DR3-1.

Input data

	31-38	OLIVINE	PLAG	CPX	DR3-1
SiO_2	50.49	39.74	46.08	52.49	48.74
TiO_2	1.00	0.04	0.01	0.28	0.61
Al_2O_3	14.87	0.07	34.51	2.96	21.51
FeO*	9.04	13.42	0.37	4.21	5.69
MgO	8.63	45.99	0.24	18.39	6.40
CaO	12.89	0.40	17.47	20.93	14.89
Na_2O	2.48	0.01	1.31	0.20	1.73
K_2O	0.18	0.01	0.01	0.01	0.11
		Fo 85.93	An 88.00	Wo 42.03	
		Fa 14.07	Ab 11.94	En 51.37	
			Or 0.06	Fs 6.60	

Least squares approximation

	DR3-1			MIX		
	OBS.	CALC.	DIFF.	COMP.	Wt.%	S.D.
SiO_2	48.74	48.77	0.03	31.38	56.21	1.13
TiO_2	0.61	0.58	-0.03	OLIVINE	1.25	0.33
Al_2O_3	21.51	21.50	-0.01	PLAG	37.65	0.59
FeO*	5.69	5.59	-0.10	CPX	4.84	0.70
MgO	6.40	6.41	0.01			
CaO	14.89	14.84	-0.05	TOTAL	99.95	1.49
Na_2O	1.73	1.90	0.17			
K_2O	0.11	0.11	-0.00			

Sum of squares of residuals = 0.043

Table 3-21: Predicted and observed trace element content of DR3-1 using results of the least squares approximation given in Table 3-20.

DISTRIBUTION COEFFICIENTS

as in Table 3-19.

TRACE ELEMENT MATCH

	31-38	DR3-1	
	OBS.	Calc.	OBS.
Zr	53	31	35
Nb	8.8	5.0	5.7
Y	21.9	14.9	14.0
Rb	4.4	2.5	1.9
Ba	50	28.1	23.8
Sr	108	125	122
Sc	39	27.8	30.6
Ga	14.3	13.4	13.0
Ni*	74	71	83.4
Co	52	35	34.1
Cr*	87	234	242

* Ni was calculated using the observed average NiO content of 0.16% and 0.035% in DR3-1 olivine and clinopyroxene respectively. Cr calculated using the observed average Cr_2O_3 content (0.56%) in DR3-1 pyroxenes.

indicates that 31-38 is itself probably a derivative liquid relative to some common 'parent'. Since we are, however, discussing a linear accumulation model, the absence of an intermediate parent is unimportant for most elements. Exceptions are Ni, Cr, Sr and Co which will be affected to a certain extent by this approximation due to their high distribution coefficients.

As discussed earlier, it is unlikely that simple fractional crystallisation and accumulation of phenocrysts were the only processes operative during the evolution of these early lavas in the FAMOUS area. This is borne out by the fact that not all samples comprising this suite can be simply related, with respect to both major and trace elements, to the plagioclase-pyroxene basalts. For example, though DR10-101C appears to be closely related to the other plagioclase-phyric basalts and the plagioclase-pyroxene basalts with respect to diagnostic incompatible element ratios such as Zr/Nb and to the NiO content pf phenocryst olivines, models using observed phenocryst phases fail to account for both major and trace element variations satisfactorily. As in the case of DR2-301, it appears that additional processes such as varying degrees of partial melting and/or magma mixing have left an additional chemical imprint on some of these lavas.

In summary, quantitative modelling of both major and trace elements indicates that the plagioclase-pyroxene basalts and plagioclase-phyric basalts of the FAMOUS area comprise a consanguinous suite of lavas that can be related to a large extent by fractional crystallisation and/or accumulation of plagioclase, olivine and clinopyroxene. Inconsistencies observed for some samples suggest that the magma chamber, from which these early FAMOUS lavas derived, experienced periodic impulses of new

primitive batches of magma (formed by slightly varied degrees of partial melting), which were then mixed with the existing magma in the chamber. No primitive parental magmas related to this suite have been identified. A simplified schematic representation of the proposed petrogenetic relationship of the plagioclase-pyroxene and plagioclase-phyric basalts is presented in Fig. 3-21.

7.3 Olivine Basalts

The number of samples comprising the suite of olivine basalts and the very fresh condition of the rocks affords the opportunity of rigorously applying current approaches for the quantitative modelling of major and trace element variations. The relationship between the various olivine basalts will therefore be evaluated as rigorously as possible.

Trace element variations within the olivine basalts, and specifically within those comprising this study, are qualitatively in accord with those that could be expected to result from fractional crystallisation. The possible contribution of fractional crystallisation to the observed compositional variations has been investigated quantitatively and a summary of selected least squares approximations for possible parent-daughter pairs is given in Table 3-22. For the purposes of the mixing calculations, samples DR4-303 and DR1-122 have been averaged, as have DR4-329 and DR4. Inspection of Table 3-22 reveals some salient features:

(1) The models relating the most primitive of the olivine basalts (DR4-303, DR1-122) to the rest are not really satisfactory, as exemplified by the high sum of the squares of residuals (0.24 to 0.49). The remaining solutions are generally satisfactory, all

PARENT	OLIVINE	PLAGIOCLASE	CLINOPYROXENE	DAUGHTER	F	ΣR^2
DR4-303/DR1-122	-0.0193(Fo_{89})			DR9-322	0.9902	0.49
DR4-303/DR1-122	-0.0326(Fo_{89})	-0.0435(An_{86})		DR9-308	0.9327	0.44
DR4-303/DR1-122	-0.0337(Fo_{87})	-0.0117(An_{86})	-0.0304*	11-18	0.9306	0.24
DR4-303/DR1-122	-0.0505(Fo_{87})	-0.0805(An_{86})	-0.0507*	DR4-329/DR4	0.8250	0.47
DR9-322	-0.0096(Fo_{89})	-0.0334(An_{86})		DR9-308	0.9555	0.08
DR9-322	-0.0098(Fo_{87})		-0.0374*	11-18	0.9458	0.07
DR9-322	-0.0279(Fo_{87})	-0.0769(An_{86})	-0.0575*	DR4-329/DR4	0.8396	0.11
DR9-308	-0.0203(Fo_{87})	-0.0362(An_{86})	-0.0427*	DR4-329/DR4	0.8988	0.06
11-18	-0.0179(Fo_{87})	-0.0735(An_{86})	-0.0213*	DR4-329/DR4	0.8877	0.06
DR4-329/DR4	-0.0144(Fo_{84})	-0.0402(An_{84})	-0.0226†	DR2-174	0.9277	0.07

* $Wo_{42}En_{51}Fs_7$

† $Wo_{40}En_{51}Fs_9$

Table 3-22: Summary of least squares approximations relating various olivine basalts from the FAMOUS region. Mineral proportions and F (residual liquid) given in weight fractions.

giving low sums of the squares of residuals (<0.11).

(2) Clinopyroxene fractionation appears to play an important role in relating the olivine basalt major element compositions. Plagioclase comprises the dominant proportion of the calculated fractionates, with olivine comprising the lowest proportion. Dungan and Rhodes (1978) have noted the apparent chemical imprint of clinopyroxene fractionation on trapped melt inclusions from ocean floor basalts, even in the absence of clinopyroxene phenocrysts. They suggest that this can be accomplished by underplating of gabbro onto the upper walls of a subvolcanic magma chamber as it evolves between mixing events involving the addition of unfractionated magma to the chamber. The feasibility of clinopyroxene fractionation in the FAMOUS lavas is indicated by both the occurrence of abundant clinopyroxene phenocrysts in the slightly more evolved olivine basalts (DR4, DR4-329, 11-18) and the experimental work of Bender et al. (1978) and Dungan et al. (1978), who found clinopyroxene crystallisation follows olivine and plagioclase by 50 to 100°C. This temperature interval decreases with increasing pressure and at 10.5 kbar clinopyroxene replaces olivine as the liquidus phase (Bender et al., 1978).

Though some of the mixing calculations relating the different olivine basalts are apparently successful with respect to major elements (Table 3-22), not all these mixes explain the observed trace element variation adequately. Two mixes relating one of the more primitive olivine basalts, DR9-322, and two of the relatively evolved olivine basalts, DR4-329/DR4 and 11-18, are presented in Tables 3-23 and 3-25. The models satisfy both the major element and trace element variations

Table 3-23: Least squares approximation relating olivine basalt DR9-322 to olivine basalt DR4-329/DR4

Input data

	DR9-322	OLIVINE	PLAG	CPX	DR4-329/DR4
SiO_2	50.02	40.02	45.74	52.49	50.79
TiO_2	1.00	0.03	0.03	0.28	1.15
Al_2O_3	15.49	0.03	34.29	2.96	15.30
FeO*	8.66	12.36	0.37	4.21	9.62
MgO	9.65	46.98	0.24	18.39	8.69
CaO	12.45	0.32	17.72	20.93	11.82
Na_2O	2.18	0.01	1.59	0.20	2.05
K_2O	0.16	0.01	0.02	0.01	0.18
		Fo 87.17	An 85.93	Wo 42.03	
		Fa 12.83	Ab 13.95	En 51.37	
			Or 0.12	Fs 6.60	

Least squares approximation

	DR9-322			MIX		
	OBS.	CALC.	DIFF.	COMP.	Wt.%	S.D.
SiO_2	50.02	50.04	0.02	DR4-329/DR4	83.96	1.67
TiO_2	1.00	0.98	-0.02	OLIVINE	2.68	0.54
Al_2O_3	15.49	15.50	0.01	PLAG	7.22	0.93
FeO*	8.66	8.68	0.02	CPX	5.75	1.06
MgO	9.65	9.63	-0.02			
CaO	12.45	12.42	-0.03	TOTAL	99.61	2.25
Na_2O	2.18	1.85	-0.33			
K_2O	0.16	0.15	-0.01			

Sum of squares of residuals = 0.11

Table 3-24: Predicted and observed trace element content of DR4-329/DR4 using results of least squares approximation given in Table 3-23, and distribution coefficients from Table 3-19.

	DR9-322	DR4-329/DR4	
	OBS.	Calc.	OBS.
Zr	58	68	65
Nb	7.0	8.3	7.9
Y	22.4	25.4	23.6
Rb	3.1	3.7	4.2
Ba	34.3	40.9	38.6
Sr	100	102.	113
Sc	39	40	39
Ga	15.1	16.4	15.9
Ni	209 ($D^{Ni}_{Ol} = 12.62$)*	155	158
Co	52 ($D^{Co}_{Ol} = 3.0$)†	53	54

* D^{Ni}_{Ol} calculated from; $D^{Ni}_{Ol} = \frac{124}{MgO} - 0.9$ (Hart and Davis, 1977)

where MgO = 9.17% (average of DR9-322 and DR4-329/DR4).

† D^{Co}_{Ol} calculated from; $D^{Co}_{Ol} = \frac{9676}{T(K)} - 5.23$ (Leeman and Scheidegger, 1977)

where $T(^{o}C)$ = 1250 (calculated liquidus T of DR9-322, Table 3-10)

Table 3-25: Least squares approximation relating olivine basalt 11-18 to olivine basalt DR4-329/DR4.

Input data

	11-18	OLIVINE	PLAG	CPX	DR4-329/DR4
SiO_2	50.34	40.02	45.74	52.49	50.79
TiO_2	1.02	0.03	0.03	0.28	1.15
Al_2O_3	16.14	0.03	34.29	2.96	15.30
FeO*	8.73	12.36	0.37	4.21	9.62
MgO	8.96	46.98	0.24	18.39	8.69
CaO	12.15	0.32	17.72	20.93	11.82
Na_2O	2.10	0.01	1.59	0.20	2.05
K_2O	0.16	0.01	0.02	0.01	0.18
		Fo 87.17	An 85.93	Wo 42.03	
		Fa 12.83	Ab 13.95	En 51.37	
			Or 0.12	Fs 6.60	

Least squares approximation

	11-18			MIX		
	OBS.	CALC.	DIFF.	COMP.	Wt.%	S.D.
SiO_2	50.34	50.28	-0.06	DR4-329/DR4	88.77	1.22
TiO_2	1.02	1.03	0.01	OLIVINE	1.79	0.39
Al_2O_3	16.14	16.17	0.03	PLAG	7.35	0.68
FeO*	8.73	8.88	0.15	CPX	2.13	0.77
MgO	8.96	8.97	0.01			
CaO	12.15	12.25	0.10	TOTAL	100.04	1.64
Na_2O	2.10	1.94	-0.16			
K_2O	0.16	0.16	0.00			

Sum of squares of residuals = 0.063

Table 3-26: Predicted and observed trace element content of DR4-329/DR4 using results of least squares approximation given in Table 3-25, and distribution coefficients from Table 3-19.

	11-18	DR4-329/DR4	
	OBS.	Calc.	OBS.
Zr	57	64	65
Nb	6.7	7.5	7.9
Y	22.8	24.9	23.6
Rb	2.5	2.8	4.2
Ba	36.0	40.6	38.6
Sr	110	107	113
Sc	34.4	37	39
Ga	14.7	15.3	15.9
Ni	174 ($D_{Ol}^{Ni} = 13.15$)*	148	158
Co	50 ($D_{Ol}^{Co} = 3.3$)†	52	54

* Calculated from Hart and Davis (1977) using an average MgO content of 8.83%.

† Calculated from Leeman and Scheidegger (1977) using an olivine crystallisation temperature of 1230°C.

Table 3-27: Least squares approximation relating olivine basalt DR4-329/DR4 to most evolved olivine basalt DR2-174.

Input data

	DR4-329/DR4	OLIVINE	PLAG	CPX	DR2-174
SiO_2	50.79	39.98	47.00	52.89	50.71
TiO_2	1.15	0.03	0.04	0.32	1.38
Al_2O_3	15.30	0.03	33.31	2.65	15.02
FeO*	9.62	14.85	0.40	5.81	10.13
MgO	8.69	44.35	0.27	18.18	8.25
CaO	11.82	0.32	17.18	19.87	11.66
Na_2O	2.05	0.01	1.78	0.25	2.14
K_2O	0.18	0.01	0.02	0.01	0.26
		Fo 84.19	An 84.08	Wo 40.00	
		Fa 15.81	Ab 15.81	En 50.88	
			Or 0.12	Fs 9.12	

Least squares approximation

	DR4-329/DR4			MIX		
	OBS.	CALC.	DIFF.	COMP.	Wt.%	S.D.
SiO_2	50.79	50.71	-0.08	DR2-174	92.77	1.44
TiO_2	1.15	1.29	0.14	OLIVINE	1.44	0.46
Al_2O_3	15.30	15.34	0.04	PLAG	4.03	0.79
FeO*	9.62	9.76	0.14	CPX	2.26	0.89
MgO	8.69	8.71	0.02			
CaO	11.82	11.96	0.14	TOTAL	100.50	1.93
Na_2O	2.05	2.06	0.01			
K_2O	0.18	0.24	0.06			

Sum of squares of residuals = 0.071

Table 3-28: Predicted and observed trace element content of evolved olivine basalt DR2-174 using results of the least squares approximation given in Table 3-27.. Distribution coefficients are given in Table 3-19.

	DR4-329/DR4		DR2-174	
	OBS.		Calc.	OBS.
Zr	65		70	82
Nb	7.9		8.5	10.9
Y	23.6		25.0	27.4
Rb	4.2		4.5	4.8
Ba	39		42	59
Sr	113		113	114
Sc	39		40	41
Ga	15.9		16.4	17.5
Ni	158	(D_{Ol}^{Ni} = 13.74)*	136	123
Co	54	(D_{Ol}^{Co} = 3.3)†	54	52

* D_{Ol}^{Ni} calculated from Hart and Davis (1977) using an average MgO of 8.47%.

† D_{Ol}^{Co} calculated assuming a crystallisation temperature of 1230°C and using equation from Leeman and Scheidegger (1977).

in these samples by the fractional crystallisation of plagioclase, clinopyroxene and olivine in the proportions 17 : 46 : 37 and 16 : 65 : 19 respectively. The success of these models in predicting the trace element contents of the 'daughter' compositions (Tables 3-24 and 3-26) attests to their consistency.

It is possible to account successfully for the major element difference between sample DR4-329/DR4 and the most evolved olivine basalt, DR2-174, by the fractional crystallisation of 1.4% olivine (Fo_{84}), 4.0% plagioclase (An_{84}) and 2.3% clinopyroxene ($Wo_{40}En_{51}Fs_{9}$) (Table 3-27). This mix, however, fails to account for the trace element content of DR2-174 (Table 3-28). Although many of the compatible trace element abundances are correctly predicted, a large discrepancy occurs between predicted and observed incompatible elements (e.g. Zr, Nb and Ba). Since the predicted incompatible element abundances are unaffected by choice of distribution coefficients, and since at least Zr and Nb are not affected by weathering processes (Pearce and Cann, 1973), this discrepancy is regarded as invalidating this simple fractional crystallisation model.

An attempt has been made to show that although many of the compositional variations shown by the olivine basalts can be attributed to simple factional crystallisation processes, not all samples have this simple relationship. Diagnostic incompatible element ratios (e.g. Zr/Nb) suggest that the olivine basalts have been derived from a single source and in general the trace element variations describe systematic trends suggesting that the olivine basalts comprise a consanguinous suite of lavas. Coupling this information to the demonstrated inconsistency of many of the major and trace element calculations, it is suggested that

the discrepancies in the quantitative modelling can be attributed to open system fractional crystallisation acting within a magma chamber that experiences periodic replenishment by new 'primitive' magma (possibly derived by varying degrees of partial melting) which then incompletely mixes with existing magma. Usselman and Hodge (1978) have outlined a model for thermal control of open system low-pressure fractionation. Periodic replenishment by additional parental liquid can result in a steady thermal fractionating state being achieved which allows a fractionating-mixing magma chamber to remain active for an indefinite period of time and maintains a constant temperature interval bracketing a cotectic boundary. Such a situation would result in the buffering of the major elements and compatible trace elements (whose bulk $D = \pm 1.0$) in the liquid, but would result in a decoupling and apparent excessive enrichment in incompatible elements in lavas tapped at progressive stages.

In summary, a model is proposed in which the olivine basalts from the FAMOUS area comprise a consanguinous suite of lavas related by open system fractional crystallisation within a magma chamber that has reached a steady thermal state, probably at the olivine-plagioclase-pyroxene saturation surface. Periodic replenishment of this chamber by magma derived by slightly different degrees of partial melting (e.g. Langmuir et al., 1977) and subsequent incomplete mixing has resulted in an apparent decoupling of major and trace elements. Such processes would be ineffective in fractionating incompatible element ratios but would account for apparent excessive enrichment in absolute abundances of incompatible elements in some of the more evolved lavas. The primitive nature of many of the FAMOUS olivine basalts suggests that some magma

reaches the surface without excessive fractionation. This is further discussed in a later section.

7.4 Picritic basalts

On the basis that the picrites represent olivine + minor Cr-spinel cumulus-enriched rocks, and from a study of melt inclusions in Cr-spinel phenocrysts, a major element parental composition (P_1) for the picrites was calculated (Section 6.). Using this average composition, it is possible to predict accurately the amount of olivine accumulation necessary to account for the compositions of DR8 and 10-03C, utilizing a least squares approximation technique and average olivine phase compositions. The proportions of cumulate olivine can then be used to 'back-calculate' the trace element content of the hypothetical parent from the whole rock trace element contents.

A summary of the major element least squares approximation is presented in Table 3-29, and it can be seen that it is necessary to accumulate 11.09% and 32.46% olivine to account for the compositions of DR8 and 10-03C respectively. Cr-spinel has been excluded from the calculations due to its extremely low abundance (<1.0%), but it would theoretically contribute minor Al_2O_3, MgO and FeO* to the cumulate. These values have been used individually to back-calculate the trace element content of this hypothetical parent from the whole rock compositions of DR8 and 10-03C. Results of this calculation are presented in Table 3-29 and show remarkably good agreement for the two cases. With the exception of Y($D^{Y}_{ol} = 0.13$), Zn($D^{Zn}_{ol} = 0.86$, Bougault and Hekinian, 1974) and Ni, all trace elements were assigned a distribution coefficient of zero. Values for Y and Zn were calculated using equation (4) (Chapter II) to predict the concentration in the cumulating

Table 3-29: A. Summary of least squares approximation for the derivation of picrites DR8 and 10-03c from the postulated 'primary' magma P_1 (see section 6·0).

B. The predicted trace element content of this hypothetical 'primary' magma P_1 derived by 'back-calculation' from DR8 and 10-03c. See text for further discussion.

A. Summary of major element least squares approximation.

DR8 = 88.32% PAR + 11.09% Fo_{89} ($\Sigma R^2 = 0.07$)

10-03c = 66.95% PAR + 32.46% Fo_{90} ($\Sigma R^2 = 0.16$)

B. Predicted trace element content of parent.

	From DR8	From 10-03c	Average
Zr	34.1	33.0	33.5
Nb	2.99	2.60	2.8
Y	18.4	16.80	17.6
Rb	1.90	-	1.9
Ba	27.3	17.5	22.4
Sr	78.6	71.8	75.2
Sc	42.2	42.0	42.1
Ga	12.3	13.1	12.7
Ni	-	396	396
V	205	199	202
Zn	61	55	58
Cu	113	130	122

olivine (two iterations were required) and then a simple mass balance calculation was performed to determine the concentration in the parent. Ni was predicted by first calculating an applicable D_{ol}^{Ni} for the given MgO content of the parent. This was calculated using an equation from Smith et al. (in press), i.e.

$$D_{ol}^{Ni} = \frac{111.33}{MgO} - 1.71$$

This equation has been suggested (Smith et al., in press) to be more applicable than the relationship of Hart and Davis (1978) at high MgO contents. The calculated D_{ol}^{Ni} (7.33) was then divided into the highest NiO content (0.37%) observed in an olivine in 10-03C, on the assumption that the olivine with highest NiO content would reflect the liquidus composition. An inherent assumption in this procedure is that the olivines are products of Rayleigh crystallisation rather than equilibrium crystallisation. Considering the relatively unzoned nature of the olivines, this assumption might not be strictly valid, but is regarded as sufficing as a first approximation.

The possibility that this hypothetical composition might represent the 'parental' magma from which either the olivine basalts or plagioclase-pyroxene basalts evolved will now be considered. The variations in NiO with Fo content in phenocryst olivines suggest that the picrites, and by inference the hypothetical parent, are related to the plagioclase-pyroxene basalts. Although least squares modelling of the major elements supports such a model, the trace element abundances negate such a relationship. This is most strongly reflected in the different Zr/Nb ratios of the picrites (Zr/Nb = 10.5) and plagioclase-pyroxene basalts (Zr/Nb = 6). To change the Zr/Nb ratio by this amount would require

over 98% clinopyroxene ($D^{Zr}_{cpx} = 0.2$, $D^{Nb}_{cpx} = 0.03$, Table A2-5) crystallisation, a clearly unrealistic requirement. A simple low pressure fractional crystallisation relationship between the picrites and plagioclase-pyroxene basalts is therefore ruled out.

Though the picrites have, within experimental error, similar Zr/Nb ratios to the olivine basalts, major element modelling does not account for the compositional differences between these lavas. The significantly different NiO content in the phenocryst olivines similarly rules out a direct relationship via olivine accumulation. The different NiO content of the olivines with similar Mg/Fe ratios suggests that they derived from magma with inherently different Mg-Ni-Fe contents. A simple genetic relationship between the picrites (and the hypothetical parent) and the olivine basalts via olivine fractionation and accumulation, can therefore be ruled out. Partial melting, however, offers a mechanism in which major elements, and trace elements with high distribution coefficients, are buffered relative to the more incompatible trace elements and so the possible effects of partial melting will now be considered.

7.5 Partial Melting

To evaluate the possibility that two lavas may be related by different degrees of partial melting of a similar source, rather than by fractional crystallisation, it is necessary to consider only compositions that could represent primary magmas, i.e. magmas unmodified in composition since derivation from their source. Since basaltic magmas are generally regarded as deriving from the upper mantle, of which olivine is thought to comprise a considerable proportion, any potential primary magma should have a composition that could have been in equilibrium

with residual mantle olivine. The Mg-number of a magma may therefore be regarded as a criterion for recognising potential primary magmas e.g. Green, 1971; Kesson, 1973). The characteristics of such primary magmas in terms of absolute concentrations, specifically with respect to MgO, is however much debated. For example, O'Hara (1968), O'Hara et al. (1975), Clarke (1970) favour generation of extremely magnesian liquids (20-25% MgO) by partial melting, which then evolve via olivine fractionation to produce mid-ocean ridge basalt with characteristic 8-10% MgO. From a study of ophiolites, Elthon (1979) has postulated that MORB is the product of olivine and gabbro fractionation from a parental magma having approximately 18% MgO. Hart and Davis (1978) have argued from a consideration of Ni partitioning in olivine that primary magmas have between 11 and 13% MgO and not 20-25% MgO as suggested by others. Hanson and Langmuir (1978) have put forward the concept of modelling major elements - and specifically Mg and Fe - in terms of trace element equations for equilibrium partial melting. Assuming a pyrolite source, they conclude that primary magmas to ocean floor basalts must contain less than $\pm$ 15.5% MgO and $\pm$ 8.2% FeO. There appears therefore to be a general consensus that primary ocean floor basaltic magmas probably have greater than 11% MgO. Least differentiated basalts with 10-11% MgO, however, may well have experienced only limited olivine fractionation.

The most Mg-rich olivine basalts, DR4-303 and DR1-122, have approximately 10.5 and 10.4% MgO respectively. An analysis of another fragment of DR4-303 by Bougault and Hekinian (1974) gave 11.3% MgO, with similar concentrations of other elements. The average major element composition of these three analyses has been taken as representative of

a possible primary magma. This composition has 10.7% MgO and the average trace element content has been taken as the average of DR4-303 and DR1-122 (this study). This parental composition (P_2) is presented together with the hypothetical parent (P_1) calculated for the picrites in Table 3-30. A model will now be constructed which will attempt to show that these respective parental magmas may have been generated from a homogeneous source by different degrees of partial melting. It is unlikely that either parent can be regarded as a true primary magma, but it is suggested that they might have experienced as little as 3% olivine fractionation since equilibration with their source area. The model will be based on quantitative modelling of trace elements and selected major elements. A possible model for accounting for the different NiO content of the olivine observed in the picrites and olivine basalts will finally be proposed.

Any quantitative partial melting model requires estimates of a number of parameters, most of which are still poorly known. Such parameters include initial (or residual) mantle mineralogy, proportions of phases entering the melt, the degree and type of melting, temperature and pressure of melting, concentration of elements in the source region and applicable distribution coefficients. The approach that has been used is first to determine to what extent the two 'parental' magmas of interest, P_1 and P_2, truly represent primary magmas. This has been done following the approach of Hanson and Langmuir (1978) for modelling Fe-Mg relationships (see Chapter II, Section 3.2 for details), combined with modelling of Ni distributions. This is then followed by modelling selected trace elements by simple non-modal equilibrium melting (Shaw, 1970). Though the more complex dynamic melting proposed by Langmuir et

Table 3-30: Compositions of postulated primary magmas. P_1 has been calculated from melt inclusion data and consideration of Fe-Mg distribution in picrites DR8 and 10-03c. P_2 is the average composition of the most Mg-rich olivine basalts, DR4-303 and DR1-122.

	P_1	P_2
SiO_2	48.81	50.48
TiO_2	0.63	0.87
Al_2O_3	15.77	15.33
FeO*	8.00	8.36
MnO	0.15	0.15
MgO	12.33	10.72
CaO	12.57	11.84
Na_2O	1.54	1.88
K_2O	0.08	0.17
P_2O_5	0.06	0.09
Zr	33.5	49.2
Nb	2.8	6.1
Y	17.3	19.0
Rb	1.9	3.4
Ba	22.4	41.6
Sr	74.8	114
Co	-	53.1
Cr	-	583
Ni	396	270
V	202	198
Zn	58	69.0
Cu	122	74.7
Sc	41.9	35.4
Ga	12.7	15.2

al. (1977) is possibly more realistic, the simple equilibrium melting model satisfies most variations and due to the unconstrained nature of many of the parameters, it is felt that the more complex approach is not warranted at this stage.

The modal mineralogy of the source area has been assumed to be similar to that predicted for the source of Mauna Loa, Hawaii (Leeman et al., 1977). The mineral proportions are: olivine 58; orthopyroxene 22; clinopyroxene 14; garnet 6. These are assumed to enter the melt in the proportions 10 : 10 : 40 : 40 respectively (Leeman et al., 1977) until all garnet is exhausted and then in the proportions 20 : 20 : 60 (Kushiro, 1968, 1969). The choice of garnet in preference to spinel (or plagioclase) as the aluminous phase is based on a number of criteria:

(1) The geochemically 'enriched' nature of the lavas suggests derivation from an undepleted source. In accord with generally accepted mantle models (e.g. Hanson, 1977; Sun and Hanson, 1975a), this is assumed to be below the depth of generation of depleted MORB (i.e. below $\pm$ 68 km, Bottinga and Steinmetz, 1979) and possibly within the upper reaches of the garnet stability field. At the position of the M.A.R. the garnet peridotite-spinel peridotite phase transition is assumed to be at approximately 68 km depth (Bottinga and Steinmetz, 1979).

(2) Langmuir et al. (1977) have postulated dynamic melting of a garnet-bearing source to account for the REE distributions in the FAMOUS lavas.

(3) The model presented by Nisbet and Fowler (1978) for the FAMOUS region postulates initiation of melting at depth within a rising diapir. The depth of initial melting might well be within the

garnet stability field (Nisbet and Fowler, 1978).

The predicted compositions of P_1 and P_2 are, however, not affected in the model by the presence of garnet as the aluminous phase as this phase is exhausted at the required degrees of melting. The exhaustion of garnet prior to clinopyroxene is in accord with melting occurring at low pressures within the garnet stability field (Yoder, 1976). Temperatures of last equilibration of the primary melt with the residual mantle have been assumed to be not significantly greater than the observed liquidus of the basalts (Yoder, 1976). Bender et al. (1978) have shown that the liquidus of one of the most primitive FAMOUS glasses is 1268°C and the calculated liquidus temperature for DR4-303 and DR1-122, on the basis of olivine Fe-Mg partitioning, is 1268°C (Table 3-10), and on the basis of Mn partitioning is 1245-1274°C (Table 3-3). Consequently the temperature of last equilibration with residual mantle has been assumed to be approximately 1300°C. Hanson and Langmuir (1978) have shown that, given the temperature of melting, FeO and MgO of the source and degree of melting, it is possible to calculate the FeO and MgO contents of an equilibrium melt (see Chapter II, Section 3.2). Ni abundances may similarly be predicted for such melts using the equilibrium partial melting equation for non-modal melting (Shaw, 1970). D_{ol}^{Ni} was calculated using the equation of Smith et al. (in press) relating D_{ol}^{Ni} to MgO content of the melt. Distribution coefficients for Ni in orthopyroxene, clinopyroxene and garnet were assumed constant ($D_{opx}^{Ni} = 3$, $D_{cpx}^{Ni} = 1.5$, $D_{gt}^{Ni} = 0.1$). A mantle composition similar to that proposed by Sun and Nesbitt (1977) for Archean mantle has been adopted for the calculations (i.e. 37.6% MgO, 9.04% FeO). Fig. 3-20 shows a partial melting grid giving predicted Ni and FeO/MgO+FeO ratios in

primary magmas derived by various degrees of partial melting (from 12 to 28%) at temperatures ranging from 1300 to 1400°C.

From Fig. 3-20 it can be seen that P_2 (the most primitive olivine basalt) is unlikely to represent a primary magma but could be derived by $\pm$ 3.5% olivine fractionation from a primary melt formed by $\pm$ 17% melting (the choice of the value 17% is based on additional trace element constraints - see later) at 1300°C. The characteristics of this primary melt would be: $\pm$ 12.11% MgO, $\pm$ 8.38% FeO and 365 ppm Ni. The olivine fractionation paths were calculated following the method of Pearce (1978) using a program kindly provided by Dr. K.G. Cox, and a value for $K_D^{Fe+Mg} = 0.30$ for the partitioning of Fe and Mg between olivine and liquid (Roeder and Emslie, 1970). The upper fractionation path is based on D_{ol}^{Ni} calculated from the equation of Smith et al. (in press) and the lower using the equation of Hart and Davis (1978). P_2 (the hypothetical parent composition giving rise to the picrites), however, could well represent a primary magma as it falls within the partial melting grid. Alternatively, it may have experienced as little as 1% olivine fractionation from a melt derived by 28% partial melting (value again based on trace element data - see later) at 1320°C. The characteristics of this primary melt would be: $\pm$ 13.13% MgO, $\pm$ 8.25% FeO and $\pm$ 419 ppm Ni.

The results of these calculations, depicted graphically in Fig. 3-20, reflect some important implications with respect to magma generation, some of which have been reported by Hanson and Langmuir (1978):

(1) At a given temperature, increase in the degree of melting results in a relatively small increase in Ni and MgO and relatively large decrease in FeO. Resultant liquids would therefore show a range in Mg/Fe ratio (increasing Mg-number) with similar Ni contents.

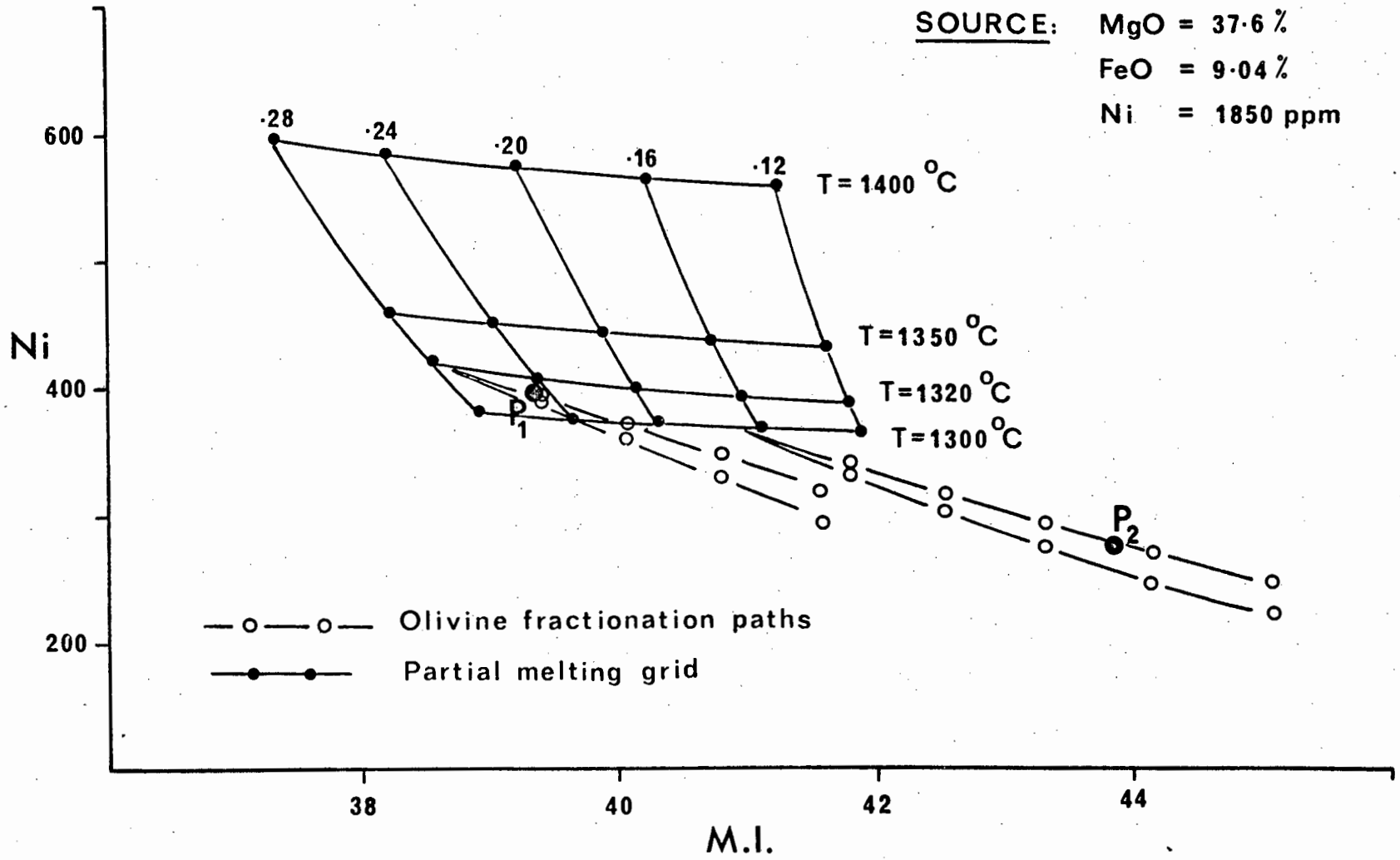

Fig. 3-20: Partial melting grid showing the variation of Ni with M.I. in liquids derived by various degrees of partial melting of a garnet peridotite source. The degree and temperature of melting and initial source concentrations are indicated. The compositions of primary magmas P_1 and P_2 are also indicated. Open symbols on olivine fractionation paths indicate increments of 1% olivine fractionation. See text for further discussion.

(2) An increase in temperature of melting results in a relatively large increase in MgO and Ni and a relatively small increase in FeO for a given degree of melting (e.g. at F = 0.16 at 1300°C MgO = 12.1%, FeO = 8.4%, Ni = 364 ppm and at 1400°C - MgO = 16.9%, FeO = 11.3%, Ni = 561 ppm). Consequently melts produced at higher temperatures have a greater Mg-number for a given F.

(3) The predicted concentration of Ni in the melt is very sensitive to the choice of D_{ol}^{Ni} and consequently, although the relative relationships in Fig. 3-20 would be unaffected, absolute values may vary significantly.

(4) Hanson and Langmuir (1978) have in addition pointed out that the effect of increasing the pressure at which partial melting occurs would tend to result in progressively more MgO and FeO-rich liquids.

An attempt has been made to show that of the two postulated parental magmas, P_1 and P_2, only P_1 possibly reflects the composition of a true primary magma. P_2 may, however, have experienced as little as 3.5% olivine fractionation since derivation from its source. All the trace elements considered in the partial melting study (Table 3-31) are basically incompatible with respect to olivine. Olivine fractionation would therefore result in only a small absolute enrichment in these elements and would have no effect on their mutual ratios. Since 3.5% fractional crystallisation is equivalent to about a 1% difference in degree of partial melting at the 17% melting level, which is well within the uncertainties of the data, both P_1 and P_2 have been regarded as representing primary magmas.

Due to the 'enriched' nature of the FAMOUS lavas, i.e. their

Table 3-31: Selected trace element distribution coefficients used in partial melting modelling (Table 3-32). Source of data are Tables A2-1, A2-5, A2-6, A2-7.

	Olivine	Opx	Cpx	Garnet
Zr	0.01	0.01	0.20	1.2
Nb	0.01	0.01	0.03	0.01
Y	0.10	0.10	0.50	3.00
Rb	0.01	0.01	0.011	0.015
Ba	0.01	0.01	0.013	0.023
Sr	0.01	0.01	0.10	0.01
Sc	0.15	0.40	2.00	10.0
Ga	0.01	0.01	0.40	0.01
K_2O	0.01	0.01	0.011	0.015
P_2O_5	0.01	0.01	0.01	0.10
TiO_2	0.01	0.02	0.20	0.20

trace element contents and incompatible element ratios are more akin to oceanic island basalts than to MORB, a relatively pristine mantle composition is preferred to a more depleted one that might characterise the source of MORB. For the elements in question the best available estimate of such a composition appears to be that postulated by Sun and Nesbitt (1977) for Archean mantle. Selected values from the ranges given in their compilation have been used in the proposed model. The selected source concentration chosen for Nb (1.00 ppm) is somewhat higher than that proposed by Sun and Nesbitt (1977) (0.53-0.72 ppm) but is not unrealistic. Applicable distribution coefficients for the elements have been selected from Tables A2-1, A2-5, A2-6 and A2-7 and are presented in Table 3-31. With the exception of Sc, all the elements have bulk solid-melt distribution coefficients significantly less than 1 and so are not sensitive to small uncertainties in the selected values.

Table 3-32 presents the proposed melting model whereby P_2 can be generated by 17% equilibrium melting and P_1 by 27% equilibrium melting of a homogeneous source, leaving residual olivine, orthopyroxene and clinopyroxene. Garnet is consumed after 15% melting. The initial trace element content of the source is given, together with observed and calculated values for the two proposed parental compositions. Residual mineralogy at the time of melt extraction is given for $F = 0.17$ and $F = 0.27$. As mentioned earlier, correction for 3.5% olivine fractionation from P_1 would require that the degree of melting giving rise to this composition would increase to 18%. It must be stressed that the values of $F = 0.17$ and $F = 0.27$ are values applicable for equilibrium melting. If a model based on continuous melting (Langmuir et al., 1977) is developed, significantly different F values can be obtained. For

Table 3-32: Comparison of predicted and observed trace element contents of parental magmas P_1 and P_2 derived by 27% and 17% equilibrium partial melting respectively of a homogeneous source. Initial source mineral assemblage has been taken from Leeman et al. (1977) and the calculated residual mineral assemblage is given for each model. Initial source concentrations have been taken from Sun and Nesbitt (1977). See text for additional discussion.

Element	Conc. in source	P_2 (F = 0.17)		P_1 (F = 0.27)	
		OBS.	CALC.	OBS.	CALC.
Zr	9.4	49.2	49.3	33.5	33.7
Nb	1.0	6.1	5.6	2.8	3.6
Y	5.5	19.0	19.7	17.3	15.9
Rb	0.57	3.4	3.2	1.9	2.06
Ba	7.1	41.6	39.8	22.4	25.6
Sr	21.0	114	113	74.8	75.5
Sc	17.0	35.4	36.1	41.9	38.7
Ga†	3.1	15.2	15.1	12.7	11.1
K_2O	0.03	0.17	0.17	0.08	0.11
P_2O_5	0.018	0.09	0.10	0.06	0.06
TiO_2	0.18	0.87	0.93	0.63	0.64

Mineral proportions

Mineral	Initial	Residue	Residue
Olivine	0.58	0.6742	0.7281
OPX	0.22	0.2420	0.2468
CPX	0.14	0.0838	0.0251
Garnet (or spinel or plag.)	0.06	-	-

† Assumed from data in Willis (1979).

example, for continuous melting, which proceeds to 12% before melt extraction, which then occurs in 4% increments, an equally acceptable solution for the derivation of P_1 by 20% melting would be obtained. In either event, the excellent agreement between observed and calculated trace element concentrations for both parent compositions supports their derivation from a single homogeneous source by different degrees of partial melting.

One, of possibly several, possible explanations for the significantly different NiO contents in the olivines crystallising from these two parent magmas is evident from Fig. 3-20. Increasing the degree of partial melting results in an increase in Mg/Fe ratio of the liquid with little change in absolute Ni content. Olivines crystallising from these liquids, or their derivatives, would therefore reflect these primary differences in Mg-Fe-Ni of the parental magmas. Although not entirely satisfactory, this model requires that the apparent coherency of the NiO in the olivines from the picrites with those of the plagioclase-pyroxene basalts and plagioclase-phyric basalts is fortuitous. The fact that the trends have maintained their uniqueness still requires the operation of distinct 'magma-chamber systems' for the generation of the picrites (by olivine accumulation) and the evolution of the olivine basalts.

The relationship of the plagioclase-pyroxene basalts and plagioclase-phyric basalts to the olivine basalts is not well determined as quantitative modelling is frustrated by the lack of a suitable plagioclase-pyroxene basalt primary magma. Any suitable model would have to account for the different Zr/Nb ratios (Fig. 3-13) and different NiO contents in the olivines (Fig. 3-16). Trace element analyses of coexisting garnet and clinopyroxene for Zr (Shimizu and Allègre, 1978)

and Zr and Nb (this study, Chapter II) suggest that garnet might prove a suitable phase for the fractionation of the Zr/Nb ratio. Assuming applicable distribution coefficients (Table 2-9), a source with initial Zr/Nb = 9.4 (similar to that of the postulated source for the olivine basalts), containing 8% residual garnet, could give rise to a melt, derived by 15% equilibrium partial melting, having a Zr/Nb ratio of approximately 6 (similar to that of the plagioclase-pyroxene basalts). Yoder (1976) has shown that at low pressures within the garnet stability field, garnet is exhausted before clinopyroxene during melting, while at higher pressures clinopyroxene is consumed first. Generation of a primary magma, which subsequently gave rise to the plagioclase-pyroxene basalts, at higher pressure from a source with similar composition and by similar or slightly lesser degrees of partial melting as that proposed for the olivine basalts, might result in residual garnet rather than clinopyroxene being present (Yoder, 1976). Equilibration against this residual garnet would be a possible mechanism for accounting for the lower Zr/Nb ratio of the plagioclase-pyroxene basalts. A greater contribution by clinopyroxene to the melt would similarly be qualitatively in accord with the relatively higher CaO content of the plagioclase-pyroxene basalts. The lower Zr/Nb ratio in the plagioclase-pyroxene basalts could alternatively be accounted for by postulating a lower degree of partial melting, leaving both clinopyroxene and garnet in the source. However, this would not account for the observed low NiO content in the olivines of the plagioclase-pyroxene basalts as lower degrees of partial melting would result in the production of a relatively more Fe-rich magma with similar Ni content.

Taking into account the possible effect of pressure on K_D's for MgO and FeO, Hanson and Langmuir (1978,

Fig. 4) suggest that melts derived at higher pressure would have a higher Mg-number than those derived at lower pressure. It would seem possible therefore that the variation in MgO-FeO-Ni of primary melts derived at higher pressure might be similar to variations due to higher degrees of partial melting at constant pressure. If this is correct, then it would be consistent with the olivines in derivative magmas having lower NiO content for a given forsterite content than those from magmas derived by melting at lower pressure. Such a model is preferred to one in which dynamic melting is the sole cause of the fractionation of the Zr/Nb ratio as one would then expect a continuous range in Zr/Nb ratio rather than two distinct groups. In addition, the similar Sr isotope ratios of the olivine basalts (DR4), picrites (DR8) and plagioclase-phyric basalt (DR3-1) suggest derivation from a homogeneous source area rather than from chemically distinct source areas.

7.6 Summary

Quantitative modelling of whole rock compositions from the FAMOUS area indicates that generation of all observed lava types is not possible from a single magma chamber. Evidence against such an hypothesis can be summarised as follows:

(1) The NiO contents of liquidus olivine and Cr-spinel from the various lava types describe two distinct 'fractionation' paths indicating evolution from two distinctly different 'parental' magma compositions. This distribution clearly distinguishes between the olivine basalts on the one hand and the plagioclase-pyroxene, plagioclase-phyric and picritic basalts on the other.

(2) The distinct Zr/Nb ratios (which are not readily fractionated by low pressure fractionation processes) of the olivine basalts and

plagioclase-olivine basalt ($Zr/Nb = \pm 8.4$), the plagioclase-pyroxene basalts ($Zr/Nb = \pm 6$) and the picrites ($Zr/Nb = \pm 10$), suggest derivation of these magma types from distinct 'parental' magmas.

(3) Least square approximations indicate that low pressure fractional crystallisation within an open system magma chamber can account for intra-group compositional variations, but fails to account for inter-group variations.

Zonation within a central magma chamber, as proposed by Hekinian et al. (1976), White and Bryan (1977) and Bryan et al. (1979), is unlikely to account for these differences. Consequently it is proposed that during the evolution of the FAMOUS region at least three distinct 'parental' magmas have experienced low pressure, open system fractional crystallisation resulting in the overall compositional variation of the lava types. A simplified schematic representation of the proposed genetic relationships of the FAMOUS lavas is presented in Fig. 3-21. Following this scheme, the plagioclase-phyric basalts are related to the plagioclase-pyroxene basalts by low pressure accumulation of dominantly plagioclase. These magmas are characterised by having a low Zr/Nb ratio and are derivatives of a primary magma which possibly formed by $\pm$ 10-15% partial melting of a peridotitic source leaving residual garnet. On the basis of their lower Zr/Nb ratio and lower NiO content of the olivines and Cr-spinel, these magmas can be distinguished from the olivine basalts and picrites, which are postulated to derive from a chemically similar source, but at lower pressure. The compositional range of the olivine basalts is suggested to be a function of open system fractionation of plagioclase, clinopyroxene and olivine in a magma chamber which

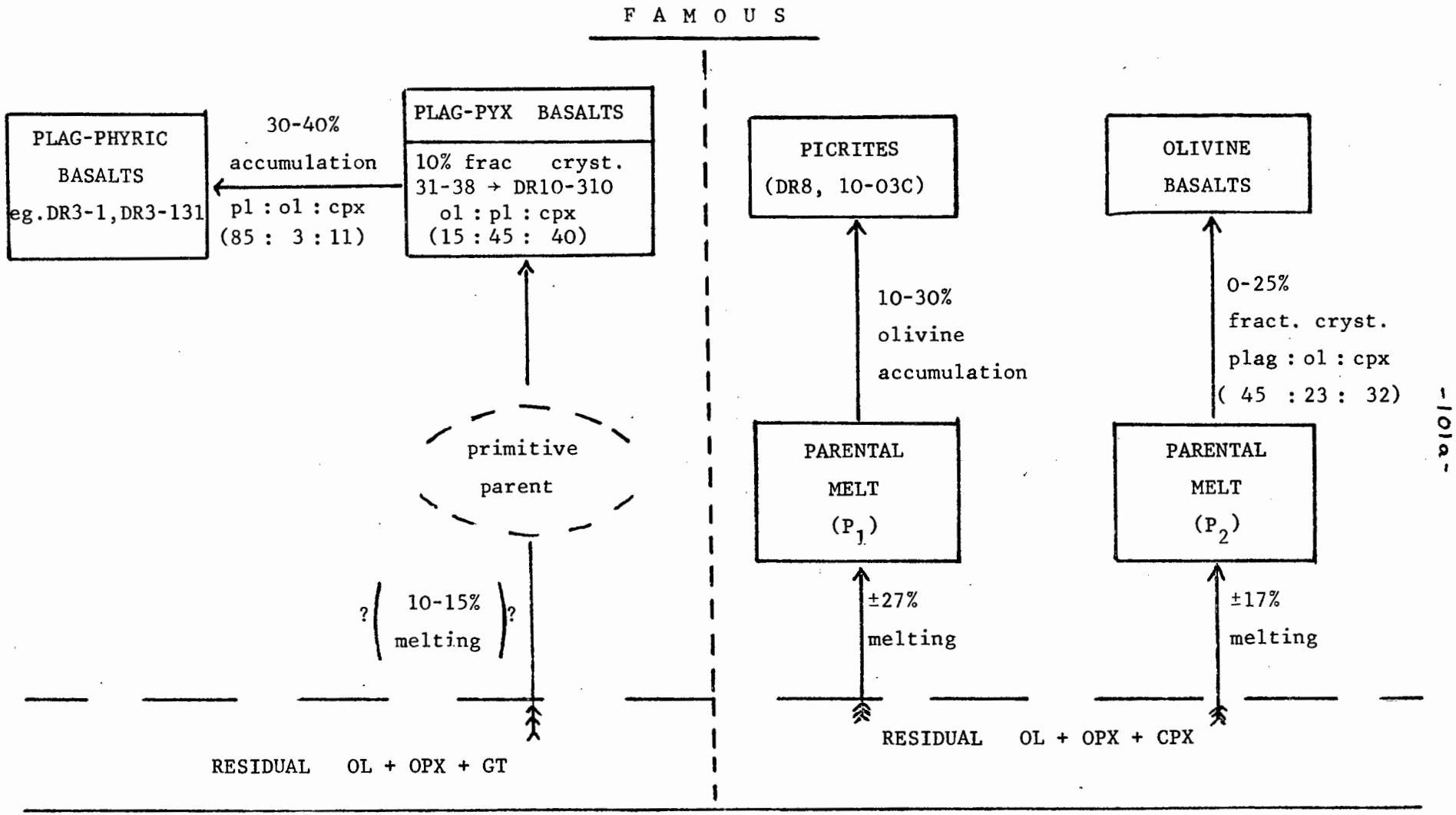

Fig. 3-21: Simplified schematic representation of the proposed petrogenetic scheme to account for some of the observed compositional variations in the FAMOUS region.

is periodically refilled by new batches of 'primary' magma. These new magma batches are probably derived by successively greater degrees of partial melting. Two of the most primitive olivine basalts from the present study could represent 'primary' magmas which have experienced as little as 3.5% olivine fractionation since derivation from their source area. The trace element composition of these samples is consistent with derivation from an 'Archean-type' mantle by $\pm$ 17% equilibrium partial melting.

The study of melt inclusions in phenocryst phases in the picrite basalts enables the prediction of a hypothetical parent composition which could have given rise to the picrites by olivine accumulation. This magma is more primitive than the most MgO-rich olivine basalts sampled and could represent a true primary magma. The trace element composition of this primary magma is consistent with its derivation by $\pm$ 27% partial melting of a similar source to that of the olivine basalts.

The distinct NiO contents of the olivine and Cr-spinel phenocrysts of these three 'types' of FAMOUS lavas, in conjunction with their distinct Zr/Nb ratios, indicate that much of the magmatic activity in the FAMOUS region has been separated in time or space.

CHAPTER IV

THE ISLAS ORCADAS AND CONRAD FRACTURE ZONES

1. INTRODUCTION

The Bouvet triple junction at 55°S, 1°W marks the site of the divergence of the South American, Anarctica and African plates and is situated just to the west of Bouvet Island (Fig. 4-1). To the west of the triple junction the America-Antarctica Ridge marks the boundary between the South American and Antarctica plates, and to the east is the Southwest Indian Ocean Ridge which separates the African and Antarctica plates. Sclater et al. (1976, 1978), Bergh and Norton (1976) and Norton (1976) have conducted geophysical studies of the area and note that both ridges are slow spreading (<1 cm/yr half spreading rate) and are characterised by long deep transform faults offsetting short ridge sections.

During cruise 11/76 of the R.V. "Islas Orcadas", which took place in December 1976, the ridge system in the vicinity of the Bouvet triple junction was surveyed and dredging was carried out at three locations: at the Islas Orcadas fracture zone near 54°5'S and 6°4'E, at the ridge crest at 11°E and at the Conrad fracture zone near 55°40'S and 3°51'W. Dredge locations are indicated in Fig. 4-2. Basaltic fragments from these dredges were made available to the University of Cape Town's Geochemistry Department by H.J.B. Dick (assistant chief scientist during the cruise) as part of a collaborative study of the South Atlantic ridge system involving the Woods Hole Oceanographic Institution, U.S.A., and the U.C.T. Geochemistry Department. A study of the mineralogy and geochemistry of the basaltic fragments from this collection comprises the dominant portion of this chapter.

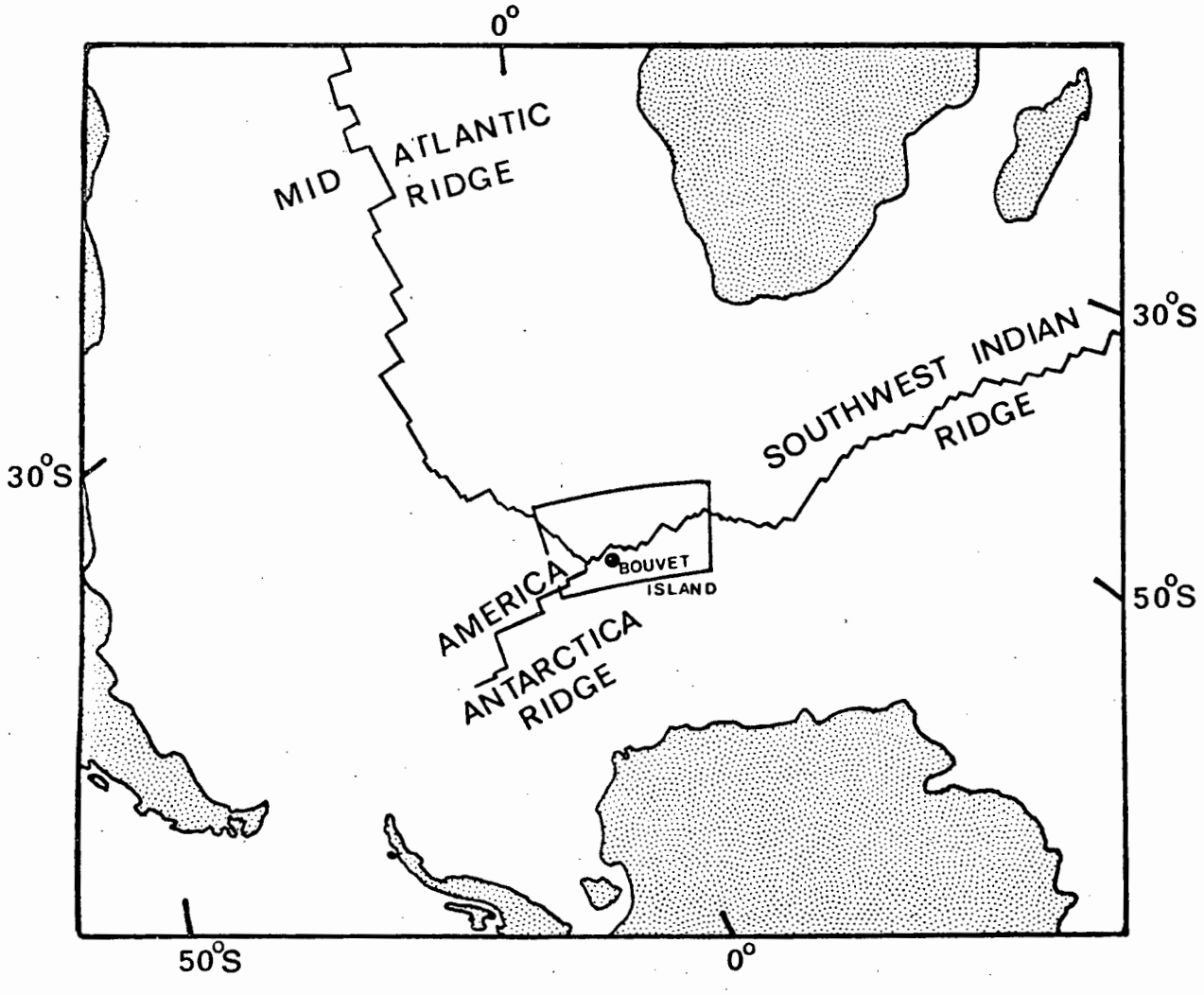

Fig. 4-1: A sketch map of the plate boundaries between the South American, African and Antarctic plates (after Sclater et al., 1978). The Bouvet triple junction and study area are shown by the open box.

2. GEOLOGICAL SETTING AND SAMPLE LOCATION

Preliminary results relating to the tectonic structure and petrology of the area of interest have been presented by Sclater et al. (1978). The survey of the Southwest Indian Ocean Ridge led to the discovery of an en echelon suite of four large fracture zones situated between Bouvet Island and 14°E (Sclater et al., op. cit.). Fig. 4-2 shows the location of these fracture zones which have been named, from west to east, "Moshesh', "Islas Orcadas", "Shaka" and "Dingaan" (Sclater et al., 1978). The Islas Orcadas fracture zone, the second largest, is over 100 km long and has a vertical relief of 3000 m. Three of the six successful dredge stations on the Islas Orcadas fracture zone, which recovered basaltic fragments, are depicted in Fig. 4-3B. Samples considered in this study are nine from Station 62/Dredge 13, and two from Station 63/Dredge 14 on the northwest wall, and three from Station 60/Dredge 11 on the southeast wall. Sample numbers have the prefix I062-, I063- and I060- respectively. A single sample (I075-2) of aphyric basalt from Station 75/Dredge 15 on the Southwest Indian Ocean Ridge crest at 11°E is also included in this study.

The Conrad fracture zone cuts the American-Antarctica Ridge just to the west of the Bouvet triple junction. Two successful dredges were made on the northern wall of this fracture zone, the locations of which are shown in Fig. 4-3A. Twenty samples recovered from Station 45/Dredge 3 on the lower half of the northern wall, and 8 samples from Station 47/Dredge 4 towards the top of the northern wall, have been studied. Sample numbers have the prefix I045- and I047- respectively. More detailed information regarding the positioning, depth and success of the various dredges is given in Sclater et al. (1978).

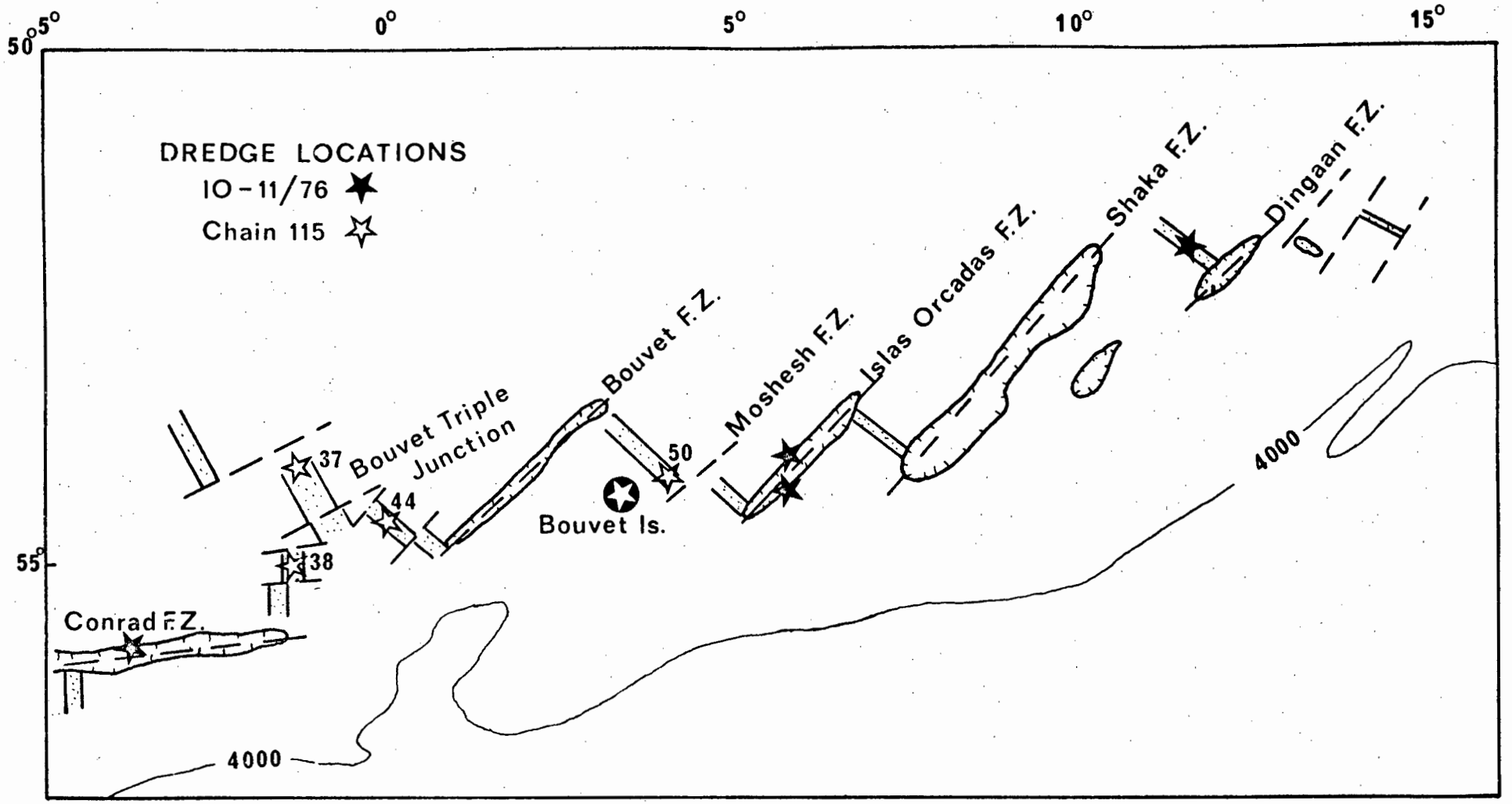

Fig. 4-2: Sketch of the fracture zone system between the Bouvet triple junction and 11°E (from H.J.B. Dick, pers. comm.) Dredge locations of the Islas Orcadas (IO11/76) and Chain (115) cruises are indicated. Station numbers of Chain 115 dredges are taken from Dickey et al. (1977).

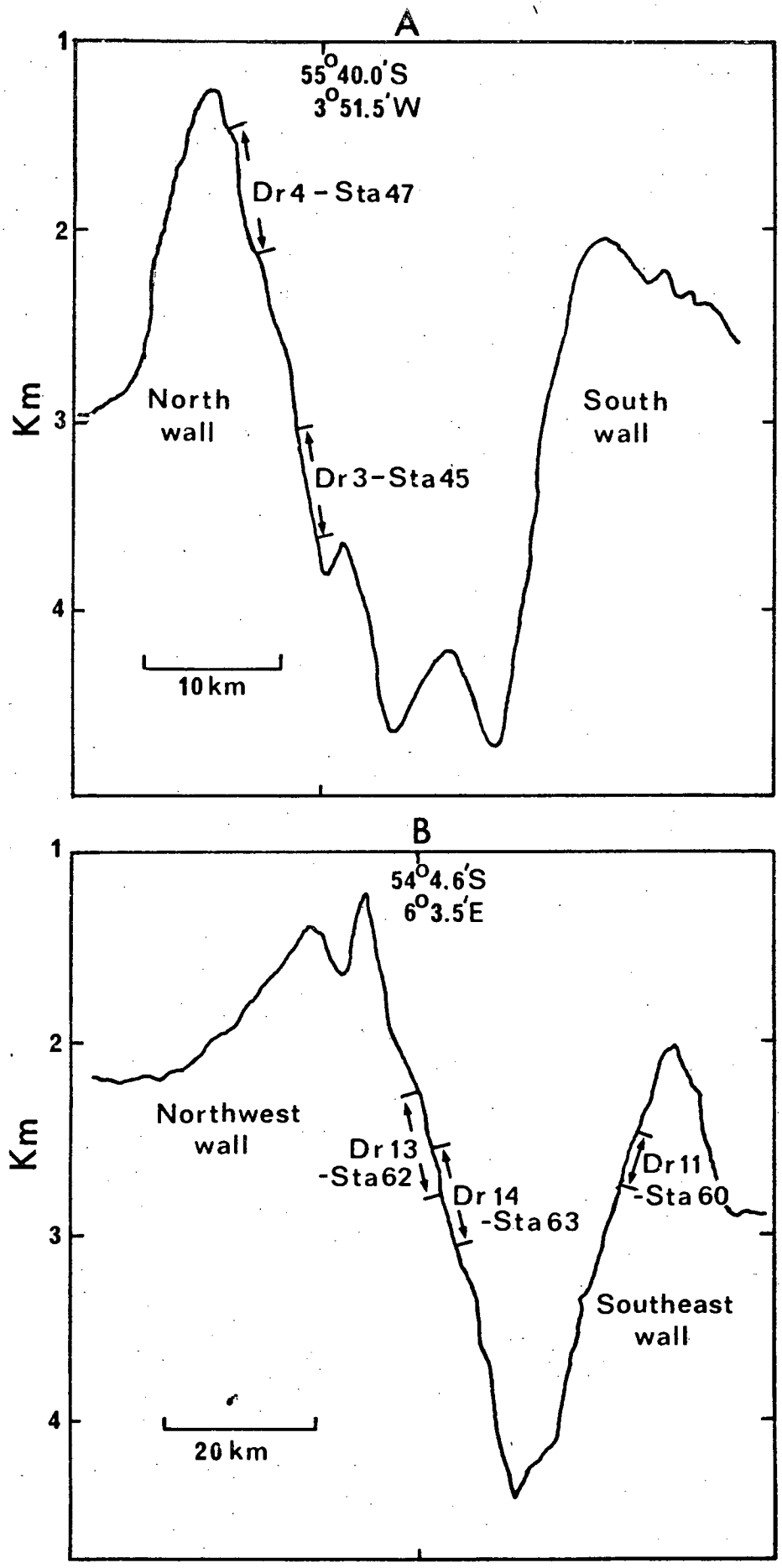

Fig. 4-3: A. The sites of two successful dredge stations on the Conrad fracture zone (from Sclater et al., 1978).
B. The sites of three successful dredge stations on the Islas Orcadas fracture zone (from Sclater et al., 1978).

3. ISLAS ORCADAS FRACTURE ZONE

3.1 Petrography and Mineralogy

The basaltic fragments recovered from the Islas Orcadas fracture zone (IOFZ) have been investigated optically, and phenocryst and microphenocryst phases from the majority of the samples have been analysed by electron microprobe. In selected cases secondary minerals have been analysed. Individual analyses are presented in microfiche tables (see appendix for list of tables) and only selected analyses are included in the text. Mineral phases in samples I063-3, I062-49 and I062-1A have not been analysed.

3.1.1 Station 60/Dredge 11:

Only three samples were recovered from Dredge 11. Two of these (I060-1 and I060-3) are plagioclase phyric with subordinate olivine and clinopyroxene, while the third (I060-2) is highly olivine phyric. Individual mineral analyses for these samples are given in microfiche Tables F4-1 to F4-3.

In basalt I060-2 olivine occurs as fractured euhedral to subhedral phenocrysts (1.0-1.5 mm) and microphenocrysts (Plate 4-1A). The phenocrysts show negligible zoning and range in composition from Fo_{85} to Fo_{80}, and microphenocrysts have an average composition of Fo_{76} (Table 4-1). The calculated K_D for the partitioning of Fe and Mg between olivine and liquid, using the most Mg-rich olivine in I060-2 and the whole rock Fe/Mg ratio, gives a value of 0.33 (assuming an Fe_2O_3/FeO ratio for the whole rock of 0.15). This compares favourably with an equilibrium value of 0.30 ± 0.03 (Roeder and Emslie, 1970), indicating that the olivine phenocrysts could have crystallised from a liquid with a composition similar to that of the whole rock, and that the abundant

T A B L E 4-1

ISLAS ORCADAS F.Z: SELECTED MINERAL ANALYSES. SAMPLE I060-2

	1	2	3	4	5	6
SIO2	39.33	38.74	38.47	.17	.14	.09
TIO2	.03	.05	.07	2.73	2.97	1.08
AL203	.07	.08	.07	25.96	26.01	33.54
CR203	-	-	-	23.33	22.28	24.26
FE203	-	-	-	15.46	16.01	10.65
FEO	14.74	18.25	22.18	19.58	21.15	15.67
MNO	.18	.27	.29	-	-	-
MGO	45.16	41.94	39.06	12.34	11.54	14.80
CAO	.25	.28	.47	.02	.02	ND
NA2O	-	-	-	-	-	-
K2O	-	-	-	-	-	-
TOTAL	99.76	99.61	100.61	99.59	100.12	100.10

* * ATOMIC PROPORTIONS BASED ON SELECTED NO. OF OXYGENS * *

OXYGEN	4	4	4	4	4	4
SI	.990	.993	.995	.005	.004	.003
AL	.002	.002	.002	.940	.942	1.154
TI	.001	.001	.001	.063	.069	.024
CR	-	-	-	.566	.541	.560
FE3+	-	-	-	.357	.370	.234
FE2+	.310	.391	.480	.503	.544	.382
MN	.004	.006	.006	-	-	-
MG	1.694	1.603	1.505	.565	.529	.644
CA	.007	.008	.013	.001	.001	-
NA	-	-	-	-	-	-
K	-	-	-	-	-	-
SUM	3.008	3.004	3.003	3.000	3.000	3.000
	FO 84.52	FO 80.37	FO 75.83	CR .38	CR .36	CR .33
	FA 15.48	FA 19.63	FA 24.17	MG .53	MG .49	MG .63
				FE .19	FE .20	FE .12

* * * S A M P L E D I R E C T O R Y * * *

ANALYSIS NO.	DESCRIPTION
1	OLIVINE PHENO, MG-RICH
2	OLIVINE PHENO, FE-RICH
3	OLIVINE MICROPHENO
4	CR-SPINEL IN OLIVINE 2
5	CR-SPINEL IN OLIVINE 3
6	CR-SPINEL IN OLIVINE 6

** ND = NOT DETECTED **

olivine phenocrysts do not necessarily imply phenocryst enrichment. Plagioclase occurs mainly as microphenocrysts in an intersertal texture set in a hyalocrystalline matrix (Plate 4-1A). Representative analyses are presented in Table 4-1 and depicted in Fig. 4-4. Equant Cr-spinel microphenocrysts occur poikilitically enclosed within olivine phenocrysts (Plate 4-1B), and have a chemistry typical of spinels found in alkali basalt. Representative analyses are given in Table 4-1 and depicted graphically in Fig. 4-5. Relative to the compositional range of spinels from the M.A.R. (Sigurdsson and Schilling, 1976; Sigurdsson, 1977), these spinels are significantly enriched in FeO, calculated Fe_2O_3 and TiO_2 and have unusually low Cr_2O_3 contents. High Fe_2O_3 and TiO_2 contents in Cr-spinels are typical of alkali basalts (Gunn et al., 1970; Wass, 1973), though they have been reported in tholeiitic basalts with 'alkaline' affinities (Sigurdsson and Schilling, 1976) and in a tholeiite from Snake River Plain (Thompson, 1973). Evans and Wright (1972) have reported Cr-spinels from Kilauea lavas with comparable TiO_2 (2.2-3.2%) and Fe_2O_3 (10.4-11.2%), though they are richer in Cr_2O_3 (38-44%) and poorer in Al_2O_3 (12.9-13.5%). Arculus (1974) has reported a nearly complete series from chromite to titanomagnetite from island arc basalts. That complete solid solution does exist between Cr-spinel and titaniferous magnetite has been demonstrated experimentally at basaltic temperatures and at oxygen fugacities above 10^{-8} atm. (Hill and Roeder, 1974). At lower fO_2, clinopyroxene crystallisation may interrupt that of chromite due to a reaction involving chromite, silicate liquid and clinopyroxene (Irvine, 1967). The occurrence of titaniferous, Fe_2O_3-rich Cr-spinels coexisting with olivine (Fo_{80}) in I060-2 suggest relatively high oxygen fugacities during the crystallisation of this basalt.

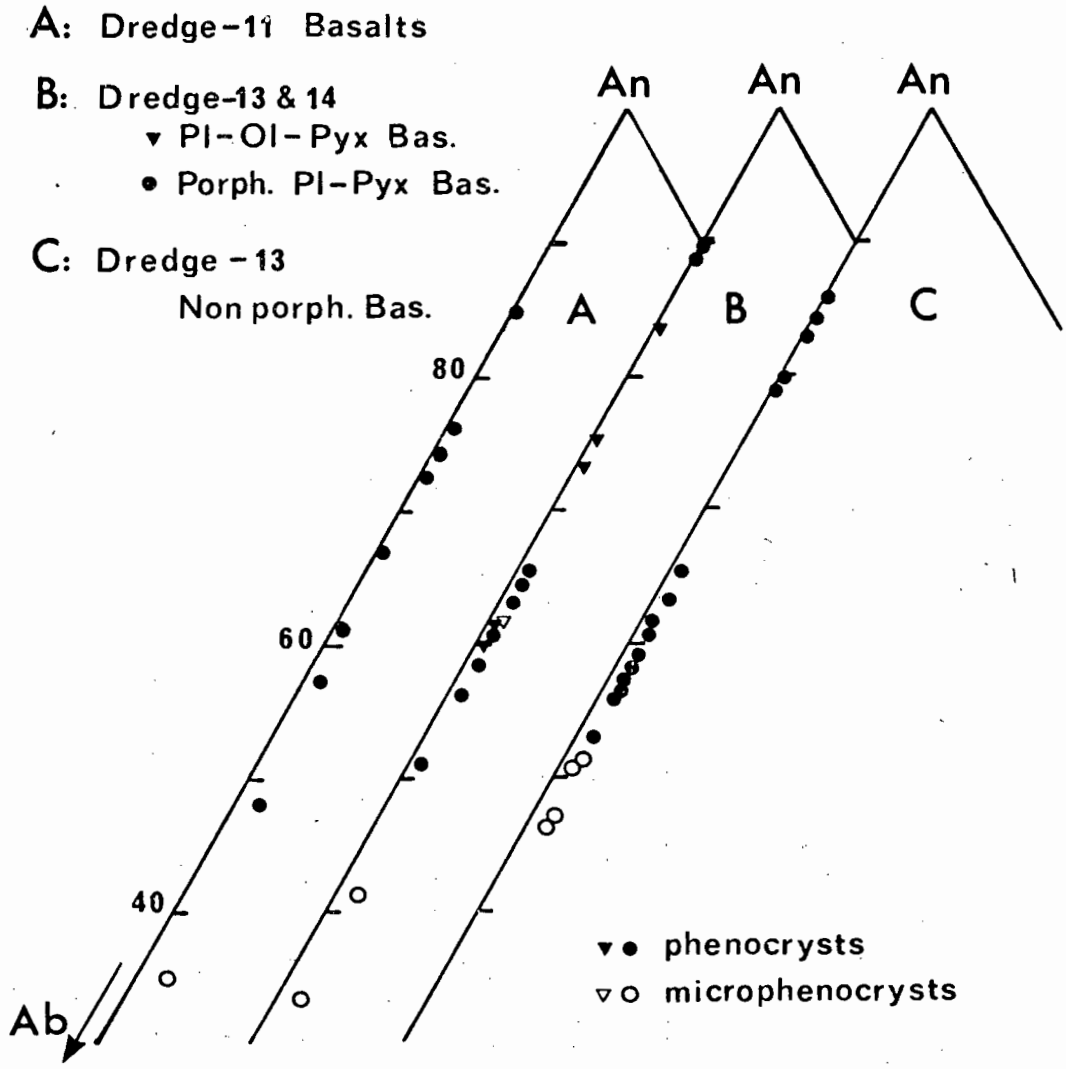

Fig. 4-4: Variation in end-member compositions of plagioclase phenocrysts and microphenocrysts from Islas Orcadas fracture zone basalts.

Fig. 4-5: Analysis of I060-2 spinels plotted on two faces of the spinel compositional prism (Irvine, 1967). The compositional fields of alpine peridotite spinels, lherzolite spinels, MAR spinels and high-Al spinels are taken from Sigurdsson and Schilling (1976). Fields designated 1, 11 and 111 correspond to high-Al spinels, MAR spinels and titaniferous magnesiochromites respectively (Sigurdsson and Schilling, 1976).

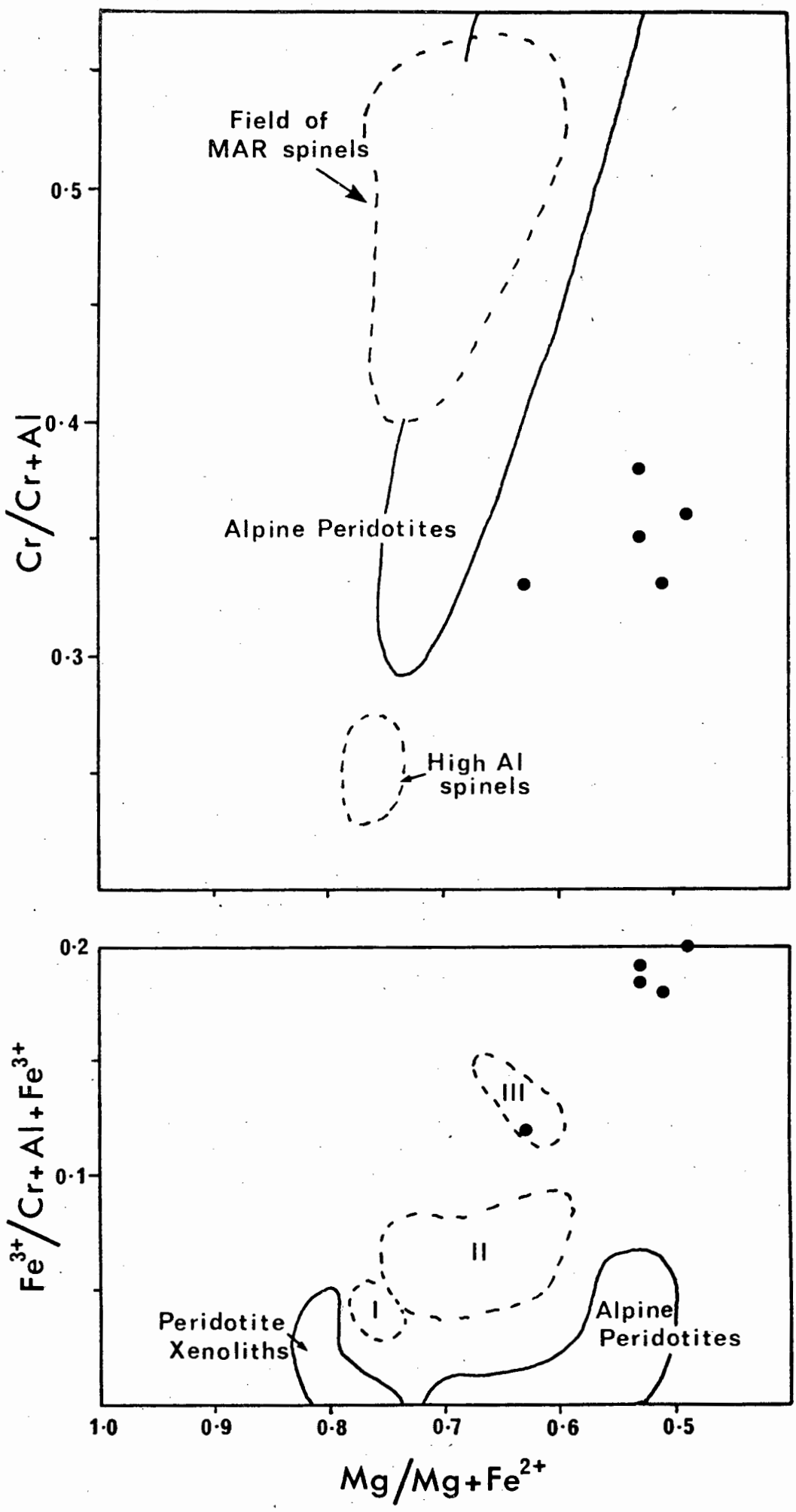
Field of
MAR spinels
Alpine Peridotites
High Al
spinels
Cr/Cr+Al
0·5
0·4
0·3
Fe3+/Cr+Al+Fe3+
0·2
0·1
III
II
I
Peridotite
Xenoliths
Alpine
Peridotites
1·0
0·9
0·8
0·7
0·6
0·5
Mg/Mg+Fe2+

Sample I060-1 is characterised by extremely abundant 'sieve textured' plagioclase phenocrysts and glomerocrysts (1-2 mm) with central 'cores' charged with trapped melt inclusions (Plate 4-1C). Some plagioclase phenocrysts show complex oscillatory zoning and range in composition from An_{72} to An_{48} (Table 4-2, Fig. 4-4). Olivine occurs as relatively sparse subhedral phenocrysts (1-2 mm) and microphenocrysts and ranges in composition from Fo_{81} to Fo_{74} (Table 4-2). Assuming a whole rock Fe_2O_3/FeO ratio of 0.15, the calculated K_D for the distribution of Fe and Mg between the most Mg-rich olivine and whole rock is 0.29. Comparison to an equilibrium value of 0.30 ± 0.03 (Roeder and Emslie, 1970) indicates that the olivines are in equilibrium with the host rock. The relatively low CaO content of the olivines (0.16 wt.%) distinguishes these olivines from those found in the other Dredges 11 and 13 basalts (.e.g. Tables 4-1, 4-3 and 4-4). Brownish-green clinopyroxene occurs as discrete phenocrysts (0.5-1.0 mm) and in aggregates with plagioclase and are relatively restricted in composition, $Wo_{43}En_{45}Fs_{12}$ to $Wo_{47}En_{40}Fs_{13}$ (Table 4-2). The unusual occurrence of titanomagnetite microphenocrysts (0.1-0.2 mm) poikilitically enclosed within olivine (Plate 4-1D), clinopyroxene and occasionally plagioclase, as well as in the matrix, is a feature of this rock. Representative titanomagnetite analyses are presented in Table 4-2, and inspection of the compositions indicates subtle differences which can be related to the mode of occurrence. Those occurring within olivine are poorer in TiO_2 (10.7-11.2%) and FeO (33.8-34.7%) and richer in Cr_2O_3 (0.80-1.6%), Al_2O_3 (5.3-6.3%), Fe_2O_3 (41.3-42.1%) and MgO (4.7-5.3%) than those occurring within clinopyroxene (TiO_2 - 15.3%, FeO - 39.1%, Cr_2O_3 - 0.79%, Al_2O_3 - 2.8%, Fe_2O_3 - 36.6% and MgO - 3.9%). Both varieties are distinguishable from those occurring

T A B L E 4-2

ISLAS ORCADAS F.Z: SELECTED MINERAL ANALYSES. SAMPLE I060-1

	1	2	3	4	5	6	7	8	9
SIO2	53.37	55.68	38.75	38.04	51.08	49.83	.19	.17	.12
TIO2	.13	.16	ND	.04	.72	1.23	10.74	15.33	17.63
AL203	28.42	27.23	.07	.11	3.76	4.78	6.27	2.84	2.28
CR203	-	-	-	-	.07	.02	1.28	.79	.70
FE203	-	-	-	-	-	-	41.50	36.64	33.03
FEO	.79	.75	17.32	23.62	7.33	7.91	34.72	39.05	41.69
MNO	-	-	.12	.31	.14	.15	.35	.46	.55
MGO	.09	.07	42.50	38.58	16.08	13.77	4.68	3.94	3.64
CAO	12.14	10.36	.16	.16	21.38	22.37	.04	.23	.05
NA20	4.89	5.94	-	-	.43	.36	-	-	-
K20	.29	.43	-	-	-	-	-	-	-
TOTAL	100.12	100.62	98.93	100.86	100.99	100.42	99.77	99.45	99.69

* * ATOMIC PROPORTIONS BASED ON SELECTED NO. OF OXYGENS * *

OXYGEN	8	8	4	4	6	6	4	4	4
SI	2.427	2.508	.995	.988	1.874	1.850	.007	.006	.004
ALIV	1.523	1.446	.002	.003	.126	.150	.263	.122	.098
ALVI	-	-	-	-	.037	.060	-	-	-
TI	.004	.005	-	.001	.020	.034	.288	.420	.483
CR	-	-	-	-	.002	.001	.036	.023	.020
FE3+	-	-	-	-	-	-	1.112	1.004	.906
FE2+	.030	.028	.372	.513	.225	.246	1.034	1.189	1.271
MN	-	-	.003	.007	.004	.005	.011	.014	.017
MG	.006	.005	1.627	1.493	.879	.762	.248	.214	.198
CA	.592	.500	.004	.004	.841	.890	.002	.009	.002
NA	.431	.519	-	-	.031	.026	-	-	-
K	.017	.025	-	-	-	-	-	-	-
SUM	5.031	5.036	3.003	3.010	4.039	4.023	3.000	3.000	3.000
	AN 56.90	AN 47.92	FO 81.39	FO 74.43	WO 43.22	WO 46.90	US 34.09	US 45.54	US 51.62
	AB 41.48	AB 49.72	FA 18.61	FA 25.57	EN 45.21	EN 40.15	MT 65.91	MT 54.46	MT 48.38
	OR 1.62	OR 2.37			FS 11.57	FS 12.94			

* * * S A M P L E D I R E C T O R Y * * *

ANALYSIS NO.	DESCRIPTION
1	PLAGIOCLASE PHENO
2	PLAGIOCLASE PHENO
3	OLIVINE PHENO
4	OLIVINE PHENO
5	CPX PHENO (IN PLAGIOCLASE)
6	CPX PHENO
7	TI-MGT (IN OLIVINE)
8	TI-MGT (IN CPX)
9	TI-MGT (DISCRETE)

** ND = NOT DETECTED **

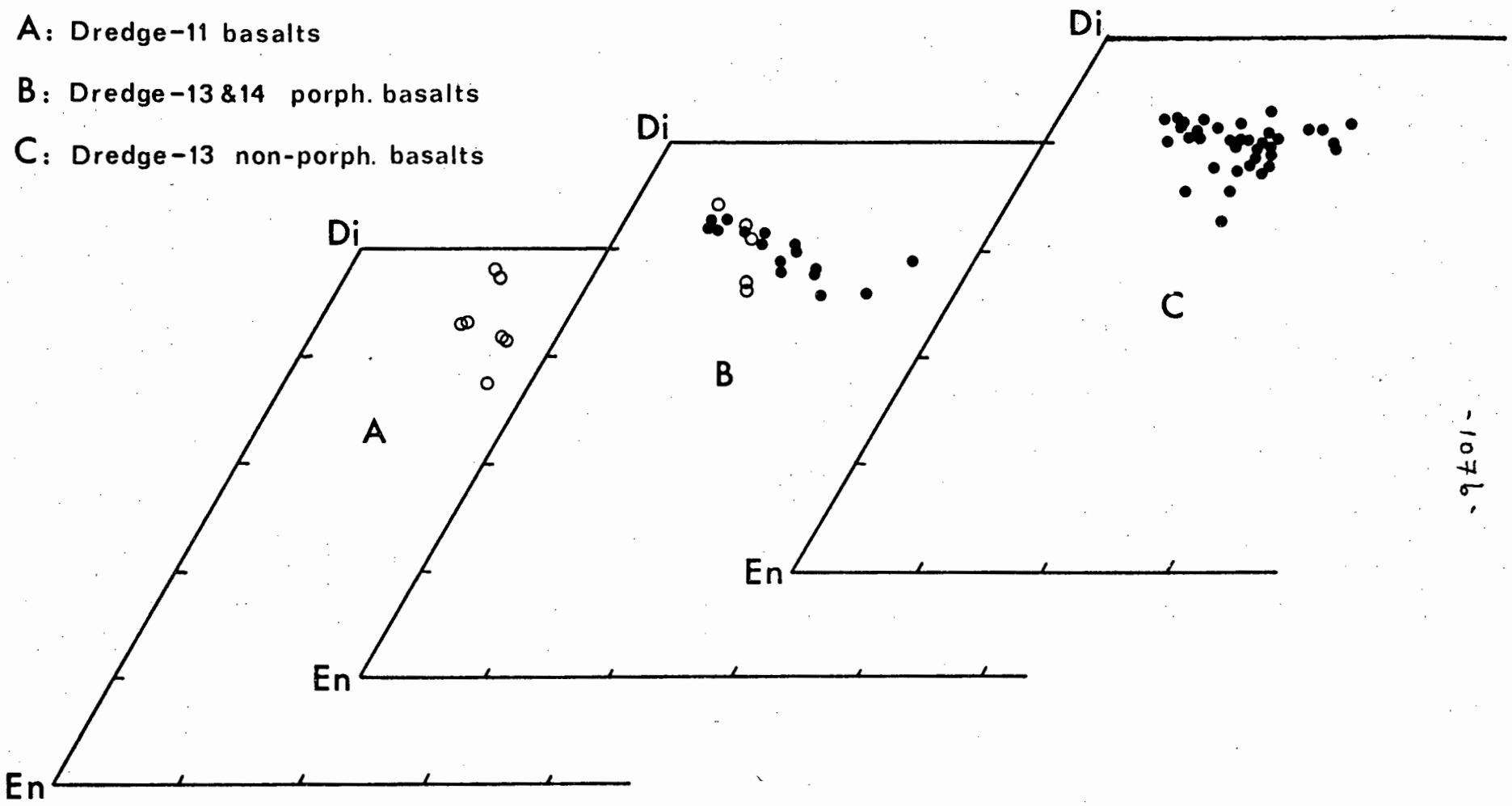

Fig. 4-6: Compositional variation of clinopyroxenes from IOFZ basalts. Open symbols represent samples containing olivine.

in the matrix which are richer in TiO_2 (17.0-17.6%) and ferrous iron (41.5-41.7%) and poor in Al_2O_3 (2.3-2.4%), Fe_2O_3 (33.0-33.8%), Cr_2O_3 (0.7%) and MgO (3.5-3.6%). The Cr_2O_3 content of the titanomagnetite included within olivine is significantly higher than that commonly found in 'late stage' titanomagnetite crystallising from ocean floor basalts (e.g. Conrad fracture zone, this study). The occurrence of 'early' titanomagnetite in sample I060-1 is suggestive of relatively high fO_2 conditions during the crystallisation of this basalt.

I060-3 is a holocrystalline basalt (hypabyssal?) comprising large (1-5 mm) plagioclase phenocrysts set in a fairly even grained (0.2-0.5 mm) matrix of orientated plagioclase laths with dispersed olivine and clinopyroxene and Fe-Ti oxides (Plate 4-1E). Plagioclase phenocrysts range in composition from An_{85} to An_{61}, with microphenocrysts being significantly more sodic, An_{35} (Table 4-3, Fig. 4-4). Olivine occurs only as microphenocrysts and is significantly more Fe-rich than that in the other Dredge 11 basalts, ranging in composition from Fo_{64} to Fo_{37} (Table 4-3). Clinopyroxene microphenocrysts have a restricted compositional range and a representative composition is given in Table 4-3. Both ilmenite and titanomagnetite occur as microphenocrysts in the groundmass and representative analyses are presented in Table 4-3. The presence of coexisting ilmenite and titanomagnetite allows the use of the experimental T-fO_2-X relations (Buddington and Lindsley, 1964) to determine the temperature and oxygen fugacity of last equilibration of the oxide phases in I060-3. Using the curves of Buddington and Lindsley (1964), an fO_2 of 10^{-11} atm. at 1000°C is indicated. The lack of exsolution and restricted compositional range of the Fe-Ti oxides suggest that this might represent crystallisation conditions rather than post extrusion alteration.

T A B L E 4-3

ISLAS ORCADAS F,Z: SELECTED MINERAL ANALYSES. SAMPLE I060-3

	1	2	3	4	5	6	7	8
SIO2	46.72	52.86	59.25	36.44	34.04	50.94	.13	.24
TIO2	.03	.06	.13	.02	.05	1.36	48.77	22.54
AL203	34.21	29.59	25.04	.06	.12	2.20	.29	2.08
CR203	-	-	-	-	-	-	ND	-
FE203	-	-	-	-	-	-	7.64	22.49
FEO	.65	.62	.86	31.34	43.02	10.19	40.08	50.25
MNO	-	-	-	.40	.67	.20	.47	.48
MGO	.06	.09	.07	30.94	21.36	15.03	1.84	1.03
CAO	17.42	12.99	7.72	.28	.34	20.23	.14	.10
NA2O	1.70	4.13	7.71	-	-	.34	-	-
K2O	.05	.11	.43	-	-	-	-	-
TOTAL	100.84	100.45	101.21	99.48	99.60	100.49	99.37	99.21

* * ATOMIC PROPORTIONS BASED ON SELECTED NO. OF OXYGENS * *

OXYGEN	8	8	8	4	4	6	3	4
SI	2.136	2.392	2.636	.999	.993	1.899	.003	.009
ALIV	1.844	1.578	1.313	.002	.004	.097	.009	.091
ALVI	-	-	-	-	-	-	-	-
TI	.001	.002	.004	.000	.001	.038	.920	.631
CR	-	-	-	-	-	-	-	-
FE3+	-	-	-	-	-	-	.144	.630
FE2+	.025	.023	.032	.718	1.050	.318	.841	1.563
MN	-	-	-	.009	.017	.006	.010	.015
MG	.004	.006	.005	1.264	.929	.835	.069	.057
CA	.854	.630	.368	.008	.011	.808	.004	.004
NA	.151	.362	.665	-	-	.025	-	-
K	.003	.006	.024	-	-	-	-	-
SUM	5.017	5.001	5.048	3.000	3.004	4.026	2.000	3.000
	AN 84.74	AN 63.07	AN 34.80	FO 63.76	FO 46.94	WO 41.21	IL 85.80	US 66.70
	AB 14.97	AB 36.29	AB 62.89	FA 36.24	FA 53.06	EN 42.59	GK 6.93	MT 33.30
	OR .29	OR .64	OR 2.31			FS 16.20	HM 7.27	

* * * S A M P L E D I R E C T O R Y * * *

ANALYSIS NO.	DESCRIPTION
1	PLAGIOCLASE PHENO
2	PLAGIOCLASE PHENO
3	PLAGIOCLASE MICROPHENO
4	OLIVINE MICROPHENO
5	OLIVINE MICROPHENO
6	CPX MICROPHENO
7	ILMENITE
8	TI-MGT

** ND = NOT DETECTED **

PLATE 4-1

A: Photomicrograph of dredge-11 basalt I060-2 showing numerous olivine phenocrysts and plagioclase microphenocrysts.

B: Fractured olivine phenocryst in I060-2 containing a small Cr-spinel inclusion.

C: Photomicrograph of plagioclase phyric dredge-11 basalt I060-1. Note the abundant trapped melt inclusions in the plagioclase phenocrysts. Crossed polars.

D: Fractured, anhedral olivine phenocryst in I060-1, containing titanomagnetite inclusions.

E: Photomicrograph of dredge-11 basalt I060-3 showing the porphyritic texture of large plagioclase phenocrysts set in a matrix of orientated plagioclase laths. Crossed polars.

F: Photomicrograph showing the plagioclase phyric nature of dredge-13 basalt I062-42A. Crossed polars.

G: Subhedral olivine phenocryst in subophitic relationship with plagioclase in I062-42A. Crossed polars.

H: Photomicrograph of I062-42A showing subophitic relationship of plagioclase and clinopyroxene. Crossed polars.

PLATE 4-1

A

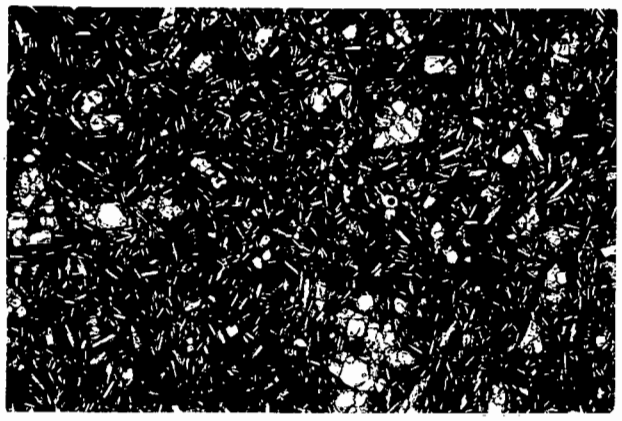

4mm

B

0·5mm

C

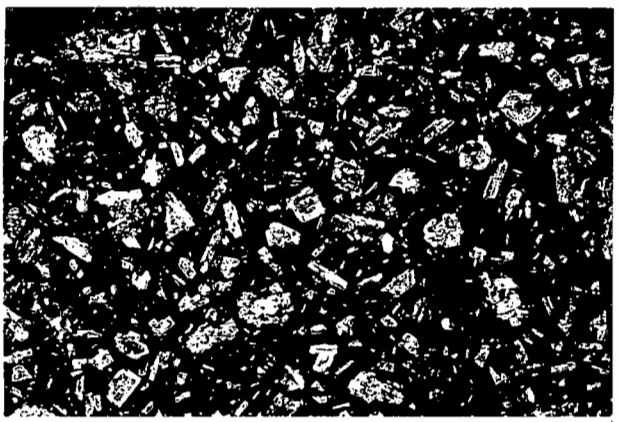

5mm

D

1 mm

E

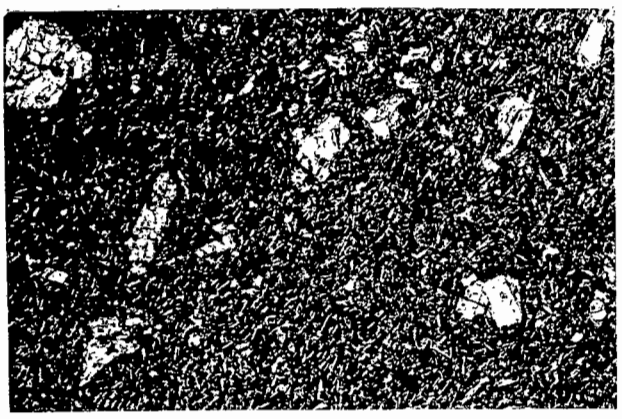

6mm

F

6mm

G

2·5mm

H

2·5mm

3.1.2 Stations 62/63, Dredges 13/14

Since both these Dredges are closely situated on the north-western wall and since only two basaltic fragments from Dredge 14 have been studied, the samples have been combined for descriptive purposes. Of the 12 samples studied from these Dredges, two are highly plagioclase phyric with subordinate olivine and clinopyroxene and the remainder are characterised by the presence of only plagioclase and clinopyroxene phenocrysts.

(a) Olivine-plagioclase-pyroxene basalts:

Samples I062-42A (Plate 4-1F) and I062-49 have a porphyritic texture, with large plagioclase phenocrysts and glomerocrysts (1-4 mm) set in a microcrystalline matrix of plagioclase laths and pyroxene sheaves in an arborescent texture. Fe-Ti oxides occur as minute grains and dendrites filling the interstices in the groundmass. Plagioclase phenocrysts are characterised by containing abundant trapped 'melt' inclusions and have core compositions ranging from An_{89} to An_{73}. Zoning is extensive and ranges to compositions similar to that of the groundmass plagioclase, An_{62}. Representative analyses are presented in Table 4-4 and are depicted graphically in Fig. 4-4. Olivine phenocrysts (0.5-2.0 mm) show minor zoning and range in composition from Fo_{87} to Fo_{83} (Table 4-4). Some of the larger olivine phenocrysts partially or totally enclose plagioclase phenocrysts (Plate 4-1G). Assuming a whole rock Fe_2O_3/FeO ratio of 0.15, the calculated olivine-host rock K_D for the most Mg-rich olivines is 0.20. This is significantly less than the equilibrium range (Roeder and Emslie, 1970) and indicates that the olivines are too Mg-rich to have crystallised from a liquid with a composition equal to that of the host rock. The low K_D suggests therefore

T A B L E 4-4

ISLAS ORCADAS F.Z: SELECTED MINERAL ANALYSES. SAMPLE I062-42A

	1	2	3	4	5	6	7	8	9	10
SIO2	44.91	51.88	46.31	48.92	51.77	40.20	40.04	39.52	52.74	51.68
TIO2	.04	.10	.05	.05	.13	-	-	-	.54	.90
AL2O3	34.66	29.63	33.63	31.83	29.73	-	-	-	3.10	3.28
CR2O3	-	-	-	-	-	-	-	-	.45	.03
FEO	.33	.78	.35	.48	.82	12.28	13.15	15.74	4.34	7.44
MNO	-	-	-	-	-	.16	-	.22	.10	.19
MGO	.21	.21	.20	.19	.21	47.42	46.79	44.50	17.53	16.45
CAO	18.48	13.09	17.40	15.41	13.22	.34	.33	.30	21.60	20.17
NA2O	1.18	4.39	1.84	3.05	4.38	-	-	-	.27	.34
K2O	.03	.15	.07	.06	.15	-	-	-	-	-
NIO	-	-	-	-	-	.18	.17	.09	-	-
TOTAL	99.84	100.23	99.85	99.99	100.41	100.58	100.48	100.37	100.67	100.48

* * ATOMIC PROPORTIONS BASED ON SELECTED NO. OF OXYGENS * *

OXYGEN	8	8	8	8	8	4	4	4	6	6
SI	2.080	2.363	2.139	2.244	2.356	.993	.993	.994	1.911	1.898
ALIV	1.892	1.591	1.831	1.721	1.595	-	-	-	.089	.102
ALVI	-	-	-	-	-	-	-	-	.044	.040
TI	.001	.003	.002	.002	.004	-	-	-	.015	.025
CR	-	-	-	-	-	-	-	-	.013	.001
FE2+	.013	.030	.014	.018	.031	.254	.273	.331	.132	.228
MN	-	-	-	-	-	.003	-	.005	.003	.006
MG	.014	.014	.014	.013	.014	1.745	1.729	1.667	.947	.900
CA	.917	.639	.861	.757	.645	.009	.009	.008	.839	.794
NA	.106	.388	.165	.271	.386	-	-	-	.019	.024
K	.002	.009	.004	.004	.009	-	-	-	-	-
NI	-	-	-	-	-	.004	.003	.002	-	-
SUM	5.026	5.036	5.029	5.031	5.040	3.007	3.007	3.006	4.011	4.018
	AN 89.49	AN 61.71	AN 83.60	AN 73.38	AN 61.99	FO 87.31	FO 86.38	FO 83.44	WO 43.75	WO 41.28
	AB 10.34	AB 37.45	AB 16.00	AB 26.28	AB 37.17	FA 12.69	FA 13.62	FA 16.56	EN 49.39	EN 46.83
	OR .17	OR .84	OR .40	OR .34	OR .84				FS 6.86	FS 11.89

* * * S A M P L E D I R E C T O R Y * * *

ANALYSIS NO.	DESCRIPTION
1	PLAGIOCLASE PHENO (CORE)
2	PLAGIOCLASE PHENO (RIM)
3	PLAGIOCLASE PHENO (CORE)
4	PLAGIOCLASE PHENO (CORE)
5	PLAGIOCLASE MICROPHENO
6	OLIVINE PHENO (CORE)
7	OLIVINE PHENO (RIM)
8	OLIVINE PHENO (CORE)
9	CPX PHENO, MG-RICH
10	CPX PHENO, FE-RICH

that 1062-42A has experienced olivine enrichment, but the small proportion of olivine present (<2 vol. %) is unlikely to have significantly affected the whole rock Fe/Mg ratio. Clinopyroxene occurs as large clear phenocrysts, commonly in ophitic relationships with plagioclase (Plate 4-1H). Phenocryst compositions range from $Wo_{44}En_{49}Fs_7$ to $Wo_{41}En_{47}Fs_{12}$, with microphenocrysts being slightly more iron-rich and Ca-poor ($Wo_{36}En_{51}Fs_{13}$; Table 4-4, Fig. 4-6). Individual mineral analyses are reported in microfiche Table F4-4.

(b) Plagioclase-pyroxene basalts:

The dominant variety of basalt recovered from the IOFZ is saturated in plagioclase and clinopyroxene. Two petrographically distinguishable varieties occur: one with a porphyritic texture (I062-51, I063-2 and I063-3), and the other with an even grained, non-porphyritic texture (I062-5, I062-12, I062-15, I062-30, I062-31, I062-42B and I062-1A).

The porphyritic variety has large plagioclase (2-4 mm) and clinopyroxene (1-3 mm) phenocrysts set in a medium grained matrix of intersertal plagioclase and clinopyroxene (Plate 4-2A). Titanomagnetite occurs in the interstices in the matrix. The plagioclase phenocrysts have a uniform composition, An_{88}-An_{90} (Table 4-5) and are typically surrounded by a thin rim of more albitic plagioclase, An_{60} (Plate 4-2B, Table 4-5). Plagioclase microphenocrysts have a composition of An_{41}-An_{34} (Table 4-5). Compositional variation is depicted in Fig. 4-4B and individual analyses are presented in microfiche Tables F4-5 and F4-6. Some zoned clinopyroxene phenocrysts occur in subophitic relationship with plagioclase and have a range in composition from $Wo_{43}En_{50}Fs_7$ to $Wo_{36}En_{43}Fs_{22}$ (Table 4-5). Microphenocrysts are somewhat more Fe-rich (Table 4-5). Clinopyroxene compositional variation is presented in

T A B L E 4-5

ISLAS ORCADAS F.Z: SELECTED MINERAL ANALYSES. PORPH. PLAG - PYX BASALTS

	1	2	3	4	5	6	7	8	9	10
SIO2	45.38	45.49	52.17	58.70	53.19	50.76	49.87	51.25	47.47	63.84
TIO2	ND	ND	.07	.09	.38	.99	1.24	.72	2.34	-
AL2O3	35.54	35.58	30.50	26.03	2.27	2.02	3.82	2.20	4.01	18.96
CR2O3	-	-	-	-	.32	.02	.02	.09	.12	-
FEO	.31	.30	.73	.72	4.77	13.36	10.75	9.76	14.79	.08
MNO	-	-	-	-	.11	.31	.23	.30	.39	-
MGO	.26	.29	.21	.08	18.26	14.78	15.55	15.89	12.00	ND
CAO	18.12	17.85	12.33	7.19	20.90	17.27	18.10	19.45	18.28	.04
NA2O	1.16	1.23	4.34	7.62	.23	.32	.38	.45	.49	.10
K2O	.02	.02	.12	.30	-	-	-	-	-	16.40
TOTAL	100.80	100.77	100.47	100.73	100.43	99.83	99.96	100.11	99.89	99.43

* * ATOMIC PROPORTIONS BASED ON SELECTED NO. OF OXYGENS * *

OXYGEN	8	8	8	8	6	6	6	6	6	8
SI	2.077	2.081	2.361	2.615	1.931	1.917	1.864	1.910	1.822	2.971
ALIV	1.917	1.918	1.627	1.367	.069	.083	.136	.090	.178	1.040
ALVI	-	-	-	-	.028	.007	.033	.007	.003	-
TI	-	-	.002	.003	.010	.028	.035	.020	.068	-
CR	-	-	-	-	.009	.001	.001	.003	.004	-
FE2+	.012	.011	.028	.027	.145	.422	.336	.304	.475	.003
MN	-	-	-	-	.003	.010	.007	.009	.013	-
MG	.018	.020	.014	.005	.988	.832	.866	.883	.686	-
CA	.889	.875	.598	.343	.813	.699	.725	.777	.752	.002
NA	.103	.109	.381	.658	.016	.023	.028	.033	.036	.009
K	.001	.001	.007	.017	-	-	-	-	-	.974
SUM	5.016	5.015	5.017	5.036	4.013	4.021	4.030	4.036	4.036	5.000
	AN 89.51	AN 88.81	AN 60.66	AN 33.70	WO 41.78	WO 35.79	WO 37.62	WO 39.56	WO 39.30	AN .20
	AB 10.37	AB 11.07	AB 38.64	AB 64.63	EN 50.77	EN 42.60	EN 44.95	EN 44.95	EN 35.88	AB .92
	OR .12	OR .12	OR .70	OR 1.67	FS 7.44	FS 21.61	FS 17.44	FS 15.49	FS 24.82	OR 98.88

* * * S A M P L E D I R E C T O R Y * * *

ANALYSIS NO.	DESCRIPTION
1	PLAGIOCLASE PHENO (CORE, I062-51)
2	PLAGIOCLASE PHENO (NEAR RIM, I062-51)
3	PLAGIOCLASE PHENO (EXTREME RIM, I062-51)
4	PLAGIOCLASE MICROPHENO (I062-51)
5	CPX PHENO (CORE, I063-2)
6	CPX PHENO (RIM, I063-2)
7	CPX PHENO (I063-2)
8	CPX PHENO (I062-51)
9	CPX MICROPHENO (I062-51)
10	K-FSP IN CPX PHENO (I063-2)

** ND = NOT DETECTED **

Fig. 4-6B, and individual analyses are presented in microfiche Tables F4-5 and F4-6. Sample I063-2 shows evidence of extensive alteration with the majority of plagioclase, including that ophitically enclosed within pyroxene (Plates 4-2C and 4-2D), being replaced by K-feldspar (Table 4-5). Fodor et al. (1978) and Mathews (1971) have reported similar occurrences of K-feldspar in ocean floor basalts from the Rio Grande Rise and the Swallow Bank (an abyssal hill in the NE Atlantic) respectively. K-feldspar replacement of plagioclase is also extremely common in many of the samples from the Conrad fracture zone (see Section 4.1). Additional K-feldspar analyses are presented in microfiche Table F4-6.

The even grained non-porphyritic variety comprises small (0.5-1.0 mm) zoned plagioclase phenocrysts (An_{83}-An_{61}) in subophitic relationships with zoned clinopyroxene (Plate 4-2E). Rare large plagioclase phenocrysts occur in some samples (I062-31, I062-42B). Plagioclase and clinopyroxene commonly occur in 'rosette'-type aggregates (Plate 4-2F) of elongate plagioclase laths intergrown with smaller anhedral clinopyroxene grains. Clinopyroxene phenocrysts range in composition from $Wo_{43}En_{49}Fs_{8}$ to $Wo_{41}En_{37}Fs_{22}$ (Fig. 4-6C) with compositional zoning of up to 4 mole % ferrosilite. Microphenocryst compositions are typically $Wo_{38}En_{44}Fs_{19}$ to $Wo_{40}En_{37}Fs_{23}$. Plagioclase phenocrysts range in composition from An_{85} to An_{53} (Fig. 4-4C), with microphenocrysts being slightly less calcic, An_{52}-An_{46}. Representative mineral analyses are presented in Table 4-6 and individual analyses in microfiche Tables F4-7 to F4-11. The matrix comprises sheaves of plagioclase and clinopyroxene in an arborescent texture with abundant dendritic titanomagnetite. Segregation vesicles (Smith, 1967) are common and are typically filled with Fe-rich magmatic residue (Plate 4-2G).

In primitive basalts (i.e. Mg-number >0.68), spinel compositions are potentially informative with respect to the earliest stages of magmatic crystallisation (e.g. Sigurdsson and Schilling, 1976; this work, Chapter III), while clinopyroxene is potentially useful with respect to the middle and late stages of crystallisation (La Bas, 1962; Nisbet and Pearce, 1977; Schweitzer et al., 1978, 1979; Coish and Taylor, 1979). Pyroxenes are especially useful for indicating the alkaline or tholeiitic affinities of a magma from which they crystallised (Schweitzer et al., 1978, 1979; La Bas, 1962; Nisbet and Pearce, 1977). Schweitzer et al. (op. cit.) have noted, for example, that alkalic pyroxenes are depleted in Cr_2O_3 and enriched in TiO_2 and Na_2O relative to tholeiitic pyroxenes. Pyroxenes from the IOFZ show a wide range in composition but have a tendency to be slightly more alkaline in nature (i.e. have higher TiO_2 and Na_2O contents) than those from typical abyssal tholeiites or those from the Conrad fracture zone. The slight enrichment in Na relative to 'tholeiitic' pyroxenes is shown in Fig. 4-7A, where most IOFZ pyroxenes fall within the 'alkali' pyroxene field. The divisions in Fig. 4-7A have been estimated by the writer from the distribution given by Schweitzer et al. (1979).

The close correlation between Na, Ti and Al^{IV} in the IOFZ pyroxenes is shown in Fig. 4-8. The correlation coefficients for the trends shown in Fig. 4-8 range from 0.806 (Na vs Ti) to 0.947 (Al^{IV} vs Ti), indicating the close association of these elements in the pyroxene structure. The well known positive correlation between Ti and Al (Kushiro et al., 1970; La Bas, 1962; Ross et al., 1970; Schweitzer et al., 1978, 1979) is clearly shown by the IOFZ pyroxenes and relates to the substitution of Al^{IV} for Si in the tetrahedral site coupled with the

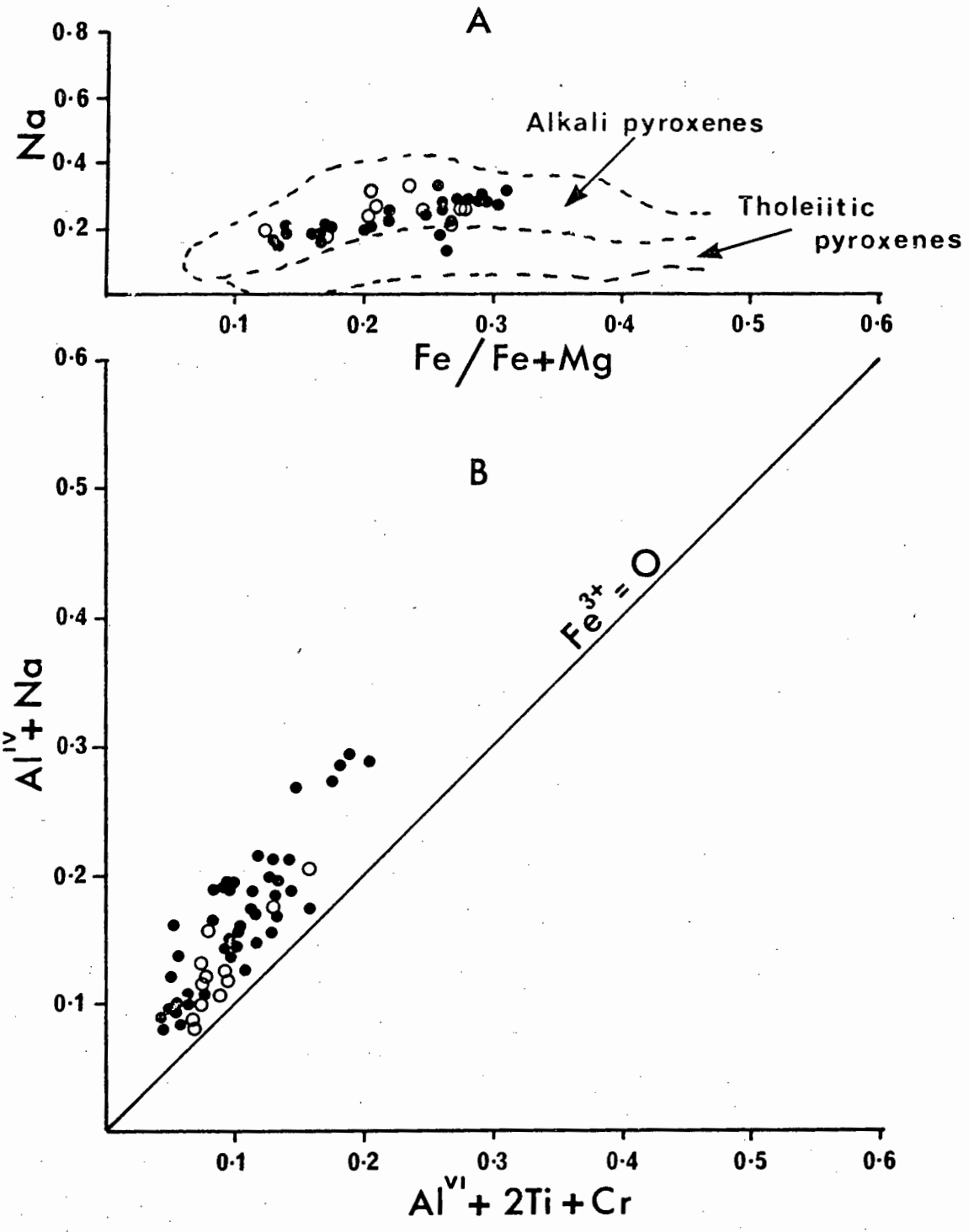

Fig. 4-7: A. Plot of Na against Fe/Fe+Mg ratio for IOFZ pyroxenes (units are atomic proportions calculated on the basis of 6 oxygens). Designated fields were taken from Schweitzer et al. (1979).

B. Plot of charge deficiencies (Y-axis) versus charge excess (X-axis) for IOFZ pyroxenes. Units are cations per 6 oxygens. Open symbols indicate pyroxenes from olivine bearing basalt I062-42A.

PLATE 4-2

A: Photomicrograph of porphyritic dredge-13 basalt I062-51 showing large plagioclase phenocrysts set in a crystalline matrix. Crossed polars.

B: Plagioclase glomerocryst in I062-51 containing melt inclusions and surrounded by a distinct rim with a more albitic composition. Crossed polars.

C: Clinopyroxene phenocryst in dredge-14 basalt I063-2, subophitically enclosing plagioclase laths which have been totally replaced by K-feldspar.

D: Large plagioclase phenocryst in I063-2 which has been totally replaced by K-feldspar and albite.

E: Photomicrograph of non-porphyritic plagioclase-pyroxene basalt I062-12.

F: 'Rosette' of intergrown plagioclase laths and anhedral clinopyroxene in I062-12.

G: Partially filled segregation vesicle in I062-15. Note the tangentially arranged plagioclase microlites.

PLATE 4-2

A

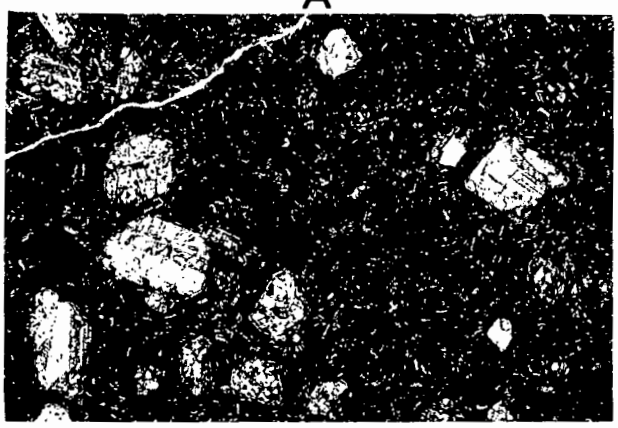

7mm

B

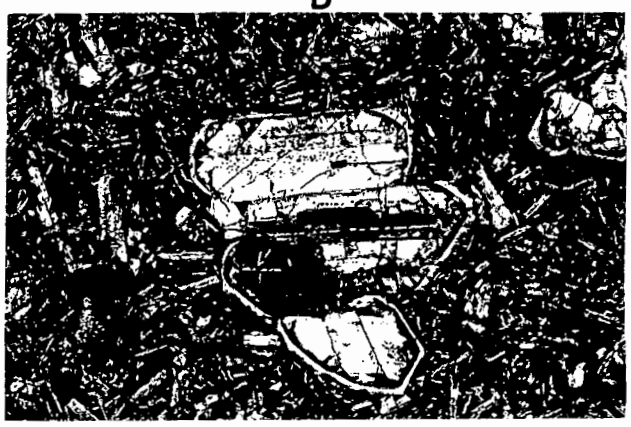

2 mm

C

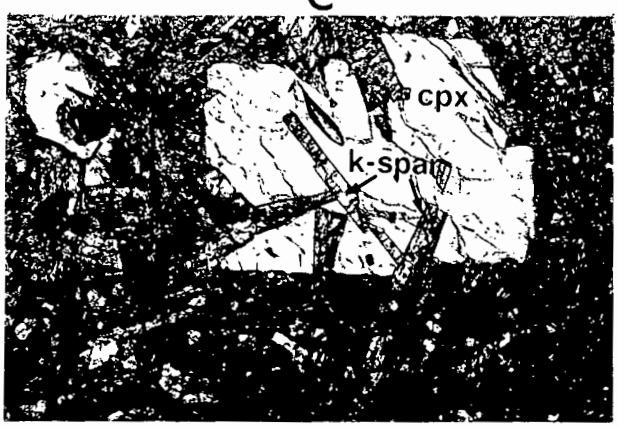

1·5mm

D

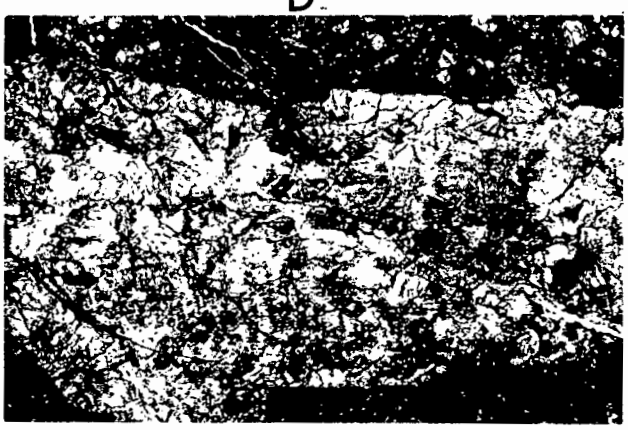

1·5mm

E

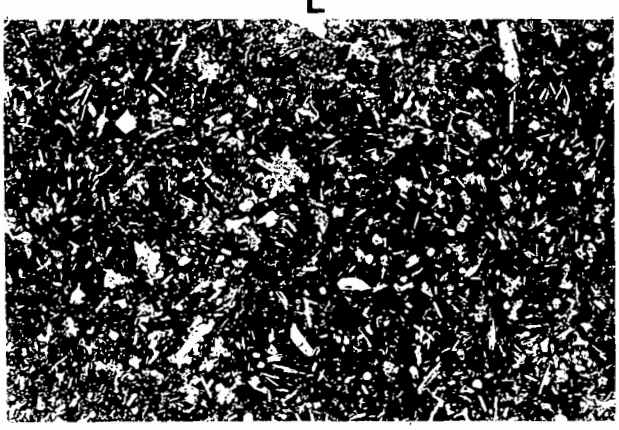

6·5mm

F

0·9mm

G

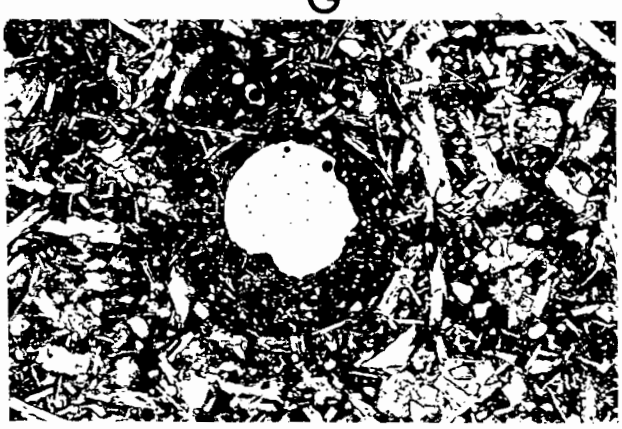

1·3mm

substitution of Ti for Mg in the octahedral M1 site (Schweitzer et al., 1978, 1979). Substitutional couples involving Na-Ti and Na-Al^{IV} (either directly or indirectly) are also indicated in the IOFZ pyroxenes (Fig. 4-8). Ti, Na and Al^{IV} also show extremely good negative correlations with Mg in the IOFZ pyroxenes (Fig. 4-9), with correlation coefficients of -0.937, -0.853 and -0.872 respectively. Schweitzer et al. (1979) have noted that common substitutions in ocean floor pyroxenes are: Al for Si in the tetrahedral site coupled with Ti or Fe^{3+} for Mg or Fe^{2+} respectively in the octahedral M1 site. The preference of Ti and apparently Na for the Mg-site rather than the Fe^{2+}-site is indicated by the significantly better correlation coefficients between Ti, Na and Mg (-0.937 and -0.853 respectively), than those between Ti, Na and Fe (0.843 and 0.689 respectively). The good correlation between Al^{IV} and Mg (Fig. 4-9) is regarded as indirectly reflecting the correlation between Al^{IV} and Ti. The lesser degree of correlation of Ti and Na with Fe is possibly partly due to the fact that total Fe was plotted rather than Fe^{2+}. The occurrence of significant Fe^{3+} in the IOFZ pyroxenes is indicated by a plot of charge deficiencies (Al^{IV} + Na) versus charge excess (Al^{VI} + 2Ti + Cr) (Fig. 4-7B). The fact that the majority of IOFZ pyroxenes fall to the left of the 'charge balance' line (Fe^{3+} = 0) indicates that a significant portion of the Fe is present as Fe^{3+} (Schweitzer et al., 1979). The inherent errors in the estimation of the amount of Fe^{3+} in pyroxenes (e.g. Papike et al., 1974) makes it difficult to assess the correlation of Ti and Na with Fe^{2+} more rigorously.

La Bas (1962) suggested that the substitution of Al and Ti into the pyroxene structure may be used to characterise volcanic rocks. Fig. 4-10 shows a plot of Al^{IV} (x 50) vs TiO_2, and SiO_2 vs Al_2O_3 with the

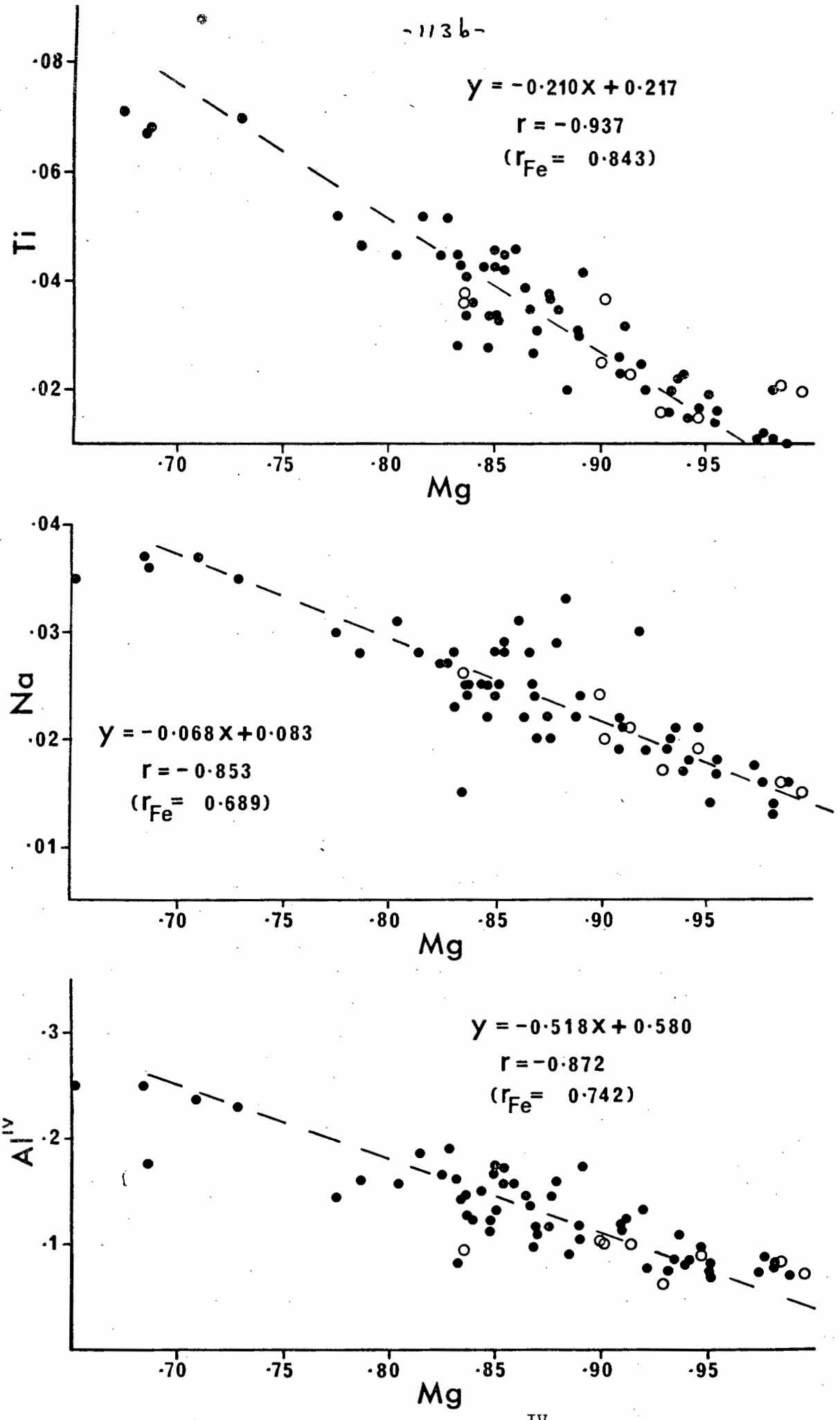

Fig. 4-9: Correlation of Ti, Na and Al^{IV} with Mg in IOFZ pyroxenes. Correlation coefficients for the variation with Fe are given for comparison. Symbols and units as in Fig. 4-8.

non-alkaline, alkaline and peralkaline fields as defined by La Bas (1962). The IOFZ pyroxenes straddle the alkaline/non-alkaline dividing line, again indicating their slightly alkaline nature relative to typical ocean floor tholeiites. Pyroxenes from the Conrad fracture zone are restricted to the non-alkaline field, while the pyroxenes from Bouvet Island hawaiites tend to be more alkaline (Fig. 4-10) and are relatively enriched in TiO_2 and depleted in SiO_2 for a given Al content. In this regard it should be noted that Coish and Taylor (1979) have stressed the effect of cooling rate on pyroxene composition and note that Ti and Al contents of pyroxenes increase with increased cooling rate. In an attempt to overcome this problem, only cores of phenocrysts have been plotted in Fig. 4-10. If all pyroxene compositions are plotted, the data points extend significantly further into the alkaline field.

Bryan (1974) has investigated the Fe-Mg relationships in plagioclase from ocean floor basalts. From considerations of the stoichiometry of the plagioclase samples that he studied, Bryan concluded that the substitution of divalent Fe and Mg is best described by a formula unit of the type $Ca(Mg,Fe)\ Si_3O_8$, i.e. Mg and Fe substitute for Al in the plagioclase structure. Similar conclusions have been reached by Neibuhr et al. (1973), Crawford (1973) and Wenke and Wilde (1973). The substitution of Fe and Mg is reportedly favoured by decreasing temperatures (Bryan, 1974).

The variation in Fe and Mg (calculated on the basis of 8 oxygens) with An content in plagioclase from the IOFZ is shown in Fig. 4-11. Though there is considerable scatter in the data, there is a definite trend of increasing Fe and decreasing Mg (and consequently increasing Fe/Mg ratio) with decreasing An content. The Fe/Mg ratio in plagioclase

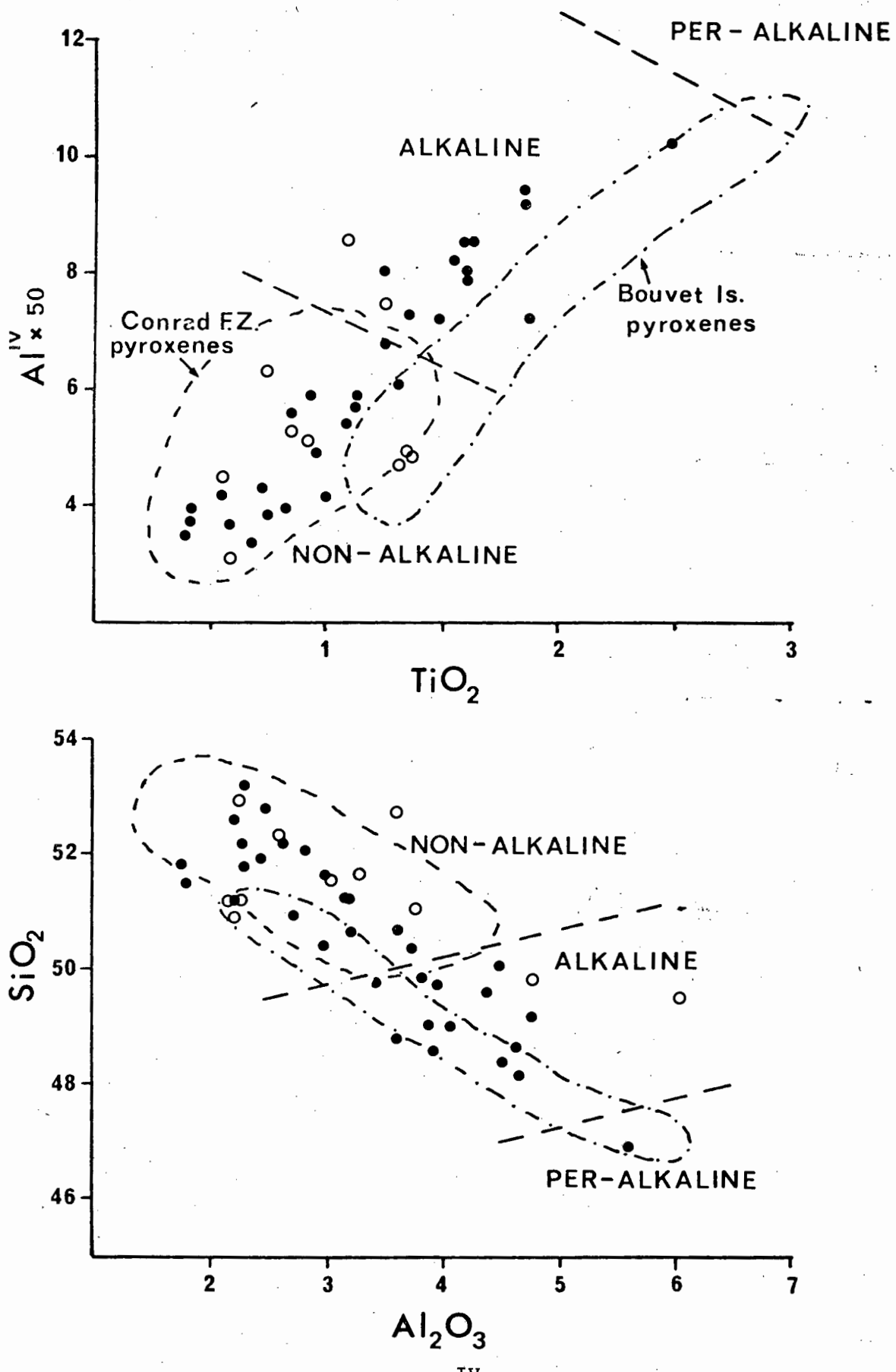

Fig. 4-10: Variation of Al^{IV} and SiO_2 with TiO_2 and Al_2O_3 respectively in IOFZ pyroxenes. Non-alkaline, alkaline and per-alkaline fields are taken from la Bas (1962). Compositional fields of Conrad F.Z. and Bouvet Island pyroxenes are shown for comparison. Symbols as in Fig. 4-8.

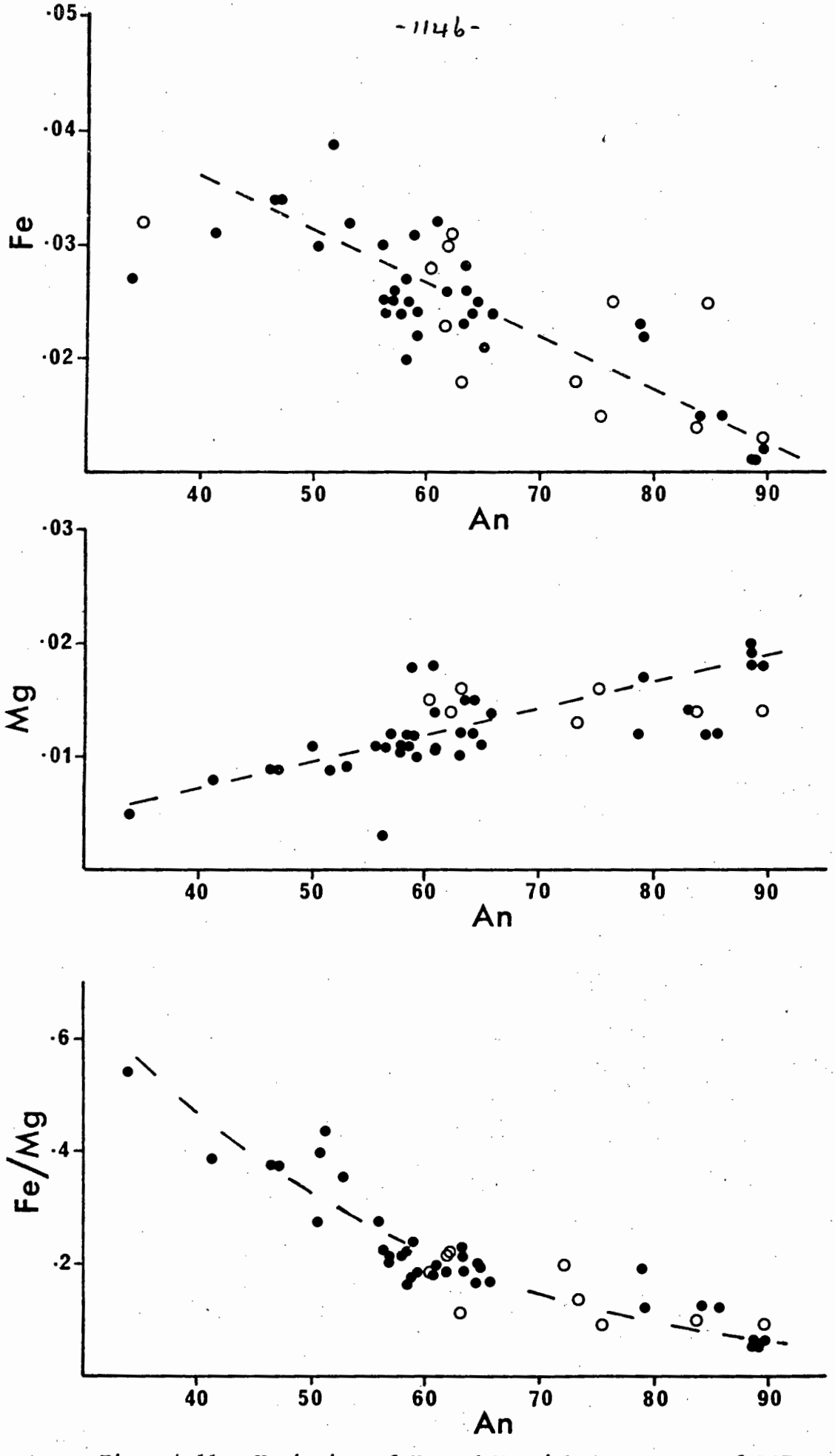

Fig. 4-11: Variation of Fe and Mg with An content of IOFZ plagioclase. Symbols as in Fig. 4-8, units are atomic proportions on the basis of 8 oxygens.

is generally regarded as reflecting the Fe/Mg ratio of the magma at the time of crystallisation, an interpretation consistent with the observed increasing ratio with increasing albite content in the IOFZ plagioclase (Fig. 4-11). In addition it is interesting to note that zoned plagioclase shows a far greater variation in Fe than in Mg. To investigate the site occupancy of Fe and Mg in the IOFZ plagioclase, the approach used by Bryan (1974) has been adopted and is outlined below.

A variety of substitutions can balance charges in the plagioclase structure. For the albite end-member the common substitution is of the type $R^{+}R^{3+}Si_3O_8$ (or $R^{2+}R^{2+}Si_3O_8$) and in the anorthite end-member charges are balanced by a substitution of the type $R^{2+}(R^{3+})_2Si_2O_8$.

If all Ca is combined as formula units of the anorthite type, the following two expressions will be fulfilled:

$$Ca = Al - 1.0 \quad \text{and} \quad Ca = -1.0Si + 3.0.$$

Substitution of Fe and/or Mg can theoretically occur for either Ca, in an anorthite-type molecule, resulting in the following relations:

$$Ca+Mg+Fe = Al - 1.0 \quad \text{and} \quad Ca+Mg+Fe = -1.0Si + 3.0$$

or for Al, in an albite-type molecule, where:

$$Ca = (Al+2Fe+2Mg) - 1 \quad \text{and} \quad Ca = -1.0(Si-Fe-Mg) + 3.0.$$

(Though only one divalent ion is required to balance Ca in an albite-type substitution, the amounts of Fe and Mg must be doubled to satisfy the expected relation for pure anorthite-albite mixtures.)

Utilising the above relations, Bryan (1974) found that a plot of Ca vs Al showed an excess of Ca over Al, which increased in the less calcic feldspars. An excess of Ca over Si was also indicated. From considerations of various possible substitutions, Bryan (1974) concluded that the data were best satisfied by the substitution of Fe and Mg for

Al in an albite-type formula unit, i.e. according to the relations:

$$Ca = (Al+2Mg+2Fe) - 1.0 \quad \text{and} \quad Ca = -1.0(Si-Fe-Mg) + 3.0.$$

Manipulation of the IOFZ plagioclase data in a similar fashion reveals additional possible Fe, Mg substitutions. Figs. 4-12A and 4-12B show the variation of Ca with Al and Si respectively in IOFZ plagioclase. Analagous to the findings of Bryan (1974) Ca shows a slight excess over Al (specifically at low Ca contents), but contrary to Bryan's findings, Si is slightly deficient relative to Ca (Fig. 4-12B). Assumption that all Fe (as divalent Fe) and Mg substitutes for Al in an albite-type formula unit, as suggested by Bryan (1974), results in an even greater discrepancy between the calculated regression lines and the expected relations (Figs. 4-12C and 4-12D). If all Fe is regarded as being trivalent, the discrepancy is slightly reduced, but is still significant. Of the various other possible substitutions, that which was found to satisfy the data best was the substitution of Mg for Ca in an anorthite-type formula unit, coupled with the substitution of Fe for Al in an albite-type formula unit. In Figs. 4-12E and 4-12F it is assumed that all Fe is divalent and substitutes for Al, with Mg substituting for Ca. The calculated regression equations are very close to the ideal relation and are as follows:

$$Ca + Mg = 1.002(Al+2Fe) - 1.018$$

and

$$Ca + Mg = -1.02(Si-Fe) + 3.028.$$

An even closer agreement is obtained between the calculated regression equations and the expected trends if some Fe is assumed to substitute directly for Al as trivalent Fe. Figs. 4-12G and 4-12H show the close relation between the expected trends and the calculated regression lines assuming that half the Fe is present as Fe^{3+}; the regression equations

Fig. 4-12: Substitutional relationships of Fe and Mg in IOFZ plagioclase. Units are cations per 8 oxygens. Solid lines represent the predicted relations for pure albite-anorthite mixtures; dashed lines represent linear regression lines for data set. The slopes, intercepts and correlation coefficients are given for the regression lines. See text for further discussion.

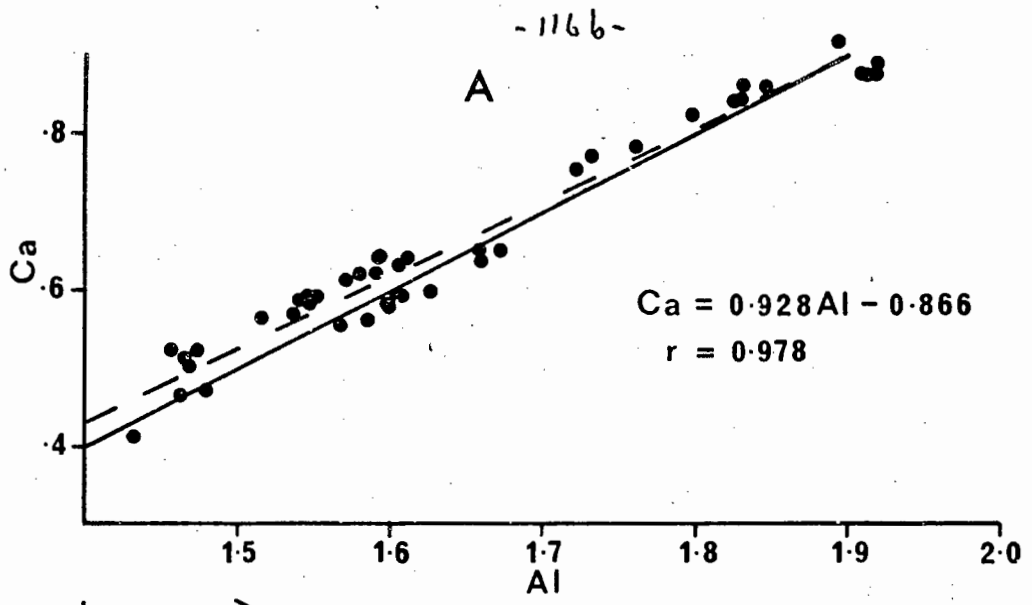
A
Ca = 0·928Al − 0·866
r = 0·978
Ca
·8
·6
·4
1·5
1·6
1·7
1·8
1·9
2·0
Al

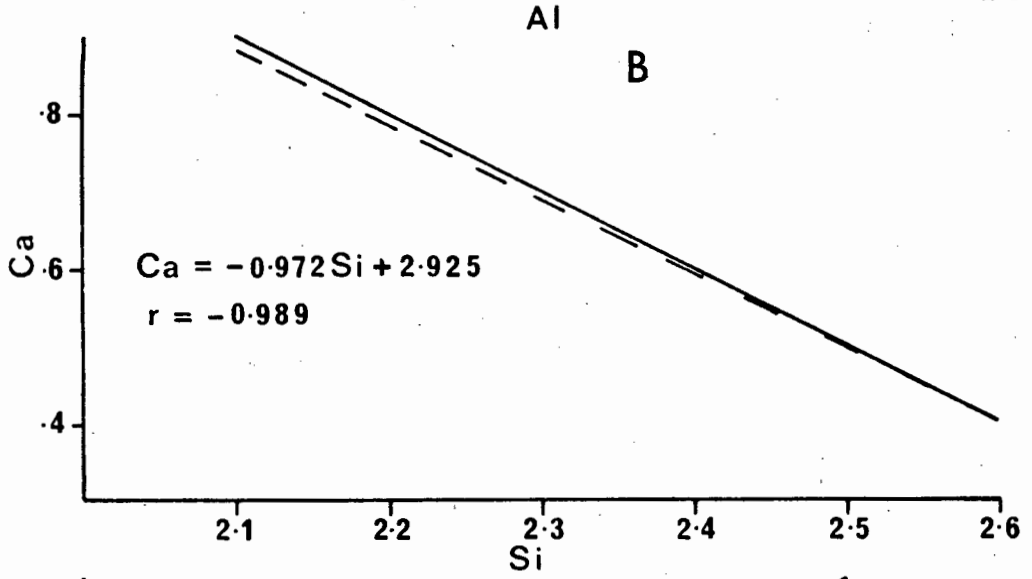
B
Ca = −0·972Si + 2·925
r = −0·989
Ca
·8
·6
·4
2·1
2·2
2·3
2·4
2·5
2·6
Si

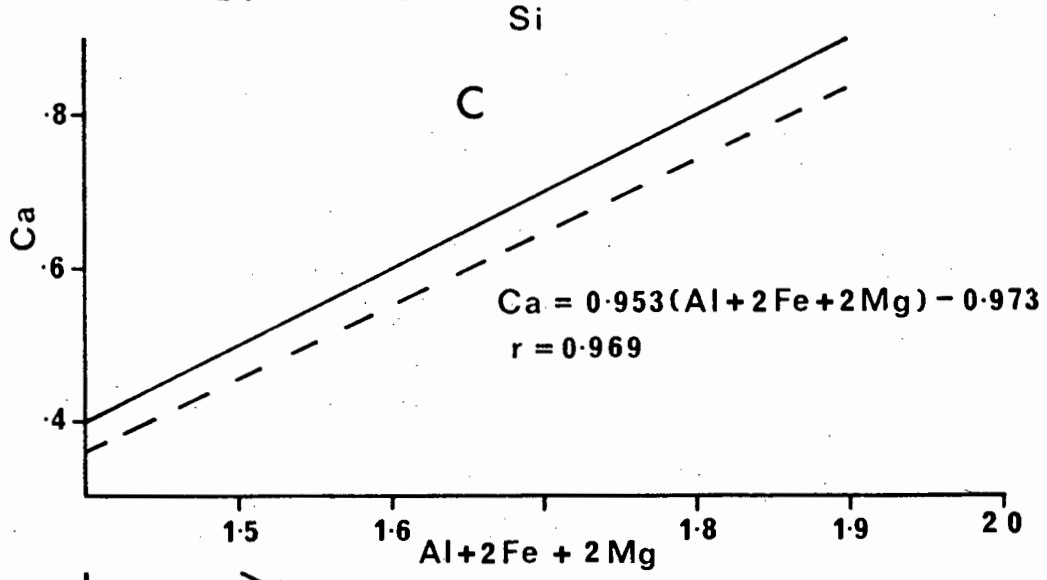
C
Ca = 0·953(Al + 2Fe + 2Mg) − 0·973
r = 0·969
Ca
·8
·6
·4
1·5
1·6
1·8
1·9
2 0
Al + 2Fe + 2Mg

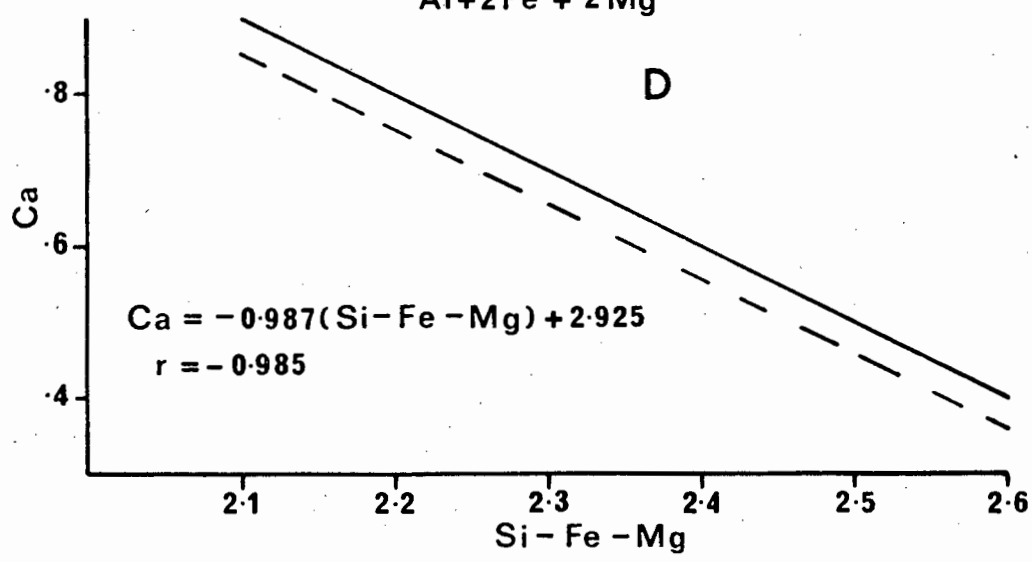
D
Ca = −0·987(Si − Fe − Mg) + 2·925
r = −0·985
Ca
·8
·6
·4
2·1
2·2
2·3
2·4
2·5
2·6
Si − Fe − Mg

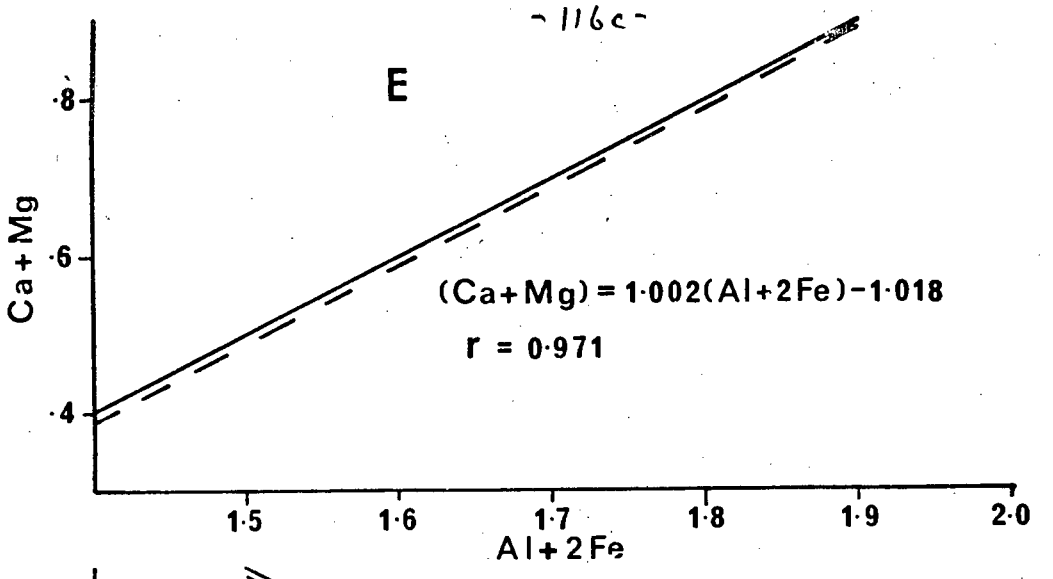
E
(Ca+Mg) = 1·002(Al+2Fe)−1·018
r = 0·971
Ca+Mg
·8
·6
·4
1·5
1·6
1·7
1·8
1·9
2·0
Al+2Fe

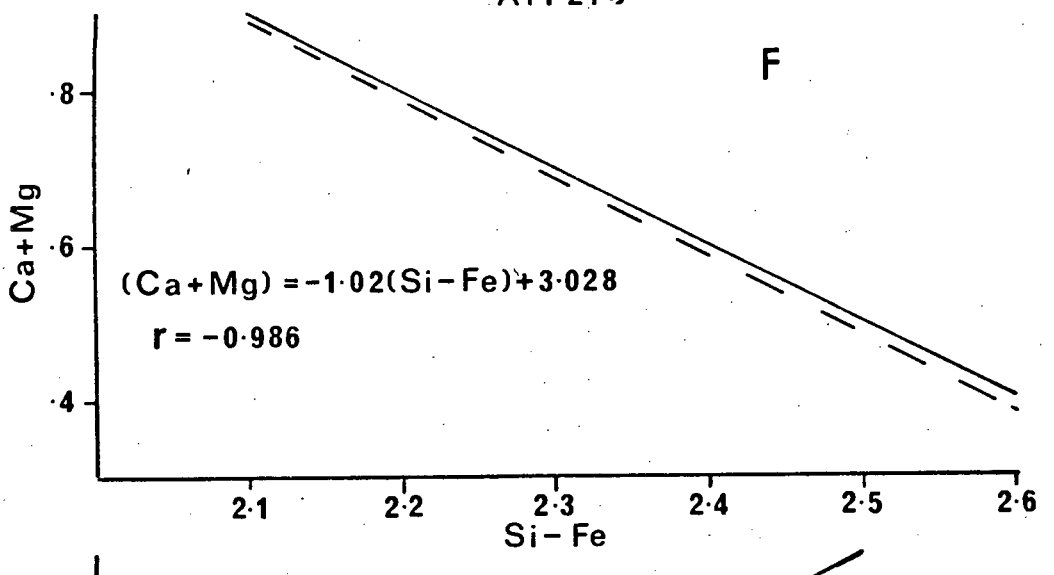
F
(Ca+Mg) = −1·02(Si−Fe)+3·028
r = −0·986
Ca+Mg
·8
·6
·4
2·1
2·2
2·3
2·4
2·5
2·6
Si−Fe

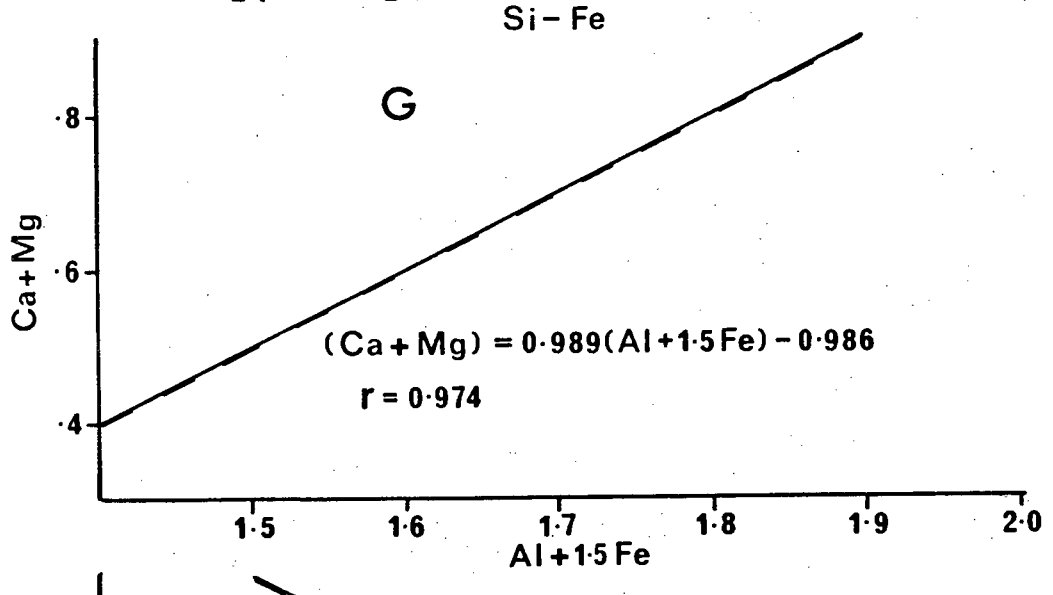
G
(Ca+Mg) = 0·989(Al+1·5Fe) − 0·986
r = 0·974
Ca+Mg
·8
·6
·4
1·5
1·6
1·7
1·8
1·9
2·0
Al+1·5Fe

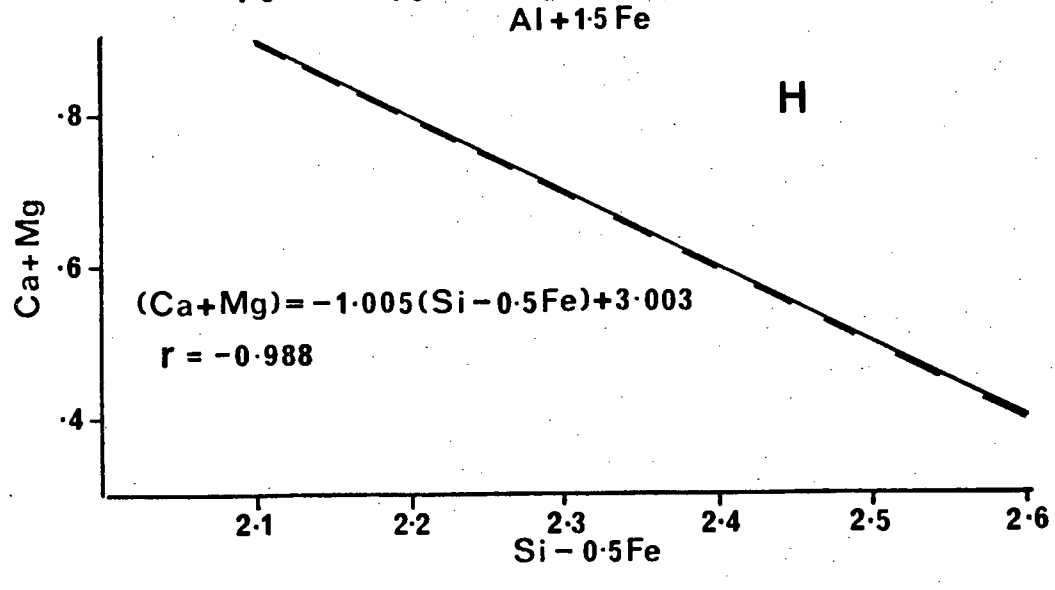
H
(Ca+Mg) = −1·005(Si−0·5Fe)+3·003
r = −0·988
Ca+Mg
·8
·6
·4
2·1
2·2
2·3
2·4
2·5
2·6
Si−0·5Fe

are:

$$Ca + Mg = 0.989(Al+1.5Fe) - 0.986$$

and $$Ca + Mg = -1.005(Si-0.5Fe) + 3.003.$$

The above clearly indicates that, at least in some instances, Fe and Mg substitute in different sites in the plagioclase structure. Due to the different crystallo-chemical effects of the tetrahedral (Al) site and 8-fold co-ordinated Ca site, the Fe/Mg ratio of plagioclase is therefore unlikely to reflect directly the Fe/Mg ratio of the magma from which it crystallised.

3.1.3 Alteration:

The detailed mineralogy of the alteration products of the IOFZ basalts has not been considered to fall within the scope of this study; however, a brief description of the degree of alteration is of relevance. Most samples from the IOFZ show varying degrees of alteration, ranging from the minor development of chlorite through to the extensive replacement of matrix and phenocryst phases by secondary hydrous minerals and K- and Na-feldspar.

The development of hydrous minerals in the Dredge 13 non-porphyritic plagioclase-pyroxene basalts and the plagioclase-phyric olivine basalts is restricted to the matrix with the plagioclase and clinopyroxene phenocrysts and microphenocrysts being generally free of alteration. Olivine phenocrysts in I062-42A and I062-49 are, however, characteristically surrounded by a brown alteration rim (bowlingite/iddingsite?). The Dredge 13 and 14 porphyritic plagioclase-pyroxene basalts are more extensively altered as indicated by the widespread development of chlorite, actinolite and other secondary hydrous minerals in the matrix and by the common replacement of plagioclase phenocrysts by chlorite

(I062-51, I063-2) and/or K- and Na-feldspar (I063-2).

The basalts from Dredge 11 on the southeast wall tend to be less altered than those recovered in Dredges 13 and 14 from the northwest wall, with alteration being restricted to the minor development of hydrous minerals in the matrix.

3.2 Whole Rock Chemistry

Major and fourteen trace element analyses, CIPW norms and selected element ratios for fifteen IOFZ samples and a single sample from the Southwest Indian Ocean Ridge crest at 11°E (I075-2) are presented in Table 4-7. CIPW norms were calculated after normalising the data to 100%, volatile-free, and assuming an Fe_2O_3/FeO ratio of 0.15.

Most of the samples show varying degrees of alteration when examined in thin section. This is also evident in the significant values measured for LOI (or H_2O^+) in most samples (Table 4-7). A number of recent studies (e.g. Hart et al., 1974; Andrews, 1977; Baragar et al., 1977; Humphris and Thompson, 1978a,b; Mottl and Holland, 1978) have been concerned with the chemical changes that take place during low temperature alteration of sea floor basalts. Major element variations commonly ascribed to sea floor weathering are: depletion in SiO_2, CaO, Al_2O_3 and Na_2O, and increase in MgO, Fe_2O_3, total Fe, K_2O and H_2O^+. TiO_2 and P_2O_5 are regarded as being immobile (Pearce and Cann, 1973; Hart et al., 1974). Of the analysed trace elements, Rb, Sr, Ba, Cu, Ni and Co show varying degrees of mobility during weathering, while Zr, Nb, Y, Ga, Cr, V and Zn are relatively unaffected by alteration processes (Pearce and Cann, 1973; Frey et al., 1974; Hart et al., 1974; Humphris and Thompson, 1978b). In the light of the relatively high volatile content (1.9-3.5%) of most of the IOFZ rocks, the following discussion below will emphasise the less mobile major and trace elements.

TABLE 4-7

TSLAS ORCADAS F.Z: WHOLE ROCK ANALYSES, CIPW NORMS & SELECTED RATIOS

	I060-1	I060-2	I060-3	I062-49	I062-42A	I062-51	I063-2	I062-5	I062-12	I062-15
SIO2	53.65	47.13	49.69	49.47	49.18	49.61	48.99	48.67	49.85	49.60
TIO2	1.17	2.11	3.18	1.49	1.60	1.61	1.86	2.41	2.55	2.35
AL203	19.59	14.66	15.51	16.35	16.60	16.34	14.42	14.06	14.66	14.09
FE203	.89	1.41	1.48	1.07	1.19	1.21	1.43	1.54	1.45	1.60
FEO	5.93	9.42	9.87	7.14	7.91	8.03	9.51	10.27	9.67	10.66
MNO	.13	.15	.19	.13	.19	.14	.18	.22	.20	.19
MGO	4.15	9.61	4.78	5.85	6.18	6.79	6.48	5.19	4.50	5.04
CAO	8.61	9.00	9.60	12.09	12.15	9.71	8.02	9.29	9.76	8.75
NA2O	4.51	3.03	3.76	2.73	2.70	2.77	2.62	2.90	3.41	3.40
K2O	.94	1.03	1.08	.50	.41	.74	2.73	.66	.76	.80
P2O5	.20	.39	.46	.19	.32	.20	.25	.34	.31	.31
H2O+	.52	1.17	.60	1.59	1.57	2.33	2.80	1.61	2.60	2.92
H2O-	.14	.80	.19	.96	.35	.51	.32	1.87	.51	.50
CO2	-	-	-	-	-	-	.12	.41	-	-
TOTAL	100.43	99.91	100.39	99.56	100.35	99.99	99.73	99.44	100.23	100.21
				* * * C.I.P.W. NORMS * * *						
Q	.00	.00	.00	.00	.00	.00	.00	.65	.00	.00
NE	.00	.75	.00	.00	.00	.00	.00	.00	.00	.00
OR	5.53	6.18	6.41	3.01	2.48	4.49	16.72	4.08	4.61	4.90
PL	68.80	48.63	54.26	56.09	55.65	54.97	43.21	50.18	52.82	51.22
DI	9.07	15.40	18.54	23.01	21.78	14.15	15.90	17.77	20.49	17.66
HY	7.81	.00	2.09	9.88	9.27	17.64	3.47	19.37	13.49	15.83
OL	4.83	21.92	9.38	3.04	5.21	3.31	14.29	.00	.71	2.64
MT	1.29	2.10	2.16	1.59	1.75	1.80	2.15	2.33	2.16	2.39
IL	2.23	4.08	6.06	2.92	3.10	3.15	3.67	4.79	4.99	4.62
AP	.48	.97	1.11	.44	.78	.50	.62	.85	.76	.76
				* * * TRACE ELEMENTS * * *						
ZR	159.	160.	234.	112.	113.	118.	136.	171.	182.	186.
NB	7.0	25.5	32.0	12.6	13.6	12.1	16.0	22.0	23.6	23.6
Y	19.7	22.2	32.9	24.8	34.8	27.3	32.3	40.2	41.6	44.7
RB	12.8	9.9	18.5	8.5	5.8	45.8	73.0	13.0	14.4	22.0
BA	156.	148.	207.	70.9	70.9	71.0	361.	99.6	282.	138.
SR	626.	546.	453.	221.	237.	181.	566.	208.	231.	191.
CO	27.3	60.2	39.6	43.4	43.2	43.1	47.0	45.7	42.5	41.0
CR	43.0	335.	38.8	215.	170.	78.8	65.1	52.1	45.6	65.2
NI	43.3	207.	36.8	67.1	73.8	43.8	44.9	28.3	24.4	37.3
V	207.	195.	265.	227.	242.	235.	269.	339.	345.	294.
ZN	68.7	96.8	108.	75.8	88.1	86.2	89.0	125.	126.	141.
CU	79.3	50.2	30.8	63.0	50.0	64.0	54.3	42.2	45.2	60.5
SC	24.4	24.6	27.5	31.9	36.0	34.4	31.7	34.9	36.3	34.6
TH	-	-	-	-	-	-	-	-	-	-
PB	-	-	-	-	-	-	-	-	-	-
GA	-	-	-	-	16.3	16.6	16.2	19.2	19.8	19.6

T A B L E 4-7 (CONTINUED)

ISLAS ORCADAS F.Z: WHOLE ROCK ANALYSES, CIPW NORMS & SELECTED RATIOS

	I060-1	I060-2	I060-3	I062-49	I062-42A	I062-51	I063-2	I062-5	I062-12	I062-15
					* * * ELEMENT RATIOS * * *					
ZR/NB	22.7	6.27	7.30	8.89	8.35	9.76	8.53	7.75	7.75	7.88
ZR/BA	1.02	1.08	1.13	1.58	1.60	1.66	.377	1.71	.648	1.35
ZR/Y	8.09	7.19	7.11	4.52	3.26	4.33	4.22	4.24	4.38	4.16
K/RB	610.	866.	486.	487.	590.	134.	311.	422.	438.	301.
K/BA	50.0	57.8	43.3	58.6	48.0	86.5	62.7	55.0	22.4	48.2
K/ZR	49.1	53.4	38.3	37.1	30.0	52.1	167.	32.1	34.6	35.8
Y/NB	2.81	.872	1.03	1.97	2.56	2.26	2.02	1.83	1.77	1.90
CA/Y	3.132+003	2.892+003	2.085+003	3.488+003	2.493+003	2.545+003	1.777+003	1.652+003	1.676+003	1.401+003
TI/ZR	44.1	79.1	81.5	79.8	84.6	81.8	81.9	84.7	83.8	75.9
TI/NB	1.003+003	496.	595.	709.	706.	799.	699.	656.	649.	598.
TI/Y	357.	569.	579.	361.	275.	354.	346.	359.	367.	316.
TI/P	8.04	7.43	9.50	10.8	6.87	11.1	10.2	9.74	11.3	10.4
CR/V	.208	1.72	.147	.949	.700	.335	.242	.154	.132	.222
NI/CO	1.58	3.44	.931	1.55	1.71	1.02	.956	.619	.575	.910
M.I.	62.2	53.0	70.4	58.4	59.6	57.6	62.8	69.5	71.2	70.9
MG#	.555	.645	.463	.594	.582	.601	.548	.474	.453	.457
D.I.	43.9	31.6	38.4	26.7	25.7	28.6	39.7	30.5	34.3	34.6

T A B L E 4-7 (CONTINUED)

ISLAS ORCADAS F.Z: WHOLE ROCK ANALYSES, CIPW NORMS & SELECTED RATIOS

	I062-30	I062-31	I062-42B	I067-1A	I063-3	I075-2
SIO2	49.51	48.59	50.25	50.34	53.99	50.18
TIO2	2.51	2.47	2.51	2.52	.85	2.21
AL2O3	14.71	14.06	15.02	14.78	18.75	14.96
FE2O3	1.47	1.60	1.37	1.48	1.08	1.76
FEO	9.79	10.63	9.12	9.84	7.19	8.82
MNO	.24	.27	.19	.21	.19	.18
MGO	5.05	5.15	4.64	4.89	2.87	5.41
CAO	9.90	9.46	9.99	9.69	7.26	10.06
NA2O	3.43	3.15	3.42	3.21	3.36	3.80
K2O	.68	.71	.68	.72	.32	.85
P2O5	.30	.34	.31	.30	.08	.35
H2O+	2.60	2.67	2.59	2.24	3.53	.92
H2O-	.39	.57	.42	-	.68	.17
CO2	-	-	-	-	-	-
TOTAL	100.58	99.67	100.51	100.22	100.15	99.67
				* * * C.I.P.W. NORMS * * *		
Q	.00	.00	.06	.35	8.89	.00
NE	.00	.00	.00	.00	.00	.00
OR	4.14	4.37	4.14	4.34	2.01	5.02
PL	53.00	50.59	53.93	51.90	66.24	53.41
DI	20.70	19.50	20.32	19.60	.31	21.76
HY	9.80	13.79	13.92	16.03	19.06	.94
OL	4.58	3.69	.00	.00	.00	10.42
MT	2.17	2.39	2.03	2.18	1.63	1.99
IL	4.88	4.86	4.88	4.87	1.68	4.20
AP	.73	.83	.76	.74	.20	.83
				* * * TRACE ELEMENTS * * *		
ZR	177.	176.	179.	172.	40.0	190.
NB	21.1	22.2	21.6	19.6	ND	24.0
Y	40.1	41.6	39.1	37.7	17.5	34.8
RB	13.3	15.4	9.2	15.0	5.3	16.5
BA	190.	95.9	286.	157.	82.1	167.
SR	226.	210.	229.	225.	184.	278.
CO	41.0	69.4	38.1	39.6	28.6	43.9
CR	65.1	44.8	49.5	57.0	33.4	68.9
NI	28.5	31.4	22.5	31.8	13.1	36.3
V	294.	343.	341.	358.	225.	284.
ZN	132.	126.	122.	125.	93.1	95.0
CU	52.2	44.6	44.6	54.9	87.8	61.3
SC	33.8	37.6	36.8	35.2	41.9	37.0
TH	-	-	-	-	-	-
PB	-	-	-	-	-	-
GA	19.3	19.5	19.6	-	-	19.6

** ND = NOT DETECTED **

T A B L E 4-7 (CONTINUED)

ISLAS ORCADAS F.Z: WHOLE ROCK ANALYSES, CIPW NORMS & SELECTED RATIOS

	I062-30	I062-31	I062-428	I067-1A	I063-3	I075-2
			* * * ELEMENT RATIOS * * *			
ZR/NB	8.38	7.93	8.27	8.77	-	7.95
ZR/BA	.933	1.84	.624	1.09	.488	1.14
ZR/Y	4.41	4.23	4.57	4.57	2.29	5.47
K/RB	424.	383.	611.	398.	504.	426.
K/BA	29.8	61.5	19.7	38.0	32.4	42.2
K/ZR	31.9	33.5	31.6	34.8	66.4	37.1
Y/NB	1.90	1.88	1.81	1.92	-	1.45
CA/Y	1.765+003	1.624+003	1.827+003	1.839+003	2.967+003	2.067+003
TI/ZR	85.0	84.1	84.2	87.8	127.	69.6
TI/NB	712.	667.	697.	770.	-	553.
TI/Y	375.	356.	385.	401.	291.	381.
TI/P	11.5	9.98	11.1	11.5	14.6	8.67
CR/V	.221	.131	.145	.159	.149	.242
NI/CO	.694	.453	.590	.804	.456	.827
M.I.	69.0	70.4	69.3	69.8	74.2	66.2
MG#	.479	.463	.476	.470	.416	.522
D.I.	33.8	32.0	33.9	32.3	40.7	37.2

3.2.1 Major Elements:

All but one sample (I060-2) from the IOFZ are hypersthene normative basalts, indicating their tholeiitic affinities. All but four basalts (I063-2, I062-42B, I062-1A and I063-3) are olivine normative, and of the four quartz normative samples, only I063-3 has significant normative quartz (8.9%, Table 4-7). Although sample I060-2 is nepheline normative (0.75% Ne) and can therefore be strictly classified as an alkali basalt (Yoder and Tilley, 1962), it is preferred not to distinguish this basalt specifically from the other IOFZ basalts which have a transitional to mildly alkaline chemistry. The single sample from the ridge crest at 11°E is olivine normative with very minor (0.94%) normative hypersthene. In terms of total normative pyroxene, plagioclase and olivine (Fig. 4-13), the majority of the IOFZ samples from Dredges 13 and 14 from the northwest wall (i.e. the plagioclase-pyroxene basalts and the two plagioclase-phyric olivine basalts I062-42A and I062-49) lie slightly to the plagioclase side of the inferred olivine-plagioclase cotectic of Shido et al. (1971). In contrast, the samples from Dredge 11 on the southeast wall show extreme scatter (Fig. 4-13). Basalt I060-2 is displaced, relative to the others, towards the olivine apex, in accord with its more primitive chemical composition, while the plagioclase-phyric olivine basalts I060-1 and I060-3 are displaced towards the plagioclase apex. The aphyric 11°E sample is similarly displaced towards plagioclase and away from the pyroxene field. Relative to the field of FAMOUS glasses (Bryan et al., 1976), the IOFZ basalts are displaced towards the plagioclase field, and the plagioclase-pyroxene basalts and Dredge 13 olivine basalts extend the range of off-ridge extrusives and intrusives (from Bryan et al., 1976) to olivine-poorer compositions (Fig. 4-13).

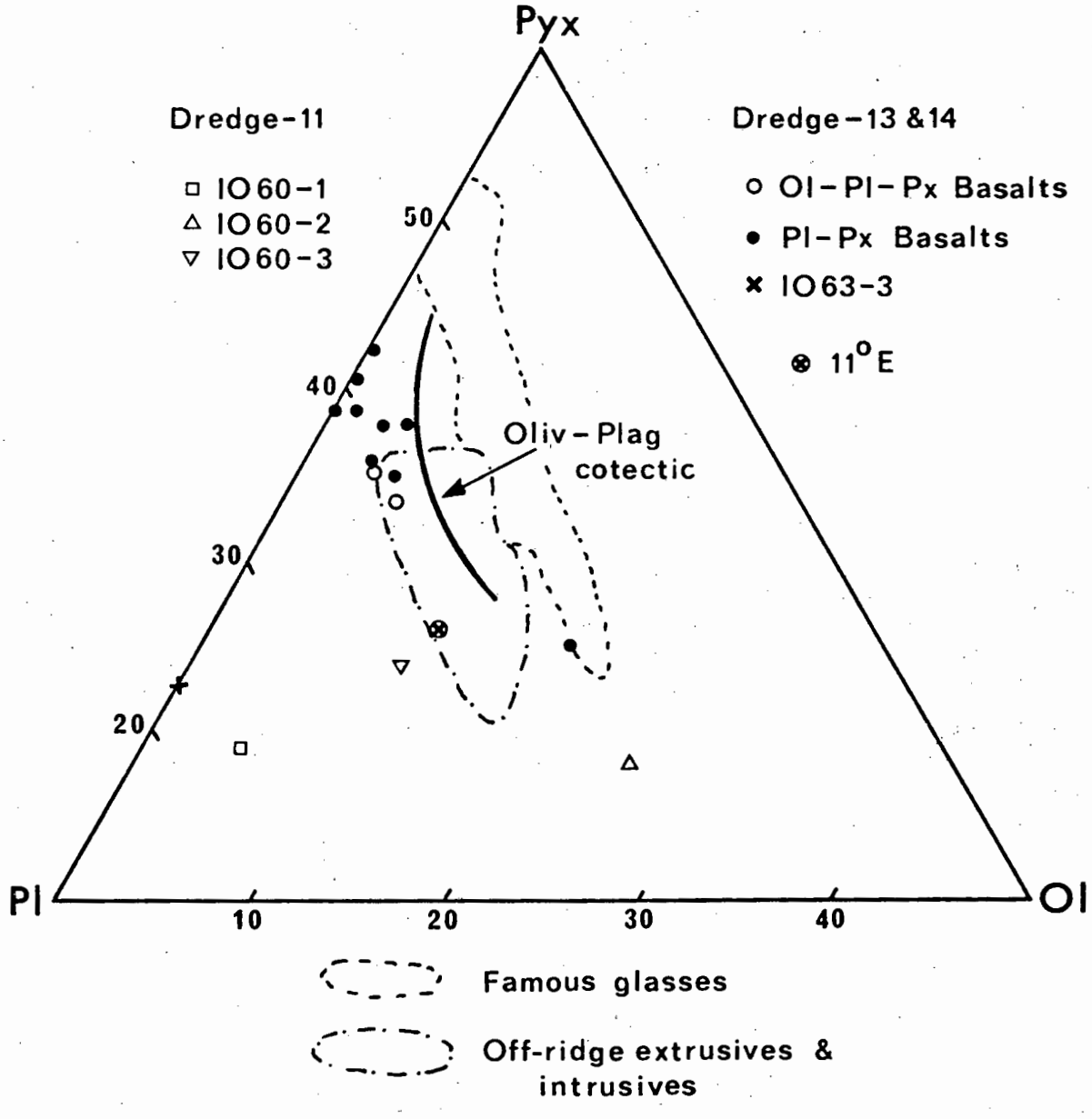

Fig. 4-13: Total normative pyroxene, plagioclase and olivine variation in IOFZ basalts and the single basalt from 11°E. The olivine-plagioclase cotectic is taken from Shido et al. (1971). Fields of FAMOUS glasses and off-ridge extrusives and intrusives are taken from Bryan et al. (1976).

The variation in total alkalis with respect to SiO_2 content is illustrated in Fig. 4-14. The Dredge 13 basalts are enriched in total alkalis relative to the Conrad fracture zone basalts (Section 4.2) and typical MORB (Dickey et al., 1977), and fall close to the field of Bouvet Island hawaiites (Verwoerd et al., 1974; this study, Chapter V). The displacement of plagioclase-pyroxene basalt I063-2 into the alkali field is due to the abundant secondary K-feldspar in this sample. Sample I063-3 from Dredge 14 has an unusually high SiO_2 content (56 wt.%, volatile-free) and extremely low MgO content (3.0 wt.%, Table 4-7), and in this respect differs from all other IOFZ basalts. The distinctive compositions of the Dredge 11 basalts are clearly evident in Fig. 4-14. The $11^{o}E$ sample lies on the Irvine and Baragar (1971) alkali basalt-tholeiite dividing line, and since the rock is relatively fresh, its alkali content is regarded as a true reflection of its primary composition.

The compositional variation in terms of an AFM diagram is shown in Fig. 4-15, together with designated fields for Atlantic fracture zone basalts, Atlantic rift valley volcanics and aseismic ridges (Hekinian and Thompson, 1976). The more iron-rich basalts from both walls of the fracture zone extend the total field of fracture zone basalts to more Mg-depleted compositions. Basalt I060-2 has the least evolved composition (in terms of the MgO/FeO* ratio) of the IOFZ basalts. The relative enrichment in alkalis in the highly altered I063-2 is evident: the apparent enrichment in alkalis in I060-1 is attributed to the highly plagioclase phyric nature of this sample. The $11^{o}E$ sample is poorer in MgO and richer in alkalis than typical Atlantic rift valley volcanics (Fig. 4-15).

In accord with previous studies on fracture zone basalts (e.g. Shibata and Fox, 1975; Hekinian and Thompson, 1976; Shibata et al., 1979a), the IOFZ basalts have an evolved major element chemistry relative to abyssal tholeiites. The most 'primitive' basalt recovered is the alkali basalt (I060-2) from Dredge 11 on the southeast wall, which has a Mg-number of 0.65, with an absolute MgO content of 9.8% (Table 4-7). All other samples are significantly more evolved, with Mg-numbers ranging down to 0.42 (Table 4-7) and with MgO contents of 7.0 to 2.9%. The most primitive basalts from Dredge 13 are the two olivine basalts and the porphyritic plagioclase-pyroxene basalt I062-51 (Mg-numbers = 0.58-0.60). Since all are highly plagioclase phyric, their absolute MgO contents have been diluted.

The evolved nature of the tholeiitic basalts is clearly illustrated by the high degree of enrichment attained by the incompatible major elements. TiO_2 concentrations range from 0.9 to 3.2% and P_2O_5 from 0.08 to 0.46%. K_2O contents are likewise high for abyssal tholeiites, but since K_2O is highly mobile and in view of the secondary alkali feldspar present in I063-2, little significance is attached to the observed variation. The FeO* and TiO_2-rich nature of the IOFZ basalts is illustrated in Fig. 4-16 in a plot of TiO_2 versus FeO*/MgO. The non-porphyritic plagioclase-pyroxene basalts from Dredge 13 all plot within the field of ferrotholeiites from the Ninetyeast Ridge (Frey et al., 1976). They do not however attain the extreme FeO*-, TiO_2-rich compositions of some of the Conrad fracture zone basalts (see Section 4.2). The olivine tholeiites and porphyritic plagioclase-pyroxene basalts have compositions similar to the more evolved FAMOUS glasses (Bryan et al., 1976). Basalt I063-3 is significantly depleted in TiO_2

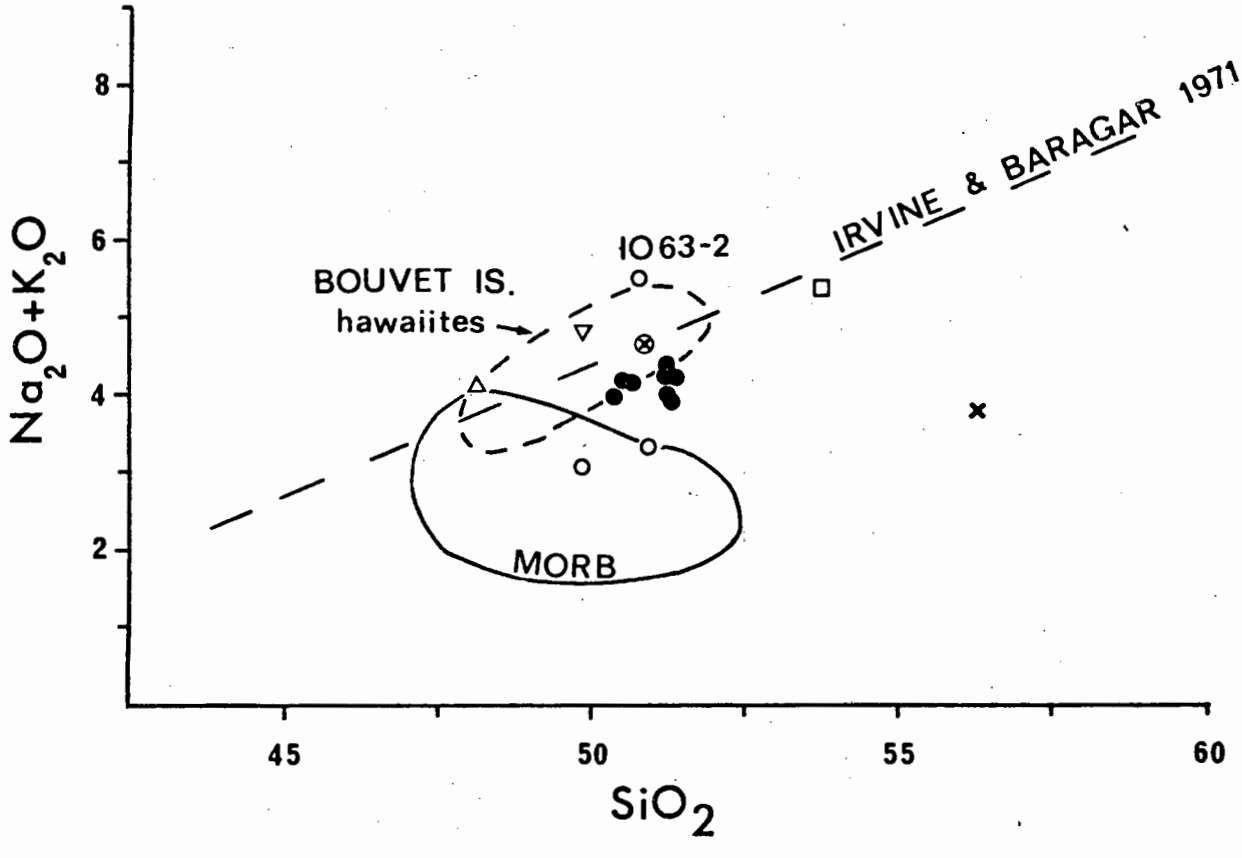

Fig. 4-14: Total alkalies - SiO_2 plot of IOFZ basalts and the 11°E basalt. Field of mid-ocean ridge basalt (MORB) is taken from Dickey et al. (1977), and the field of Bouvet Island hawaiites is shown for comparison. Symbols as in Fig. 4-13.

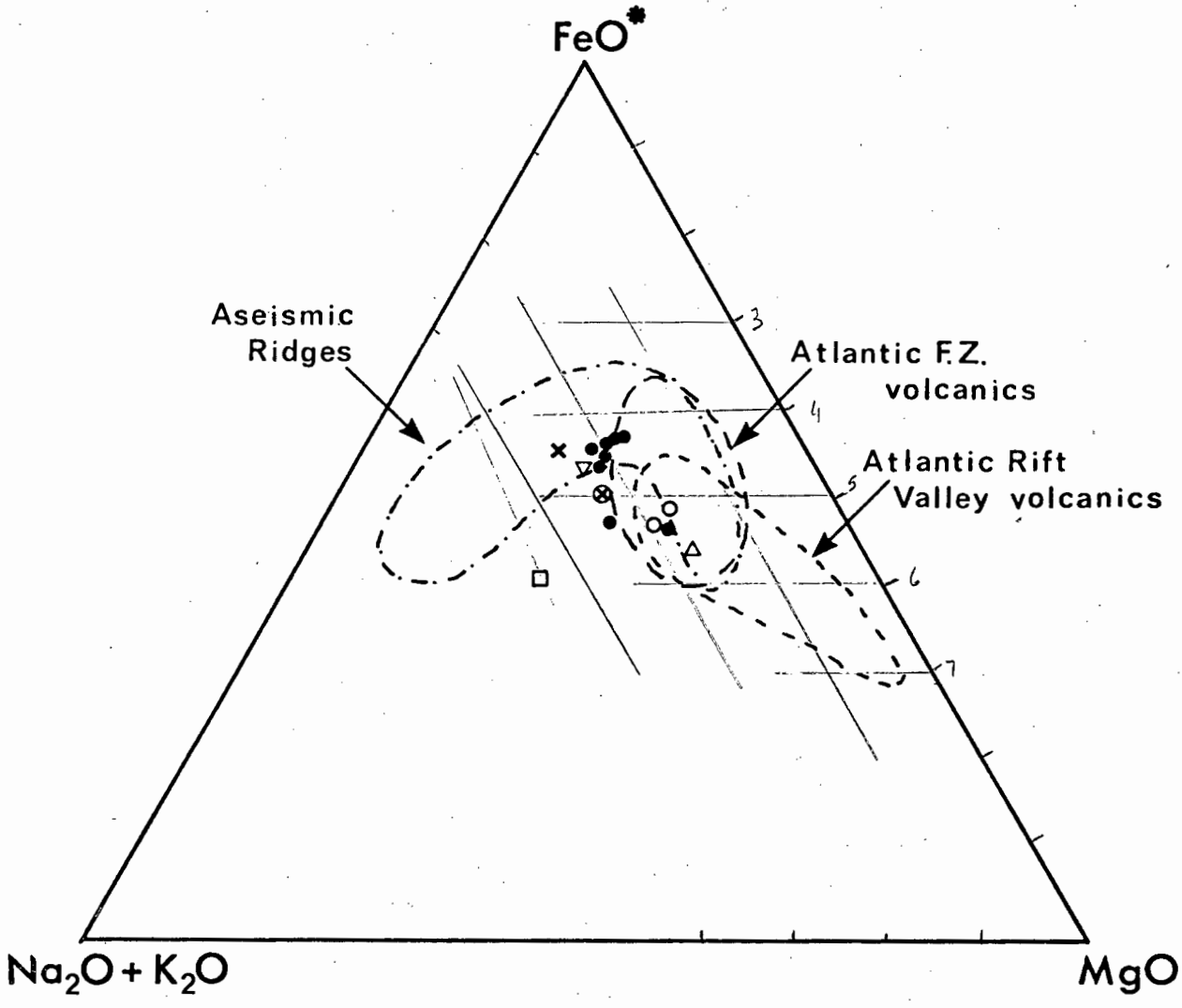

Fig. 4-15: A-F-M diagram showing the compositional variation of IOFZ basalts and the 11°E basalt. Compositional fields of asiesmic ridge, Atlantic fracture zone and Atlantic rift valley volcanics are taken from Hekinian and Thompson (1976). Symbols as in Fig. 4-13.

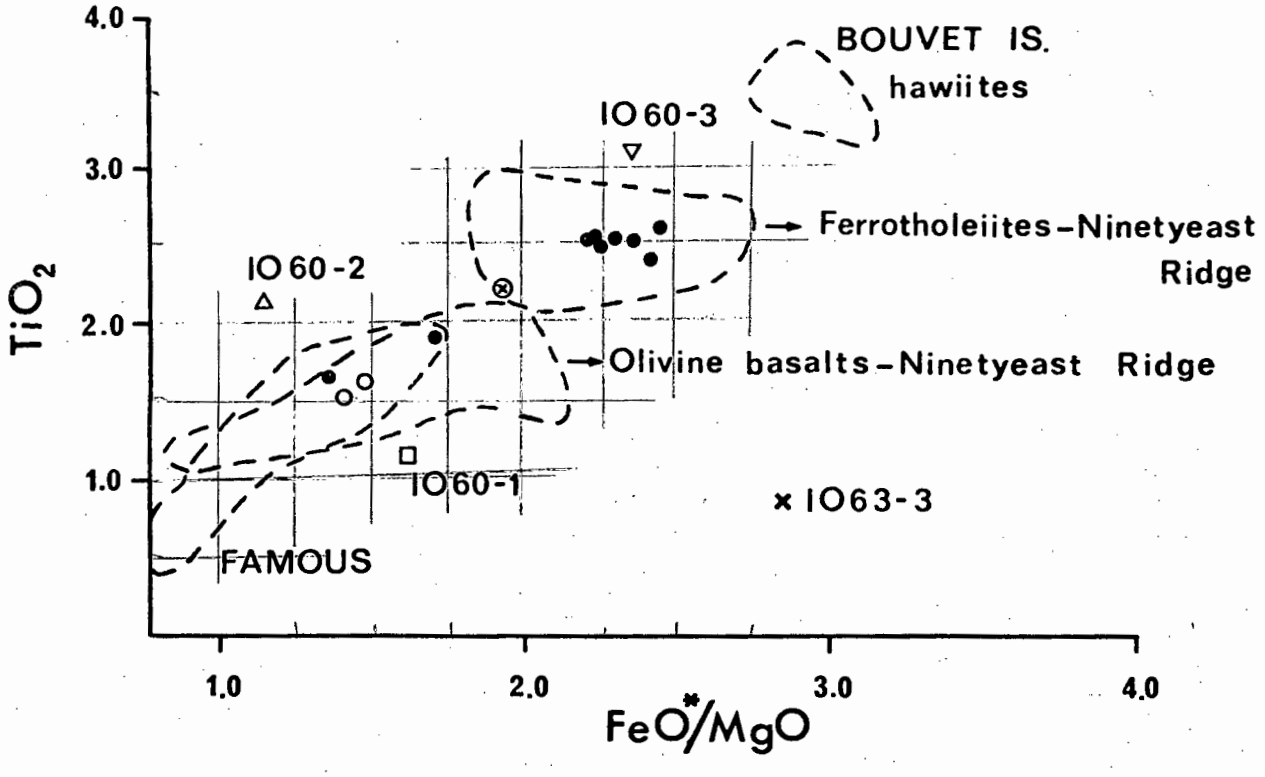

Fig. 4-16: Plot of TiO_2 versus FeO*/MgO for IOFZ and 11°E basalts. Compositional fields for Ninetyeast Ridge basalts were taken from Frey et al. (1976) and the field of FAMOUS glasses is taken from Bryan et al. (1976). The field of Bouvet Island hawaiites is shown for comparison. Symbols as in Fig. 4-13.

for its FeO*/MgO ratio. The Dredge 11 basalts show a range in composition in terms of TiO_2 and FeO*/MgO, with I060-3 being highly enriched in TiO_2 and basalt I060-2 relatively depleted in FeO* (Fig. 4-16). The 11°E basalt is also relatively FeO*- and TiO_2rich and falls within the field of the Ninetyeast Ridge ferrotholeiites.

The variation of some major elements with M.I. (mafic index = $FeO+Fe_2O_3/FeO+Fe_2O_3+MgO$) is shown in Fig. 4-17. Significant scatter is observed for the oxides CaO, Al_2O_3, Na_2O and K_2O with no systematic trends being defined. However, TiO_2 and P_2O_5 in Dredge 13 basalts do show a uniform enrichment with increasing M.I. The high P_2O_5 content of olivine basalt I062-42A is anomalous, especially in light of the fact that it has a nearly identical composition with respect to all other elements (majors and traces) to olivine basalt I062-49. Porphyritic plagioclase-pyroxene basalt I063-2 (Dredge 14) falls within the trends defined by the Dredge 13 basalts, but SiO_2-rich basalt I063-3 is significantly displaced. The Dredge 11 basalts are similarly displaced from these trends.

Since the mutual ratios of incompatible elements are largely unaffected by fractionation processes (e.g. Gast, 1968; Erlank and Kable, 1976), the covariance of such elements is useful in the investigation of the genetic relationships within a suite of samples. With respect to the observed phenocryst mineral assemblages in the IOFZ basalts, P_2O_5 and to a lesser extent TiO_2 are two such major elements. These two elements are plotted versus Zr (also an immobile incompatible element) in Fig. 4-18, where most samples define excellent correlations. In the plot of TiO_2 versus Zr, only basalt I060-1 is significantly displaced from the main trend, having a relatively low TiO_2

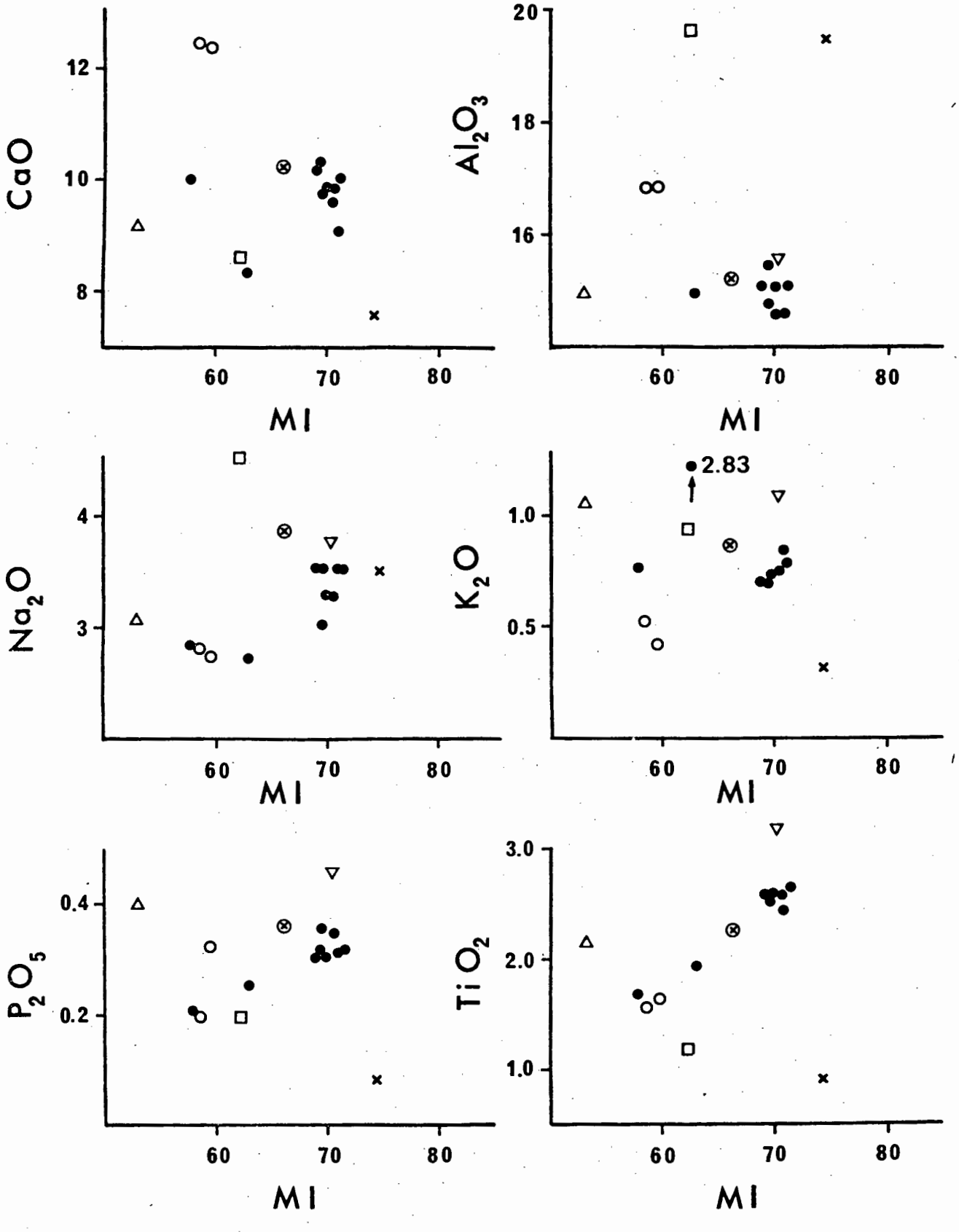

Fig. 4-17: Major element variation of the IOFZ basalts and the 11°E basalt with respect to M.I. as index of differentiation. Symbols as in Fig. 4-13.

content. The average Ti/Zr ratio of the IOFZ basalts (excluding I060-1) is 82.6 $\pm$ 3, which is significantly lower than typical MORB (Ti/Zr = 100-110; Pearce and Cann, 1973; Sun et al., 1979) but very similar to the Conrad fracture zone basalts and dolerites (Ti/Zr = 87.5). The Dredge 13 and 14 basalts similarly define a good correlation between P_2O_5 and Zr (Fig. 4-18), with an average P/Zr ratio of 7.9 $\pm$ 6. This ratio is somewhat higher than both MORB (P/Zr = 6.55; Sun and Nesbitt, 1977) and the Conrad fracture zone basalts and dolerites (P/Zr = 6.97) and more like that observed in Archean basalts (P/Zr = 7.2; Nesbitt and Sun, 1976). Although Dredge 11 basalt I060-3 has a similar P/Zr ratio to the Dredge 13 and 14 basalts, basalts I060-1 and I060-2 are clearly distinguished by their P/Zr ratios (Fig. 4-18). The very distinct P/Zr ratios of these latter two samples, both with respect to one another and to the main trend, clearly indicate that either P and Zr are not behaving as true incompatible elements, or that distinct source regions are involved in the production of the IOFZ basalts. It is interesting to note that the 11°E sample plots very close to the TiO_2-Zr and P_2O_5-Zr trends (Fig. 4-18) defined by Dredge 13 and 14 basalts, suggesting derivation from a source with similar ratios of these three elements.

In summary, the suite of samples from the IOFZ are dominantly tholeiitic basalts, though a single nepheline normative basalt was recovered. The basalts have a more evolved composition than normal MORB and tend towards a transitional or mildly alkaline chemical composition. The interelement variation of immobile elements suggests derivation of the Dredge 13 and 14 basalts from a relatively homogeneous source which is apparently distinct from that giving rise to the Dredge 11 basalts.

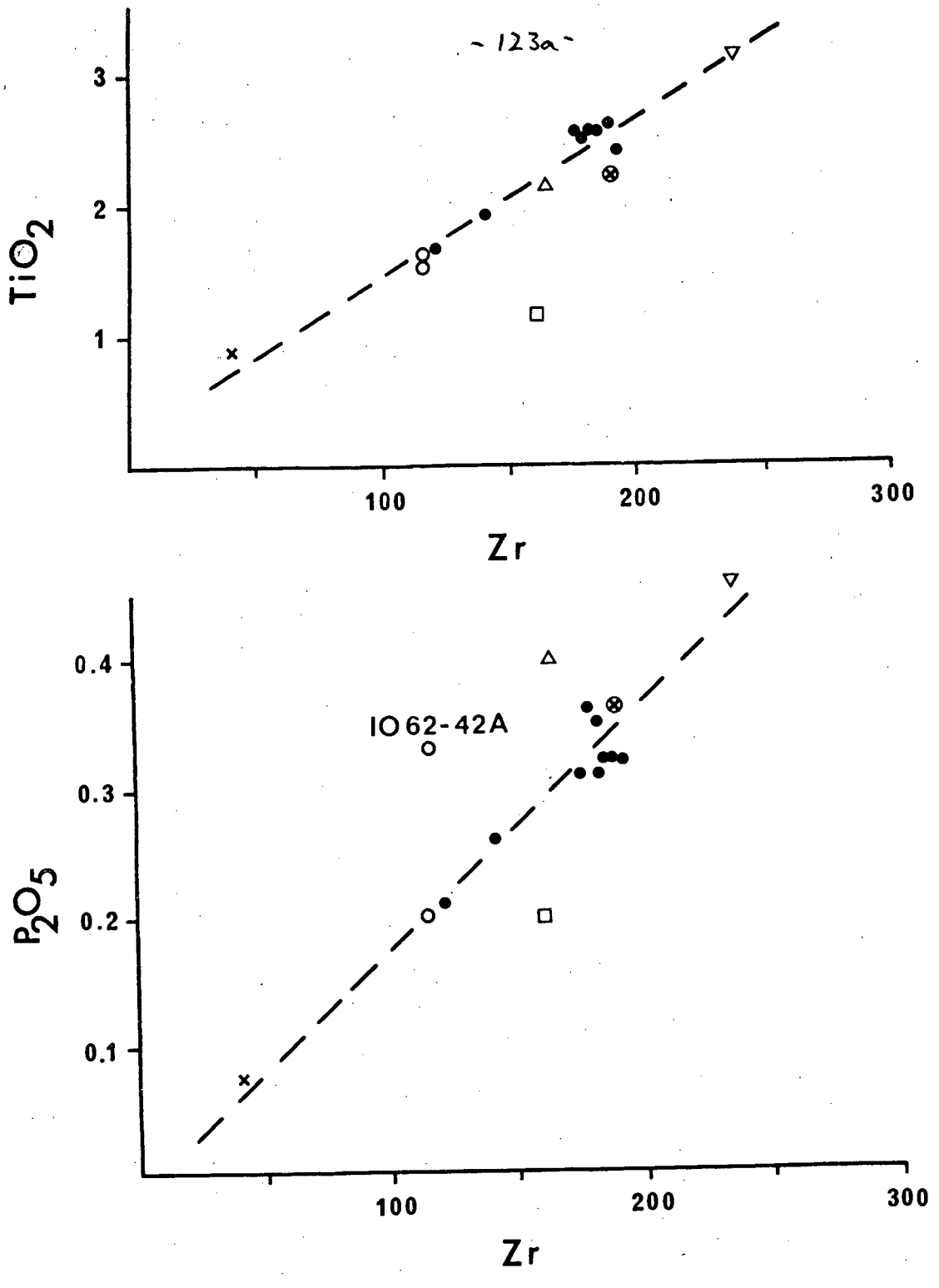

Fig. 4-18: Variation of TiO_2 and P_2O_5 with respect to Zr in IOFZ basalts. The single 11°E basalt is plotted for comparison. Symbols as in Fig. 4-13.

The large range in absolute concentrations of incompatible elements and the evolved compositions of the basalts suggest that fractional crystallisation has played a significant role in the evolution of these basalts. No potential primary abyssal basalts have been recovered from the IOFZ.

3.2.2 Trace Elements:

In accord with their relatively evolved, somewhat transitional major element compositions, the IOFZ basalts are characterised by high concentrations of incompatible trace elements and low concentrations of the compatible ferromagnesian trace elements. To illustrate the trace element variations, selected elements are plotted against Zr (as a measure of differentiation) in Figs. 4-19 and 4-20. Zr has been used as a measure of differentiation in preference to M.I. to avoid the effect of alteration on the FeO*/MgO ratio (Humphris and Thompson, 1978a).

The mobile incompatible elements Rb and Ba are present in high concentrations (6-75 ppm and 70-373 ppm respectively) and define a broad increase (with much scatter) with increasing Zr (Fig. 4-19). Sr concentrations are more restricted (180-250 ppm) in the Dredge 13 and 14 basalts and, with the exception of highly altered I063-2, can be readily distinguished from the Sr-rich (457-630 ppm) Dredge 11 basalts (Fig. 4-19, Table 4-7). Dredge 13 and 14 basalts are also clearly distinguished from the Dredge 11 basalts by their higher Sc content (Fig. 4-19, Table 4-7).

Relatively immobile, Sc, Ga, V and Zn all show systematic increases with differentiation in the Dredge 13 and 14 basalts, while Ni, Cr and Cu define somewhat more scattered trends, decreasing with increasing differentiation. Ga increases from 16 to 21 ppm, V from 240

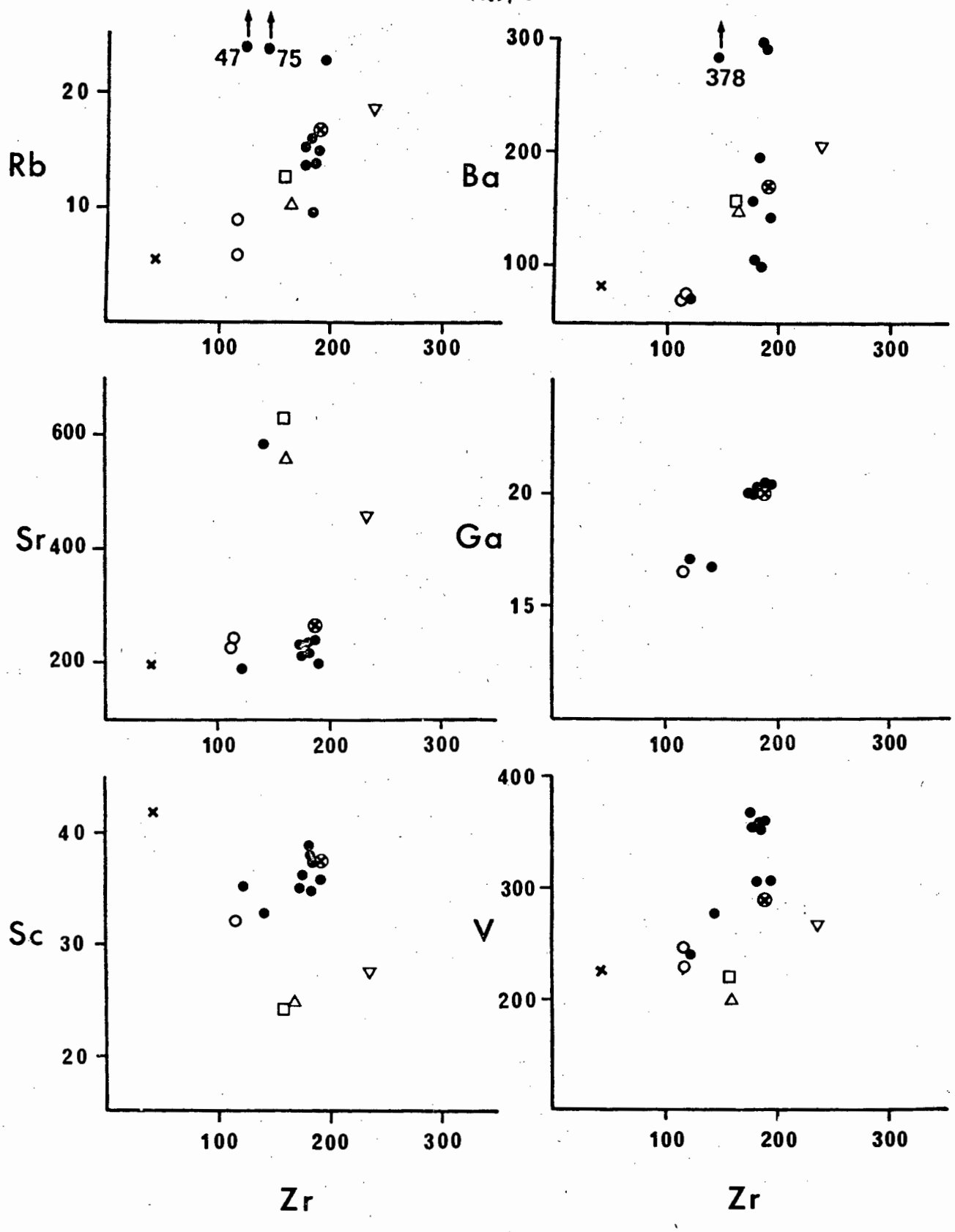

Fig. 4-19: Variation of selected trace elements in IOFZ basalts with respect to Zr as a measure of differentiation. The single 11°E basalt is shown for comparison. Symbols as in Fig. 4-13.

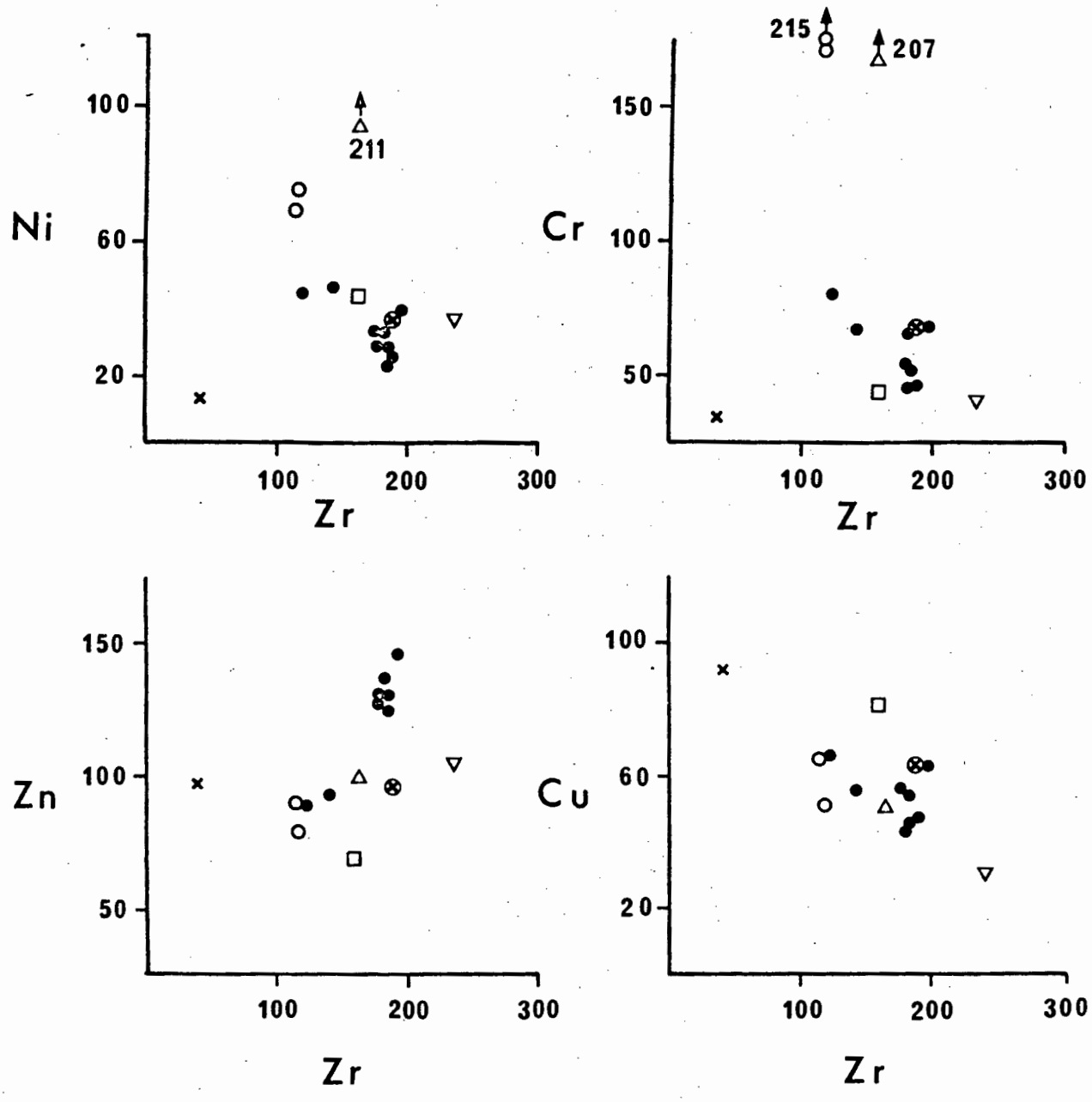
Ni
100
60
20
211
100
200
300
Zr
Cr
215
207
150
100
50
100
200
300
Zr
Zn
150
100
50
100
200
300
Zr
Cu
100
60
20
100
200
300
Zr

Fig. 4-19 (Cont.):

to 360 ppm, and Zn from 55 to 140 ppm, as Zr increases from 115 to 190 ppm with differentiation in the Dredge 13 and 14 basalts. The SiO_2-rich I063-3 is distinguished from the other basalts by having a relatively high Sc (41 ppm) and Zn (90 ppm) content for its low Zr content (42 ppm). Ni and Cr abundances are low, with all tholeiitic basalts having less than 80 ppm Ni and most having less than 80 ppm Cr. The olivine basalts from Dredge 13 are characterised by high Cr contents - in qualitative accord with the abundance of clinopyroxene phenocrysts. The unusual composition of SiO_2-rich I063-3 is also illustrated by the low Ni (14 ppm) and Cr (35 ppm) contents, in relation to its low Zr content (42 ppm), relative to the other IOFZ basalts. Olivine-rich basalt I060-2 has the highest Ni content (211 ppm) which, in conjunction with its high Mg-number, illustrates its primitive composition. With respect to the trace elements depicted in Fig. 4-19, the sample from $11^{o}E$ is compositionally similar to the non-porphyritic plagioclase-pyroxene basalts from Dredge 13 on the northwestern wall of the IOFZ.

In contrast to the more mobile incompatible elements, Zr, Nb and Y show an excellent degree of correlation in the Dredge 13 and 14 basalts (Fig. 4-20). The plot of Nb versus Zr clearly distinguishes the Dredge 11 olivine-rich and plagioclase-rich basalts from the remaining basalts which describe a well defined trend. This trend cuts the Zr axis some distance from the origin, indicating that Zr is significantly less incompatible than Nb. Nb concentrations range from 12 to 24 ppm in the Dredge 13 and 14 basalts with a corresponding change in Zr from 115 to 192 ppm. The Dredge 11 olivine basalt I060-3 is the sample most enriched in Nb and plots close to the main trend in Fig. 4-20. Relative to this trend, the olivine-phyric basalt I060-2 is enriched in

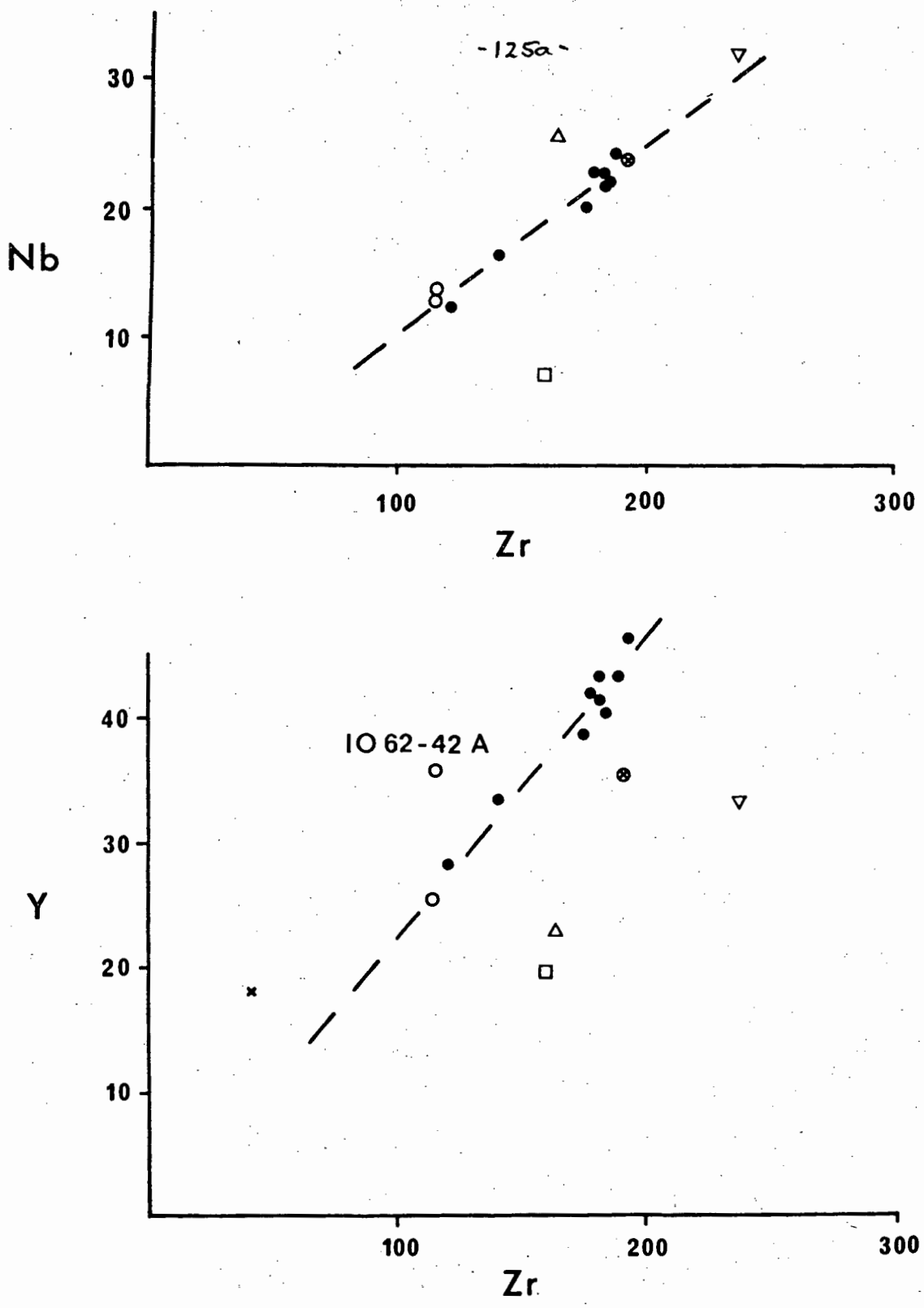

Fig. 4-20: Plot of Nb and Y against Zr in the IOFZ basalts and the single 11°E basalt. Symbols as in Fig. 4-13.

Nb for its Zr content, while I060-1 is depleted in Nb for its Zr content. The 11°E sample is characterised by its similar Nb content and lower Y content than the Dredge 14 plagioclase-pyroxene basalts. The Y-Zr variation similarly serves to distinguish between the Dredge 13 and 14 basalts, the Dredge 11 olivine- and plagioclase-rich basalts (Fig. 4-20). Plagioclase-phyric olivine basalt I062-42A is anomalous in its high Y content and, taken together with previously noted high P_2O_5 content, it seems possible that this sample may have experienced contamination from a superficial marine phosphorous-rich deposit. SiO_2-rich I063-3 is similarly displaced from the main trend defined by the Dredge 13 and 14 samples.

Several incompatible element ratios have been shown to be diagnostic of source region characteristics. Such ratios (e.g. K/Rb, K/Ba, Zr/Nb, Y/Nb, Zr/Y, Sm/La, La/Ta) can serve as a measure of the degree of depletion of the source region (Gast, 1968; Hart, 1971; Pearce and Cann, 1973, Erlank and Kable, 1976; Bougault et al., 1979). From this group of ratios the first two are susceptible to alteration and consequently have little value for the fairly altered IOFZ basalts. The Dredge 13 and 14 basalts have an average Zr/Nb = 8.4 $\pm$.6, which is significantly lower than typical MORB (Zr/Nb = 37; Erlank and Kable, 1976) and the Conrad fracture zone basalts (Zr/Nb = 21), but identical to the olivine basalts from the FAMOUS region (Zr/Nb = 8.4, this study) and similar to that commonly associated with tholeiitic basalts from oceanic islands (ave. Zr/Nb = 6.6; Erlank and Kable, 1976). Bouvet Island hawaiites have, for example, an average Zr/Nb ratio of 6.6 (this work), similar to that characteristic of an undepleted or incompatible element enriched source (e.g. Erlank and Kable, 1976). Two of the Dredge 11

basalts have similar though slightly lower Zr/Nb ratios (I060-2 - Zr/Nb = 6.3; I060-3 - Zr/Nb = 7.3) to the Dredge 13 and 14 basalts, while the third (I060-1) has a significantly higher ratio (Zr/Nb = 22.7). The Dredge 11 basalts (excluding I060-1) can also be distinguished by their higher Zr/Y ratio (7.5) and lower Y/Nb (0.95) relative to the Dredge 13 and 14 basalts (Zr/Y = 4.2 $\pm$ 0.4; Y/Nb = 1.98 $\pm$ 0.2). The low Y/Nb ratio of these basalts illustrates the transitional to mildly alkaline nature of these IOFZ basalts (e.g Pearce and Cann, 1973). The sample from 11°E is similarly characterised by having low Zr/Nb (7.95) and Y/Nb (1.45) ratios.

A single Dredge 13 basalt, I062-30, has been analysed for the REE at the Australian National University, Canberra, by A.R. Duncan, and the data are given in Table 4-8. In contrast to the typical LREE-depleted patterns of MORB (e.g. Bryan et al., 1976) and in accord with the low Zr/Nb ratios characterizing the IOFZ basalts, I062-30 has a strongly LREE-enriched pattern (Fig. 4-21). Such a highly fractionated REE pattern (La/Yb = 3.39) probably requires the primary magma, which gave rise to the evolved I062-30, to have been in equilibrium with residual garnet during partial melting.

In summary, the trace element variations in the IOFZ basalts distinguish these basalts from normal depleted MORB. The basalts are characterised by high absolute concentrations of the incompatible elements, attesting to their evolved compositions. Diagnostic incompatible element ratios (e.g. Zr/Nb, Y/Nb, La/Yb) suggest that these lavas have slightly transitional to mildly alkaline compositions and that they derived from a relatively undepleted (or possibly enriched) mantle. Certain trace elements (e.g. Sr, Sc, Nb, Y) serve to distinguish the

Table 4-8. Rare earth element concentrations and chondritic normalised values for IOFZ basalt I060-30. Concentrations were normalised using the values for Leedy chondrite divided by 1.2 (Sun & Hanson, 1976).

	I062-30	
	ppm	chondritic
La	20.0	63.49
Ce	44.0	54.12
Pr	5.2	44.83
Nd	24.0	40.20
Sm	6.2	32.29
Eu	1.91	26.53
Gd	6.10	23.55
Tb	1.13	23.06
Dy	7.50	23.08
Ho	1.70	23.29
Er	4.60	21.60
Tm	0.59	19.67
Yb	3.90	18.75
† CH La/Sm		1.966
CH La/Yb		3.386
Eu/Eu*		0.962

† CH = chondritic

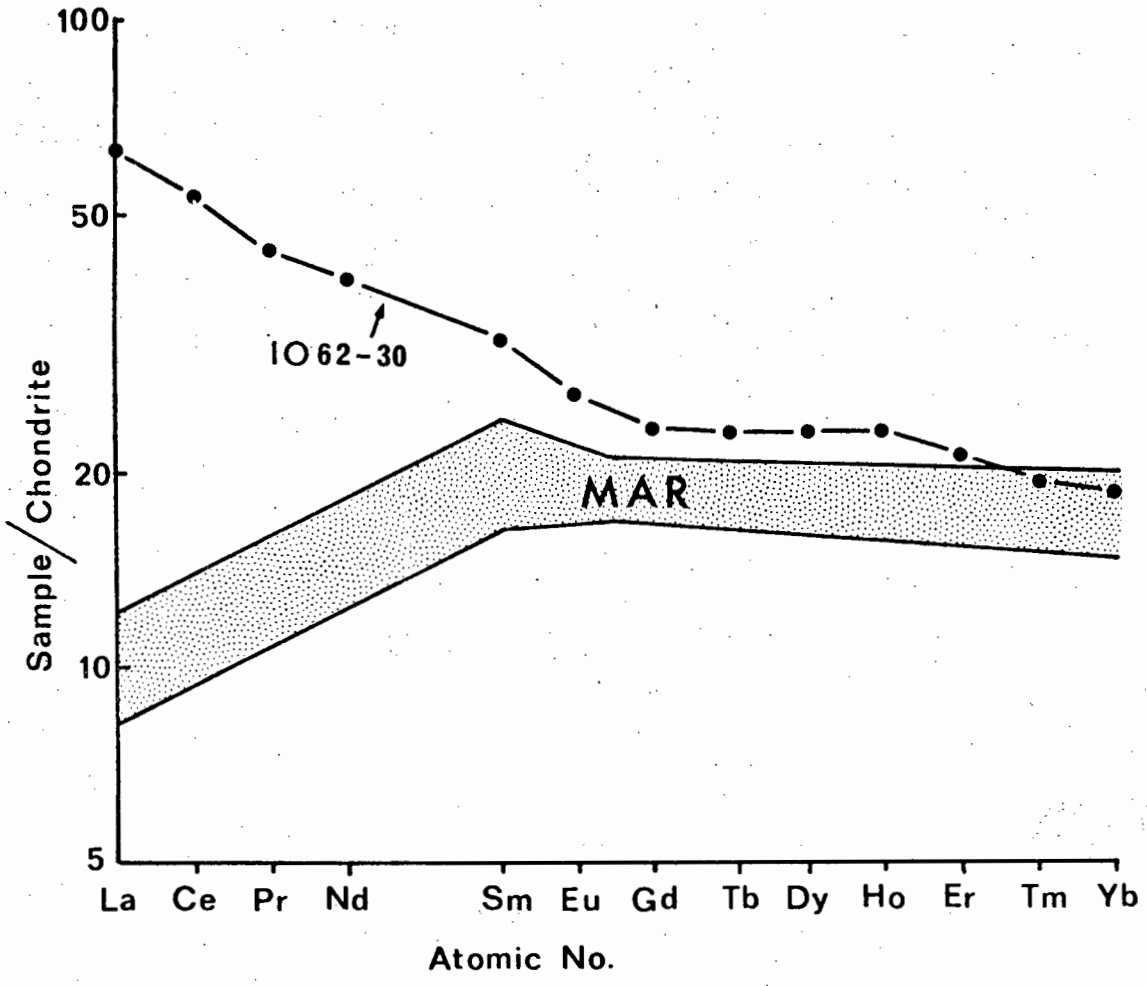

Fig. 4-21: Chondrite normalised REE variation in a single IOFZ basalt. Concentrations were normalised using the values for Leedy chondrite divided by 1.2 (Sun & Hanson, 1976). Field average of MAR basalts (Frey et al., 1974) is shown for comparison.

Dredge 13 and 14 basalts from the Dredge 11 basalts. Possible genetic relationships among the IOFZ basalts will be considered in the following section.

3.3 Petrogenesis

3.3.1 Fractional Crystallisation:

Qualitatively, the trend depicted in Figs. 4-18 and 4-20 suggest a consanguinous relationship for many of the IOFZ basalts. However, consideration of the variation of a few critical elements and element ratios indicates that some samples are clearly distinctive and must be derived from compositionally distinct source regions. Possible genetic relationships among various samples via fractional crystallisation of observed phenocryst phases have been quantitatively evaluated utilising the least squares approximation technique of Bryan et al. (1969). As before, whole rock compositions and average mineral compositions have been normalised to 100% volatile-free and all iron expressed as FeO. P_2O_5 and K_2O have been excluded from the mixing calculations due to the low concentrations of the former and the high mobility during alteration of the latter. P_2O_5 has been treated as a trace element and used as an independent check on the calculated major element models. Due to the already noted distinct differences in composition between the Dredge 11 and the Dredge 13 and 14 basalts, the two groups will at first be considered separately.

(1) Dredge 13 and 14 Basalts:

With the exception of the SiO_2-rich Dredge 14 basalt, I063-3, the Dredge 13 and 14 basalts display systematic trends in terms of the immobile incompatible trace elements (e.g. Fig. 4-20). In order to evaluate the extent to which the observed compositional variation can

be attributed to fractional crystallisation, the seven evolved Dredge 13 basalts have been grouped and an average composition (referred to as ferrobasalt) has been used for the purposes of modelling. The least evolved plagioclase-phyric olivine-bearing basalts, I062-42A and I062-49, have similarly been averaged. In terms of absolute incompatible element contents, the Dredge 13 and 14 basalts can then be ordered in the following differentiation scheme (average Zr contents are given in brackets):

I063-3 →	I062-42A/I062-49 →	I062-51 →	I063-2 →	Ferrobasalt
(42)	(116)	(121)	(141)	(183)

Since none of the above basalts can be regarded as representing 'primary' magmas, in view of their low Mg-numbers and low Ni and Cr contents (Table 4-7), the choice of a suitable parental composition is somewhat arbitrary and all possible parent-daughter pairs have been considered. Although I063-3 has the lowest incompatible element content (Table 4-7), its very high SiO_2 content, low MgO and low ferromagnesian trace element contents are in conflict with this sample being representative of a possible parental magma. In fact, the above-mentioned compositional characteristics preclude any simple fractional crystallisation relationship relating this basalt to any of the other IOFZ basalts and, considering the numerous glacial erratics recovered during dredging (Sclater et al., 1978), the possibility exists that this rock may be an erratic.

A summary of least squares approximations relating various Dredge 13 and 14 parent-daughter pairs is given in Table 4-9. Inspection of Table 4-9 shows that it is not possible to relate all the major element compositional variations to low pressure fractionation of a

No.	PARENT	PLAG	CPX	OLIV	OPX	DAUGHTER	F	ΣR^2
1	62-42A/62-49	$-.2300(An_{75})$	$-.1547^{c}$	$-.0102(Fo_{81})$	---	ferrobasalt	0.6043	0.08
1b	"	$-.2167(An_{75})$	$-.1523^{a}$	$-.0144(Fo_{77})$	---	ferrobasalt	0.6179	0.10
2	"	$-.2050(An_{75})$	$-.1949^{a}$	$+.0301(Fo_{75})$	---	I063-2	0.6141	0.75
3	"	$-.0779(An_{75})$	$-.1380^{a}$	$+.0417(Fo_{75})$	---	I062-51	0.8110	0.95
4	I062-51	$-.1220(An_{76})$	$-.0851^{a}$	---	---	ferrobasalt	0.7998	4.87
5	"	$-.2293(An_{75})$	$-.0119^{a}$	---	$-.1455^{b}$	ferrobasalt	0.6156	0.03
6	"	$-.1444(An_{76})$	$-.0803^{a}$	---	---	I063-2	0.7713	0.32
7	I063-2	$+0.0342(An_{70})$	---	---	---	ferrobasalt	1.0485	5.74

[a] Cpx = $Wo_{39}En_{47}Fs_{14}$ [b] Opx = $Wo_{3}\ En_{69}Fs_{27}$ [c] Cpx = $Wo_{37}En_{17}Fs_{16}$

Table 4-9: Summary of least squares approximations relating various dredge-13 and -14 parent-daughter combinations. Mineral proportions and F are given in weight fractions.

single 'parental' magma. Considering only the sum of squares of residuals of the models presented in Table 4-9, it is evident that only four models, No's 1, 1b, 5 and 6, are at all acceptable. Although the sum of squares of residuals for model-6 is somewhat high, the model is regarded as acceptable in light of the highly altered state of I063-2 (see Section 3.1).

The derivation of the ferrobasalt from I062-42A/I062-49 by the fractionation of 23.0% plagioclase, 15.5% clinopyroxene and 1.0% olivine is shown in more detail in Table 4-10 as an example. The major element fit is generally good and the proportions of fractionating minerals are realistic in terms of observed modal proportions in the rocks, but two points required elaboration. Firstly, the 'parental' composition in any modelling calculation should ideally represent a 'liquid' composition. The plagioclase phyric nature of I062-42A and I062-49 and the already noted minor olivine accumulation suggests that this composition might not represent a true 'liquid'. However, since the major element modelling is linear, accumulation effects in the 'parent' will be transparent providing the introduced phases are derived from the same magma system. In essence, the model indicates that I062-42A/I062-49 was derived by partial cumulus enrichment from a 'parental liquid' which in turn fractionated to give the evolved ferrobasalts. The second point is that the required pyroxene composition is somewhat more Fe-rich than is desirable when compared to observed phenocryst compositions. Use of a slightly more Fe-rich olivine (e.g. Fo_{77}) results in a slightly more realistic pyroxene composition ($Wo_{39}En_{47}Fs_{14}$) since it is intermediate between that observed in the parent ($Wo_{39}En_{50}Fs_{11}$) and that observed in the daughter ($Wo_{41}En_{43}Fs_{16}$). The olivine composition is, however, then

significantly more Fe-rich than that observed in the parent (Fo_{83}-Fo_{86}). The results of the respective mixing calculations are virtually identical (Table 4-9, models 1 and 1b). In a similar study on the formation of ferro-basalt at East Pacific mid-ocean spreading centres, Clague and Bunch (1976) were forced to postulate the fractionation of an Fe-rich pyroxene ($Wo_{36}En_{43}Fs_{21}$) to satisfy their mixing calculations. These authors suggested that minor pyrrhotite fractionation might serve to account for the Fe discrepancy.

To illustrate the consistency of the model presented in Table 4-10, the results have been used to calculate a predicted trace element content of the IOFZ ferrobasalt. The trace elements have been modelled assuming Rayleigh fractionation (Equation 1, Chapter II) and using distribution coefficients selected from Tables A2-1, A2-2 and A2-5 in the appendix and given in Table 4-11. Predicted and observed trace element concentrations in the IOFZ ferrobasalt (Table 4-11) generally show excellent agreement and attest to the consistency of the model. Only the relatively immobile trace elements have been modelled due to the already noted alteration of many of the IOFZ basalts. Any cumulation effects in I062-42A/I062-49 will affect the predicted concentrations of the more compatible trace elements, Sr, Ni and Sc, due to the difference between exponential (fractional crystallisation) and linear (cumulation) variations. The small differences that might be produced are, however, within the known uncertainty in the values of these compatible trace element distribution coefficients.

It is not possible to relate the IOFZ ferrobasalt to the plagioclase-phyric I062-51 via fractionation of the observed phenocryst phases (Table 4-9). However, if orthopyroxene fractionation is invoked

Table 4-11: Calculated and observed trace element concentrations in the IOFZ ferrobasalts using the results from the major element model presented in Table 4-11. Distribution coefficients have been selected from the compilation in Tables A2-1, A2-2 and A2-5 in the appendix.

Distribution coefficients

	PLAG	CPX	OLIV
Zr	.01	.24	.01
Nb	.01	.05	.01
Y	.18	.50	.12
Sr	2.0	.12	.01
Sc	.01	2.2	.01
Ga	1.0	.40	.01
Ni	.01	5.0	21*
V	.01	1.0	.01
P_2O_5	.01	.01	.01

* calc. from the equation of Hart and Davis (1978).

Trace element model

	I062-42A/I062-49	Ferrobasalt	
	OBS.	CALC.	OBS.
Zr	116	183	183
Nb	13	21	23
Y	30	43	42
Sr	235	211	224
Sc	34	36	37
Ga	17	19	20
Ni	72	34	30
V	247	335	337
P_2O_5	0.20%	0.33%	0.33%

in addition to plagioclase and clinopyroxene, then it is possible to derive the ferrobasalts from I062-51 (Table 4-9, model 5), at least in terms of the major elements. Orthopyroxene fractionation in ocean floor basalts is not totally unrealistic as Bender et al. (1978) have, for example, identified orthopyroxene as a coliquidus phase in a FAMOUS basalt in certain of their run products at 15 kb. In a study of the fractionation of Leg 37 basalts, Flower et al. (1977) found it necessary to postulate substantial orthopyroxene fractionation to satisfy major element variations in certain magma groups. Although no orthopyroxene gabbro has been dredged from the IOFZ, a hypersthene gabbro has been dredged from the Conrad fracture zone (see Section 4.1) consistent with the possibility of orthopyroxene fractionation in some ocean floor basalts.

The remaining sample in the Dredge 13 and 14 fractionation trend, I063-2, can be related to I062-51 by the fractionation of 14.4% plagioclase and 8.0% clinopyroxene. Although the sum of squares of residuals is somewhat high (0.32, Table 4-9), the sample is highly altered (see Section 3.1) and the major element match is regarded as being within the uncertainty of the true composition. Most of the mismatch is in MgO (-0.40) and Na_2O (-0.29), elements which are both mobile during sea floor alteration (e.g. Humphris and Thompson, 1978a), while TiO_2, which is relatively immobile (e.g. Pearce and Cann, 1973), is almost perfectly matched.

The consistency of the above models has been independently tested by using the results to calculate the predicted immobile trace element contents of the daughter magmas, i.e. I063-2 and the ferrobasalt. The predicted and observed trace element compositions are compare in Table

4-12 where it can be seen that a generally excellent agreement is obtained. There is a slight discrepancy in Zr in both models, with the predicted Zr being somewhat high, while the predicted Nb and Sc contents of the ferrobasalt are slightly low and high respectively. With the exception of these two discrepancies, the trace element calculations support the major element mixes. It would appear therefore that orthopyroxene fractionation may well be a feasible mechanism in controlling the composition of certain ocean floor basalts.

Attempts at relating the plagioclase-phyric olivine basalt I062-42A/I062-49 to either I062-51 or I063-2 have proved unsuccessful (e.g. Table 4-9), even if orthopyroxene fractionation is invoked.

In summary then, the compositional variations of all but one (I063-3) of the Dredge 13 and 14 basalts can be described by fractional crystallisation of observed phenocryst phases. One proposed model requires substantial orthopyroxene fractionation. The amount of fractionation required to account for the range in compositions varies from 23% to 40% and the fractionating phases comprise dominantly plagioclase and clinopyroxene. As noted by Clague and Bunch (1976), the importance of these two phases in controlling the evolution of ocean floor basalt to ferrobasalt is clearly illustrated.

(2) Dredge 11 Basalts:

Of the three Dredge 11 basalts, I060-1 can be readily distinguished by its significantly higher SiO_2 content and specifically by its very much higher Zr/Nb ratio (Table 4-7). Since it is extremely difficult to fractionate this immobile incompatible element ratio by fractional crystallisation, it is unlikely that this sample is genetically related to any of the other IOFZ basalts. Although ilmenite and/or titanomagnetite

Table 4-12: Calculated and observed trace element compositions of I063-2 and IOFZ ferrobasalt using the results of models 5 and 6 in Table 4-9. Distribution coefficients have been selected from Tables A2-2, A2-5 and A2-6 in the appendix.

Distribution coefficients

	PLAG	CPX	OPX
Zr	.01	.35	.10
Nb	.01	.05	.01
Y	.18	.5	.12
Sc	.01	2.2	1.4
Ga	1.0	.4	.01
Ni	.01	2.5	5.0
V	.01	1.0	1.0
P_2O_5	.01	.01	.01

Trace element check

PARENT = I062-51

	PARENT	I063-2		FERROBASALT	
	OBS.	OBS.	CALC.	OBS.	CALC.
Zr	121	141	151	183	191
Nb	12.4	17	15	23	20
Y	28	33	34	42	42
Sc	35	36	37	37	42
Ga	17	20	18	20	21
Ni	45	46	46	30	28
V	242	278	285	337	323
P_2O_5	.21%	.26%	.27%	.33%	.34%

fractionation is theoretically capable of increasing the Zr/Nb ratio due to the high D^{Nb}_{ilm} and D^{Nb}_{mgt} (Tables A2-8 and A2-9), over 40% titanomagnetite fractionation ($D^{Nb}_{mgt} = 2.16$, $D^{Zr}_{mgt} = 0.24$) or 12-30% ilmenite fractionation ($D^{Nb}_{ilm} = 7\text{-}22$, $D^{Zr}_{ilm} = 0.19\text{-}1.38$) would be required to change the Zr/Nb ratio by the required amount. This is clearly unrealistic, and consequently it is concluded that I060-1 is genetically unrelated to the IOFZ basalts and must be derived from a separate source area and may represent an erratic.

A least squares approximation relating the Dredge 11 basalt I060-2 to basalt I060-3 is presented in Table 4-13. The results indicate that although the parent magma is slightly nepheline normative, fractional crystallisation of 14.2% plagioclase (An_{68}), 14.1% olivine (Fo_{81}), 4.2% clinopyroxene ($Wo_{39}En_{47}Fs_{14}$) and minor titanomagnetite (0.6%) can give rise to a hypersthene normative magma similar to I060-3. With the possible exception of TiO_2, the low sum of squares of residuals attests to the consistency of the mixing calculation. If this mix is then used to calculate a predicted trace element content of I060-3, the concentrations of the majority of trace elements are adequately accounted for (Table 4-14). Closer inspection of the results presented in Table 4-14, however, indicates some subtle differences between the observed and calculated contents of Nb, Rb, P_2O_5 and possibly Sr. Although the discrepancy in Sr can be accounted for by selection of a slightly higher though not unrealistic D^{Sr}_{plag} (e.g. 3.5), and the Rb difference can possibly be attributed to minor alteration, the discrepancies in Nb and P_2O_5 are significantly greater than the uncertainties in the data. Both elements are immobile during alteration (e.g. Pearce and Cann, 1973) and both are highly incompatible with extremely low bulk

Table 4-13: Least squares approximation relating basalt I060-2 to dredge-11 olivine basalt I060-3.

Input data

	I060-3	PLAG	CPX	OLIV	Ti-Mt	I060-2
SiO_2	50.43	51.19	51.16	39.14	0.25	48.90
TiO_2	3.22	0.01	0.88	0.03	23.25	2.18
Al_2O_3	15.74	31.34	3.43	0.06	2.15	15.21
FeO*	11.37	0.58	8.74	17.68	72.71	11.10
MnO	0.19	0.01	0.20	0.22	0.51	0.15
MgO	4.85	0.13	16.03	42.69	1.06	9.97
CaO	9.75	13.66	18.59	0.31	0.10	9.34
Na_2O	3.82	3.63	0.33	0.01	0.01	3.14
		An 67.53	Wo 38.97	Fo 81.14		
		Ab 32.47	En 46.73	Fa 18.86		
			Fs 14.30			

Least squares approximation

	I060-2			MIX		
	OBS.	CALC.	DIFF.	COMP.	Wt.%	S.D.
SiO_2	48.90	48.90	.00	I060-3	67.29	1.63
TiO_2	2.18	2.35	.17	PLAG	14.22	0.94
Al_2O_3	15.21	15.21	.00	CPX	4.23	0.86
FeO*	11.10	11.04	-.06	OLIV	14.11	0.36
MnO	0.15	0.17	.02	TiMgt	0.61	0.22
MgO	9.97	9.99	.02			
CaO	9.34	9.33	-.01	TOTAL	100.46	2.11
Na_2O	3.14	3.10	-.04			

Sum of squares of residuals = 0.04

Table 4-14: Calculated and observed trace element concentrations in dredge -11 olivine basalt I060-3; using the results of the major element model in Table 4-13, and distributions given below. Source of distribution coefficients are Tables A2-1, A2-2, A2-5 and A2-9.

Distribution coefficients

	PLAG	CPX	OLIV	Ti-Mgt
Zr	.01	.24	.01	.24
Nb	.01	.05	.01	2.16
Y	.18	.50	.13	.17
Rb	.01	.01	.01	.01
Ba	.10	.01	.01	.01
Sr	3.0 (3.5)	.12	.01	.01
Sc	.01	2.5	.01	5.0
Ni	.01	2.5	12	10.0
P_2O_5	.01	.01	.01	.01

Trace element check

	I060-2	I060-3	
	OBS.	CALC.	OBS.
Zr	163	238	236
Nb	26	38	32
Y	23	32	33
Rb	10	15	19
Ba	148	216	207
Sr	557	493 (453)	457
Sc	25	31	28
Ni	211	34	37
P_2O_5	0.40%	.59%	.46%

distribution coefficients. Variations in selected D's will therefore not significantly affect the calculation. Furthermore, in contrast to the commonly found underestimation of incompatible element enrichment in fractionation models for ocean floor basalts (e.g. Bryan et al., 1976; Bryan, 1979; Bryan et al., 1979), the proposed model results in excessive enrichment in Nb and P_2O_5. Though apatite has not been identified in I060-2, a qualitative scan with the electrom microprobe indicates its presence in the matrix of I060-3; minor apatite (0.20%) fractionation could adequately account for the P_2O_5 discrepancy. The Nb anomaly, however, remains unaccounted for, and although one is reluctant to reject a model on the basis of one (or two) elements, the discrepancy in Nb (and possibly P_2O_5) does cast doubt on the consistency of this model.

(3) Variation between Dredges:

Chemical characteristics of the Dredge 11 basalts and the Dredge 13 and 14 basalts (Section 3.2.2) preclude any simple fractional crystallisation relationship between the basalts of these dredge hauls from opposite walls of the IOFZ. The differences (excluding the obviously distinct I063-3 and I060-1) can be summarised as follows:

Northwest Wall	Southeast Wall
Zr/Nb = 8.39	Zr/Nb = 6.80
Y/Nb = 1.98	Y/Nb = 0.95
Zr/Y = 4.26	Zr/Y = 7.15
Sc relatively high	Sc relatively low
Y relatively high	Y relatively low

These differences cannot readily be accounted for by any low pressure fractionation scheme. For example, over 50% fractionation of clino-

pyroxene alone would be required to increase the Zr/Y ratio by the required amount. Differences in certain incompatible element ratios of the basalts from the southeastern wall and those from the northwestern wall therefore preclude a direct relationship via fractional crystallisation.

3.3.2 Partial Melting:

Although none of the IOFZ basalts can be regarded as primary magmas (with the possible exception of IO60-2), the incompatible element ratios of these lavas should still closely reflect those in the parental magmas. A brief qualitative evaluation of the effect of partial melting on these ratios, with the objective of accounting for the observed differences between basalts from opposite walls of the IOFZ (see above), is given below.

The incompatible element ratios which serve to distinguish between the basalts from the southeastern and northwestern walls are: Zr/Nb, Zr/Y and Y/Nb. None of these ratios is easily changed by low pressure fractional crystallisation. Consideration of distribution coefficients for suitable residual mantle phases indicates that these ratios can, however, be fractionated by equilibration against residual garnet (Table 2-9). Approximate distribution coefficients for these elements with garnet are as follows (selected from Chapter II, Table 2-9): $D_{gt}^{Zr} = 1.2$; $D_{gt}^{Nb} = 0.1$; $D_{gt}^{Y} = 3.3$. Assuming residual garnet in the source, it is clear that Zr and Y will be substantially fractionated from Nb, and Zr will be fractionated relative to Y. In order to illustrate this fractionation, Zr/Y, Zr/Nb and Y/Nb ratios have been calculated for different degrees of partial melting (10% and 15%), with a residual assemblage of ol + opx, cpx and gt in the proportions

87 : 8 : 5 and 93 : 5 : 2. Assuming applicable mineral-liquid distribution coefficients (e.g. Table 3-31) and suitable initial concentrations in the source region (e.g. Zr = 13 ppm, Nb = 1.2 ppm, and Y = 4.6 ppm; Sun and Nesbitt, 1977), the mutual ratios of these elements in the melt would be:

	15% melt	10% melt
Zr/Nb	9.3	6.6
Y/Nb	1.94	0.97
Zr/Y	4.8	6.6

If these ratios are compared to those given previously as characteristic of the basalts from the opposite walls of the IOFZ, it is clear that the apparent differences are readily explained in terms of different degrees of partial melting of the same garnet-bearing source.

4. CONRAD FRACTURE ZONE

4.1 Petrography and Mineral Chemistry

The suite of samples from the Conrad fracture zone (F.Z.) can, in terms of texture, be broadly subdivided into apparently extrusive and apparently intrusive varieties. The extrusive rocks and the majority of intrusive rocks are basaltic in composition and are classified as basalts and dolerites respectively. In addition to the dolerites, an intrusive ferrodiorite and hypersthene gabbro were recovered from the Conrad F.Z. and are included in this study.

4.1.1 Extrusive Rocks (Basalts):

The Conrad F.Z. basalts range in texture from highly phyric to aphyric and on the basis of phenocryst type can be subdivided into: (1) olivine-plagioclase-pyroxene basalts, and (2) plagioclase-pyroxene basalts. These subdivisions are purely descriptive and carry no genetic implications.

T A B L E 4-15

CONRAD F.7: SELECTED MINERAL ANALYSES. OLTV - PLAG - PYX BASALTS

	1	2	3	4	5	6	7	8	9	10
SIO2	40.11	39.48	38.95	39.89	38.33	39.44	38.81	46.18	47.35	48.33
TIO2	-	-	.02	ND	.04	.02	.02	.04	.04	.05
AL2O3	-	-	.03	.03	.05	.05	.04	33.23	33.08	32.45
CR2O3	-	-	.04	ND	ND	.02	.03	-	-	-
FEO	14.41	17.43	15.91	14.26	20.29	16.07	19.78	.36	.48	.55
MNO	.22	.25	.21	-	.26	.22	.27	-	-	-
MGO	44.97	42.08	44.64	46.22	40.00	44.24	40.79	.31	.29	.33
CAO	.33	.36	.33	.32	.29	.33	.31	17.96	16.47	15.91
NA2O	-	-	-	-	-	-	-	1.54	2.20	2.55
K2O	-	-	-	-	-	-	-	ND	.02	.03
NIO	.16	.12	-	-	-	-	-	-	-	-
TOTAL	100.20	99.72	100.13	100.74	99.27	100.39	100.05	99.63	99.93	100.20

* * ATOMIC PROPORTIONS BASED ON SELECTED NO. OF OXYGENS * *

OXYGEN	4	4	4	4	4	4	4	8	8	8
SI	1.003	1.006	.984	.991	.996	.993	.997	2.139	2.179	2.214
AL	-	-	.001	.001	.002	.001	.001	1.815	1.794	1.753
TI	-	-	.000	-	.001	.000	.000	.001	.001	.002
CR	-	-	.001	-	-	.000	.001	-	-	-
FE2+	.301	.372	.336	.296	.441	.338	.425	.014	.018	.021
MN	.005	.005	.004	-	.006	.005	.006	-	-	-
MG	1.676	1.598	1.680	1.711	1.549	1.659	1.562	.021	.020	.023
CA	.009	.010	.009	.009	.008	.009	.009	.892	.812	.781
NA	-	-	-	-	-	-	-	.138	.196	.227
K	-	-	-	-	-	-	-	-	.001	.002
NI	.003	.002	-	-	-	-	-	-	-	-
SUM	2.997	2.994	3.015	3.008	3.002	3.006	3.001	5.021	5.022	5.022
	FO 84.76	FO 81.14	FO 83.33	FO 85.24	FO 77.84	FO 83.07	FO 78.61	AN 86.52	AN 80.44	AN 77.38
	FA 15.24	FA 18.86	FA 16.67	FA 14.76	FA 22.16	FA 16.93	FA 21.39	AB 13.42	AB 19.44	AB 22.44
								OR .06	OR .12	OR .17

* * * S A M P L E D I R E C T O R Y * * *

ANALYSIS NO.	DESCRIPTION
1	OLIVINE, PHENO (CORE, 1045-152)
2	OLIVINE, PHENO (AS ABOVE, RIM)
3	OLIVINE, PHENO (CORE, 1045-152).
4	OLIVINE, PHENO (CORE, 1045-97)
5	OLIVINE, PHENO (CORE, 1045-97)
6	OLIVINE, PHENO (CORE, 1045-97)
7	OLIVINE, PHENO (CORE, 1045-161)
8	PLAG, PHENO (CORE, 1045-97)
9	PLAG, PHENO (CORE, 1045-97)
10	PLAG, PHENO (AS ABOVE, RIM)

** ND = NOT DETECTED **

TABLE 4-15 (CONTINUED)

CONRAD F.Z: SELECTED MINERAL ANALYSES. OLTV - PLAG - PYX BASALTS

	11	12	13	14	15	16	17	18	19
SIO2	50.00	48.24	52.21	51.35	50.16	50.72	51.73	52.80	51.96
TIO2	.04	.04	.08	.50	.63	.69	.82	.34	.10
AL2O3	31.37	32.36	29.18	2.56	3.25	3.79	3.69	2.45	5.00
CR2O3	-	-	-	.65	.75	.85	.29	.45	.08
FEO	.44	.48	.75	6.00	6.46	6.41	8.57	5.23	29.51
MNO	-	-	-	.15	.15	.14	.19	.13	.03
MGO	.31	.24	.22	17.80	17.26	16.71	18.55	17.35	3.97
CAO	15.13	16.41	12.75	20.31	20.44	19.68	16.45	21.57	.38
NA2O	3.13	2.80	4.22	.31	.33	.29	.16	-	.06
K2O	.03	.04	.05	-	-	-	-	-	4.74
TOTAL	100.45	100.61	99.46	99.63	99.43	99.28	100.45	100.32	95.83

* * ATOMIC PROPORTIONS BASED ON SELECTED NO. OF OXYGENS * *

OXYGEN	8	8	8	6	6	6	6	6	22
SI	2.278	2.207	2.388	1.896	1.865	1.879	1.889	1.927	7.770
ALIV	1.684	1.745	1.573	.104	.135	.121	.111	.073	.230
ALVI	-	-	-	.008	.007	.045	.048	.032	.651
TI	.001	.001	.003	.014	.018	.019	.023	.009	.011
CR	-	-	-	.019	.022	.025	.008	.013	.009
FE2+	.017	.018	.029	.185	.201	.199	.262	.160	3.691
MN	-	-	-	.005	.005	.004	.006	.004	.004
MG	.021	.016	.015	.980	.956	.923	1.009	.944	.885
CA	.739	.805	.625	.804	.814	.781	.644	.843	.061
NA	.276	.248	.374	.022	.024	.021	.011	-	.017
K	.002	.002	.003	-	-	-	-	-	.904
SUM	5.018	5.044	5.011	4.036	4.047	4.017	4.011	4.005	14.234
	AN 72.64	AN 76.24	AN 62.36	WO 40.82	WO 41.30	WO 41.06	WO 33.61	WO 43.33	
	AB 27.19	AB 23.54	AB 37.35	EN 49.76	EN 48.51	EN 48.50	EN 52.72	EN 48.47	
	OR .17	OR .22	OR .29	FS 9.41	FS 10.19	FS 10.44	FS 13.67	FS 8.20	

* * * S A M P L E D I R E C T O R Y * * *

ANALYSIS NO.	DESCRIPTION
11	PLAG, PHENO (CORE, I045-152)
12	PLAG, PHENO (AS ABOVE, RIM)
13	PLAG, MICROPHENO (I045-161)
14	CPX, PHENO (CORE, I045-152)
15	CPX, PHENO (AS ABOVE, RIM)
16	CPX, PHENO (CORE, I045-97)
17	CPX, PHENO (CORE, I045-97)
18	CPX, PHENO (CORE, I045-161)
19	BROWN FILLING OF VESCILE (I045-97)

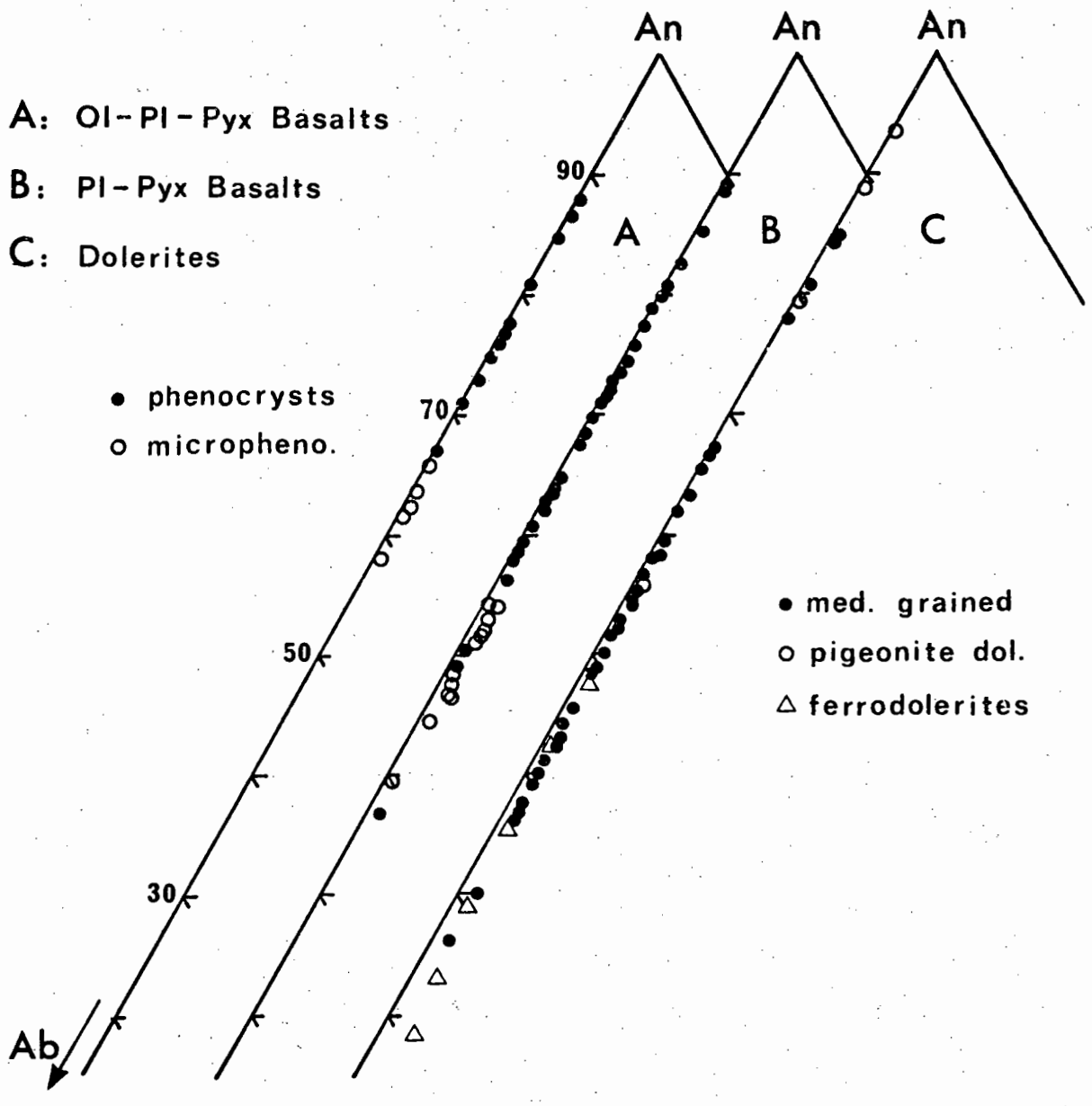

Fig. 4-22: End-member variation of plagioclase phenocrysts and microphenocrysts from Conrad F.Z. basalts and dolerites.

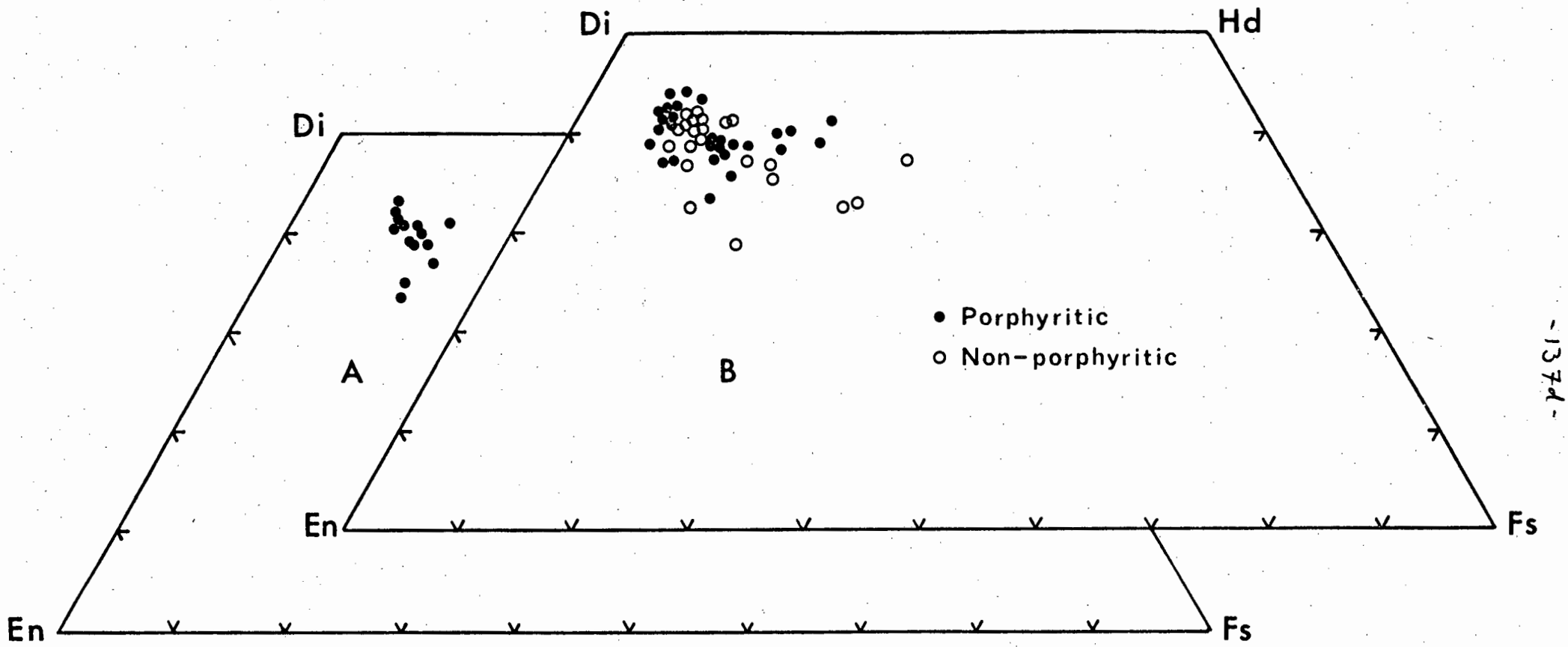

Fig. 4-23: End-member variation of clinopyroxene from Conrad F.Z. basalts.

(i) Olivine-plagioclase-pyroxene basalts:

Only three samples fall into this group, I045-97, I045-152 and I045-161, of which the latter comprises a fragment of the glassy rind of a pillow. The former two samples are porphyritic with phenocrysts of olivine (0.5-1.0 mm), plagioclase (0.5-2.0 mm) and clinopyroxene (0.5-1.0 mm) set in a groundmass with an arborescent texture of sub-microscopic sheaves of plagioclase and pyroxene with fine grained titanomagnetite filling the interstices (Plate 4-3A). Olivine occurs as fractured euhedral to subhedral phenocrysts and microphenocrysts which generally range in composition from Fo_{85} to Fo_{78} (Table 4-15). One of the microphenocrysts analysed in I045-97 had a composition of Fo_{68}. Zoning is minimal but some grains show a range of up to 3 mol % fosterite. A brown/green alteration product (bowlingite/iddingsite?) occurs surrounding some olivine phenocrysts. Plagioclase occurs as elongate laths and in glomerocrysts and aggregates with olivine and/or clinopyroxene are not uncommon (Plate 4-3B). Complex oscillatory zoning is characteristic and many of the larger plagioclase phenocrysts contain abundant trapped melt inclusions (Plate 4-3C). Variation in plagioclase phenocryst composition (An_{87}-An_{67}) and microphenocrysts (An_{58}-An_{65}) is depicted in Fig. 4-22A, and representative analyses are presented in Table 4-15. Reverse zoning of up to 4 mol % An is found in some phenocrysts (Table 4-15, No's 11 and 12). Clinopyroxene (diopsidic augite) occurs as discrete euhedral to subhedral phenocrysts or in subophitic intergrowth with plagioclase (Plate 4-3D). Compositions range from $Wo_{43}En_{49}Fs_{8}$ to $Wo_{37}En_{48}Fs_{15}$ (Fig. 4-23A) with the greatest variation occurring in the proportions of Wo and Fs. The substitution of Ca-Fe in these pyroxenes can be attributed to conditions of rapid crystallisation

(Smith and Lindsley, 1971). Representative analyses are presented in Table 4-15. Segregation vesicles (Smith, 1967) occur in the matrix and are generally filled with Fe-rich magmatic residue. Sparse, secondary orange/brown minerals (K-Fe chlorophaite, celadonite?) occur in the matrix or partially filling vesicles in I045-97. A representative analysis of this secondary mineral is presented in Table 4-15 (No. 19). Individual olivine, plagioclase and pyroxene analyses from the olivine basalts are presented in microfiche Table F4-12.

The porphyritic nature of I045-97 and I045-152 implies the possibility that these samples might have experienced phenocryst redistribution. Calculation of the Fe-Mg K_D between the most Mg-rich olivine phenocrysts (Fo_{85}) and whole rock compositions of I045-97 and I045-152, gives values of 0.24 and 0.25 respectively. Compared to an equilibrium value of 0.30 (Roeder and Emslie, 1970), this would suggest that the most magnesium olivines are too Mg-rich to have crystallised from the host rock. A liquidus olivine composition of Fo_{83} (similar to the dominant olivine composition) gives a K_D of 0.29. Coexisting olivine microphenocryst-quench glass pairs in sample I045-161 similarly give an average K_D of 0.29 (assuming an Fe_2O_3/FeO ratio for the glass = 0.15). Additional evidence that I045-97 and I045-152 might have experienced phenocryst redistribution is found in the occurrence of strongly reversed zoned plagioclase phenocrysts (Table 4-15, No's 11 and 12).

(ii) Plagioclase-pyroxene Basalts:

The remaining basalts (I045-91, I045-130B, I045-151, I045-161B, I045-173, I045-14, I045-106, I047-62, I047-64) are all characterised by the presence of only two phenocryst phases - plagioclase and clinopyroxene. These basalts show great variations in texture, ranging from

PLATE 4-3

A: Photomicrograph of olivine-plagioclase-pyroxene basalt I045-152, showing plagioclase, olivine and clinopyroxene phenocrysts set in a hyalocrystalline matrix. Crossed polars.

B: Aggregate of olivine, plagioclase and clinopyroxene in basalt I045-97. Crossed polars.

C: Large euhedral plagioclase phenocryst in I045-97 with abundant trapped melt inclusions. An olivine-plagioclase aggregate can be seen in the lower right hand corner. Partially crossed polars.

D: Elongate clinopyroxene phenocryst in I045-152 showing subophitic relationship with plagioclase. Crossed polars.

E: Photomicrograph showing the coarsely porphyritic texture of plagioclase-pyroxene phyric basalt I045-130B.

F: Photomicrograph showing the porphyritic texture of plagioclase-pyroxene basalt I047-64. The large phenocrysts include both plagioclase and clinopyroxene.

G: Photomicrograph showing the texture of plagioclase-pyroxene basalt I045-91.

H: Photomicrograph showing the texture of plagioclase-pyroxene basalt I045-151.

PLATE 4-3

A

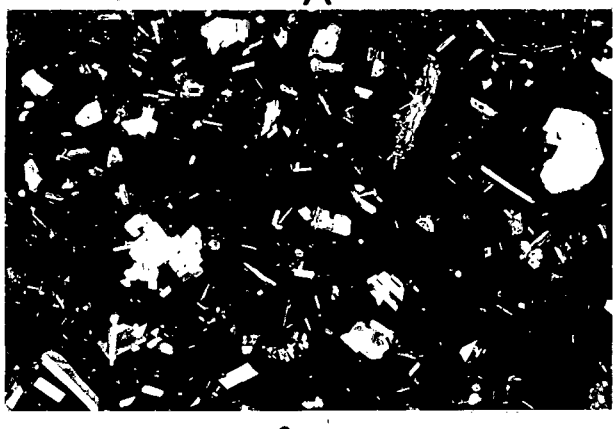

6 mm

B

2·5mm

C

1·7mm

D

2·5mm

E

3mm

F

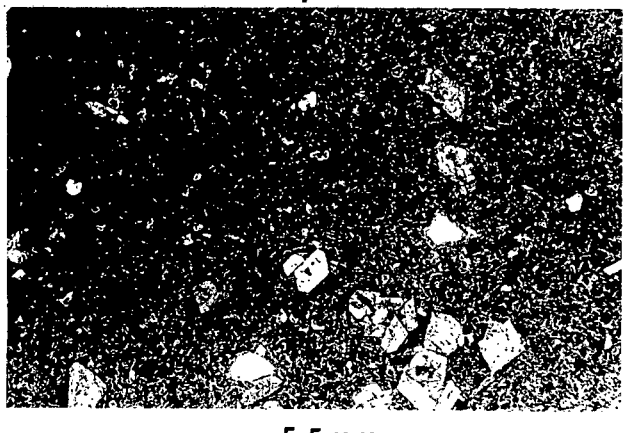

5·5mm

G

3mm

H

3·7mm

coarsely porphyritic (I045-130B, I045-173, I047-64, I047-62), with large phenocrysts (1-4 mm) and glomerocrysts of plagioclase and clinopyroxene, through intermediate varieties (I045-91, I045-151, I045-161B, I045-106), to microporphyritic (I045-14). Some of the more typical textures are shown in Plates 4-3E to H and Plates 4-4A and B. The matrix of the samples commonly comprises intergrown sheaves of plagioclase and pyroxene with Fe-Ti oxides occurring as finely disseminated, equant grains filling the voids between the groundmass plagioclase and clinopyroxene. Some samples (e.g. I047-64) have an intersertal matrix of plagioclase laths with interstitial clinopyroxene and opaque oxides. The groundmass ferromagnesian minerals show varied degrees of alteration.

In the porphyritic varieties plagioclase and clinopyroxene occur as large euhedral to subhedral phenocrysts, often in subophitic relationship (Plate 4-4C). In contrast, samples I045-91, I045-151 and I047-62 are characterised by the occurrence of aggregates (1.0-3.0 mm) of radiating plagioclase laths (0.5-1.0 mm) intergrown with anhedral brownish clinopyroxene (0.2-0.5 mm) in a 'rosette' type structure (Plate 4-4D). Sample I045-151 is typified by the presence of abundant vesicles.

The variation in plagioclase composition is depicted in Fig. 4-22B. The majority of phenocrysts range in composition from An_{89} to An_{60}, though zoning can occur to compositions as sodic as An_{36}. Zoning is generally normal, but reverse zoning does occur in some phenocrysts. For example, a large subhedral plagioclase phenocryst (An_{48}) in I045-91 is bounded by a sharp contact from a rim of calcic plagioclase (An_{67}). Microphenocrysts generally range in composition from An_{60} to An_{45}.

T A B L E 4-16

CONRAD F.7: SELECTED MINERAL ANALYSES. PLAG - PYX BASALTS

	1	2	3	4	5	6	7	8	9	10
SIO2	45.64	48.57	49.73	54.52	46.78	55.19	52.91	49.33	52.48	52.09
TIO2	ND	.03	.05	.08	.02	.07	.09	.06	.07	-
AL203	33.98	31.86	31.23	28.04	34.22	27.89	29.42	31.99	29.51	30.20
CR203	-	-	-	-	-	-	-	-	-	-
FEO	.36	.65	.45	.78	.53	.62	.57	.51	.83	.55
MNO	-	-	-	-	-	-	-	-	-	-
MGO	.20	.13	.23	.09	.16	.07	.15	.23	.28	-
CAO	17.33	15.02	14.63	10.72	17.72	10.67	12.57	15.14	12.61	13.30
NA20	1.66	2.88	3.28	5.50	1.17	5.64	4.42	3.08	4.48	4.02
K20	ND	.03	.03	.12	.15	.14	.08	.04	.06	.04
TOTAL	99.19	99.17	99.63	99.85	100.75	100.29	100.21	100.38	100.32	100.20

* * ATOMIC PROPORTIONS BASED ON SELECTED NO. OF OXYGENS * *

OXYGEN	8	8	8	8	8	8	8	8	8	8
SI	2.121	2.244	2.282	2.472	2.139	2.489	2.399	2.251	2.382	2.365
AL	1.861	1.735	1.689	1.499	1.844	1.482	1.572	1.721	1.579	1.616
TI	-	.001	.002	.003	.001	.002	.003	.002	.002	-
CR	-	-	-	-	-	-	-	-	-	-
FE2+	.014	.025	.017	.030	.020	.023	.022	.019	.032	.021
MN	-	-	-	-	-	-	-	-	-	-
MG	.014	.009	.016	.006	.011	.005	.010	.016	.019	-
CA	.863	.744	.719	.521	.868	.516	.611	.740	.613	.647
NA	.150	.258	.292	.484	.104	.493	.389	.273	.394	.354
K	-	.002	.002	.007	.009	.008	.005	.002	.003	.002
SUM	5.023	5.017	5.019	5.021	4.995	5.018	5.009	5.024	5.025	5.005
	AN 85.18	AN 74.11	AN 71.02	AN 51.50	AN 88.53	AN 50.71	AN 60.83	AN 72.92	AN 60.66	AN 64.49
	AB 14.76	AB 25.71	AB 28.81	AB 47.81	AB 10.58	AB 48.50	AB 38.71	AB 26.85	AB 39.00	AB 35.28
	OR .06	OR .18	OR .17	OR .69	OR .89	OR .79	OR .46	OR .23	OR .34	OR .23

* * * S A M P L E D I R E C T O R Y * * *

ANALYSIS NO.	DESCRIPTION
1	PLAG, PHENO (CORE, I045-130B)
2	PLAG, PHENO (AS ABOVE, RIM)
3	PLAG, PHENO (CORE, I045-130B)
4	PLAG, MICROPHENO (I045-130B)
5	PLAG, PHENO (CORE, I045-173)
6	PLAG, PHENO (CORE, I045-173)
7	PLAG, PHENO (CORE, I047-64)
8	PLAG, PHENO (CORE, I045-91)
9	PLAG, PHENO (AS ABOVE, RIM)
10	PLAG, PHENO (CORE, I045-151)

** ND = NOT DETECTED **

TABLE 4-16 (CONTINUED)

CONRAD F.Z: SELECTED MINERAL ANALYSES. PLAG - PYX BASALTS

	11	12	13	14	15	16	17	18	19	20
SIO2	45.16	52.19	52.86	54.12	51.84	52.91	53.14	52.02	51.21	49.00
TIO2	.04	.11	.09	.09	.42	.32	.44	.64	.51	1.06
AL2O3	34.65	29.72	29.47	29.01	3.69	1.94	1.93	2.30	2.87	1.77
CR2O3	-	-	-	-	.83	.18	.20	.12	.64	.03
FEO	.35	.72	.60	.81	4.71	6.27	6.89	8.24	6.23	18.82
MNO	-	-	-	-	.12	.16	.16	.20	.16	.49
MGO	.24	.24	.16	.09	17.59	18.79	18.89	17.33	17.25	11.20
CAO	17.94	12.42	12.04	11.38	20.47	18.57	18.53	19.02	21.40	17.62
NA2O	1.25	4.34	4.65	5.22	.28	.21	.20	.22	.24	.25
K2O	ND	.11	.10	.13	-	-	-	-	-	-
TOTAL	99.64	99.85	99.97	100.85	99.95	99.35	100.38	100.09	100.51	100.24

* * ATOMIC PROPORTIONS BASED ON SELECTED NO. OF OXYGENS * *

OXYGEN	8	8	8	8	6	6	6	6	6	6
SI	2.092	2.377	2.400	2.435	1.893	1.942	1.936	1.918	1.882	1.900
ALIV	1.892	1.596	1.577	1.538	.107	.058	.064	.082	.118	.081
ALVI	-	-	-	-	.052	.026	.019	.018	.007	-
TI	.001	.004	.003	.003	.012	.009	.012	.018	.014	.031
CR	-	-	-	-	.024	.005	.006	.003	.019	.001
FE2+	.014	.027	.023	.030	.144	.193	.210	.254	.192	.610
MN	-	-	-	-	.004	.005	.005	.006	.005	.016
MG	.017	.016	.011	.006	.957	1.028	1.026	.952	.945	.647
CA	.890	.606	.586	.549	.801	.731	.723	.752	.843	.732
NA	.112	.383	.409	.455	.020	.015	.014	.016	.017	.019
K	-	.006	.006	.007	-	-	-	-	-	-
SUM	5.018	5.016	5.015	5.024	4.014	4.012	4.015	4.020	4.041	4.037
	AN 88.75	AN 60.87	AN 58.52	AN 54.24	WO 42.11	WO 37.44	WO 36.93	WO 38.38	WO 42.58	WO 36.79
	AB 11.19	AB 38.49	AB 40.90	AB 45.02	EN 50.33	EN 52.69	EN 52.36	EN 48.64	EN 47.74	EN 32.53
	OR .06	OR .64	OR .58	OR .74	FS 7.56	FS 9.87	FS 10.72	FS 12.98	FS 9.68	FS 30.67

* * * SAMPLE DIRECTORY * * *

ANALYSIS NO.	DESCRIPTION
11	PLAG, PHENO (CORE, I045-14)
12	PLAG, PHENO (AS ABOVE, RIM)
13	PLAG, PHENO (CORE, I047-62)
14	PLAG, PHENO (EUHEDRAL, I045-106)
15	CPX, GLOMERO. (I045-130B)
16	CPX, PHENO (CORE, I045-130B)
17	CPX, PHENO (CORE, I047-64)
18	CPX, PHENO (AS ABOVE, RIM)
19	CPX, PHENO (I045-173)
20	CPX, MICROPHENO (I045-173)

** ND = NOT DETECTED **

T A B L E 4-16 (CONTINUED)

CONRAD F.7: SELECTED MINERAL ANALYSES. PLAG - PYX BASALTS

	21	22	23	24	25	26	27	28	29
SIO2	50.46	50.06	52.21	49.84	51.47	.12	.22	.10	.10
TIO2	.76	1.17	.57	1.31	.41	50.24	13.36	50.45	19.84
AL2O3	3.87	3.63	2.19	4.34	3.11	.12	.49	.11	1.09
CR2O3	.20	-	.20	.03	.40	.10	-	-	.08
FE2O3	-	-	-	-	-	3.89	41.12	4.13	27.23
FEO	7.25	12.61	7.19	11.12	5.99	43.85	42.95	43.31	48.39
MNO	.15	.26	.18	.27	.13	1.40	.43	2.13	.56
MGO	17.74	18.06	17.22	14.60	17.77	.03	ND	ND	ND
CAO	18.61	14.00	19.68	18.95	19.90	-	-	-	-
NA2O	.18	.18	.26	.34	.15	-	-	-	-
K2O	-	-	-	-	-	-	-	-	-
TOTAL	99.22	99.97	99.70	100.80	99.33	99.75	98.58	100.24	97.30

* * ATOMIC PROPORTIONS BASED ON SELECTED NO. OF OXYGENS * *

OXYGEN	6	6	6	6	6	3	4	3	4
SI	1.870	1.864	1.927	1.854	1.899	.003	.008	.003	.004
ALIV	.130	.136	.073	.146	.101	.004	.022	.003	.050
ALVI	.039	.023	.022	.044	.035	-	-	-	-
TI	.021	.033	.016	.037	.011	.957	.386	.957	.575
CR	.006	-	.006	.001	.012	.002	-	-	.002
FE3+	-	-	-	-	-	.074	1.189	.078	.790
FE2+	.225	.393	.222	.346	.185	.929	1.380	.913	1.560
MN	.005	.008	.006	.009	.004	.030	.014	.045	.018
MG	.980	1.002	.947	.809	.977	.001	-	-	-
CA	.739	.559	.778	.755	.787	-	-	-	-
NA	.013	.013	.019	.025	.011	-	-	-	-
K	-	-	-	-	-	-	-	-	-
SUM	4.028	4.030	4.016	4.026	4.021	2.000	3.000	2.000	3.000
	WO 38.02	WO 28.59	WO 39.97	WO 39.53	WO 40.37	IL 96.16	US 39.37	IL 96.03	US 59.29
	EN 50.41	EN 51.30	EN 48.64	EN 42.36	EN 50.14	GK .11	MT 60.63	GK .04	MT 40.71
	FS 11.56	FS 20.10	FS 11.40	FS 18.11	FS 9.49	HM 3.73		HM 3.93	

* * * S A M P L E D I R E C T O R Y * * *

ANALYSIS NO.	DESCRIPTION
21	CPX, PHENO (CORE, I045-91)
22	CPX, MICROPHENO (I045-91)
23	CPX, PHENO (CORE, I047-62)
24	CPX, PHENO (I047-62)
25	CPX, (I045-14)

ANALYSIS NO.	DESCRIPTION
26	ILMENITE (I045-130B)
27	TI-MAGNETITE (I045-130B)
28	ILMENITE (I047-62)
29	TI-MAGNETITE (I047-62)

** ND = NOT DETECTED **

Representative plagioclase analyses are presented in Table 4-16, and individual analyses are given in microfiche Tables F4-13 to F4-21. Relative to the olivine-plagioclase-pyroxene basalts, the plagioclase compositions extend to more sodic varieties (Figs. 4-22A and B).

Cores of the larger clinopyroxene phenocrysts have a relatively restricted range in composition: $Wo_{42}En_{51}Fs_7$ to $Wo_{37}En_{52}Fs_{11}$, but some are zoned to more Fe-rich compositions at the extreme rims, e.g. $Wo_{41}En_{46}Fs_{13}$ to $Wo_{38}En_{46}Fs_{16}$. Smaller phenocryst and microphenocrysts range in composition from $Wo_{38}En_{47}Fs_{15}$ to $Wo_{37}En_{32}Fs_{31}$. Representative analyses are presented in Table 4-16 and individual analyses are depicted in Fig. 4-23B.

Unlike the IOFZ pyroxenes, pyroxenes from the Conrad F.Z. basalts do not show systematic minor element variations, suggesting the lack of a simple genetic relationship between all the various basalts. In a plot of Al^{IV} versus TiO_2 and SiO_2 versus Al_2O_3 (Fig. 4-24), the Conrad F.Z. basalt pyroxenes show considerable scatter but fall within the 'non-alkaline' field of La Bas (1962), attesting to their tholeiitic affinities. In terms of Al^{IV}, TiO_2 and SiO_2, the pyroxenes from the dolerites of the Conrad F.Z. are indistinguishable from those occurring in the basalts (Fig. 4-24). This contrasts, however, with the pyroxenes from the IOFZ which show considerable displacement into the 'alkaline' field (Figs. 4-24 and 4-10).

Fe-Ti oxides occur as finely disseminated grains in all the samples. Though they are generally too small for accurate microprobe analyses, semi-quantitative analyses indicate the presence of both ilmenite (I045-130B, I045-173, I047-62) and titanomagnetite (I045-130B, I045-91, I045-151, I045-161B, I047-62). Analyses of ilmenite grains in

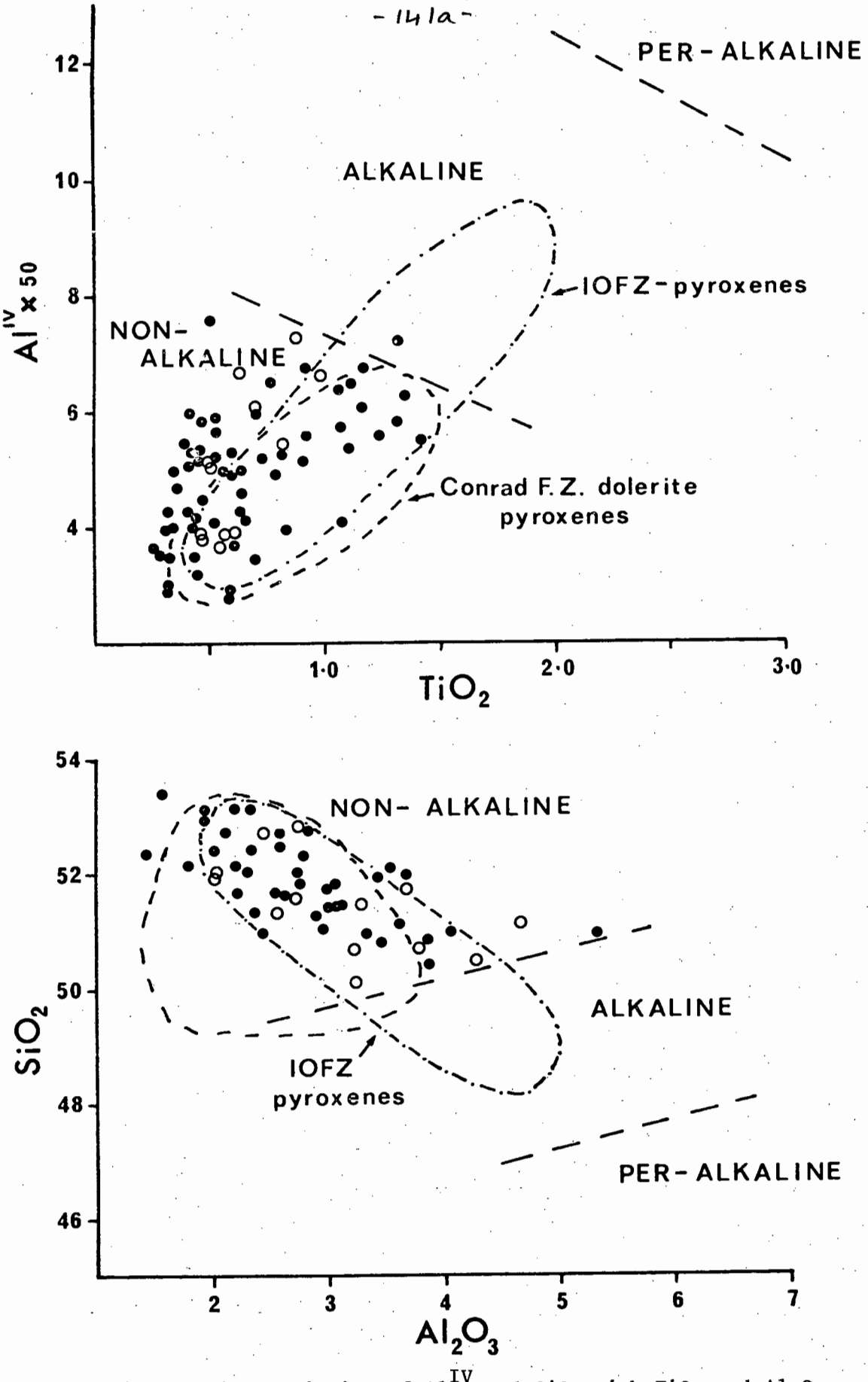

Fig. 4-24: Variation of Al^{IV} and SiO_2 with TiO_2 and Al_2O_3 respectively in pyroxenes from Conrad F.Z. basalts. Non-alkaline, alkaline and per-alkaline fields are taken from La Bas (1962). Compositional fields of IOFZ pyroxenes and pyroxenes from Conrad F.Z. dolerites are shown for comparison. Open symbols represent pyroxenes from basalts containing olivine.

PLATE 4-4

A: Photomicrograph of sparsely porphyritic plagioclase-pyroxene basalt I047-62. The larger phenocrysts consist of both plagioclase and clinopyroxene.

B: Photomicrograph of microporphyritic plagioclase-pyroxene basalt I045-14.

C: Clinopyroxene phenocryst subophitically intergrown with plagioclase in plagioclase-pyroxene basalt I045-130B. Crossed polars.

D: 'Rosette' comprising radially orientated plagioclase laths intergrown with anhedral clinopyroxene in plagioclase-pyroxene basalt I045-91. Crossed polars.

E: Photomicrograph showing the texture of medium grained dolerite I045-159, comprising interlocking plagioclase and clinopyroxene grains with dispersed Fe-Ti oxides. The vein cutting across the field of view consists of K-feldspar.

F: Photomicrograph of medium grained dolerite I045-34 showing large plagioclase crystals set in a matrix of interlocking plagioclase and clinopyroxene grains.

G: Photomicrograph of ferrodolerite I045-68 comprising a crystalline intergrowth of plagioclase and dominantly altered clinopyroxene. The vein cutting across the field of view in the lower left hand corner consists of analcite.

H: Photomicrograph showing the contact between porphyritic plagioclase-pyroxene basalt I045-130B and medium grained dolerite I045-130D.

PLATE 4-4

A

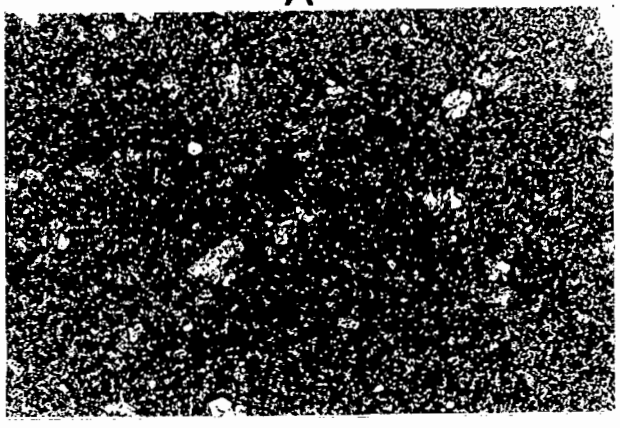

4·7 mm

B

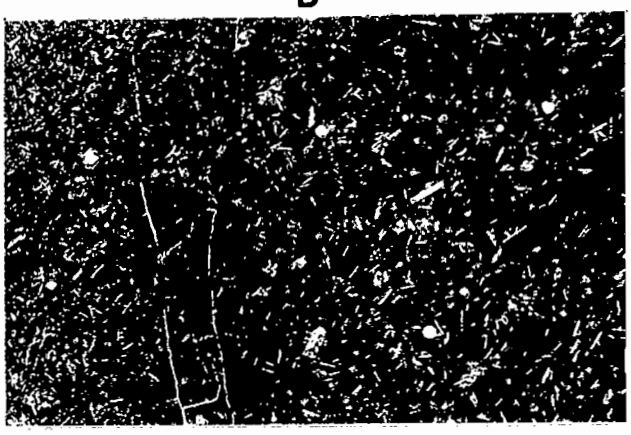

4·4 mm

C

2·2 mm

D

·75 mm

E

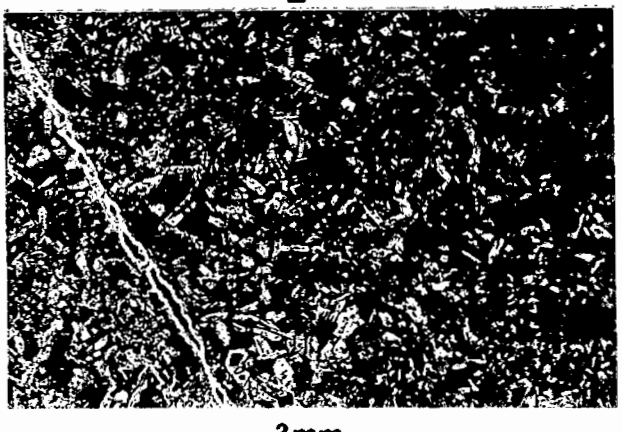

3mm

F

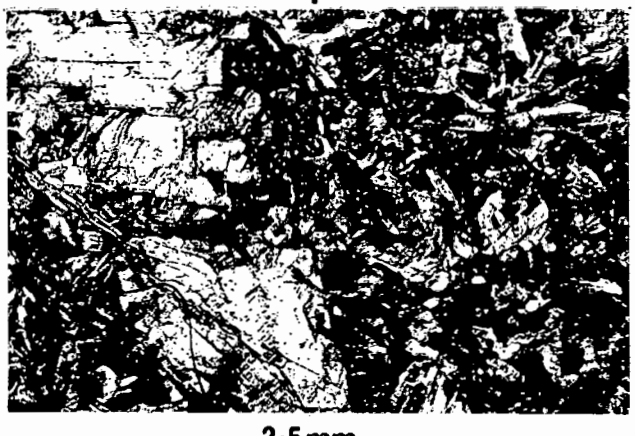

2·5mm

G

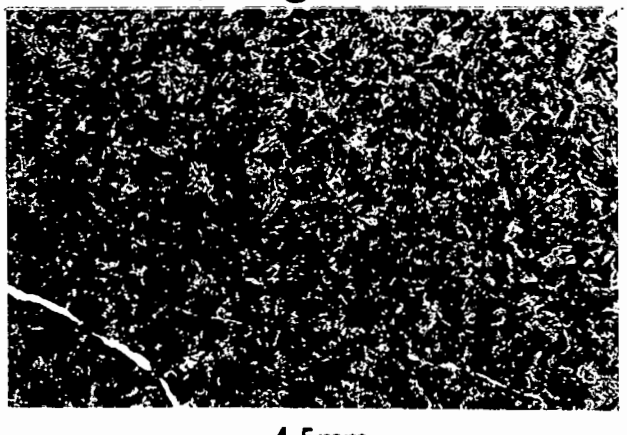

4·5mm

H

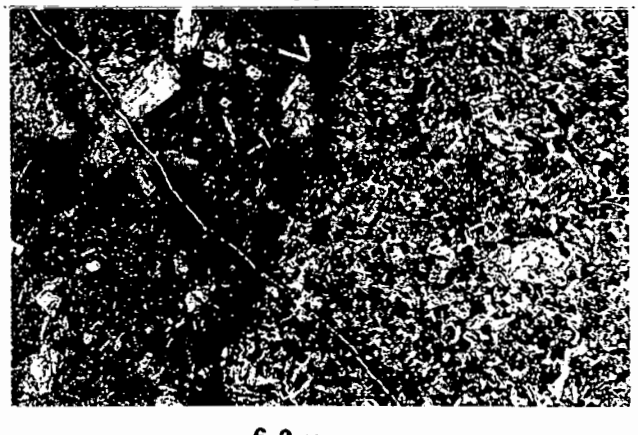

6·3mm

samples I045-130B and I047-62 show them to be of very similar composition ($Il_{96}Hm_4$; Table 4-16) in terms of major components, but the ilmenite from I045-130B is relatively enriched in Mn (Table 4-16). It was possible to analyse only a single coexisting titanomagnetite in each of the above two samples (I045-130B, I047-62) and in both cases the total was extremely low (Table 4-16). The two compositions differ significantly (Us_{40} and Us_{60} respectively), but whether this is a primary feature or a result of post-consolidation oxidation (e.g. Haggerty, 1976) is difficult to assess. A factor favouring the latter is the extremely low temperature and oxygen fugacity obtained for the coexisting compositions in I045-130B. Using the T-fO_2-X curves of Buddington and Lindsley (1964), and equilibration temperature of 750°C at an fO_2 of 10^{-17} atm. is indicated for the coexisting ilmenite-titanomagnetite in I045-130B. The coexisting Fe-Ti oxides in I047-62 indicate a temperature of 850°C at 10^{-14} atm.

4.1.2 Intrusive Rocks:

Twelve hypabyssal basalts (dolerites), one ferrodiorite and a hypersthene gabbro have been studied from the Conrad F.Z. The three varieties are described separately below.

(i) Dolerites

The majority of dolerites (samples I045-34, I045-49, I045-130D, I045-148, I045-159, I045-160, I047-12, I047-32 and I047-101) are medium grained (0.5-2.0 mm), and comprise varying proportions of plagioclase and clinopyroxene forming an interlocking meshwork, with sparse large phenocrysts and glomerocrysts of plagioclase and clinopyroxene. Some typical textures are shown in Plates 4-4E to H. Plagioclase varies in composition from calcic bytownite to andesine (Fig. 4-22C, Table 4-17) and is marked by extreme compo-

TABLE 4-17

CONRAD F.Z: SELECTED MINERAL ANALYSES. MEDIUM GRAINED DOLERITES

	1	2	3	4	5	6	7	8	9	10
SIO2	45.92	50.50	50.30	54.63	54.48	61.77	55.63	59.14	46.41	56.79
TIO2	.04	.08	-	.11	-	-	.10	.06	.04	.05
AL203	34.15	30.28	31.29	27.71	28.70	24.42	27.71	25.67	33.95	26.76
CR203	-	-	-	-	-	-	-	-	-	-
FEO	.36	.65	.49	.68	.66	.50	.68	.45	.34	.41
MNO	-	-	-	-	-	-	-	-	-	-
MGO	.21	.18	-	.10	.16	.08	.11	.03	.25	.04
CAO	17.81	13.46	14.84	10.85	11.38	5.73	10.66	7.76	16.80	8.58
NA2O	1.70	3.91	3.53	5.48	5.31	7.56	5.48	7.06	1.59	6.75
K2O	.02	.06	.06	.12	.11	.25	.12	.16	ND	.15
TOTAL	100.21	99.12	100.51	99.68	100.80	100.31	100.49	100.33	99.39	99.53

* * ATOMIC PROPORTTONS BASED ON SELECTED NO. OF OXYGENS * *

OXYGEN	8	8	8	8	8	8	8	8	8	8
SI	2.116	2.326	2.290	2.481	2.450	2.732	2.501	2.637	2.145	2.564
AL	1.855	1.644	1.679	1.483	1.521	1.273	1.468	1.349	1.849	1.424
TI	.001	.003	-	.004	-	-	.003	.002	.001	.002
CR	-	-	-	-	-	-	-	-	-	-
FE2+	.014	.025	.019	.026	.025	.018	.026	.017	.013	.015
MN	-	-	-	-	-	-	-	-	-	-
MG	.014	.012	-	.007	.011	.005	.007	.002	.017	.003
CA	.879	.664	.724	.528	.548	.272	.514	.371	.832	.415
NA	.152	.349	.312	.483	.463	.648	.478	.610	.142	.591
K	.001	.004	.003	.007	.006	.014	.007	.009	-	.009
SUM	5.032	5.026	5.028	5.018	5.024	4.963	5.004	4.997	5.001	5.022
	AN 85.17	AN 65.32	AN 69.67	AN 51.89	AN 53.88	AN 29.07	AN 51.45	AN 37.44	AN 85.33	AN 40.91
	AB 14.71	AB 34.34	AB 29.99	AB 47.43	AB 45.50	AB 69.42	AB 47.86	AB 61.64	AB 14.61	AB 58.24
	OR .11	OR .35	OR .34	OR .68	OR .62	OR 1.51	OR .69	OR .92	OR .06	OR .85

* * * S A M P L E D I R E C T O R Y * * *

ANALYSIS NO.	DESCRIPTION
1	PLAG, PHENO (CORE, I045-34)
2	PLAG, PHENO (AS ABOVE, RIM)
3	PLAG, PHENO (I045-49)
4	PLAG, PHENO (I045-130D)
5	PLAG, PHENO (CORE, I045-159)
6	PLAG, PHENO (AS ABOVE, RIM)
7	PLAG, PHENO ,(CORE, I047-12)
8	PLAG, PHENO (AS ABOVE, RIM)
9	PLAG, PHENO (CORE, I047-32)
10	PLAG, PHENO (AS ABOVE, RIM)

** ND = NOT DETECTED **

T A B L E 4-17 (CONTINUED)

CONRAD F.Z: SELECTED MINERAL ANALYSES. MEDIUM GRAINED DOLERITES

	11	12	13	14	15	16	17	18	19	20
SIO2	52.88	52.30	50.49	52.40	50.81	50.36	52.05	50.34	51.17	50.30
TIO2	.36	.66	.62	.47	.79	.99	.73	1.23	.77	.93
AL2O3	2.46	2.58	1.29	2.77	3.26	2.26	2.79	2.26	3.14	1.87
CR2O3	.61	.16	.54	.41	.18	ND	.11	.02	.60	.04
FEO	4.28	8.07	17.29	5.65	7.74	13.08	7.55	14.33	7.11	15.63
MNO	.13	.19	.42	.12	.20	.27	.18	.29	.14	.37
MGO	17.91	16.67	11.71	17.72	16.48	14.23	16.97	13.28	16.66	14.06	
CAO	20.76	19.31	17.32	20.88	19.33	17.80	18.93	17.32	20.10	16.92
NA2O	.24	.30	.32	.23	.23	.32	.27	.33	.25	.26
K2O	-	-	-	-	-	-	-	-	-	-
TOTAL	99.63	100.24	100.00	100.65	99.02	99.32	99.58	99.40	99.94	100.38

* * ATOMIC PROPORTIONS BASED ON SELECTED NO. OF OXYGENS * *

OXYGEN	6	6	6	6	6	6	6	6	6	6
SI	1.932	1.924	1.942	1.909	1.894	1.913	1.921	1.918	1.890	1.909
ALIV	.068	.076	.058	.091	.106	.087	.079	.082	.110	.084
ALVI	.038	.036	.001	.028	.038	.014	.042	.020	.027	-
TI	.010	.018	.018	.013	.022	.028	.020	.035	.021	.027
CR	.018	.005	.016	.012	.005	-	.003	.001	.018	.001
FE2+	.131	.248	.556	.172	.241	.415	.233	.457	.220	.496
MN	.004	.006	.014	.004	.006	.009	.006	.009	.004	.012
MG	.975	.914	.671	.962	.916	.805	.933	.754	.917	.795
CA	.813	.761	.714	.815	.772	.724	.749	.707	.796	.688
NA	.017	.021	.024	.016	.017	.024	.019	.024	.018	.019
K	-	-	-	-	-	-	-	-	-	-
SUM	4.005	4.010	4.014	4.021	4.017	4.020	4.006	4.008	4.020	4.031
	WO 42.36	WO 39.57	WO 36.77	WO 41.81	WO 40.03	WO 37.24	WO 39.09	WO 36.87	WO 41.17	WO 34.76
	EN 50.83	EN 47.52	EN 34.58	EN 49.36	EN 47.46	EN 41.41	EN 48.74	EN 39.32	EN 47.46	EN 40.18
	FS 6.82	FS 12.91	FS 28.65	FS 8.83	FS 12.51	FS 21.36	FS 12.17	FS 23.81	FS 11.37	FS 25.06

* * * S A M P L E D I R E C T O R Y * * *

ANALYSIS NO.	DESCRIPTION
11	CPX, PHENO (1045-34)
12	CPX, PHENO (CORE, 1045-34)
13	CPX, PHENO (AS ABOVE, RIM)
14	CPX, PHENO (ADJ. TO PLAG INCL. 1045-49)
15	CPX, PHENO (1045-130D)
16	CPX, PHENO (1045-130D)
17	CPX, PHENO (1045-159)
18	CPX, PHENO (CORE, 1045-159)
19	CPX, LARGE PHENO (CORE, 1047-12)
20	CPX, PHENO (AS ABOVE, RIM)

** ND = NOT DETECTED **

T A B L E 4-17 (CONTINUED)

CONRAD F.Z: SELECTED MINERAL ANALYSES. MEDIUM GRAINED DOLERITES

	21	22	23	24	25	26	27	28	29	30
SIO2	.04	ND	-	-	-	.15	.50	.15	.13	.12
TIO2	48.62	50.80	23.94	25.53	50.63	47.53	50.09	20.78	26.12	24.94
AL203	.04	.02	1.07	1.23	ND	.17	.22	1.01	1.90	.82
CR203	-	-	-	-	-	-	-	-	-	-
FE203	7.93	2.82	20.83	17.30	3.80	9.58	2.91	27.20	15.39	20.17
FEO	42.46	44.41	52.57	54.09	44.38	41.69	43.90	50.00	54.74	53.38
MNO	1.24	1.11	.59	.47	1.05	1.04	1.39	.67	.73	1.11
MGO	.03	.09	ND	ND	.05	.10	.19	-	.04	.04
CAO	-	-	-	-	-	-	-	-	-	.17
NA20	-	-	-	-	-	-	-	-	-	-
K20	-	-	-	-	-	-	-	-	-	-
TOTAL	100.36	99.26	99.01	98.63	99.92	100.26	99.20	99.81	99.05	100.75

* * ATOMIC PROPORTIONS BASED ON SELECTED NO. OF OXYGENS * *

OXYGEN	3	3	4	4	3	3	3	4	4	4
SI	.001	-	-	-	-	.004	.013	.006	.005	.004
AL	.001	.001	.048	.055	-	.005	.007	.045	.084	.036
TI	.923	.972	.680	.726	.964	.903	.956	.587	.736	.696
CR	-	-	-	-	-	-	-	-	-	-
FE3+	.151	.054	.592	.492	.072	.182	.056	.769	.434	.563
FE2+	.896	.945	1.661	1.711	.939	.880	.932	1.572	1.716	1.657
MN	.027	.024	.019	.015	.023	.022	.030	.021	.023	.035
MG	.001	.003	-	-	.002	.004	.007	-	.002	.002
CA	-	-	-	-	-	-	-	-	-	.007
NA	-	-	-	-	-	-	-	-	-	-
K	-	-	-	-	-	-	-	-	-	-
SUM	2.000	2.000	3.000	3.000	2.000	2.000	2.000	3.000	3.000	3.000
	IL 92.34	IL 96.96	US 69.67	US 74.68	IL 96.19	IL 90.46	IL 96.45	US 60.43	US 77.23	US 71.19
	GK .11	GK .34	MT 30.33	MT 25.32	GK .19	GK .38	GK .73	MT 39.57	MT 22.77	MT 28.81
	HM 7.54	HM 2.70			HM 3.62	HM 9.16	HM 2.82			

* * * S A M P L E D I R E C T O R Y * * *

ANALYSIS NO.	DESCRIPTION
21	ILMENTIE, (1045-34)
22	ILMENTIE, (1045-34)
23	TI-MAGNETITE (1045-49)
24	TI-MAGNETITE (1045-49)
25	ILMENTIE (1045-49)
26	TLMENITE (1045-49)
27	ILMENITE (1045-159)
28	TI-MAGNETITE (1045-159)
29	TI-MAGNETITE (1045-159)
30	TI-MAGNETITE (1047-32)

** ND = NOT DETECIED **

sitional zoning (e.g. I047-32; An_{85}(core) - An_{41}(rim)). Representative analyses are given in Table 4-17 and individual analyses in microfiche Tables F4-22 to F4-28. Clinopyroxenes range in composition from diopsidic augite to ferro-augite. The range in composition ($Wo_{42}En_{51}Fs_{7}$-$Wo_{36}En_{33}Fs_{31}$) is depicted graphically in Fig. 4-25 and representative analyses are given in Table 4-17. With the exception of a greater proportion of Fe-rich pyroxenes, the compositional spread is very similar to that observed for the pyroxenes of the Conrad F.Z. plagioclase-pyroxene basalts (Fig. 4-23B).

Ilmenite and/or titanomagnetite occur in the matrix of all the medium grained dolerite samples. Titanomagnetite ranges in composition from $Us_{60}Mt_{40}$ to $Us_{77}Mt_{23}$ (Table 4-17) and generally has well developed exsolution, resulting in an apparent range of compositions within one thin section. Most of the exsolution observed conforms to the 'trellis type' (Haggerty, 1976) and can be attributed to post emplacement oxidation. Ilmenite varies in composition from $Il_{90}Hm_{10}$ to $Il_{98}Hm_{2}$ (Table 4-17) and generally has a more uniform composition than coexisting titanomagnetite. Though coexisting titanomagnetite-ilmenite occurs in samples I045-49, I045-130D and I045-159, the exsolved nature of the titanomagnetite restricts its potential use in calculating temperatures and oxygen fugacities.

Sample I047-28 has an even grained microdoleritic texture of interlocking plagioclase laths (0.5 mm) and fine grained augitic pyroxene, interspersed with equant ilmenite grains (Plate 4-5B). Plagioclase varies in composition from An_{51} to An_{37} (Fig. 4-22C); representative analyses are presented in Table 4-18 and individual analyses in microfiche Table F4-29. Clinopyroxene has an Fe-rich composition

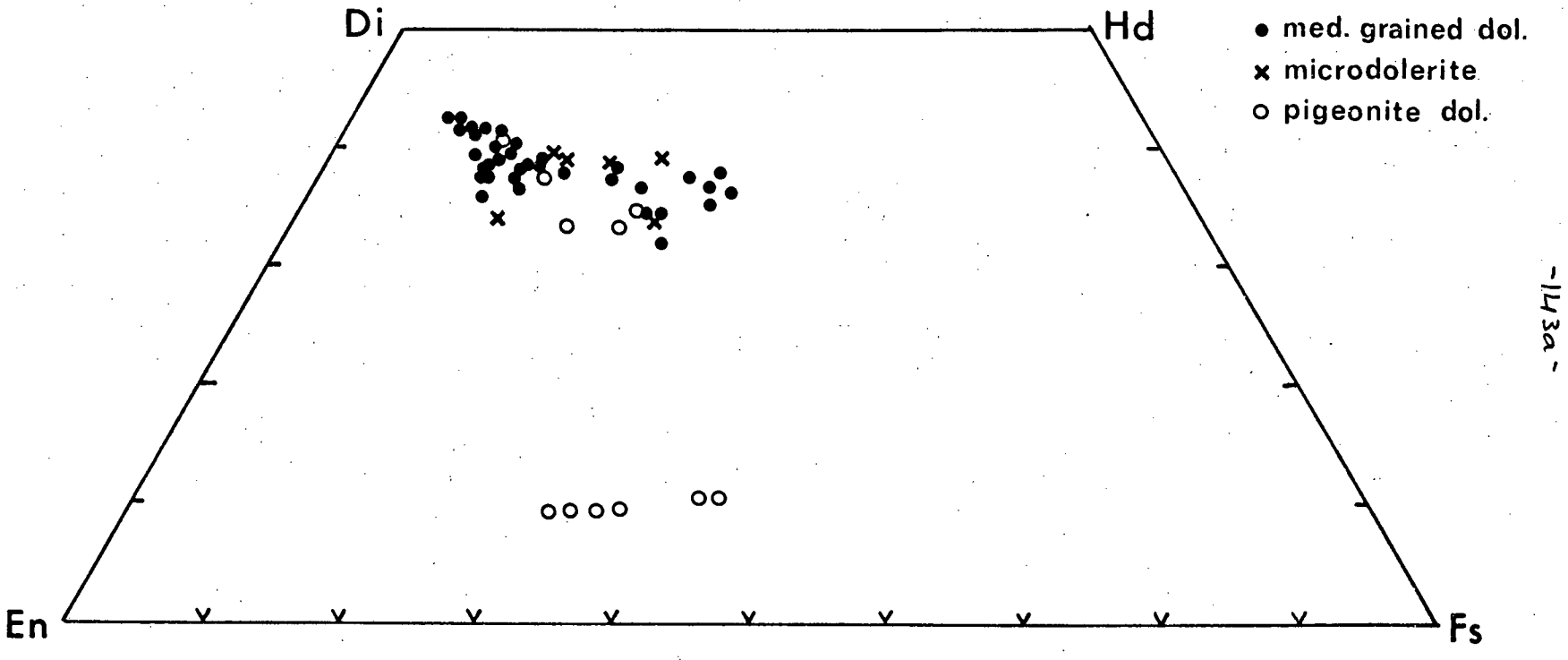

Fig. 4-25: Compositional variation of pyroxenes from Conrad F.Z. dolerites.

($Wo_{35}En_{51}Fs_{14}$ to $Wo_{34}En_{40}Fs_{26}$); the compositional variation is depicted in Fig. 4-25. Ilmenite is extremely uniform in composition ($Il_{94}Hm_{6}$) and is distinguished from the ilmenite of the other dolerites by its extremely high MnO content, 5.1-6.5% (Table 4-18).

A single sample of pigeonite dolerite (I047-72) was dredged from the Conrad F.Z. Abundant large plagioclase phenocrysts (1.0-2.0 mm) are set in a matrix of smaller plagioclase laths and small (0.2 mm) anhedral augitic pyroxene and pigeonite (Plate 4-5A). Relatively large (0.2-0.5 mm), equant to irregular Fe-Ti oxides occur dispersed throughout the matrix. Plagioclase varies in composition from An_{93} to An_{55} (Fig. 4-22C) and shows marked compositional zoning (e.g. An_{89}-An_{55}). Larger plagioclase phenocrysts commonly have abundant trapped melt inclusions and poikilitically enclosed pyroxene grains (Plate 4-5C). Representative analyses are presented in Table 4-18 and individual analyses in microfiche Table F4-30. Pigeonite ranges in composition from $Wo_{9}En_{60}Fs_{31}$ to $Wo_{10}En_{47}Fs_{43}$ (Fig. 4-25) and coexists with zoned augitic pyroxene ranging from $Wo_{41}En_{47}Fs_{12}$ to $Wo_{35}En_{41}Fs_{24}$ (Fig. 4-25, Table 4-18).

Sample I045-68 can be classified as a ferro-dolerite with a fine even grained texture of plagioclase (andesine to oligoclase) laths intergrown with extremely altered augitic pyroxene (Plate 4-4G). Titanomagnetite (exsolving ilmenite) and fine apatite needles occur in the matrix. Individual plagioclase analyses are depicted in Fig. 4-22C and representative mineral analyses are given in Table 4-18. Individual analyses are reported in microfiche Table F4-31.

In terms of Al^{IV} versus TiO_2 and SiO_2 versus Al_2O_3 (Fig. 4-26), the pyroxenes from the Conrad F.Z. dolerites are very similar to those

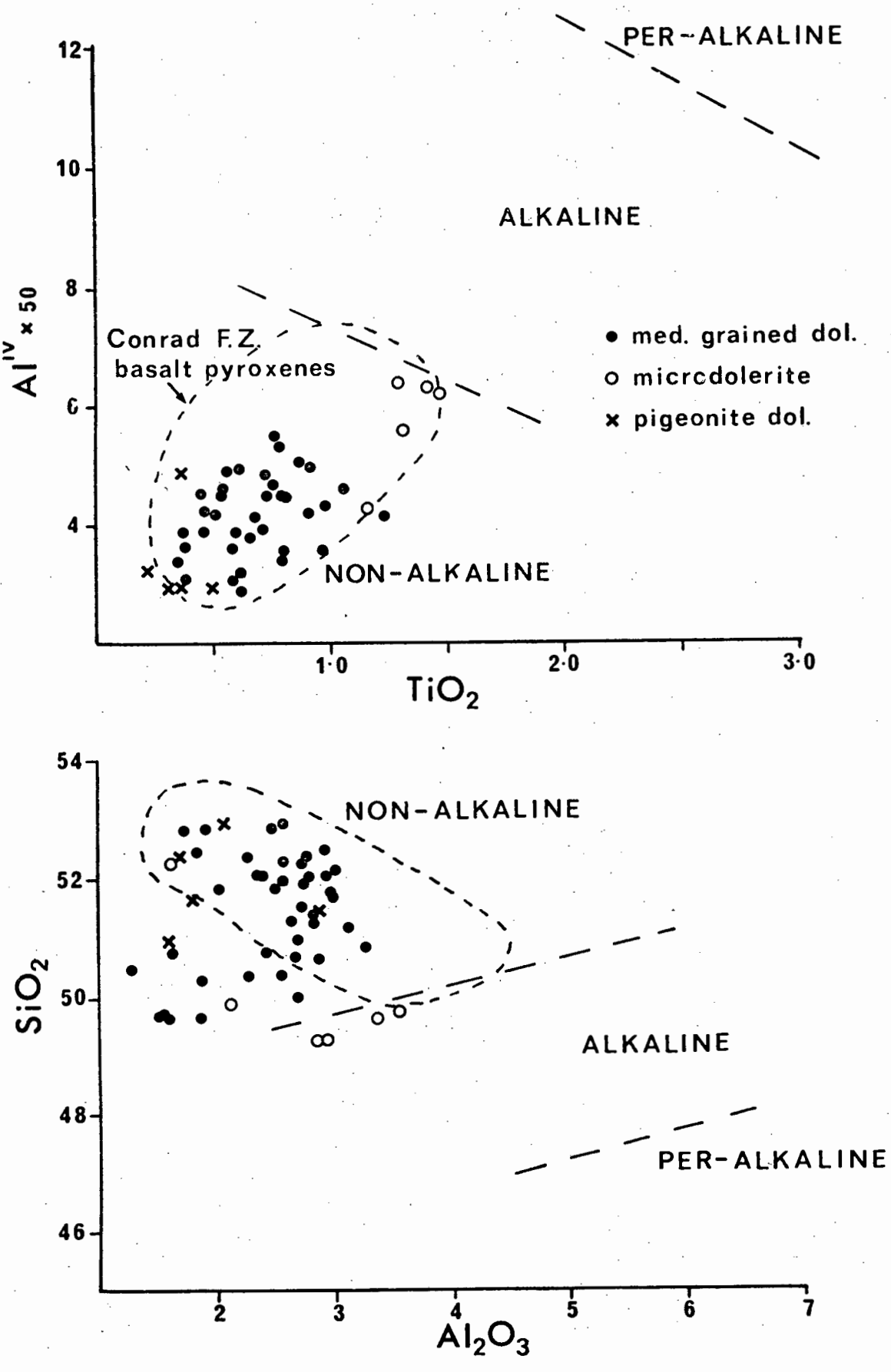

Fig. 4-26: Variation of Al^{IV} and SiO_2 with TiO_2 and Al_2O_3 respectively in pyroxenes from Conrad F.Z. dolerites. Non-alkaline, alkaline and per-alkaline fields are taken from La Bas (1962). The compositional field of pyroxenes from Conrad F.Z. basalts is shown for comparison. Symbols as indicated.

TABLE 4-18

CONRAD F.Z: SELECTED MINERAL ANALYSES. SELECTED DOLERITES

	1	2	3	4	5	6	7	8	9	10
SIO2	53.21	59.15	52.27	49.24	.33	44.01	53.23	53.14	51.17	51.47
TIO2	ND	.04	.62	1.31	48.92	.02	.06	.14	.27	.37
AL203	29.22	25.21	1.63	2.85	.13	35.09	28.11	.84	1.17	2.89
CR203	-	-	.39	.04	-	-	-	-	-	.05
FE203	-	-	-	-	6.92	-	-	-	-	-
FEO	.76	.52	8.93	15.59	37.36	.55	1.06	19.91	26.40	10.48
MNO	-	-	.44	.64	6.52	-	-	.49	.62	.28
MGO	.12	.24	17.99	13.45	.02	.03	.10	21.63	16.13	16.49
CAO	12.24	7.61	17.02	15.93	.30	18.72	11.58	4.63	4.97	18.62
NA20	4.51	7.12	.25	.32	-	.73	5.06	.03	.03	.16
K20	.09	.18	-	-	-	ND	.13	-	-	-
TOTAL	100.16	100.07	99.54	99.37	100.50	99.16	99.33	100.81	100.76	100.81

* * ATOMIC PROPORTIONS BASED ON SELECTED NO. OF OXYGENS * *

OXYGEN	8	8	6	6	3	8	8	6	6	6
SI	2.412	2.645	1.937	1.887	.008	2.055	2.438	1.965	1.958	1.902
ALIV	1.561	1.329	.063	.113	.004	1.931	1.517	.035	.042	.098
ALVI	-	-	.008	.016	-	-	-	.002	.011	.028
TI	-	.001	.017	.038	.924	.001	.002	.004	.008	.010
CR	-	-	.011	.001	-	-	-	-	-	.001
FE3+	-	-	-	-	.131	-	-	-	-	-
FE2+	.029	.019	.277	.500	.785	.021	.041	.616	.845	.324
MN	-	-	.014	.021	.139	-	-	.015	.020	.009
MG	.008	.016	.993	.768	.001	.002	.007	1.192	.920	.908
CA	.595	.365	.676	.654	.008	.936	.568	.183	.204	.737
NA	.396	.617	.018	.024	-	.066	.449	.002	.002	.011
K	.005	.010	-	-	-	-	.008	-	-	-
SUM	5.007	5.003	4.014	4.022	2.000	5.013	5.030	4.014	4.009	4.030
	AN 59.68	AN 36.75	WO 34.73	WO 34.03	IL 93.31	AN 93.35	AN 55.43	WO 9.21	WO 10.35	WO 37.44
	AB 39.79	AB 62.22	EN 51.05	EN 39.97	GK .08	AB 6.59	AB 43.83	EN 59.86	EN 46.73	EN 46.12
	OR .52	OR 1.03	FS 14.22	FS 26.00	HM 6.61	OR .06	OR .74	FS 30.92	FS 42.92	FS 16.45

* * * S A M P L E D I R E C T O R Y * * *

ANALYSIS NO.	DESCRIPTION
1	PLAG (I047-28)
2	PLAG (I047-28)
3	CPX (I047-28)
4	CPX (I047-28)
5	ILMENITE (I047-28)
6	PLAG, PHENO (CORE, I047-72)
7	PLAG, PHENO (AS ABOVE, RIM)
8	PIGEONITE (I047-72)
9	PIGEONITE, (I047-72)
10	CPX (I047-72)

** ND = NOT DETECTED **

T A B L E 4-18 (CONTINUED)

CONRAD F.Z: SELECTED MINERAL ANALYSES. SELECTED DOLERITES

	11	12	13	14	15
SIO2	50.98	57.04	64.12	59.44	51.34
TIO2	.49	.06	.02	.04	.74
AL2O3	1.58	26.48	22.22	25.50	2.41
CR2O3	ND	-	-	-	.22
FEO	14.94	.51	.19	.42	8.97
MNO	.39	-	-	-	.23
MGO	14.10	.08	.10	.03	16.60
CAO	16.81	8.97	3.57	7.61	18.95
NA2O	.21	6.67	9.61	7.62	.23
K2O	-	.15	.47	.16	-
TOTAL	99.51	99.96	100.30	100.82	99.69

* * ATOMIC PROPORTIONS BASED ON SELECTED NO. OF OXYGENS * *

OXYGEN	6	8	8	8	6
SI	1.941	2.568	2.829	2.641	1.910
ALIV	.059	1.405	1.156	1.335	.090
ALVI	.012	-	-	-	.016
TI	.014	.002	.001	.001	.021
CR	-	-	-	-	.006
FE2+	.476	.019	.007	.016	.279
MN	.013	-	-	-	.007
MG	.800	.005	.007	.002	.920
CA	.686	.433	.169	.362	.755
NA	.016	.582	.822	.656	.017
K	-	.009	.026	.009	-
SUM	4.017	5.023	5.017	5.023	4.022
	WO 34.96	AN 42.27	AN 16.59	AN 35.25	WO 38.64
	EN 40.79	AB 56.88	AB 80.81	AB 63.87	EN 47.08
	FS 24.25	OR .84	OR 2.60	OR .88	FS 14.28

* * * S A M P L E D I R E C T O R Y * * *

ANALYSIS NO.	DESCRIPTION
11	CPX (I047-72)
12	PLAG (I045-68)
13	PLAG (I045-68)
14	PLAG (I045-68)
15	CPX (I045-68)

** ND = NOT DETECTED **

PLATE 4-5

A: Pigeonite dolerite I047-72 showing abundant plagioclase phenocrysts. Crossed polars.

B: Photomicrograph of microdolerite I047-28 showing intergranular texture.

C: Plagioclase phenocrysts in I047-72. Crystal on the right has trapped melt inclusions in a zone separating the central core from the rim. The large phenocryst in the center has poikilitically enclosed pigeonite.

D: Hypersthene gabbro I045-172 with interlocking plagioclase orthopyroxene and clinopyroxene.

E: Photomicrograph of ferrodiorite I045-51 showing interlocking plagioclase, pyroxene and Fe-Ti oxides with dark patches of altered mesostases.

F: Subhedral 'brown' amphibole adjacent to a granophyric intergrowth of quartz, alkali feldspar and apatite needles. A slightly altered fayatitic olivine occurs in the center of the granophyric intergrowth.

G: Photomicrograph showing the typical occurrence of a pigeonite core surrounded by a mantle of Fe-rich clinopyroxene which is in turn mantled by 'secondary' green amphibole.

H: Plagioclase phenocryst in I047-64 showing partial alteration to K-feldspar and albite. Partially crossed polars.

PLATE 4-5

A

4mm

B

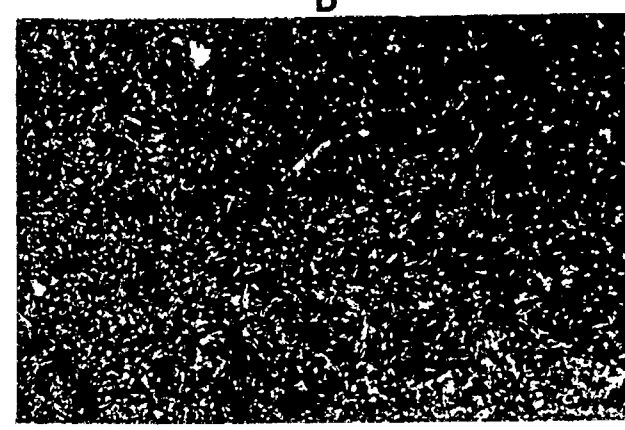

3mm

C

0·9mm

D

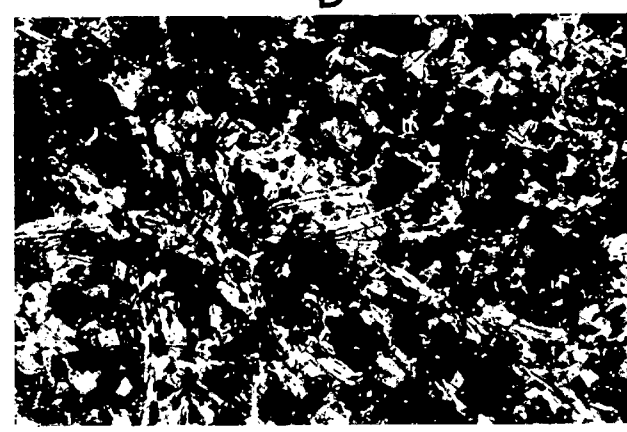

3·6mm

E

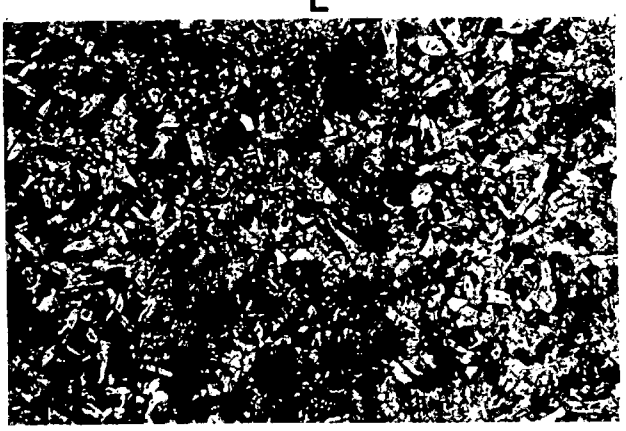

5mm

F

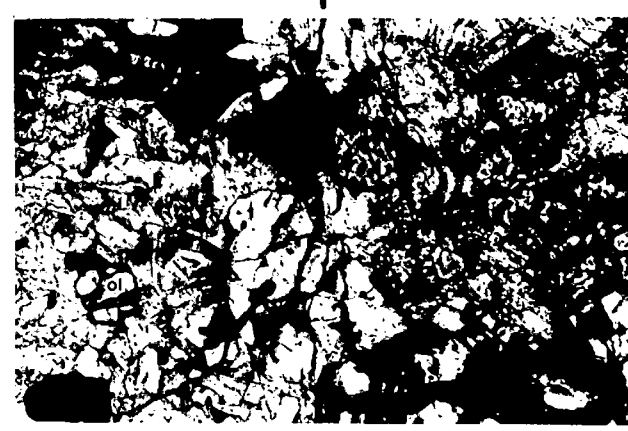

1·2 mm

G

1mm

H

1mm

occurring in the basalts (Fig. 4-24). Like the basalt pyroxenes, they are restricted to the non-alkaline compositional field (La Bas, 1962), with the pigeonite dolerite augitic pyroxenes having the lowest Al^{IV} and TiO_2 contents and the micro-dolerite pyroxenes having the highest.

(ii) Gabbro

A single sample of hypersthene gabbro (I045-172) was recovered from the Conrad F.Z. (Plate 4-5D). The rock comprises interlocking grains of primary plagioclase (An_{47}-An_{65}), clinopyroxene ($Wo_{46}En_{43}Fs_{11}$), orthopyroxene ($Wo_1En_{64}Fs_{35}$) and accessory ilmenite (Il_{90}-Il_{93}). Secondary minerals include brown ple ochroic amphibole, commonly replacing orthopyroxene and sparse flakes of biotite commonly associated with ilmenite. Representative mineral analyses are presented in Table 4-19 and individual analyses are given in microfiche Table F4-32.

(iii) Ferrodiorite

A single sample of ferrodiorite (I045-51) was recovered from the Conrad F.Z. Though evolved rocks of similar composition have previously been reported from the ocean floor (e.g. Aumento, 1969; Hart, 1971; Frey et al., 1976; Subbaro and Hekinian, 1978; Fodor et al., 1977; Viswanatha Reddy et al., 1978), numerous glacial erratics were recovered during dredging (Sclater et al., 1978) and the possibility exists that this rock may represent an erratic. Dickey et al. (1977) have reported on a rock with similar composition (basaltic andesite) from the dredge station just to the north of the Conrad F.Z. These authors concluded that the chemical characteristics of the rock were such as to indicate that it was an erratic. However, the interesting mineral chemistry of I045-51 warrants further discussion.

Ferrodiorite I045-51 is a medium grained rock (Plate 4-5E) with

T A B L E 4-19

CONRAD F.Z: SELECTED MINERAL ANALYSES. HYPERSTHENE GABBRO I045-172

	1	2	3	4	5	6	7	8
SIO2	54.53	55.03	51.20	52.26	52.10	52.54	52.36	.03
TIO2	-	-	.08	.07	.07	.22	.21	49.40
AL2O3	29.01	28.00	30.68	1.03	1.15	1.68	1.78	.04
CR2O3	-	-	-	.14	.18	.24	.21	-
FE2O3	-	-	-	-	-	-	-	6.35
FEO	.04	.11	.66	23.36	22.38	7.20	7.59	43.60
MNO	-	-	-	.34	.35	.12	.14	.34
MGO	-	-	.21	23.04	22.92	15.29	15.01	.29
CAO	11.14	10.24	13.75	.44	.92	23.08	23.05	-
NA2O	5.49	6.11	3.99	-	-	.36	.40	-
K2O	.06	.08	.04	-	-	-	-	-
TOTAL	100.27	99.57	100.61	100.68	100.07	100.73	100.75	100.05

★ ★ ATOMIC PROPORTIONS BASED ON SELECTED NO. OF OXYGENS ★ ★

OXYGEN	8	8	8	6	6	6	6	3
SI	2.455	2.493	2.324	1.945	1.945	1.938	1.935	.001
ALIV	1.540	1.495	1.641	.045	.051	.062	.065	.001
ALVI	-	-	-	-	-	.011	.013	-
TI	-	-	.003	.002	.002	.006	.006	.938
CR	-	-	-	.004	.005	.007	.006	-
FE3+	-	-	-	-	-	-	-	.121
FE2+	.002	.004	.025	.727	.699	.222	.235	.921
MN	-	-	-	.011	.011	.004	.004	.007
MG	-	-	.014	1.278	1.275	.841	.827	.011
CA	.537	.497	.669	.018	.037	.912	.913	-
NA	.479	.537	.351	-	-	.026	.029	-
K	.003	.005	.002	-	-	-	-	-
SUM	5.016	5.030	5.029	4.029	4.025	4.029	4.032	2.000
	AN 52.68	AN 47.87	AN 65.42	WO .87	WO 1.83	WO 46.19	WO 46.24	IL 92.86
	AB 46.98	AB 51.69	AB 34.35	EN 63.18	EN 63.42	EN 42.56	EN 41.88	GK 1.09
	OR .34	OR .45	OR .23	FS 35.95	FS 34.75	FS 11.25	FS 11.88	HM 6.04

★ ★ ★ S A M P L E D I R E C T O R Y ★ ★ ★

ANALYSIS NO.	DESCRIPTION
1	PLAGIOCLASE (CORE)
2	PLAGIOCLASE (RIM)
3	PLAGIOCLASE
4	ORTHOPYROXENE
5	ORTHOPYROXENE
6	CLINOPYROXENE
7	CLINOPYROXENE
8	ILMENITE

an extremely complex mineral paragenesis. Primary minerals include plagioclase, augitic pyroxene, pigeonite, olivine (fayalite), titanomagnetite, ilmenite, alkali feldspar, apatite, quartz and possibly amphibole. Secondary minerals include biotite and a second amphibole. Quartz occurs as discrete anhedral grains up to 1.0 mm in size or in granophyric intergrowth with alkali feldspar ($Or_7Ab_{27}An_2$) and is commonly in close spatial association with fayalitic olivine (Fo_9). The olivine occurs as small anhedral grains with slightly altered grain boundaries (Plate 4-5F). Apatite needles occur dispersed throughout the rock and are particularly abundant in the granophyric intergrowths. Two varieties of amphibole are present: a brown variety (pleochroic in two shades of brown) and a green variety. The former occurs as discrete subhedral grains (Plate 4-5F), while the latter occurs both as discrete grains and as overgrowths on clinopyroxene (Plate 4-5G). Chemically the two varieties can be distinguished by their different TiO_2 contents; the brown variety having 1.5-1.7 wt.% TiO_2 and the green variety 0.5-0.9 wt.% TiO_2 (Table 4-20). Plagioclase shows a range in composition from An_{57} to An_{23} and some grains are considerably zoned (An_{48}-An_{24}) (Table 4-20).

Coexisting ilmenite and titanomagnetite occur in 'sandwich' or 'composite' intergrowths (as defined by Haggerty, 1976) and have fairly uniform compositions. Ilmenite compositions range from Il_{97} to Il_{99} and titanomagnetite ranges in composition from $Us_{40}Mt_{60}$ to $Us_{42}Mt_{58}$ (a single grain having a composition of $Us_{48}Mt_{52}$). Representative analyses are given in Table 4-20 and individual analyses are given in microfiche Table F4-33. The estimated temperature and oxygen fugacity during the crystallisation of these Fe-Ti oxides, using the T-fO_2-X curves of Buddington and Lindsley (1964), are 650°C and 10^{-21} atm. respectively.

TABLE 4-20

CONRAD F.Z: SELECTED MINERAL ANALYSES. FERRODIORITE I045-51

	1	2	3	4	5	6	7	8	9	10
SIO2	30.10	30.01	53.56	55.46	61.77	64.84	.09	.19	.09	.85
TIO2	.11	.06	.06	.05	ND	ND	13.60	14.34	50.99	51.12
AL203	ND	ND	29.55	27.16	23.28	19.50	1.26	1.00	.06	.12
CR203	-	-	-	-	-	-	-	-	-	-
FE203	-	-	-	-	-	-	-	-	-	-
FEO	65.01	64.49	.85	.74	.15	.03	40.73	39.24	2.88	1.19
MNO	.87	.83	-	-	-	-	43.54	44.23	45.61	46.33
MGO	3.37	3.69	.17	.03	ND	ND	.29	.31	.14	.48
CAO	.14	.08	11.73	9.99	5.32	.42	ND	ND	.10	.06
NA20	-	-	4.72	5.94	8.92	2.81	.03	.03	.02	.05
K20	-	-	.25	.32	.35	11.71	-	-	-	-
TOTAL	99.61	99.17	100.89	99.69	99.81	99.33	99.55	99.35	99.89	100.20

* * ATOMIC PROPORTIONS BASED ON SELECTED NO. OF OXYGENS * *

OXYGEN	4	4	8	8	8	8	4	4	3	3
SI	.998	.997	2.411	2.516	2.754	2.967	.003	.007	.002	.021
AL	-	-	1.568	1.452	1.223	1.052	.056	.045	.002	.004
TI	.003	.001	.002	.002	-	-	.388	.410	.969	.966
CR	-	-	-	-	-	-	-	-	-	-
FE3+	-	-	-	-	-	-	1.162	1.122	.055	.022
FE2+	1.802	1.793	.032	.028	.006	.001	1.380	1.405	.964	.973
MN	.024	.023	-	-	-	-	.009	.010	.003	.010
MG	.166	.183	.011	.002	-	-	-	-	.004	.002
CA	.005	.003	.566	.486	.254	.021	.001	.001	.001	.001
NA	-	-	.412	.523	.771	.249	-	-	-	-
K	-	-	.014	.019	.020	.684	-	-	-	-
SUM	2.999	3.001	5.016	5.027	5.029	4.974	3.000	3.000	2.000	2.000
	FO 8.46	FO 9.25	AN 57.03	AN 47.30	AN 24.32	AN 2.16	US 40.03	US 42.21	IL 96.87	IL 98.62
	FA 91.54	FA 90.75	AB 41.53	AB 50.90	AB 73.78	AB 26.15	MT 59.97	MT 57.79	GK .38	GK .23
			OR 1.45	OR 1.80	OR 1.90	OR 71.69			HM 2.75	HM 1.15

* * * S A M P L E D I R E C T O R Y * * *

ANALYSIS NO.	DESCRIPTION
1	OLIVINE
2	OLIVINE
3	PLAGIOCLASE, CENTER
4	PLAGIOCLASE, CORE
5	PLAGIOCLASE, SAME GRAIN RIM
6	ALKALI FELDSPAR
7	TI-MAGNETITE
8	TI-MAGNETITE
9	ILMENITE
10	ILMENITE

** ND = NOT DETECTED **

TABLE 4-20 (CONTINUED)

CONRAD F.Z: SELECTED MINERAL ANALYSES. FERRODIORITE I045-51

	11	12	13	14	15	16	17	18	19	20
SIO2	49.43	48.02	47.72	48.04	47.14	46.54	50.24	49.62	48.50	47.44
TIO2	.63	.38	.32	.53	.43	.33	.36	.37	.35	.40
AL2O3	1.56	.91	.64	1.06	.67	.40	.98	1.00	.80	.65
CR2O3	-	-	-	-	-	-	-	-	-	-
FE2O3	-	-	-	-	-	.06	-	-	-	-
FEO	20.13	31.60	36.44	29.59	37.94	43.00	25.77	31.03	34.36	39.69
MNO	.39	.49	.61	.45	.62	.72	.39	.50	.53	.67
MGO	11.81	5.96	5.83	6.66	4.71	4.76	16.18	12.75	9.81	6.34
CAO	15.59	12.37	8.93	13.48	8.43	3.86	5.12	5.39	5.44	5.19
NA2O	.13	.13	.05	.14	.09	.04	ND	.06	.10	.02
K2O	-	-	-	-	-	-	-	-	-	-
TOTAL	99.67	99.86	100.54	99.95	100.03	99.71	99.05	100.72	99.89	100.40

* * ATOMIC PROPORTIONS BASED ON SELECTED NO. OF OXYGENS * *

OXYGEN	6	6	6	6	6		6	6	6	6
SI	1.924	1.956	1.956	1.943	1.957	-	1.954	1.949	1.957	1.957
ALIV	.072	.044	.031	.051	.033	-	.045	.046	.038	.032
ALVI	-	-	-	-	-	-	-	-	-	-
TI	.018	.012	.010	.016	.013	-	.011	.011	.011	.012
CR	-	-	-	-	-	-	-	-	-	-
FE3+	-	-	-	-	-	.000	-	-	-	-
FE2+	.655	1.076	1.249	1.001	1.317	-	.838	1.019	1.160	1.370
MN	.013	.017	.021	.015	.022	.000	.013	.017	.018	.023
MG	.685	.362	.356	.401	.291	-	.938	.746	.590	.390
CA	.650	.540	.392	.584	.375	.000	.213	.227	.235	.229
NA	.010	.010	.004	.011	.007	-	-	.005	.008	.002
K	-	-	-	-	-	-	-	-	-	-
SUM	4.027	4.016	4.020	4.022	4.017	.000	4.013	4.019	4.017	4.015
	WO 32.66	WO 27.29	WO 19.63	WO 29.41	WO 18.90		WO 10.73	WO 11.38	WO 11.85	WO 11.54
	EN 34.42	EN 18.29	EN 17.83	EN 20.21	EN 14.69		EN 47.14	EN 37.46	EN 29.72	EN 19.60
	FS 32.92	FS 54.42	FS 62.54	FS 50.38	FS 66.41		FS 42.13	FS 51.16	FS 58.42	FS 68.86

* * * SAMPLE DIRECTORY * * *

ANALYSIS NO.	DESCRIPTION
11	CA-RICH PYROXENE
12	CA-RICH PYROXENE
13	CA-RICH PYROXENE, CORE
14	CA-RICH PYROXENE, RIM
15	CA-RICH PYROXENE, CORE
16	CA-RICH PYROXENE, RIM
17	CA-POOR PYROXENE
18	CA-POOR PYROXENE
19	CA-POOR PYROXENE, CORE
20	CA-POOR PYROXENE, RIM

** ND = NOT DETECTED **

T A B L E 4-20 (CONTINUED)

CONRAD F.Z: SELECTED MINERAL ANALYSES. FERRODIORITE I045-51

	21	22	23	24	25
SIO2	41.27	41.94	43.88	42.26	33.85
TIO2	1.67	1.51	.56	.87	4.24
AL2O3	8.53	7.58	8.87	7.90	12.57
CR2O3	-	-	-	-	-
FEO	27.94	26.79	26.00	27.42	32.05
MNO	.21	.26	.19	.19	.17
MGO	5.03	5.73	5.45	5.83	3.84
CAO	10.29	10.36	10.54	10.24	.03
NA2O	1.91	1.77	1.91	1.73	.24
K2O	1.34	1.34	1.09	1.26	8.56
TOTAL	98.19	97.28	98.49	97.70	95.55

* * ATOMIC PROPORTIONS BASED ON SELECTED NO. OF OXYGENS * *

OXYGEN	23	23	23	23	22
SI	6.550	6.681	6.812	6.702	5.529
ALIV	1.450	1.319	1.188	1.298	2.420
ALVI	.146	.104	.435	.179	-
TI	.199	.181	.065	.104	.521
CR	-	-	-	-	-
FE2+	3.709	3.569	3.376	3.637	4.378
MN	.028	.035	.025	.026	.024
MG	1.190	1.360	1.261	1.378	.935
CA	1.750	1.768	1.753	1.740	.005
NA	.588	.547	.575	.532	.076
K	.271	.272	.216	.255	1.784
SUM	15.882	15.836	15.706	15.849	15.670

* * * S A M P L E D I R E C T O R Y * * *

ANALYSIS NO.	DESCRIPTION
21	AMPHIBOLE, (BROWN)
22	AMPHIBOLE, (BROWN)
23	AMPHIBOLE, (GREEN)
24	AMPHIBOLE, (GREEN)
25	BIOTITE

Clinopyroxene and pigeonite occur as subhedral grains in sub-ophitic relation with plagioclase. Pigeonite occurs both separately and as cores mantled by clinopyroxene (Plate 4-5G), many of which are in turn mantled by green amphibole (Plate 4-5G). The pyroxenes of I045-51 have unusual compositions and show zonal variations more typical of some lunar pyroxenes than of terrestrial pyroxenes.

Fig. 4-27A illustrates the unusual compositional variation of Ca-rich and Ca-poor pyroxenes in ferrodiorite I045-51, relative to the trends shown by Skaergaard and Bushveld Complex pyroxenes (Brown, 1957; Brown and Vincent, 1963; Atkins, quoted in Lindsley and Munoz, 1969). Representative analyses are presented in Table 4-20 and individual analyses in microfiche Table F4-33. The most marked features of the pyroxenes in I045-51 are their extremely Fe-rich nature (Fs comprises up to 75 mol.%), the lack of a pyroxene minimum in the 'Ca-rich' trend, and the corresponding subcalcic nature of the more evolved ferro-augites. Though similar Fe-rich 'pigeonites' have been reported from the Bjirkrem Sogndal massif (Duchesne, 1972), the coexisting Ca-rich pyroxenes follow a normal tholeiitic crystallisation trend, i.e. crystallisation towards hedenbergite. Iron-rich 'pigeonite' associated with similar subcalcic augite has, however, been reported from the Trough bands of the Skaergaard Intrusion (Yin Yin Nwe, 1975). The nearest analogy to the Ca-rich pyroxene trend has been found in the lunar literature where subcalcic augite from lunar rocks 12021 (Boyd and Smith, 1971; Ross et al., 1973) and 12022 (Bence and Papike, 1972) define a similar compositional trend towards the pyroxenoid pyroxferroite.

The presence of the pyroxene minimum in the crystallisation trend of tholeiitic pyroxenes is closely related to the cessation of Ca-poor

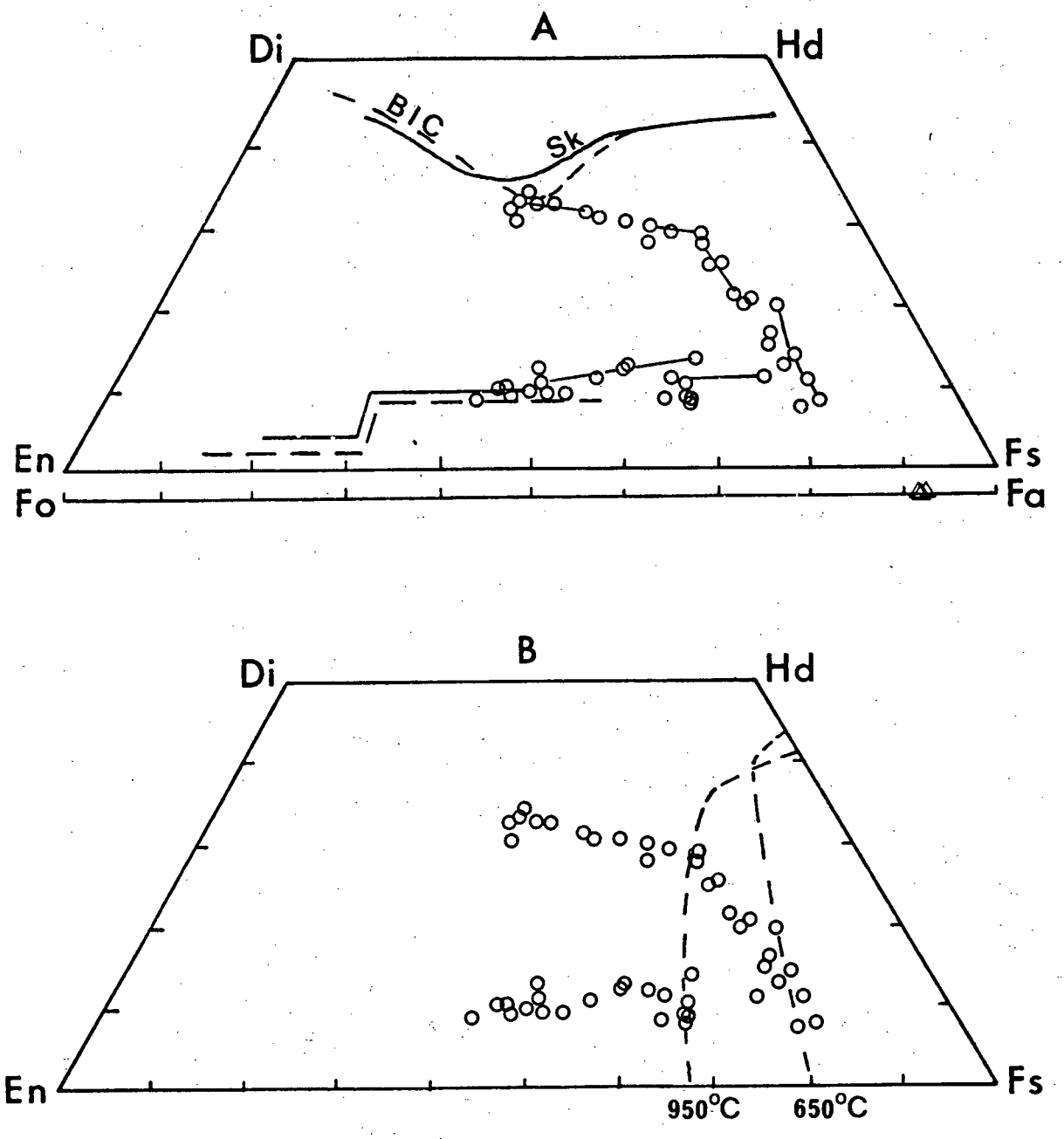

Fig. 4-27: A. Compositional variation in pyroxenes from ferrodiorite I045-51. Solid lines joining data points indicate extent of zoning. The solid trend lines (SK) represent the variation Skaergaard pyroxenes, and dashed lines (BIC) represent the variation in Bushveld Complex pyroxenes (taken from Lindsley and Munoz, 1969).

B. Compositional variation of I045-51 pyroxenes in relation to the position of the pyroxene 'forbidden zone'. The position of the 'forbidden zone' at 950°C is taken from Smith (1971) and the position of 650°C curve is estimated from the experimental data from Smith (1971) for compositions along the En-Fs join.

pyroxene crystallisation, which in turn is closely related to the position of the so-called 'forbidden zone' in the pyroxene quadrilateral (Lindsley and Munoz, 1969; Smith, 1971, 1972; Campbell and Nolan, 1974). The position of the 'forbidden zone' marks the composition of the most Fe-rich low-Ca pyroxene that is stable under the given temperature and pressure conditions, after which Ca-poor pyroxene breaks down according to the reaction (Lindsley and Munoz, 1969; Campbell and Nolan, 1974):

$$\underset{\text{in Ca-poor pyroxene}}{2FeSiO_3} = \underset{\text{in olivine}}{Fe_2SiO_4} + \underset{\text{in the melt}}{SiO_2} \quad \ldots\ldots\ldots (1)$$

to give fayalitic olivine and quartz coexisting with Ca-rich clinopyroxene. At this point in the pyroxene crystallisation sequence the high-Ca pyroxenes continue to crystallise and become progressively more Ca-rich (Campbell and Nolan, 1974).

The extent of the forbidden zone is not well known, but is reportedly a function of pressure, temperature, a_{SiO_2} and a_{FeO} (Smith, 1971; Lindsley and Munoz, 1969; Smith, 1972; Campbell and Nolan, 1974; Mori, 1978). Decreasing temperature or increasing pressure results in a contraction of the forbidden zone along the En-Fs join (Smith, 1971, 1972; Mori, 1978), while increase in a_{SiO_2} also results in Ca-poor pyroxene compositions extending to higher Fe/Mg ratios (Campbell and Nolan, 1974).

A possible explanation for the continuation of crystallisation of low-Ca pyroxene in I045-51 to extremely iron-rich compositions ($Wo_9En_{15}Fs_{76}$) is in the interplay of the abovementioned factors. The effect of pressure on the crystallisation of I045-51 is difficult to assess, but if one assumes that the sample is not an erratic (borne out to a certain extent by the bulk composition), then the pressure is

unlikely to have been very high. The effects of temperature a_{SiO_2} and a_{FeO} are more readily assessed and are more likely to be of importance. The extremely iron-rich nature of the magma is an extremely important initial factor. The initial high a_{FeO} (whole rock FeO*/MgO = 7.5) resulted in the initial pyroxene compositions being themselves very iron-rich (Fig. 4-27). Campbell and Nolan (1974) have demonstrated that the presence of free quartz (as found in I045-51) implies that the a_{SiO_2} is such as to stabilise low-Ca high-Fe pyroxene. Consequently low-Ca pyroxene crystallisation continues until the limiting point of the forbidden zone for the given temperature and pressure of crystallisation. If the activity of SiO_2 is such that free quartz does not crystallise, then low-Ca pyroxene breaks down to olivine at lower Fe/Mg ratios. The presence of abundant modal quartz in I045-51 is consistent with continuous crystallisation of low-Ca pyroxene until the limiting point of the forbidden zone was reached. The extremely low temperature of final crystallisation of I045-51 ($\pm$ 650°C), as indicated by the coexisting Fe-Ti oxides, would result in the forbidden zone only extending a short way along the Fs-En join. Data from Smith (1971) indicates that the limiting composition of the forbidden zone along this join at 600-700°C is $En_{20}Fs_{80}$ which, if superimposed on the pyroxene quadrilateral (Fig. 4-27B), corresponds closely to the most Fe-rich pyroxenes from I045-51. It is apparent from Fig. 4-27B that by this stage of crystallisation the high-Ca pyroxene trend had simultaneously reached the limit of the forbidden zone. From this stage onwards further crystallisation involved precipitation of olivine (Fa_{92}) and quartz in place of low-Ca pyroxene and should theoretically have resulted in the composition of the final Ca-rich pyroxene moving towards the Hd-Di join, along a path defined by

the extent of the forbidden zone (Lindsley and Munoz, 1969). The absence of a trend towards higher Ca content in the high-Ca pyroxenes can possibly be attributed to the crystallisation of a metastable highly subcalcic ferroaugite because of local compositional heterogeneities and low diffusion rates in the magma, which by this stage was nearly totally crystalline. The presence of primary amphibole suggests a local build-up of pH_2O and possibly during the final stage of crystallisation amphibole was stabilised relative to Ca-rich pyroxene, accounting for the cessation of Ca-rich pyroxene crystallisation on reaching the forbidden zone. Alternatively the presence of 'secondary' amphibole mantles on many of the Ca-rich pyroxenes (Plate 4-5G) might mask the presence of originally more calcic rims.

4.1.3 Alteration:

Most samples from the Conrad F.Z. show varying degrees of alteration ranging from minor development of chlorite, through chlorite-actinolite intergrowths, to a greenschist facies assemblage of chlorite-actinolite-epidote-albite. Such assemblages are fairly typical of altered sea-floor basalts (Humphris and Thompson, 1978a), and especially typical of fracture zone basalts (e.g. Bonatti et al., 1971; Melson and Thompson, 1971; Thompson and Melson, 1972).

(i) Chlorite-actinolite

Chlorite and/or actinolite are present in many of the basalts (I045-14, I045-106, I045-130B, I045-173, I047-62, I047-64) and in all the dolerites. The extent of chlorite/actinolite development varies from sample to sample but when present is fairly extensive and is significantly greater in the hypabyssal rocks (pigeonite dolerite I047-72 excepted). The chlorite and actinolite occur separately or as patchy

intergrowths and replace both clinopyroxene and plagioclase. Representative analyses are presented in Table 4-21. In the presentation of the analyses, all iron has been expressed as FeO.

(ii) Epidote

Epidote is present as small irregular grains in the matrix of only one sample (I045-106) in which most of the primary mineral assemblage has been replaced by secondary minerals. A representative epidote analysis is presented in Table 4-21. In accord with Deer, Howie and Zussman (1966), all iron has been expressed as ferric iron.

(iii) Alkali feldspar-analcite

Partial or total replacement of plagioclase (both groundmass and phenocryst) by alkali feldspar occurs in numerous samples. The alkali feldspar is either nearly pure albite (I047-62, I047-28, I047-101) with compositions ranging from $An_7Ab_{92}Or_1$ to $An_2Ab_{78}Or_{20}$, or nearly pure K-feldspar (I047-62, I047-64, I047-32, I045-14, I045-34, I045-159, I045-160, I047-12, I047-28) with compositions of $Or_{90}Ab_{10}$ to $Or_{99}Ab_1$. Analcite has been identified in samples I045-14, I045-68 and I045-160. Representative analyses are presented in Table 4-21. The alkali feldspar and analcite occur as patchy (or total) replacement of plagioclase, and both albite and K-feldspar can occur together as distinct patches within a single plagioclase crystal (Plate 4-5H). A second mode of occurrence is as veins of alkali feldspar and/or analcite (Plate 4-4 E and G). Similar replacement of plagioclase by K-feldspar and analcite has been reported in samples dredged from the Rio Grande Rise (Fodor et al., 1977) and in basalts from the Swallow Bank, an abyssal hill in the NE Atlantic (Mathews, 1971).

The abundance of secondary alkali feldspar in the Conrad F.Z.

T A B L E 4-21

CONRAD F.Z: SELECTED ANALYSES OF ALTERATION MINERALS

	1	2	3	4	5	6	7	8	9	10
SIO2	29.36	26.65	42.08	52.06	37.52	66.05	67.96	54.98	63.64	64.20
TIO2	.10	.10	.19	.16	.23	.03	ND	ND	-	-
AL2O3	17.26	16.91	9.30	3.12	23.75	21.09	20.30	22.22	19.55	18.36
CR2O3	-	-	-	-	.03	-	-	-	-	-
FE2O3	-	-	-	-	13.34	-	-	-	-	-
FEO	22.45	29.46	19.96	16.00	-	.08	.03	ND	.06	.02
MNO	.16	.19	.20	.23	.15	-	-	-	-	-
MGO	16.38	13.33	13.24	13.67	.03	ND	ND	ND	-	-
CAO	1.45	.05	7.49	11.73	23.05	1.59	.37	.06	.04	.02
NA2O	.09	.02	.27	.32	.04	11.12	11.62	13.27	1.12	.07
K2O	.03	.05	.07	.06	.02	.06	.05	.02	15.55	16.82
TOTAL	87.28	86.76	92.80	97.35	98.16	100.03	100.35	90.58	99.96	99.49

* * ATOMIC PROPORTIONS BASED ON SELECTED NO. OF OXYGENS * *

OXYGEN	28	28	23	23	12	8	8	7	8	8
SI	6.118	5.824	6.637	6.865	2.861	2.903	2.962	2.372	2.944	2.991
ALIV	4.239	4.356	1.363	1.135	2.134	1.092	1.043	1.130	1.066	1.008
ALVI	-	-	.367	.904	-	-	-	-	-	-
TI	.016	.016	.023	.016	.013	.001	-	-	-	-
CR	-	-	-	-	.002	-	-	-	-	-
FE3+	-	-	-	-	.765	-	-	-	-	-
FE2+	3.912	5.385	2.633	1.764	-	.003	.001	-	.002	.001
MN	.028	.035	.027	.026	.010	-	-	-	-	-
MG	5.087	4.342	3.112	2.686	.003	-	-	-	-	-
CA	.324	.012	1.266	1.657	1.883	.075	.017	.003	.002	.001
NA	.036	.008	.083	.082	.006	.948	.982	1.110	.100	.006
K	.008	.014	.014	.010	.002	.003	.003	.001	.918	1.000
SUM	19.769	19.992	15.524	15.146	7.679	5.026	5.009	4.618	5.032	5.008
						AN 7.30	AN 1.72		AN .19	AN .10
						AB 92.37	AB 98.00		AB 9.85	AB .63
						OR .33	OR .28		OR 89.96	OR 99.27

* * * S A M P L E D I R E C T O R Y * * *

ANALYSIS NO.	DESCRIPTION
1	CHLORITE, (I045-130B)
2	CHLORITE, (I045-159)
3	CHLORITE/ACTINOLITE INTERG. (I045-106)
4	ACTINOLITE, (I045-68)
5	EPIDOTE, (I045-106)

ANALYSIS NO.	DESCRIPTION
6	ALBITE, (I047-62)
7	ALBITE, (I047-101)
8	ANALCITE, (I045-68)
9	K-FELDSAPR, (I045-34)
10	K-FELDSAPR, (I045-159)

** ND = NOT DETECTED **

samples, and in accord with the commonly more altered nature of fracture zone basalts relative to rift valley basalts (Melson and Thompson, 1971; Thompson and Melson, 1972; Bryan, 1979), suggests the alteration is associated with the movement of alkali-enriched hydrothermal fluids within the fracture zones rather than simple interaction with seawater. This significant introduction of alkalis (K, Na, Rb and Ba) clearly limits the use of these key elements in any meaningful petrogenetic interpretation.

4.2 Whole Rock Chemistry

Major and fourteen trace elements, CIPW norms and selected element ratios are presented for 12 Conrad F.Z. basalts in Table 4-22 and for 12 dolerites, one ferrodiorite and one hypersthene gabbro in Table 4-23. CIPW norms were calculated after normalising the data to 100%, volatile-free, and assuming an Fe_2O_3/FeO ratio of 0.15.

As discussed in the previous section, most of the samples show varied degrees of alteration in thin section. This is clearly evident in the significant values for LOI (up to 3.9 wt.%) and, in selected cases, for H_2O^+ and CO_2 (Tables 4-22 and 4-23). The chemical changes associated with low temperature alteration have been summarised in Section 3.2 (IOFZ basalts). The Conrad F.Z. samples are on average more altered than those from the IOFZ, and secondary K- and Na-feldspar are abundant in many of the samples. The degree of mobility in some elements is shown by analyses I045-91I and I045-91R (Table 4-22) which are from the exterior and interior portions respectively of a single sample. In hand specimen the only distinction between the two zones is the slightly darker (oxidised) nature of the exterior zone. Chemically, the exterior zone is enriched in Rb (factor of 3), K_2O (factor of 1.5) and total Fe,

TABLE 4-22

CONRAD F.Z: WHOLE ROCK ANALYSES, CIPW NORMS & SELECTED RATIOS OF BASALTS

	I045-97	I045-152	I045-161	I045-91T	I045-91R	I045-130B	I045-151	I045-161	I045-173	I047-64
SIO2	49.84	50.32	52.55	51.21	50.17	49.23	52.30	51.33	48.45	49.96
TIO2	1.42	1.53	1.77	1.62	1.57	1.01	1.73	1.69	1.66	1.86
AL203	16.52	15.55	13.36	14.93	14.41	16.86	15.30	14.61	15.37	13.85
FE203	1.22	1.23	1.56	1.13	1.47	1.11	1.08	1.18	1.39	1.52
FEO	8.14	8.22	10.41	7.55	9.81	7.39	7.21	7.90	9.28	10.15
MNO	.16	.17	.18	.18	.18	.16	.17	.19	.18	.23
MGO	6.29	6.42	6.26	6.76	6.44	7.60	6.14	6.92	7.15	6.79
CAO	11.96	11.88	11.06	11.94	11.45	12.26	12.10	11.76	11.64	8.38
NA20	2.66	2.64	2.98	3.06	2.80	2.34	2.89	3.05	2.40	2.44
K20	.34	.45	.25	.28	.48	.31	.41	.28	.25	.65
P205	.19	.19	-	.16	.17	.10	.20	.17	.19	.23
H20+	.49	.79	-	1.48	1.79	2.31	.43	1.25	2.56	2.50
H20-	.51	.80	-	.39	.20	.11	.17	.31	.08	.84
C02	.10	.29	-	-	-	-	.16	-	-	.10
TOTAL	99.84	100.48	100.38	100.69	100.94	100.79	100.29	100.64	100.60	99.50
				* * * C.I.P.W. NORMS * * *						
Q	.00	.00		.00	.00	.00	1.71	.00	.00	2.51
CO	.00	.00		.00	.00	.00	.00	.00	.00	.00
OR	2.01	2.72		1.65	2.90	1.89	2.42	1.65	1.54	4.02
PL	55.33	52.32		52.72	49.52	55.28	52.25	51.66	51.78	47.43
DI	21.53	23.68		26.41	25.32	21.17	25.53	26.25	21.85	12.98
HY	12.92	14.61		11.95	11.96	11.03	12.74	13.26	13.40	26.54
OL	3.22	1.47		2.12	4.72	6.82	.00	1.81	5.72	.00
MT	1.80	1.81		1.67	2.16	1.64	1.58	1.74	2.06	2.29
IL	2.73	2.94		3.11	3.02	1.96	3.30	3.25	3.21	3.68
AP	.45	.45		.38	.40	.24	.47	.40	.45	.57
				* * * TRACE ELEMENTS * * *						
ZR	110.	112.		111.	106.	63.7	113.	115.	125.	144.
NB	6.4	5.7		5.5	5.1	ND	6.0	5.3	4.9	7.0
Y	33.2	34.2		36.1	32.6	23.4	36.4	36.8	37.4	40.6
RB	5.9	6.6		3.2	10.4	6.3	2.2	2.9	4.1	13.1
BA	36.9	42.6		60.8	38.3	62.5	67.4	62.5	28.3	203.
SR	142.	138.		157.	135.	113.	153.	162.	116.	109.
CO	45.4	52.9		83.7	43.7	47.6	53.8	70.8	45.2	47.1
CR	216.	207.		158.	142.	370.	137.	131.	237.	105.
NT	76.7	93.6		134.	39.5	97.9	39.7	94.1	85.1	55.8
V	241.	266.		289.	278.	220.	310.	296.	286.	313.
ZN	86.9	89.6		96.0	87.2	95.4	105.	95.7	99.4	158.
CU	77.9	67.7		119.	67.8	46.8	87.0	99.7	50.6	56.5
SC	36.5	37.0		42.4	39.1	42.7	42.1	42.7	39.0	38.7
TH	-	-		-	-	-	-	-	-	-
PB	-	-		-	-	-	-	-	-	-
GA	16.9	16.8		17.0	16.3	15.3	17.8	17.4	16.6	19.0

** ND = NOT DETECTED **

T A B L E 4-22 (CONTINUED)

CONRAD F.Z: WHOLE ROCK ANALYSES, CIPW NORMS & SELECTED RATIOS OF BASALTS

	I045-97	I045-152	I045-161	I045-91I	I045-91R	I045-130B	I045-151	I045-161	I045-173	I047-64
* * * ELEMENT RATIOS * * *										
ZR/NB	17.1	19.5	-	20.2	20.8	-	18.9	21.7	25.2	20.5
ZR/BA	2.99	2.62	-	1.82	2.78	1.02	1.68	1.84	4.41	.709
ZR/Y	3.32	3.27	-	3.07	3.26	2.72	3.10	3.13	3.34	3.54
K/RB	479.	587.	-	738.	383.	410.	1.561+003	796.	510.	413.
K/BA	76.5	87.7	-	38.2	104.	41.2	50.5	37.2	73.4	26.6
K/ZR	25.6	33.4	-	21.0	37.5	40.4	30.1	20.2	16.6	37.5
Y/NB	5.15	5.87	-	6.59	6.40	-	6.08	6.95	7.55	5.78
CA/Y	2.574+003	2.480+003	-	2.366+003	2.507+003	3.746+003	2.376+003	2.282+003	2.226+003	1.475+003
TI/ZR	77.1	82.0	-	87.8	88.5	95.0	91.8	88.0	79.8	77.5
TI/NB	1.320+003	1.601+003	-	1.775+003	1.846+003	-	1.731+003	1.912+003	2.010+003	1.586+003
TI/Y	256.	268.	-	269.	288.	259.	285.	275.	266.	275.
TI/P	10.3	11.1	-	13.9	12.7	13.9	11.9	13.7	12.0	11.1
CR/V	.896	.780	-	.546	.511	1.68	.441	.443	.828	.336
NI/CO	1.69	1.77	-	1.60	.903	2.06	.737	1.33	1.88	1.19
M.I.	59.8	59.5	65.7	56.2	63.7	52.8	57.4	56.7	59.9	63.2
MG#	.579	.582	.517	.615	.539	.647	.603	.610	.579	.544
D.I.	24.8	25.4	-	27.9	26.8	22.0	28.7	27.7	22.3	28.0

T A B L E 4-22 (CONTINUED)

CONRAD F.Z: WHOLE ROCK ANALYSES, CIPW NORMS & SELECTED RATIOS OF BASALTS

	I045-14	I045-106	I047-62
SIO2	50.08	49.48	50.02
TIO2	1.26	1.93	2.49
AL2O3	14.12	14.41	12.98
FE2O3	1.34	1.46	1.76
FEO	8.91	9.76	11.74
MNO	.20	.24	.40
MGO	7.36	7.05	5.71
CAO	10.72	9.02	7.13
NA2O	2.87	2.98	3.58
K2O	.38	.44	.63
P2O5	.12	.24	.32
H2O+	2.62	3.30	2.90
H2O-	.14	.14	.57
CO2	-	-	-
TOTAL	100.12	100.45	100.23
			* * * C.I.P.W. NORMS * * *
Q	.00	.00	.00
CO	.00	.00	.00
OR	2.30	2.66	3.84
PL	50.13	51.39	49.37
DI	23.48	15.68	13.60
HY	14.22	20.82	23.99
OL	5.13	2.91	.90
MT	1.99	2.19	2.64
IL	2.45	3.78	4.88
AP	.28	.59	.78
			* * * TRACE ELEMENTS * * *
ZR	78.0	167.	201.
NB	ND	8.9	11.0
Y	31.1	44.7	52.8
RB	7.4	9.5	12.6
BA	33.9	46.1	122.
SR	119.	136.	112.
CO	47.5	40.5	37.2
CR	176.	228.	36.1
NI	69.2	69.4	31.4
V	285.	292.	328.
ZN	87.5	131.	251.
CU	56.9	20.8	35.9
SC	44.4	39.3	38.8
TH	-	-	-
PB	-	-	-
GA	15.3	17.0	18.4

** ND = NOT DETECTED **

T A B L E 4-22 (CONTINUED)

CONRAD F.Z: WHOLE ROCK ANALYSES, CIPW NORMS & SELECTED RATIOS OF BASALTS

	I045-14	I045-106	I047-62
		* * * ELEMENT RATIOS * * *	
ZR/NB	-	18.9	18.2
ZR/BA	2.30	3.63	1.65
ZR/Y	2.51	3.75	3.80
K/RB	428.	384.	413.
K/BA	93.1	79.3	42.9
K/ZR	40.5	21.8	26.0
Y/NB	-	5.05	4.79
CA/Y	2.462+003	1.443+003	964.
TI/ZR	96.9	69.1	74.3
TI/NB	-	1.307+003	1.353+003
TI/Y	243.	259.	282.
TI/P	14.4	11.0	10.7
CR/V	.619	.783	.110
NI/CO	1.46	1.72	.844
M.I.	58.2	61.4	70.3
MG#	.595	.563	.464
D.I.	27.3	28.6	35.2

T A B L E 4-23

CONRAD F.Z: WHOLE ROCK ANALYSES, CIPW NORMS & SELECTED RATIOS OF INTRUSIVES

	I045-34	I045-49	I045-68	I045-130D	I045-148	I045-159	I045-160	I047-12	I047-28A	I047-32
SIO2	49.15	49.81	48.67	49.57	49.27	49.55	49.75	51.41	48.08	51.47
TIO2	1.70	1.59	3.49	1.84	1.85	1.90	1.49	2.08	2.39	1.54
AL203	15.17	15.09	12.03	14.40	14.59	14.03	14.98	13.68	13.98	14.93
FE203	1.36	1.30	2.16	1.46	1.47	1.48	1.31	1.64	1.59	1.36
FEO	9.04	8.67	14.37	9.70	9.82	9.88	8.73	10.92	10.62	9.08
MNO	.18	.18	.26	.19	.24	.19	.18	.21	.22	.18
MGO	6.70	7.26	4.38	6.68	6.96	6.71	7.45	5.10	6.50	6.03
CAO	10.08	11.28	7.00	10.19	9.44	9.94	11.32	7.15	7.90	8.29
NA20	2.80	2.25	3.52	3.15	2.70	2.58	2.63	3.66	2.69	3.18
K20	.65	.17	1.02	.62	.67	.96	.20	.61	1.67	1.31
P205	.21	.19	.43	.17	.21	.22	.16	.35	.28	.18
H20+	2.39	1.52	2.62	2.57	2.82	1.53	1.68	2.74	3.24	2.57
H20-	.27	.21	.30	.14	.31	.37	.17	.52	.63	.41
CO2	.12	.10	-	-	-	.08	.07	-	-	-
TOTAL	99.82	99.62	100.25	100.68	100.35	99.42	100.12	100.07	99.79	100.53
				* * * C.I.P.W. NORMS * * *						
Q	.00	1.17	.00	.00	.00	.00	.00	1.81	.00	.00
CO	.00	.00	.00	.00	.00	.00	.00	.00	.00	.00
OR	3.96	1.00	6.20	3.72	4.08	5.85	1.18	3.72	10.28	7.92
PL	52.15	50.74	45.01	51.04	49.96	46.90	51.67	51.71	45.14	50.74
DI	18.39	20.18	15.54	21.95	16.68	20.26	22.21	12.15	13.97	14.70
HY	14.39	21.44	19.26	8.31	19.50	17.50	16.13	23.24	13.74	19.47
OL	5.26	.00	2.96	8.86	3.48	3.07	3.62	.00	8.47	1.71
MT	2.03	1.93	3.22	2.16	2.19	2.20	1.93	2.45	2.41	2.03
IL	3.32	3.10	6.82	3.57	3.61	3.70	2.89	4.08	4.73	3.00
AP	.52	.45	1.04	.40	.52	.54	.38	.85	.69	.43
				* * * TRACE ELEMENTS * * *						
ZR	119.	99.3	270.	119.	140.	122.	92.8	238.	170.	206.
NB	4.2	4.1	14.4	4.9	6.9	5.8	4.1	12.3	9.0	8.0
Y	34.6	30.8	70.6	31.3	42.2	37.6	29.7	62.2	47.8	46.9
RB	13.6	2.3	24.9	12.6	13.1	24.9	4.1	17.7	33.6	24.0
BA	77.5	45.3	199.	163.	62.3	121.	27.9	126.	459.	268.
SR	164.	143.	116.	173.	114.	137.	124.	118.	110.	120.
CO	44.0	46.7	42.1	42.9	47.4	51.3	48.8	40.5	50.3	35.0
CR	178.	227.	14.7	141.	180.	80.3	191.	107.	223.	121.
NI	60.5	75.4	16.5	47.5	76.7	41.8	68.3	42.4	76.3	50.1
V	264.	273.	428.	293.	303.	326.	272.	211.	348.	222.
ZN	67.7	88.7	147.	101.	107.	224.	83.9	154.	185.	116.
CU	64.1	31.8	57.2	65.0	43.0	72.4	62.8	52.8	53.4	61.7
SC	37.7	39.5	42.9	39.5	38.9	39.4	38.1	34.8	38.9	34.0
TH	-	-	-	-	-	-	-	-	-	-
PB	-	-	-	-	-	-	-	-	-	-
GA	17.9	17.2	21.1	16.6	17.7	17.7	16.5	19.1	18.3	17.8

T A B L E 4-23 (CONTINUED)

CONRAD F.Z: WHOLE ROCK ANALYSES, CIPW NORMS & SELECTED RATIOS OF INTRUSIVES

	I045-34	I045-49	I045-68	I045-130D	I045-148	I045-159	I045-160	I047-12	I047-28A	I047-32
* * * ELEMENT RATIOS * * *										
ZR/NB	28.6	24.2	18.7	24.5	20.4	21.2	22.6	19.3	18.8	25.8
ZR/BA	1.54	2.19	1.35	.728	2.25	1.01	3.33	1.89	.369	.768
ZR/Y	3.44	3.22	3.82	3.80	3.33	3.24	3.12	3.83	3.55	4.38
K/RB	395.	619.	340.	409.	425.	320.	410.	286.	413.	453.
K/BA	69.6	31.2	42.5	31.6	89.3	66.0	59.5	40.3	30.2	40.6
K/ZR	45.3	14.2	31.4	43.3	39.6	65.3	17.9	21.3	81.7	52.9
Y/NB	8.30	7.50	4.89	6.45	6.13	6.53	7.24	5.04	5.30	5.88
CA/Y	2.082+003	2.614+003	709.	2.328+003	1.600+003	1.888+003	2.719+003	822.	1.182+003	1.262+003
TI/ZR	85.6	96.0	77.6	92.8	79.0	93.4	96.3	52.4	84.5	44.9
TI/NB	2.444+003	2.319+003	1.449+003	2.274+003	1.612+003	1.978+003	2.173+003	1.011+003	1.590+003	1.157+003
TI/Y	294.	309.	297.	353.	263.	303.	300.	201.	300.	197.
TI/P	11.1	11.5	11.1	14.9	12.1	11.9	12.8	8.16	11.7	11.8
CR/V	.675	.831	3.444-002	.479	.595	.246	.705	.504	.641	.543
NI/CO	1.38	1.61	.392	1.11	1.62	.815	1.40	1.05	1.52	1.43
M.I.	60.8	57.9	79.1	62.6	61.9	62.9	57.4	71.1	65.3	63.4
MG#	.569	.599	.352	.551	.558	.548	.603	.454	.522	.542
D.I.	28.4	21.6	36.8	31.0	27.6	28.3	23.9	37.5	34.0	35.5

T A B L E 4-23 (CONTINUED)

CONRAD F.Z: WHOLE ROCK ANALYSES, CIPW NORMS & SELECTED RATIOS OF INTRUSIVES

	1047-72	1047-101	1045-51	1045-172
SIO2	53.08	51.73	58.30	52.72
TIO2	.65	2.51	1.92	.60
AL2O3	17.66	12.06	11.97	10.76
FE2O3	1.27	1.72	1.83	1.46
FEO	8.45	11.48	12.21	9.74
MNO	.20	.29	.19	.18
MGO	5.02	5.58	1.86	12.42
CAO	10.43	5.75	6.36	9.30
NA2O	2.55	3.38	2.75	1.94
K2O	.27	.13	2.08	.49
P2O5	.05	.73	.34	.11
H2O+	.95	3.87	.83	.16
H2O-	.41	.22	.08	.13
CO2	-	-	-	.31
TOTAL	100.99	99.45	100.72	100.32
			* * * C.I.P.W. NORMS * * *	
Q	4.61	7.43	13.96	.00
CO	.00	.00	.00	.00
OR	1.60	.83	12.29	2.90
PL	57.75	48.17	37.54	35.74
DI	12.89	5.55	13.12	21.34
HY	19.97	28.64	15.99	35.93
OL	.00	.00	.00	.59
MT	1.84	2.62	2.65	2.12
IL	1.23	4.99	3.65	1.14
AP	.12	1.82	.81	.26
			* * * TRACE ELEMENTS * * *	
ZR	31.1	359.	253.	57.1
NB	ND	20.0	11.5	ND
Y	17.4	91.7	56.7	15.4
RB	4.8	1.2	81.6	13.9
BA	55.5	7.6	507.	197.
SR	135.	43.6	142.	151.
CO	33.1	33.3	34.6	70.4
CR	22.2	43.4	12.1	1043.
NI	8.5	15.5	11.3	306.
V	291.	161.	171.	194.
ZN	81.0	228.	125.	81.6
CU	85.7	82.7	244.	57.3
SC	34.8	38.1	33.1	29.8
TH	-	-	-	-
PB	-	-	-	-
GA	15.8	22.7	19.9	12.2

** ND = NOT DETECTED **

T A B L E 4-23 (CONTINUED)

CONRAD F.Z: WHOLE ROCK ANALYSES, CIPW NORMS & SELECTED RATIOS OF INTRUSIVES

	I047-72	I047-101	I045-51	I045-172
			* * * ELEMENT RATIOS * * *	
ZR/NB	-	18.0	22.0	-
ZR/BA	.561	47.0	.499	.290
ZR/Y	1.79	3.91	4.46	3.71
K/RB	464.	922.	212.	293.
K/BA	40.4	141.	34.1	20.7
K/ZR	72.1	3.01	68.3	71.2
Y/NB	-	4.59	4.93	-
CA/Y	4.284+003	448.	802.	4.322+003
TI/ZR	125.	41.9	45.5	63.0
TI/NB	-	753.	1.002+003	-
TI/Y	224.	164.	203.	234.
TI/P	17.9	4.72	7.76	7.49
CR/V	7.612-002	.270	7.042-002	5.37
NI/CO	.257	.464	.327	4.35
M.I.	65.9	70.3	88.3	47.4
MG#	.514	.464	.214	.694
D.I.	27.9	38.2	49.6	19.4

and depleted in Sr, Ba, Cu, SiO_2, Al_2O_3, CaO and Na_2O. The marked difference in Ni, Co and Cr are attributed to contamination from the saw blade during sectioning. The difference in FeO/MgO+FeO ratio of the two zones is also noteworthy. Quantitative interpretation of bulk rock chemical variations is thus severely limited. In an attempt to 'see through' compositional variations introduced by secondary alteration, petrologic interpretations will, in most instances, be placed on the less mobile major and trace elements (i.e. TiO_2, P_2O_5, Zr, Nb and Y).

4.2.1 Major Elements:

The tholeiitic affinity of all the samples from the Conrad F.Z. is indicated by their normative hypersthene content. All but two basalts (I045-151 and I047-64) and four dolerites (I045-49, I047-12, I047-72 and I047-101) are also olivine normative (Tables 4-22 and 4-23). In terms of total normative pyroxene, plagioclase and olivine, both basalts and dolerites straddle the inferred olivine-plagioclase cotectic of Shido et al. (1971) (Fig. 4-28) and are displaced towards plagioclase relative to the field of FAMOUS glasses (Bryan et al., 1976). Relative to the IOFZ basalts, the Conrad F.Z. samples are not as plagioclase-rich, but like the IOFZ basalts, they extend the range of off-ridge extrusives and intrusives (Bryan et al., 1976) to olivine-poor compositions (Fig. 4-28).

The variation in total alkalis with respect to SiO_2 is shown in Fig. 4-29. The Conrad F.Z. basalts fall within, or close to, the field of MORB, while the dolerites appear to be significantly enriched in both SiO_2 and total alkalis. Basalt I047-62 and dolerites are significantly enriched in alkalis and/or SiO_2 relative to MORB and some of this variation may be attributed to secondary alkali feldspar. In terms of an

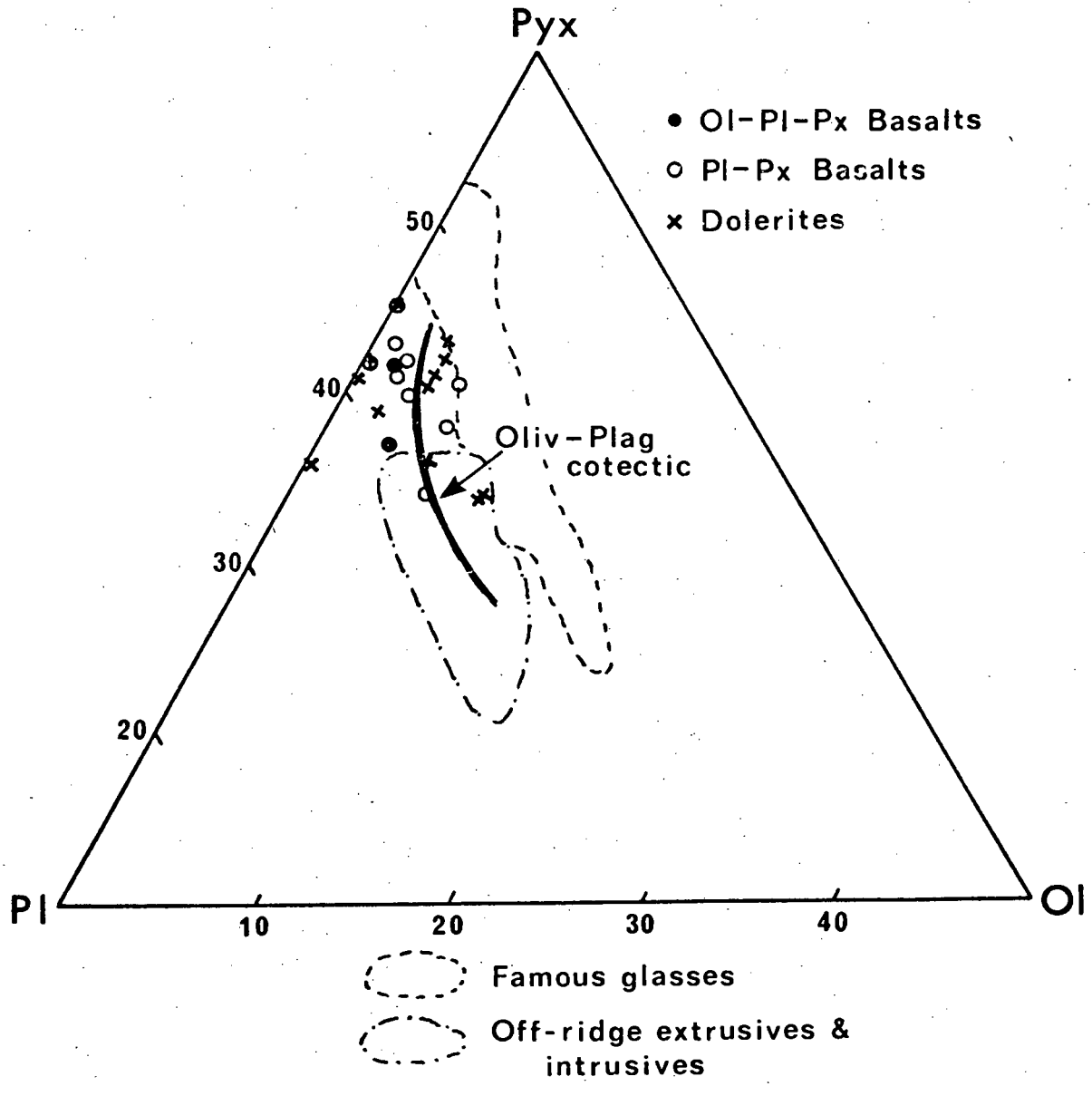

Fig. 4-28: Variation in total normative pyroxene, plagioclase and olivine for Conrad F.Z. basalts and dolerites. The position of the olivine-plagioclase cotectic is taken from Shido et al. (1971). Composition fields of FAMOUS glasses and off-ridge extrusives and intrusives are from Bryan et al. (1976).

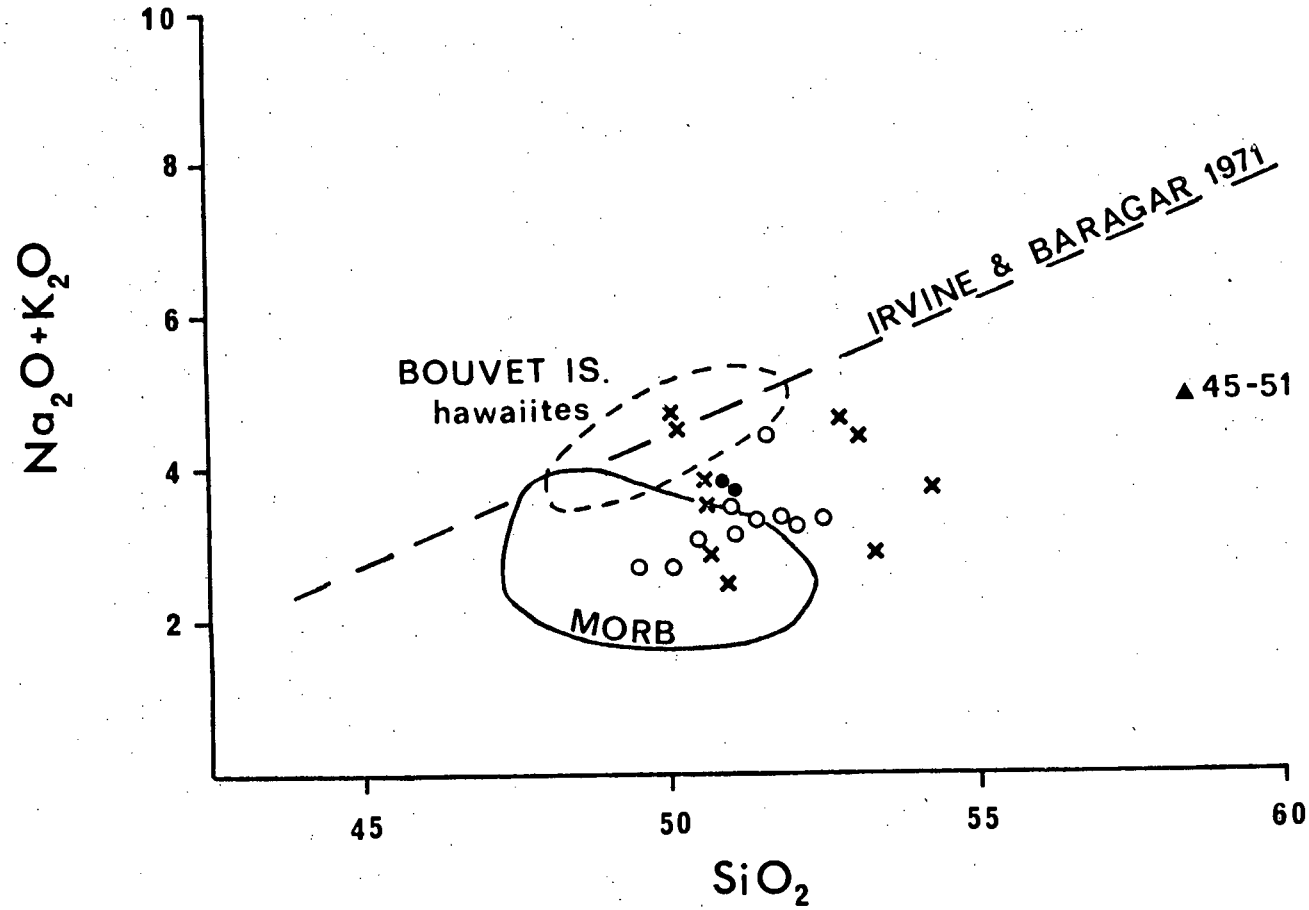

Fig. 4-29: Total alkalis - SiO_2 variation in Conrad F.Z. basalts and dolerites. Field of mid-ocean ridge basalt (MORB) is taken from Dickey et al. (1977). Symbols as in Fig. 4-28.

AFM diagram (Fig. 4-30), the Conrad F.Z. samples describe a broad iron enrichment trend and fall within the field of Atlantic F.Z. basalts as defined by Hekinian and Thompson (1976).

In accord with previous studies on fracture zone basalts (e.g. Shibata and Fox, 1975; Hekinian and Thompson, 1976; Shibata et al., 1979a), the Conrad F.Z. basalts and dolerites not only have evolved major element compositions relative to abyssal tholeiites, but also show an extreme range in compositions. No 'primitive' basalts have been recovered and MgO contents range from 7.6% to 5.7%, with a corresponding range in Mg-number from 0.65 to 0.46 (Table 4-22). The dolerite compositions extend to slightly lower MgO contents and range from 7.5% to 4.4% with Mg-numbers ranging from 0.60 to 0.35 (Table 4-23). It is relevant to note that the basalts with modal olivine (I045-97, I045-152 and I045-161) do not have the highest MgO contents or Mg-numbers, suggesting that the suite of rocks does not conform to a single simple fractionation sequence.

The evolved nature of the basalts and dolerites is clearly illustrated by the extreme enrichment attained by the incompatible major elements, e.g. TiO_2 and P_2O_5. TiO_2 concentrations range from 1.0% to 2.5% in the basalts and from 1.5% to 3.5% in the dolerites (one dolerite, I047-72, has 0.65% TiO_2). P_2O_5 shows a similar degree of enrichment, ranging from 0.10% to 0.32% in the basalts and from 0.16% to 0.44% in the majority of dolerites (samples I047-72 and I047-101 have 0.05% and 0.79% P_2O_5 respectively). Little importance is attached to the K_2O variations due to occurrence of secondary K-feldspar in many of the samples. The FeO and TiO_2-rich nature of the Conrad F.Z. samples is readily displayed in a plot of TiO_2 versus FeO*/MgO (Fig. 4-31). The

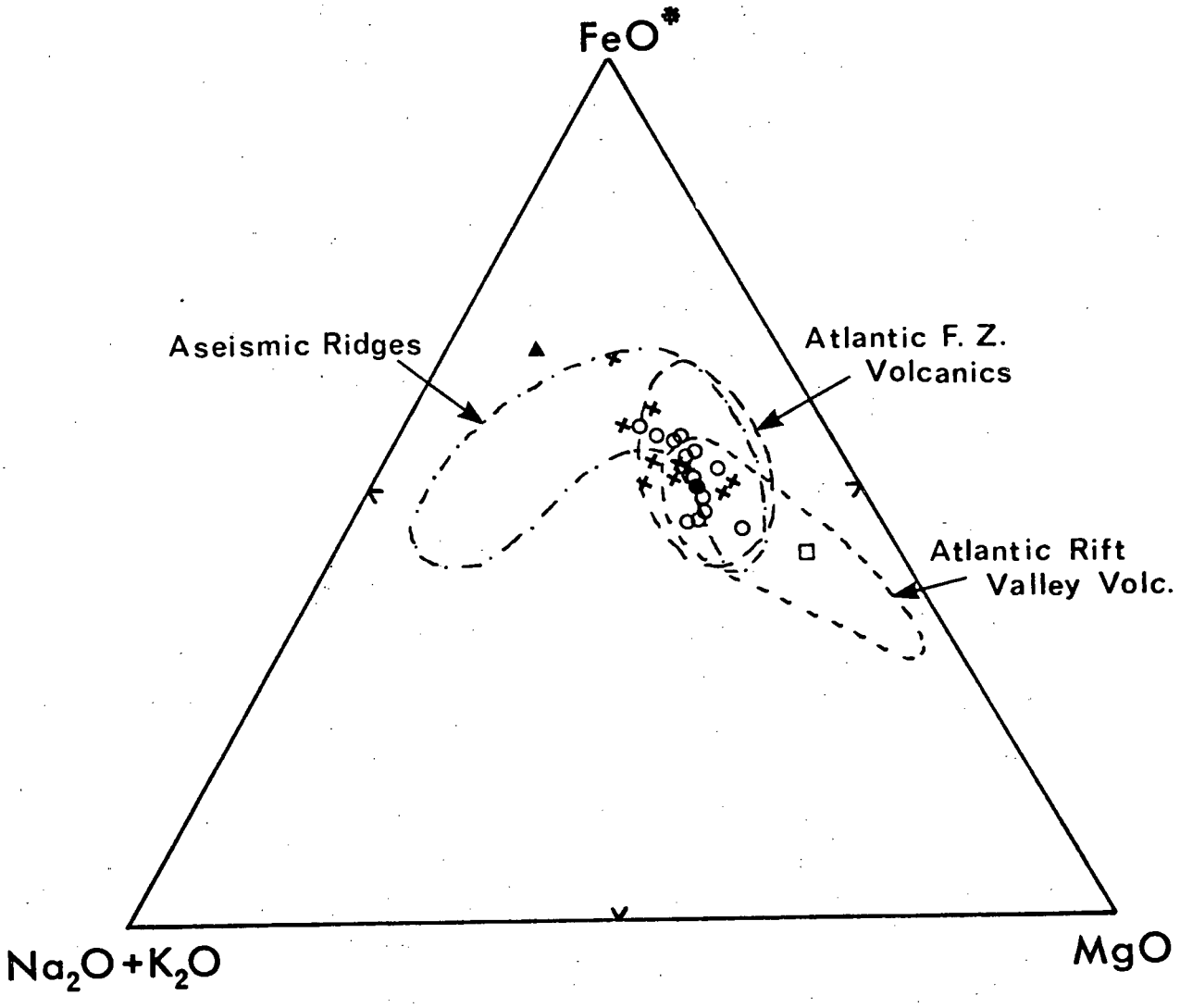

Fig. 4-30: A-F-M diagram showing the compositional variation of Conrad F.Z. basalts and dolerites. Fields of aseismic ridge, Atlantic fracture zone and Atlantic rift valley volcanics are taken from Hekinian and Thompson (1976). Closed triangle represents ferrodiorite I045-51, open square represents hypersthene gabbro I045-172, other symbols as in Fig. 4-28.

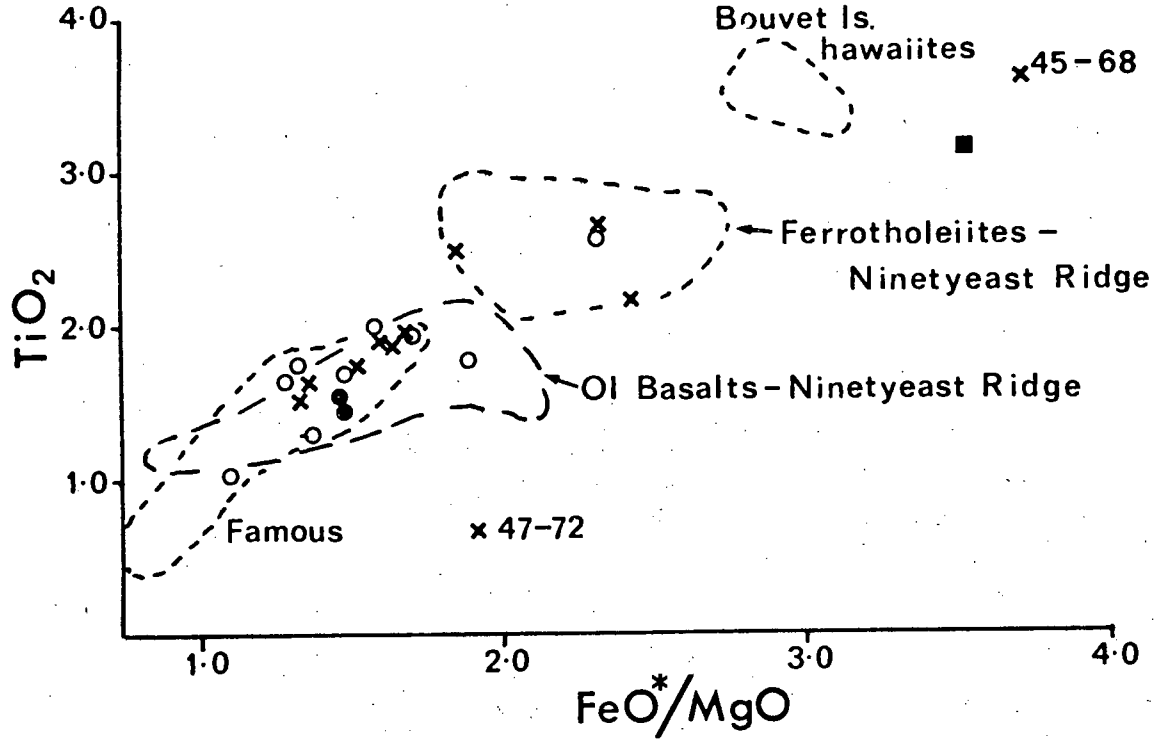

Fig. 4-31: Plot of TiO_2 against FeO^*/MgO ratio of Conrad F.Z. basalts and dolerites. Solid square represents the most TiO_2 rich ferrobasalt from the Galapagos Spreading Center (Claque and Bunch,1976). The field of FAMOUS glasses is taken from Bryan et al. (1976), the fields of Ninetyeast Ridge basalts are taken from Frey et al. (1976). Symbols as in Fig. 4-28.

majority of basalts and dolerites plot towards the upper extreme of the field of FAMOUS glasses (Bryan et al., 1976) and within the field of olivine basalts from the Ninetyeast Ridge (Frey et al., 1976). However, basalt I047-62 and dolerites I047-12, I047-28A and I047-101 correspond closely to the compositional field of ferrotholeiites from the Ninety-east Ridge (Frey et al., 1976), while ferrodolerite I045-68 is even more enriched in TiO_2 and FeO*/MgO (Fig. 4-31) than the extremely iron-rich differentiates from the Galapagos Spreading Center (Clague and Bunch, 1976).

The variations of some major elements with mafic index are illustrated in Fig. 4-32. Bearing in mind the altered nature of many of the samples, CaO and Al_2O_3 show an overall decrease with increasing M.I., while Na_2O shows a tendency to increase. The Na_2O and K_2O variations, and to a lesser extent CaO and Al_2O_3, are strongly influenced by the presence or absence of alkali feldspar, a factor contributing to the considerable scatter observed. In contrast, the variation of the immobile, incompatible elements P_2O_5 and TiO_2 in the majority of samples describe remarkably systematic positive trends with M.I. (Fig. 4-32). As mentioned earlier, it is noteworthy that the basalts with modal olivine do not have the lowest concentrations of TiO_2 and P_2O_5, elements which are preferentially partitioned into the liquid. Another feature in the compositional variations shown in Fig. 4-32 is that although the basalts and dolerites have a similar range, the dolerites tend towards more differentiated compositions, i.e. higher TiO_2, P_2O_5, M.I. and lower CaO, Al_2O_3. Pigeonite dolerite I047-72 is consistently displaced off the main trends described by the other Conrad F.Z. samples, being relatively depleted in TiO_2 and P_2O_5 and enriched in CaO and Al_2O_3 for a

given M.I., while I047-101 is conversely enriched in P_2O_5 and depleted in CaO and Al_2O_3 (Fig. 4-32). These variations are qualitatively in accord with the effects of substantial plagioclase accumulation (in accord with the high proportion of modal plagioclase in pigeonite dolerite I047-72) and of plagioclase fractionation respectively.

The covariation of 'incompatible' elements is potentially useful in investigating genetic relationships within a suite of samples since the mutual ratio is largely unaffected by fractionation processes (e.g. Gast, 1968; Erlank and Kable, 1976). With respect to observed phenocryst mineral assemblages in the basaltic rocks from the Conrad F.Z., P_2O_5 and Zr are two such incompatible elements. The excellent correlation between these two elements (Fig. 4-33) provides compelling evidence for a simple genetic relationship among most of the basaltic rocks. Two notable exceptions are evident: these are dolerites I047-32 and I047-101 (Fig. 4-33), which fall well off the main trend. It is interesting to note that the ferrodiorite (I045-51) and hypersthene gabbro (I045-172) plot very close to the basalt trend. The average P/Zr ratio of the Conrad F.Z. basaltic rocks (excluding I047-32 and I047-101) is 6.97, intermediate between that observed for average MORB (P/Zr = 6.55; Sun and Nesbitt, 1977) and archean basalts (P/Zr = 7.21; Nesbitt and Sun, 1976). The variation in TiO_2 and Zr is also shown in Fig. 4-33, where a similar close linear correlation is defined for the majority of the samples. Dolerites I047-32 and I047-101 (highly altered) are again displaced from the average trend, as is dolerite I047-12. Since ilmenite and titanomagnetite are crystallising phases in the more evolved rocks, TiO_2 does not behave as an incompatible element at this stage and consequently the displacement of these samples from the main trend can be explained. The

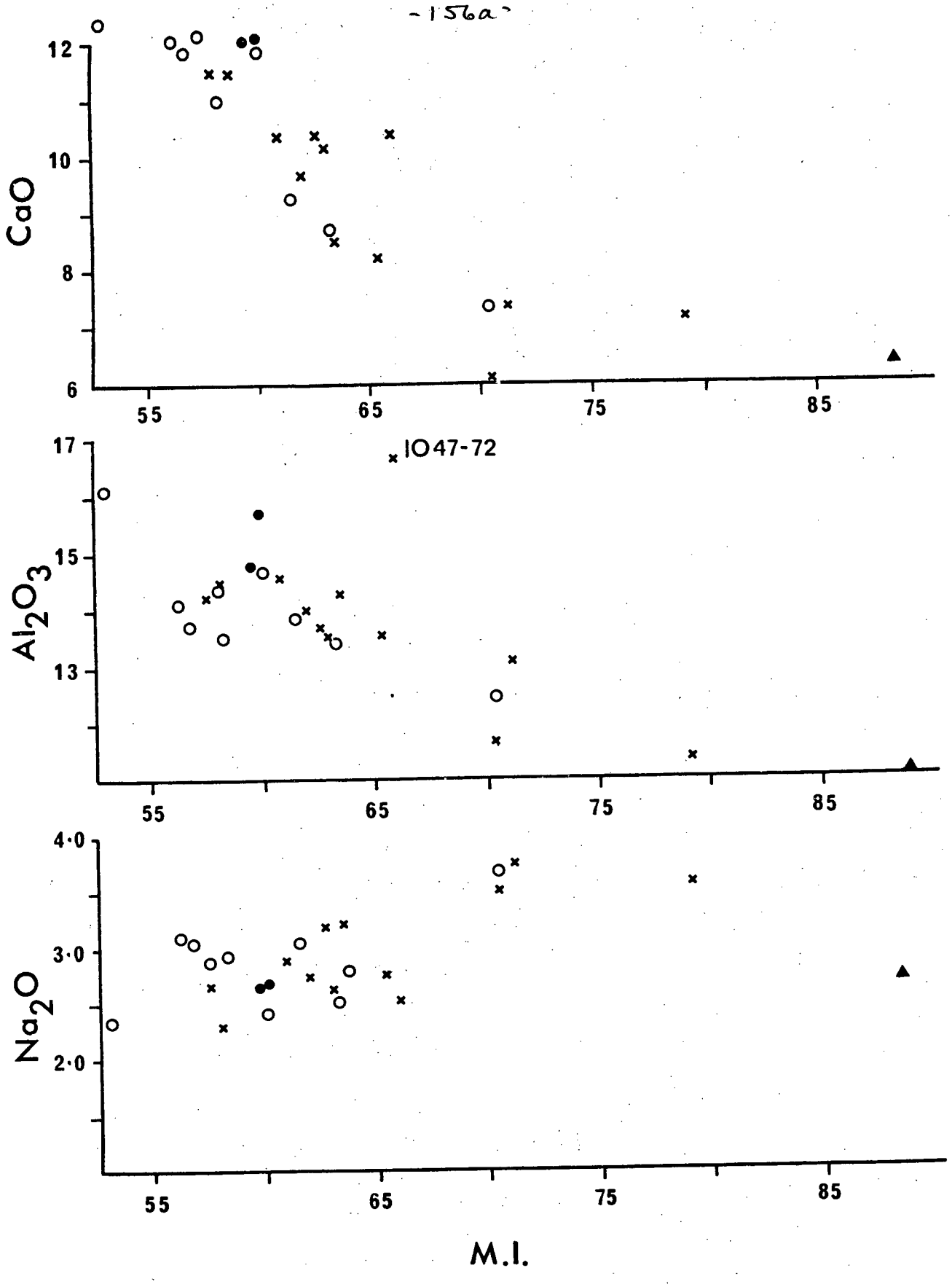

Fig. 4-32: Major element variation in Conrad F.Z. basalts and dolerites with respect to M.I. as index of differentiation. Open circles = plag-pyx basalts, closed circles = ol-plag-pyx basalt, crosses = dolerites, closed triangle = ferrodiorite.

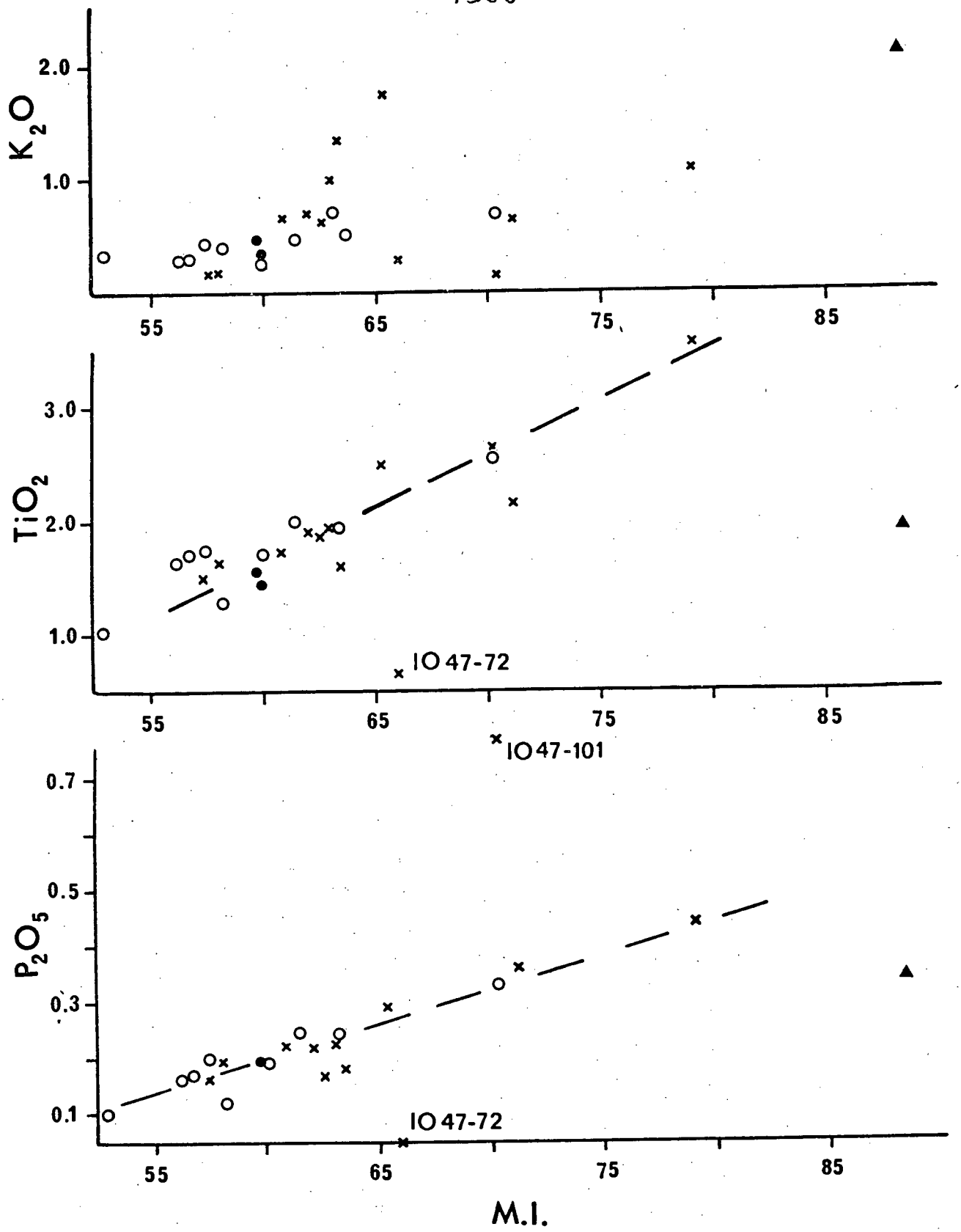
K_2O
2.0
1.0
55
65
75
85
TiO_2
3.0
2.0
1.0
IO47-72
IO47-101
P_2O_5
0.7
0.5
0.3
0.1
M.I.

Fig. 4-32 (Cont.):

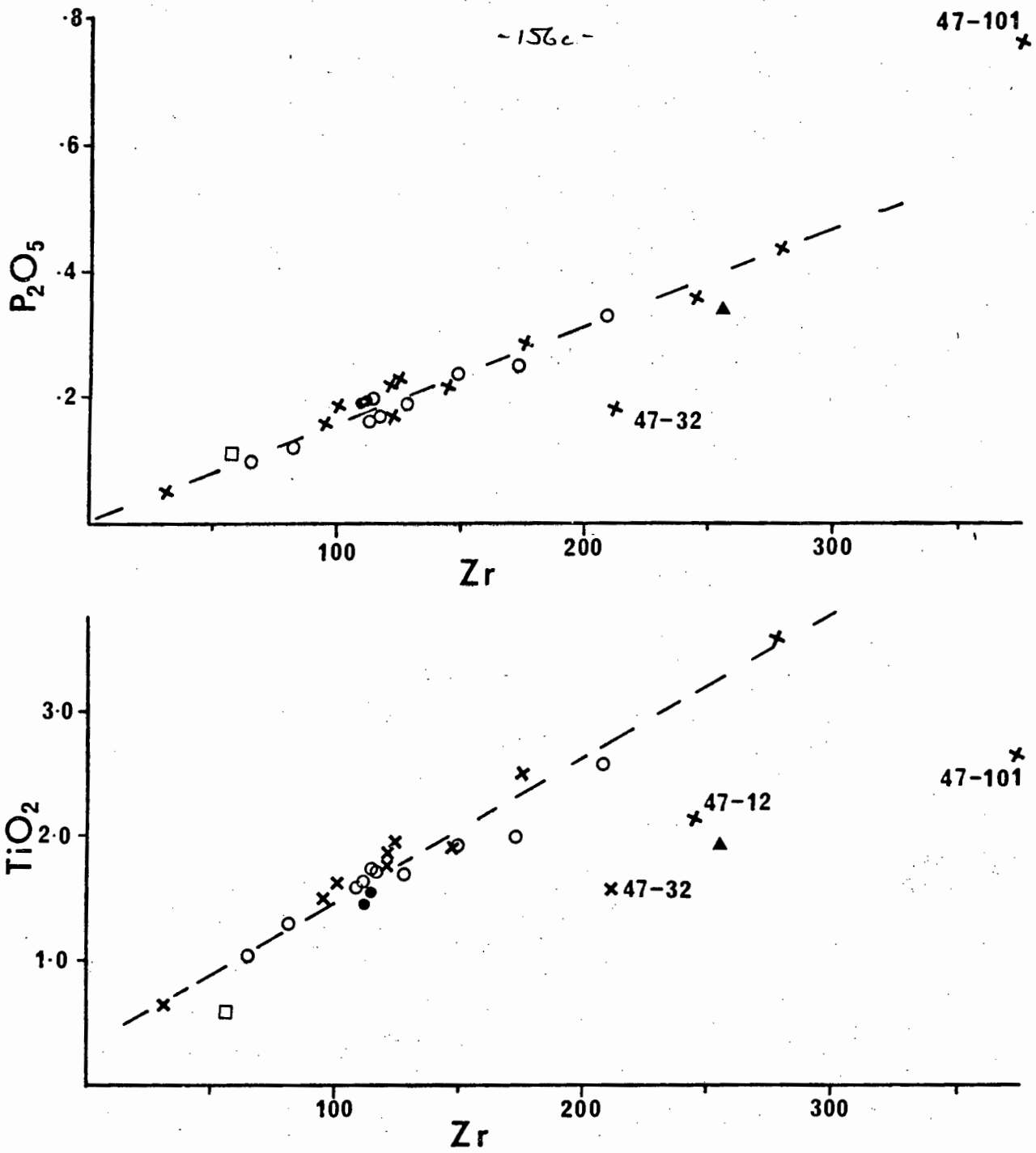

Fig. 4-33: Plot showing the correlation of P_2O_5 and TiO_2 with Zr in Conrad F.Z. basalts and dolerites. Symbols as in Fig. 4-32.

average Ti/Zr ratio of the majority of Conrad F.Z. basalts and dolerites is 87.5, significantly lower than that characteristic of MORB (Ti/Zr = 100-110; Pearce and Cann, 1973; Sun et al., 1979), but similar to the IOFZ basalts.

In summary, the major element characteristics indicate compositional similarity between the Conrad F.Z. basalts and dolerites, with the dolerites however extending to somewhat more evolved compositions. Chemical variations among the immobile elements suggest that the majority of samples (both basalts and dolerites) are genetically related and derive from a homogeneous source, at least in terms of TiO_2, P_2O_5 and Zr. Secondary alteration has extensively altered the distribution of some of the more mobile elements. The large compositional variations in terms of absolute incompatible element concentrations (variation by more than a factor of 3) suggest that intensive fractionation has taken place during the evolution of these basalts.

4.2.2 Trace Elements:

In accord with their evolved major element compositions, the Conrad F.Z. basalts and dolerites are characterised by low concentrations of compatible ferromagnesian trace elements and high concentrations of incompatible trace elements, relative to MORB. The extreme degree of differentiation within the suite is also well illustrated by the trace element variations. This variation is illustrated in Figs. 4-34 and 4-35 where selected trace elements are plotted against Zr as a measure of differentiation (Zr has been used in preference to M.I. to avoid the effect of alteration on the FeO*/MgO ratio; Humphris and Thompson, 1978a).

Unlike the well defined enrichment trends described by the

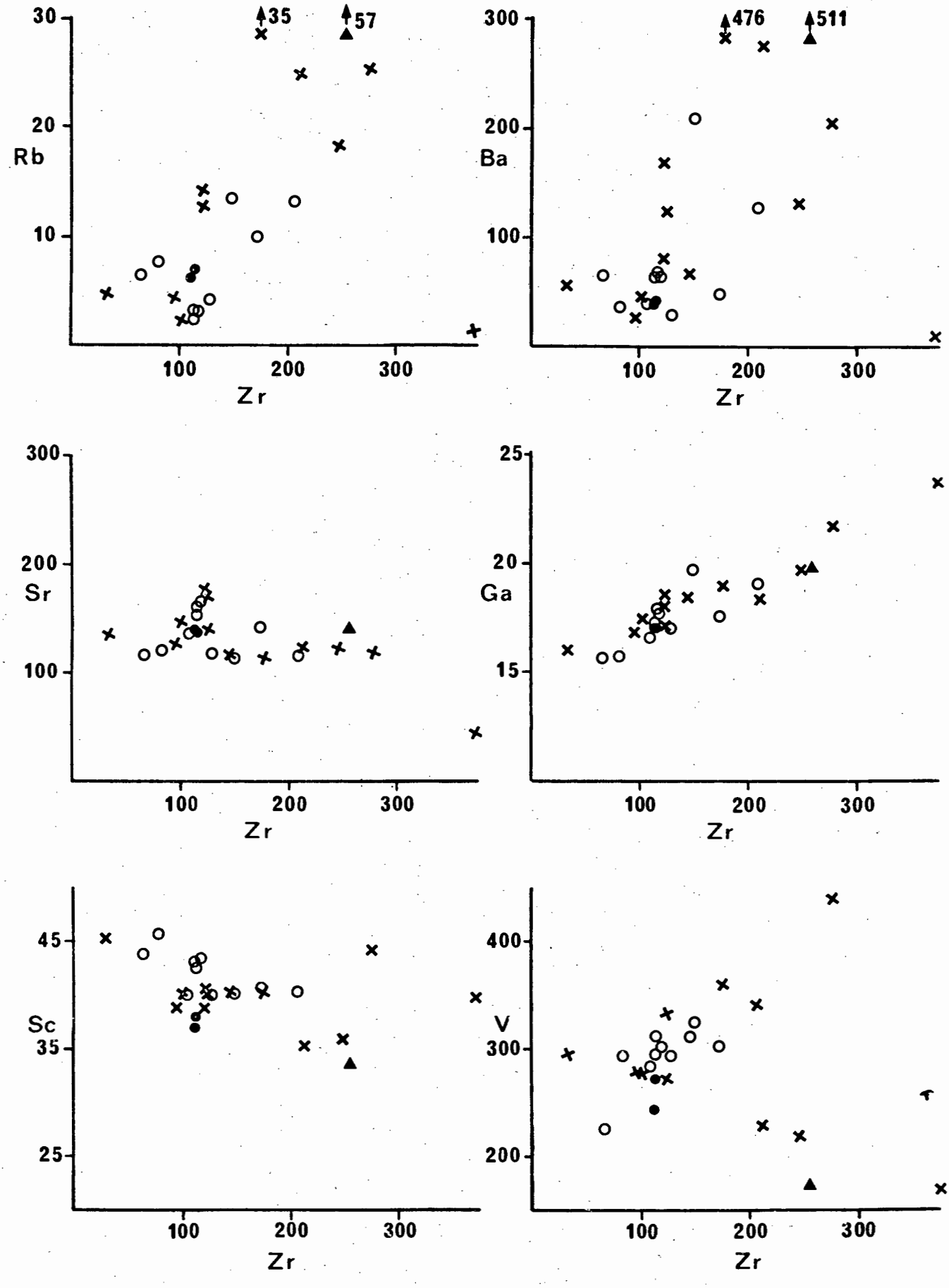

Fig. 4-34: Variation of selected trace elements with respect to Zr as index of differentiation in Conrad F.Z. basalts and dolerites. Symbols as in Fig. 4-32.

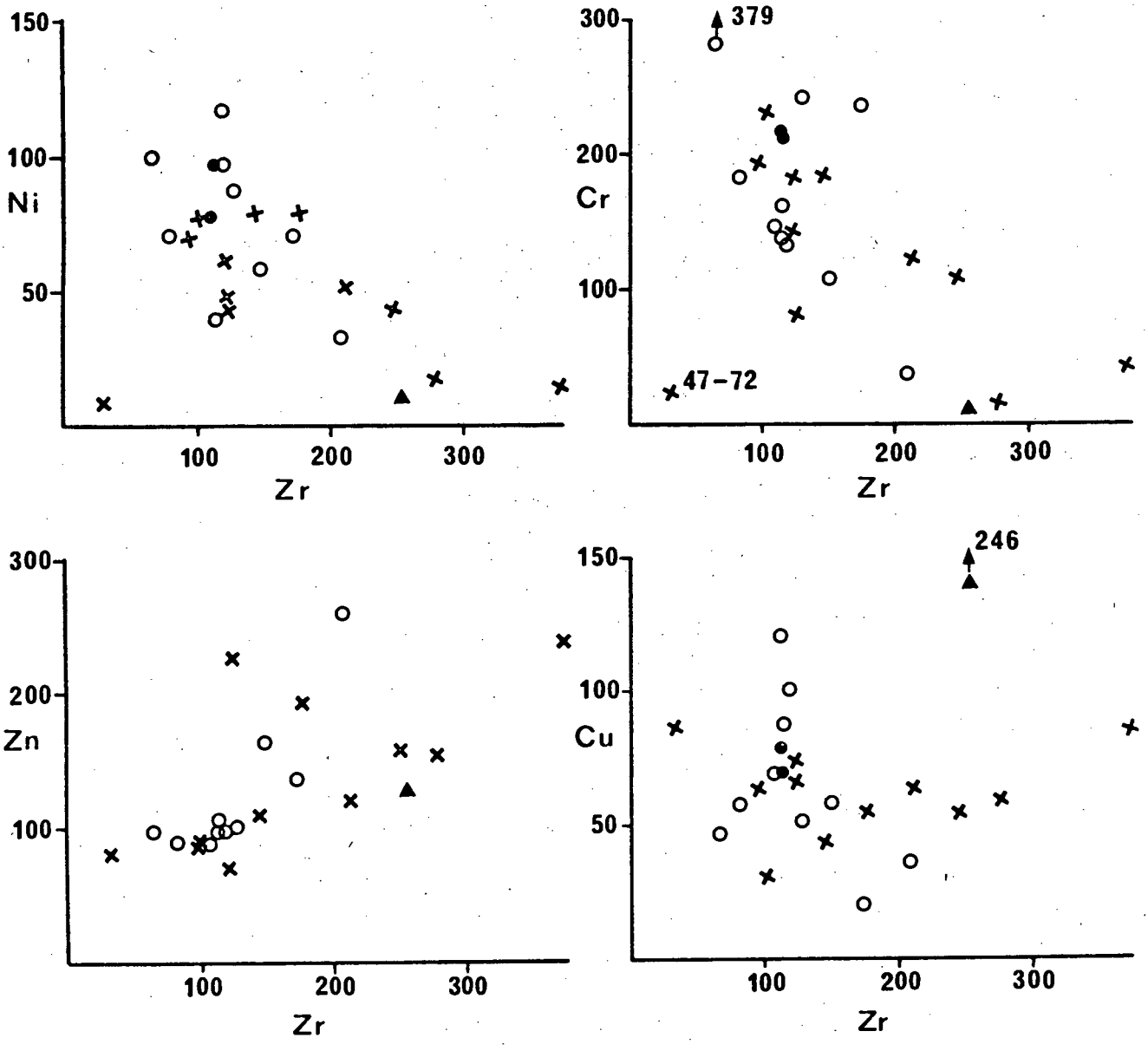
150
100
Ni
50
100
200
300
Zr
300
379
200
Cr
100
47-72
100
200
300
Zr
300
200
Zn
100
100
200
300
Zr
150
246
100
Cu
50
100
200
300
Zr

Fig. 4-34 (Cont.):

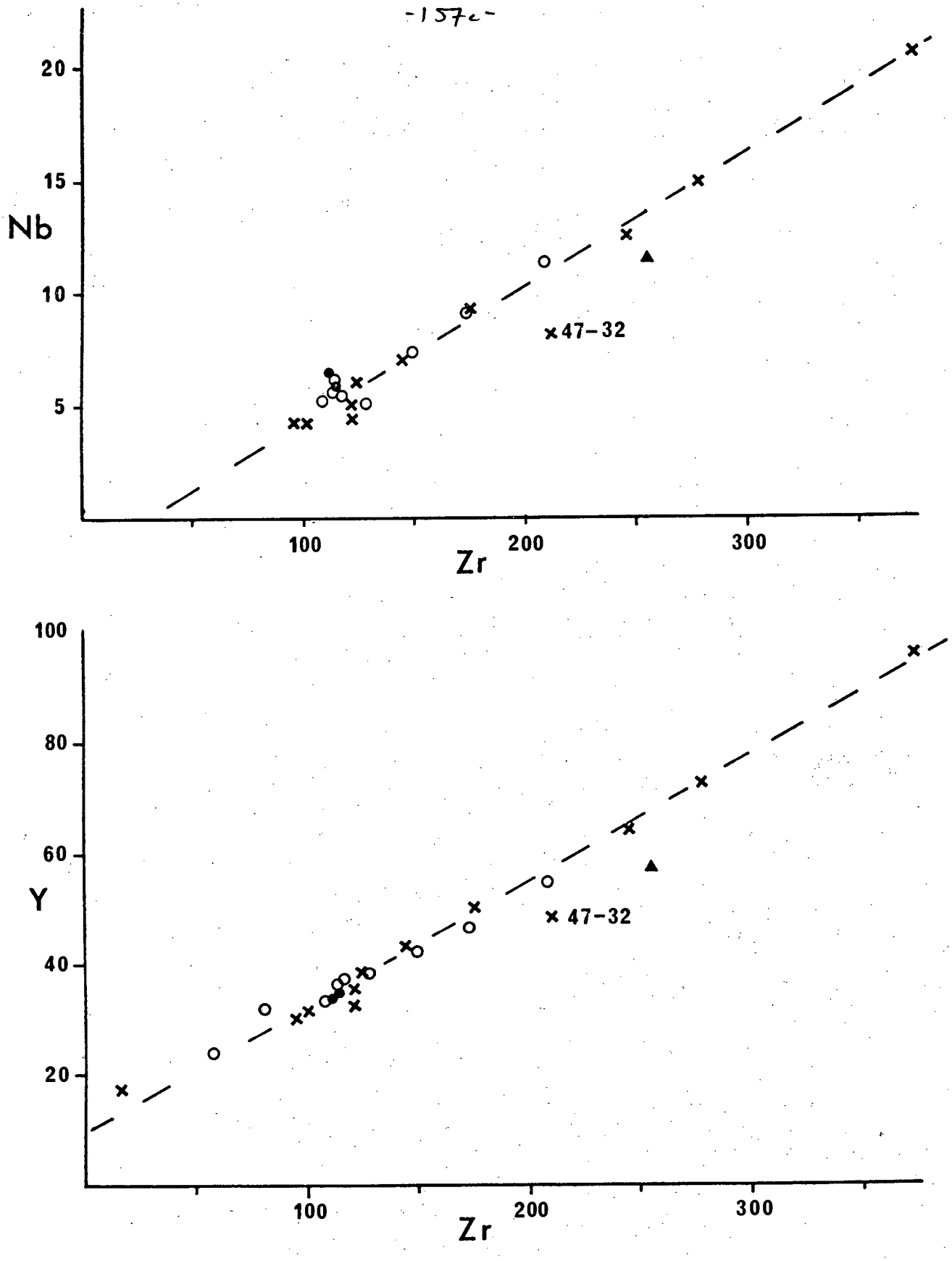

Fig. 4-35: Plot showing the correlation of Nb and Y with Zr in Conrad F.Z. basalts and dolerites. Symbols as in Fig. 4-32.

immobile incompatible major elements (TiO_2 and P_2O_5) with Zr (Fig. 4-33), the incompatible trace elements Rb and Ba (Fig. 4-34) do not describe coherent trends. The considerable scatter observed in these plots and the extreme range in concentration of these elements (Rb, 1-35 ppm; Ba, 8-476 ppm) is attributed primarily to alteration effects. Rb is known to be highly mobile during ocean floor weathering, but Ba and Sr, which shows a relatively restricted compositional range (Fig. 4-34) in most Conrad F.Z. samples (between 110 and 180 ppm Sr), are generally considered to be only moderately mobile. The high mobility of Ba and Rb is regarded as being related to the hydrothermal alteration (by possibly an alkali-rich brine) that resulted in the K-feldspar, Na-feldspar and analcite replacement observed in many of the samples. In contrast to the common practice of using Rb and Ba as sensitive indicators of petrogenetic relationships (e.g. consideration of K/Rb and K/Ba ratios; Gast, 1968; Hart et al., 1974), these elements, including possibly Sr, will clearly be of little use in assessing any genetic relationships within the Conrad F.Z. basalts and dolerites.

In contrast to the above elements, Ga shows a relatively well defined positive correlation with Zr, with concentrations increasing from 16 ppm to 22 ppm (Fig. 4-34). Sc and V show considerable scatter, though if some of the more evolved dolerites (I047-32, I047-12, I047-101) are excluded, V does define a broad increase with differentiation. Both Sc and V are readily incorporated in clinopyroxene and Fe-Ti oxides (e.g. Ewart et al., 1973; Lindstrom, 1976; Leeman et al., 1978a,b), a factor which would contribute substantially to the observed scatter in the data. Specifically the low V content of some of the more evolved dolerites could reflect Fe-Ti oxide fractionation.

Ni and Cr abundances are characteristically low (100-15 ppm and 380-15 ppm respectively) and define broad negative correlations with increasing differentiation (Fig. 4-34), emphasising the evolved nature of these rocks. The highest Ni and Cr contents (100 ppm and 380 ppm respectively) are observed in a highly plagioclase-pyroxene phyric basalt (I045-130B). The significant displacement of pigeonite dolerite I047-72 from the main Cr and Ni trends (Fig. 4-34) is in qualitative accord with the abundant modal plagioclase in this rock representing cumulus plagioclase, a feature in accord with the major element composition. Zn and Cu both show considerable scatter with Zn varying from 70 to 260 ppm and Cu from 40 to 140 ppm. Much of the Cu variation can probably be attributed to the effect of alteration, but Zn is commonly regarded as being relatively immobile during weathering.

Unlike the variation of the more mobile incompatible elements, the immobile incompatible elements Y, Nb and Zr show an excellent degree of correlation (Fig. 4-35) over an extremely large concentration range. The concentration ranges of Zr from 30 to 375 ppm, Nb from <3 to 21 ppm, and Y from 19 to 96 ppm, indicate the exceptionally large degree of differentiation reflected by these basalts and dolerites. Further inspection of Fig. 4-35 shows the previously noted feature that the dolerites span the basalt compositional range and extend to significantly more evolved compositions. Dolerite I047-32 is once again displaced from the average trends, indicating the possibility that this rock may represent a glacial erratic.

The ferrodiorite I045-51 plots within the framework of the observed variations for most of the trace elements (Fig. 4-34). However, with respect to Zr, Nb and Y variations (Fig. 4-35), it lies somewhat off

the main enrichment trend and, in terms of absolute abundances, is not as enriched in these elements as would be expected from its major element composition. The possibility of this ferrodiorite being genetically related to the Conrad F.Z. suite of basalts is discussed in a later section.

The absolute abundance of incompatible elements in a suite of lavas can be used to estimate the degree of fractionation, or phenocryst accumulation, that may have taken place during evolution of the lava suite. Within the suite of basalts and dolerites from the Conrad F.Z., the immobile incompatible elements Zr, Nb, Y, Ti and P all show excellent correlations, suggesting that a genetic relationship exists among the various samples. From the above-mentioned elements, Nb and P, and to a slightly lesser extent Zr, are the most 'incompatible' with respect to the observed phenocryst phases (Table 2-1, Anderson and Greenland, 1969; Clague and Bunch, 1976). The two samples with the lowest incompatible element concentrations are I047-72 and I045-130B. The petrography of these samples suggests that both might be cumulus-enriched (a factor qualitatively borne out by diagnostic compositional variations, Figs. 4-32 and 4-34). The low concentrations are therefore not features of a 'liquid' composition. If the remainder of the range of compositional variation was to be attributed solely to fractional crystallisation of a single 'parental' magma, it would require approximately 80% crystallisation to account for the 4.5 to 6.5-fold enrichment in incompatible elements.

Although the absolute abundance of incompatible elements in a suite of lavas is a function of the degree of partial melting and subsequent fractional crystallisation, several incompatible element ratios

have been shown to be diagnostic of source region characteristics and in particular may serve as a measure of the degree of depletion of the source region. Of the trace element ratios used in this manner (e.g. K/Rb, K/Ba, Zr/Nb, Y/Nb, Sm/La and La/Ta (Gast, 1968; Hart, 1971; Pearce and Cann, 1973; Erlank and Kable, 1976; Bougault et al., 1979)), the first two are susceptible to alteration and consequently have little application to the altered Conrad F.Z. samples. The latter ratios, however, involve more immobile elements and so are more applicable to the Conrad F.Z. basalts. The Conrad F.Z. basalts and dolerites have an average Zr/Nb ratio of 21 $\pm$ 3 which, though somewhat lower than typical MORB (Zr/Nb = 37; Erlank and Kable, 1976), contrasts with the low Zr/Nb ratio ($\pm$ 8.4) of the IOFZ basalts. The Zr/Nb ratio of the Conrad F.Z. basalts is however similar to that of the Juan de Fuca basalts (Zr/Nb = 23; Kable, 1972) and the basalts from the Blanko Fracture Zone (Zr/Nb = 17; Kable, 1972). The higher Y/Nb (6.1 $\pm$ 1.0) and lower Zr/Y (3.44 $\pm$ 0.47) ratios of the Conrad F.Z. also serve to distinguish these basalts from the IOFZ basalts (Y/Nb = 1.98, Zr/Y = 4.36).

Two Conrad F.Z. samples (I045-68, I047-12) have been analysed for the REE's. The analyses were performed at the Australian National University, Canberra, by Dr. A.R. Duncan, and the data are given in Table 4-24. In contrast to the typical LREE depletion observed in MORB (e.g. Bryan et al., 1976), dolerite I047-12 is characterised by having a flat REE pattern (Fig. 4-36) with a pronounced Eu anomaly (Eu/Eu* = 0.78). In comparison ferrodolerite I045-68 has a slightly LREE-enriched pattern (La/Yb = 1.42) and possibly a very minor Eu anomaly (Eu/Eu* = 0.91). The overall absolute abundance of the REE in these samples relato that commonly found in MORB emphasises the evolved nature of these rocks (Fig. 4-36).

Table 4-24: Rare earth element concentrations and chondrite normalised values for Conrad F.Z. samples I047-12 and I045-68. Concentrations were normalised using the values for Leedy chondrite divided by 1.2 (Sun and Hanson, 1976).

	I047-12		I045-68	
	ppm	chondritic*	ppm	chondritic*
La	11.80	37.46	15.90	50.48
Ce	34.00	41.82	45.00	55.35
Pr	5.10	43.97	6.30	54.31
Nd	26.00	43.55	35.00	58.63
Sm	7.70	40.10	8.50	44.27
Eu	2.12	29.44	2.71	37.64
Gd	9.20	35.52	10.00	38.61
Tb	1.70	34.69	1.80	36.73
Dy	11.00	33.85	12.20	37.54
Ho	2.60	35.62	2.70	36.99
Er	7.50	35.21	7.60	35.68
Tm	1.01	33.67	1.02	34.00
Yb	7.00	33.65	7.40	35.58
† CH La/Sm		.934		1.140
CH La/Yb		1.113		1.419
Eu/Eu*		.780		.910

† CH = chondritic

* Chondrite normalised

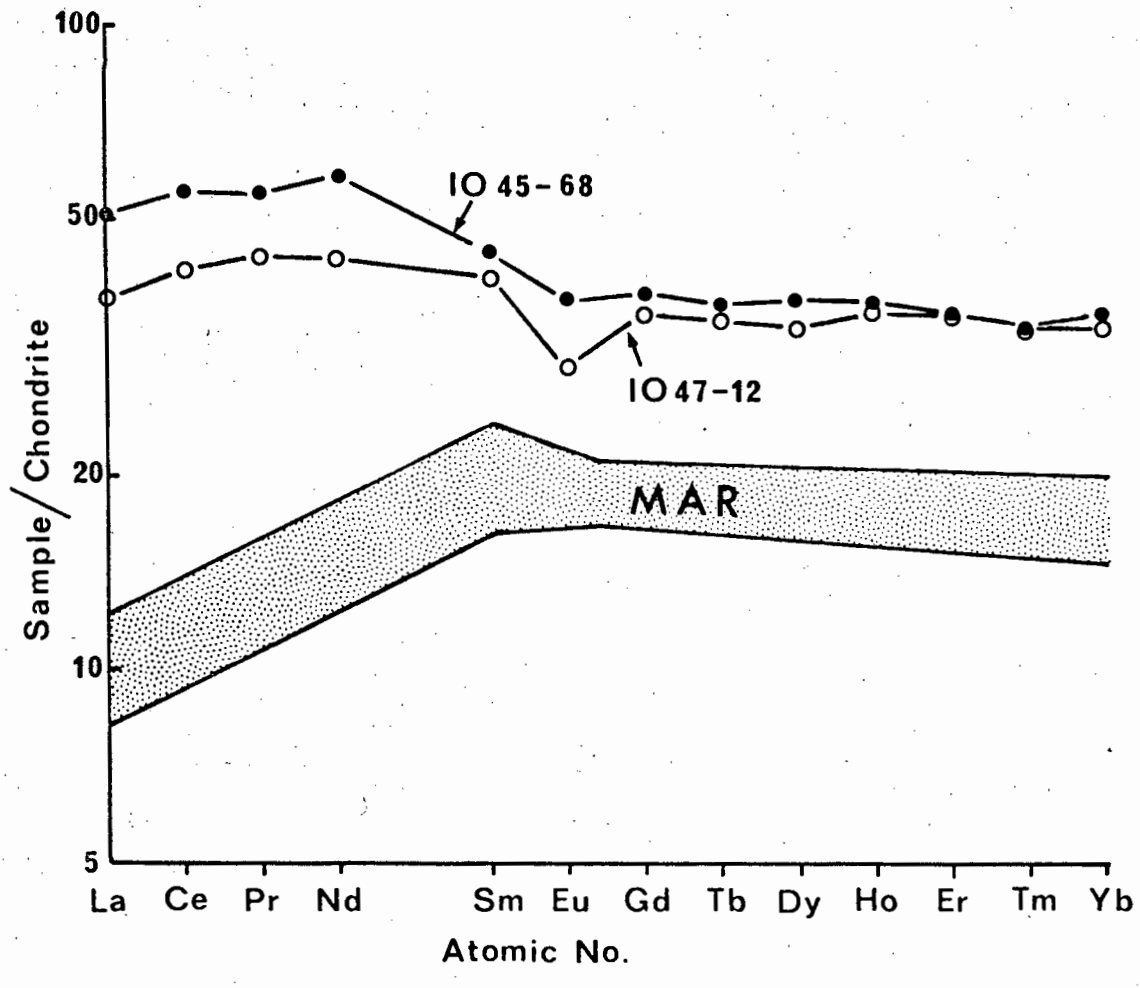

Fig. 4-36: Chondrite normalised REE variation in two Conrad F.Z. samples. Concentrations were normalised using values from Leedy chondrite divided by 1.2 (Sun & Hanson, 1976). The field of average MAR basalts (Frey et al., 1974) is shown for comparison.

4.3 Petrogenesis

It has been shown in the previous section that the immobile incompatible major and trace elements of the Conrad F.Z. basalts and dolerites describe extremely systematic trends (e.g. Figs. 4-33, 4-35). These trends strongly suggest that the majority of samples dredged from the Conrad F.Z. are genetically related through either fractional crystallisation or partial melting processes. The constant ratios of the immobile incompatible elements (e.g. Zr/Nb, Y/Nb, Zr/Y) suggest that if more than one parental magma is involved in giving rise to the range in compositions, then the source area for these magmas was homogeneous with respect to these elements.

4.3.1 Fractional Crystallisation:

Consideration of the Ni contents (100-15 ppm) and Mg-numbers (0.65-0.35) of the basaltic rocks from the Conrad F.Z. clearly indicates that these rocks cannot be regarded as 'primary magmas' (e.g. Green, 1971; Kesson, 1973; Bougault et al., 1979; this work, Chapter III). The range in compositions is therefore in large part a consequence of fractional crystallisation, of one or more parental magmas. The extent to which the compositional variations in the Conrad F.Z. can be attributed to low pressure fractional crystallisation can be evaluated quantitatively from the participating minerals and the relative importance of the fractionating phases, using a least squares approximation technique (Bryan et al., 1969). All input data to the least squares calculations were normalised to 100%, volatile-free, and all iron was expressed as FeO. Due to the low concentration of P_2O_5 and the susceptibility to alteration of K, these two elements were excluded from the calculations.

(i) Basaltic Rocks

In order to accommodate the large number of samples (both basalts and dolerites) which contribute towards the compositional spread, those samples with very similar compositions have been grouped and their average composition used. Samples that have been averaged in this fashion are: olivine-plagioclase-pyroxene basalts I045-97 and I045-152 (referred to as 45-97/45-152), plagioclase-pyroxene basalts I045-91, I045-151 and I045-161 (referred to as 45-91/45-151/45-161), dolerites I045-49 and I045-160 (referred to as 45-49/45-160), dolerites I045-34 and I045-130D (referred to as 45-34/45-130D), and samples I047-64 and I045-148 (referred to as 47-64/45-148). For the purposes of modelling no distinction has been made between supposedly intrusive and extrusive varieties, though it is appreciated that the coarser grained samples may well reflect the effects of minor flow differentiation (e.g. le Roex and Reid, 1978). These effects are, however, likely to be small relative to the extreme range of overall differentiation. For the remainder of this section all samples will be referred to as basalts.

Since none of the Conrad F.Z. basalts are potential candidates for primary magmas, and since a fairly continuous compositional range is observed, the choice of a suitable parental magma is not well constrained. For the purposes of moedlling therefore, the more evolved basalts have been regarded as potential derivatives of <u>any</u> of the less evolved basalts. On this assumption all possible parent-daughter pairs have been evaluated. The results of this evaluation indicate certain parent-daughter pairs are not permitted and that it is not possible to relate all samples to a single parent. Most of the compositional variation can be ascribed to varying degrees of fractional crystallisation of two potential 'parental'

magmas, 45-91/45-151/45-161 and 45-49/45-160. A summary of the successful least squares approximations relating the more evolved basalts to these two parental magmas is given in Table 4-25 and depicted schematically in Fig. 4-37, where the samples are arranged in order of increasing Zr content (as a measure of differentiation).

Before consideration of selected models in more detail, it should be noted that since large degrees of crystallisation are involved in the proposed models, with only two phases (plagioclase and clinopyroxene) contributing over 97% of the fractionate, the mixing calculations are not tightly constrained. Calculated degrees of crystallisation were found to be very sensitive to small variations in mineral composition, especially the minor components of clinopyroxene (TiO_2, Al_2O_3). In many cases variation of the mineral compositions resulted in significantly different predicted degrees of crystallisation, without significantly detracting from the acceptibility of the model (i.e. the sum of squares of differences remained small). Consequently mineral compositions were selected so as to fall within the observed compositional ranges and best satisfy both the major element variations and the required degree of crystallisation as indicated by the immobile incompatible elements. The selected mineral compositions are presented in Table 4-26.

Inspection of Table 4-25 and Fig. 4-37 shows that it is possible to relate the four most evolved Conrad F.Z. basalts to the 'parental' composition 45-91/45-151/45-161 by substantial fractionation of plagioclase and clinopyroxene with or without minor titanomagnetite. The amount of crystallisation varies from 53% (to produce I047-62) to 76% (to produce I047-101); clinopyroxene and plagioclase each comprise approximately 50% of the fractionate. With the exception of sample

No.	PARENT	PLAG	CPX	Ti-Mgt	DAUGHTER	F	ΣR^2
1	45-91/45-151/45-161	-0.4034(An_{53})	-0.3288	-0.0283(Mt_{30})	I047-101	0.2405	0.33
2	"	-0.3580(An_{56})	-0.3009	---	I045-68	0.3387	0.04
3	"	-0.2905(An_{56})	-0.2783	-0.0110(Mt_{30})	I047-12	0.4202	0.02
4	"	-0.2808(An_{59})	-0.2580	---	I047-62	0.4652	0.11
5	45-49/45-160	-0.2389(An_{61})	-0.2238	-0.0142(Mt_{30})	I047-28	0.5329	0.10
6	"	-0.1809(An_{68})	-0.1709	-0.0124(Mt_{30})	I047-64/I045-148	0.6381	0.02
7	"	-0.0826(An_{68})	-0.1065	-0.0042(Mt_{30})	I045-34/I045-130D	0.8124	0.14

Table 4-25: Summary of selected least squares approximations relating the various Conrad F.Z. basalts. Mineral proportions and F-values are given in weight fractions.

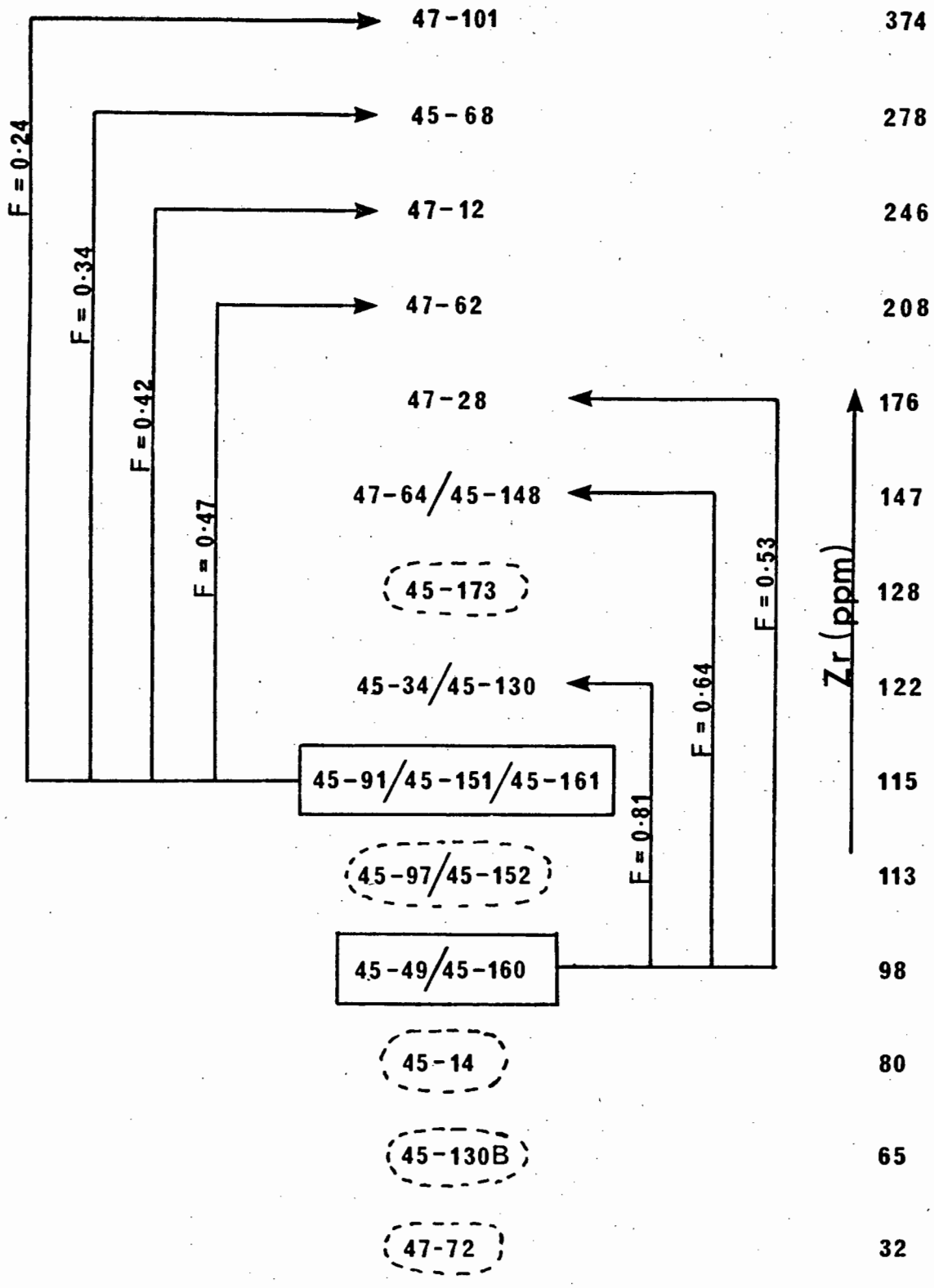

Fig. 4-37: Schematic representation of the possible fractional crystallisation relationships relating the Conrad F.Z. basalts. Samples are arranged in order of increasing Zr content. F equals the weight fraction of residual liquid calculated by least squares approximation. Samples enclosed by stipled lines cannot readily be related to the other samples by fractional crystallisation.

T A B L E 4-26

CONRAD F.Z: MINERAL COMPOSITIONS USED IN MIXING CALCULATIONS

	1	2	3	4	5	6	7	8	9	10
SIO2	50.80	54.29	53.89	53.02	52.34	51.80	51.40	50.89	51.38	.20
TIO2	.05	.08	.08	.08	.07	.70	1.30	1.12	.80	24.62
AL2O3	31.27	28.91	29.09	29.75	29.43	2.22	2.02	2.85	3.17	1.35
CR2O3	-	-	-	-	-	-	-	-	-	-
FEO	.50	.67	.50	.50	.83	9.21	9.21	8.46	7.92	72.94
MNO	ND	ND	ND	ND	ND	.23	.23	.18	.16	.49
MGO	.13	.12	.13	.13	.28	17.19	17.19	15.94	16.99	.38
CAO	13.69	10.65	11.34	11.91	12.58	18.42	18.42	20.32	19.35	ND
NA2O	3.55	5.27	4.97	4.61	4.47	.24	.24	.24	.22	ND
K2O	-	-	-	-	-	-	-	-	-	-
TOTAL	100.00	100.00	100.01	100.01	100.01	100.01	100.01	100.00	99.99	100.00

* * ATOMIC PROPORTIONS BASED ON SELECTED NO. OF OXYGENS * *

OXYGEN	8	8	8	8	8	6	6	6	6	32
SI	2.313	2.453	2.437	2.402	2.382	1.918	1.906	1.891	1.896	.063
ALIV	1.678	1.539	1.550	1.588	1.579	.082	.088	.109	.104	.500
ALVI	-	-	-	-	-	.015	-	.016	.034	-
TI	.002	.003	.003	.003	.002	.019	.036	.031	.022	5.819
CR	-	-	-	-	-	-	-	-	-	-
FE2+	.019	.025	.019	.019	.032	.285	.286	.263	.244	19.171
MN	-	-	-	-	-	.007	.007	.006	.005	.130
MG	.009	.008	.009	.009	.019	.948	.950	.883	.934	.178
CA	.668	.516	.549	.578	.614	.731	.732	.809	.765	-
NA	.313	.462	.436	.405	.395	.017	.017	.017	.016	-
K	-	-	-	-	-	-	-	-	-	-
SUM	5.003	5.006	5.003	5.004	5.023	4.023	4.022	4.024	4.021	25.871
	AN 68.06	AN 52.76	AN 55.77	AN 58.81	AN 60.86	WO 37.20	WO 37.20	WO 41.39	WO 39.36	
	AB 31.94	AB 47.24	AB 44.23	AB 41.19	AB 39.14	EN 48.28	EN 48.28	EN 45.16	EN 48.07	
	OR .00	OR .00	OR .00	OR .00	OR .00	FS 14.52	FS 14.52	FS 13.45	FS 12.57	

* * * S A M P L E D I R E C T O R Y * * *

ANALYSIS NO.	DESCRIPTION
1	PLAGIOCLASE
2	PLAGIOCLASE
3	PLAGIOCLASE
4	PLAGIOCLASE
5	PLAGIOCLASE
6	CLINOPYROXENE - 1
7	CLINOPYROXENE - 2
8	CLINOPYROXENE - 3
9	CLINOPYROXENE - 4
10	TI-MAGNETITE

** ND = NOT DETECTED **

I045-173, the remaining 'evolved' basalts (I047-28, 47-64/45-148 and 45-34/45-130D) can all be related to 'parental' composition 45-49/45-160 by fractional crystallisation, varying in amount from 19% to 47% (Table 4-25, Fig. 4-37). The fractionates comprise plagioclase, clinopyroxene and titanomagnetite in the average proportions 47:50:3. Two of the least squares approximations presented in Table 4-25 are given in detail in Tables 4-27 and 4-28. Table 4-27 shows the derivation of the extremely Fe-Ti-rich ferrodolerite I045-68 from parental composition 45-91/45-151/45-161 by 66% fractional crystallisation. The fractionating minerals comprise 35.8% plagioclase (An_{56}) and 30.1% clinopyroxene ($Wo_{37}En_{48}Fs_{15}$). The good major element agreement between predicted and observed compositions (as illustrated by the low sum of squares of residuals) and the low standard deviations of the components attest to the consistency of the calculation. The derivation of 45-34/45-130D from parental composition 45-49/45-160 by 19% fractional crystallisation of plagioclase (8.3%), clinopyroxene (10.7%) and minor titanomagnetite (0.4%) is shown in Table 4-28. Although the error in Na_2O is greater than desirable, it is well within the uncertainty associated with the effects of alteration observed in these samples. In this regard it should also be noted that the apparently high sum of squares of residuals (0.33) in calculation (1), Table 4-25 associated with the derivation of I047-101, is also within the uncertainty in the original composition of this sample due to its highly altered state.

The remaining samples illustrated in Fig. 4-37 cannot be related to one or other of these two fractionation schemes, and appear to be compositionally distinct. Two of these five samples have distinct modal mineralogy: 45-97/45-152 are the only samples with modal olivine, and

Table 4-27: Least squares approximation relating ferrodolerite I045-68 to plagioclase-pyroxene basalt 45-91/45-151/45-161.

Input data

	45-91/45-151/45-161	PLAG	CPX	I045-68
SiO_2	52.06	53.89	51.40	50.88
TiO_2	1.70	.08	1.30	3.65
Al_2O_3	15.18	29.09	2.02	12.58
FeO*	8.64	0.50	9.21	17.05
MnO	0.18	0.01	0.23	0.27
MgO	6.66	0.13	17.19	4.58
CaO	12.04	11.34	18.42	7.32
Na_2O	3.03	4.97	0.24	3.62
		An 55.77	Wo 37.20	
		Ab 44.23	En 48.28	
			Fs 14.52	

Least squares approximation

	45-91/45-151/45-161			MIX		
	OBS.	CALC.	DIFF.	COMP.	Wt.%	S.D.
SiO_2	52.06	51.99	-.07	I045-68	33.87	.60
TiO_2	1.70	1.66	-.04	PLAG	35.80	.37
Al_2O_3	15.18	15.28	.10	CPX	30.09	.42
FeO*	8.64	8.72	.08			
MnO	0.18	0.16	-.02	TOTAL	99.76	.82
MgO	6.66	6.77	.11			
CaO	12.04	12.08	.04			
Na_2O	3.03	3.08	.05			

Sum of squares of residuals = .040

Table 4-28: Least squares approximation relating 45-34/45-130D to 45-49/45-160.

Input data

	45-49/45-160	PLAG	CPX	Ti-Mgt	45-34/45-130D
SiO_2	50.80	50.80	51.38	0.20	50.63
TiO_2	1.58	0.05	0.80	24.62	1.82
Al_2O_3	15.34	31.27	3.17	1.35	15.17
FeO*	10.08	0.50	7.92	72.94	10.91
MnO	0.18	0.01	0.16	0.49	0.19
MgO	7.51	0.13	16.99	0.38	6.86
CaO	11.53	13.69	19.35	0.01	10.40
Na_2O	2.49	3.55	0.22	0.01	3.06
		An 68.06	Wo 39.36		
		Ab 31.94	En 48.07		
			Fs 12.57		

Least squares approximation

	45-49/45-160			MIX		
	OBS.	CALC.	DIFF.	COMP.	Wt.%	S.D.
SiO_2	50.80	50.80	.00	45-34/45-130D	81.24	3.04
TiO_2	1.58	1.67	.09	PLAG	8.26	1.59
Al_2O_3	15.34	15.25	-.09	CPX	10.65	1.52
FeO*	10.08	10.05	-.03	Ti-Mgt	.42	.38
MnO	0.18	0.17	-.01			
MgO	7.51	7.40	-.11	TOTAL	100.57	3.77
CaO	11.53	11.64	.11			
Na_2O	2.49	2.80	.31			

Sum of squares of residuals = 0.138

I047-72 is a pigeonite-bearing, plagioclase-rich rock. The former can however be related to ferrodolerite I045-68 with respect to both major and trace elements, but not to any of the other samples in the series. Plagioclase-pyroxene basalt I045-173, microporphyritic basalt I045-14 and plagioclase-pyroxene phyric basalt I045-130B are all compositionally unique in the sense that they cannot be related one to another or to any other samples by least squares modelling. Although these samples are apparently unrelated in terms of fractional crystallisation to the majority of Conrad F.Z. basalts, their very similar incompatible element ratios and in general their similar compositional variations suggest that they represent differentiation products of magma(s) derived from the same source region.

A least squares calculation relating the two proposed parental magmas 45-91/45-151/45-161 and 45-49/45-160 is given in Table 4-29. The inability of fractional crystallisation of the observed phenocryst phases to account for the compositional variation, specifically the trace elements, is clearly evident.

To test the consistency of the mixing calculations given in Table 4-25, the results have been used to calculate predicted trace element contents of the differentiated basalts. Owing to the already noted mobility of many of the analysed trace elements, only the relatively immobile elements, Zr, Nb, Y, Sc, Ga and P_2O_5 have been modelled. Though elements such as Cr, Ni, Co and V are also relatively immobile during ocean floor alteration (e.g. Humphris and Thompson, 1978b), they have extremely high and varied distribution coefficients for clinopyroxene (e.g. D^{Cr}_{cpx} = 0.8-87; Lindstrom, 1976; Table A2-5), and Fe-Ti oxides (e.g. D^{Ni}_{mt} = 5-77, D^{Cr}_{mt} = 20-620, D^{V}_{mt} = 4-190; see Table A2-9).

Table 4-29: Attempted least squares approximation and corresponding trace element model relating 'parental' magmas 45-91/45-151/45-161 and 45-49/45-160.

A. Least squares approximation.

	45-191/45-151/45-161			MIX		
	OBS.	CALC.	DIFF.	COMP.	Wt.%	S.D.
SiO_2	52.06	51.95	-.11	45-49/45-160	45.67	12.39
TiO_2	1.70	1.75	.05	PLAG (An_{36})	29.52	6.38
Al_2O_3	15.18	15.35	.17	Cpx (Fs_{13})	22.39	5.18
FeO*	8.64	8.62	-.02	Ti-MGT (Mt_{30})	2.86	1.12
MnO	0.18	0.14	-.04			
MgO	6.66	7.04	.38	TOTAL	100.43	14.91
CaO	12.04	12.00	-.04			
Na_2O	3.03	3.36	.33			

Sum of squares of residuals = 0.30

B. Trace element check.

	45-91/45-151/45-161	45-49/45-160	
	OBS.	CALC.	OBS.
Zr	115	231	98
Nb	5.6	11	4.2
Y	37	64	31
Sc	43	42	40
Ga	17	20	17
P_2O_5	.18%	.39%	.17%

Calculations involving these elements are therefore totally unconstrained by the major element models and have consequently been omitted.

Predicted and observed trace element contents for the two proposed fractionation series are given in Tables 4-30A and B. Values were calculated assuming Rayleigh fractionation (Equation 1, Chapter II) and using distribution coefficients given in Table 4-31. It was found that it was necessary to select two values for D^{Zr}_{cpx} (0.22 and 0.35) to satisfy the Zr variations, with the lower value being used when Fe-Ti oxide fractionation was involved. The lower value is similar to that determined for clinopyroxene from a mineral separate from Gough Island (Chapter II) and the higher value is intermediate between this value and the values reported for Hf (D^{Hf}_{cpx} = 0.20-0.55; Schock, 1978), which has a very similar geochemical behaviour (e g. Erlank et al., 1978a,b). It was also necessary to select three very slightly different values for D^{Sc}_{cpx} (2.0, 2.1 and 2.2) to account for all the variations, but again these values are well within the known uncertainty (e.g. Table A2-5). Data for D^{Ga}_{plag} is relatively sparse (Goodman, 1972; Willis, 1979) and the two slightly different values are probably well within the likely range. Inspection of Table 4-30 shows that in nearly all cases the agreement between observed and predicted values is excellent with only P_2O_5 having a tendency to be somewhat high in the predicted values. Qualitative scans with the electron microprobe across the matrix of I045-68 have indicated the presence of minor apatite. The small P_2O_5 discrepancies in this and other samples can likely be accounted for by minor apatite fractionation (<0.1%). The trace element calculations therefore confirm the consistency of the major element mixing calculations.

On the basis of the major and trace element modelling, it is

A. PARENT = 45-91/45-151/45-161

	PARENT	(4) I047-62		(3) I047-12		(2) I045-68		(1) I047-101	
	OBS.	OBS.	CALC.	OBS.	CALC.	OBS.	CALC.	OBS.	CALC.
Zr	115	208	217	246	248	278	284	374	378
Nb	5.6	11	12	13	13	15	16	21	20
Y	37	55	62	64	66	72	77	96	98
Sc	43	40	41	36	38	44	45	24	23
Ga	17	19	20	20	21	22	23	40	40
P_2O_5	.18%	.33%	.39%	.36%	.43%	.44%	.52%	.77%	.75%

B. PARENT = 45-49/45-160

	PARENT	(7)I045-34/I045-130D		(6)I047-64/I045-148		(5) I047-28	
	OBS.	OBS.	CALC.	OBS.	CALC.	OBS.	CALC.
Zr	98	122	117	147	146	176	171
Nb	4.2	5	5	7	6	9	7
Y	31	34	35	43	42	50	47
Sc	40	40	38	40	39	40	38
Ga	17	18	18	19	19	19	20
P_2O_5	.17%	.20%	.21%	.23%	.27%	.29%	.32%

Table 4-30: Predicted and observed trace element contents of differentiated Conrad F.Z. basalts.

Table 4-31: Distribution coefficients used in the trace element calculations presented in Table 4-30. The values have been selected from Tables A2-2, A2-5 and A2-9. See text for further discussion.

	Plagioclase	clinopyroxene	Ti-magnetite
Zr	.01	.35, .22'	.24
Nb	.01	.05	2.16
Y	.18	.50	.17
Sc	.01	2.0, 2.1^2, 2.2^3	4.0
Ga	1.0, 1.1^4	.4	2.0
P_2O_5	.01	.01	.01

Superscripts: 1 = value used in models 3, 7, 6, 5
2 = " " " " 2
3 = " " " " 4, 3
4 = " " " " 4

suggested that most of the compositional variation observed in the Conrad F.Z. basalts can be attributed to varying degrees of low pressure fractional crystallisation of two distinct 'parental' magmas. These 'parental' magmas do not have primary compositions and must themselves be derivatives of more primitive magmas not yet sampled. The calculations indicate that the fractionation involved dominantly plagioclase and clinopyroxene which were removed in approximately equal proportions throughout the differentiation series, together with minor (<3%) titanomagnetite. The extensive fractionation (the calculations indicate that the most evolved ferrobasalts represent as little as 24 to 34% residual magma) suggests that the magmas must have resided in shallow chambers for a considerable length of time.

It is intersting to compare the results of this study to those of Clague and Bunch (1976) who did similar geochemical modelling of ferrobasalt petrogenesis from the East Pacific mid-ocean spreading centers. These authors found that, in contrast to previously inferred olivine-plagioclase fractionation, clinopyroxene played a dominant role in the generation of the highly fractionated ocean floor basalts from these areas. In the postulated models for the generation of the East Pacific ferrobasalts, plagioclase and clinopyrxene contributed approximately equally towards the fractionate and comprised over 90% of the total, a feature in common with that found for the Conrad F.Z. Clague and Bunch (1976) found, however, that the best least squares solutions were obtained by postulating the fractionation of a "..... pyroxene composition more iron-rich than can be reasonably expected". This pyroxene composition ($Wo_{35}En_{43}Fs_{21}$) is significantly more iron-rich than that used in the Conrad F.Z. calculations ($Wo_{41}En_{45}Fs_{13}$ - $Wo_{37}En_{48}Fs_{15}$). The

compositions used in this study are within the compositional range observed in the actual samples.

Strongly fractionated ocean floor basalts are generally regarded as being associated with fast spreading ridges (e.g. East Pacific Rise, Juan de Fuca Ridge), while slow spreading ridges (e.g. Mid-Atlantic Ridge) generally lack extensively fractionated basalts (Bass, 1971; Scheidegger, 1973; Clague and Bunch, 1976). This has been attributed to the fact that thermal models for the formation of oceanic crust (Sleep, 1975; Kusznir and Bott, 1976) suggests that the latent heat of basalt in the top 5 km of the oceanic crust at slow spreading ridges is insufficient to maintain a large steady-state magma chamber (Nisbet and Fowler, 1978). The thermal regime at fast spreading ridges is however more favourable for the maintenance of a large magma chamber, thus allowing more extensive fractionation. Fracture zones, however, appear to be an exception, even if cutting slow spreading ridges. For example, Bonatti et al. (1971), Melson and Thompson (1971), Thompson and Melson (1972), Shibata and Fox (1975), Hekinian and Thompson (1976) and Shibata et al. (1979a) have all reported extensively fractionated basalts from fracture zones cutting the slow spreading Mid-Atlantic Ridge. The results of this study provide further documentation of highly fractionated basalts occurring in a fracture zone which cuts a slow spreading ridge. Quantitative modelling of the compositional variations observed in the present study indicates that extensive fractional crystallisation has resulted in the development of evolved basalt compositions, implying the existence of a large magma chamber.

(ii) Ferrodiorite

Hart (1971) has demonstrated that oceanic andesite dredged from

Table 4-32: Least squares approximation relating ferrodiorite I045-51 to olivine-plagioclase-pyroxene basalt 45-152/45-97.

Input data

	45-152/45-97	PLAG	OLIV	CPX	IL	I045-51
SiO_2	51.12	53.89	35.26	49.61	.15	59.97
TiO_2	1.51	0.08	.03	1.48	47.85	1.97
Al_2O_3	16.23	29.09	.06	2.96	.17	12.31
FeO*	9.48	.50	38.21	12.75	50.65	14.25
MnO	0.17	.01	.22	.45	1.04	.20
MgO	6.49	.13	25.86	14.13	.10	1.91
CaO	12.17	11.34	.33	18.20	.01	6.54
Na_2O	2.71	4.97	.01	.37	.01	2.83
		An 55.77	Fo 54.67	Wo 38.07		
		Ab 44.23	Fa 45.33	En 41.11		
				Fs 20.82		

Least squares approximation

	45-152/45-97			MIX		
	OBS.	CALC.	DIFF.	COMP.	Wt.%	S.D.
SiO_2	51.12	51.14	.02	I045-51	11.99	.79
TiO_2	1.51	1.58	.07	PLAG	47.29	.58
Al_2O_3	16.23	16.20	-.03	OL	6.40	.39
FeO*	9.48	9.42	-.06	CPX	32.64	.60
MnO	0.17	0.21	.04	IL	1.71	.18
MgO	6.49	6.56	.07			
CaO	12.17	12.11	-.06	TOTAL	100.02	1.22
Na_2O	2.71	2.81	.10			

Sum of squares of residuals = .030

the East Pacific Rise can be derived from average oceanic tholeiite by approximately 60% crystallisation of plagioclase, olivine, clinopyroxene and minor titanomagnetite. Attempts at relating ferrodiorite I045-51 to any of the basaltic rocks recovered from the Conrad F.Z. have however only proved partially successful. A least squares approximation relating ferrodiorite I045-51 to olivine-plagioclase-pyroxene basalt 45-152/45-97 is shown in Table 4-32. The results indicate that it is quite feasible to derive a magma of composition similar to that of the ferrodiorite by the fractionation of 47.3% plagioclase (An_{56}), 32.6% clinopyroxene ($Wo_{38}En_{41}Fs_{21}$), 6.4% olivine (Fo_{54}) and 1.7% ilmenite (Il_{90}). The exceptionally large degree of crystallisation required to satisfy the major elements (88%) is however in conflict with the observed enrichment in incompatible trace elements. Using the distribution coefficient data from Tables A2-1, A2-2, A2-5 and A2-8, some selected trace element predictions for I045-51 using this model are as follows:

	Observed	Calculated
Zr	255	700
Nb	12	38
Y	57	127
Sc	33	32
Ga	20	33

The excessive amount of crystallisation is clearly illustrated. The choice of alternate parents can equally satisfy the major element variations, but likewise fails to account for the observed enrichment in incompatible trace elements.

The relationship of the ferrodiorite to the Conrad F.Z. basalts remains therefore unresolved. The unusual mineral chemistry of this

sample (Section 4.1.2) may however indicate unusual conditions of crystallisation, a factor which may have resulted in the apparent decoupling of the major and trace elements. Alternatively, the sample may be a glacial erratic, unrelated to the other fracture zone samples.

5. DISCUSSION

5.1 Islas Orcadas and Conrad Fracture Zones

Comparison of the general characteristics of the two suites of fracture zone samples reveals a number of similarities. Basaltic rocks from both fracture zones are petrographically similar in that the dominant mineral assemblage comprises plagioclase and clinopyroxene with or without minor Fe-Ti oxides. Subordinate triply saturated olivine-plagioclase-pyroxene basalts do occur. This contrasts with the characteristic olivine-plagioclase assemblage in typical MORB (e.g. Bryan et al., 1976). Also, in contrast to typical MORB, the majority of the fracture zone basalts are holocrystalline with quench glass being relatively scarce. In addition, a high proportion of intrusive mafic rocks were recovered from the Conrad F.Z., though none were dredged from the IOFZ. The samples from both fracture zones show a high degree of alteration, especially the intrusive varieties from the Conrad F.Z. The alteration process involved the formation of hydrous secondary minerals and in many cases the replacement of phenocryst and groundmass plagioclase by K-feldspar, Na-feldspar or analcite. Comparison of the mineral compositions of the extrusive rocks indicates a similar range in plagioclase phenocryst compositions (An_{90}-An_{50}) and clinopyroxene compositions ($Wo_{44}En_{49}Fs_{7}$ - $Wo_{42}En_{37}Fs_{21}$). Plagioclase from the Conrad F.Z. intrusive rocks, however, extends to more sodic compositions (An_{30}). Higher concentrations of minor elements (Ti, Al, Na) in the IOFZ

pyroxenes distinguishes these from the Conrad F.Z. pyroxenes and emphasises their more alkaline affinity. The petrographic features of the Conrad F.Z. basalts indicate a similarity to fractionated Group I ocean floor basalts as defined by Bryan et al. (1976), while the IOFZ basalts show a closer similarity to Group II basalts.

Basaltic rocks from both fracture zones are characterised by their evolved compositions and extreme compositional variation. This factor has previously been proposed as a characteristic feature of fracture zone basalts, in contrast to the less evolved compositions and minor range of differentiation of typical MORB (e.g. Hekinian and Thompson, 1976; Shibata et al., 1979b). The evolved nature of the Conrad F.Z. and IOFZ basalts is illustrated by the absence of any potential primary magmas (i.e. magmas with Mg-number >0.67) and by their high FeO*/MgO ratios (1.1-3.7) relative to unfractionated Mid-Atlantic Ridge basalt (FeO*/MgO = 0.8-1.8; Bryan et al., 1976). This evolved nature is further illustrated by the high concentrations of immobile incompatible elements (e.g. Ti, Zr, Nb, Y, P) and low concentrations of the ferromagnesian trace elements (Cr, Ni). Most of the observed compositional variation in both fracture zones can be attributed to the fractional crystallisation of plagioclase and clinopyroxene in approximately equal proportions, with or without minor Fe-Ti oxides. The degree of crystallisation required to account for the compositional spread in the individual fracture zones does however differ, with the Conrad F.Z. basalts reflecting far greater differentiation. Least squares calculations indicate that the most evolved Conrad F.Z. basalts can be accounted for by up to 76% fractional crystallisation of a postulated parental magma, while the most evolved IOFZ basalts represent the pro-

ducts of at least 40% fractional crystallisation of a parental magma. Similar large degrees of fractionation have been proposed by Shibata and Fox (1975) and Shibata et al. (1979a) to account for the observed compositional variation in basalts from the Oceanographer fracture zone (MAR, 35°N). The fractionating phases, and relative proportions, involved in the evolution of the Conrad and IOFZ basalts are very similar to those required to account for the production of ferrobasalt at some East Pacific spreading centers (Clague and Bunch, 1976). As noted by these authors, fractionation of plagioclase and clinopyroxene appears to be an important mechanism for the generation of highly evolved ocean floor ferrobasalts. The extensive fractionation observed in the fracture zone basalts implies the presence of large magma chambers, which are not normally regarded as being stable under the thermal regime of slow spreading ridges (e.g. Nisbet and Fowler, 1978).

The above-mentioned similarities in petrography, bulk major element composition and differentiation products are all related to high level processes such as mode of emplacement and fractional crystallisation. Comparison of selected incompatible element ratios (e.g. Zr/Nb, Y/Nb, Zr/Y, La/Yb) however reveals some important differences between the two fracture zones. Such ratios have been shown to be diagnostic of source region characteristics, and in particular may serve as a measure of depletion of the source region (e.g. Gast, 1968; Hart, 1971; Pearce and Cann, 1973; Erlank and Kable, 1976; Bougault et al., 1979; Pearce and Norry, 1979). The Conrad F.Z. basalts and dolerites have an average Zr/Nb ratio of 21 $\pm$ 3 which, though somewhat lower than MORB (ave. Zr/Nb = 37; Erlank and Kable, 1976), contrasts with the low Zr/Nb ratio (8.4 $\pm$ 0.6) of the IOFZ basalts (Fig. 4-38). The Zr/Nb ratio of the

Conrad F.Z. is similar to that of the Juan de Fuca Ridge basalts (ave. Zr/Nb = 23; Kable, 1972) and the basalts from the Blanco fracture zone (ave. Zr/Nb = 17; Kable, 1972). The low Zr/Nb ratio of the IOFZ is similar to that characteristic of oceanic island tholeiites (Zr/Nb = 6.6; Erlank and Kable, 1976) and to ocean floor basalts from the vicinity of postulated mantle plumes (e.g. 45°N (MAR) Zr/Nb = 6.6; Erlank and Kable, 1976; FAMOUS (MAR) Zr/Nb = 8.4, Chapter III). The higher Y/Nb (6.1 $\pm$ 1.0) and lower Zr/Y (3.4 $\pm$ 0.47) ratios of the Conrad F.Z. basalts (Fig. 4-38) also serves to distinguish them from the IOFZ basalts (Y/Nb = 1.98 $\pm$ 0.2, Zr/Y = 4.36 $\pm$ 0.4). The low Y/Nb ratio of the IOFZ basalts is a reflection of their more alkaline chemistry (Pearce and Cann, 1973), a feature commonly associated with fracture zone basalts (e.g. Bonatti et al., 1971; Hekinian and Thompson, 1976; Shibata et al., 1979b).

Although REE data are available for only three of these basalts, the Conrad F.Z. basalts can be readily distinguished from the IOFZ basalts by their flat to slightly enriched LREE patterns (La/Yb = 1.1-1.4) relative to the strongly LREE-enriched pattern of the IOFZ basalt (La/Yb = 3.4). Both patterns are distinguishable from the LREE-depleted patterns characteristic of MORB. The REE variations are in accord with the previously discussed incompatible element ratios and further illustrate that the Conrad F.Z. basalts are transitional between Group I (La/Yb = 0.4-1.0) and Group II (La/Yb = 1.4-13.6) oceanic basalts (Bryan et al., 1976), while the IOFZ basalts are more similar to the variable Group II basalts. Although complex partial melting processes such as dynamic melting (e.g. Langmuir et al., 1977; Wood, 1979) can give rise to small variations in the incompatible element ratios, the large

differences observed between ratios, such as Zr/Nb, Y/Nb and La/Yb, imply derivation of the IOFZ and Conrad F.Z. basalts from two very distinct source regions. The source region of the Conrad F.Z. is characterised by ratios similar to those in chondrites (cf. chondritic Zr/Nb = 16, Graham and Mason, 1972; flat REE patterns), while those from the IOFZ are more similar to the LIL element-enriched source regions associated with oceanic islands and mantle plumes (e.g. Schilling, 1973, 1975a). The two IOFZ Dredge 11 basalts with low Zr/Nb ratios have virtually identical Zr/Nb, Y/Nb and Zr/Y ratios to those of Bouvet Island hawaiites (Fig. 4-38), illustrating their close similarity to these nearby island basalts and suggesting derivation from similar source regions.

5.2 Bouvet Triple Junction Basalts

The data from the detailed study of the two fracture zones, the sample from the ridge crest at 11°E and the samples described by Dickey et al. (1977) from the vicinity of the Bouvet triple junction allow a wider study of the geochemistry of this South Atlantic ridge system. To avoid laboratory bias and to facilitate a more direct comparison of the data, the samples described by Dickey et al. (1977) (kindly provided by Dr. J.S. Dickey) have been re-analysed for 13 trace elements by XRF. These new data, together with the whole rock major element analyses (from Dickey et al., 1977) are presented in Table 4-33. Sample numbers e.g. 37/1D-1) reflect the station number and dredge number and correspond to those given in Dickey et al. (1977). Also given in Table 4-33 is a whole rock and glass analysis (by electron microprobe) of an additional sample (50/35D) from Station 50, Dredge 35D also provided by Dr. J.S. Dickey. The dredge locations of the various samples which will be dis-

TABLE 4-33

WHOLE ROCK ANALYSES OF BOUVET TRIPLE JUNCTION SAMPLES PROVIDED BY J.S.DICKEY

	50/35D	50/35D-G	50/8D-1	37/1D-1	37/1D-2	37/1D-3	38/3D-1	38/3D-2	44/5D-1	44/5D-2
SIO2	49.91	50.73	51.97	50.95	51.21	50.05	60.40	49.83	52.51	51.27
TIO2	1.22	1.69	1.71	2.06	2.09	2.12	.65	.91	2.54	2.50
AL203	20.33	15.22	15.66	15.11	15.01	14.46	14.80	19.13	14.67	14.64
FE203	.87	1.50	-	1.30	1.43	-	1.60	.66	1.41	2.05
FEO	5.78	7.50	8.52	8.93	8.60	11.18	5.30	6.05	9.55	8.49
MNO	.12	.15	.19	.15	.19	.14	.10	.13	.15	.20
MGO	5.83	7.23	7.29	7.27	7.49	7.25	5.24	7.22	5.60	5.32
CAO	13.54	11.96	11.52	10.45	10.41	10.64	7.79	12.88	9.54	10.08
NA20	2.04	2.75	2.59	2.61	2.69	3.04	2.67	2.28	2.61	3.63
K20	.37	.58	.45	.56	.45	.66	1.59	.07	.77	.83
P205	.15	-	-	-	-	-	-	-	-	-
H20+	.60	-	-	-	-	-	-	-	-	-
H20-	.03	-	-	-	-	-	-	-	-	-
CO2	-	-	-	-	-	-	-	-	-	-
TOTAL	100.79	99.31	99.90	99.39	99.57	99.54	100.14	99.16	99.35	99.01
				* * * C.I.P.W. NORMS * * *						
Q	.17		.93	.03	.35	.00	14.08	.00	4.56	.00
CO	.00		.00	.00	.00	.00	.00	.00	.00	.00
OR	2.19		2.66	.33	2.67	3.91	9.38	.42	4.58	4.95
PL	62.40		51.66	50.23	50.51	49.71	46.21	51.54	48.42	52.42
DI	17.02		22.22	19.70	19.70	23.75	12.12	18.08	17.66	23.85
HY	14.31		17.48	20.83	20.64	6.46	14.60	13.21	17.83	8.37
OL	.00		.00	.00	.00	9.75	.00	3.98	.00	2.57
MT	1.26		1.75	1.90	2.08	2.31	2.31	.96	2.06	3.00
IL	2.32		3.25	3.94	3.99	4.04	1.23	1.74	4.85	4.79
AP	.36		.00	.00	.00	.00	.00	.00	.00	.00
				* * * TRACE ELEMENTS * * *						
ZR	96.2		92.4	154.	154.	157.	114.	60.4	236.	207.
NB	9.9		9.6	13.3	13.5	14.2	3.6	ND	25.6	21.5
Y	19.7		18.0	32.6	32.7	32.5	25.1	24.9	38.6	35.0
RB	6.3		5.0	6.6	6.8	9.0	52.8	1.9	15.1	11.8
BA	64.9		65.9	85.9	86.7	86.5	275.	11.6	164.	160.
SR	272.		275.	193.	194.	201.	154.	119.	291.	289.
CO	34.8		34.3	50.6	50.8	52.3	27.2	41.3	44.8	45.3
CR	97.0		134.	252.	252.	239.	157.	333.	63.0	76.6
NI	42.1		38.8	105.	113.	118.	49.5	124.	43.7	36.4
V	183.		181.	278.	280.	266.	151.	192.	238.	263.
ZN	52.1		73.6	122.	132.	118.	91.5	81.6	144.	138.
CU	30.7		35.4	58.7	58.6	57.5	34.6	65.1	63.9	56.0
SC	32.2		31.2	38.3	38.4	33.7	29.2	32.1	34.8	35.2
TH	-		-	-	-	-	-	-	-	-
PB	-		-	-	-	-	-	-	-	-
GA	14.9		-	-	-	-	-	-	-	-

** ND = NOT DETECTED **

T A B L E 4-33 (CONTINUED)

WHOLE ROCK ANALYSES OF BOUVET TRIPLE JUNCTION SAMPLES PROVIDED BY J.S.DICKEY

	50/35D	50/35D-G	50/8D-1	37/1D-1	37/1D-2	37/1D-3	38/3D-1	38/3D-2	44/5D-1	44/5D-2
				* * * ELEMENT RATIOS * * *						
ZR/NB	9.73	-	9.62	11.6	11.4	11.1	31.7	-	9.22	9.63
ZR/BA	1.48	-	1.40	1.79	1.78	1.81	.414	5.20	1.44	1.29
ZR/Y	4.89	-	5.12	4.72	4.71	4.83	4.54	2.43	6.12	5.92
K/RB	487.	-	741.	700.	553.	608.	250.	309.	422.	586.
K/BA	47.3	-	56.7	54.1	43.1	63.3	47.9	50.1	38.9	43.0
K/ZR	31.9	-	40.4	30.2	24.3	34.9	116.	9.62	27.1	33.3
Y/NB	1.99	-	1.88	2.45	2.42	2.29	6.98	-	1.51	1.63
CA/Y	4.915+003	-	4.566+003	2.290+003	2.275+003	2.339+003	2.215+003	3.697+003	1.769+003	2.059+003
TI/ZR	76.0	-	111.	80.2	81.4	81.0	34.2	90.3	64.5	72.4
TI/NB	740.	-	1.068+003	928.	928.	895.	1.082+003	-	595.	697.
TI/Y	371.	-	569.	379.	383.	391.	155.	219.	395.	428.
TI/P	11.2	-	-	-	-	-	-	-	-	-
CR/V	.532	-	.742	.907	.900	.897	1.04	1.73	.264	.292
NI/CO	1.21	-	1.13	2.07	2.22	2.26	1.82	3.00	.974	.805
M.I.	53.3	55.5	53.9	58.5	57.2	60.7	56.8	48.2	66.2	66.5
MG#	.643	.632	.604	.592	.608	.536	.638	.680	.511	.528
D.I.	19.6	-	-	-	-	-	-	-	-	-

cussed are shown in Fig. 4-2.

The overall chemical and petrographic features of the basalts dredged from the Bouvet triple junction have been described by Dickey et al. (1977), and these authors have noted that the basalts dredged from Station 50 (east of Bouvet Island), Station 44 (Spiess Ridge) and Station 37 (MAR) differ from normal MORB. These basalts are LIL element-enriched, have high $^{87}Sr/^{86}Sr$ ratios, and clinopyroxene is a common phenocryst mineral. In contrast, the basalts dredged from Station 38 (Scotia Ridge) to the west of the Conrad F.Z. resemble typical MORB. The trace element analyses from this study support these conclusions. The variation of selected trace elements (Zr, Nb, Y) from all basalts dredged from this South Atlantic ridge system is illustrated in Fig. 4-38 and is compared with the range of Bouvet Island hawaiites and FAMOUS basalts in some instances.

All basaltic rocks (both ridge and fracture zone basalts) that have been dredged from the Southwest Indian Ocean Ridge in the vicinity of Bouvet Island, i.e. from the triple junction area to 11°E (Fig. 4-2), are characterised by having low Zr/Nb, low Y/Nb and high Zr/Y ratios (Fig. 4-38). The available REE data (Fig. 4-39) and the negative correlation between Zr/Nb and La/Sm ratios (Sun et al., 1979) suggests that this portion of the ridge is also characterised by being LREE-enriched, in contrast to the LREE depletion commonly associated with ocean ridge basalts. Although many of the samples are highly altered, the positive correlation between Zr/Nb and K/Ba in ocean ridge basalts (Erlank and Kable, 1976) would suggest that the basalts to the east of the triple junction would also have low K/Ba ratios. Basalts dredged from the Conrad F.Z. and from Station 38 (Fig. 4-2) to the west of the triple

junction, on the American-Antarctic Ridge, are characterised by having interelement ratios more like normal mid-ocean ridge basalts, i.e. high Zr/Nb, Y/Nb, low Zr/Y and flat to LREE-depleted REE patterns (Figs. 4-38, 4-39).

Dickey et al. (1977) noted the apparent LIL enrichment in the basalts dredged from the immediate vicinity of the Bouvet triple junction and they attributed the composition of the lavas to the influence of a mantle plume situated beneath Bouvet Island (Morgan, 1971, 1972, 1973). The results of this study confirm this conclusion and indicate that not only do basalts in the immediate vicinity of Bouvet Island carry a 'plume-enriched' chemical imprint, but basalts dredged from as far east as 11°E have a LIL element-enriched chemistry. This suggests that the chemistry of the Southwest Indian Ocean ridge from the triple junction to at least 11°E can be likenened to the well known LIL element-enrichment along the MAR in the vicinity of the postulated Azores plume (e.g. Schilling, 1975; White et al., 1976; White and Bryan, 1977; White and Schilling, 1978) and to the Reykjanes Ridge in the vicinity of the postulated Iceland plume (e.g. Schilling, 1973). Mantle plumes have been envisaged as representing the manifestation of convection in the lower mantle, which brings up heat and primordial material to the asthenosphere and provides the driving force for the separation of the lithospheric plates during continental drift (Morgan, 1971, 1972, 1973). Anderson (1975) suggests that plumes represent sites of anomalously deep melting, induced possibly by high concentrations of radioactive elements. Either model offers an explanation for the more 'pristine' or enriched LIL element compositions of the lavas generated by this mechanism. If Bouvet Island is indeed the site of a mantle plume, originally giving rise to the

Fig. 4-38: Variation of Nb, Y and Y/Nb ratio with respect to Zr in basalts from the vicinity of the Bouvet triple junction. The field of FAMOUS basalts is taken from this study and the Nb-Zr variation in MAR basalts from Kable (1972). Symbols are as follows;

- ✚ Bouvet Island hawaiites
- ● Islas Orcadas fracture zone basalt
- O Conrad fracture zone basalt
- △ Spiess Ridge - Station 44
- ▲ Ridge axis east of Bouvet Island - Station 50
- □ MAR in vicinity of the Bouvet triple junction - Station 37
- ▽ Scotia Ridge - Station 38
- ⊗ Southwest Indian Ocean Ridge - at 11°E.

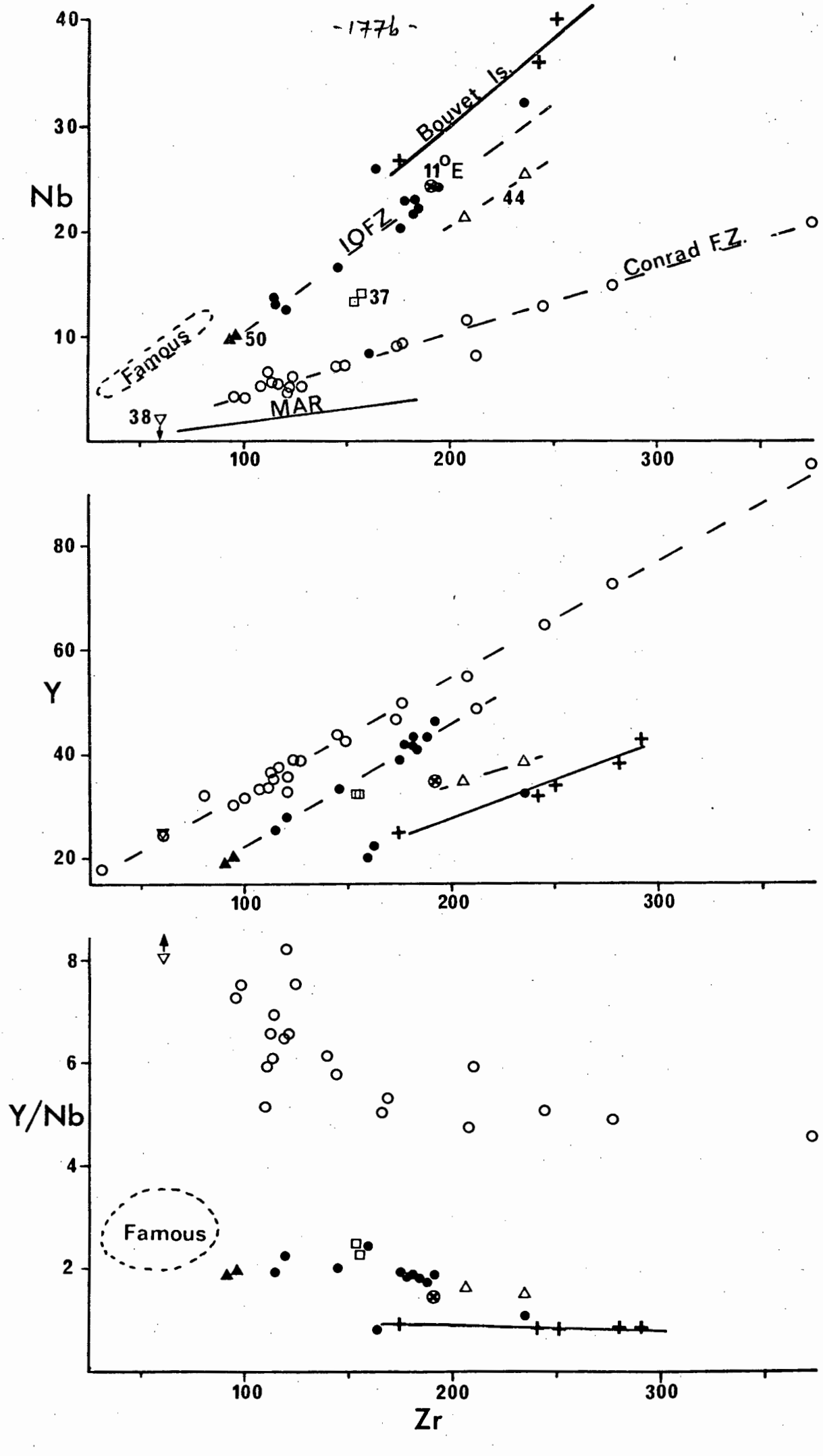
Nb
Y
Y/Nb
Zr
Bouvet Is.
11°E
44
IOFZ
37
Conrad F.Z.
Famous
50
MAR
38
Famous
100
200
300
10
20
30
40
60
80
2
4
6
8

break-up of Gondwanaland (Morgan, 1971, 1972, 1973), then the similarity in compositions (e.g. LREE, Zr/Nb, Y/Nb ratios) of the Southwest Indian Ocean Ridge basalts and the Bouvet Island hawaiites (Figs. 4-38, 4-39) suggests that the ocean floor basalts and the island basalts have been derived from a very similar source region. This is supported by the similar $^{87}Sr/^{86}Sr$ isotope ratios of the Stations 44 and 50 basalts (0.70325 to 0.70372; Dickey et al., 1977), and those from Bouvet Island (0.70368±3; O'Nions and Pankhurst, 1974). The low $^{87}Sr/^{86}Sr$ ratios, LREE depletion and low LIL element concentrations in basalts from the American-Antarctic Ridge indicates that the effect of the 'Bouvet plume' does not extend to the west of the triple junction.

CHAPTER V

BOUVET ISLAND

1. INTRODUCTION

Bouvet Island (lat. 54°26'S, long. 3°25'E) is situated at the southern end of the Mid-Atlantic Ridge (MAR) immediately to the west of the triple junction of the African, Anarctic and South American plates (Fig. 5-1).

This southernmost island on the MAR has been suggested by Johnson et al. (1973) to be an especially high peak in the western rift mountains. Bouvet is a stratovolcano covering an area of 51 km^2 and rising to a height of 780 m above sea level, with a centrally situated caldera (Verwoerd et al., 1974). Gradual slopes characterise the leeward southern and eastern sides, while precipitous sea cliffs typify the western and southern margins. Verwoerd et al. (1974) have shown that the island is built up of volcanic rocks of the series hawaiite, mugearite and benmoreite with minor rhyolite. Hawaiite is the predominant rock type, though exposure is poor with over 95% of the island being covered by ice.

Bouvet is a young oceanic island, with published maximum ages ranging from 1 m.y. to 6 m.y. Verwoerd et al. (1974) suggest a maximum age of 1 m.y. on the basis of the normal magnetisation of orientated specimens (Snape, 1971), whilst Imsland et al. (1977) argue that a maximum age of 6 m.y. is indicated on the basis of a half-spreading rate of 0.83 cm/yr (Sclater et al., 1976) and a distance of 50 km from the ridge crest. The volcanism giving rise to Bouvet Island has been

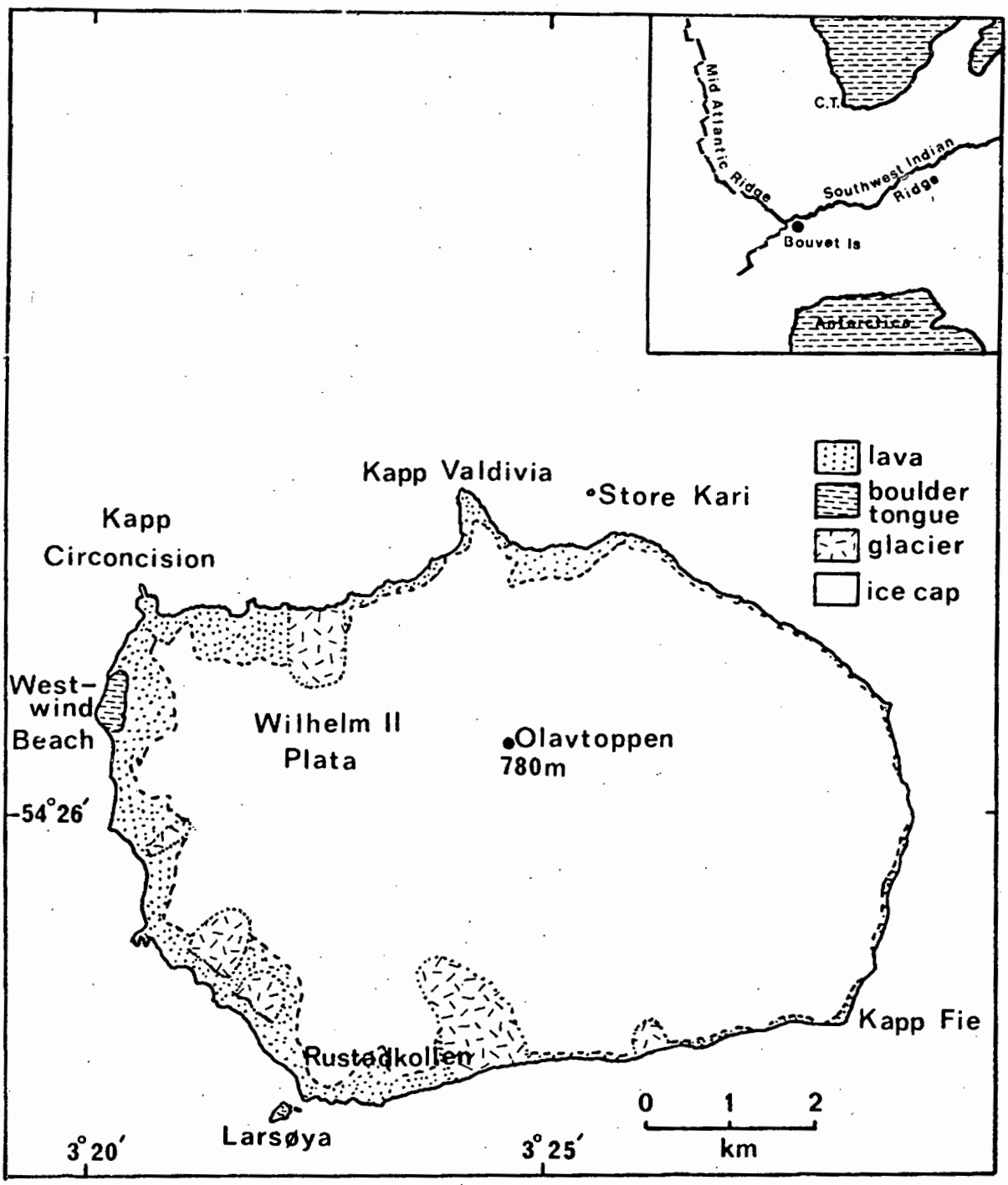

Fig. 5-1: Sketch map of Bouvet Island, simplified from Verwoerd et al. (1974). Norwegian names in the form approved by the Antarctic Place-names Committee.

PLATE 5-1

A: Photomicrograph of plagioclase phyric hawaiite WJ8B. Phenocrysts in field of view include plagioclase and clinopyroxene. Crossed polars.

B: Plagioclase phenocryst in WJ8B showing resorption features and a subhedral clinopyroxene phenocryst poikilitically enclosing plagioclase laths. Crossed polars.

C: Photomicrograph of sparsely phyric hawaiite WJ2B showing large plagioclase glomerocryst and subhedral olivine phenocrysts, in a fine grained matrix of orientated plagioclase laths. Partially crossed polars.

D: Photomicrograph of aphyric mugearite WJ1B showing intergranular texture of plagioclase and clinopyroxene.

E: Porphyritic texture of benmoreite WJ10B. Phenocrysts comprise plagioclase, clinopyroxene, olivine and titanomagnetite set in a dense hyalocrystalline matrix. Crossed polars.

F: Photomicrograph showing the poikilitic relationship between plagioclase and clinopyroxene in benmoreite WJ10B.

G: 'Atoll' type and subhedral to euhedral growth forms in plagioclase phenocrysts in benmoreite WJ10B. A clinopyroxene phenocryst containing poikilitically enclosed titanomagnetite is shown in the lower left hand corner. Partially crossed polars.

H: Photomicrograph of rhyolite WJ18B showing subhedral anorthoclase phenocrysts enclosed in a glassy groundmass of microlites with a well developed flow structure. Crossed polars.

PLATE 5-1

A

4 mm

B

2·2 mm

C

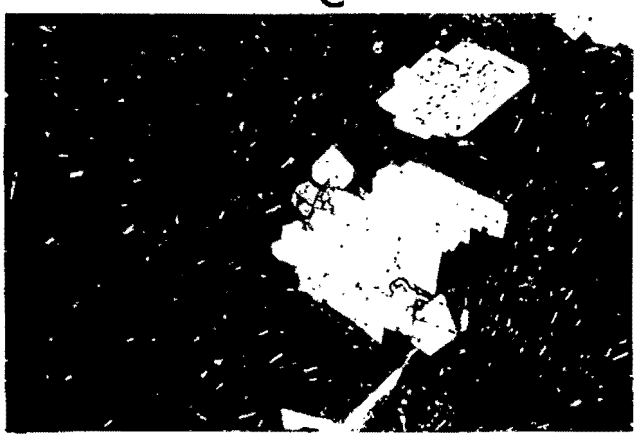

4 mm

D

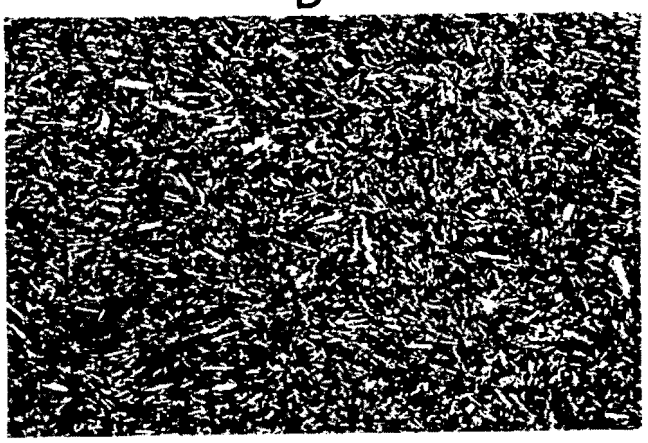

5 mm

E

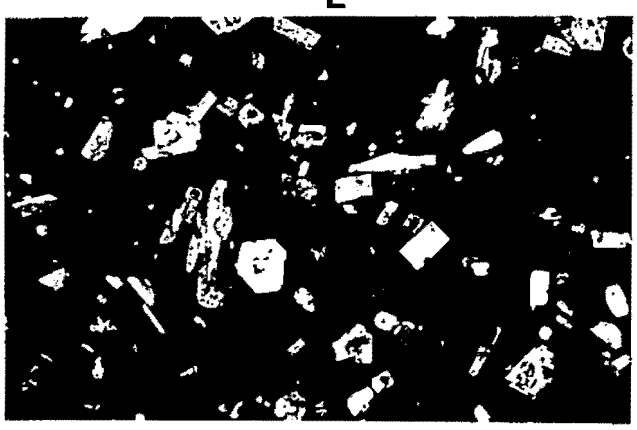

6 mm

F

2 mm

G

2·3 mm

H

5·5 mm

altered subhedral phenocrysts. Minor olivine occurs as inclusions in, or attached to, plagioclase phenocrysts. Titanomagnetite occurs as discrete euhedral to subhedral phenocrysts (up to 0.5 mm in size) and also commonly as inclusions in clinopyroxene (Plate 5-1G) and plagioclase. Apatite (CaO 56.16%, P_2O_5 42.48%) forms acicular needles in the matrix or occurs as inclusions in clinopyroxene, opaque oxides and plagioclase. The mutual poikilitic relationships between the various phenocryst phases is taken as evidence of co-precipitation of these phases. Modal proportions (determined by point counting) of the phenocryst phases are as follows: (vol.%) plagioclase 18.0; clinopyroxene 3.0; titanomagnetite 2.0; olivine 1.0.

3.4 Rhyolite

The single sample of rhyolite (WJ18B) is a fine-grained, sparsely porphyritic lava, with anorthoclase phenocrysts set in very fine-grained matrix of alkali-feldspar microlites which exhibit well developed flow structures (Plate 5-1H). Verwoerd et al. (1974) report the presence of aegerine and soda hornblende crystallites. The sample of obsidian is a black quench glass and lacks any detectable crystallites.

4. CHEMISTRY

4.1 General Statement

With the exception of the sample of obsidian analysed by the writer, all major element data were taken from Verwoerd et al. (1974). Certain trace elements (Zr, Nb, Y, Rb, Ba and Sr) were redetermined on the original briquettes together with Sc. The remaining trace element data were taken from Verwoerd et al. (op. cit.).

Major and trace elements, CIPW norms and selected element ratios are presented in Table 5-2. The CIPW norms were calculated volatile-

T A B L E 5-2

BOUVET ISLAND: WHOLE ROCK ANALYSES, CIPW NORMS & SELECTED RATIOS

	WJ 8B	WJ 17B	WJ 2B	WJ 7B	WJ 14B	WJ 16B	WJ 1B	WJ 18B	OBSID	WJ 10B
SIO2	48.45	49.41	50.13	46.98	48.53	49.66	54.37	69.56	70.58	59.12
TIO2	2.18	2.94	3.50	3.78	3.65	3.27	1.95	.30	.29	1.09
AL203	19.93	17.08	15.38	14.68	14.84	15.85	15.55	13.29	12.65	14.26
FE203	3.99	4.22	3.39	5.24	4.92	3.90	2.89	1.84	1.77	3.32
FEO	4.12	6.00	8.92	7.17	7.56	8.25	8.35	2.70	2.60	5.41
MNO	.10	.15	.19	.18	.18	.21	.21	.12	.11	.24
MGO	3.43	3.75	4.30	4.13	4.08	3.78	2.17	.09	.07	1.00
CAO	11.44	9.73	8.72	8.91	8.62	7.54	5.98	.76	.67	3.79
NA20	3.43	3.31	3.36	3.21	3.48	3.60	4.32	5.33	5.23	4.62
K20	.72	1.04	1.31	1.05	1.25	1.29	2.25	4.85	4.76	3.06
P205	.37	.48	.49	.43	.44	.62	.65	.01	.01	.35
H20+	-	.85	.27	1.73	.93	1.43	.76	-	-	-
H20-	.37	.83	.06	.78	.42	.39	.29	.02	.67	.25
C02	1.71	-	-	1.98	.97	.56	.56	.29	-	1.67
TOTAL	100.24	99.79	100.02	100.25	99.87	100.35	100.30	99.16	99.41	98.18
* * * C.T.P.W. NORMS * * *										
Q	.00	.39	.20	.00	.00	.56	2.62	17.60	21.01	9.03
OR	4.37	6.26	7.80	6.50	7.62	7.80	13.47	29.01	28.48	18.85
AB	29.35	28.60	28.60	28.43	30.29	31.14	37.06	41.90	39.06	40.70
AN	37.66	29.32	23.06	23.64	21.76	23.82	16.64	.00	.00	9.49
AC	.00	.00	.00	.00	.00	.00	.00	2.17	2.08	.00
NS	.00	.00	.00	.00	.00	.00	.00	.31	.00	.00
NE	.14	.00	.00	.00	.00	.00	.00	.00	.00	.00
DI	14.67	13.90	14.26	16.39	16.00	8.61	7.80	3.33	2.94	6.66
HY	.00	12.28	15.38	11.40	10.33	17.40	14.43	5.09	4.94	10.15
OL	6.80	.00	.00	2.10	2.90	.00	.00	.00	.00	.00
MT	1.94	2.46	2.96	3.07	3.03	2.96	2.74	.00	.00	2.15
IL	4.19	5.63	6.61	7.43	7.04	6.27	3.72	.56	.55	2.12
AP	.90	1.16	1.16	1.07	1.07	1.49	1.56	.02	.02	.88
* * * TRACE ELEMENTS * * *										
ZR	172.	237.	281.	256.	246.	286.	466.	1188.	1326.	663.
NB	26.3	35.5	43.5	37.1	39.4	42.6	68.8	155.	180.	96.9
Y	24.5	31.4	37.7	33.8	33.3	37.7	52.0	90.1	104.	61.6
RB	11.7	11.3	20.2	13.3	20.9	19.0	39.8	105.	117.	59.2
BA	130.	206.	250.	190.	226.	246.	439.	298.	180.	579.
SR	566.	491.	434.	421.	446.	424.	413.	14.5	11.7	304.
CO	29.0	34.0	44.0	44.0	45.0	37.0	18.0	4.0	-	4.0
CR	22.0	35.0	20.0	30.0	23.0	13.0	7.0	4.0	-	3.0
NI	19.0	16.0	21.0	23.0	16.0	10.0	ND	9.0	-	3.0
V	175.	230.	278.	304.	318.	271.	47.0	3.0	-	9.0
ZN	-	-	-	-	-	-	-	-	-	-
CU	-	-	-	-	-	-	-	-	-	-
SC	19.8	33.4	27.9	29.3	27.9	27.5	14.7	1.3	.9	12.4
TH	2.0	2.9	2.9	2.9	3.0	3.0	5.8	16.2	-	7.8
PB	.5	.7	.9	.7	.8	.7	1.6	4.8	4.0	2.1
GA	21.0	21.0	23.0	22.0	23.0	22.0	26.0	31.0	32.2	27.0

T A B L E 5-2 (CONTINUED)

BOUVET ISLAND: WHOLE ROCK ANALYSES, CIPW NORMS & SELECTED RATIOS

	WJ 8B	WJ 17B	WJ 2B	WJ 7B	WJ 14B	WJ 16B	WJ 1B	WJ 18B	OBSID	WJ 10B
				* * * ELEMENT RATIOS * * *						
ZR/NB	6.54	6.69	6.46	6.90	6.23	6.71	6.77	7.67	7.36	6.84
ZR/BA	1.32	1.16	1.12	1.35	1.08	1.16	1.06	3.99	7.37	1.15
ZR/Y	7.00	7.57	7.46	7.58	7.36	7.58	8.95	13.2	12.7	10.8
K/RB	513.	767.	538.	653.	497.	563.	470.	382.	337.	429.
K/BA	46.1	42.0	43.5	46.0	45.8	43.6	42.5	135.	220.	43.9
K/ZR	34.8	36.4	38.7	34.1	42.3	37.5	40.1	33.9	29.8	38.3
Y/NB	.935	.884	.865	.911	.845	.886	.756	.582	.579	.635
CA/Y	3.330+003	2.217+003	1.655+003	1.885+003	1.847+003	1.430+003	822.	60.3	45.9	440.
TI/ZR	76.1	74.2	74.7	88.5	89.1	68.7	25.1	1.51	1.31	9.85
TI/NB	497.	497.	482.	611.	555.	461.	170.	11.6	9.65	67.4
TI/Y	532.	562.	557.	671.	656.	520.	225.	20.0	16.6	106.
TI/P	8.09	8.41	9.81	12.1	11.4	7.25	4.12	41.2	39.8	4.28
CR/V	.126	.152	7.194-002	9.868-002	7.233-002	4.797-002	.149	1.33	-	.333
NI/CO	.655	.471	.477	.523	.356	.270	5.556-004	2.25	-	.750
M.I.	70.3	73.2	74.1	75.0	75.4	76.3	83.8	98.1	98.4	89.7
MG#	.597	.527	.462	.507	.490	.449	.317	5.607-002	4.578-002	.248
D.I.	33.9	35.2	36.6	34.9	37.9	39.5	53.2	88.5	88.6	68.6

TABLE 5-2 (CONTINUED)

BOUVET ISLAND: WHOLE ROCK ANALYSES, CIPW NORMS & SELECTED RATIOS

	WJ 5B	WJ 11B	N 420A	N 421A
SIO2	60.59	59.72	60.24	60.17
TIO2	1.10	1.14	1.20	1.34
AL203	15.65	14.59	14.69	14.72
FE203	1.63	2.83	1.71	6.49
FEO	7.29	6.30	8.03	3.18
MNO	.28	.24	.33	.27
MGO	.99	1.13	1.08	.88
CAO	4.32	3.91	3.91	3.61
NA20	4.42	4.85	4.73	4.76
K20	2.98	2.88	2.93	2.90
P205	.32	.37	.39	.37
H20+	.30	-	.19	.87
H20-	.05	.04	.20	.84
C02	-	.58	-	-
TOTAL	99.92	98.58	99.63	100.40
			* * * C.I.P.W. NORMS * * *	
Q	9.77	8.17	9.52	9.63
OR	17.67	17.37	17.25	17.43
AB	35.57	41.97	40.61	41.04
AN	14.14	9.74	10.30	10.42
AC	.00	.00	.00	.00
NS	.00	.00	.00	.00
NE	.00	.00	.00	.00
DI	4.59	6.58	4.64	4.64
HY	11.28	10.87	11.00	11.14
OL	.00	.00	.00	.00
MT	2.17	2.22	2.23	2.26
IL	2.07	2.20	2.53	2.55
AP	.76	.90	.88	.90
			* * * TRACE ELEMENTS * * *	
ZR	635.	637.	690.	676.
NB	94.6	94.0	98.0	95.0
Y	59.4	61.0	62.0	61.0
RB	55.8	57.8	61.0	58.0
BA	584.	574.	577.	575.
SR	315.	313.	313.	321.
CO	5.0	5.0	6.0	5.0
CR	6.0	4.0	14.0	6.0
NI	4.0	5.0	ND	5.0
V	9.0	11.0	10.0	11.0
ZN	-	-	-	-
CU	-	-	-	-
SC	13.8	14.0	13.7	14.2
TH	8.6	7.9	8.8	-
PB	2.0	2.2	2.4	-
GA	28.0	28.0	28.0	29.0

T A B L E 5-2 (CONTINUED)

BOUVET ISLAND: WHOLE ROCK ANALYSES, CIPW NORMS & SELECTED RATIOS

	WJ 5B	WJ 11B	N 420A	N 421A
			* * * ELEMENT RATIOS * * *	
ZR/NB	6.72	6.78	7.04	7.12
ZR/BA	1.09	1.11	1.20	1.18
ZR/Y	10.7	10.4	11.1	11.1
K/RB	443.	414.	398.	415.
K/BA	42.4	41.7	42.2	41.9
K/ZR	38.9	37.5	35.3	35.6
Y/NB	.628	.649	.633	.642
CA/Y	520.	458.	451.	423.
TI/ZR	10.4	10.7	10.4	11.9
TI/NB	69.7	72.7	73.4	84.6
TI/Y	111.	112.	116.	132.
TI/P	4.72	4.23	4.23	4.98
CR/V	.667	.364	1.40	.545
NI/CO	.800	1.00	1.667-003	1.00
M.I.	90.0	89.0	90.0	91.7
MG#	.195	.242	.193	.330
D.I.	63.0	67.5	67.4	68.1

free, with Fe_2O_3/FeO adjusted to 0.20 (Verwoerd et al., 1974). The analyses presented in Imsland et al. (1977) are similar to those used in this study with minor differences (possibly laboratory bias) occurring in some trace elements.

4.2 Whole Rock Chemistry

The chemical variations in the Bouvet Island lavas have been previously discussed by Verwoerd et al. (1974) and Imsland et al. (1977). Consequently only the more salient features will be discussed here.

4.2.1 Major Elements:

The essential major element composition of the Bouvet Island lavas is shown on AFM diagram in (Fig. 5-2), where a strong Mg depletion is associated with an enrichment in total alkalis through the sequence hawaiite to rhyolite. The trend for Gough Island lavas (A. le Roex, unpublished data) is shown for comparison. In a total alkalis-silica diagram (Fig. 5-3) the lavas are seen to straddle the alkali-basalt-tholeiite dividing line of Irvine and Baragar (1971) attesting to their previously reported transitional to mildly alkaline nature (Verwoerd et al., 1974; Imsland et al., 1977). The compositional field of Gough Island lavas is again shown for comparison.

Some important features of the evolution of the Bouvet Island lavas are demonstrated by the behaviour of a few selected major elements: CaO, TiO_2 and P_2O_5. These elements are plotted versus mafic index (M.I. = Fe_2O_3+FeO/Fe_2O_3+FeO+MgO) in Fig. 5-4. The increasing M.I. of the lavas through the sequence hawaiite to rhyolite indicates that if these lavas can be related by low pressure fractional crystallisation, then a ferromagnesian mineral such as olivine and/or clinopyroxene must have played an important role. The continual decrease in CaO, the

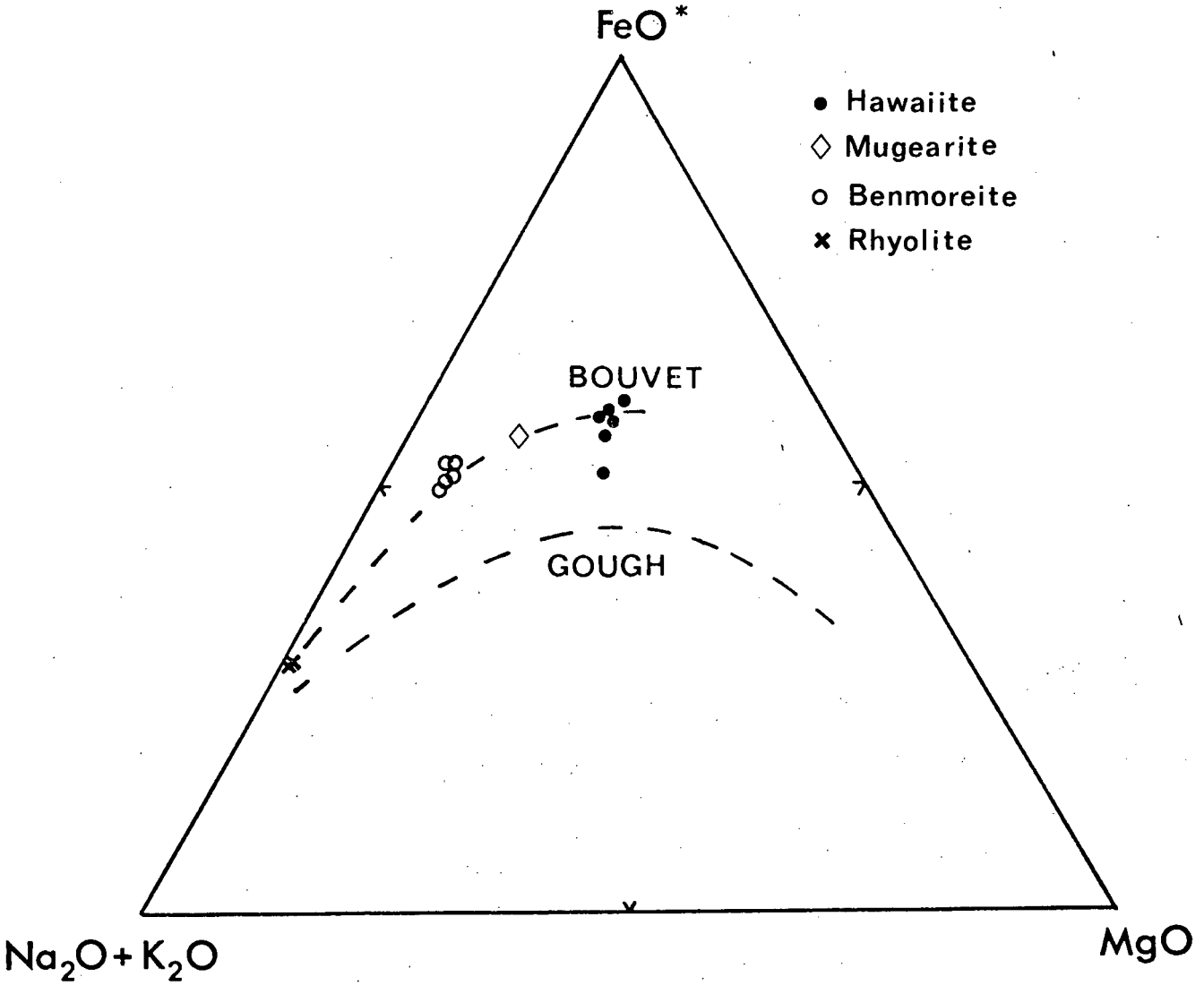

Fig. 5-2: A-F-M diagram showing the compositional variation of Bouvet Island lavas. Trend line for Gough Island (A.P. le Roex, unpubl. data) is shown for comparison.

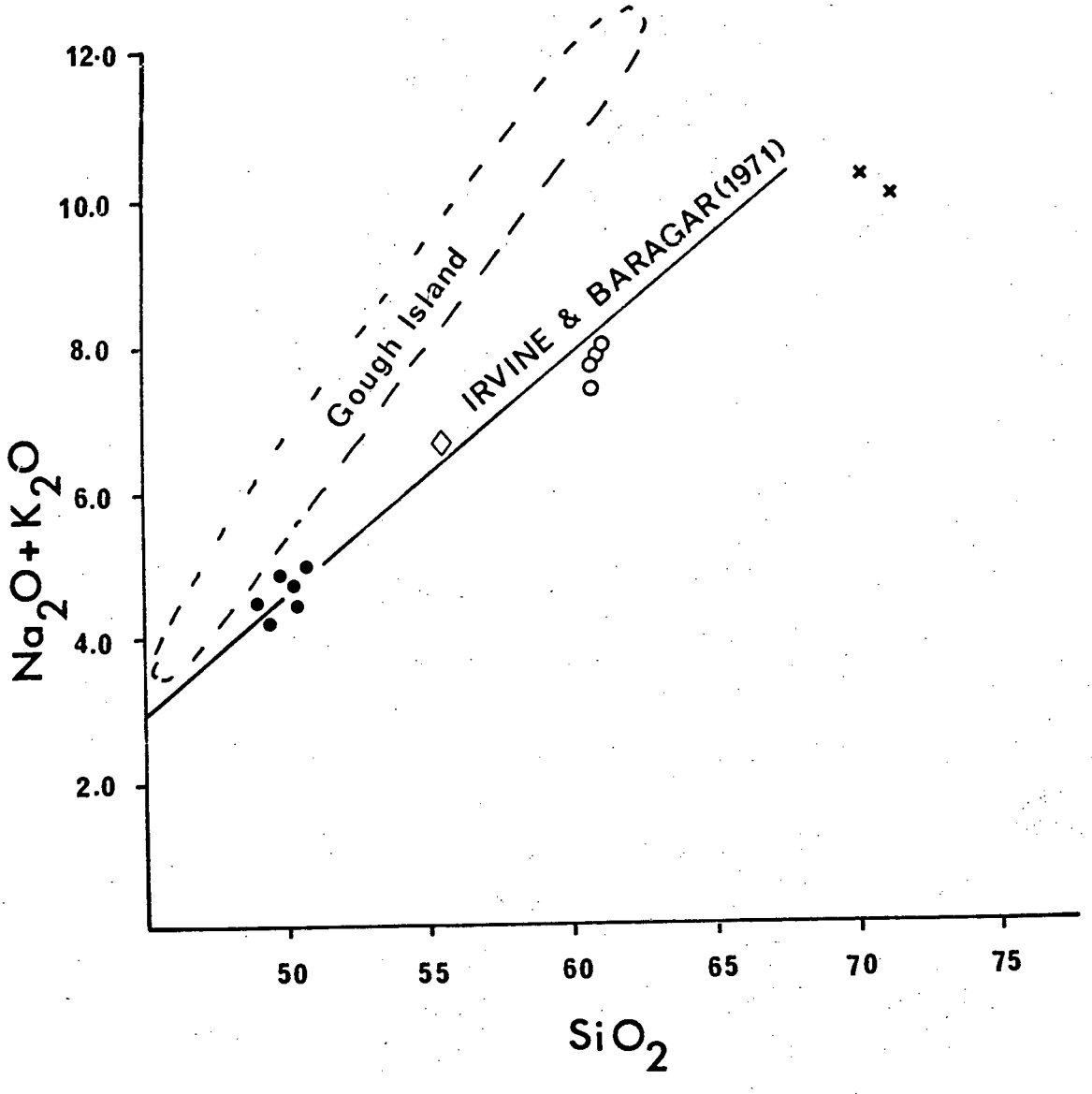

Fig. 5-3: Total alkalies - SiO_2 diagram showing the compositional spread of Bouvet Island lavas. Field of Gough Island lavas (A.P. le Roex, unpubl. data) is shown for comparison. Symbols as in Fig. 5-2.

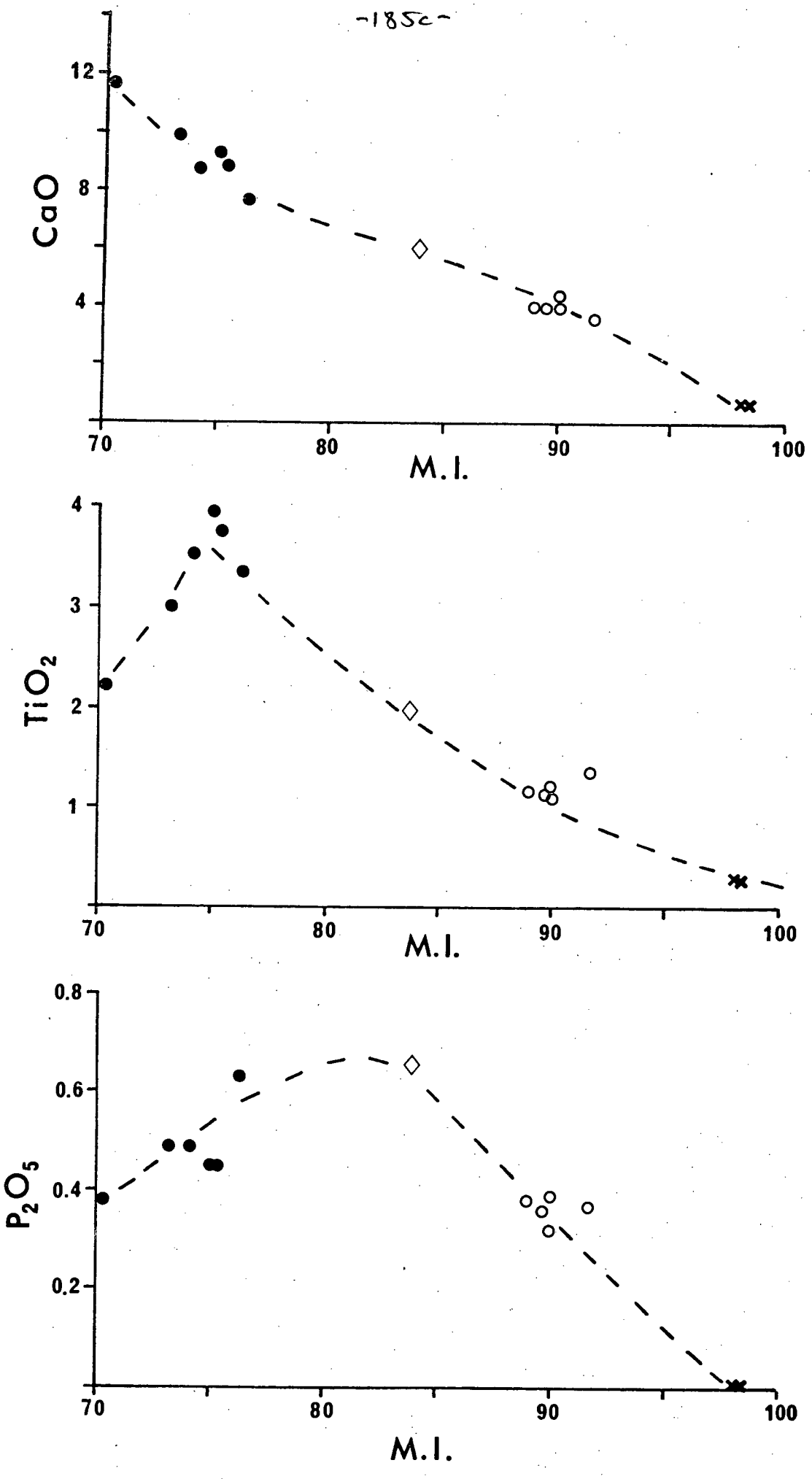

Fig. 5-4: Variation of CaO, TiO_2 and P_2O_5 with differentiation (expressed in terms of M.I.) in Bouvet Island lavas. Symbols as in Fig. 5-2.

initial increase in P_2O_5 from hawaiite to mugearite followed by a decrease through benmoreite to rhyolite and continual decrease in TiO_2 from the sparsely phyric hawaiites through to rhyolite provide constraints on other possible fractionating phases.

The variation in Ca indicates that plagioclase and/or clinopyroxene must comprise a significant proportion of any fractionate, while the initial enrichment of P_2O_5 followed by a depletion indicates that apatite must become an important crystallising phase in the later stages. The decrease in TiO_2 throughout the series similarly indicates the fractionation of a TiO_2-bearing phase. The decrease in TiO_2 in the highly phyric hawaiites WJ8B and WJ17B (M.I. = 70.3 and 73.2 respectively) can probably be attributed to a dilution effect involving plagioclase. The overall major element variation of the Bouvet Island lavas therefore shows well defined trends which are in qualitative accordance with a fractional crystallisation model involving plagioclase, clinopyroxene, titanomagnetite, with possibly minor olivine and apatite.

4.2.2 Trace Elements:

Trace elements in the Bouvet Island lavas similarly show well defined trends with increasing M.I. (Figs. 5-5A to C), again suggestive of a simple fractionation process having given rise to the spectrum of observed lavas. The general behaviour of the trace elements will be discussed on the assumption of such a model and in terms of two groups: those showing incompatible behaviour and those showing compatible behaviour.

(1) Incompatible Trace Elements

In the Bouvet Island lavas the following trace elements exhibit varying degrees of incompatibility (arranged in order of decreasing

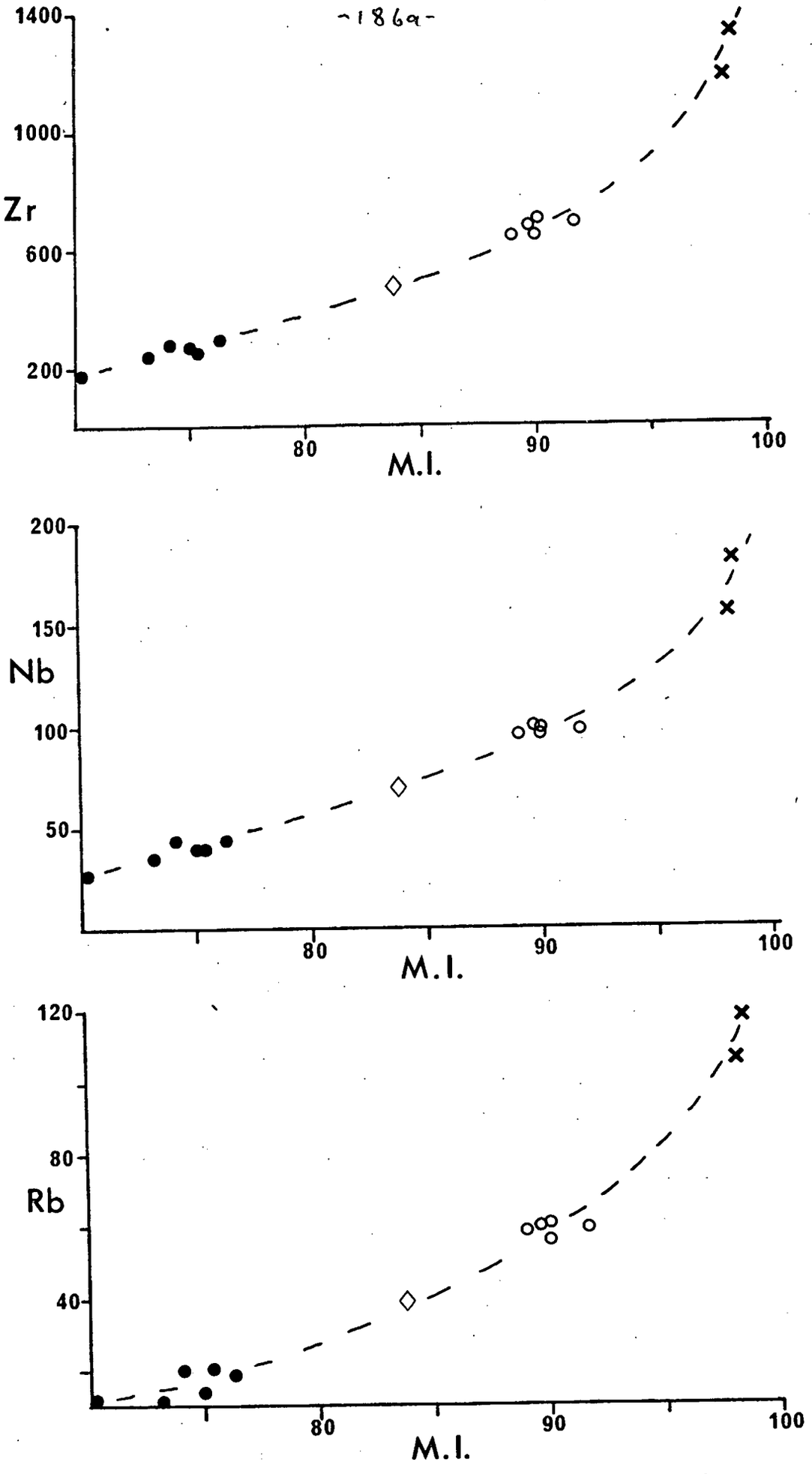

Fig. 5-5: Variation in selected trace elements with differentiation (expressed in terms of M.I.) in Bouvet Island lavas. Symbols as in Fig. 5-2.

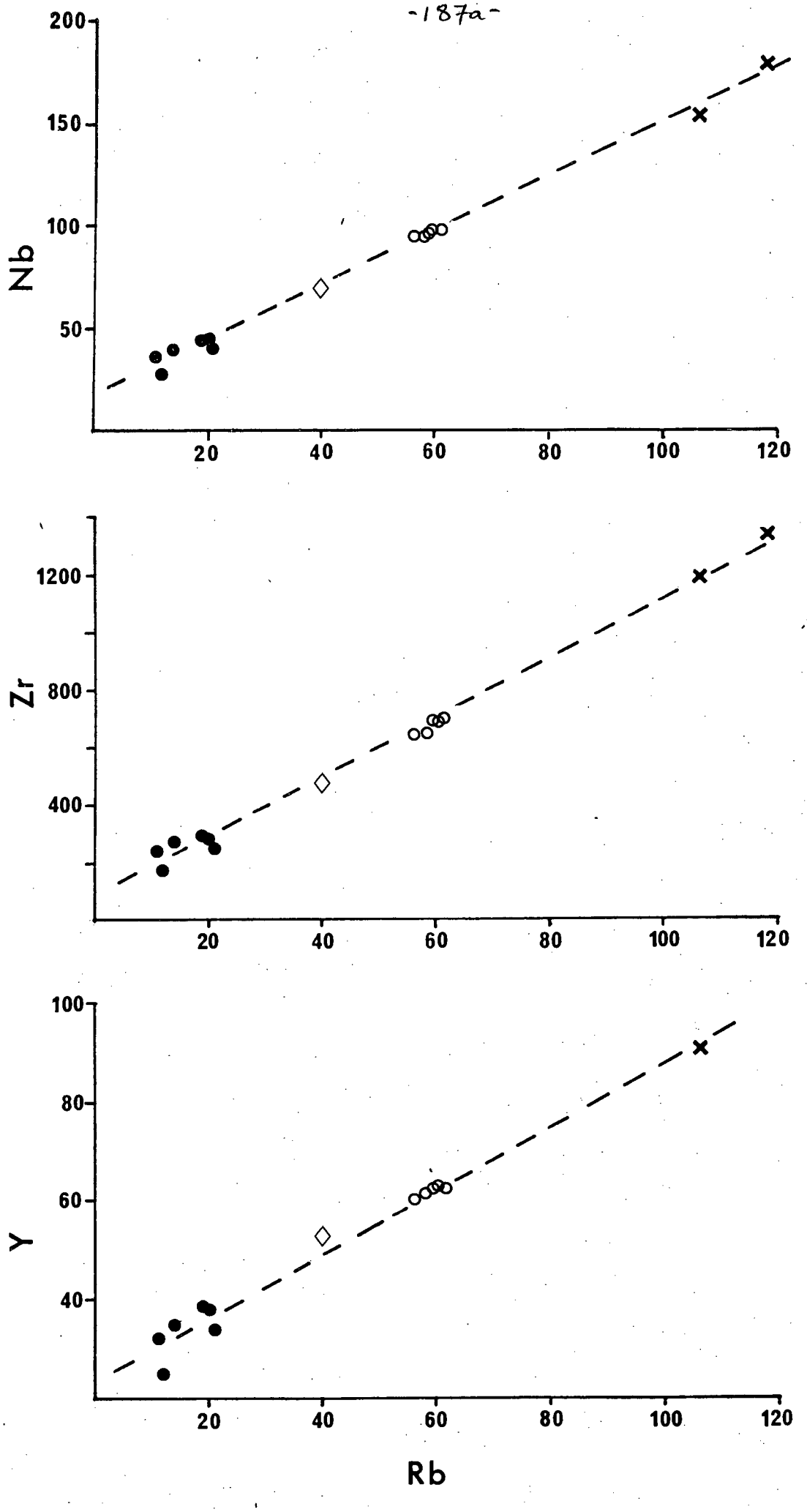

Fig. 5-6: Correlation of Nb, Zr and Y with Rb in Bouvet Island lavas. Symbols as in Fig. 5-2.

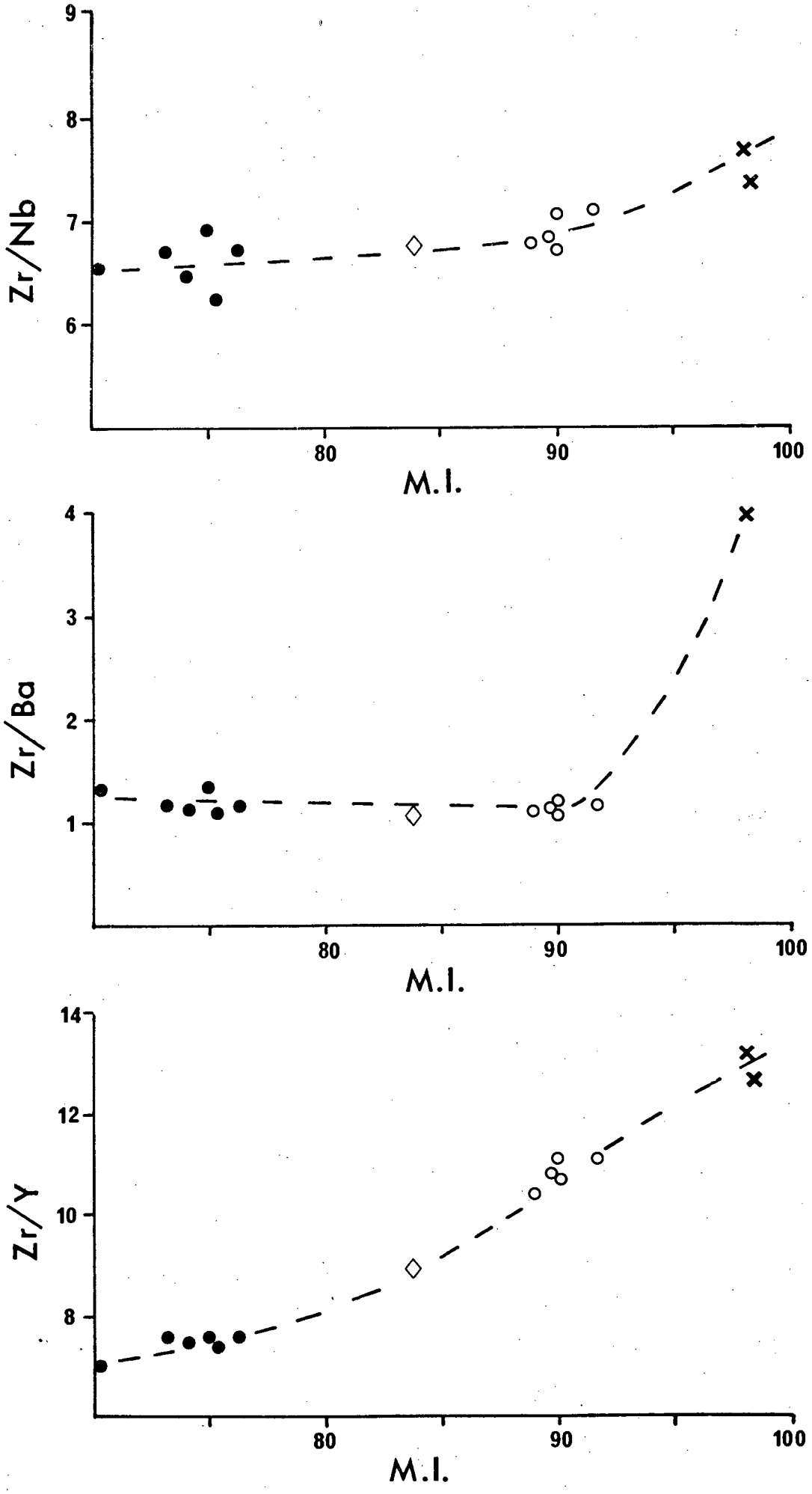

Fig. 5-7: Variation in selected incompatible element ratios with M.I. in Bouvet Island lavas. Symbols as in Fig. 5-2.

If an element is completely incompatible (i.e. $D \sim 0$), then the concentration of that element in the residual liquid (C^L) is inversely proportional to F (the amount of liquid remaining), i.e.

$$\frac{C^L}{C^o} = \frac{1}{F}$$

where C^o = concentration in the initial liquid. Assuming Th to have the lowest bulk D and that the range in composition from hawaiite to rhyolite can be explained in terms of fractional crystallisation, it would be necessary to crystallise approximately 82% of the parental hawaiite to account for the observed enrichment of wholly incompatible elements in the rhyolite.

In the early part of the sequence, hawaiite to benmoreite, Ba behaves as an incompatible element and increases with differentiation. However, the rhyolite has a significantly lower Ba content than the benmoreites (Fig. 5-5B), and if the rhyolite comprises the end product of a fractional crystallisation sequence, it would be necessary to invoke the crystallisation of a phase in which Ba was compatible. The presence of anorthoclase phenocrysts in the rhyolite is in qualitative accord with this ($D^{Ba}_{anorth} \sim 5$; Sun and Hanson, 1976). The change in bulk distribution coefficient for Ba between the benmoreites and the rhyolite is also shown by the Zr/Ba ratio (Fig. 5-7) which remains constant from the hawaiites through mugearite to the benmoreites and then rapidly increases. Any fractionation scheme must obviously account adequately for this variation.

(2) Compatible Trace Elements

The variation of the compatible trace elements (Sr, Sc, V, Co, Cr, Ni) in the Bouvet Island lavas can be used to place qualitative

restraints on the type and proportion of possible fractionating minerals compatible with the observed compositional variations. The continuous decrease in Sr and Sc (Fig. 5-5B) throughout the series requires that plagioclase (D^{Sr}_{plag} = 2-3; Korringa and Noble, 1971) and clinopyroxene (D^{Sc}_{cpx} = 1-8; Lindstrom, 1976; Ewart et al., 1973; Dale and Henderson, 1972) comprise significant proportions of any fractionating assemblage. Minor magnetite fractionation could also contribute to the decreasing Sc (D^{Sc}_{mgt} = 1-8; Leeman et al., 1978; Ewart et al., 1973; Lindstrom, 1976).

The decrease in Co, V (Fig. 5-5C), Cr and Ni requires the crystallisation of clinopyroxene (D^{Co}_{cpx} = 0.5-7.0; D^{V}_{cpx} = 1-8; D^{Cr}_{cpx} = 1-32, and D^{Ni}_{cpx} = 1-14; Lindstrom, 1976; Ewart et al., 1973; Lindstrom and Weill, 1978), olivine (D^{Co}_{ol} = 2-5; D^{Ni}_{ol} = 8-25; Lindstrom, 1976; Dale and Henderson, 1977; Hart and Davis, 1978), and/or titanomagnetite (D^{V}_{mgt} = 5-100; D^{Co}_{mgt} = 3-17; D^{Ni}_{mgt} = 5-77; and D^{Cr}_{mgt} = 20-600; Lindstrom, 1976; Ewart et al., 1973; Leeman et al., 1978). It is clear that relatively minor amounts of titanomagnetite fractionation could result in large decreases in the elements V, Cr, Co and Ni. The initial decrease in Co, V and Sc in the highly phyric hawaiites (Figs. 5-5B,C, M.I. = 70.3 and 73.2) reflects a dilution effect by plagioclase, the accumulation of which simultaneously results in an increase in Sr (Fig. 5-5B).

4.2.3 Rare Earth Elements:

Rare earth elements (REE) have been determined on eight Bouvet Island samples by E.D.J. Kable using neutron activation techniques. Average values, normalised to the Leedy chondrite / 1.20 (Sun and Hanson, 1976) are presented in Table 5-3 and REE variations are illustrated in Fig. 5-8.

	WJ8B	WJ2B	WJ7B	WJ16B	WJ1B	WJ5B	WJ10B	WJ18B
La	19.4	32.3	26.9	31.8	51.8	65.7	64.4	104.0
Ce	34.4	49.7	47.8	54.5	89.4	105.8	108.4	174.6
Sm	6.2	9.75	9.20	10.2	15.3	16.0	16.4	23.4
Eu	2.09	3.14	2.85	3.35	4.55	4.64	4.64	3.09
Tb	0.91	1.41	1.42	1.53	2.22	2.63	2.75	4.17
Yb	2.06	2.88	2.76	3.09	4.77	5.55	5.63	9.19
Lu	0.24	0.38	0.38	0.40	0.60	0.72	0.75	1.13
Ta	2.05	3.00	2.88	3.00	4.66	6.20	6.21	10.35
Hf	4.30	6.77	6.52	7.29	11.03	14.43	15.60	28.40
CH La/Sm	1.91	2.02	1.78	1.90	2.06	2.50	2.39	2.71
Zr/Hf	40.00	41.51	39.26	39.23	42.25	44.01	42.50	41.83
Nb/Ta	12.83	14.50	12.88	14.20	14.76	15.26	15.60	14.98
La/Ta	9.46	10.77	9.34	10.60	11.12	10.60	10.37	10.05

Table 5-3: REE element, Ta and Hf contents of selected Bouvet Is. lavas. All elements were determined by INAA at the Nuclear Physics Research Institution, University of the Witwatersrand, by E.J.D. Kable.

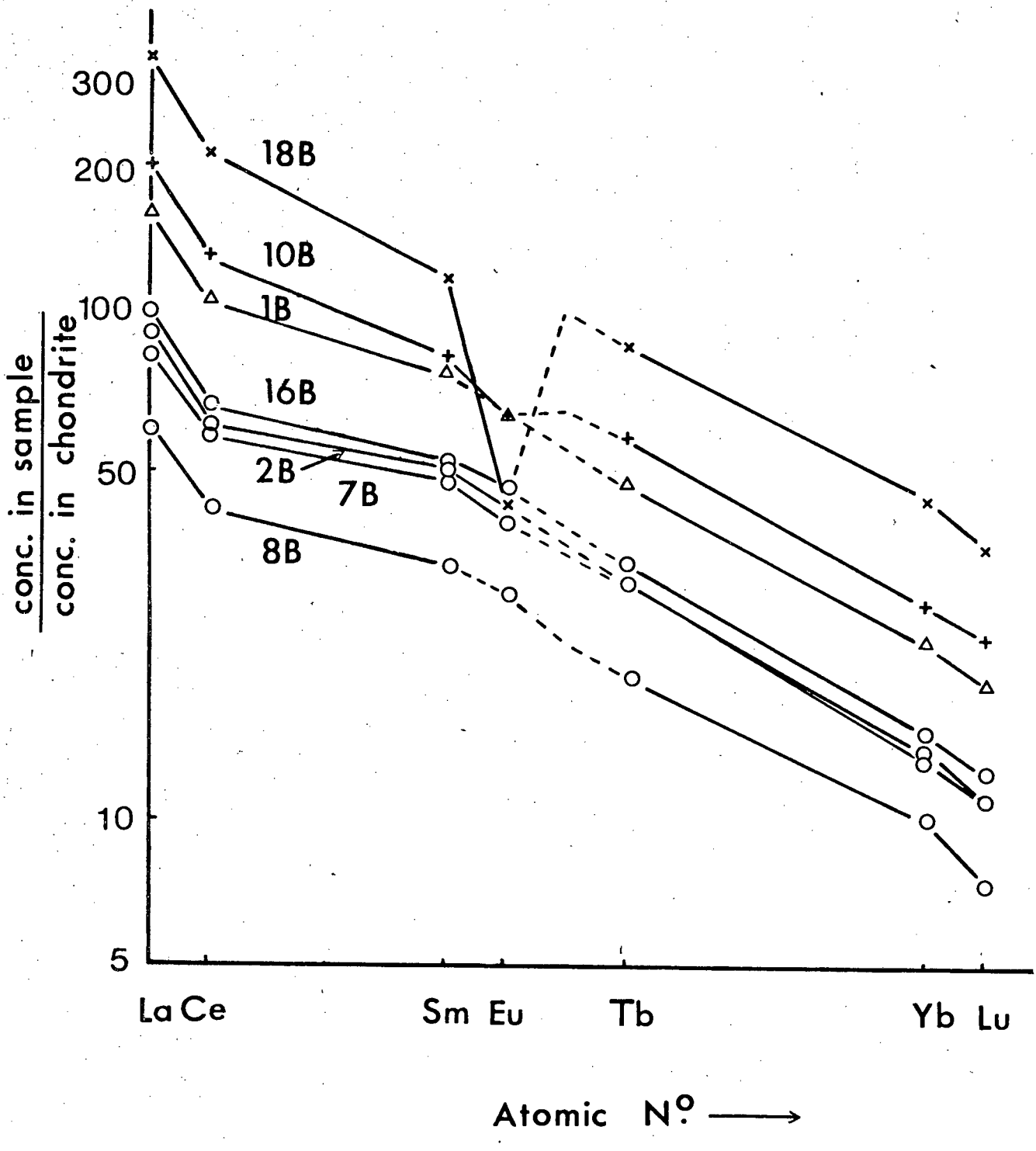

Fig. 5-8: Chondrite normalised REE variation in selected Bouvet Island lavas. Concentrations were normalised using values for Leedy chondrite, divided by 1.2 (Sun and Hanson, 1976).

TABLE 5-4

BOUVET ISLAND: REPRESENTATIVE OLIVINE ANALYSES.

	1	2	3	4	5	6
SIO2	38.15	38.21	36.63	33.08	31.79	31.43
TIO2	.04	-	-	.18	.10	.08
AL2O3	.03	-	-	.08	.02	.04
CR2O3	ND	-	-	-	-	-
FEO	22.17	21.93	33.66	47.05	53.62	55.37
MNO	.31	.36	.53	.79	1.15	1.59
MGO	38.71	39.44	27.91	18.21	12.19	10.83
CAO	.28	.28	.32	.36	.53	.48
NA2O	-	-	-	-	-	-
K2O	-	-	-	-	-	-
NIO	.07	.07	.05	-	-	-
TOTAL	99.77	100.29	99.10	99.75	99.40	99.82

* * ATOMIC PROPORTIONS BASED ON SELECTED NO. OF OXYGENS * *

OXYGEN	4	4	4	4	4	4
SI	.996	.991	1.019	.987	.991	.987
AL	.001	-	-	.003	.001	.001
TI	.001	-	-	.004	.002	.002
CR	-	-	-	-	-	-
FE2+	.484	.476	.783	1.174	1.398	1.454
MN	.007	.008	.012	.020	.030	.042
MG	1.506	1.525	1.157	.809	.566	.507
CA	.008	.008	.010	.012	.018	.016
NA	-	-	-	-	-	-
K	-	-	-	-	-	-
NI	.001	.001	.001	-	-	-
SUM	3.003	3.009	2.981	3.008	3.006	3.010
	FO 75.68 FA 24.32	FO 76.22 FA 23.78	FO 59.64 FA 40.36	FO 40.82 FA 59.18	FO 28.83 FA 71.17	FO 25.85 FA 74.15

* * * S A M P L E D I R E C T O R Y * * *

ANALYSIS NO.	DESCRIPTION
1	AVERAGE OLIVINE PHENO, HAWAIITE - WJ 2B
2	OLIVINE PHENO CORE, HAWAIITE - WJ 2B
3	OLIVINE PHENO RIM, HAWAIITE - WJ 2B
4	OLIVINE MICROPHENO, HAWAIITE - WJ 2B
5	AVERAGE OLIVINE, MUGEARITE - WJ 1B
6	AVERAGE OLIVINE PHENO, BENMOREITE

** ND = NOT DETECTED **

The Bouvet Island lavas show strong LREE enrichment typical of ocean island basalts (e.g. Schilling and Winchester, 1969; Zielinsky and Frey, 1970; Flower, 1971). The overall parallel trends show increasing enrichment in all REE from hawaiite through to rhyolite, with the highly phyric hawaiite (WJ8B) having the lowest overall REE content. Superimposed on these general smooth trends is a marked negative Eu anomaly in rhyolite WJ18B and a lesser anomaly is present in benmoreite WJ10B. The REE trend for the highly phyric hawaiite has the suggestion of a slight positive Eu anomaly.

The continuous enrichment in total REE through the sequence hawaiite to rhyolite is in accord with a fractional crystallisation model relating the composition of the lavas as the REE have bulk D's for the observed phenocryst assemblages of less than unity. The negative Eu anomalies in the benmoreite and rhyolite support the earlier conclusions, on the basis of Sr contents, that plagioclase fractionation played an important role in the evolution of the Bouvet Island lavas. The small positive Eu anomaly in the highly phyric lava is in accord with accumulation of calcic plagioclase in which the D^{Eu}_{plag} is still relatively low (Arth, 1976).

4.3 Mineral Chemistry

4.3.1 General Statement:

Microprobe analyses of phenocryst, microphenocryst and matrix phases were made on six samples (WJ8B, WJ2B, WJ7B, WJ1B, WJ10B and WJ18B) selected to span the spectrum of whole rock compositions on Bouvet Island. In any low pressure fractionation scheme mineral compositions should show relatively smooth compositional variations throughout the sequence (Baker et al., 1977). One of the objects of the study therefore has been to

monitor mineral compositional variations through the sequence hawaiite to rhyolite. A second objective is to obtain compositional ranges for use in quantitative modelling. Finally, selected trace elements have been determined for some minerals in an attempt to determine and utilise calculated trace element distribution coefficients.

4.3.2 Olivine:

Olivine is present in WH2B (hawaiite), WJ1B (mugearite) and WJ10B (benmoreite). Average olivine analyses for the Bouvet Island lavas are presented in Table 5-4, and individual analyses can be found in microfiche Tables F5-1, F5-4 and F5-5. The range in compositions is depicted in Fig. 5-12. The average olivine phenocryst in WJ2B (hawaiite) has a composition of Fo_{75} (Table 5-4, No. 1) and a typical phenocryst shows strong zoning from Fo_{75} to Fo_{60} (Table 5-4, No's. 2 and 3). Olivine microphenocrysts are significantly more iron-rich with compositions corresponding to Fo_{41} (Table 5-4, No. 4).

Calculation of an olivine-liquid Fe-Mg K_D (Roeder and Emslie, 1970) (see Chapter III, Section 5.2 for full discussion) for hawaiite WJ2B gives a value of 0.24. This is obtained using the whole rock FeO/MgO ratio (as representative of the liquid composition, with Fe_2O_3/FeO adjusted to 0.20) and the core of the most Mg-rich olivine (as representing the liquidus olivine composition). This value is outside the range (0.30 ± 0.03) observed by Roeder and Emslie (1970) for equilibrium assemblages, and though Bender et al. (1978) and Longhi et al. (1978) have suggested that the Fe-Mg K_D decreases with increasing temperature and is to a certain extent composition-dependent, it is unlikely that the hawaiite had a sufficiently high liquidus temperature to lower the K_D to the observed level. Knutson and Green (1975) have,

for example, found the liquidus temperature of a typical hawaiite (water-free) to be 1150°C, which is at the low end of the range of temperatures used by Roeder and Emslie (1970).

Adjustment of the Fe_2O_3/FeO ratio has a small effect on the K_D, but to raise the calculated K_D to 0.29, the Fe_2O_3/FeO ratio would have to be raised to approximately 0.55, which is significantly higher than even the observed Fe_2O_3/FeO ratio of WJ2B, which is all probability reflects post consolidation oxidation. The selected Fe_2O_3/FeO value of 0.20 is probably a maximum value, since Fe-Ti oxide data suggest a value closer to 0.13 (see Section 4.3.5). On the basis of the above arguments, it is suggested that the olivine phenocrysts in WJ2B are too fosteritic to have crystallised from a magma with the composition of WJ2B. Their presence suggests the existence of a slightly more Mg-rich precursor to the hawaiites on Bouvet Island, of which they are relict phenocrysts. An olivine of composition Fo_{70} would be expected to crystallise from a magma of composition similar to WJ2B. The bulk composition of WJ2B is probably not significantly altered by the presence of these scarce phenocrysts due to their low modal abundance (< 1%).

Olivines present in the mugearite sample show a relatively restricted compositional range of Fo_{31} to Fo_{27}; an average olivine composition is given in Table 5-4 (No. 5). The benmoreite WJ10B is characterised by similar Fe-rich phenocryst olivines (Table 5-4, No. 6) which also show a limited compositional range (Fo_{28}-Fo_{25}) and negligible zoning.

Fig. 5-9 shows the variation of MnO, TiO_2 and CaO with fosterite content of all the Bouvet Island olivines. As might be expected, MnO shows a strong enrichment with increasing fayalite content, while CaO

Fig. 5-9: Minor element variation with respect to forsterite content in olivines from Bouvet Island lavas. Symbols are as follows;

●	Hawaiite	WJ2B
◇	Mugearite	WJ1B
O	Benmoreite	WJ10B

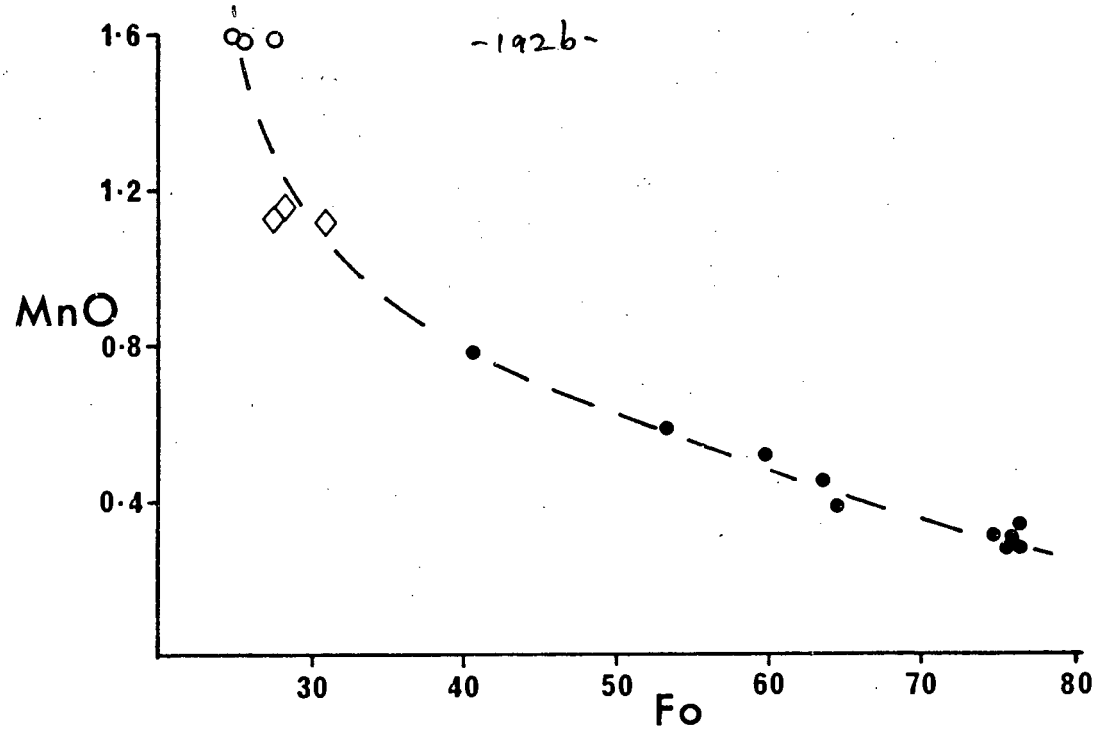
1·6
1·2
MnO
0·8
0·4
30
40
50
60
70
80
Fo

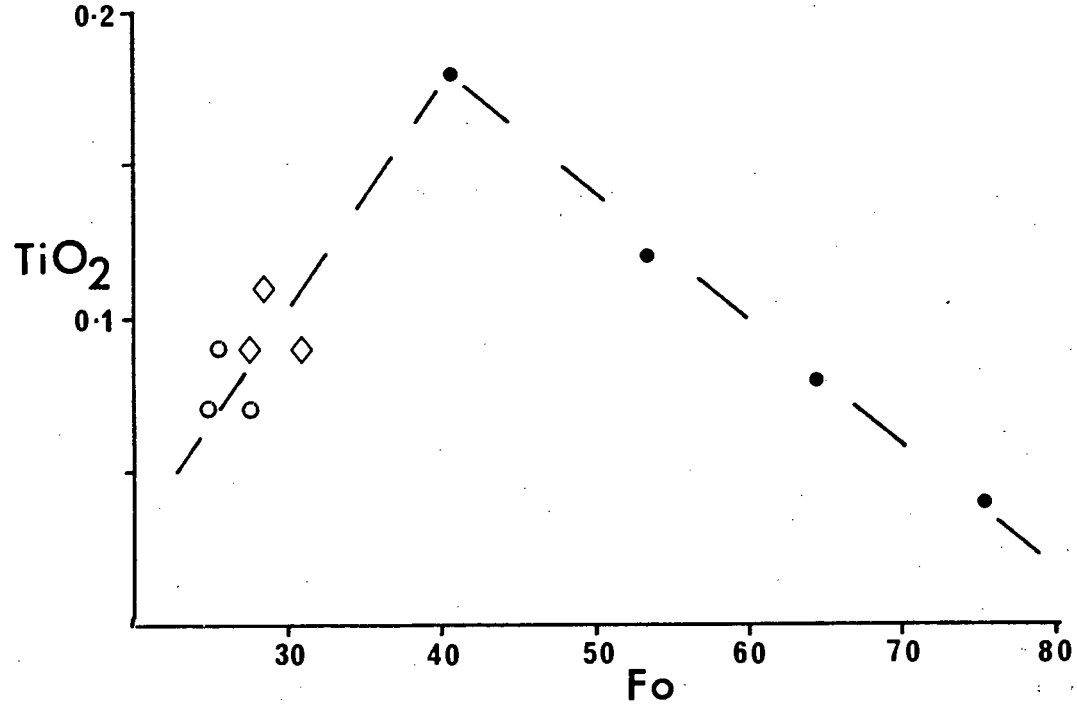
0·2
TiO2
0·1
30
40
50
60
70
80
Fo

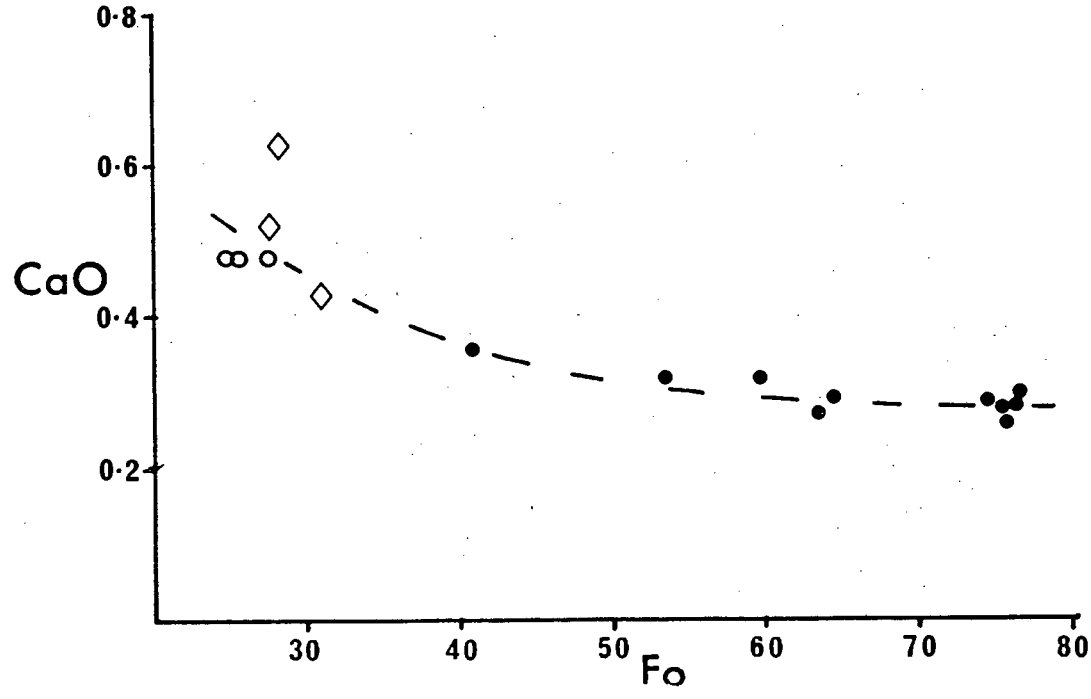
0·8
0·6
CaO
0·4
0·2
30
40
50
60
70
80
Fo

shows only a slight enrichment in the very iron-rich olivines of the mugearite and benmoreite. The CaO content of the olivines (0.3% and greater) suggests all observed olivines are relatively 'low pressure' phases (Simkin and Smith, 1970). TiO_2 shows a strong correlation with fayalite content in the olivines of WJ2B, although there are fewer analyses of TiO_2 than CaO and MgO in olivines from hawaiite WJ2B (TiO_2 was not determined in selected cases where NiO was analysed), and then a sharp drop towards the mugearite and benmoreite olivines, reflecting the onset of the crystallisation of oxide phases.

Numerous authors have recently studied the distribution of Mn between olivine and silicate liquids (e.g. Roeder, 1974; Duke, 1976; Watson, 1977; Leeman and Sch eidegger, 1977) as a function of temperature. It was suggested earlier that the 'liquidus olivine' of WJ2B would have a composition of approximately Fo_{70}. Interpolation from Fig. 5-9 gives a corresponding MnO content of 0.33%. Using this value with a whole rock MnO value of 0.19 (Table 5-2) gives a $D_{Mn}^{ol\text{-}liq}$(wt.%) of 1.74 and a $D_{Mn}^{ol\text{-}liq}$ (mol.%) of 1.41. Insertion of these values in the relevant equations relating temperature to $D_{Mn}^{ol\text{-}liq}$ enables the calculation of the liquidus temperature of the Bouvet Island hawaiite WJ2B. The equation, authors and corresponding values are given below (calculated errors for these equations are in general $\pm$ 50°C):

1. Roeder (1974) : $\log D \text{ (wt.\%)} = \frac{3850}{T(K)} - 2.59$

   $T = 1087^{\circ}C$

2. Duke (1976) : $D \text{ (wt.\%)} = 0.00388\ T\ (^{\circ}C) + 5.856$

   $T = 1060^{\circ}C$

3. Watson (1977) : $\ln D \text{ (mol.\%)} = -0.00329\ T\ (^{\circ}C) + 4.02$

   $T = 1117^{\circ}C$

4. Leeman and Scheidegger (1977) : $\ln D\ (wt.\%) = \frac{12184}{T(K)} - 7.96$

$T = 1158^{o}C$

Although the calculated temperatures show a range of $100^{o}C$, all are within one standard deviation of the mean value of $1106^{o}C$. This value is close to the predicted liquidus temperature ($1122^{o}C$) using an equation derived by H.S. Smith (unpublished data) relating MgO content of a magma to liquidus temperature as follows:

$$T^{o}C = 18.79\ MgO + 1042$$

It also corresponds favourably to the experimental work of Knutson and Green (1975) who found the 'dry' liquidus temperature of a typical hawaiite to be $1150^{o}C$, while the 'wet' liquidus' with 2% H_2O present was $1080^{o}C$. The order of crystallisation in both instances was olivine - olivine + plagioclase - olivine + plagioclase + clinopyroxene which corresponds to the observed petrography of the Bouvet Island hawaiites.

NiO was determined in a few selected olivine phenocrysts of hawaiite WJ2B. Concentrations vary from 0.07% NiO (Fo_{76}) (Table 5-4, No. 2) to 0.03% NiO (Fo_{63}). NiO shows normal zoning in the olivine phenocrysts with a maximum decrease of about 0.02% NiO from core to rim. In view of the already noted disequilibrium between olivine phenocryst and bulk rock composition of hawaiite WJ2B (on the basis of Fe-Mg distributions), no attempt has been made to utilise the observed Ni distribution between the analysed phenocrysts and the bulk rock.

4.3.3 Feldspar:

Bouvet Island lavas show a range in feldspar composition from An_{84} to An_{20} and Or_{20} to Or_{30} (Fig. 5-10). Individual analyses are presented in microfiche Tables F5-1 to F5-6, while average compositions and ranges are presented in Table 5-5.

T A B L E 5-5

BOUVET ISLAND: REPRESENTATIVE PLAGIOCLASE ANALYSES.

	1	2	3	4	5	6	7	8	9	10
SIO2	46.90	53.45	49.98	54.33	54.93	48.93	50.78	55.33	56.68	56.25
TIO2	.06	.16	.12	.16	.23	.07	.09	.17	.13	.09
AL2O3	33.58	29.08	31.18	28.46	27.72	32.36	31.53	27.59	27.19	27.59
CR2O3	-	-	-	-	-	-	-	-	-	-
FEO	.61	.67	.63	.75	.83	.48	-	.66	.56	.48
MNO	-	-	-	-	-	-	-	-	-	-
MGO	.08	.13	.12	.13	.12	.11	.14	.12	.08	ND
CAO	17.19	12.09	14.59	11.14	10.58	15.64	14.55	10.29	9.58	9.63
NA2O	1.98	4.94	3.27	5.27	5.69	2.70	3.35	5.99	6.34	6.19
K2O	.04	.30	.12	.33	.46	.12	.13	.49	.63	.49
TOTAL	100.44	100.82	100.01	100.57	100.56	100.41	100.57	100.64	101.19	100.73

* * ATOMIC PROPORTIONS BASED ON SELECIED NO. OF OXYGENS * *

OXYGEN	8	8	8	8	8	8	8	8	8	8
SI	2.153	2.412	2.287	2.451	2.479	2.234	2.301	2.493	2.533	2.522
AL	1.817	1.547	1.681	1.514	1.475	1.742	1.684	1.465	1.432	1.458
TI	.002	.005	.004	.005	.008	.002	.003	.006	.004	.003
CR	-	-	-	-	-	-	-	-	-	-
FE2+	.023	.025	.024	.028	.031	.018	-	.025	.021	.018
MN	-	-	-	-	-	-	-	-	-	-
MG	.005	.009	.008	.009	.008	.007	.009	.008	.005	-
CA	.846	.585	.715	.539	.512	.765	.706	.497	.459	.463
NA	.176	.432	.290	.461	.498	.239	.294	.523	.549	.538
K	.002	.017	.007	.019	.026	.007	.008	.028	.036	.028
SUM	5.025	5.033	5.017	5.026	5.038	5.015	5.005	5.045	5.039	5.030
	AN 82.56	AN 56.53	AN 70.65	AN 52.87	AN 49.38	AN 75.67	AN 70.06	AN 47.39	AN 43.94	AN 44.97
	AB 17.21	AB 41.80	AB 28.66	AB 45.26	AB 48.06	AB 23.64	AB 29.19	AB 49.92	AB 52.62	AB 52.31
	OR .23	OR 1.67	OR .69	OR 1.86	OR 2.56	OR .69	OR .75	OR 2.69	OR 3.44	OR 2.72

* * * S A M P L E D I R E C T O R Y * * *

ANALYSIS NO.	DESCRIPTION
1	MOST CALCIC PLAG PHENO, HAWAIITE
2	MOST SODIC PLAG PHENO, HAWAIITE
3	PLAG PHENO CORE, HAWAIITE - WJ 7B
4	PLAG PHENO RIM HAWAIITE - WJ 7B
5	AVERAGE PLAG MICROPHENO, HAWAIITE
6	PLAG PHENO CORE, CUMULATE - WJ 8B
7	PLAG PHENO RIM, CUMULATE - WJ 8B
8	PLAG MICROPHENO, CUMULATE - WJ 8B
9	PLAG PHENO EXTREME RIM, CUMULATE - WJ 8B
10	MOST CALCIC PLAGIOCLASE, MUGEARITE

** ND = NOT DETECTED **

TABLE 5-5 (CONTINUED)

BOUVET ISLAND: REPRESENTATIVE PLAGIOCLASE ANALYSES.

	11	12	13	14	15	16	17	18
SIO2	62.66	66.57	56.46	61.33	64.27	66.32	66.39	66.56
TIO2	.14	.12	.08	.06	.23	.04	.04	.04
AL2O3	22.38	19.40	26.99	24.50	21.48	19.43	19.37	19.55
CR2O3	-	-	-	-	-	-	-	-
FEO	.66	.79	.46	.39	1.26	.33	.22	.31
MNO	-	-	-	-	-	-	-	-
MGO	.06	.06	.06	.03	.06	ND	ND	ND
CAO	4.06	1.76	9.19	5.78	3.86	.52	.51	.56
NA2O	7.67	6.84	5.89	7.86	6.61	7.96	7.91	8.30
K2O	2.34	4.38	.48	.89	1.98	4.88	5.28	4.54
TOTAL	99.97	99.92	99.61	100.84	99.75	99.49	99.73	99.87

* * ATOMIC PROPORTIONS BASED ON SELECTED NO. OF OXYGENS * *

OXYGEN	8	8	8	8	8	8	8	8
SI	2.800	2.964	2.550	2.713	2.859	2.968	2.969	2.965
AL	1.179	1.018	1.437	1.278	1.126	1.025	1.021	1.027
TI	.005	.004	.003	.002	.008	.001	.001	.001
CR	-	-	-	-	-	-	-	-
FE2+	.025	.029	.017	.014	.047	.012	.008	.012
MN	-	-	-	-	-	-	-	-
MG	.004	.004	.004	.002	.004	-	-	-
CA	.194	.084	.445	.274	.184	.025	.024	.027
NA	.665	.591	.516	.674	.570	.691	.686	.717
K	.133	.249	.028	.050	.112	.279	.301	.258
SUM	5.005	4.943	5.000	5.008	4.911	5.002	5.012	5.007
	AN 19.59	AN 9.09	AN 45.00	AN 27.44	AN 21.23	AN 2.51	AN 2.42	AN 2.67
	AB 66.97	AB 63.96	AB 52.20	AB 67.53	AB 65.80	AB 69.47	AB 67.80	AB 71.57
	OR 13.44	OR 26.95	OR 2.80	OR 5.03	OR 12.97	OR 28.02	OR 29.78	OR 25.76

* * * SAMPLE DIRECTORY * * *

ANALYSIS NO.	DESCRIPTION
11	MOST SODIC PLAGIOCLASE, MUGEARITE
12	AVERAGE 'ANORTHOCLASE', MUGEARITE
13	AVERAGE CALCIC PLAG PHENO, BENMOREITE
14	AVERAGE SODIC PLAG PHENO, BENMOREITE
15	AVERAGE PLAG MICROPHENO, BENMOREITE
16	AVERAGE ANORTHOCLASE PHENO, RHYOLITE
17	ANORTHOCLASE PHENO CORE, RHYOLITE
18	ANORTHOCLASE PHENO RIM, RHYOLITE

** ND = NOT DETECTED **

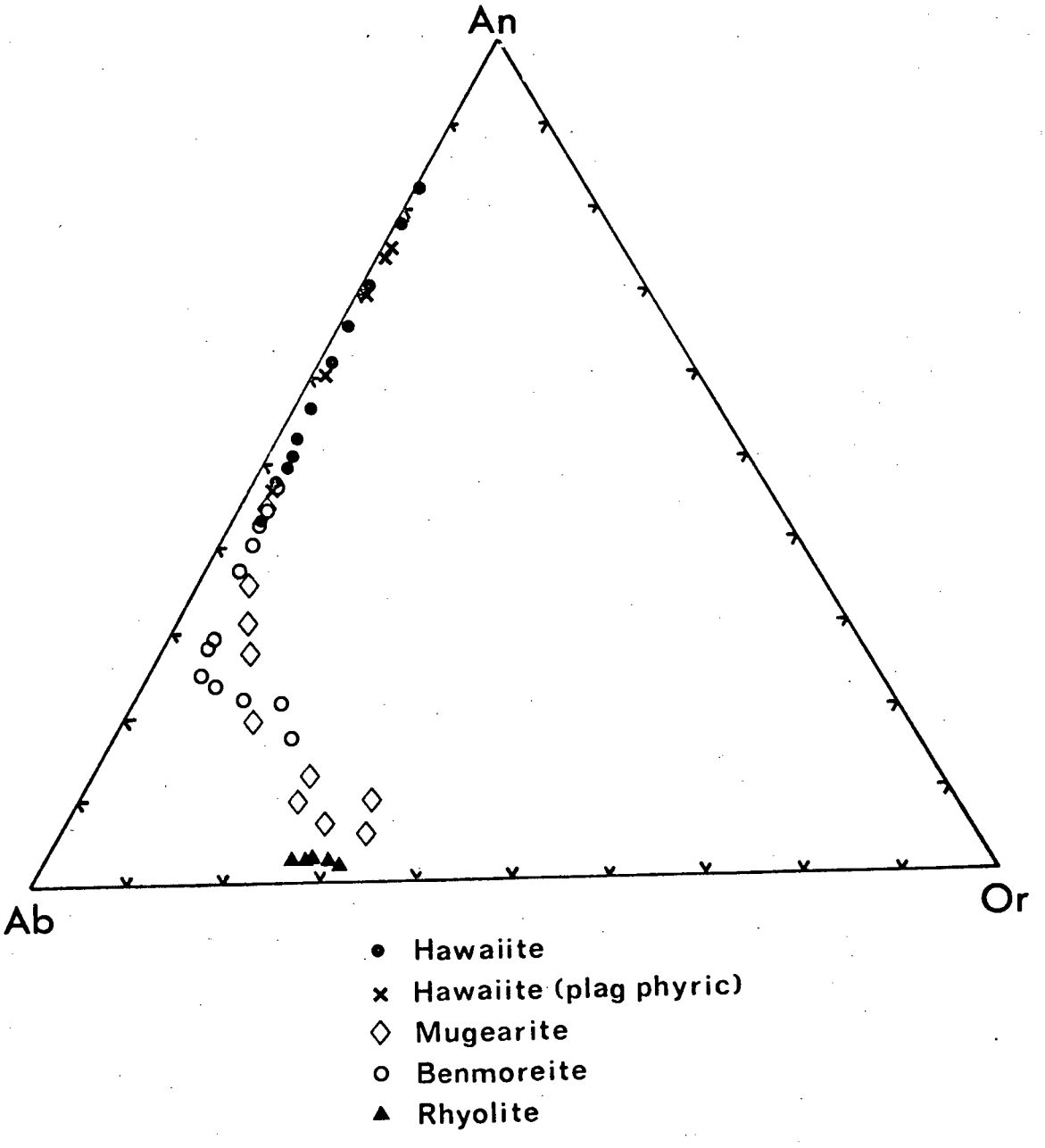

Fig. 5-10: Compositional variation of plagioclase and alkali-feldspar from Bouvet Island lavas.

Plagioclase phenocrysts and glomerocrysts in the Bouvet Island hawaiites range in composition from An_{83} to An_{56} (Table 5-5, No's. 1 and 2) with zoning typically being quite marked (An_{70}-An_{53}) (Table 5-5, No's. 3 and 4). There is little difference in composition between the glomerocysts and the phenocrysts, but the plagioclase microlites are significantly more sodic (An_{49}, Table 5-5, No. 5). The plagioclase in the porphyritic hawaiite WJ8B is of similar composition to those in the sparsely phyric hawaiites and ranges from An_{78} to An_{60}. Zoning of the large plagioclase grains is typically from An_{75} (core) to An_{70} (rim) (Table 5-5, No's 6 and 7) with some of the larger phenocrysts being surrounded by a thin rim of andesine (An_{44}, Table 5-5, No. 9). Microphenocrysts have a composition of An_{47}.

Feldspars in the mugearite show variable composition and range from An_{45} through An_{20} to anorthoclase - $An_9Ab_{64}Or_{26}$ (Table 5-5, No's. 10, 11 and 12). Though only a limited number of plagioclase analyses are available from the benmoreite sample, there appears to be a possible grouping of compositions into a more calcic variety (which is generally more euhedral) of average composition An_{45} (Table 5-5, No. 13), and a more sodic variety, An_{27} (Table 5-5, No. 14). Those phenocrysts showing 'atoll-type' growth forms generally fall into the latter group.

Anorthoclase phenocrysts of rhyolite WJ18B show a limited range in composition ($Or_{30}Ab_{68}An_2$ - $Or_{27}Ab_{70}An_3$) and commonly show a small degree of zoning ($Or_{30}Ab_{68}$ - $Or_{26}Ab_{72}$; Table 5-5, No's. 17 and 18). A typical anorthoclase microlite has composition $Or_{31}Ab_{67}An_2$.

The distribution of Sr in plagioclase phenocrysts and microphenocrysts has been determined by electron probe microanalysis (see Appendix for a description of the analytical techniques). The object of

Table 5-6: Sr and Na_2O concentrations measured by electron microprobe in plagioclase and clinopyroxene phenocrysts and microphenocrysts. A single matrix determination is presented.

I. Plagioclase	Sr(ppm)	Na_2O(%)
A. Hawaiite(WJ 2B): Whole rock Sr = 435 ppm		
Large euhedral pheno. (core)	796	2.42
Same grain (rim)	814	2.92
Anhedral pheno. (core)	734	2.44
Glomerocryst (core)	820	3.31
Microphenocryst	865	4.66
B. Hawaiite (WJ8B): Whole rock Sr = 578 ppm		
Phenocryst (core)	823	3.30
" (rim)	898	-
Glomerocryst (core)	855	2.70
" (rim)	867	3.35
Small phenocryst	877	-
Phenocryst	870	-
Plag. pheno enclosing cpx	848	4.50
Microphenocryst	832	6.0
Microphenocryst	880	6.0
C. Mugearite (WJ1B): Whole rock Sr = 419 ppm		
Phenocryst (core)	1278	5.34
Large phenocryst	1061	5.06
Small phenocryst	1128	5.67
'Anorthoclase'	754	7.31
'Anorthoclase'	597	-
D. Benmoreite (WJ10B): Whole rock Sr = 309 ppm		
Euhedral phenocryst (core)	1139	6.66
" " (rim)	1115	6.51
" " (core)	1151	5.62
" " (rim)	1256	6.19
" " (core)	1310	5.61
" " (rim)	1130	6.54

Table 5-6 (continued):

	Sr(ppm)	Na_2O(%)
D. Benmoreite (WJ10B): Whole rock Sr = 309 ppm (continued)		
Embayed phenocryst	1068	6.75
Euhedral phenocryst (core)	1067	6.56
Plag. enclosing cpx	1184	5.72
Microphenocryst	929	7.15

II. Clinopyroxene	Sr(ppm)
Hawaiite (WJ1B)	
Phenocryst	101
Benmoreite (WJ10B)	114,105
Phenocrysts	
Hawaiite (WJ8B)	
Phenocrysts	86,89,108

III. Matrix	
Benmoreite (WJ10B)	151

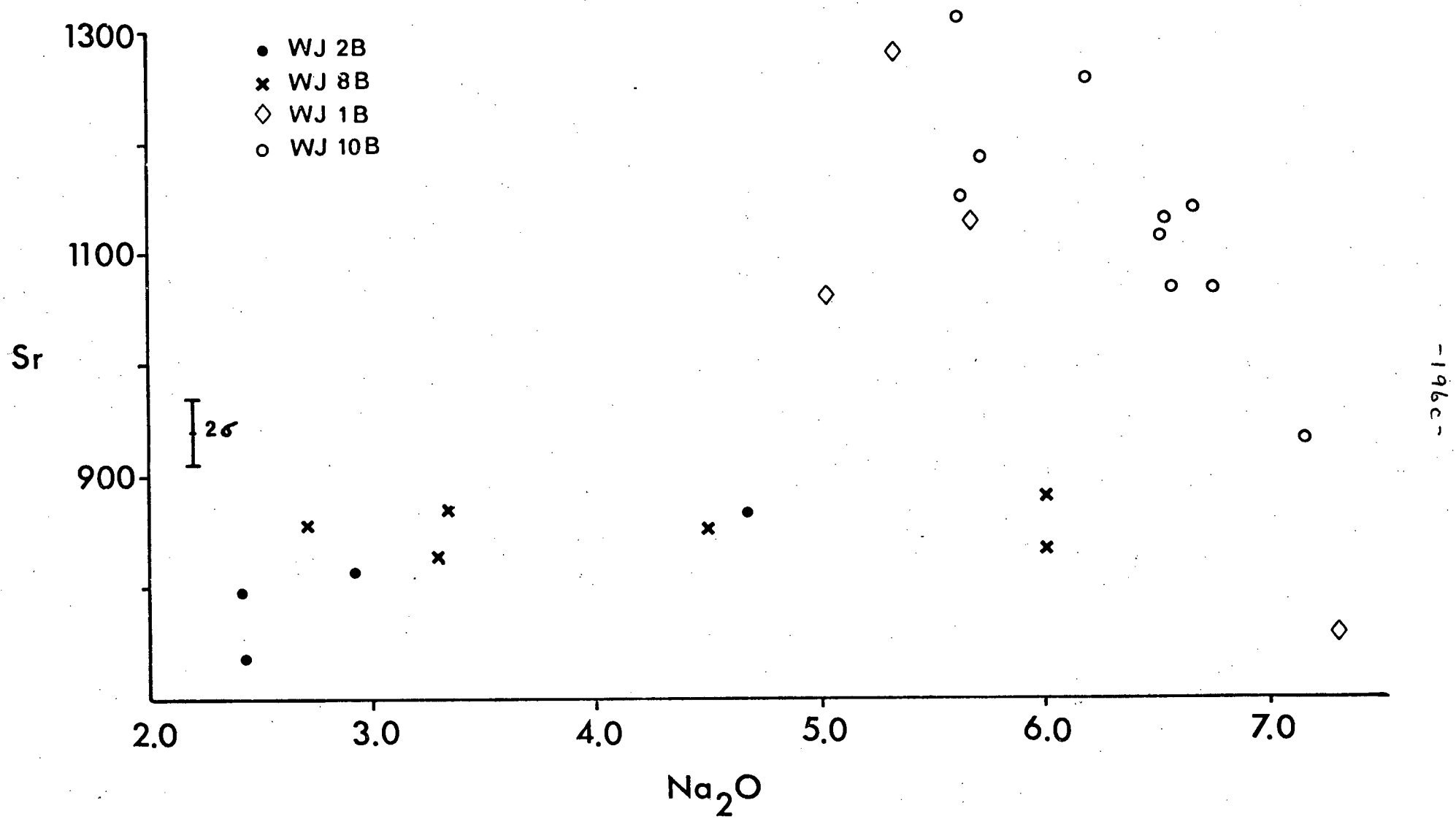

Fig. 5-11: Variation of Sr with Na_2O content in Bouvet Island plagioclase.

microphenocryst/matrix pair from benmoreite WJ10B, a $D^{Sr}_{plag} = 6.15$ (An_{24}) is obtained, again in reasonable agreement with data from Korringa and Noble (1971) who give $D^{Sr}_{plag} = 7.0$ (An_{30}).

4.3.4 Clinopyroxene:

Average clinopyroxene analyses are presented in Table 5-7 and individual analyses are depicted in Fig. 5-12 where the trends for Skaergaard 'tholeiite' pyroxenes and Tristan da Cunha 'alkali' pyroxenes are shown for comparison.

Titaniferous augite is the typical clinopyroxene of hawaiite WJ2B and shows a relatively constant composition of $Wo_{43}En_{40}Fs_{17}$ (Table 5-7, No. 1). Microphenocrysts show slight depletion in wollastonite component relative to enstatite but have a similar ferrosilite composition (Table 5-7, No. 2). Clinopyroxene phenocrysts, present as subophitic intergrowths with plagioclase, are chemically indistinguishable from those forming discrete grains.

The clinopyroxenes of the highly phyric hawaiite (WJ8B) are significantly more magnesian and are also near constant in composition, averaging $Wo_{44}En_{44.5}Fs_{11.5}$ (Table 5-7, No. 3). With respect to minor elements, the clinopyroxenes of WJ8B are depleted in TiO_2 and Al_2O_3 and enriched in Cr_2O_3 relative to WJ2B clinopyroxenes.

Mugearite WJ1B is characterised by augitic clinopyroxene showing a limited compositional range and having average composition $Wo_{41}En_{31}Fs_{22}$ (Table 5-7, No. 4). Clinopyroxene phenocrysts in benmoreite WJ10B show a range in composition from $Wo_{41}En_{34}Fs_{25}$ to $Wo_{41}En_{27}Fs_{32}$ (Table 5-7, No's. 5 and 6). With respect to minor elements, they are depleted in TiO_2 and Al_2O_3 relative to those present in the mugearite. A small degree of zoning is present in some grains and reverse zoning of appro-

T A B L E 5-7

BOUVET ISLAND: REPRESENTATIVE CLINOPYROXENE ANALYSES.

	1	2	3	4	5	6
SIO2	48.05	48.62	50.48	50.58	50.16	49.88
TIO2	2.34	2.38	1.23	1.09	1.06	.49
AL203	4.56	4.26	3.19	2.12	1.89	.86
CR203	.02	-	.18	-	-	-
FEO	10.48	10.42	7.13	13.44	15.01	19.06
MNO	.17	.23	.17	.38	.49	.68
MGO	13.50	14.12	15.49	12.52	11.74	8.92
CAO	20.04	19.15	21.17	19.03	19.19	19.01
NA20	.45	.39	.34	.37	.36	.36
K20	-	-	-	-	-	-
TOTAL	99.61	99.57	99.38	99.53	99.90	99.26

* * ATOMIC PROPORTIONS BASED ON SELECTED NO. OF OXYGENS * *

OXYGEN	6	6	6	6	6	6
SI	1.817	1.832	1.883	1.927	1.921	1.962
ALIV	.183	.168	.117	.073	.079	.038
ALVI	.021	.022	.023	.022	.007	.002
TI	.067	.067	.035	.031	.031	.014
CR	.001	-	.005	-	-	-
FE2+	.331	.328	.222	.428	.481	.627
MN	.005	.007	.005	.012	.016	.023
MG	.761	.793	.861	.711	.670	.523
CA	.812	.773	.846	.777	.788	.801
NA	.033	.029	.025	.027	.027	.027
K	-	-	-	-	-	-
SUM	4.031	4.020	4.022	4.008	4.019	4.017
	WO 42.64	WO 40.81	WO 43.85	WO 40.55	WO 40.63	WO 41.06
	EN 39.95	EN 41.85	EN 44.62	EN 37.10	EN 34.57	EN 26.80
	FS 17.41	FS 17.33	FS 11.53	FS 22.35	FS 24.80	FS 32.14

* * * S A M P L E D I R E C T O R Y * * *

ANALYSIS NO.	DESCRIPTION	ANALYSIS NO.	DESCRIPTION
1	AVERAGE PHENOCRYST, HAWAIITE - WJ 2B	4	AVERAGE PHENOCRYST, MUGEARITE
2	AVERAGE MICROPHENOCRYST, HAWAIITE-WJ 2B	5	MOST MG-RICH PHENOCRYST, BENMOREITE
3	AVERAGE PHENOCRYST, CUMULATE - WJ 8B	6	MOST FE-RICH PHENOCRYST, BENMOREITE

ximately 2 mol.% Fs is not uncommon. There is little compositonal difference between clinopyroxene present as inclusions in plagioclase and those present as discrete grains, both showing a range in composition.

The major end-member components (Wo, En, Fs) of the Bouvet Island clinopyroxenes describe a smooth compositional variation of iron enrichment with associated slight Ca depletion through the sequence hawaiite-mugearite-benmoreite (Fig. 5-12). The Bouvet Island trend is midway between that typical for alkaline magmas (i.e. a trend parallel to the Di-Hd join; Barberi et al., 1971) and that characterising typical tholeiitic pyroxenes (e.g. Skaergaard, which follows a trend of marked initial decrease in calcium content with iron enrichment).

Minor and/or trace element contents of minerals are often more sensitive indicators of consanguinity within a lava series than major element contents. Fig. 5-13 depicts variations of selected minor elements as a function of ferrosilite content. Though there is a relatively large degree of scatter in the plots, two salient features can be noted.

(1) There is a smooth variation with increasing ferrosilite component through the series hawaiite to benmoreite, with a decrease in Al_2O_3, Na_2O and TiO_2 and an increase in MnO.

(2) The clinopyroxenes of the highly phyric hawaiite WJ8B are displaced from these trends.

The variation in TiO_2 and SiO_2 with Al_2O_3 is also shown in Fig. 5-13. The decreasing Al_2O_3 content with increasing SiO_2 in the Bouvet Island pyroxenes in going from hawaiite through to benmoreite can be attributed to increasing degree of silican saturation (La Bas, 1962), while the well documented close correlation between Al_2O_3 and TiO_2 (La Bas, 1962;

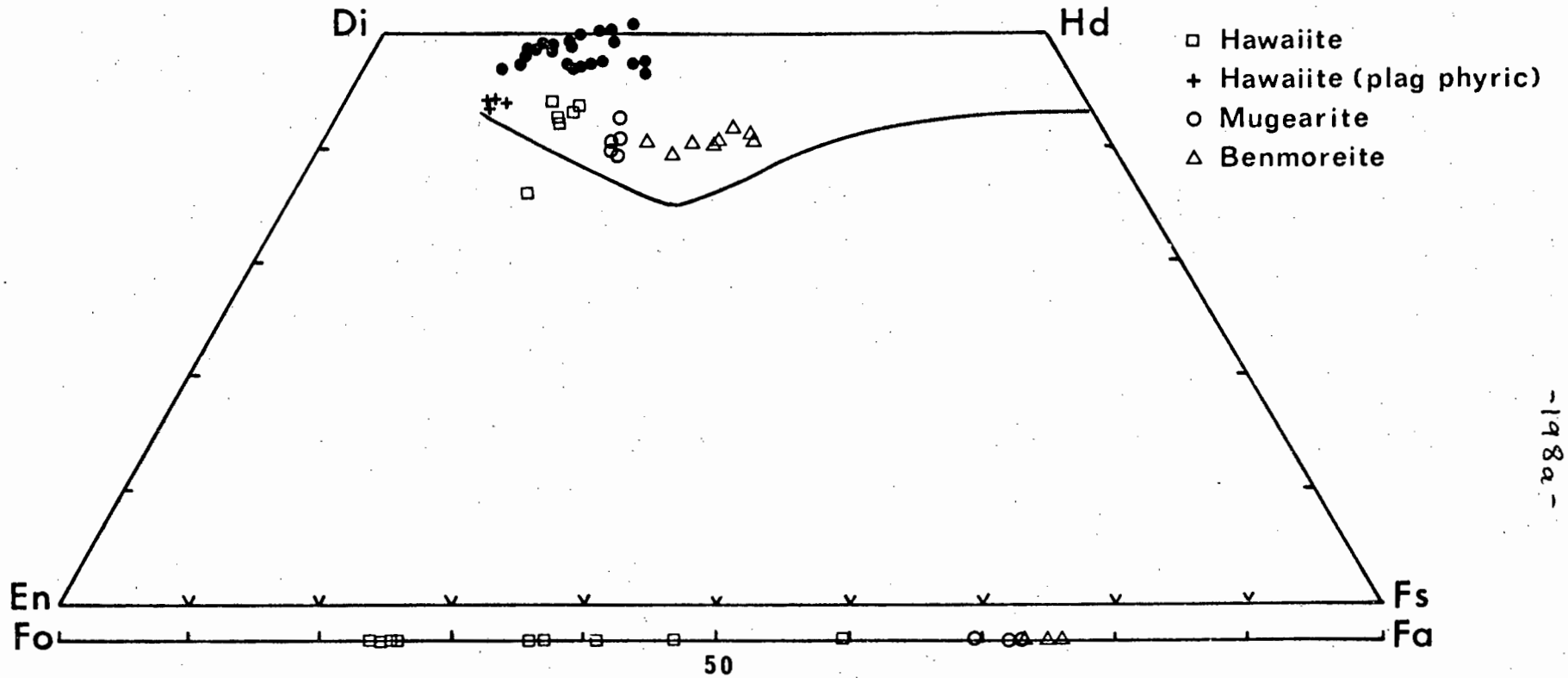

Fig. 5-12: Pyroxene and olivine compositional variation in Bouvet Island lavas. Solid trend line reflects the variation observed in clinopyroxene from the Skaergaard Intrusion. Filled circles show the variation in pyroxene composition from Tristan da Cunha (A.P. le Roex, unpubl. data).

Fig. 5-13: Minor element variation with respect ferrosilite and Al_2O_3 content in pyroxenes from Bouvet Island. Symbols are as follows;

- ● Hawaiite
- ✖ Hawaiite (plag. phyric)
- ◇ Mugearite
- O Benmoreite

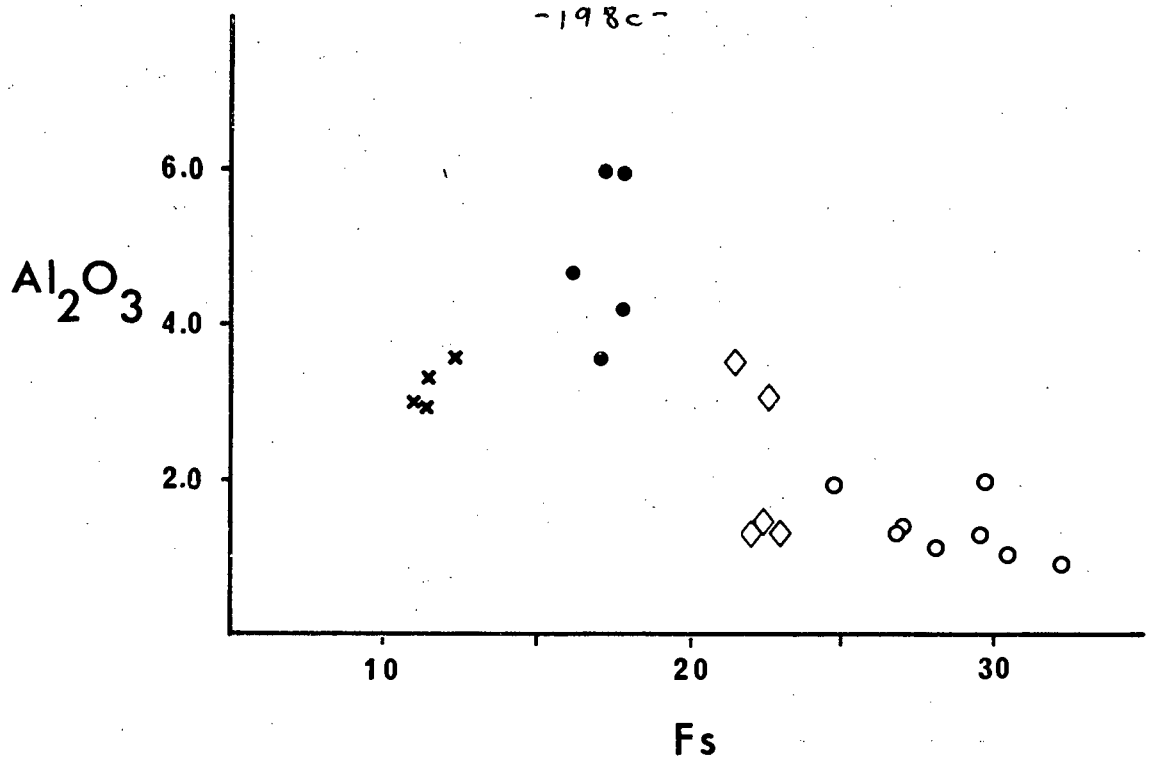
Al_2O_3
6.0
4.0
2.0
10
20
30
Fs

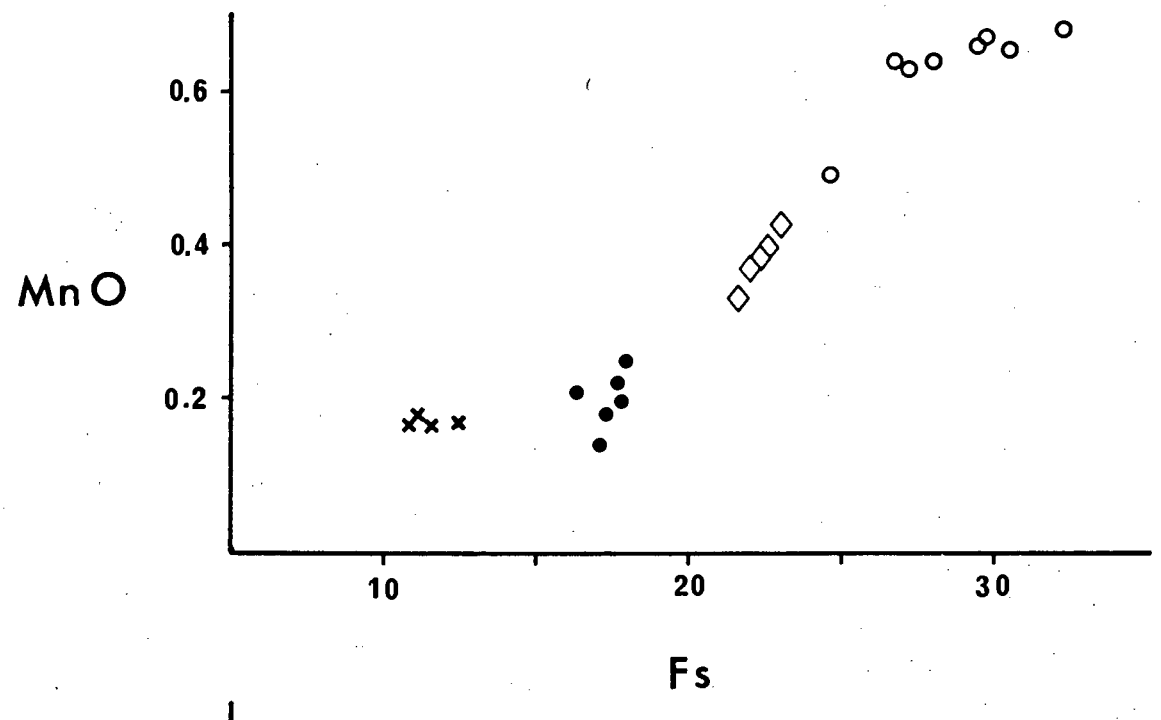
MnO
0.6
0.4
0.2
10
20
30
Fs

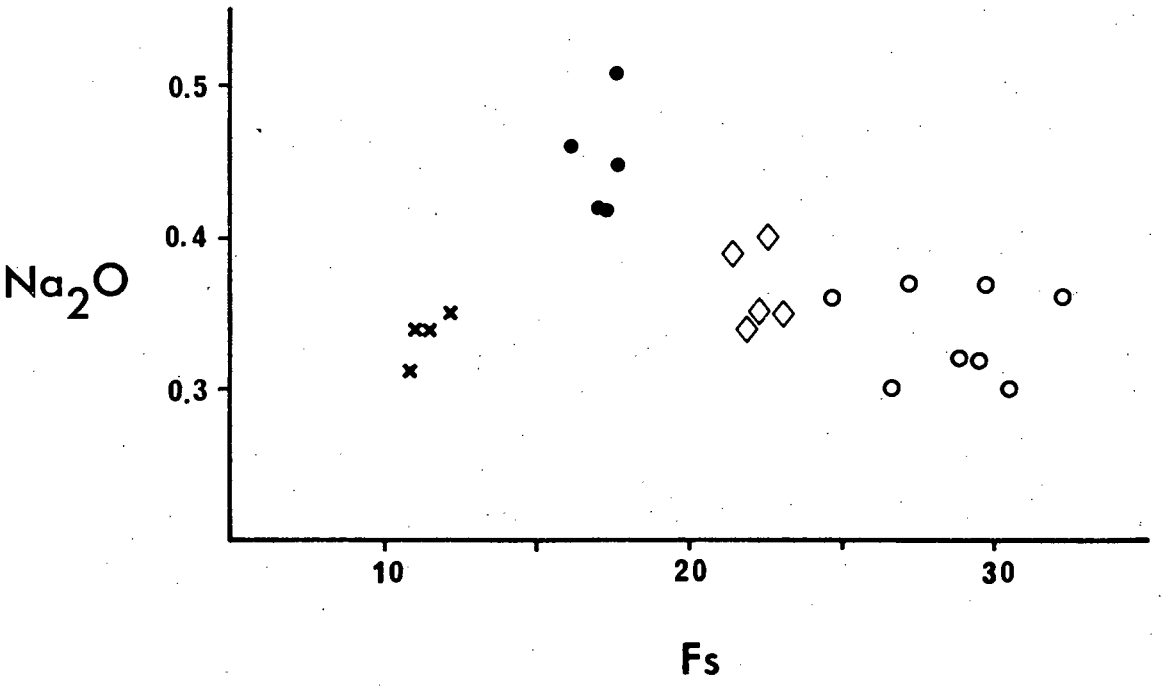
Na_2O
0.5
0.4
0.3
10
20
30
Fs

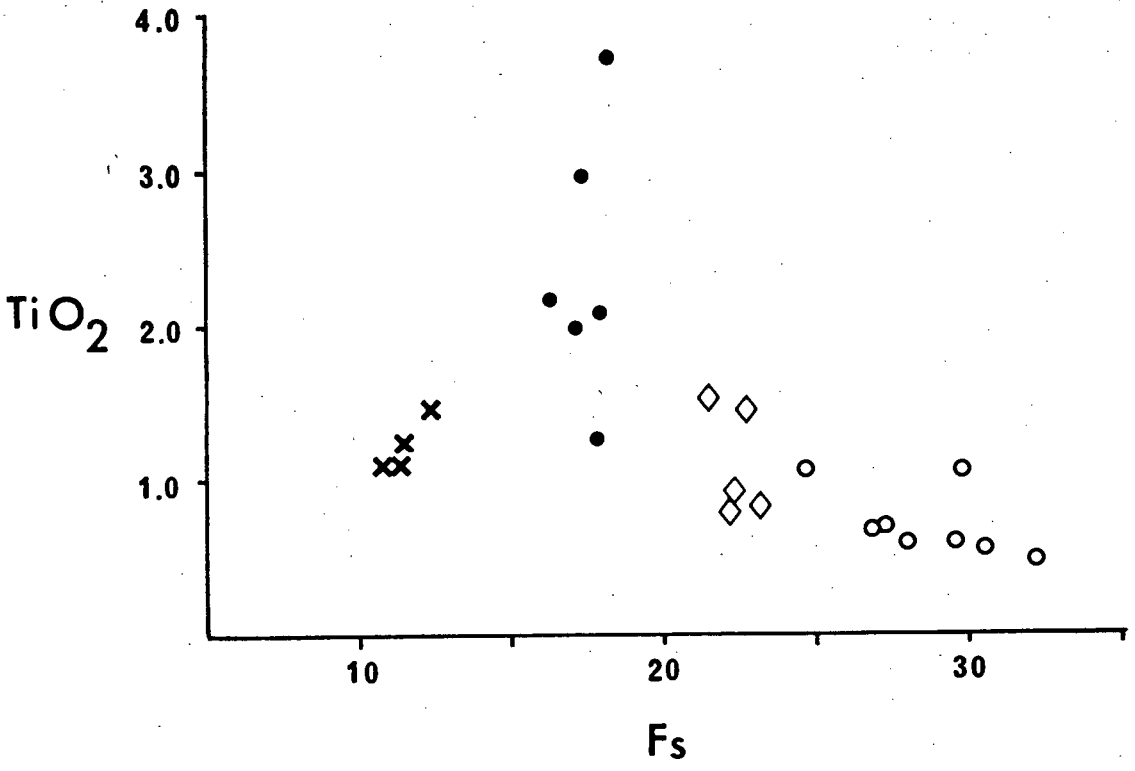
4.0
3.0
2.0
1.0
TiO2
10
20
30
Fs

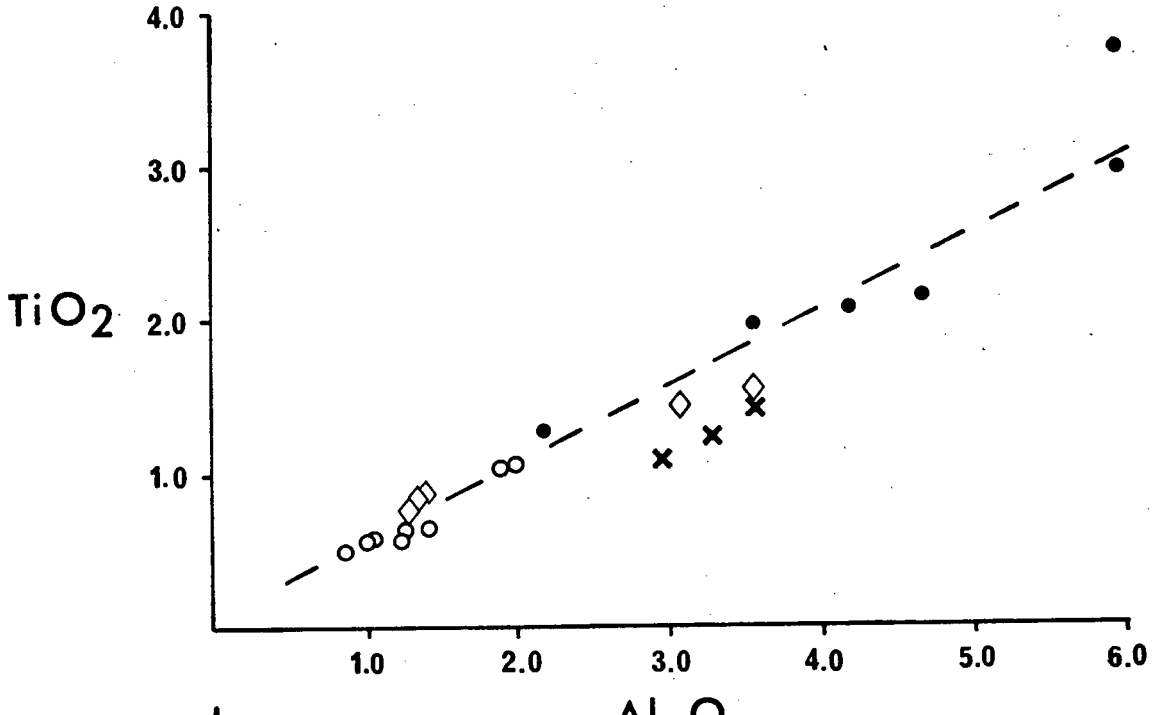
4.0
3.0
2.0
1.0
TiO2
1.0
2.0
3.0
4.0
5.0
6.0
Al2O3

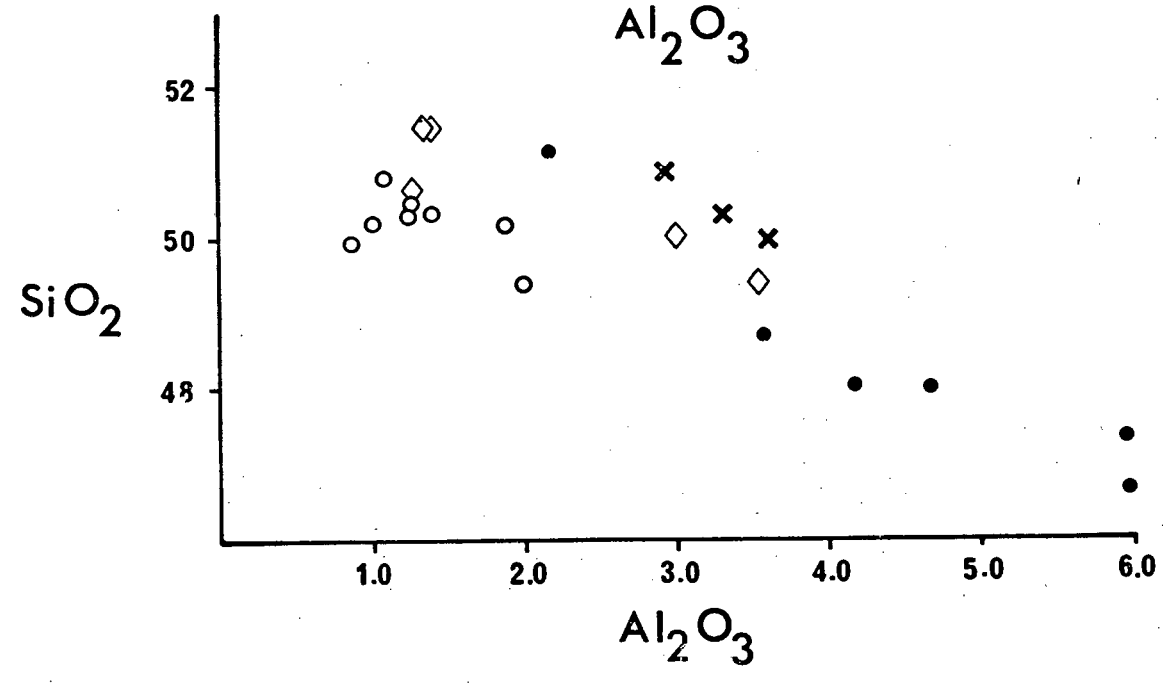
52
50
48
SiO2
1.0
2.0
3.0
4.0
5.0
6.0
Al2O3

Kushiro et al., 1970; Ross et al., 1970) has been suggested to be directly controlled by silica content (Verhoogen, 1962). Schweitzer et al. (1979) have suggested that a common substitution in pyroxenes is Al for Si in a tetrahedral site, combined with Ti for Mg in an octahedral site. In both these figures the anomalous composition of the pyroxenes from the highly phyric hawaiite WJ8B is again evident. As for the Bouvet Island olivines, there is a smooth variation in the composition of the Bouvet Island clinopyroxenes from hawaiite through to benmoreite, supporting the postulation of a relatively simple differentiation model for the evolved Bouvet Island lavas. The minor element composition of clinopyroxenes from the highly phyric hawaiite WJ8B, however, appears to preclude a simple plagioclase cumulation model relating these lavas to the sparsely phyric hawaiites.

An attempt was made to determine the Sr contents of Bouvet clinopyroxenes. Typical concentrations range from 86 to 114 ppm (Table 5-6), which is only just above the detection limit (70 ppm) and, considering that the statistical error is $\pm$ 30 ppm, any meaningful interpretation is severely limited. Calculated mineral/bulk rock distribution coefficients range from 0.15 to 0.37, increasing from hawaiite through mugearite to benmoreite.

4.3.5 Fe-Ti Oxides:

With the exception of the rhyolite, Fe-Ti oxides are ubiquitous in all the Bouvet Island lavas. The hawaiites are characterised by the presence of both ilmenite and titanomagnetite, or only ilmenite (WJ8B), whereas the mugearite and benmoreites have titanomagnetite as the opaque phase. Average compositions of the oxide minerals are presented in Table 5-8.

TABLE 5-8

BOUVET ISLAND: REPRESENTATIVE FE-TI OXIDE ANALYSES.

	1	2	3	4	5	6	7
SIO2	.14	.30	.12	.27	.22	.32	.25
TIO2	50.11	22.97	47.80	19.97	48.20	23.81	23.41
AL2O3	.10	1.51	.08	.73	.09	.59	1.63
CR2O3	-	-	-	-	-	-	-
FE2O3	6.51	22.73	10.10	28.81	9.61	21.55	21.76
FEO	41.41	50.58	41.23	48.81	41.27	52.10	50.62
MNO	.48	.66	.95	.27	.52	.57	.81
MGO	1.74	1.09	.38	.43	.75	.42	1.16
CAO	.19	.11	.21	.15	.37	.22	.09
NA2O	-	-	-	-	-	-	-
K2O	-	-	-	-	-	-	-
TOTAL	100.68	99.95	100.87	99.44	101.03	99.58	99.73

* * ATOMIC PROPORTIONS BASED ON SELECTED NO. OF OXYGENS * *

OXYGEN	3	4	3	4	3	4	4
SI	.003	.011	.003	.010	.005	.012	.009
AL	.003	.066	.002	.032	.003	.026	.071
TI	.934	.639	.901	.565	.903	.671	.652
CR	-	-	-	-	-	-	-
FE3+	.121	.633	.190	.816	.180	.608	.606
FE2+	.859	1.566	.864	1.537	.860	1.633	1.568
MN	.010	.021	.020	.009	.011	.018	.025
MG	.064	.060	.014	.024	.028	.023	.064
CA	.005	.004	.006	.006	.010	.009	.004
NA	-	-	-	-	-	-	-
K	-	-	-	-	-	-	-
SUM	2.000	3.000	2.000	3.000	2.000	3.000	3.000
	IL 87.44	US 66.89	IL 89.01	US 58.08	IL 88.13	US 68.83	US 68.26
	GK 6.46	MT 33.11	GK 1.42	MT 41.92	GK 2.80	MT 31.17	MT 31.74
	HM 6.10		HM 9.56		HM 9.07		

* * * SAMPLE DIRECTORY * * *

ANALYSIS NO.	DESCRIPTION
1	AVERAGE ILM, HAWAIITE - WJ 2B
2	AVERAGE TI-MGT, HAWAIIIE - WJ 2B
3	AVERAGE ILM, HAWAIITE - WJ 7B
4	AVERAGE TI-MGT, HAWAIITE - WJ 7B
5	AVERAGE ILM, CUMULATE - WJ 8B
6	AVERAGE TI-MGT, MUGEARITE
7	AVERAGE TI-MGT, BENMOREITE

The oxides of WJ2B are confined to the groundmass and are relatively uniform in composition with ilmenite having an average composition of $Il_{88}Gk_6Hm_6$ (Table 5-8, No. 1) and titanomagnetite an average composition of $Us_{66}Mt_{33}$ (Table 5-8, No. 2). Hawaiite WJ7B similarly has both ilmenite and titanomagnetite microphenocrysts. Average ilmenite ($Il_{89.0}Gk_{1.4}Hm_{9.6}$) and titanomagnetite ($Us_{58}Mt_{42}$) are presented in Table 5-8 (No's. 3 and 4).

Sample WJ8B is characterised by the presence of only ilmenite of average composition $Il_{88}Gk_3Hm_9$ (Table 5-8, No. 5). In terms of minor elements, the ilmenites from sample WJ2B are enriched in MgO (i.e. geikelite molecule) relative to those from WJ7B and WJ8B, while titanomagnetite from WJ2B is enriched in both MgO and Al_2O_3 relative to that of WJ7B. The distribution of Mg between oxides and silicates is primarily controlled by the magma composition, and secondly by the paragenetic sequence, temperature of formation and on rates and paths of equilibration (Haggerty, 1976). Due to the extreme similarity in bulk composition of WJ2B and WJ7B, the latter factors are probably dominant in causing differing MgO contents.

Titanomagnetite from the mugearite sample has an average composition of $Us_{69}Mt_{31}$ (Table 5-8, No. 6) and that from the benmoreite a composition of $Us_{68}Mt_{32}$ (Table 5-8, No. 7).

Comparison of the minor element components of the Bouvet Island titanomagnetites shows that those from the benmoreites are slightly enriched in MgO and Al_2O_3 relative to those from the mugearites and similar to those from hawaiite WJ2B. Those from the mugearite are most similar to the titanomagnetite from hawaiite WJ7B.

The presence of coexisting ilmenite and titanomagnetite in

hawaiites WJ2B and WJ7B enable the calculation of crystallisation temperatures and oxygen fugacities for these lavas using the method of Buddington and Lindsley (1964).

To bring natural oxide compositions into accord with the experimental data on pure end-members, the effect of minor constituents (MgO, MnO, Al_2O_3, Cr_2O_3) must be taken into account. Buddington and Lindsley (1964) discuss the problem and suggest a procedure for recalculating natural ilmenites and titanomagnetites in terms of the pure end-members. The minor element content of the Bouvet Island titanomagnetite is, however, sufficiently low to have little effect on the final ulvospinel component. There is, however, significant MgO in the ilmenites necessitating these formulae to be recalculated MgO-free as shown by Buddington and Lindsley (1964).

Using the contours on the T(^{o}C), log fO_2 projection given by Buddington and Lindsley (1964, p. 316), the average ilmenite-titanomagnetite composition of $Il_{93.5}$ - Us_{67} for hawaiite WJ2B gives an estimated oxygen fugacity of $10^{-11.1}$atm. and temperature of $\pm$ 1000^{o}C. Average data for hawaiite WJ7B (Il_{90} - Us_{58}) suggests an fO_2 of $10^{-10.7}$atm. and a temperature of $\pm$ 1000^{o}C.

From the above it can be concluded that the Bouvet Island hawaiites crystallised at an average temperature of 1000^{o}C and at an oxygen fugacity of 10^{-11}atm. This temperature is in good agreement with the experimental work of Knutson and Green (1975) who found a typical hawaiite to be quadruply saturated (olivine-plagioclase-clinopyroxene-opaque) at $\pm$ 1040^{o}C at 5kbar and 2% H_2O.

A number of relationships have been suggested for relating oxygen fugacity and Fe^{3+}/Fe^{2+} ratio (e.g. Fudali, 1965; Roeder and Emslie,

1970; Lindstrom, 1976). Those reported by Fudali (1965) and Roeder and Emslie (1970) relate fO_2 to Fe^{2+}/Fe^{3+} at constant temperature (1200°C), while the relationship reported by Lindstrom (1976):

$$\log \frac{Fe^{2+}}{Fe^{3+}} = \frac{-6300}{T(K)} + 3.01 - \tfrac{1}{4} \log fO_2$$

incorporates a temperature effect as well.

Using Lindstrom's (1976) relationship, an Fe_2O_3/FeO ratio of 0.17 is calculated for the hawaiites at the time of extrusion. This, however, is unlikely to be a liquidus Fe_2O_3/FeO ratio as cooling can be regarded as a process of oxidation, even though cooling causes a decrease in fO_2 (Verhoogen, 1962). An idea of the Fe_2O_3/FeO ratio at liquidus temperatures can be obtained at the cost of two assumptions. Firstly, it is necessary to assume a liquidus temperature. It has been argued (Section 4.3.2) that olivine compositions suggest a temperature of 1100°C. Assuming olivine to be the liquidus phase (and this is supported by experimental data of Knutson and Green, 1975), this temperature can be used as an approximate liquidus temperature. Secondly, the oxygen fugacity at the time of olivine crystallisation must be assumed. This can be derived using the data of Kennedy (1948) which show a change in fO_2 of approximately an order of magnitude for every 100°C in temperature (Fudali, 1965). On this basis the liquidus fO_2 would be 10^{-10} atm. Insertion of this parameter into Lindstrom's (1976) relationship gives an Fe_2O_3/FeO ratio of 0.13 at liquidus temperatures.

5. PETROGENESIS

5.1 General Statement

The overall whole rock chemical variations with respect to both major and trace elements in the Bouvet Island lavas, coupled with the

observed smooth variations in mineral chemistry are strongly suggestive of a consanguineous lava suite. Further evidence for a close genetic relationship among the lavas is found in the similar $^{87}Sr/^{86}Sr$ ratios (0.70369 $\pm$ 3) of the hawaiites and benmoreites (O'Nions and Pankhurst, 1974).

In the following section a fractional crystallisation model is quantitatively investigated and shown to describe adequately the observed compositional variations in the Bouvet Island lavas. Though partial melting could theoretically account for at least the trace element variations, the evolved nature of the lavas, i.e. low Mg-numbers (atomic Mg/Mg+Fe) and low Ni contents preclude their direct derivation from typical mantle (see Chapter III, Section 7). Furthermore, it is generally accepted that more evolved alkaline rocks, including hawaiites, mugearites and benmoreites have formed by crystal fractionation at low or high pressure from more primitive basaltic magma (Green and Ringwood, 1967; Ito and Kennedy, 1967; and Green et al., 1974). Considering the successful application of fractional crystallisation models to other lava suites of similar composition, e.g. Reunion Island (Ludden, 1978a, 1978b) and Kenya Rift (Baker et al., 1977) and the successful accounting of the variation in the Bouvet Island lavas by this means, it is felt to be unwarranted to turn to more complicated partial melting melting models of undetermined source areas. Baker et al. (1977) examined a similar problem with respect to the benmoreites and trachytes of the Kenya Rift and found that partial melting models could not adequately account for the trace element abundances.

5.2 Choice of Parental Magma Composition

The most primitive lavas yet returned from Bouvet Island are the

Table 5-10: Predicted and observed trace element content of the Bouvet Is. Mugearite using the results of the least squares approximation given in Table 5-9. The sources of the distribution coefficients used are discussed in the text.

A. Distribution coefficients.

Element	PLAG	OL	CPX	IL	Ti-MGT	APAT.
Zr	0.01	0.01	0.21	0.28	0.24	0.01
Nb	0.01	0.01	0.09	0.8	2.16	0.01
Y	0.20	0.12	0.70	0.1	0.17	16.9
Rb	0.01	0.01	0.01	0.01	0.01	0.01
Ba	0.01	0.01	0.01	0.01	0.01	0.10
Sr	2.30	0.01	0.12	0.01	0.01	2.0
Ga	1.1	0.03	0.4	0.14	2.0	0.01
Co	0.04	10.7	4.5	2.2	10.0	0.20
Sc	0.15	0.20	5.0	1.8	3.0	0.22
V	0.01	0.04	4.0	12.0	45.0	0.01
Th	0.01	0.01	0.01	0.01	0.01	1.3
U	0.01	0.01	0.01	0.01	0.01	4.0

B. Trace element check.

	HAWAIITE	MUGEARITE	
	OBS.	CALC.	OBS.
Zr	268	451	473
Nb	42	68	70
Y	36	50	53
Rb	21	38	40
Ba	243	433	446
Sr	448	415	419
Ga	23	27	26
Co	45	15	18
Sc	28	16	15
V	303	54	48
Th	3.0	5.3	5.9
U	0.9	1.6	1.6
P_2O_5	.47%	0.68%	0.66%

present in the mugearite. Therefore it is feasible that apatite might comprise an extremely small (0.2%) portion of the crystal fractionate.

Though all trace elements show good agreement, many of the data are not tightly constrained due to the wide ranges in published distribution coefficients. The trace elements which are most tightly constrained are those for which distribution coefficients are extremely small for all mineral phases present (i.e. are totally incompatible). The elements which satisfy these requirements in the passage from hawaiite to mugearite are Rb, Ba, Th and U. Though Th and U possibly have significant D's for apatite (values estimated from data in Ludwig and Stuckless, 1978), the extremely small amount of apatite fractionation has little effect on the bulk D. The extremely good agreement for these elements is therefore a good test of the model.

Distribution coefficients used in the calculations presented in Table 5-10 have been selected from Tables A2-1, A2-2, A2-5, A2-8, A2-9 and A2-11 as being realistic estimates similar to, or within ranges of, published distribution coefficients. Where a choice has been available within these criteria, those values giving the better trace element match have been selected. Values of 0.01 have been arbitrarily assigned to cases where a given element is generally regarded as being totally excluded from a given mineral.

The slightly low predicted Zr in the mugearite is dominantly controlled by the distribution coefficient used for clinopyroxene. The value used is that obtained from two mineral separates from Gough Island lavas (Chapter II) which corresponds to the upper limit of the experimentally determined values of McCallum and Charette (1978). Using the lower limit of their range ($D^{Zr}_{cpx} = 0.05$) gives a value of 464 ppm which

is in closer accord with that observed (473 ppm). The choice of values for ilmenite (taken from McCallum and Charette, 1978) and titanomagnetite (taken from this study, Chapter II) have only a small influence on the predicted Zr due to their relatively low weight fraction in the crystal fractionate.

Selection of data for Y was somewhat more arbitrary. The dominant control on Y variation is the small fraction of apatite required to satisfy P_2O_5 variations. It has been assumed that D^{Y}_{ap} is possibly similar to D^{Dy}_{ap} on the basis of the well known chemical coherency of Y with the heavy rare earth elements (e.g. Frey et al., 1978). Nagasawa and Schnetzler (1971) report a $D^{Dy}_{ap} = 16.9$ for dacitic rocks and this value has been arbitrarily selected as an approximation to D^{Y}_{ap}. The value of $D^{Y}_{plag} = 0.18$ is that obtained for a mineral separate from Gough Island (Chapter II), in preference to the significantly lower experimental results of Drake and Weill (1975) ($D^{Y}_{plag} = 0.01$-0.03): the resultant difference in calculated Y is small. The value of 0.7 for D^{Y}_{cpx} is similarly taken from the average mineral separate from Gough Island and corresponds to phenocryst/matrix data of Ewart and Taylor (1969). There is therefore a significant choice in the selection of distribution coefficients for Y, any combination of which could yield the desired result. The chosen values are felt to be the most realistic.

Rb and Ba have been regarded as being totally incompatible, while Sr enters plagioclase to a significant degree and clinopyroxene to a lesser extent. D^{Sr}_{plag} of 2.30 is in agreement with data from Philpotts and Schnetzler (1970) and Berlin and Henderson (1968) for plagioclase of similar composition, but significantly less than that obtained by Korringa and Noble (1971) ($D^{Sr}_{plag} = 3.8$; An_{60}). The range in published

data, coupled with the probable effect of factors such as temperature and magma composition on D^{Sr}_{plag} (Drake and Weill, 1975), makes the choice of a suitable D somewhat arbitrary within reasonable limits. It should, however, be noted that while the major element model predicts an average plagioclase composition of An_{58}, the fractionating plagioclase is likely to have continually changed in composition from $\pm$ An_{75} (ave. hawaiite) to $\pm$ An_{40} (ave. mugearite), with a corresponding change in D^{Sr}_{plag}. The estimate of $D^{Sr}_{plag} = 2.3$ is therefore not thought to be unreasonable.

Co readily enters all ferromagnesian minerals and opaques with large and variable D's. Values for titanomagnetite, ilmenite and plagioclase have been taken from Paster et al. (1974) and Lindstrom (1976). Published data on clinopyroxene indicate a strong compositional and/or temperature effect on D^{Co}_{cpx} (Lindstrom, 1976; Ewart et al., 1973). The data from Lindstrom (1976) suggests a $D^{Co}_{cpx} = 4.5$ for a temperature of 1000°C, which is a reasonable estimate of the temperature at which fractionation took place (Section 4.3.5). The formula relating temperature to D^{Co}_{ol} given by Leeman and Scheidegger (1977),

$$\ln D^{Co}_{ol} = \frac{9676}{T(K)} - 5.23$$

gives a D^{Co}_{ol} of 10.7 for a temperature of 1000°C. These values have therefore been selected as the most realistic values to use in the fractionation model.

The distribution of the REE's enables a further test for the validity of the fractionation model. Although the REE's have been determined on hawaiites WJ2B, WJ16B and WJ7B, the latter was excluded due to its anomalously low La value relative to the former two, and the average of samples WJ2B and WJ16B has been taken as representative of

Table 5-11: A. Phenocryst/liquid distribution coefficients for the REE used in crystal fractionation calculations. Values are from Ludden (1978a) except for the apatite data which are from Nagasawa and Schnetzler (1971). La and Tb values were extrapolated from Ce and Gd respectively.

B. Chondrite normalised REE check for fractionation model relating the average Bouvet Is. hawaiite to the Bouvet Is. mugearite using the results of the least squares approximation given in Table 5-9.

A. Distribution coefficients.

Element	PLAG	OL	CPX	IL+MT	APAT
La	0.12	0.01	0.10	0.05	14.0
Ce	0.11	0.009	0.12	0.05	16.6
Sm	0.11	0.006	0.38	0.05	20.7
Eu	*	0.006	0.39	0.05	14.5
Tb	0.10	0.010	0.50	0.05	19.3
Yb	0.10	0.010	0.60	0.05	9.4
Lu	0.10	0.010	0.60	0.05	7.9

* D^{Eu}_{plag} An_{60} = 0.60, An_{53} = 0.70

B. REE check

	HAWAIITE	MUGEARITE	
	OBS.	CALC.	OBS.
La	101	165	164
Ce	64	103	109
Sm	51	79	79
Eu	44	60	63
Tb	31	46	46
Yb	14	21	22
Lu	12	18	18

the hawaiites. Results of the modelling calculations are presented in Table 5-11B, with the applicable distribution coefficients listed in Table 5-11A.

The excellent agreement between the predicted and observed REE content of the mugearite further attests to the consistency of the proposed fractionation model. The slight discrepancy in Ce is difficult to explain as the Ce distribution coefficient is relatively small for all phases except apatite. However, D^{Ce}_{ap} would have to be lowered to zero to produce the required enrichment, which is obviously not justified. The slight discrepancy for Eu could easily be accounted for by a selection of slightly lower D^{Eu}_{plag}. Though the value of 0.60 for D^{Eu}_{plag} was selected as corresponding to a plagioclase composition of An_{60} (Ludden, 1978), the distribution coefficient is also dependent on factors such as temperature and oxygen fugacity (Drake and Weill, 1975) and so selection of a slightly lower value would not necessarily be unrealistic ($D^{Eu}_{plag} = 0.50$ gives an estimated Eu content of 62.5 ppm in contrast to 60.8 ppm, Table 5-11).

The success of the proposed model in relating the major element compositions of the average Bouvet Island hawaiite to the mugearite, coupled with the excellent agreement obtained for the trace elements, attests to the consistency of the proposed low pressure fractionation model relating these lava types.

5.4.2 Benmoreites:

The Bouvet Island benmoreites have been suggested to represent a very recent (between 1955 and 1958) eruption (Baker and Tomblin, 1964), and various petrogenetic schemes can theoretically be suggested for their evolution from the more basic rock types. Two such models are

presented schematically below:

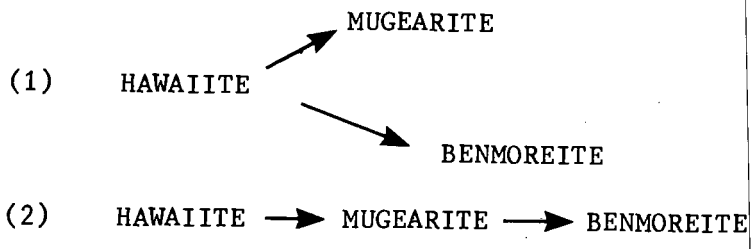

In model (1) hawaiite differentiates directly to give benmoreite, while in model (2) hawaiite differentiates to mugearite which in turn experiences further differentiation to give benmoreite.

A least squares approximation representing model (1), i.e. direct derivation of the benmoreites from a parental hawaiite is presented in Table 5-12, together with the input data. The benmoreite composition used is the average of the five benmoreites analysed (Table 5-2).

The model suggests that to produce a magma with a composition of the average Bouvet Island benmoreite, it is necessary to fractionally crystallise 63.7% of the parental hawaiite. The crystallising minerals comprise 32.5% plagioclase (An_{53}), 4.7% olivine (Fo_{57}), 18.3% clinopyroxene ($Wo_{43}En_{39}Fs_{18}$), 3.4% ilmenite (Il_{86}), and 4.6% titanomagnetite (Us_{66}). To satisfy the P_2O_5 content of the benmoreite, it is necessary for apatite to comprise 0.78% of the fractionate. The abundance of apatite needles poikilitically enclosed in clinopyroxene, plagioclase and opaque oxides in benmoreite WJ10B attests to the feasibility of minor apatite fractionation. The small amount of apatite necessary will have negligible effect on the major element least squares approximation.

It is interesting to note that, with the exception of plagioclase which has a slightly more evolved composition, the minerals fractionating to produce the benmoreite are identical to those required for the

Table 5-12: Least squares approximation relating the average Bouvet Is. hawaiite to the average Bouvet Is. benmoreite.

Input data

	HAWAIITE	PLAG	OL	CPX	IL	Ti-MGT	BENMOREITE
SiO_2	50.47	54.02	35.28	48.68	0.15	0.23	61.40
TiO_2	3.66	0.16	0.11	2.03	50.00	23.61	1.20
Al_2O_3	15.46	28.30	0.06	3.90	0.07	0.48	15.13
FeO*	12.25	0.75	36.25	10.69	47.02	74.44	9.13
MnO	0.19	0.01	0.51	0.17	0.53	0.51	0.28
MgO	4.28	0.13	27.29	13.54	2.04	0.22	1.04
CaO	8.87	11.08	0.31	20.51	0.18	0.51	4.00
Na_2O	3.50	5.24	0.01	0.47	0.01	0.01	4.79
K_2O	1.31	0.33	0.01	0.01	0.01	0.01	3.02

An 53.37	Fo 57.29	Wo 43.01
Ab 45.68	Fa 42.7	En 39.49
Or 0.95		Fs 17.50

Least squares approximation

	HAWAIITE			MIX		
	OBS.	EST.	DIFF.	COMP.	Wt.%	S.D.
SiO_2	50.47	50.48	0.01	BENMOREITE	36.30	.46
TiO_2	3.66	3.66	0.00	PLAG	32.55	.43
Al_2O_3	15.46	15.45	-0.01	OL	4.73	.30
FeO*	12.25	12.25	0.00	CPX	18.33	.35
MnO	0.19	0.20	0.01	IL	3.43	.20
MgO	4.28	4.27	-0.01	Ti-MGT	4.58	.23
CaO	8.87	8.86	-0.01			
Na_2O	3.50	3.53	0.03	TOTAL	99.91	.84
K_2O	1.31	1.21	-0.10			

Sum of squares of differences = 0.011

derivation of the less evolved mugearite. Furthermore, the relative proportions of the minerals are very similar in both cases (mugearite: plagioclase:clinopyroxene:olivine:opaque = 47:32:9:12, and benmoreite: 51:29:7:12). These factors suggest that the Bouvet Island hawaiites correspond in composition to a five-phase saturation surface plag + cpx + ol + opaque + liq and that the differentiated lavas resulted from differing degrees of crystallisation on this surface.

Comparison of predicted and observed trace element abundances in the Bouvet Island benmoreites (Table 5-13) using the results of the major element modelling verifies the feasibility of a fractional crystallisation model. Distribution coefficients used in the calculations are, with the exception of Ba, Sr and Eu, the same as those used for the modelling of the mugearite trace element variations (Tables 5-10 and 5-11).

Although it is generally assumed that Ba is incompatible with respect to plagioclase feldspar, a number of studies (e.g. Hart and Brooks, 1974; Paster et al., 1974; Nagasawa and Schnetzler, 1971; Sun and Hanson, 1976; Ewart and Taylor, 1969; Ewart et al., 1973) have found that Ba can show significant plagioclase/liquid distribution coefficients. This is also borne out by the mineral separate from Gough Island which gives a $D^{Ba}_{plag} = 0.3$ (Chapter II).

To satisfy the Ba content in the benmoreite, it is necessary to postulate a $D^{Ba}_{plag} = 0.25$ which, though well within the range of published data (Table A2-2), is inconsistent with the value used for the modelling of the mugearite ($D^{Ba}_{plag} = 0.01$). Though it is generally found that crystal/liquid distribution coefficients increase with increasing polymerization of a silicate melt (e.g. Henderson, 1977; Watson, 1977;

Lindstrom, 1976), Ryerson and Hess (1978) have shown that Ba partitioning is relatively unaffected by polymerization and that D^{Ba}_{plag} values are similar for ferropyroxenetic liquids and granitic liquids. Korringa and Noble (1971) have, however, found that D^{Ba}_{plag} varies linearly with plagioclase composition, with D^{Ba}_{plag} increasing slightly with sodic content of the plagioclase. The similarity in average plagioclase composition (An_{58}-An_{53}), however, precludes such a significant change in distribution coefficient. The similar mineral compositions in the two models suggest a reasonably similar temperature of crystallisation and so significantly lower temperature is unlikely to account for the observed discrepancy. It should be noted, however, that use of an average value, say $D^{Ba}_{plag} = 0.12$, results in only a 6% relative error in both cases and, considering the large F-steps and other assumptions, this is thought to be not unreasonable.

It is well documented that the distribution coefficients of Sr between plagioclase and liquid is very sensitive to plagioclase composition (Philpotts and Schnetzler, 1970; Korringa and Noble, 1971; Drake and Weill, 1975; Sun et al., 1974). The D^{Sr}_{plag} for the benmoreite modelling has therefore been assumed to be slightly higher ($D^{Sr}_{plag} = 2.6$) than that for the mugearite considering the slight but significant difference in plagioclase compositions used.

The REE modelling similarly shows excellent agreement between predicted and observed concentrations for the benmoreite (Table 5-13B). Distribution coefficients used are those given in Table 5-11A, with $D^{Eu}_{plag} = 0.7$ being selected as corresponding to the plagioclase composition An_{53}.

The results of this quantitative modelling therefore suggest it

is quite feasible for the Bouvet Island benmoreites to be derived directly from the average hawaiite by fractional crystallisation of plagioclase, olivine, clinopyroxene, ilmenite, titanomagnetite and minor apatite. The derivation of the benmoreites from the mugearite magma (Model (2)) has been quantitatively tested and found to be improbable for a number of reasons. Firstly, with respect to the major element least squares approximation, it is necessary to postulate the fractionation of a small amount of alkali-feldspar, which is not a phenocryst phase in either lava, though does occur as a late-stage groundmass phase in the mugearite. If, however, the major element model is accepted, then the degree of fractionation (55%) is in conflict with the observed enrichment in incompatible elements. Assuming Th to be totally incompatible (i.e. $\bar{D} \sim 0.01$), then only 30% crystallisation is required to account for the enrichment in the benmoreites, a value which is borne out by other (possibly slightly less) incompatible elements such as Rb, U, Nb and Zr. This large discrepancy in degree of crystallisation therefore invalidates the derivation of the Bouvet Island benmoreites from the less evolved mugearite.

5.4.3 Rhyolite:

The most evolved rock type present on Bouvet Island is rhyolite and in the postulated fractionation scheme is the logical end product of extensive fractional crystallisation of the less differentiated lavas. Three possible petrogenetic schemes may be suggested for their evolution:

(1) BENMOREITE ⟶ RHYOLITE

(2) MUGEARITE ⟶ RHYOLITE

(3) HAWAIITE ⟶ RHYOLITE

i.e. derivation of the rhyolite by fractional crystallisation of the benmoreite (Model (1)), by fractional crystallisation of the mugearite (Model (2)), or direct extensive fractional crystallisation of the hawaiite (Model (3)). The latter case is difficult to assess due to the large degree of fractionation required and the extreme change in mineral composition. Models (1) and (2) can, however, be investigated more readily.

In terms of major elements it is possible to derive the rhyolite from the average benmoreite (Model (1)) by fractional crystallisation of 25% plagioclase (An_{47}), 4% olivine (Fo_{26}), 6% clinopyroxene ($Wo_{40}En_{30}Fs_{30}$) and 4% titanomagnetite (Us_{66}). The plagioclase composition (An_{47}) required for this model is, however, unrealistic for two reasons. Firstly, the most calcic plagioclase in the benmoreite corresponds to this composition with the majority of the phenocrysts being significantly more albitic (An_{27}), and so it is unlikely that the average plagioclase fractionated would have a composition of An_{47}. The second even more limiting factor to fractionating such a calcic plagioclase is the marked decreased in Sr and Ba in the passage from benmoreite to rhyolite. Distribution coefficients for Ba in plagioclase are small (generally less than 0.4; Table A2-2), and to satisfy the observed decrease in Ba, a distribution coefficient of $\pm$ 4 for plagioclase (Ba is essentially incompatible for all other phases) is required. Such a value is more in keeping with a feldspar of anorthoclase composition (Sun and Hanson, 1976). To account for the Sr decrease, a $D^{Sr}_{plag} = 10$ is required, which is even greater than typical values for alkali-feldspar (e.g. Korringa and Noble, 1971). The required degree of fractionation, 39%, is also insufficient to enrich the more incompatible

trace elements, e.g. Zr, Nb, Rb, Th and U, to the required extent. It can therefore be concluded that the derivation of the Bouvet Island rhyolites by fractional crystallisation of the average benmoreite is improbable.

The evolution of the mugearite by fractional crystallisation can, however, give rise to a magma of similar composition to the rhyolite (i.e. Model (2)). A preferred least squares approximation relating rhyolite WJ18B to mugearite WJ1B is presented in Table 5-14 together with the input data. The olivine, clinopyroxene and titanomagnetite have been selected as typical compositions present in the mugearite (these phases are absent from the rhyolite). Feldspars in the mugearite range in composition from plagioclase (An_{44}) to 'anorthoclase' ($Or_{27}Ab_{64}An_{9}$), while those present in the rhyolite are anorthoclase ($Or_{30}Ab_{68}An_{2}$). The feldspar used in the modelling therefore corresponds to a combination of the two end-members in the approximate proportion of 80:20 (plagioclase:anorthoclase). To derive the rhyolite from a mugearite parent, it is necessary to crystallise 69% of the mugearite by fractionating 44.3% 'feldspar', 4.4% olivine, 12.6% clinopyroxene and 7.7% titanomagnetite. The realistic mineral proportions, their composition and low sum of squares of differences attests to the consistency of this least squares approximation. To account for the marked decrease in P_2O_5 from mugearite (0.55%) to rhyolite (0.01%) requires the additional removal of 1.5% apatite during fractional crystallisation.

Selection of distribution coefficients to model the differentiation of mugearite to rhyolite in terms of trace elements proves somewhat of a problem in the light of the large major element compositional change. It is well documented that distribution coefficients show a

Table 5-14: Least squares approximation relating Bouvet Is. mugearite WJ1B to rhyolite WJ18B.

Input data

	MUGEARITE	FSP	OL	CPX	Ti-MGT	RHYOLITE
SiO_2	55.62	58.42	31.83	51.08	0.23	70.51
TiO_2	2.00	0.01	0.09	0.78	23.61	0.30
Al_2O_3	15.90	26.02	0.02	1.30	0.48	13.47
FeO*	11.21	0.08	53.95	13.62	74.44	4.41
MnO	0.21	0.01	1.15	0.37	0.51	0.12
MgO	2.22	0.01	12.49	12.94	0.22	0.09
CaO	6.12	7.57	0.46	19.57	0.51	0.77
Na_2O	4.42	6.06	0.01	0.34	0.01	5.40
K_2O	2.30	1.72	0.01	0.01	0.01	4.92

An 36.98	Fo 29.21	Wo 40.60
Ab 53.28	Fa 70.79	En 37.34
Or 9.95		Fs 22.06

Least square approximation

	MUGEARITE				MIX	
	OBS.	EST.	DIFF.	COMP.	Wt.%	S.D.
SiO_2	55.62	55.62	0.00	RHYOLITE	31.07	.13
TiO_2	2.00	2.01	0.01	FSP	44.26	.13
Al_2O_3	15.90	15.90	0.00	OL	4.42	.12
FeO*	11.21	11.21	0.00	CPX	12.58	.09
MnO	0.21	0.18	-0.03	Ti-MGT	7.66	.07
MgO	2.22	2.23	0.01			
CaO	6.12	6.11	-0.01	TOTAL	100.00	.25
Na_2O	4.42	4.40	-0.02			
K_2O	2.30	2.29	-0.01			

Sum of squares of differences = 0.002

Table 5-15: Predicted and observed trace element content of the Bouvet Is. rhyolite using the results of the least squares approximation given in Table 5-14. The sources of the given distribution coefficients are discussed in the text.

A. Distribution coefficients

Element	FSP	OL	CPX	Ti-MGT	APATITE
Zr	.01	.01	.6	.8	.01
Nb	.01	.01	.2	2.5	.01
Y	.1	.12	.7	.17	16.9
Rb	.30	.01	.01	.01	.01
Ba	2.1	.01	.01	.01	.10
Sr	5.8	.01	.12	.01	5
Ga	0.9	.03	.40	2.0	.01
Co	.04	10.7	4.5	10.0	.20
Sc	.15	.20	10.0	5.0	.50
V	.01	.04	4.0	45	.01
Th	.01	.01	.01	.01	1.3 (5.0)
U	.01	.01	.01	.01	4.0

B. Trace element check.

	MUGEARITE	RHYOLITE	
	OBS.	CALC.	OBS.
Zr	473	1198	1190
Nb	70	155	155
Y	53	88	90
Rb	40	107	106
Ba	446	301	299
Sr	419	16	15
Ga	26	30	31
Co	18	2.6	4.0
Sc	15	2.6	1.3
V	48	<1.0	3.0
Th	5.9	18.4 (16.8)	16.3
U	1.6	4.7	4.8
P_2O_5	0.66%	0.02%	0.01%

relative to alkali-feldspar by a factor of approximately 2 (Willis, 1979), and so a slightly lower D^{Ga}_{fsp} than that used for the more basic end of the fractionation series is warranted.

Distribution coefficients for Co, Sc and V are so large and variable in the ferromagnesian phases (specifically titanomagnetite) that slight modifications of these D's to accommodate compositional changes are felt to be unwarranted. Similar D's to those used previously have therefore been selected. Data for the partitioning of Th and U between apatite and liquid is lacking in the literature, but estimates for D^{Th}_{ap} from data given by Ludwig and Stuckless (1978) suggest a D^{Th}_{ap} of greater than 1.0. To satisfy the observed Th enrichment, however, it is necessary to postulate a D of 5 which, though relatively high, might not be too unrealistic. The value of $D^{U}_{ap} = 4$ is similarly taken from Ludwig and Stuckless (1978).

Predicted and observed REE contents of rhyolite WJ18B are presented in Table 5-16B and distribution coefficients used are those presented in Table 5-16A. With the exception of Eu for which a D more typical of alkali-feldspar has been chosen (Arth, 1976), the distribution coefficients are the same as those used in modelling the less differentiated rocks. Though use of these D's does not predict the REE's in the rhyolite as well as they do for the less evolved rocks, the small discrepancies do not warrant significant changes in individual values of distribution coefficients. Due to the extremely large degree of fractionation, the results of the calculations are extremely sensitive to very small changes in D for feldspar, apatite and to a lesser extent clinopyroxene. With the exception of Tb and Ce for which predicted values are too low, there is a slight tendency for the values to be on

Table 5-16: A. Phenocryst/liquid distribution coefficients for the REE used in the crystal fractionation calculations. Values are from Ludden (1978a) except for the apatite data which are from Nagasawa and Schnetzler (1971). La and Tb values were extrapolated from Ce and Gd respectively.

B. Predicted and observed chondrite normalised REE content of the Bouvet Is. rhyolite using the results of the least squares approximation given in Table 5-15.

A. Distribution coefficients

Element	FSP	OL	CPX	Ti-MGT	APAT
La	.12	.01	0.10	.05	14.0
Ce	.11	.009	0.12	.05	16.6
Sm	.11	.006	0.38	.05	20.7
Eu	1.50*	.006	0.39	.05	14.5
Tb	0.10	.010	0.50	.05	19.3
Yb	0.10	.010	0.60	.05	9.4
Lu	0.10	.010	0.60	.05	7.9

* Selected from Arth (1976).

B. REE check.

	MUGEARITE	RHYOLITE	
	OBS.	CALC.	OBS.
La	164	334	330
Ce	109	210	214
Sm	79	130	121
Eu	63	42	42
Tb	46	77	88
Yb	22	47	44
Lu	18	40	34

the high side. Slight increase in the D's would therefore be indicated in accord with the general tendency for D's to increase with polymerization of the melt. The slight increase indicated is, however, significantly lower than that usually observed for silecious liquids (e.g. Arth, 1976). A possible explanation for the small increase is the high P_2O_5 content of the mugearite (0.66%) which has been suggested to lower mineral/liquid distribution coefficients for the REE (Ryerson and Hess, 1978).

On the basis of the above evaluation, it is concluded therefore that the Bouvet Island rhyolites have evolved by fractional crystallisation of a parental mugearite and would comprise the residual 17% of the initial hawaiite magma.

5.5 Highly Phyric Hawaiites

The highly plagioclase phyric nature of samples WJ8B and WJ17B suggests the presence of cumulus plagioclase, derived perhaps from the more aphyric hawaiites. Mixing calculations relating WJ8B to the average hawaiite support this contention, although minor yet consistent discrepancies occur in some elements, e.g. Na_2O, P_2O_5, Ba and Sr. The calculated degree of accumulation is 40% (comprising 34% plagioclase and 6% clinopyroxene) and is in agreement with the modal proportion of plagioclase and clinopyroxene ($\pm$ 37 and $\pm$ 3 vol.% respectively). Incompatible elements other than Ba are adequately accounted for by this crystal accumulation model.

The distinct minor element content of clinopyroxene phenocrysts in plagioclase phyric WJ8B (Section 4.3.4) relative to those in the sparsely phyric hawaiites, however, argues against a direct relationship via simple crystal accumulation. The apparent difference in minor

element chemistry of the pyroxenes might be related to polybaric crystallisation. Knutsen and Green (1975) have shown, for example, that at pressures of 10 kbar under 'dry' conditions clinopyroxene is the liquidus phase of hawaiite, followed by plagioclase. Clinopyroxene crystallised under these conditions could conceivably have a slightly different minor element composition than the more evolved low pressure varieties.

Although the mixing calculations are not as satisfactory as those for the differentiated lavas, it is suggested that the plagioclase phyric hawaiites are probably related to the more sparsely phyric varieties via plagioclase and minor clinopyroxene accumulation. In view of the distinct minor element content of the clinopyroxene in plagioclase phyric WJ8B, it is probable that the crystal accumulation occurred under different conditions (P,T and/or fO_2) from those pertaining to the evolution of the differentiated lavas.

5.6 Discussion

An attempt has been made to show that fractional crystallisation of observed phenocryst phases can account adequately for the observed compositional range in the Bouvet Island lavas. Of the fractionating phenocrysts (plagioclase + olivine + clinopyroxene + Fe-Ti oxide + apatite), plagioclase plays the dominant role in controlling the lava composition. The ability of plagioclase to 'sink' or 'float' in a magma has been experimentally demonstrated by Walker and Hays (1977) and Campbell et al. (1978) and has been shown to be critically dependent on bulk magma composition and the presence or absence of a fluid phase. Calculated volatile-free liquid densities (following Bottinga and Weill, 1970) for the average Bouvet Island hawaiite, mugearite and benmoreite

are given below, together with calculated plagioclase densities:

	1100°C	1000°C
Hawaiite	2.67 (2.60)	2.69 (2.62)
Mugearite	2.51	2.52
Benmoreite	2.46	2.47
Plag (An_{75})	2.68	2.68
(An_{58})	2.66	2.66
(An_{44})	2.64	2.64
(Ab_{100})	2.56	2.56

Partial molar volumes were taken from Bottinga and Weill (1970) and extrapolated to 1100 and 1000°C. Coefficients of expansion for plagioclase were taken from Clark (1966) and applied to densities at 20°C from Deer et al. (1966). The values in brackets were calculated assuming 1% H_2O in the hawaiite magma. Comparison of these data suggests that it is quite feasible for plagioclase of composition similar to the observed phenocrysts to 'sink' in the mugearite and benmoreite magmas and that in the presence of minor H_2O a plagioclase of composition An_{75} would tend to be more dense than the hawaiite magma. The common occurrence of clinopyroxene inclusions in plagioclase would tend to raise the effective density of the plagioclase and so further facilitate 'sinking'. Removal of plagioclase by gravitational settling is therefore feasible in the Bouvet Island lavas.

Experimental data on a natural hawaiite give some indication of the possible depth at which fractionation took place. Knutsen and Green (1975) found that plagioclase crystallisation is restricted to pressures of less than 6 kbar under hydrous conditions. Clinopyroxene is the liquidus phase, followed by plagioclase under dry conditions at 10 kbar.

Olivine and plagioclase are the liquidus phases at 5 kbar under anhydrous conditions. The presence of olivine, plagioclase and clinopyroxene phenocrysts in the sparsely phyric hawaiites limits the depth of fractionation to less than 10 kbar under anhydrous conditions and to less than 6 kbar in the presence of minor H_2O.

The proposed model for the evolution of the Bouvet Island lavas is summarised in Fig. 5-14 and involves the fractional crystallisation of a 'parental' hawaiite at moderate to low pressure on a multiply saturated (olivine + plagioclase + clinopyroxene + Fe-Ti oxide + apatite + liquid) surface. Crystallisation of 44% of this 'parental' hawaiite gave rise to a magma of mugearite composition which, following partial extrusion, experienced a further 69% crystallisation to give rise to minor amounts of rhyolite. Extensive ($\pm$ 64%) crystallisation of the 'parental' hawaiite magma (at shallow depths?) allowed the formation of the Bouvet Island benmoreites. The suggestion of Baker and Tomblin (1964) that the benmoreite represents the product of recent volcanic activity on Bouvet Island is circumstantial support for the postulated petrogenetic scheme presented above and in Fig. 5-14. The possible evolution of the Bouvet Island hawaiites will now be considered.

6. SOURCE AREA CHARACTERISTICS

6.1 Primary Magmas

Chemical characteristics of 'primary' magmas that have not experienced any significant change in composition since derivation from their source area have been discussed in Chapter III. Some diagnostic features are: high Ni (250-400 ppm) and Cr (400-600 ppm) contents and high Mg-numbers (0.68-0.77) (e.g. Green, 1971; Dungan and Rhodes, 1978; Sato, 1977; Bougault et al., 1979). Verwoerd et al. (1974) have noted

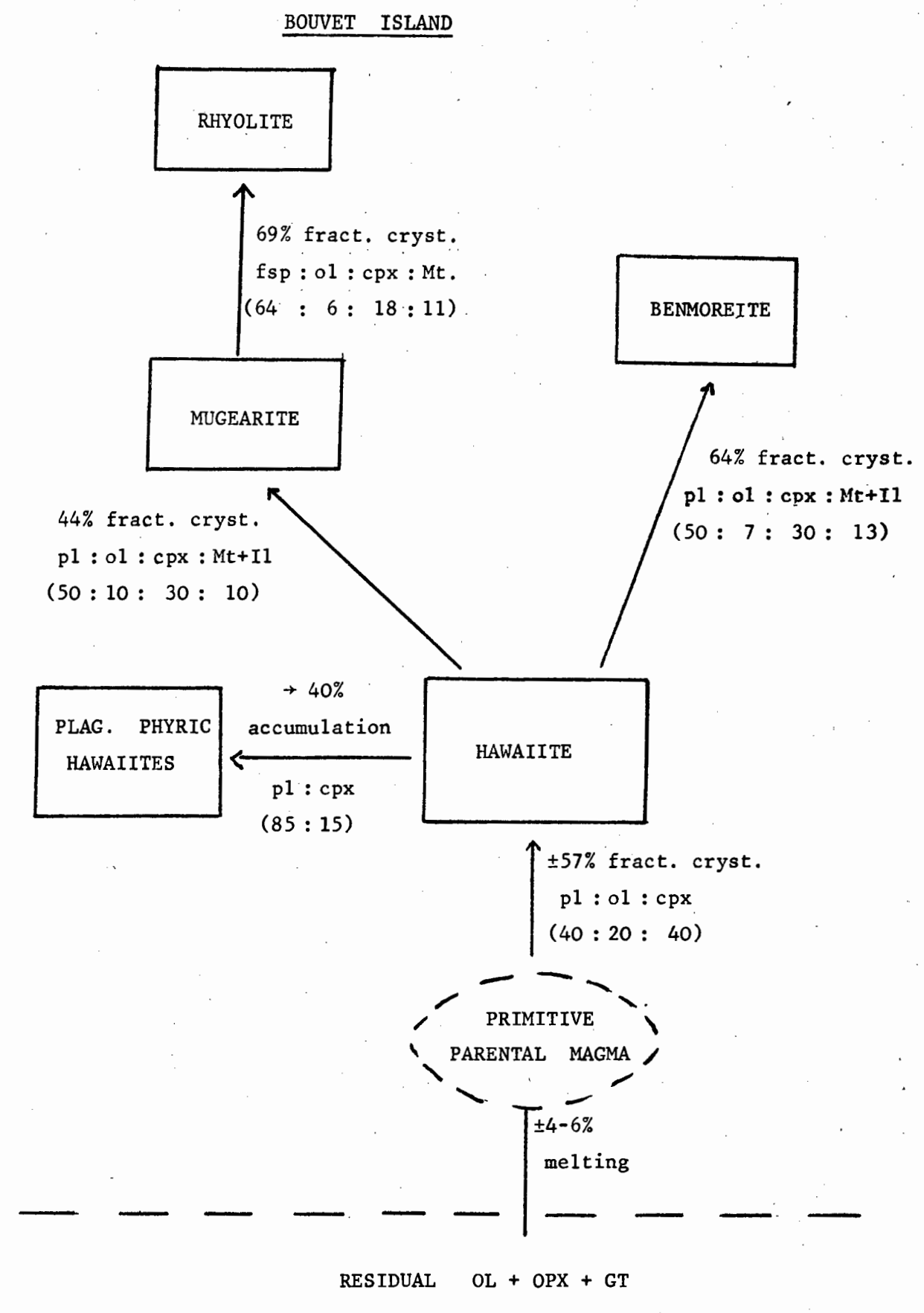

Fig. 5-14: Simplified schematic representation of the proposed petrogenetic model to account for some of the observed compositional variations in Bouvet Island lavas.

that several chemical features of the Bouvet Island hawaiites attest to their being evolved rather than 'primary' magmas. These features include their low Ni (19 ppm) and Cr (22 ppm) contents and their low Mg-numbers ($\pm$ 0.42); characteristics which clearly exclude Bouvet Island hawaiites as representing primary magmas. The above factors suggest that the hawaiites have experienced significant fractional crystallisation prior to eruption and that they are themselves derivative magmas from some more primitive basalt precursor. Verwoerd et al. (1974) showed that fractionation of olivine $\pm$ Cr-spinel from a more basaltic precursor could account for the low MgO, Ni and Cr abundances in the Bouvet Island hawaiites. Green et al. (1974) have suggested that many hawaiite magmas might derive from alkali-olivine basalt by fractional crystallisation, involving kaersutite, within the upper mantle, while Ludden (1978) concluded that the hawaiite lavas of Reunion Island are the result of low pressure fractionation involving olivine, plagioclase, clinopyroxene and magnetite from a primitive olivine basalt. Price and Taylor (1973) have similarly invoked low level fractionation of basalt to give rise to the more differentiated hawaiites of the Dunedin Volcano, New Zealand.

To enable some constraints to be placed on the trace element composition of the source area of Bouvet Island lavas, and in the absence of any potential 'primary' magma sampled from Bouvet Island, a model will be developed in which an estimate is made of the trace element character of a hypothetical primitive precursor to the evolved Bouvet Island hawaiites. This composition will then be used to place some constraints on the composition of the source area. The construction of the model is based firstly on the assumption that the hawaiites are evolved lavas and have therefore experienced a degree of fractional crystallisa-

tion since generation in their source area, and secondly that melting was initiated at depths below present day convection in the mantle (e.g. Sun and Hanson, 1975a). This is in accordance with Morgan's (1971, 1972) conclusion that Bouvet Island is the surface expression of a mantle plume originating at great depth.

In order to 'back calculate' the trace element content of a hypothetical parental magma, it is necessary to know not only the fractionating phases involved, but also their proportions. This can be achieved on the assumption that since the major elements (excluding TiO_2, K_2O and P_2O_5) are to a certain extent buffered during partial melting processes (e.g. Irvine and Kushiro, 1976), they are not unduly sensitive to varying degrees of partial melting. This assumption allows one to postulate an hypothetical parental composition with respect to major elements, which will then allow the calculation, by least squares approximation, of the approximate degree of fractional crystallisation required to generate the average hawaiite. This calculation will also give some idea of the type and proportion of fractionating minerals.

The choice of an hypothetical major element parental composition was made on the assumption that it would have a transitional to mildly alkaline chemistry in accord with the observed overall chemistry of the hawaiites, rather than being similar to the typically more alkaline lavas of most oceanic islands. Although no primitive magmas have been sampled from Bouvet Island, Watson (1976) has postulated a primary magma composition for this area from a study of melt inclusions in lavas dredged from the ridge crest just to the east of Bouvet Island. Considering the chemical similarity, with respect to diagnostic trace element ratios, of these Southwest Indian Ocean ridge basalts with those from Bouvet Island

(Dickey et al., 1977; this work, Chapter IV), this major element composition has been selected as representing a possible parental magma to the Bouvet Island hawaiites.

Possible fractional crystallisation schemes relating this hypothetical 'primary' magma to the average Bouvet Island hawaiite are briefly evaluated in the following section. The results are then used to place some constraints on the type of mantle and the degree of partial melting required to give rise to a primary basaltic precursor to the Bouvet Island hawaiites.

6.2 Fractional Crystallisation

Three possible fractionation schemes were investigated: (1) high pressure, (2) low pressure, and (3) a combination of (1) and (2) via an intermediate parent. Of these three, only low pressure fractionation provided realistic results. Models (1) and (3) both require substantial garnet fractionation (in addition to clinopyroxene and possibly kaersutite) to satisfy the major element variation, and this leads to a number of serious inconsistencies when back-calculating the trace element content of this hypothetical parent magma. For example, combining known distribution coefficients with the required proportions of fractionating minerals leads to a calculated Sc content in the primary magma of $\pm$ 1150 ppm and an Y content of $\pm$ 62 ppm, both of which are well outside the range observed in any primitive basaltic rocks. The calculated Ni content of 119 ppm in such a scheme is significantly lower than the 250-400 ppm Ni of primary melts (e.g. Sato, 1977; this work, Chapter III).

'Low' pressure fractionation of 26% plagioclase, 6% olivine and 30% clinopyroxene from this hypothetical parent magma results in a reasonable approximation to the major element composition of the average

Bouvet Island hawaiite. The trace element composition of the hypothetical Bouvet Island parental magma has been calculated using these mineral proportions, applicable distribution coefficients (Table 5-17), and assuming Rayleigh fractionation. This predicted composition is given in Table 5-18 and appears to be realistic when compared to the compositional range of typical 'primitive' olivine basalt.

6.3 Source Area Composition

It is possible to calculate the trace element composition of a source region that could give rise to a magma with the observed trace element content of the hypothetical parent, providing the residual mineral assemblage is known. In the absence of any specific knowledge of the source mineralogy, an arbitrary residual mineral assemblage of 57% olivine, 26% orthopyroxene, 15% clinopyroxene and 2% garnet has been assumed. These proportions are similar to those required to satisfy the REE variations in lavas from Mauna Loa, Hawaii, assuming that the lavas were generated by between 10 and 20% partial melting (Leeman et al., 1977). The initial source concentration can then be calculated by rearrangement of Shaw's (1970) equation for equilibrium partial melting as follows:

$$C_o = C^l F + C^l D (1-F)$$

where C_o = concentration in the source

C^l = concentration in the liquid

F = degree of melting

D = bulk distribution coefficient based on the residual mineral assemblage.

Calculated mantle compositions, which could give rise to the parental magma by 6% and 7% equilibrium melting, are presented in Table 5-18. With the exception of Nb and Sr, the calculated composition com-

Table 5-17: Distribution coefficients used in fractional crystallisation and equilibrium partial melting models for the derivation of a hypothetical 'primary' Bouvet Is. magma. Values have been selected from Tables A2-1, A2-2, A2-5 to A2-7. Where two values are given the value in brackets has been used in the partial melting calculations.

	PLAG	OLIV	CPX	OPX	GARNET
Ni	.01	18 (11)	4.0 (1.98)	4.0	0.5
Co	.01	6.0 (3.0)	1.0	2.0	1.0
Rb	.01	.01	.01	.01	.01
Ba	.01	.01	.01	.01	.01
Zr	.01	.01	.20	.01	1.2
Nb	.01	.01	.09 (.03)	.01	.03
Y	.18	.10	.50	.10	3.0
Sr	1.9	.01	.12	.01	.01
Sc	.10	.15	2.0	.40	10.0
Ga	1.0	.01	0.4	.01	.01
$K_2O\%$	.01	.01	.01	.01	.01
$P_2O_5\%$	.01	.01	.01	.01	.10
$TiO_2\%$	.01	.01	.20	.02	.20

Table 5-18: Calculated trace element composition of a postulated 'primitive' Bouvet Island magma, and predicted mantle composition assuming 6% and 7% equilibrium partial melting. Residual mantle mineralogy is indicated.

	PRIMITIVE MELT	PREDICTED MANTLE		MANTLE*
		F=0.06	F=0.07	
Ni	253	1827	1810	1600-2000
Co	48	111	111	100
Rb	8.0	0.56	0.63	0.57-0.78
Ba	91	6.3	7.2	7.1
Zr	112	13.3	14.3	9.7-13.0
Nb	17	1.2	1.4	0.53-0.72
Y	19	5.0	5.2	4.2 - 5.8
Sr	383	32.5	36.3	19 - 26
Sc	28	19.8	19.9	14 - 20
Ga	16	2.9	3.1	3.4†
K_2O%	0.49	.034	.039	0.024-0.033
P_2O_5%	0.18	.012	.014	0.018-0.024
TiO_2%	1.65	0.17	0.18	0.18 - 0.24

RESIDUAL MANTLE:	OLIVINE	57%
	OPX	26%
	CPX	15%
	GARNET	2%

* From Sun and Nesbitt (1977)

† Assumed from data in Willis (1979).

pares very favourably with the postulated primitive mantle composition (Table 5-18) of Sun and Nesbitt (1977). Bearing in mind the assumptions made and the hypothetical nature of the model, it is suggested that the Bouvet Island hawaiites have been derived from a primitive olivine basalt magma with a trace element composition similar to that presented in Table 5-18. Such a magma could be generated by 6-7% partial melting of a mantle composition similar to that postulated by Sun and Nesbitt (1977), leaving residual garnet in the source.

CHAPTER VI

DISCUSSION

The preceding chapters have embodied the detailed petrogenetic modelling of oceanic lava suites from three distinct tectonic environments: mid-ocean ridge, fracture zone and oceanic island. The results of these studies have been summarised in the individual chapters and will not be repeated here, but rather an attempt will be made to consider some of these results collectively in terms of the relationship between rock type and tectonic setting. Some important questions in this respect can be summarised as follows:

(1) Do rock types from ridge systems and fracture zones show consistent differences?

(2) Do the differences in igneous rock suites (e.g. ridge systems and fracture zones) reflect source area differences or differences introduced by differentiation processes, and how do these relate to the tectonic setting?

(3) To what extent can systematic geochemical differences be attributed to the action of mantle plumes?

In order to evaluate the extent to which observed geochemical differences of oceanic rocks from different tectonic environments can be attributed to source area characteristics and/or tectonic control, it is important to take into account first the effect of second order magmatic processes. Such second order processes include fractional crystallisation, magma mixing and variation in type and degree of partial melting. Of these processes, fractional crystallisation is the most readily

evaluated and a large portion of this study has been concerned with investigating the extent to which the observed compositional variation in these oceanic basalts can be attributed to low pressure fractional crystallisation. The lava suites that have been studied include samples from the Mid-Atlantic Ridge at $36^{o}49'N$ (FAMOUS), from the Islas Orcadas Fracture Zone on the Southwest Indian Ocean Ridge, from the Conrad Fracture Zone on the Antarctica-America Ridge and from Bouvet Island. The samples from these areas range from some of the most primitive (e.g. the picrites and olivine basalts from FAMOUS) to some of the most evolved (e.g. the ferrobasalts from the IOFZ and Conrad F.Z.) basalts ever recovered from the ocean floor. The compositional variation of the Bouvet Island lava suite further extends this range to highly evolved rhyolitic compositions.

It has long been recognised that the suboceanic mantle is to a first approximation composed of at least two distinct chemical units; the one giving rise to LIL element-enriched oceanic island basalts and the other to LIL element-depleted ocean ridge basalts (e.g. Gast, 1968; Kay et al., 1970; O'Nions et al., 1976; Hanson, 1977). The mantle source giving rise to oceanic island basalts is characterised by low small/large ion incompatible element ratios (e.g. K/Rb, K/Ba, Zr/Nb, Y/Nb), LREE enrichment and high $^{87}Sr/^{86}Sr$ ratios (high $^{207}Pb/^{204}Pb$ and $^{206}Pb/^{204}Pb$ ratios and low $^{143}Nd/^{144}Nd$ ratios are also characteristics; e.g. Tatsumoto, 1966; O'Nions and Pankhurst, 1974; O'Nions et al., 1977; De Paolo and Wasserburg, 1976, 1979). The chemical characteristics of most ocean ridge basalts imply derivation from a depleted source characterised by high values for the above ratios, LREE depletion and low $^{87}Sr/^{86}Sr$ ratios (low $^{207}Pb/^{204}Pb$ and $^{206}Pb/^{204}Pb$ ratios and high

$^{143}Nd/^{144}Nd$ ratios are additional characteristics; e.g. Tatsumoto, 1966; O'Nions and Pankhurst, 1974; O'Nions et al., 1977; De Paolo and Wasserburg, 1976, 1979). Although basalts derived from both types of source region have been described from the ocean floor (e.g. Erlank and Kable, 1976), there are, to the writer's knowledge, no reported occurrences of LIL element-depleted basaltic volcanism on oceanic islands.

Although a continuum of compositions probably exists, LIL element-depleted and LIL element-enriched ocean floor basalts correspond respectively to Group I and Group II type ocean floor basalts of Bryan et al. (1976). In terms of this classification, no chemical distinction is recognised between basalts extruded at fracture zones and those extruded along mid-ocean ridges. For example, basalts from the Mid-Atlantic Ridge in the FAMOUS region and from the Southwest Indian Ocean Ridge reflect the characteristics of unfractionated and fractionated Group II basalts respectively, as do the basalts from the Islas Orcadas Fracture Zone. Although the basalts from the Conrad F.Z. have a chemistry transitional between fractionated Group I and Group II basalts, they are more similar to the former. Clinopyroxene (a characteristic of Group II basalts; Bryan et al., 1976) is present in all but the most primitive of the FAMOUS basalts and is ubiquitous in the fracture zone basalts. Olivine is abundant in all the FAMOUS basalts but is rare in the fracture zone basalts. Texturally the FAMOUS lavas also differ from the fracture zone basalts in that they are characterised by the presence of abundant quench textures and quench glass rinds, while the fracture zone basalts tend to be more crystalline. These textural differences, however, reflect the extent of fractional crystallisation and mode of emplacement rather than relating to source area characteristics.

The results of the petrogenetic modelling of these lava suites indicate that fractional crystallisation is an important process occurring in all three tectonic environments, and that most of the observed compositional variation can be accounted for by crystal fractionation of one or more parental magmas. For example, the compositional range of the relatively primitive FAMOUS basalts can be accounted for by up to 25% fractional crystallisation of observed phenocryst phases, and by crystal accumulation of up to 40% plagioclase or 30% olivine. The compositional variation of the more evolved fracture zone basalts can be accounted for by up to 76% fractional crystallisation. Similar large degrees of crystal fractionation ($\pm$ 83%) are required to account for the passage from hawaiite to rhyolite on Bouvet Island. Several authors (e.g. Kay, 1970; Shido et al., 1971; Scheidegger, 1973; Schilling, 1975b; Bryan et al., 1976) have noted the importance of the cotectic crystallisation of olivine and plagioclase at low pressures in controlling the bulk chemistry of ocean floor basalts. In contrast, the results of the quantitative modelling in this study emphasise the importance of clinopyroxene fractionation in controlling the bulk chemistries of the lavas studied. This is illustrated by the average proportions of fractionating phases in the four study localities given below:

FAMOUS -	plag : ol : cpx	=	45 : 23 : 32
IOFZ -	plag : ol : cpx	=	57 : 3 : 39
CONRAD F.Z. -	plag : cpx : Fe-Ti oxides	=	51 : 46 : 3
BOUVET IS. -	plag : ol : cpx : Fe-Ti oxides	=	50 : 9 : 30 : 11

Plagioclase is clearly the most important fractionating phase in all cases, but is closely followed by clinopyroxene and only in the relatively primitive FAMOUS lavas does olivine contribute substantially

to the fractionating assemblage. The importance of clinopyroxene in controlling the bulk chemistry of certain ocean floor basalts has also been noted by Cann (1971), Byerly et al. (1975), Clague and Bunch (1976), Flower et al. (1977), Donaldson and Brown (1977), Dungan and Rhodes (1978) and Rhodes et al. (1979). Considering the abundant clinopyroxene phenocrysts in the samples studied, with the possible exception of the more primitive FAMOUS lavas, it is not necessary to invoke magma mixing (Dungan and Rhodes, 1978; Rhodes et al., 1979) to account for the significant proportion of clinopyroxene in the crystal fractionates. However, detailed consideration of trace element variations in many of the lava suites (and specifically FAMOUS) suggests that open system fractionation and magma mixing (O'Hara, 1977; Dungan and Rhodes, 1978; Rhodes et al., 1979; Bryan, 1979; Bryan et al., 1979) is apparently a more realistic fractionation process than simple closed system fractionation. This is specifically evident in the FAMOUS basalts but is possibly obscured in the fracture zone basalts (and in the Bouvet Island lavas) by the relatively greater degree of differentiation that has occurred in these basalts. The greater degree of alteration of the fracture zone basalts may also have obscured some of the subtle variations that could be attributed to magma mixing. Although fractional crystallisation has been shown to be an important process occurring at both oceanic ridges (FAMOUS) fracture zones (IOFZ, Conrad F.Z.) and oceanic islands (e.g. Bouvet Island), the extent to which this process occurs is clearly different. At the Mid-Atlantic Ridge in the FAMOUS area, the amount of differentiation is significantly less than at the fracture zones.

Consideration of the fine scale chemical variation of the FAMOUS lavas and associated phenocryst minerals indicates that the observed

compositional variation in the FAMOUS region is unlikely to have arisen from differentiation within a single magma chamber. Differentiation of at least two and possibly three distinct parental magmas, derived from two different source areas, is required to account for the observed compositional variation. This suggests either the coexistence of a number of small magma chambers which are individually tapped and experience magma mixing by addition of new 'primitive' batches of magma, yet maintain their chemical identity or, more plausibly, the existence of small temporal separated magma chambers which are created, experience crystal fractionation, magma mixing and eruption, and then disappear to be replaced by a new chamber as a consequence of some or other tectonic event (e.g. Nisbet and Fowler, 1978; Bougault et al., 1979). Such a mechanism would result in the eruption of predominantly moderately evolved magmas that have experienced relatively small degrees of fractional crystallisation (e.g. Rhodes et al., 1979).

A similar model is apparently not applicable for describing the compositional variation of the fracture zone basalts. In common with the FAMOUS lavas, it has been shown that the differentiation of more than one parental magma is required to account for the overall compositional variation observed in the fracture zone basalts. However, in contrast, the extremely evolved nature of many of these basalts and the large amount of fractional crystallisation (up to 76%) required to account for this differentiation, implies the presence of a large, stable low level magma chamber, that has existed for a significant time interval.

The presence of large magma chambers and extensive fractionation has previously been suggested to be a feature of fast-spreading ridges (e.g. Clague and Bunch, 1976; Nisbet and Fowler, 1978; Rhodes et al.,

1979). Fast spreading rates imply more frequent tapping of a magma chamber through fracturing and fissure eruptions. The incidence of fracturing and tapping of magma relative to injection and mixing of 'primitive' magma will be greater than at slow spreading ridges (e.g. MAR), and will therefore favour the sampling of the magma chamber during the quiescent fractionating part of the cycle. This will result in the more frequent eruption of highly fractionated magmas. Although such a mechanism may be applicable for fast spreading ridges, it is unlikely to be valid for the IOFZ and Conrad F.Z. as both are situated on slow spreading ridges (Sclater et al., 1978). In this respect though, it is important to bear in mind that spreading rates are generally determined over a large time scale and that they may be very variable over the short time scale more applicable for magmatic events (Bougault et al., 1979). Nisbet and Fowler (1978) have reviewed the geophysical data from mid-ocean ridges and argue that the thermal regime at slow spreading ridges is unlikely to support the presence of a large magma chamber.

The common occurrences of highly differentiated rocks in fracture zones (Hekinian and Thompson, 1976; this study), even when situated on slow spreading ridges, suggests some additional tectonic control. A possible explanation is that faulting may have exposed more fractionated basalts in fracture zones than those found in rift valleys (Hekinian and Thompson, 1976). Thompson and Melson (1972) favour the concept of so-called 'leaky' transform faults in which new oceanic crust is injected into fracture zones in response to sea floor spreading normal to that which occurs at the ridge axis. They have suggested that the chemical characteristics of this new crust differs from that formed at normal ridge crests. Assuming that volcanic activity does occur along fracture

zones, and since they are displaced from the actively spreading ridge, it is likely that the magma supply rate in fracture zones is relatively low. Under these conditions magma may well reside in chambers for a sufficient length of time and experience substantial 'closed-system' fractional crystallisation, without injection of and mixing with new batches of 'primary' magma. This would result in the extrusion of a higher proportion of differentiated basalts relative to mid-ocean ridges. It is suggested that most of the observed chemical differences between fracture zone basalts and ridge axis basalts are related to the tectonic control on magma supply rates and so indirectly the extent of possible fractional crystallisation, rather than to source area differences. The extensive differentiation that is shown by the basalt suites comprising this study emphasises the importance of comparing only incompatible element ratios (and isotope ratios where available) rather than the absolute element abundances of basalts from different tectonic environments.

With the exception of a few isolated cases (e.g. the Mid-Atlantic Ridge at $45^{o}N$), most occurrences of Group II basalts are found in the vicinity of oceanic islands. This effect of oceanic island volcanism on nearby ridge segments has been attributed to the action of mantle plumes, marked by the site of the oceanic island. Such effects have been documented near the Azores (Schilling, 1975a,b; White and Schilling, 1978), near Iceland (Schilling, 1973), near St. Paul, Amsterdam Island (Frey et al., 1976) and near Bouvet Island (Dickey et al., 1977; this study). It has been noted that the mantle source for oceanic island basalts is clearly distinguished from that for normal Group I ocean floor basalts in terms of some diagnostic trace element ratios (e.g. K/Rb, K/Ba, Zr/Nb,

Y/Nb, $^{87}Sr/^{86}Sr$, La/Yb). The similarity of these ratios in oceanic island basalts and Group II ocean floor basalts suggests derivation of the latter from a similar source area to that of oceanic islands. The very similar values for these ratios in the FAMOUS basalts, those from the Southwest Indian Ocean Ridge and from Bouvet Island support this contention. In addition, quantitative modelling of the derivation of primary magmas from the FAMOUS region and from Bouvet Island and consideration of selected incompatible element ratios of basalts from the IOFZ, indicate that basalts from these areas can all be derived from a source with composition similar to that postulated by Sun and Nesbitt (1977) for Archean mantle. The basalts from FAMOUS and the IOFZ can be derived by 10-27% partial melting of such a source, while <10% melting is required to give rise to a primary 'parental' Bouvet Island magma. The source area for the Conrad F.Z. basalts is chemically distinct and more similar to the depleted source of normal Group I basalts.

The origin of these two apparently distinct mantle sources and the maintenance of their identities, is a question of much debate. There is, however, a general consensus, on the basis of isotopic data, that the mantle source of depleted, normal mid-ocean ridge basalt has a long-term history ($\geq$1 b.y.) of depletion in incompatible elements (Sun and Hanson, 1975a; Brooks et al., 1976; Richard et al., 1976; Sun et al., 1979). Various possible depletion models have been summarised by Sun et al. (1979). Of more relevance to the present study is the origin of the LIL element enrichment in Group II ocean floor basalt and oceanic island mantle sources. The isotopic data of Group II-type ocean floor basalts indicates that the enrichment in incompatible elements is a relatively recent event (e.g. < 300 m.y.; Sun et al., 1979), i.e. such basalts are

derived from long-term depleted sources which were added to by a LIL element enriched fraction (e.g. O'Nions et al., 1977; Carlson et al., 1977; Sun et al., 1979). This enrichment event could involve the intrusion of veinlets, derived by very low degrees of melting, into existing depleted mantle (e.g. Sun and Hanson, 1975b) or involve a metasomatic process involving a fluid phase (e.g. Erlank, 1973; Aoki, 1975; Lloyd and Bailey, 1975; Erlank and Rickard, 1977).

Sun and Hanson (1975a) have suggested that the most likely source of oceanic island basalts is below the presently convecting mantle. This deeper undepleted mantle rises adiabatically as a diapir, melts and results in oceanic island type volcanism which marks the site of a so-called mantle plume. Dynamic melting (including processes such as continuous melting with incomplete removal of melt, zone refining and magma mixing) during uprise of this mantle diapir provides the necessary framework for the 'second-order' enrichment of adjacent depleted mantle. Following the model of Sun and Hanson (1975b), this enrichement might occur by the intrusion of very small fractions of melt, derived from the rising diapir, as veinlets into the adjacent mantle or by metasomatic fluid movement. Subsequent melting of this enriched mantle would produce Group II-type basalts having the chemical imprint of the more directly related plume-derived oceanic island volcanism. The mixing of plume-derived and normal mantle has, for example, been offered as an explanation for the gradual chemical change along the Mid-Atlantic Ridge southward from the Azores (Schilling, 1975a; White and Schilling, 1978). The results of the present study support a close genetic relationship between Group II ocean floor basalts and oceanic island basalts, and suggest their derivation from a similar source area.

REFERENCES

Akella J., Williams R.J. and Mullins O. (1976) Solubility of Cr, Ti, and Al in coexisting olivine, spinel and liquid at 1 atm. Proc. Seventh Lunar Sci. Conf., 1179-1194.

Albee A.L. and Ray L. (1970) Correction factors for electron probe microanalysis of silicates, oxides, carbonates, phosphates and sulfates. Anal. Chem. 42 (12), 1408-1414.

Allègre C.J., Treuil M., Minster J-F, Minster B. and Albarede F. (1977) Systematic use of trace element in igneous process. Part 1: Fractional crystallisation processes in volcanic suites. Contrib. Mineral. Petrol. 60, 57-75.

Anderson A.T. (1974) Evidence for a picritic, volatile-rich magma beneath Mt. Shasta, California. J. Petrol. 15, 243-267.

---------- (1976) Magma Mixing: Petrological process and volcanological tool. J. Volcan. Geotherm Res. 1, 3-33.

---------- and Greenland L.P. (1969) Phosphorus fractionation diagram as a quantitative indicator of crystallisation differentiation of basaltic liquids. Geochim. Cosmochim. Acta 33, 493-505.

---------- and Wright T.L. (1972) Phenocrysts and glass inclusions and their bearing on oxidation and mixing of basaltic magmas, Kilauea volcano, Hawaii. Am. Min. 57, 188-216.

Anderson D.L. (1975) Chemical plumes in the mantle. Bull. Geol. Soc. Am. 86, 1593-1600.

Andrews A.J. (1977) Low temperature fluid alteration of oceanic layer 2 basalts, DSDP Leg 37. Can. J. Earth Sci. 14 (4), 911-926.

Aoki K. (1975) Origin of phlogopite and potassic richterite bearing peridotite xenoliths from South Africa. Contrib. Mineral. Petrol. 53, 145-156.

------- and Prinz M. (1974) Chromian spinels in lherzolite inclusions from Itunome-gata, Japan. Contrib. Mineral. Petrol. 46, 249-256.

Arculus R.J. (1974) Solid solution characteristics of spinels: pleonaste-chromite-magnetite compositions in some island arc basalts. Carnegie Inst. Wash. Yearb. 73, 322-327.

Arcyana (1977) Rocks collected by bathyscaph and diving saucer in the FAMOUS area of the Mid-Atlantic Rift Valley: petrological diversity and structural setting. Deep-Sea Research 24, 565-589.

Arndt N.T. (1977a) Ultrabasic magmas and high degree melting of the mantle. Contrib. Mineral. Petrol. 64, 205-221.

---------- (1977b) Partitioning of Ni betweeen olivine and ultrabasic and basic liquids. Carnegie Inst. Wash. Yearb. 76, 553-557.

Arth J.G. (1976) Behaviour of trace elements during magmatic processes - a summary of theoretical models and their application. J. Res. U.S. Geol. Surv. 4 (1), 41-47.

Aumento F. (1969) Diorites from the Mid Atlantic Ridge at 45°N. Science 165, 1112-1113.

----------, Loncarevic B.D. and Ross D.I. (1971) Hudson Geotraverse: Geology of the Mid-Atlantic Ridge at 45°N. Phil. Trans. Roy. Soc. Lond. A268, 623-650.

Baird A.K. (1961) A pressed specimen die for the Norelco vacuum-path X-ray spectrograph. Norelco Rep. 8, 108.

Baker B.H., Goles G.G., Leeman W.P. and Lindstrom M.M. (1977) Geochemistry and petrogenesis of a Basalt-Benmoreite-Trachyte suite from the southern part of the Gregory Rift, Kenya. Contrib. Mineral. Petrol. 64, 303-332.

Baker P.E. (1965) The recent eruption on Bouvetoya with a note on magma type. Proc. Geol. Soc. Lond. 1625, 144-145.

Baker P.E. (1967) Historical and geological notes on Bouvetoya. Br. Antarct. Surv. Bull. 13, 71-84.

---------- (1973) Islands of the South Atlantic. In The Ocean basins and Margins, Vol. 1, The South Atlantic, Chap. 13, 493-553 (ed.) A.E.M. Nairn and F.G. Stehli: New York-London, Plenum Press.

---------- and Tomblin J.F. (1964) A recent volcanic eruption on Bouvetoya, South Atlantic Ocean. Nature 203, 1055-1056.

Baragar W.R.A., Plant A.G., Pringle G.J. and Mikkel Schau (1977) Petrology and alteration of selected units of Mid-Atlantic Ridge basalts sampled from sites 332 and 335, DSDP. Can. J. Earth Sci. 14 (4), 837-874.

Barberi F., Bizouard H. and Voret J. (1971) Nature of the clinopyroxene and iron enrichment in alkalic and transitional basaltic magmas. Contrib. Mineral. Petrol. 33, 93-107.

Bass M.N. (1971) Variable abyssal basalt populations and their relation to sea-floor spreading rates. Earth Planet. Sci. Lett. 11, 18-22.

Bence A.E. and Albee A.L. (1968) Empirical correction factors for the electron microanalysis of silicates and oxides. J. Geology 76, 382-403.

---------- and Papike J.J. (1977) Pyroxenes as recorders of lunar basalt petrogenesis: chemical trends due to crystal liquid interaction. Proc. Third Lunar Sci. Conf. 1, 439-469.

Bender J.F., Hodges F.N. and Bence A.E. (1978) Petrogenesis of basalts from the Project Famous: Experimental study from 0-15 kbars. Earth Planet. Sci. Lett. 41, 277-302.

Benjamin T.M., Heuser R. and Burnett D.S. (1978) Solar system actimide abundance I. Laboratory partitioning between whitlockite, diopsidic clinopyroxene and anhydrous melt (abs.) Lunar Planet. Sci. IX, 70-77.

Bergh H.W. and Norton I.O. (1976) Prince Edward fracture zone and the evolution of the Mozambique Basin. J. Geophys. Res. 81, 5221-5239.

Berlin R. and Henderson C.M.B. (1968) A reinterpretation of Sr and Ca fractionation trends in plagioclase from basic rocks. Earth Planet. Sci. Lett. 4, 79-83.

-------- and Henderson C.M.B. (1969) The distribution of Sr and Ba between the alkali feldspar, plagioclase and groundmass phases of porphyritic trachytes and phonolites. Geochim. Cosmochim. Acta 33, 247-255.

Best M.G. (1974) Contrasting types of chromium-spinel peridotite xenoliths in basanitic lavas, Western Grand Canyon, Arizona. Earth Planet Sci. Lett. 23, 229-237.

Bird M.L. (1971) Distribution of trace elements in olivines and pyroxenes -- an experimental study. Unpubl. Ph.D. thesis, Univ. of Missouri, Rolla.

Blanchard D.P., Rhodes J.M., Dungan M.A., Rodgers K.V., Donaldson C.H., Brannon J.C., Jacobs J.W. and Gibson E.K. (1976) The chemistry and petrology of basalts from Leg 37 of the Deep Sea Drilling project. J. Geophys. Res. 81, 4231-4246.

Bonatti E., Honnorez J. and Ferrara G. (1971) Peridotite-gabbro-basalt complex from the equatorial Mid-Atlantic Ridge. Phil. Trans. Roy. Soc. Lond. A 268, 385-402.

Bottinga Y. and Steinmetz L.(1979) A geophysical, geochemical, petrological model of the sub-marine lithosphere. Tectonophys. 55, 311-347.

---------- and Weill D.F. (1970) Densities of liquid silicate systems calculated from partial molar volumes of oxide components. Am. J. Sci. 269, 169-182.

Bougault H., Cambon P., Corre O., Joron J.L. and Treuil M. (1979) Evidence for variability for magmatic processes and upper mantle heterogeneity in the axial region of the Mid-Atlantic Ridge near 22°N and 36°N. Tectonophys. 55, 11-34.

---------- and Hekinian R. (1974) Rift Valley in the Atlantic ocean near 36°50' N: Petrology and geochemistry of basaltic rocks. Earth Planet Sci. Lett. 24, 249-261.

Boyd F.R. and Smith D. (1971) Compositional zoning in pyroxenes from lunar rock 12021, Oceanus Procellarum. J. Petrol. 12, 439-464.

Broch O.A. (1946) Two contributions to Antarctic petrography. I Lavas of Bouvet Island. Sci. Results Norw. Antact. Exped. 1927-1928, 25 Norsk. Vid.-Akad. Oslo, 3-26.

Brooks C.K. (1976) The Fe_2O_3/FeO ratio of basalt analyses: an appeal for standardized procedure. Bull. Geol. Soc. Denmark 25, 117-119.

Brown G.M. (1957) Pyroxenes from the early and middle stages of fractionation of the Skaergaard intrusion, East Greenland. Min. Mag. 31, 511-543.

---------- and Vincent E.A. (1963) Pyroxenes from late stages of fractionation of the Skaergaard intrusion, East Greenland. J.Petrol. 4, 175-197.

Bryan W.B. (1972) Mineralogical studies of submarine basalts. Carnegie Inst. Wash. Yearb. 71, 396-403.

---------- (1974) Fe-Mg relationships in sector-zoned submarine basalts plagioclase. Earth Planet. Sci. Lett. 24, 157-165.

---------- (1979) Regional variation and petrogenesis of basalt glasses from the FAMOUS area, Mid-Atlantic Ridge. J. Petrol. 20 (2), 293-325.

----------, Finger L.W. and Chayes F. (1969) Estimating proportions in petrologic mixing equations by least squares approximation. Science 163, 926-927.

---------- and Moore J.G. (1977) Compositional variations of young basalts in the Mid-Atlantic Ridge rift valley near lat. 36°49' N. Geol. Soc. Am. Bull. 88, 556-570.

----------, Thompson G., Frey F.A. and Dickey J.S. (1976) Inferred geologic settings and differentiation in basalts from the Deep Sea Drilling Project. J. Geophys. Res. 81, 4285- 4304.

----------, ---------- and Michael P.J. (1979) Compositional variation in a steady-state zoned magma chamber: Mid-Atlantic Ridge at 36°50' N. Tectonophys. 55, 63-85.

Buddington A.F. and Lindsley D.H. (1964) Iron-titanium oxide minerals and synthetic equivalents. J. Petrol. 5, 310-357.

Byerley G.R., Melson W.G. and Vogt P.R. (1975) Extreme differentiation of ocean ridge volcanic rocks: Galepagos Ridge and Juan de Fuca Ridge (abstract). EOS. Trans. Am. Geophys. Union. 56 (6), 469.

Cameron E.N. (1979) Titanium bearing oxide minerals of the Critical Zone of the Eastern Bushveld Complex. Am. Min. 64, 140-150.

Campbell I.H. and Nolan J. (1974) Factors affecting the stability field of Ca-poor pyroxene and the origin of the Ca-poor minimum in Ca-rich pyroxenes from tholeiitic intrusions. Contrib. Mineral. Petrol. 48, 205-219.

----------, Roeder P.L. and Dixon J.M. (1978) Plagioclase buoyancy in basaltic liquids as determined with a centrifuge furnace. Contrib. Mineral. Petrol. 67, 369-377.

Cann J.R. (1971) Major element variations in ocean floor basalts. Phil. Trans. Roy. Soc. Lond. A 268, 495-505.

Carlson R.W., Macdougal J.D. and Lugmair G.W. (1977) Differential Sm/Nd evolution in oceanic basalts. EOS. Trans. Am. Geophys. Union 58, 1250.

Cawthorne R.G., Ford C.E., Biggar G.M., Bravo M.S. and Clarke D.F. (1974) Determination of the liquid composition in experimental samples: discrepancies between microprobe analyses and other methods. Earth Planet. Sci. Lett. 21, 1-6.

Claque D.A. and Bunch T.E. (1976) Formation of ferrobasalt at East Pacific mid-ocean spreading centers. J. Geophys. Res. 81 (3), 4247-4256.

Clark S.P. (Jr). (1966) Handbook of physical constants. Geol. Soc. Am. Mem: 97

Clarke D.B. (1970) Tertiary basalts of Baffin Bay: possible primary magma from the mantle. Contrib. Mineral. Petrol. 25, 203-224.

Coish R.A. and Taylor L.A. (1979) The effects of cooling rate on texture and pyroxene chemistry in DSDP Leg 34 basalt: A microprobe study. Earth Planet. Sci. Lett. 42, 389-398.

Consolmagno G.J. and Drake M.J. (1976) Equivalence of equations describing trace element distribution during equilibrium partial melting. Geochim. Cosmochim. Acta 40, 1421-1422.

Cox K.G. and Bell J.D. (1972) A crystal fractionation model for the basaltic rocks of the New Georgia Group, British Solomon Islands. Contrib. Mineral. Petrol. 37, 1-13.

Crawford M.L. (1973) Crystallisation of plagioclase in mare basalts. Proc. Fourth Lunar Sci. Conf. 1, 705-717.

Dale I.M. and Henderson P. (1972) The partitioning of transition elements in phenocryst-bearing basalts and their implications about melt structure. 24th Inter. Geol. Congr. (1972), section 10, 105-111.

Deer W.A., Howie R.A. and Zussman J. (1966) An introduction to the rock-forming minerals. Longmans.

De Paolo D.J. and Wasserburg G.J. (1976) Inferences about magma sources and mantle structure from variations of $^{143}Nd/^{144}Nd$. Geophys. Res. Lett. 3 (12), 743-746.

---------- (1979) Petrogenetic mixing models and Nd-Sr isotopic patterns. Geochim. Cosmochim. Acta 43, 615-627.

De Pieri R. and Quareni S. (1978) Partition coefficients of alkali and alkaline earth elements between alkali-feldspar phenocrysts and their lava matrix. Min. Mag. 42, 63-67.

Dick H.J.B. (1976) Spinel in Fracture zone "B" and the Median Valley basalts, FAMOUS area, Mid-Atlantic Ridge. EOS. Trans. Am. Geophys. Union 57 (4), 341.

Dickey J.S., Frey F.A., Hart S.R., Watson E.B. and Thompson G. (1977) Geochemistry and petrology of dredged basalts from the Bouvet Triple junction South Atlantic. Geochim. Cosmochim. Acta 41, 1105-1118.

Donaldson C.H. (1976) An experimental investigation of olivine morphology. Contrib. Mineral. Petrol. 57, 187-213.

---------- and Brown R.W. (1977) Refractory megacrysts and magnesium-rich melt inclusions within spinel in oceanic tholeiites: indicators of magma mixing and parental magma composition. Earth Planet. Sci. Lett. 37, 81-89.

Dowty E. (1977) The importance of adsorption in igneous partitioning of trace elements. Geochim. Cosmochim. Acta 41, 1643-1646.

Drake M.J. and Weill D.F. (1975) Partition of Sr, Ba, Ca, Y, Eu^{2+}, Eu^{3+} and other REE between plagioclase feldspar and magmatic liquid: and experimental study. Geochim. Cosmochim. Acta 39, 689-712.

Duchesne J.C. (1972) Pyroxenes et olivines dans le massit de Bjerkrem-Sogndal (Norvege meridionale). Rept. 24th Int. Geol. Congr. Section 2, 320-328.

Duke J.M. (1976) Distribution of the period four transition elements among olivine, calcic clinopyroxene and mafic silicate liquid: experimental results. J. Petrol. 17, 499-521.

Dungan M.A., Long P.E. and Rhodes J.M. (1978) The petrography, mineral chemistry and one-atmosphere phase relations of basalts from Site 395 - Leg 45 D.S.D.P. In: Initial Reports of the Deep Sea Drilling project, 45 (in press). Washington, D.C. U.S. Government Printing Office.

---------- and Rhodes J.M. (1978) Residual glasses and melt inclusions in basalts from DSDP Legs 45 and 46: Evidence for magma mixing. Contrib. Mineral. Petrol. 67, 417-431.

Ellis D.J. and Green D.H. (1979) An experimental study of the effect of Ca upon garnet-clinopyroxene Fe-Mg exchange equilibria. Contrib. Mineral. Petrol. 71, 13-22.

Elthon D. (1979) High magnesia liquids as the parental magma for ocean floor basalts. Nature 278, 514-518.

Engel A.E., Engel C.G. and Haven R.G. (1965) Chemical characteristics of oceanic basalts and the upper mantle. Bull. Geol. Soc. Am. 76, 719-734.

Erlank A.J. (1973) Kimberlitic potassic richterite and the distribution of potassium in the upper mantle. Int. Kimb. Conf. abst. 103-106. Univ. of Cape Town.

---------- and Kable E.J.D. (1976) The significance of incompatible elements in Mid-Atlantic Ridge basalts from 45°N, with particular reference to Zr/Nb. Contrib. Mineral. Petrol. 54, 281-291.

---------- and Rickard R.S. (1977) Potassic richterite bearing peridotites from kimberlite and the evidence they provide for upper mantle metasomatis Second Int. Kimb. Conf. (ext. abst.).

----------, Smith H.S., Marchant J.W., Cardoso M.P. and Ahrens L.H. (1978a) Hafnium. In Handbook of Geochemistry, Vol. II/5, (Ed) Wedepohl K.H., Springer-Verlag, Berlin.

---------- (1978b) Zirconium. In Handbook of Geochemistry, Vol. II/5, (Ed) Wedepohl K.H., Springer-Verlag, Berlin.

Evans B.W. and Frost B.R. (1975) Chrome-spinel in progressive metamorphism - a preliminary analysis. Geochim. Cosmochim. Acta 39, 959-972.

---------- and Wright T.L. (1972) Composition of liquidus chromite from the 1959 (Kilauea Iki) and 1965 (Makaoputi) eruptions of Kilauea Volcano-Hawaii. Am. Min. 57, 217-230.

Ewart A., Bryan W.B. and Gill J.B. (1973) Mineralogy and geochemistry of the younger volcanic islands of Tonga, S.W. Pacific. J. Petrol. 14 (3), 429-465.

-------- and Taylor S.R. (1969) Trace element geochemistry of the rhyolitic volcanic rocks, Central North Island, New Zealand. Phenocryst data. Contrib. Mineral. Petrol. 22, 127-146.

Fesq H.W., Bibby D.M., Sellschop J.P.F. and Watterson J.I.W. (1973) The determination of trace element impurities in natural diamonds by instrumental neutron activation analysis. J. Radioanal. Chem. 17, 195-216.

Flower M.F.J. (1971) Rare earth element distribution in lavas and ultramafic xenoliths from the Comores Archipelago, western Indian Ocean. Contrib. Mineral. Petrol. 31, 335-346.

----------, Robinson P.T., Schmincke H.-U. and Ohnmacht W. (1977) Magma fractionation systems beneath the Mid-Atlantic Ridge at 36-37°N. Contrib. Mineral. Petrol. 64, 167-195.

Fodor R.V., Husler J.W. and Kumar N. (1977) Petrology of volcanic rocks from an aseismic ridge: Implications for the origin of the Rio Grande Rise, South Atlantic Ocean. Earth Planet. Sci. Lett. 35, 225-233.

Fowler C.M.R. (1976) Crustal structure of the Mid-Atlantic Ridge crest at 37°N. Geophys. J.R. Astr. Soc. 47, 459-491.

Frey F.A., Bryan W.B. and Thompson G. (1974) Atlantic Ocean Floor: Geochemistry and petrology of basalts from Legs 2 and 3 of the Deep-Sea Drilling Project. J. Geophys. Res. 79 (35), 5507-5526.

---------, Dickey J.S., Thompson G. and Bryan W.B. (1976) Eastern Indian Ocean DSDP sites: Correlation between petrography, geochemistry and tectonic setting. Deep Sea Drilling in the Indian Ocean, Geol. Soc. Am. Mem., in press.

--------- and Green D.H. (1974) The mineralogy, geochemistry and origin of lherzolite inclusions in Victorian basanites. Geochim. Cosmochim. Acta 38, 1023-1059.

---------, Green D.H. and Roy S.D. (1978) Integrated models of basalt petrogenesis. A study of quartz tholeiites to olivine melilitites from south eastern Australia utilizing geochemical and experimental petrological data. J. Petrol. 19 (3), 463-513.

----------, Haskin M.A., Poetz J. and Haskin L.A. (1968) Rare earth abundances in some basic rocks. J. Geophys. Res. 73, 6085-6098.

Fudali R.F. (1965) Oxygen fugacities of basaltic and andesitic magmas. Geochim. Cosmochim. Acta 29, 1063-1075.

Fujii T. (1978)Fe-Mg partitioning between olivine and spinel. Carnegie Inst. Wash. Yearb. 1976-1977, 563-569.

Gast P.W. (1965) Terrestrial ratio of potassium to rubidium, and the composition of the earth's mantle. Science 147, 858-860.

-------- (1968) Trace element fractionation and the origin of tholeiitic and alkaline magma types. Geochim. Cosmochim. Acta 32, 1057-1086.

Glassley W.E. and Piper D.Z. (1978) Cobalt and scandium partitioning versus iron content for crystalline phases in ultramafic nodules. Earth Planet. Sci. Lett. 39, 173-178.

Goodman R.J. (1972) The distribution of Ga and Rb in coexisting groundmass and phenocryst phases of some basic volcanic rocks. Geochim. Cosmochim. Acta 36, 303-317.

Graham A.L. and Mason B. (1972) Niobium in meteorites. Geochim. Cosmochim. Acta 36, 917-922.

Green D.H. (1970) A review on experimental evidence on the origin of basaltic nephelinitic magmas. Phys. Earth Planet. Inter. 3, 221-235.

---------- (1971) Compositions of basaltic magmas as indicators of conditions of origin: application to oceanic volcanism. Phil. Trans. Roy. Soc. Lond. 268, 707-725.

----------, Edgar A.D., Beasley P., Kiss E. and Ware N.G. (1974) Upper mantle source for some hawaiites, mugearites and benmoreites. Contrib. Mineral. Petrol. 48, 33-43.

---------- and Hibberson W. (1970) Experimental duplication of conditions of precipitation of high-pressure phenocrysts in a basaltic magma. Phys. Earth Planet. Inter. 3, 247-254.

---------- and Ringwood A.E. (1967) The genesis of basaltic magmas. Contrib. Mineral. Petrol. 15, 103-190.

Greenland P.L. (1970) An equation for trace element distribution during magmatic crystallisation. Am. Min. 55, 455-465.

Greenwalt D. and Taylor P.T. (1974) Deep tow measurements across the axial valley of the Mid-Atlantic Ridge. J. Geophys. Res. 79, 4401-4406.

Grutzeck M., Kridelbough S. and Weill D. (1974) Distribution of Sr and the REE between diopside and silicate liquid. Geophys. Res. Lett. 1 (6), 273-275.

Gunn B.M., Coy-Yll R., Watkins N.D., Abranson C.E. and Nougier J. (1970) Geochemistry of an Oceanite-Ankaramite-Basalt suite from East Island, Crozet Archipelago. Contrib. Mineral. Petrol. 28, 319-339.

Haggerty S.E. (1971) Compositional variations in lunar spinels. Nature Phys. Sci. 233, 156-160.

---------- (1972a) Luna 16: an opaque mineral study and a systematic examination of compositional variations of spinels from Mare Fecunditatis Earth Planet. Sci. Lett. 13, 328-352.

---------- (1972b) Solid solution characteristics of lunar spinels. Carnegie Inst. Wash. Yearb. 71, 474-480.

---------- (1976) Opaque minerals in terrestrial igneous rocks. In Oxide Minerals. Chapter 8 (Ed) D. Rumble III, Southern Printing Company.

Hakli T.A. and Wright T.L. (1967) The fractionation of Ni between olivine and augite as a geothermometer. Geochim. Cosmochim. Acta 31, 877-884.

Hanson, G.N. (1977) Geochemical evolution of the suboceanic mantle. J. Geol. Soc. Lond. 134, 235-253.

---------- and Langmuir C.H. (1978) Modelling of major elements in mantle-melt systems using trace element approaches. Geochim. Cosmochim. Acta 42, 725-741.

Hart S.R. (1971) K, Rb, Cs, Sr and Ba contents and Sr isotope ratios of ocean floor basalts. Phil. Trans. Roy. Soc. Lond. A 268, 573-587.

--------- and Brooks C. (1974) Clinopyroxene-matrix partitioning of K, Rb, Cs, Sr, Ba. Geochim. Cosmochim. Acta 38, 1799-1806.

--------- and Davis K.E. (1978) Nickel partitioning between olivine and silicate melt. Earth Planet. Sci. Lett. 40, 203-219.

---------, Erlank A.J. and Kable E.J.D. (1974) Sea floor basalt alteration: Some chemical and Sr isotope effects. Contrib. Mineral. Petrol. 44, 219-230.

Hekinian R., Moore J.G. and Bryan W.B. (1976) Volcanic rocks and processes of the Mid-Atlantic Ridge rift valley near 36°49'N. Contrib. Mineral. Petrol. 39, 301-308.

---------- and Thompson G. (1976) Comparative geochemistry of volcanics from rift valleys, transform faults and aseismic ridges. Contrib. Mineral. Petrol. 57, 145-162.

Henderson P. (1977) Effect of silicate melt structure on mineral melt partitioning. Can. Min. 15, 202.

Hertogen J. and Gijbels R. (1976) Calculation of trace element fractionation during partial melting. Geochim. Cosmochim. Acta 40, 313-322.

Hill R. and Roeder P. (1974) The crystallisation of spinel from basaltic liquid as a function of oxygen fugacity. J. Geol. 82, 709-729.

Holtedahl O. (1929) On the geology and physiography of some Antarctic and Sub-Antarctic islands. Sci. Results Norw. Antarct. Exped. 1927-1928 (3), Norsk. Vid.-Akad. Oslo, 1-172.

Humphris S.E. and Thompson G. (1978a) Hydrothermal alteration of oceanic basalts by seawater. Geochim. Cosmochim. Acta 42, 107-125.

---------- (1978b) Trace element mobility during hydrothermal alteration of oceanic basalts. Geochim. Cosmochim. Acta 42, 127-136.

Imsland P., Larsen J.G., Prestvik T. and Sigmond E. (1977) The geology and petrology of Bouvetøya , South Atlantic Ocean. Lithos 10, 213-234.

Irvine T.N. (1967) Chromian spinel as a petrogenetic indicator. Part 2. Petrologic application. Can. J. Earth. Sci. 4, 71-103.

---------- and Baragar W.R. (1971) A guide to the chemical classification of the common volcanic rocks. Can. J. Earth Sci. 8, 523-548.

---------- and Kushiro I. (1976) Partitioning of Ni and Mg between olivine and silicate liquids. Carnegie Inst. Wash. Yearb. 75, 668-675.

Irving A.J. (1978) A review of experimental studies of crystal/liquid trace element partitioning. Geochim. Cosmochim. Acta 42, 743-770.

---------- and Frey F.A. (1976) Effect of composition on the partitioning of rare earth elements, Hf, Sc and Co between garnet and liquid: experimental and natural evidence (abstract). EOS. Trans. Am. Geophys. Union 57, 339.

---------- (1977) Experimental partitioning of trace elements between garnet and hydrous acidic melt. (Abs.). International Conference on experimental trace element geochemistry, September 1977.

---------- (1978) Distribution of trace elements between garnet megacrysts and host volcanic liquids of kimberlitic to rhyolitic composition. Geochim. Cosmochim. Acta 42, 771-787.

Ito J. and Frondel C. (1967) Synthetic zirconium and titanium garnets. Am. Min. 52, 773-781.

Ito K. and Kennedy G.C. (1967) Melting and phase relations in a natural peridotite to 40 kilobars. Am. J. Sci. 265, 519-538.

Jackson E.D. (1969) Chemical variation in coexisting chromite and olivine in chromitite zones of the Stillwater Complex. Econ. Geol. Mono. 4, 41-71.

Jakobsson P., Jonsson J. and Shido F. (1978) Petrology of the Western Reykjanes Peninsula Iceland. J. Petrol. 19, 669-705.

Johnson G.L., Hey R.N. and Lowrie A. (1973) Marine geology in the environs of Bouvet Island and the South Atlantic Triple Junction. Marine Geophys. Res. 2, 23-36.

Kable E.J.D. (1972) Some aspects of the geochemistry of selected elements in basalts and associated lavas. Unpubl. Ph.D. thesis, University of Cape Town.

Kay R., Hubbard N.J. and Gast P.W. (1970) Chemical characteristics and origin of oceanic ridge volcanic rocks. J. Geophys. Res. 75, 1585-1613.

Kennedy G.C. (1948) Equilibrium between volatiles and oxides in igneous rocks. Am. J. Sci. 246, 529-549.

Kesson S.E. (1973) The primary geochemistry of the Monaro Alkaline volcanics, Southeastern Australia - evidence for upper mantle heterogeneity. Contrib. Mineral. Petrol. 42, 93-108.

---------- and Price R.C. (1972) The major and trace element chemistry of kaersutite and its bearing on the petrogenesis of alkaline rocks. Contrib. Mineral. Petrol. 35, 119-124.

Knutson J. and Green T.H. (1975) Experimental duplication of a high pressure megacryst/cumulate assemblage in a near saturated hawaiite. Contrib. Mineral. Petrol. 52, 121-132.

Korringa M.K. and Noble D.C. (1971) Distribution of Sr between natural feldspar and igneous melt. Earth Planet. Sci. Lett. 11, 147-151.

Krishnamurphy P. and Cox K.G. (1977) Picrite basalts and related lavas from the Deccan Traps of Western India. Contrib. Mineral. Petrol. 62, 53-75.

Kushiro I. (1968) Compositions of magmas formed by partial zone melting of the earths upper mantle. J. Geophys. Res. 73, 619-634.

---------- (1969) The system fosterite-diopside-silica with and without water at high pressures. Am. J. Sci. 267 A, 269-294.

----------, Nekamura Y., Haramura H. and Akimoto S. (1970) Crystallisation of some lunar mafic magmas and generation of rhyolitic liquid. Science 167, 610-612.

Kusznir N.J. and Bott M.H.P. (1976) A thermal study of the formation of oceanic crust. Geophys. J.R. Astr. Soc. 47, 83-95.

La Bas M.J. (1962) The role of aluminium in igneous clinopyroxenes with relation to their parentage. Am. J. Sci. 260, 267-288.

Langmuir C.H., Bender J.F., Bence A.E. and Hanson G.N. (1977) Petrogenesis of basalts from the FAMOUS area: Mid-Atlantic Ridge. Earth Planet. Sci. Lett. 36, 133-156.

---------- and Hanson G.N. (1977) Dynamic melting of mantle. (Abs.) International conference on experimental trace element geochemistry, September 1977.

Leeman W.P. (1974) Experimental determination of partitioning of divalent cations between olivine and basaltic liquid. Unpubl. Ph.D. thesis, University of Oregon, Part II.

---------- (1979) Partitioning of Pb between volcanic glass and coexisting sanidine and plagioclase feldspars. Geochim. Cosmochim. Acta 43, 171-175.

---------- and Lindstrom D.J. (1978) Partitioning of Ni^{2+} between basaltic and synthetic melts and olivines - an experimental study. Geochim. Cosmochim. Acta 42, 801-816.

----------, Ma M.-S, Murali A.V. and Schmitt R.A. (1978a) Empirical estimation of magnetite/liquid distribution coefficients for some transition elements. Contrib. Mineral. Petrol. 65, 269-272.

---------- (1978b) Empirical estimation of magnetite/liquid distribution coefficients for some transition elements. A correction. Contrib. Mineral. Petrol. 66, 429.

Leeman W.P., Murali A.V., Ma M.-S. and Schmitt R.A. (1977) Mineral constitution of mantle source regions for Hawaiian basalts - rare earth evidence for mantle heterogeneity. In: Oregon Dept. Geol. Mineral. Indus. Bull. 96. Proceedings of the AGU Chapman Conf. on partial melting in the Earth's upper mantle.

---------- and Scheidegger K.F. (1977) Olivine/liquid distribution coefficients and a test for crystal liquid equilibrium. Earth Planet. Sci. Lett. 35, 247-257.

le Roex A.P.and Reid D.L. (1978) Geochemistry of Karroo dolerite sills in the Calvinia district, Western Cape Province, South Africa. Contrib. Mineral. Petrol. 66, 351-360.

Lindsley D.H. and Munoz J.L. (1969) Subsolidus relations along the join hedenbergite-ferrosilite. Am. J. Sci. 267A, 295-324.

Lindstrom D.J. (1976) Experimental study of the partitioning of the transition metals between clinopyroxene and coexisting silicate liquids. Unpubl. Ph.D. thesis, University of Oregon.

---------- and Weill D.F. (1978) Partitioning of transition metals between diopside and coexisting silicate liquids. I nickel, cobalt and manganese. Geochim. Cosmochim. Acta 42, 817-831.

Littlejohn A.L. and Greenwood H.J. (1974) Lherzolite nodules in basalts from British Columbia, Canada. Can. J. Earth Sci. II, 1288-1308.

Lloyd F.E. and Bailey P.K. (1975) Light element metasomatism of the continental mantle: The evidence and consequences. Phy. Chem. Earth 9, 389-416.

Long P.E. (1978) Experimental determination of partition coefficients for Rb, Sr and Ba between alkali feldspar and silicate liquid. Geochim. Cosmochim. Acta 42, 833-846.

Longhi J., Walker D. and Hays J.F. (1978) The distribution of Fe and Mg between olivine and lunar basaltic liquids. Geochim. Cosmochim. Acta 42, 1545-1558.

Ludden J.N. (1978a) Magmatic evolution of the basaltic shield volcanoes of Reunion Island. J. Volcan. Geotherm. Res. 4, 171-198.

---------- (1978b) Fractionation trends defined by residual glasses in the lavas and xenoliths of Piton de la Fournaise, Reunion Island. Can. Min. 16, 265-276.

Ludwig K.R. and Stuckless J.S. (1978) Uranium - lead isotope systematics and apparent ages of zircons and other minerals in Precambrian granitic rocks, Granite Mountains, Wyoming. Contrib. Mineral. Petrol. 65, 243-254.

Maaløe S. (1979) Compositional range of primary tholeiitic magmas evaluated from major element trends. Lithos 12, 59-72.

Masuda A. and Kushiro I. (1970) Experimental determination of partition coefficients of ten rare earth elements and Ba between clinopyroxene and liquid in the synthetic silicate system at 20 kbar pressure. Contrib. Mineral. Petrol. 26, 42-49.

Mathews D.H. (1971) Altered basalts from Swallow Bank, an abyssal hill in the NE Atlantic, and from a nearby seamount. Phil. Trans. Roy. Soc. Lond. A 268, 551-571.

Mathez E.A. (1973) Refinement of the Kudo-Weill plagioclase thermometer and its application to basaltic rocks. Contrib. Mineral. Petrol. 41, 61-72.

McCallum I.S. and Charette M.P. (1978) Zr and Nb partition coefficients: implication for the genesis of mare basalts KREEP and sea floor basalts. Geochim. Cosmochim. Acta 42, 859-869.

McKay G.A. and Weill D.F. (1976) Petrogenesis of KREEP. Proc. Seventh Lunar Sci. Conf., 2427-2447.

---------- (1977) KREEP petrogenesis revisited. Proc. Eighth Lunar Sci. Conf., 2339-2355.

Melson W.G. and Thompson G. (1971) Petrology of a transform fault zone and adjacent ridge segments. Phil. Trans. Roy. Soc. Lond. A 268, 423-441.

Minster J.F., Minster J.B., Treuil M. and Allègre C.J. (1977) Systematic use of trace elements in igneous processes. Part II: Inverse problem of the fractional crystallisation processes in volcanic suites. Contrib. Mineral. Petrol. 61, 49-77.

Morgan W.J. (1971) Convection plumes in the lower mantle. Nature 230, 42-43.

---------- (1972) Deep mantle convection plumes and plate motions. Am. Assoc. Petrol. Geol. Bull. 56, 203-213.

---------- (1973) Plate motions and deep mantle convection. Geol. Soc. Am. Mem. 132, 7-22.

Mori T. (1978) Experimental study of pyroxene equilibria in the system $CaO-MgO-FeO-SiO_2$. J. Petrol. 19, 45-65.

Mottl M.J. and Holland H.D. (1978) Chemical exchange during hydrothermal alteration of basalt by seawater - I. Experimental results for major and minor components of seawater. Geochim. Cosmochim. Acta 42, 1103-1115.

Mysen B.O.(1975) Partitioning of iron and magnesium between crystals and partial melts in peridotitic upper mantle. Contrib. Mineral. Petrol. 52, 69-76.

--------- (1976a) Partitioning of samarium and nickel between olivine orthopyroxene, and liquid: Preliminary data at 20 kbar and 1025°C. Earth Planet. Sci. Lett. 31, 1-7.

--------- (1976b) Nickel partitioning between upper mantle crystals and partial melts as a function of pressure, temperature and nickel concentration. Carnegie Inst. Wash. Yearb. 75, 662-668.

--------- (1978) Experimental determination of nickel partition coefficients between liquid, pagasite and garnet peridotite minerals and concentration limits of behaviour according to Henry's law at high pressure and temperature. Am. J. Sci. 278, 217-243.

---------- (1979) Trace element partitioning between garnet peridotite minerals and water-rich vapour: experimental data from 5 to 30 kbar. Am. Min. 64, 274-287.

---------- and Kushiro I. (1976) Partitioning of iron, nickel and magnesium between metal, oxide and silicates in Allende meteorite as a function of fO_2. Carnegie Inst. Wash. Yearb. 75, 678-684.

---------- (1979) Pressure dependance of nickel partitioning between fosterite and aluminium silicate melts. Earth Planet. Sci. Lett. 42, 383-388.

Nagasawa H. (1970) Rare earth concentrations in zircons and apatites and their host dacites and granites. Earth Planet. Sci. Lett. 9, 359-364.

---------- (1973) Rare earth distribution in alkali rocks from Oki-Dogo Island, Japan. Contrib. Mineral. Petrol. 39, 301-308.

---------- and Schnetzler C.C. (1971) Partitioning of rare earth, alkalic and alkaline earth elements between phenocrysts and acidic igneous magma. Geochim. Cosmochim. Acta 35, 953-968.

----------, Schreiber H.D. and Blanchard D.P. (1976) Partition coefficients of REE and Sc in perovskite, melilite and spinel and their implications for Allende inclusions. (Abs.) Lunar Sci. VII, 588-590.

Needham H.D. and Francheteau J. (1974) Some characteristics of the rift valley in the Atlantic Ocean near 36°48' N. Earth Planet. Sci. Lett. 22, 29-43.

Neibuhr H.H., Zeira S. and Hafner S.S. (1973) Ferric iron in plagioclase crystals from anorthosite 15415. Proc. Fourth Lunar Sci. Conf., 971-982.

Nesbitt R.W. and Sun S.S. (1976) Geochemistry of Archean spinifex-textured peridotites and magnesian and low-magnesian tholeiites. Earth Planet. Sci. Lett. 31, 433-453.

Neumann E.R. (1976) Two refinements for the calculation of structural formulae for pyroxenes and amphiboles. Nor. Geol. Tidsskr. 56, 1-6.

Nisbet E.G. and Fowler C.M.R. (1978) The Mid-Atlantic Ridge at 37° and 45°N: some geophysical and petrological constraints. Geophys. J.R. Astr. Soc. 54, 631-660.

---------- and Pearce J.A. (1977) Clinopyroxene composition in mafic lavas from different tectonic settings. Contrib. Mineral. Petrol. 63, 149-160.

Norrish K. and Hutton J.T. (1969) An accurate X-ray spectrographic method for the analysis of a wide range of geological samples. Geochim. Cosmochim. Acta 33, 431-453.

Norton I. (1976) The present relative motion between Africa and Antarctica. Earth Planet. Sci. Lett. 33, 219-230.

O'Hara M.J. (1965) Primary magmas and the origin of basalts. Scott. J. Geol. 1, 19-40.

---------- (1968) Are ocean floor basalts primary magma? Nature 220, 683-686.

---------- (1977) Geochemical evolution during fractional crystallisation of a periodically refilled magma chamber. Nature 266, 503-507.

----------, Saunders M.J. and Mercy E.L.P. (1975) Garnet peridotite, primary ultrabasic magma and eclogite; interpretation of upper mantle processes in kimberlite. Phys. Chem. Earth 9, 571-604.

O'Nions R.K., Hamilton P.J. and Evensen N.M. (1977) Variations in $^{143}Nd/^{144}Nd$ and $^{87}Sr/^{86}Sr$ ratios in oceanic basalts. Earth Planet. Sci. Lett. 34, 13-22.

---------- and Pankhurst R.J. (1974) Petrogenetic significance of isotope and trace element variations in volcanics from the Mid-Atlantic. J. Petrol. 15, 603-634.

----------, Pankhurst R.J. and Gronwold K. (1976) Nature and development of basalt magma sources beneath Iceland and the Reykjanes Ridge. J. Petrol. 17, 315-338.

Onuma N., Higuchi H., Waikita H. and Nagasawa H. (1968) Trace element partition between two pyroxenes and the host lava. Earth Planet. Sci. Lett. 5, 47-51.

Pankhurst R.J. (1977) Open system crystal fractionation and incompatible element variations in basalts. Nature 268, 36-38.

Papike J.J., Cameron K.L. and Baldwin K. (1974) Amphiboles and pyroxenes: characterisation of other than quadrilateral components and estimates of ferric iron from microprobe data. Geol. Soc. Am. Abs. with Prog. 6, 1053-1054.

Paster T.P., Schauwecker D.S. and Haskin L.A. (1974) The behaviour of some trace elements during solidification of the Skaergaard layered series. Geochim. Cosmochim. Acta 38, 1549-1577.

Pearce J.A. and Cann J.R. (1973) Tectonic setting of basic volcanic rocks determined using trace element analysis. Earth Planet Sci. Lett. 19, 290-300.

---------- and Norry M.J. (1979) Petrogenetic implication of Ti, Zr, Y and Nb variations in volcanic rocks. Contrib. Mineral. Petrol. 69, 33-47.

Pearce T.H. (1978) Olivine fractionation equations for basaltic and ultrabasic liquids. Nature 276, 771-774.

Philpotts J.A. and Schnetzler C.C. (1970) Phenocryst-matrix partition coefficient for K, Rb, Sr and Ba, with application to anorthosite and basalt genesis. Geochim. Cosmochim. Acta 34, 307-322.

Pierozynski W.J. and Henderson C.M.B. (1978) Distribution of Sr, Ba and Rb between alkali feldspar and silicate melt. Progress in Exper. Petrol. In Fourth progress report of research supported by N.E.R.C. 1975-1978. (Ed.) Mackenzie W.S.

Platt R.G. and Mitchell R.H. (1979) The Marathon Dikes: Zirconium-rich titanian garnets and manganoan magnesian ulvöspinel-magnetite spinels. Am. Min. 64, 546-550.

Price R.C. and Taylor S.R. (1973) The geochemistry of the Dunedin Volcano, East Otogo, New Zealand: Rare earth elements. Contrib. Mineral. Petrol. 40, 195-205.

Puchelt H. and Emmermann R. (1976) Bearing of rare earth patterns of apatites from igneous and metamorphic rocks. Earth Planet. Sci. Lett. 31, 279-286.

Reid D.L. (1977) Geochemistry of Precambrian igneous rocks in the lower Orange River region. Unpubl. Ph.D. Thesis. University of Cape Town.

Rhodes J.M., Dungan M.A., Blanchard D.P. and Long P.E. (1979) Magma mixing at mid-ocean ridges: evidence from basalts drilled near 22°N on the Mid-Atlantic Ridge. Tectonophys. 55, 35-61.

Richard P., Shinizu N. and Allègre C.J. (1976) $^{143}Nd/^{146}Nd$ a natural tracer: an application to oceanic basalts. Earth Planet. Sci. Lett. 31, 269-278.

Rickard R.S. and le Roex A.P. (1977) The determination of strontium in silicate minerals using electron microprobe techniques. Proc. Electron Microscopy Soc. S.A., Vol. 7, 85-86.

Ringwood A.E. (1970) Petrogenesis of Apollo 11 basalts and implications for lunar origin. J. Geophys. Res. 75, 6453-6479.

Robie R.A. and Waldbaum D.R. (1968) Thermodynamic properties of minerals and related substances at 298.15 K and one atm. pressure and at higher temperatures. Bull. U.S. Geol. Surv. 1259.

Roeder P.L. (1974) Activity of iron and olivine solubility in basaltic liquids. Earth Planet. Sci. Lett. 23, 397-410.

----------, Campbell I.H. and Jamieson H.E. (1979) A re-evaluation of the olivine-spinel geothermometer. Contrib. Mineral. Petrol. 68, 325-334.

---------- and Emslie R.F. (1970) Olivine-liquid equilibrium. Contrib. Mineral. Petrol. 29, 275-289.

Ross M., Hubner J.S. and Dowty E. (1973) Deliniation of the one atmosphere augite-pigeonite miscibility gap for pyroxenes from lunar basalt 12021. Am. Min. 58, 619-635.

-------, Bence A.E., Dwornik E.J., Clarke J.R. and Papike J.J. (1970) Lunar clinopyroxenes: chemical composition, structural state and texture. Science 167, 628-630.

Ryerson F.J. and Hess P.C. (1978) Implications of liquid-liquid distribution coefficients to mineral-liquid partitioning. Geochim. Cosmochim. Acta 42, 921-932.

Sato H. (1977) Nickel content of basaltic magma: Identification of primary magmas and a measure of the degree of olivine fractionation. Lithos 10, 113-120.

Scheidegger K.F. (1973) Temperatures and compositions of magmas ascending along midocean ridges. J. Geophys. Res. 78, 3340-3355.

Schilling J.-G. (1971) Sea-floor evolution: Rare earth evidence. Phil. Trans. Roy. Soc. Lond. A 268, 663-706.

---------- (1973) Iceland mantle plume: rare earth evidence. Nature Phys. Sci. 242, 2-5.

---------- (1975a) Azores Mantle blob: rare earth evidence. Earth Planet. Sci. Lett. 25, 103-115.

---------- (1975b) Rare earth variations across 'normal segments' of the Reykjanes ridge, 60°-53°N, Mid-Atlantic ridge, 29°S, and East Pacific rise, 2°-19°S, and evidence on the composition of the underlying low-velocity layer. J. Geophys. Res. 80, 1459-1473.

---------- and Winchester J.W. (1967) Rare-earth fractionation and magmatic processes. In: Mantles of Earth and Terrestrial Planets, (Ed). Runcom F.R.S., pp. 267-283. Interscience.

---------- (1969) Rare earth contribution to the origin of the Hawaiian lavas. Contrib. Mineral. Petrol. 23, 27-37.

Schock H.H. (1977) Trace element partition between phenocrysts of plagioclase, pyroxenes and magnetite and their host pyroclastic matrix. J. Radioan. Chem. 38, 327-340.

Schreiber H.D. (1976) The experimental determination of redox states, properties and distribution of chromium in synthetic silicate phases and application to basalt petrogenesis. Unpubl. Ph.D. thesis. University of Wisconsin.

Schweitzer E.L., Papike J.J. and Bence A.E. (1978) Clinopyroxenes from deep-sea basalts: a statistical analysis. Geophys. Res. Lett. 5, 573-576.

---------- (1979) Statistical analysis of clinopyroxenes from deep-sea basalts. Am. Min. 64, 501-513.

Sclater J.G., Bowin C., Hey R., Haskins H., Purie J., Phillips J. and Tapscott C. (1976) The Bouvet Triple Junction. J. Geophys. Res. 81, 1857-1869.

Sclater J.G., Dick H., Norton I.O. and Woodroffe D. (1978) Tectonic structure and petrology of the Antarctic plate boundary near the Bouvet Triple Junction. Earth Planet. Sci. Lett. 37, 393-400.

Seitz M.G. (1974) Fractionation of a REE between diopside and basalt at 20 kbar pressure. Carnegie Inst. Wash. Yearb. 73, 547-551.

Seitz M.G. and Shimizu N. (1972) Partitioning of uranium in the Di-Al-An system and a spinel lherzolite system by fission track mapping. Carnegie Inst. Wash. Yearb. 71, 548-553.

Seward T.M. (1971) The distribution of transition elements in the system $CaMgSi_2O_6$- $Na_2Si_2O_5$-H_2O at 1000 bars pressure. Chem. Geol. 7, 73-95.

Shaw D.M. (1970) Trace element fractionation during anatexis. Geochim. Cosmochim. Acta 34, 237-243.

Shee S.R. (1978) The mineral chemistry of xenoliths from the Orapa Kimberlite Pipe, Botswana. Unpublished M.Sc. thesis, University of Cape Town.

Shibata T. and Fox P.J. (1975) Fractionation of abyssal tholeiites. Samples from the Oceanographer fracture zone (35°N, 35°W). Earth Planet. Sci. Lett. 27, 62-72.

Shibata T., De Long S.E. and Walker D. (1979a) Abyssal tholeiites from the oceanographer fracture zone. I Petrology and fractionation. Contrib. Mineral. Petrol. 70, 89-102.

----------, Thompson G. and Frey F.A. (1979b) Tholeiitic and alkali basalts from the Mid-Atlantic Ridge at 43°N. Contrib. Mineral Petrol. 70, 127-141.

Shido F.A., Miyashiro A. and Ewing M. (1971) Crystallisation of abyssal tholeiites. Contrib. Mineral. Petrol. 31, 251-266.

Shimizu N. (1974) An experimental study of the partitioning of K, Rb, Cs, Sr and Ba between clinopyroxene and liquid at high pressure. Geochim. Cosmochim. Acta 38, 1789-1798.

---------- and Allègre C.J. (1978) Geochemistry of transition elements in garnet lherzolite nodules in kimberlites. Contrib. Mineral. Petrol. 67, 41-50.

Sigurdsson H. (1977) Spinels in Leg 37 basalts and peridotites : phase chemistry and zoning. In: Initial Reports of the Deep Sea Drilling Project, 37, Washington D.C., U.S. Government Printing Office.

---------- and Schilling J.-G. (1976) Spinels in Mid-Atlantic Ridge basalts: Chemistry and occurrence. Earth Planet. Sci. Lett. 29, 7-20.

Simkin T. and Smith J.V. (1970) Minor element distribution in olivine. J. Geol. 78, 304-325.

Sleep N.H. (1975) Formation of oceanic crust: some thermal constraints. J. Geophys. Res. 80, 4037-4042.

Smith D. (1971) Stability of the assemblage iron rich orthopyroxene-olivine-quartz. Am. J. Sci. 271, 370-382.

-------- (1972) Stability of iron-rich pyroxene in the system $CaSiO_3$-$FeSiO_3$-$MgSiO_3$. Am. Min. 57, 1413-1428.

-------- and Lindsley D.H. (1971) Stable and metastable augite crystallisation trends in a single basalt flow. Am. Min. 56, 225-233.

Smith H.S., Erlank A.J. and Duncan A.R. (in press) Geochemistry of some ultramafic komatiite lava flows from the Barberton Mountain Land, South Africa. Precambrian Res. (in press).

Smith R.E. (1967) Segregation vesicles in basaltic lava. Am. J. Sci. 265, 696-713.

Snape C. (1971) Paleomagnetism of three samples of lava from Bouvet Island. In: Marion and Prince Edward Islands. (eds) E.M. van Zinderen Bakker Sr., J.M. Winterbottom and R.A. Dyer, Cape Town, A.A. Balkema p 69-71.

Starke P. (1966) South African expedition to Bouvet Island 1966. Antarctic J. 1 (5), 232-234.

Subbaro K.V. and Hekinian R. (1978) Alkali enriched rocks from the Central Eastern Pacific Ocean. Marine Geol. 26, 249-268.

Sun C., Williams R.J. and Sun S.-S.(1974) Distribution coefficients of Eu and Sr for plagioclase-liquid and clinopyroxene-liquid equilibria in oceanic ridge basalt: an experimental study. Geochim. Cosmochim. Acta 38, 1415-1433.

Sun S.-S. and Hanson G.N. (1975a) Evolution of the mantle: Geochemical evidence from alkali basalt. Geology 3, 297-302.

---------- (1975b) Origin of Ross island basanitoids and limitations upon the heterogeneity of mantle sources for alkali basalts and nephelinites. Contrib. Mineral. Petrol. 52, 77-106.

---------- (1976) Rare earth element evidence for differentiation of McMurdo Volcanics, Ross Island, Antarctica. Contrib. Mineral. Petrol. 54, 139-155.

--------- and Nesbitt R.W. (1977) Chemical heterogeneity of the Archean Mantle: Composition of the earth and mantle evolution. Earth Planet. Sci. Lett. 35, 429-448.

--------, Nesbitt R.W. and Sharaskin A.Ya. (1979) Geochemical characteristics of Mid-ocean ridge basalts. Earth Planet. Sci. Lett. 44, 119-138.

---------, Tatsumoto M. and Schilling J.-G. (1975) Mantle plume mixing along the Reykjanes Ridge axis: lead isotope evidence. Science 190, 143-147.

Takahashi E. (1978) Partitioning of Ni^{2+}, Co^{2+}, Fe^{2+}, Mn^{2+} and Mg^{2+} between olivine and silicate melts: compositional dependence of partition coefficient. Geochim. Cosmochim. Acta 42, 1829-1844.

Tanaka T. and Nishizawa O. (1975) Partition of REE, Ba and Sr between crystal and liquid phases for a natural silicate system at 20 kb. pressure. Geochem. J. 9, 161-166.

Tatsumoto M. (1966) Genetic relations of oceanic basalts as indicated by lead isotopes. Science 153, 1094-1101.

----------, Hedge C.E. and Engel A.E.J. (1965) Potassium-rubidium, strontium, thorium, uranium, and the ratio of strontium-87 to strontium-86 in oceanic tholeiitic basalt. Science 150, 1886.

Taylor S.R. (1965) Geochemical analysis by spark source mass spectrography. Geochim. Cosmochim. Acta 29 (12), 1243-1261.

---------- (1971) Geochemical application of spark source mass spectrography-II. Photoplate data processing. Geochim. Cosmochim. Acta 35 (11), 1187-1196.

---------- and Gorton M.P. (1977) Geochemical application of spark source mass spectrography-III. Element sensitivity, precision and accuracy. Geochim. Cosmochim. Acta 41, 1375-1380.

Thompson G. and Melson W.G. (1972) The petrology of oceanic crust across fracture zones in the Atlantic ocean: evidence of a new kind of sea-floor spreading. J. Geol. 80, 526-538.

Thompson R.N. (1972) Evidence for a chemical discontinuity near the basalt-'andesite' transition in many anorogenic volcanic suites. Nature 236, 106-110.

---------- (1973) Titanian chromite and chromian titanomagnetite from a Snake River Plain basalt, a terrestrial analogue to lunar spinels. Am. Min. 58, 826-830.

---------- (1974) Primary basalts and magma genesis I. Skye, north-west Scotland. Contrib. Mineral. Petrol. 45, 317-341.

---------- (1975) Primary basalts and magma genesis, II. Snake River Plain, Idaho. Contrib. Mineral. Petrol. 52, 213-232.

Thornton C.P. and Tuttle O.F. (1960) Chemistry of igneous rocks. I: Differentiation index. Am. J. Sci. 258, 664-684.

Upton B.G.J. and Wadsworth W.J. (1972) Aspects of magmatic evolution of Reunion Island. Phil. Trans. Roy. Soc. Lond. A 271, 105-130.

Usselman T.M. and Hodge D.S. (1978) Thermal control of low-pressure fractionation processes. J. Volcan. Geotherm. Res. 4, 265-281.

Verhoogen J. (1962) Distribution of titanium between silicates and oxides in igneous rocks. Am. J. Sci. 260, 211-220.

Verwoerd W.J. (1966) Geologie en kartografie van die suidelike eilande. Tegnikon 15, 105-113.

----------(1972) Islands on the mid-ocean ridge between Africa and Antarctica (Abstr.) EOS Trans. Am. Geophys. Union 53, 168-170.

----------, Erlank A.J. and Kable E.J.D. (1974) Geology and Geochemistry of Bouvet Island. Proc. of the Symposium on 'Andean and Antarctic Volcanology Problems' (Santiago, Chile, September 1974).

Viswanatha Reddy V., Subbarao K.V., Reddy G.R., Matsuda J. and Hekinian R. (1978) Geochemistry of volcanics from the Ninetyeast Ridge and its vicinity in the Indian ocean. Marine Geol. 26, 99-117.

Walker D. and Hays J.F. (1977) Plagioclase flotation and lunar crust formation. Geology 5, 425-428.

Wass S.Y. (1973) Oxides of low pressure origin from alkalic basaltic rocks, Southern Highlands, N.S.W., and their bearing on the petrogenesis of alkali-basaltic magmas. J. Geol. Soc. Austr. 20, 427-447.

Watson E.B. (1976) Glass inclusions as samples of early magmatic liquid: determinative method and application to a South Atlantic basalt. J. Volc. Geotherm. Res. 1, 73-84.

---------- (1977) Partitioning of manganese between fosterite and silicate liquid. Geochim. Cosmochim. Acta 41, 1363-1374.

Weill D.F. and McKay G.A. (1975) The partitioning of Mg, Fe, Sr, Ce, Sm, Eu and Yb in lunar igneous systems and a possible origin of KREEP by equilibrium partial melting. Proc. Sixth Lunar Sci. Conf., 1143-1158.

Wenk H.R. and Wilde W.R. (1973) Chemical anomalies in lunar plagioclase described by substitutiton vectors and their relation to optical and structural properties. Contrib. Mineral. Petrol. 41, 89-104.

White W.M. and Bryan W.B. (1977) Sr-isotope, K, Rb, Cs, Sr, Ba, and rare-earth geochemistry of basalts from the FAMOUS area. Geol. Soc. Am. Bull. 88, 571-576.

---------- and Schilling J.-G. (1978) The nature and origin of geochemical variation in Mid-Atlantic Ridge basalts from the Central North Atlantic. Geochim. Cosmochim. Acta 42, 1501-1516.

----------, Schilling J.-G. and Hart S.R. (1976) Evidence for the Azores Mantle plume from strontium isotope geochemistry of the Central North Atlantic. Nature 263, 659-663.

Willis J.P. (1979) Some aspects of the geochemistry of gallium in silicate rocks and stony meteorites. Unpubl. Ph.D. thesis, University of Cape Town.

----------, Ahrens L.H., Danchin R.V., Erlank A.J., Gurney J.J., Hofmeyer P.K. McCarthy T.S. and Orren M.J. (1971) Some interelement relationships between lunar rocks and fines and stony meteorites. In: Proc. Second Lunar Sci. Conf., 1123-1138.

----------, Erlank A.J., Gurney J.J., Theil R.H. and Ahrens L.H. (1972) Major, minor and trace element data for some Apollo 11, 12, 14 and 15 samples. In: Proc. Third Lunar Sci. Conf., 1269-1273.

Winsnes T.S. (1966) Besøk på Bouvetøya i 1958 og 1966. Nor. Polarinst. Årbok 1965, 143-149.

Wood B.J. (1974) The solubility of alumina in orthopyroxene coexisting with garnet. Contrib. Mineral. Petrol. 46, 1-15.

--------- and Fraser D.G. (1976) Elementary thermodynamics for geologists. Oxford University Press, Oxford, pp 303.

Wood D.A. (1979) Dynamic partial melting : its application to the petrogenesis of basalts erupted in Iceland, the Faeroe Islands, the Isle of Skye (Scotland) and the Troodos Massif (Cyprus). Geochim. Cosmochim. Acta 43, 1031-1046.

Wright T.L. (1974) Presentation and interpretation of chemical data for igneous rocks. Contrib. Mineral. Petrol. 48, 233-248.

Yin Yin Nwe (1975) Two different pyroxene crystallisation trends in the Trough Bands of the Skaergaard Intrusion, East Greenland. Contrib. Mineral. Petrol. 49, 285-300.

Yoder H.S. (1976) Generation of basaltic magmas. National Academy of Sciences, Washington D.C. 1976.

---------- and Tilley C.E. (1962) Origin of basalt magmas: an experimental study of natural and synthetic rock systems. J. Petrol. 3, 342-532.

Zielinsky R.A. and Frey F.A. (1970) Gough Island: evaluation of a fractional crystallisation model. Contrib. Mineral. Petrol. 29, 242-254.

APPENDIX

A1. ANALYTICAL TECHNIQUES

A1.1 Whole rock analyses

A1.1.1 Major elements:

All major elements (with the exception of Na) were analysed by X-ray fluorescence (XRF), using the lithium tetraborate fusion method of Norrish and Hutton (1969). Na was analysed by XRF using pressed powder briquettes, prepared using the method of Baird (1961). The operating conditions used are the routine procedures adopted in the Department of Geochemistry at U.C.T: they have been described in detail by Willis et al. (1971, 1972).

Natural rock standards used for calibration include the U.S.G.S. standard set and in-house standards originally calibrated against the U.S.G.S. standard set. Estimates of the precision and detection limits for the major oxides and of the accuracy of the data (derived from the average absolute error on the standard calibration curves) are given in Table A1-1.

A1.1.2 Trace elements:

Unless otherwise noted all trace elements were analysed by XRF, using pressed powder briquettes. The procedures followed are similar to those outlined in Willis et al. (1971, 1972), and the operating conditions are those adopted for routine trace element analysis in the Department of Geochemistry at U.C.T. Natural rock standards used for calibration include the U.S.G.S. standard set and in-house standards

Table A1-1: Estimated precision and detection limits and average absolute error (accuracy) on the calibration curves for the major oxides using XRF techniques. Precision is expressed as an absolute error (2σ) on the given percentage oxide.

OXIDE	PERCENTAGE	PRECISION	ACCURACY	DETECT. LIMIT
Fe_2O_3	9.0	0.038	0.064	0.014
MnO	0.15	0.008	0.003	0.008
TiO_2	1.0	0.008	0.008	0.005
CaO	12.0	0.028	0.030	0.008
K_2O	0.20	0.002	0.022	0.002
P_2O_5	0.20	0.012	0.018	0.011
SiO_2	50.0	0.140	0.264	0.036
Al_2O_3	15.0	0.080	0.079	0.022
MgO	8.0	0.148	0.086	0.072
Na_2O	2.5	0.032	0.067	0.080
Cr_2O_3	0.5	0.008	0.012	0.007
NiO	0.3	0.008	0.005	0.006

calibrated against the U.S.G.S. standards. Estimates of the uncertainties in the data due to counting statistics are given in Table A1-2. In instances where very low detection limits and errors were required - e.g. for Nb in the picritic basalts from the FAMOUS area and in the analysis of mineral separates, counting times were increased by a factor of 6, reducing the average precision errors and detection limits (Table A1-2) by approximately a factor of 2.5.

The REE data for the Conrad and Islas Orcadas fracture zones, and the Zr, Nb and Y data, for the titanomagnetite separate from Bouvet Island, were obtained by A.R. Duncan using a direct reading spark source mass spectrograph at the Australian National University, Canberra. The procedures that were used and the associated errors have been described by Taylor (1965, 1971) and by Taylor and Gorton (1977).

The REE data for the Bouvet Island lavas was obtained by E.J.D. Kable using instrumental neutron activation analysis at the Nuclear Physics Research Institute, University of the Witwatersrand. The method has been described by Fesq et al. (1973).

A1.2 Electron Microprobe Analyses

A1.2.1 Major elements:

The major element composition of minerals and of quench glasses have been determined using a Cambridge Microscan 5 Microanalyser. Samples were prepared as polished sections on glass slides which were coated with carbon to allow conduction. Operating conditions were as follows:

Table A1-2: Counting errors and detection limits for trace elements analysed by XRF. All data in ppm. The detection limit is given at the 99% confidence level, and the counting error at the 95% confidence level.

Element	Conc. range	SD(2σ)	D.L.
Zr	40 - 400	0.9 - 1.4	1.4
Nb	4 - 150	1.0 - 1.2	1.8
Y	20 - 40	0.8 - 1.0	1.3
Rb	2.5 - 90	0.8 - 1.1	1.5
Ba	10 - 800	2.1 - 6.0	3.7
Sr	80 - 800	1.0 - 1.7	1.5
Co	18 - 100	1.9 - 2.5	4.5
Cr	25 - 350	1.5 - 2.1	2.2
Ni	10 - 208	2.5 - 3.7	4.0
V	50 - 350	2.4 - 3.7	5.5
Zn	8 - 150	0.9 - 1.7	1.4
Cu	5 - 90	1.8 - 2.1	2.9
Sc	25 - 40	1.0 - 1.2	1.2
Ga	15 - 20	0.38 -0.46	0.45

Beam current	1500 nA
Accel erating voltage	15 kV
Analysing crystals	Quartz (Fe, Mn, Ca, Ti, Cr, K); RAP (Si, Al, Mg, Na).
Detection	Flow counters with Ar/CO_2 gas mixture.

A focussed (1-2μ) beam was used for all elements, except when analysing feldspars, quench glass and hydrous minerals, when a 10-30μ 'defocussed' beam was used. Calibration was achieved using natural (e.g. Kakanui pyrope, Kakanui hornblende, Stillwater chromite, Marjalahti olivine) and synthetic (pure diopside glass, anorthite glass (GL24), and rutile) mineral standards. Raw counts were corrected for dead time and background. Standardisation was undertaken at the beginning of each analytical run and nominal concentrations were calculated from the determined K-factors (cps/% oxide). Nominal concentrations were subsequently corrected using the method of Bence and Albee (1968) with the alpha factors of Albee and Ray (1970).

The precision of the technique has been discussed by Reid (1977) and is illustrated in Table A1-3 where the standard deviation about the mean of 10 analyses of the same spot is compared with the uncertainty due to counting statistics. The data for all elements except Cr_2O_3 and MnO in Table A1-3 was determined on a pargasitic hornblende and are taken from Reid (1977). The data for Cr_2O_3 and MnO were taken from Shee (1978): the analyses were done on a garnet megacryst from the Koffiefontein Mine by P.C. Cardoso. Because of

Table A1-3: Estimation of the precision of the electron microprobe analyses for the major elements. All quantities are expressed in weight percent of the oxide.

$\bar{X}$ = Mean of 10 replicate analyses of the same spot within a pargasitic hornblende (Reid, 1977). The means for Cr_2O_3 and MnO are for 12 replicate analyses of a garnet megacryst from the Koffiefontein Mine (Shee, 1978).

S.D. = Standard deviation about the mean

ERR = 2σ error (95% confidence limits) due to counting statistics.

DL = Theoretical detection limit (99% confidence level)

OXIDE	$\bar{X}$	S.D.	ERR	D.L.
SiO_2	41.97	0.08	0.08	0.06
TiO_2	3.92	0.08	0.10	0.07
Al_2O_3	13.51	0.06	0.06	0.04
Cr_2O_3	0.78	0.02	0.02	0.03
FeO	6.82	0.15	0.16	0.10
MnO	0.26	0.01	0.01	0.03
MgO	16.34	0.07	0.10	0.05
CaO	12.10	0.07	0.08	0.05
Na_2O	2.71	0.12	0.14	0.09
K_2O	1.18	0.06	0.10	0.07

the possibility that natural mineral standards are not homogeneous on the micron scale, the absolute accuracy of the technique is difficult to establish. However, Reid (1977) notes that good agreement is achieved when analysing one natural mineral standard against another, using abundance data that were obtained by a different method (e.g. XRF data provided by B.W. Chappell, Australian National University). Comparison of XRF data for high purity mineral separates with average electron microprobe data for individual grains from this study (Table A1-4) indicates excellent agreement between the two analytical techniques. For routine analysis of those minerals whose oxides should sum close to 100 percent, analyses were generally only accepted if the total fell between 99.0 and 101.0 percent. The stability of the electron microprobe and the analytical conditions used were such that analytical totals seldom fell outside this range.

A1.2.2 Trace elements:

(i) Nickel

In selected cases where Ni had to be determined in olivine, clinopyroxene, Cr-spinel and quench glass, the operating conditions were as follows:

Accelerating voltage	25 kV
Beam current	1000 nA
Crystal	LiF (200)
Detector	sealed counter
PHA	E = 1.8 v (threshold)
	ΔE = 1.7 v (window)

Table A1-4: Comparison of analytical data (for the major oxides) obtained using XRF and electron microprobe (EMP) techniques in the Department of Geochemistry at U.C.T. Analyses are from a garnet, clinopyroxene and orthopyroxene separated from a garnet websterite (JJG1424) from the Mothae Kimberlite pipe. Electron microprobe data represent the average of four grains.

	GARNET		CLINOPYROXENE		ORTHOPYROXENE	
	XRF	EMP	XRF	EMP	XRF	EMP
SiO_2	42.78	41.86	54.57	54.57	57.18	57.63
TiO_2	0.09	0.09	0.27	0.23	0.14	0.09
Al_2O_3	23.15	23.47	3.03	2.96	1.29	1.07
Cr_2O_3	1.06	1.06	0.80	0.81	0.19	0.22
FeO^*	7.71	8.11	1.65	1.62	4.78	5.04
MnO	0.34	0.30	0.05	0.07	0.09	0.07
MgO	20.55	20.39	16.44	16.78	35.57	35.85
CaO	4.62	4.69	21.45	21.63	0.34	0.26
Na_2O	0.04	0.02	1.43	1.67	0.08	0.23

Standardisation was achieved using a natural olivine with 0.35% NiO from a kimberlite nodule as standard. For the determination of Ni in olivine, clinopyroxene and Cr-spinel, total counting times of 150 sec. on the peak and 100 sec. at the background position were used. This gave an estimated relative precision for olivine based on counting statistics of ±3.36% on 0.23% NiO (or ±78 ppm on 2300 ppm NiO) and a detection limit of 0.011% (110 ppm) NiO. These data are at the 95% and 99% confidence levels respectively. For the NiO determination in clinopyroxene the statistical error was ±35 ppm on 320 ppm (or 11% relative error). To ensure adequate precision and detection limits when analysing the quench glass, longer total counting times of 300 sec. on the peak and 300 sec. on backgrounds were used. These conditions gave an estimated statistical error of ±20% (i.e. ±40 ppm on 200 ppm) with a detection limit of 65 ppm NiO. To prevent volatilisation of the sample, a 'defocussed' beam of 20-30μ diameter was used.

(ii) Strontium

The procedure for the determination of Sr as a trace element using the electron microprobe has been described by Rickard and le Roex (1977). Subsequent to this paper two additional feldspar standards were obtained allowing a more rigorous evaluation of matrix effects. A brief description and discussion of the method is presented here.

Evaluation of various analytical conditions showed that the $Sr_{L\alpha}$ line was the most suitable analytical line to use as it is

relatively free from interference and has a more suitable excitation potential (1.806 KeV) than the $Sr_{K\alpha}$ line (14.131 KeV). The best combination of analytical conditions for the measurement of the $Sr_{L\alpha}$ line were found to be as follows:

Accelerating voltage	30 kV
Beam current	100 nA
Crystal	PET
Detector	flow counter
PHA	E = 1.6v (threshold)
	ΔE = 1.5v (window)
EHT on detector	1035 v
$Sr_{L\alpha}$	$103^{o}32'$
Background	$104^{o}00'$
Counting time	240 sec. (peak)
	240 sec. (bkg.)

A wavelength scan across the $Sr_{L\alpha}$ peak indicates that the only spectral line likely to interfere on the $Sr_{L\alpha}$ peak is the Si non-diagram in line $Si_{SK\beta'}$. The relative position of the two peaks is shown in Fig. A1-1A. If an excitation potential of 30 kV is used the $Sr_{L\alpha}$ peak is very slightly tailed by the Si nondiagram line. This tailing can be removed (Fig. A1-1A) by utilising carefully selected pulse height amplitude settings. At a lower excitation potential (e.g. 20 kV) the $Sr_{L\alpha}$ peak is tailed to a significant extent by the Si nondiagram line, due to the lower count rate ratio of Sr to Si,

Fig. A1-1: A. Wavelength scan across the $Sr_{L\alpha}$ peak using the electron microprobe with pulse height discrimination and an accelerating voltage of 30 kV. Note the position of the $Si_{SK\beta}$ non-diagram line and that the spectrum does not reach true background between the two peaks.

B. Sr calibration curves for clinopyroxene and feldspar standards using beta factor corrected counts per second. The alpha factors used to calculate the beta factors were taken from Albee and Ray (1970). Analytical conditions were as given in the text.

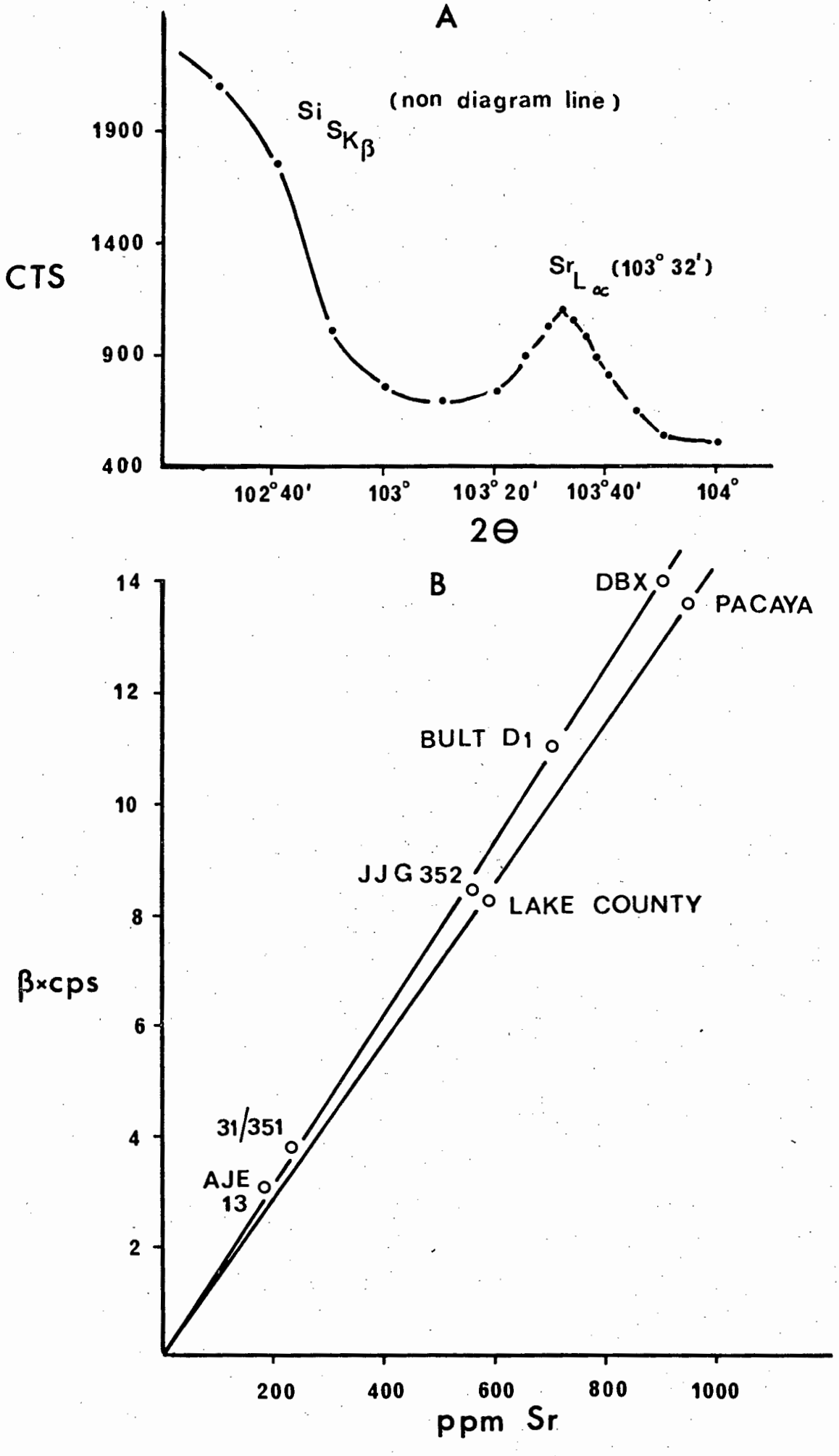
A
(non diagram line)
Si $S_{K\beta}$
$Sr_{L\alpha}$ (103° 32')
CTS
1900
1400
900
400
102°40'
103°
103°20'
103°40'
104°
2Θ
B
DBX
PACAYA
BULT D1
JJG 352
LAKE COUNTY
31/351
AJE 13
β×cps
14
12
10
8
6
4
2
200
400
600
800
1000
ppm Sr

resulting in a poorer resolution between the $Sr_{L\alpha}$ and Si nondiagram lines. This effect cannot be completely removed by pulse height amplitude selection. Inspection of Fig. A1-1A shows that although the $Sr_{L\alpha}$ is not tailed by the Si nondiagram line at 30 kV with proper PHA settings, the spectrum does not reach minimum true background level between the two peaks. Consequently the background count rate was determined at only one background position, situated at the higher angle side of the $Sr_{L\alpha}$ peak.

Calibration was achieved using natural clinopyroxenes separated from kimberlite nodules (provided by A.J. Erlank), which had previously been analysed for Sr by isotope dilution and by ion microprobe techniques, and also using two feldspar standards Lake County and Pacaya (provided by A.M. Reid). The major and trace element composition of these feldspars are given in Table A1-5. All the standards were initially used to draw up a series of working curves using (1) only the clinopyroxene standards, (2) only the feldspar standards and (3) combining all standards into one working curve. Each of the above sets of data were compared both with and without making a matrix correction using β-factors calculated from the α-factor data of Albee and Ray (1970). The results from these various working curves are summarised in Table A1-6 and two of the working curves using β-factor corrected cps. for the clinopyroxene standards and the feldspar standards are illustrated in Fig. A1-1B. Inspection of these data indicates that making a β-factor correction does not significantly improve the working curves using only clinopyroxene or only feldspar standards. If both sets of standards

Table A1-5: Composition of the feldspar standards used for calibrating the Sr working curves for the analysis of Sr by electron microprobe.
Data supplied by A.M. Reid.

	Lake County		Pacaya	
	Microprobe	XRF	Microprobe	XRF
SiO_2	51.55	49.68	45.22	45.43
TiO_2	-	0.05	-	0.02
Al_2O_3	30.99	29.77	35.45	34.93
FeO*	0.41	0.44	0.40	0.49
MgO	-	0.00	-	0.00
CaO	13.24	13.11	18.12	8.22
Na_2O	3.63	3.63	0.94	0.94
K_2O	0.13	0.12	0.03	0.06
P_2O_5	-	-	-	0.02
S	-	0.005	-	0.004
TOTAL	99.96	96.80	100.16	100.11

Trace elements - by isotope dilution (ppm)

Mg	822 ± 66	398 ± 12
K	986 ± 16	147 ± 11
Ti	230 ± 14	134 ± 11
Sr	582 ± 6	942 ± 9
Ba	63 ± 2	28.8 ± 0.9
Li	4.1±0.2	0.68±0.19

are combined then the β-factor correction does tend to improve the data (Table A1-6, part III), and it is apparent that the average absolute error on the working curve is controlled by the counting statistics (Table A1-6, parts III and IV). When the combined data are plotted on a working curve (Fig. A1-1B) then it is apparent that the two sets of standards do still tend to define separate working curves (i.e. different slopes) which suggests that either the β-factor correction is not compensating totally for the different matrix effects or that the standard values used reflect inter-laboratory bias. For this reason all Sr data were determined using the two feldspar standards only.

It was found that the count rate (which is extremely low) is extremely sensitive to the condition of the detector, the detector gas and the EHT on the detector. It was therefore necessary to check periodically that the EHT on the counter was correctly set and that no pulse shift had occurred. At the start of each analytical run it was necessary to readjust and check all the conditions. For these reasons an attempt was made to determine all data that were to be directly compared in a single analytical run. To achieve meaningful data (in terms of the statistical errors) a total counting time of 480 sec. (peak plus background) was used, which together with the high accelerating voltage necessitated use of a 'defocussed' beam (±30μ) to prevent damage to the sample. Under these conditions an average analytical error, based on counting statistics, of 4.7% (±26 ppm on 550 ppm) and a detection limit of 80 ppm was obtained.

Table A1-6: Comparison of working curve data for Sr in clinopyroxene and feldspar standards, with and without β-factor corrections. All concentrations in ppm.

I. Working curves using clinopyroxene standards only.

A. No β-factor correction.

Std.	cps.	conc.	calc.	abs. error	% error
AJE13	2.38	183	196	13	7.10
31/351	2.94	235	242	7	2.98
JJG352	6.67	558	549	-9	-1.61
BULT DI	8.67	712	714	2	0.28
DBX	10.96	904	903	-1	-0.11
	Slope = 0.01214 cps/ppm			Av. 6.4	Av. 2.42

B. With β-factor correction.

Std.	cpx x β	conc.	calc.	abs. error	% error
AJE13	3.04	183	196	13	7.10
31/351	3.75	235	242	7	2.98
JJG352	8.48	558	548	-10	-1.79
BULT DI	11.05	712	714	2	0.28
DPX	13.99	904	904	0	0
	Slope = 0.01548 cps/ppm			Av. 6.4	Av. 2.43

II. Working curves using feldspar standards only.

A. No β-factor correction.

	cps.	conc.	calc.	abs. error	% error
LAKE COUNTY	6.19	582	581	-1	-0.15
PACAYA	10.04	942	943	1	0.11
	Slope = 0.01065 cps/ppm			Av. 1	Av. 0.13

B. With β-factor correction.

	cps.	conc.	calc.	abs. error	% error
LAKE COUNTY	8.29	582	576	-6	-1.03
PACAYA	13.62	942	946	4	0.42
	Slope = 0.01440 cps/ppm			Av. 5	Av. 0.73

Table A1-6 (cont.):

III. Working curve using both clinopyroxene and feldspar standards.

A. Without β-factor correction.

Std.	cps.	conc.	calc.	abs. error	% error
AJE13	2.38	183	206	23	12.57
31/351	2.94	235	254	19	8.09
JJG352	6.67	558	577	19	3.41
BULT DI	8.67	712	749	37	5.20
DBX	10.96	904	947	43	4.76
LAKE COUNTY	6.19	582	535	-47	-8.08
PACAYA	10.04	942	868	-74	-7.87
	Slope = 0.01157 cps/ppm.			Av. 37	Av. 7.14

B. With β-factor correction.

Std.	cps.	conc.	calc.	abs. error	% error
AJE13	3.04	183	202	19	10.38
31/351	3.75	235	250	15	6.38
JJG352	8.48	558	564	6	1.07
DULT DI	11.05	712	735	23	3.23
DBX	13.99	904	931	27	2.99
LAKE COUNTY	8.29	582	552	-30	-5.15
PACAYA	13.62	942	906	-36	-3.82
	Slope = 0.01503 cps/ppm.			Av. 22	Av. 4.72

IV. Counting Statistics.

i) Av. % error = 4.87% (= 27 ppm on 550 ppm)

ii) Detection limit = 80 ppm

A2. DISTRIBUTION COEFFICIENTS

A compilation of mineral-liquid distribution coefficients taken from the literature and from this study are given in Tables A2-1 to A2-13. The tables contain the following data: element name; value of the distribution coefficient, either as specific values or as a function of a parameter such as temperature or composition; the applicable experimental conditions, if experimentally determined; the composition for which the coefficient was determined; the technique used and the reference source. Distribution coefficients have been compiled for the following minerals;

Olivine	-	Table A2-1
Plagioclase	-	Table A2-2
Anorthoclase	-	Table A2-3
Alkali-feldspar	-	Table A2-4
Clinopyroxene	-	Table A2-5
Orthopyroxene	-	Table A2-6
Garnet	-	Table A2-7
Ilmenite	-	Table A2-8
Titanomagnetite	-	Table A2-9
Spinel	-	Table A2-10
Amphibole	-	Table A2-11
Apatite	-	Table A2-12
Mica	-	Table A2-13

A3. MICROFICHE TABLES

In view of the large number of mineral analyses obtained during the course of this study, individual analyses are presented in microfiche tables as appendices to this thesis (see pocket inside back cover). Table numbers are given in the index of each microfiche card and are also given below, together with appropriate annotations.

CHAPTER III - Mid Atlantic Ridge at $36^{o}49'$ N - FAMOUS

Table		
F3-1	Olivine analyses:	Picritic basalts (DR8 and 10-03C)
F3-2	Plagioclase analyses:	Picritic basalt (DR8)
F3-3	Cr-spinel analyses:	Picritic basalts (DR8 and 10-03C)
F3-4	Olivine analyses:	Olivine basalts (DR4-303, DR1-122, DR9-322, DR9-323, DR4-329, DR4, DR2-174, 11-18)
F3-5	Plagioclase analyses:	Olivine basalts (DR4, 11-18)
F3-6	Cr-spinel analyses:	Olivine basalts (DR4, 11-18, DR9-322, DR4-303, DR1-122)
F3-7	Clinopyroxene analyses:	Olivine basalts (DR4, 11-18)
F3-8	Mineral analyses:	Plagioclase-olivine basalt (8-10)
F3-9	Plagioclase analyses:	Plagioclase phyric basalt (DR3-1)
F3-10	Clinopyroxene analyses:	Plagioclase phyric basalt (DR3-1)
F3-11	Olivine analyses:	Plagioclase phyric basalts (DR3-1, DR3-131, DR10-101C)
F3-12	Cr-spinel analyses:	Plagioclase phyric basalts (DR3-1, DR3-131)

F3-13 Plagioclase analyses: Plagioclase-pyroxene basalt (31-38)

F3-14 Clinopyroxene analyses: Plagioclase-pyroxene basalt (31-38)

F3-15 Olivine analyses: Plagioclase-pyroxene basalts (31-38, DR2-301, DR10-310)

CHAPTER IV - Islas Orcadas and Conrad Fracture Zones.

(i) Islas Orcadas Fracture Zone

Table

F4-1 Mineral analyses: Dredge-11 basalt I060-1

F4-2 " " : Dredge-11 basalt I060-2

F4-3 " " : Dredge-11 basalt I060-3

F4-4 " " : Dredge-13 basalt I062-42A

F4-5 " " : Dredge-13 basalt I062-51

F4-6 " " : Dredge-14 basalt I063-2

F4-7 " " : Dredge-13 basalt I062-5

F4-8 " " : Dredge-13 basalt I062-12

F4-9 " " : Dredge-13 basalt I062-15

F4-10 " " : Dredge-13 basalt I062-31

F4-11 " " : Dredge-13 basalt I062-42B

(ii) Conrad Fracture Zone

Table

F4-12 Mineral analyses: Ol-Plag-Pyx basalts (I045-97, I045-152, I045-161)

F4-13 Mineral analyses: Plagioclase-pyroxene basalt I045-91

F4-14 " " Plagioclase-pyroxene basalt I045-151

F5-4 Mineral analyses: Mugearite WJ1B

F5-5 " " : Benmoreite WJ10B

F5-6 " " : Rhyolite WJ18B

TABLE A2-1

OLIVINE/LIQUID DISTRIBUTION COEFFICIENTS

ELEMENT	D	CONDITIONS	COMPOSITION	TECHNIQUE	REFERENCE
NI	(124/MGO)-0.90	1250-1450C, 1 ATM	FO-AB-AN	.5% DOPING	HART & DAVIS (1978)
	EXP((10430/T)-4.79)	1225-1470C, 1 ATM	ULTRABASIC - BASIC KOMATIITE	BETA TRACK	ARNDT (1977)[b]
	13.5 - 16.8	1160-1050C, 1 ATM	BASALT (KILAUEA)	PHENOCRYST/GLASS	HAKLI & WRIGHT 1967
	EXP((7.4/RT)+0.03)				
	EXP((13160/T)-6.18)	1070-1400C, 1 ATM	BASALTIC	% LEVEL DOPING	LEEMAN & SCHEIDEGGER (1977), LEEMAN & LINDSTROM (1978), LEEMAN (1974)
	8.63 - 18.54		BASALTIC	PHENOCRYST/MATRIX	DALE & HENDERSON (1972)
	23+-2,27+-1	1114-1134C, 1 ATM	NATURAL ALKALIC BASALT, OLOLKESALIE	% LEVEL DOPING	LINDSTROM (1976)
	9.01 - 14.8	1260-1248C, 1 ATM	SYNTHETIC	% LEVEL DOPING	LINDSTROM (1976)
	2.2 - 19.5	1025C, 20KBAR	FO-AN50AB50-SIO2-H2O	PPM LEVEL DOPING BETA TRACK	MYSEN (1976)[a]
	12.2		BASALTIC	PHENOCRYST/MATRIX	BOUGAULT & HEKINIAN (1974)
	16.3		ALKALI BASALT	PHENOCRYST/MATRIX	LE ROEX (UNPUBL.)
CO	EXP((9676/T)-5.23)	1070-1400C, 1 ATM	BASALTIC	% LEVEL DOPING	LEEMAN & SCHEIDEGGER (1977)
	2.75 - 4.44		BASALTIC	PHENOCRYST/MATRIX	DALE & HENDERSON (1972)
	4.8 +-0.4	1114-1134C, 1 ATM	NATURAL ALKALIC BASALT, OLOLKESALIE	% LEVEL DOPING	LINDSTROM (1976)
	3.10		BASALTIC	MINERAL SEPARATES	PASTER ET AL (1974)

(CONTINUED ON NEXT PAGE)

T A B L E A2-1 (Cont.)

OLIVINE/LIQUID DISTRIBUTION COEFFICIENTS

ELEMENT	D	CONDITIONS	COMPOSITION	TECHNIQUE	REFERENCE
	(CONTINUED FROM PREVIOUS PAGE)				
	3.0 -		BASALTIC	PHENOCRYST/MATRIX	BOUGAULT & HEKINIAN (1974)
	5.36		ALKALI BASALT	PHENOCRYST/MATRIX	LE ROEX (UNPUBL.)
CR	0.6 +-0.2	1112-1114C, 1 ATM	NATURAL ALKALIC BASALT, OLOLKESALTE	% LEVEL DOPING	LINDSTROM (1976)
	0.72		ALKALI BASALT	PHENOCRYST/MATRIX	LE ROEX (UNPUBL.)
SC	0.37 +-0.01	1112-1134C, 1 ATM	NATURAL ALKALIC BASALT,OLORKESALIE	% LEVEL DOPING	LINDSTROM (1976)
	0.265 +-0.003	1240C, 1 ATM	SYNTHETIC LOW-K FRA MAURO BASALT	% LEVEL DOPING	MCKAY & WEILL (1977)
	0.13 - 0.22		BASALTIC	PHENOCRYST/MATRIX	DALE & HENDERSON (1972)
	0.33		BASALTIC	MINERAL SEPARATES	PASTER ET AL (1974)
	0.22		ALKALI BASALT	PHENOCRYST/MATRIX	LE ROEX (UNPUBL.)
TI	0.024 +-0.008	1112-1134C, 1 ATM	NATURAL ALKALIC BASALT,OLORKESALIE	% LEVEL DOPING	LINDSTROM (1976)
	0.07 +-0.05	1125-1250C, 1 ATM	SIO2-AL2O3-FEO-MGO-CAO-NA2O	% LEVEL DOPING	DUKE (1976)
	0.04		BASALTIC	PHENOCRYST/MATRIX	BOUGAULT & HEKINIAN (1974)
	.02, .03, .04		BASIC - ACID	COMPILATION	PEARCE & NORRY 1979
V	0.04 +-0.02	1112-1134C, 1 ATM	NATURAL ALKALIC BASALT,OLORGESALIE	% LEVEL DOPING	LINDSTROM (1976)
	0.05 +-0.03	1125-1250C, 1 ATM	SIO2-AL2O3-FEO-MGO-CAO-NA2O	% LEVEL DOPING	DUKE (1976)
	1.3	+- 1140C, 1 ATM	SYNTHETIC APOLLO 11 MARE BASALT	0.1 % DOPING	RINGWOOD (1970)
	0.09		BASALTIC	PHENOCRYST/MATRIX	BOUGAULT & HEKINIAN

(CONTINUED ON NEXT PAGE)

T A B L E A2-1 (Cont.)

OLIVINE/LIQUID DISTRIBUTION COEFFICIENTS

ELEMENT	D	CONDITIONS	COMPOSITION	TECHNIQUE	REFERENCE
	(CONTINUED FROM PREVIOUS PAGE)				
	0.11		ALKALI BASALT	PHENOCRYST/MATRIX	(1974) LE ROEX (UNPUBL.)
CU	0.47 +-0.02	1300C, 1 ATM	SIO2-AL2O3-MGO-CAO	0.5% DOPING	LINDSTROM (1976)
	0.36 +-0.02	1350C, 1 ATM			BIRD (1971)
	0.02		BASALTIC	MINERAL SEPARATES	PASTER ET AL (1974)
	0.11		BASALTIC	PHENOCRYST/MATRIX	BOUGAULT & HEKINIAN (1974)
	<0.01 -		ALKALI BASALT	PHENOCRYST/MATRIX	LE ROEX (UNPUBL.)
BA	0.005 +-0.003	1240C, 1 ATM	SYNTHETIC LOW-K FRA MAURO BASALT	% LEVEL DOPING	MCKAY & WEILL (1977)
	.0086 & .0112		OCEANITE	PHENOCRYST/MATRIX	PHILPOTTS & SCHNETZLER (1970)
	.0001		ANKARAMITE	PHENOCRYST/MATRIX	HART & BROOKS (1974)
	0.007		ALKALI BASALT	PHENOCRYST/MATRIX	LE ROEX (UNPUBL.)
SR	0.003 +-0.002	1240C, 1 ATM	SYNTHETIC LOW-K FRA MAURO BASALT	% LEVEL DOPING	MCKAY & WEILL (1977)
	.019 & .0094		OCEANITE	PHENOCRYST/MATRIX	PHILPOTTS & SCHNETZLER (1970)
	.0002		ANKARAMITE	PHENOCRYST/MATRIX	HART & BROOKS (1974)
	0.01		ALKALI BASALT	PHENOCRYST/MATRIX	LE ROEX (UNPUBL.)
RB	.0081 & .011		OCEANITE	PHENOCRYST/MATRIX	PHILPOTTS & SCHNETZLER (1970)
	.0002		ANKARAMITE	PHENOCRYST/MATRIX	HART & BROOKS (1974)
K	.006 & .008		OCEANITE	PHENOCRYST/MATRIX	PHILPOTTS & SCHNETZLER (1970)
	.0002		ANKARAMITE	PHENOCRYST/MATRIX	HART & BROOKS (1974)

(CONTINUED ON NEXT PAGE)

T A B L E A2-1 (Cont.)

OLIVINE/LIQUID DISTRIBUTION COEFFICIENTS

ELEMENT	D	CONDITIONS	COMPOSITION	TECHNIQUE	REFERENCE
(CONTINUED FROM PREVIOUS PAGE)					
GA	0.04 - 0.05		BASALTIC	PHENOCRYST/MATRIX	GOODMAN (1972)
ZN	1.80		BASALTIC	MINERAL SEPARATES	PASTER ET AL 1974
	0.86		BASALTIC	PHENOCRYST/MATRIX	BOUGAULT & HEKINIAN (1974)
	?.13		ALKALI BASALT	PHENOCRYST/MATRIX	LE ROEX (UNPUBL.)
ZR	0.03		ALKALI BASALT	PHENOCRYST/MATRIX	LE ROEX (UNPUBL.)
	0.01		BASIC - ACID	COMPILATION	PEARCE & NORRY 1979
NB	0.05		ALKALI BASALT	PHENOCRYST/MATRIX	LE ROEX (UNPUBL.)
	0.01		BASIC - ACID	COMPILATION	PEARCE & NORRY 1979
Y	0.13		ALKALI BASALT	PHENOCRYST/MATRIX	LE ROEX (UNPUBL.)
	0.01		BASIC - ACID	COMPILATION	PEARCE & NORRY 1979

TABLE A2-2

PLAGIOCLASE/LIQUID DISTRIBUTION COEFFICIENTS

ELEMENT	D	CONDITIONS	COMPOSITION	TECHNIQUE	REFERENCE
RB	0.017 +-0.008	1200C, 1 ATM	SYNTHETIC LUNAR BASALT	% LEVEL DOPING	MCKAY & WEILL (1976)
	0.08 +-0.04	1240C, 1 ATM	SYNTHETIC LOW-K FRA MARE BASALT	% LEVEL DOPING	MCKAY & WEILL (1977)
	0.041 & 0.016		DACITE	PHENOCRYST/MATRIX	NAGASAWA & SCHNETZ-LER (1971)
	0.066		TRACHYBASALT	PHENOCRYST/MATRIX	SUN & HANSON (1976)
	0.025 - 0.188		BASALT - DACITE	PHENOCRYST/MATRIX	PHILPOTTS & SCHNETZ-LER (1970)
	0.05 - 0.12		BASALTIC	PHENOCRYST/MATRIX	GOODMAN (1972)
	(0.23 & 0.50)				
	.007 - .041		RHYOLITIC(AN27-AN42)	PHENOCRYST/MATRIX	EWART & TAYLOR 1969
	0.03 - 0.008		ANDESITIC(AN81-AN69)	PHENOCRYST/MATRIX	EWART & TAYLOR 1969
	0.026		ANKARAMITE	PHENOCRYST/MATRIX	HART & BROOKS (1974)
	0.04		ALKALI BASALT	PHENOCRYST/MATRIX	LE ROEX (UNPUBL.)
K	0.20 +-0.02	1200C, 1 ATM	SYNTHETIC LUNAR BASALT	% LEVEL DOPING	MCKAY & WEILL (1977)
	0.10 & 0.076		DACITE	PHENOCRYST/MATRIX	NAGASAWA & SCHNETZ-LER (1971)
	0.019 - 0.36		BASALT-DACITE	PHENOCRYST/MATRIX	PHILPOTTS & SCHNETZ-LER (1970)
	0.18		ANKARAMITE	PHENOCRYST/MATRIX	HART & BROOKS (1974)
SR	4.4		DACITE	PHENOCRYST/MATRIX SEPARATION + I.D.	NAGASAWA & SCHNETZ-LER (1971)
	1.45		DACITE	PHENOCRYST/MATRIX SEPARATION + I.D.	NAGASAWA & SCHNETZ-LER (1971)
	4.62		TRACHYBASALT	PHENOCRYST/MATRIX	SUN & HANSON (1976)
	1.27 - 2.84		BASALT-DACITE	PHENOCRYST/MATRIX	PHILPOTTS & SCHNETZ-

(CONTINUED ON NEXT PAGE)

TABLE A2-2 (Cont.)

PLAGIOCLASE/LIQUID DISTRIBUTION COEFFICIENTS

ELEMENT	D	CONDITIONS	COMPOSITION	TECHNIQUE	REFERENCE
(CONTINUED FROM PREVIOUS PAGE)					
	2.18		BASALT	PHENOCRYST/MATRIX	LER (1970)
	3.10		LEUCITE BASANITE	PHENOCRYST/MATRIX	BERLIN & HENDERSON (1968)
	2.00		TINGUAITE	PHENOCRYST/MATRIX	BERLIN & HENDERSON (1968)
	3.45		TRACHYTE	PHENOCRYST/MATRIX	BERLIN & HENDERSON (1968)
	4.31		TRACHYTE	PHENOCRYST/MATRIX	BERLIN & HENDERSON (1968)
	3.27 - 4.31		TRACHYTES, PHONOLITES	PHENOCRYST/MATRIX	BERLIN & HENDERSON (1969)
	1.5, 2.3, 3.8		BASALT TO RHYOLITE	PHENOCRYST/MATRIX	KORRINGA & NOBLE
	5.4, 7.0		(AN90, AN75, AN60, AN45 AN30 RESPECTIVELY)		(1971)
	1.5 - 2.9		ANDESITE - DACITE	PHENOCRYST/MATRIX	EWART ET AL (1973)
	1.4 - 2.6		ANDESITE - DACITE	RAYLEIGH MODEL	EWART ET AL (1973)
	EXP(15121/T - 9.91)	1140-1190C, FO2 = 10E-8 TO 10E-14 ATM	OCEANIC BASALT	% LEVEL DOPING	SUN ET AL (1974)
	13.7 - 7.4		RHYOLITIC (AN27-AN42)	PHENOCRYST/MATRIX	EWART & TAYLOR 1969
	2.6 - 3.3		ANDESITIC (AN81-AN69)	PHENOCRYST/MATRIX	EWART & TAYLOR 1969
	2.04		ANKARAMITE	PHENOCRYST/MATRIX	HART & BROOKS (1974)
	2.44		ALKALI BASALT	PHENOCRYST/MATRIX	LE ROEX (UNPUBL.)
	4.4 - 6.5		DACITIC, AN36-AN48	PHENOCRYST/MATRIX	SCHOCK (1977)
BA	0.308		DACITE	PHENOCRYST/MATRIX	NAGASAWA & SCHNETZ-LER (1971)
	0.304		DACITE	PHENOCRYST/MATRIX	NAGASAWA & SCHNETZ-E

(CONTINUED ON NEXT PAGE)

T A B L E A2-2 (Cont.)

PLAGIOCLASE/LIQUID DISTRIBUTION COEFFICIENTS

ELEMENT	D	CONDITIONS	COMPOSITION	TECHNIQUE	REFERENCE
(CONTINUED FROM PREVIOUS PAGE)					
					LER (1971)
	1.47		TRACHYBASALT	PHENOCRYST/MATRIX	SUN & HANSON (1976)
	0.16 - 0.42		BASALT TO RHYOLITE AN30 - AN90; LINEAR	PHENOCRYST/MATRIX	KORRINGA & NOBLE (1971)
	0.72 - 1.09		TRACHYTES, PHONOLITES	PHENOCRYST/MATRIX	BERLIN & HENDERSON (1969)
	0.054 - 0.589		BASALT - DACITE	PHENOCRYST/MATRIX	PHILPOTTS & SCHNETZLER (1970)
	0.10 - 0.20		ANDESITE - DACITE	PHENOCRYST/MATRIX	EWART ET AL (1973)
	0.11 - 0.19		ANDESITE - DACITE	RAYLEIGH MODEL	EWART ET AL (1973)
	0.30 - 0.69		RHYOLITIC(AN27-AN42)	PHENOCRYST/MATRIX	EWART & TAYLOR 1969
	0.12 - 0.21		ANDESITIC(AN81-AN69)	PHENOCRYST/MATRIX	EWART & TAYLOR 1969
	0.329		ANKARAMITE	PHENOCRYST/MATRIX	HART & BROOKS (1974)
	0.68		BASALT	MINERAL SEPARATES	PASTER ET AL (1974)
	0.35		ALKALI BASALT	PHENOCRYST/MATRIX	LE ROEX (UNPUBL.)
	0.40 - 0.65		DACITIC, AN36-AN48	PHENOCRYST/MATRIX	SCHOCK (1977)
GA	0.84 - 1.27		BASALTIC	PHENOCRYST/MATRIX	GOODMAN (1972)
	0.71 - 1.7		ANDESITE - DACITE	PHENOCRYST/MATRIX	EWART ET AL (1973)
	0.95 - 1.4		RHYOLITIC(AN27-AN42)	PHENOCRYST/MATRIX	EWART & TAYLOR 1969
	1.0 - 0.88		ANDESITIC(AN81-AN69)	PHENOCRYST/MATRIX	EWART & TAYLOR 1969
	1.70		BASALT	MINERAL SEPARATES	PASTER ET AL (1974)
	0.88		ALKALI BASALT	PHENOCRYST/MATRIX	LE ROEX (UNPUBL.)
NI	0.08		ALKALI BASALT	PHENOCRYST/MATRIX	LE ROEX (UNPUBL.)
Y	0.013 TO 0.031	1150-1343C, 1 ATM	NATURAL THOLEITES & ANDESITES : DT-AB-AN	% LEVEL DOPING	DRAKE AND WEILL 1975
(CONTINUED ON NEXT PAGE)					

T A B L E A2-2 (Cont.)

PLAGIOCLASE/LIQUID DISTRIBUTION COEFFICIENTS

ELEMENT	D	CONDITIONS	COMPOSITION	TECHNIQUE	REFERENCE
(CONTINUED FROM PREVIOUS PAGE)					
	0.18		ALKALI BASALT	PHENOCRYST/MATRIX	LE ROEX (UNPUBL.)
	.03, .06, .10		BASIC - ACID	COMPILATION	PEARCE & NORRY 1979
NI	0.04 +-0.02	1170C, 1ATM	AB-AN-DI	% LEVEL DOPING	LINDSTROM (1976)
	0.09		ALKALI BASALT	PHENOCRYST/MATRIX	LE ROEX (UNPUBL.)
CO	0.049 +-0.005	1170C, 1ATM	AB-AN-DI	% LEVEL DOPING	LINDSTROM (1976)
	0.03		BASALT	MINERAL SEPARATES	PASTER ET AL (1974)
	0.04 - 0.09		DACITIC, AN36-AN48	PHENOCRYST/MATRIX	SCHOCK (1977)
SC	0.065 +-0.011	1170C, 1 ATM	NATURAL ALKALIC BASALT, OLOLKESALIE	% LEVEL DOPING	LINDSTROM (1976)
	0.01		BASALT	MINERAL SEPARATES	PASTER ET AL (1974)
	0.26		ALKALI BASALT	PHENOCRYST/MATRIX	LE ROEX (UNPUBL.)
	0.01 - 0.05		DACITIC, AN36-AN48	PHENOCRYST/MATRIX	SCHOCK (1977)
TI	0.045 +-0.003	1135C, 1 ATM			LINDSTROM (1976)
	.04, .05, .05		BASIC - ACID	COMPILATION	PEARCE & NORRY 1979
MN	0.05 +-0.02	1135C, 1 ATM			LINDSTROM (1976)
CU	0.08 - 0.32		ANDESITE - DACITE	PHENOCRYST/MATRIX	EWART ET AL (1973)
	0.07 - 0.38		ANDESITE - DACITE	RAYLEIGH MODEL	EWART ET AL (1973)
	0.004		BASALT	MINERAL SEPARATES	PASTER ET AL (1974)
	0.44		ALKALI BASALT	PHENOCRYST/MATRIX	LE ROEX (UNPUBL.)
ZN	0.13		BASALT	MINERAL SEPARATES	PASTER ET AL (1974)
	0.05		ALKALI BASALT	PHENOCRYST/MATRIX	LE ROEX (UNPUBL.)

(CONTINUED ON NEXT PAGE)

TABLE A2-2 (Cont.)

PLAGIOCLASE/LIQUID DISTRIBUTION COEFFICIENTS

ELEMENT	D	CONDITIONS	COMPOSITION	TECHNIQUE	REFERENCE
(CONTINUED FROM PREVIOUS PAGE)					
HF	0.01 - 0.12		DACITIC, AN36-AN48	PHENOCRYST/MATRIX	SCHOCK (1977)
TA	0.02 - 0.06		DACITIC, AN36-AN48	PHENOCRYST/MATRIX	SCHOCK (1977)
ZR	0.03		ALKALI BASALT	PHENOCRYST/MATRIX	LE ROEX (UNPUBL.)
	.01, .03, .10		BASIC - ACID	COMPILATION	PEARCE & NORRY 1979
NB	0.03		ALKALI BASALT	PHENOCRYST/MATRIX	LE ROEX (UNPUBL.)
	.01, .025, .06		BASIC - ACID	COMPILATION	PEARCE & NORRY 1979
TH	0.01 - 0.07		DACITIC, AN36-AN48	PHENOCRYST/MATRIX	SCHOCK (1977)
U	0.01 - 0.07		DACITIC, AN36-AN48	PHENOCRYST/MATRIX	SCHOCK (1977)
CR	0.05		ALKALI BASALT	PHENOCRYST/MATRIX	LE ROEX (UNPUBL.)
V	0.04		ALKALI BASALT	PHENOCRYST/MATRIX	LE ROEX (UNPUBL.)
PB	0.11 - 0.78		BASALTIC-RHYOLITE	I.D. PHENO/MATRIX	LEEMAN (1979)

TABLE A2-3

ANORTHOCLASE/LIQUID DISTRIBUTION COEFFICIENTS

ELEMENT	D	CONDITIONS	COMPOSITION	TECHNIQUE	REFERENCE
BA	5.04		PHONOLITE	PHENOCRYST/MATRIX	SUN & HANSON (1976)
SR	5.57		PHONOLITE	PHENOCRYST/MATRIX	SUN & HANSON (1976)
RB	0.450		PHONOLITE	PHENOCRYST/MATRIX	SUN & HANSON (1976)

TABLE A2-4

ALKALI FELDSPAR/LIQUID DISTRIBUTION COEFFICIENTS

ELEMENT	D	CONDITIONS	COMPOSITION	TECHNIQUE	REFERENCE
SR	3.87		RHYODACITE K-FELDSPAR	PHENOCRYST/MATRIX	PHILPOTTS & SCHNETZLER (1970)
	0.48 - 8.09		RHYOLITE	PHENOCRYST/MATRIX	DE PIERI & QUARENI (1978)
	0.70 - 25.60		RHYOLITE	PHENOCRYST/MATRIX	DE PIERI & QUARENI (1978)
	3 - 4		SODIC ALKALI FSP/ SALIC MELT	PHENOCRYST/MATRIX	KORRINGA & NOBLE (1971)
	1.2 - 5.0	720-780C, 8KB	GRANITIC	% LEVEL DOPING	LONG (1978)
BA	6.12		RHYODACITE K-FELDSPAR	PHENOCRYST/MATRIX	PHILPOTTS & SCHNETZLER (1970)
	1.2 - 2.80		TRACHYTES, PHONOLITES SANIDINE	PHENOCRYST/MATRIX	BERLIN & HENDERSON (1969)
	1.17 - 8.95		TRACHYTES, PHONOLITES SANIDINE	PHENOCRYST/MATRIX	BERLIN & HENDERSON (1969)
	3 TO 5		SODIC ALKALI FSP/ SALIC MELT	PHENOCRYST/MATRIX	KORRINGA & NOBLE (1971)
	0.46 - 18.04		RHYOLITE	PHENOCRYST/MATRIX	DE PIERI & QUARENI (1978)
	0.14 - 12.86		RHYOLITE	PHENOCRYST/MATRIX	DE PIERI & QUARENI (1978)
	6.4 - 14.0	720-780C, 8KB	GRANITIC	% LEVEL DOPING	LONG (1978)
RB	0.659		RHYODACITE K-FELDSPAR	PHENOCRYST/MATRIX	PHILPOTTS & SCHNETZLER (1970)
	0.11 - 0.74		RHYOLITE	PHENOCRYST/MATRIX	DE PIERI & QUARENI (1978)
	0.17 - 0.88		RHYOLITE	PHENOCRYST/MATRIX	DE PIERI & QUARENI (1978)
PB	0.84 - 1.37		RHYOLITE	PHENOCRYST/MATRIX ID	LEEMAN (1978)

TABLE A2-5

CALCIC PYROXENE/LIQUID DISTRIBUTION COEFFICIENTS

ELEMENT	D	CONDITIONS	COMPOSITION	TECHNIQUE	REFERENCE
NI	2.22 - 4.4		BASALTIC (KILAUEA)	PHENOCRYST/GLASS	HAKLI & WRIGHT 1967
	EXP((24.8/RT)-7.85)				
	1.42 - 2.11		BASALTIC	PHENOCRYST/MATRIX	DALE & HENDERSON (1972)
	6.2 - 10.0		ANDESITE - DACITE	PHENOCRYST/MATRIX	EWART ET AL (1973)
	5.6 - 8.4		ANDESITE - DACITE	RAYLEIGH MODEL	EWART ET AL (1973)
	1.98	1270-1296C, 1 ATM	AB-AN-DI	% LEVEL DOPING	LINDSTROM (1976)
	8.69 - 1.51	1182-1340C, 1 ATM	AB-AN-DI	% LEVEL DOPING	LINDSTROM (1976)
	1.5 - 14.0	1110-1360C	AB-AN-DI	% LEVEL DOPING	LINDSTROM & WEILL (1978)
	5.2, 3.5		ANDESITIC	PHENOCRYST/MATRIX	EWART & TAYLOR 1969
	4.4		BASALTIC	PHENOCRYST/MATRIX	BOUGAULT & HEKINIAN (1974)
	1.77		ALKALI BASALT	PHENOCRYST/MATRIX	LE ROEX (UNPUBL.)
	4 - 2			COMPILATION	FREY ET AL (1978)
CO	0.68 - 1.22		BASALTIC	PHENOCRYST/MATRIX	DALE & HENDERSON (1972)
	1.6 - 6.8		ANDESITE - DACITE	PHENOCRYST/MATRIX	EWART ET AL (1973)
	1.8 - 4.9		ANDESITE - DACITE	RAYLEIGH MODEL	EWART ET AL (1973)
	1.12 +-0.07		BASALT	PHENOCRYST/MATRIX	ONUMA ET AL (1968)
	0.69	1270-1296C, 1 ATM	AB-AN-DI	% LEVEL DOPING	LINDSTROM (1976)
	0.50 - 2.0	1110-1360C	AB-AN-DI	% LEVEL DOPING	LINDSTROM & WEILL (1978)
	2.3, 8.0		ANDESITIC	PHENOCRYST/MATRIX	EWART & TAYLOR 1969
	6.6 - 11.0		DACITIC	PHENOCRYST/MATRIX	SCHOCK (1977)

(CONTINUED ON NEXT PAGE)

T A B L E A2-5 (Cont.)

CALCIC PYROXENE/LIQUID DISTRIBUTION COEFFICIENTS

ELEMENT	D	CONDITIONS	COMPOSITION	TECHNIQUE	REFERENCE
(CONTINUED FROM PREVIOUS PAGE)					
	1.32		BASALTIC	PHENOCRYST/MATRIX	BOUGAULT & HEKINIAN (1974)
	1.30		ALKALI BASALT	PHENOCRYST/MATRIX	LE ROEX (UNPUBL.)
	1.2			COMPILATION	FREY ET AL (1978)
SC	2.38 - 3.23		BASALTIC	PHENOCRYST/MATRIX	DALE & HENDERSON (1972)
	2.2 - 12.0		ANDESITE - DACITE	PHENOCRYST/MATRIX	EWART ET AL (1973)
	2.5 - 8.7		ANDESITE - DACITE	RAYLEIGH MODEL	EWART ET AL (1973)
	2.92 +-0.12		BASALT	PHENOCRYST/MATRIX	ONUMA ET AL (1968)
	0.84 - 8.75	1320-1171C, 1 ATM	AB-AN-DI	% LEVEL DOPING	LINDSTROM (1976)
	4.5, 17.0		ANDESITIC	PHENOCRYST/MATRIX	EWART & TAYLOR 1969
	17.7 - 28.0		DACITIC	PHENOCRYST/MATRIX	SCHOCK (1977)
	4.98		ALKALI BASALT	PHENOCRYST/MATRIX	LE ROEX (UNPUBL.)
	3.1			COMPILATION	FREY ET AL (1978)
CR	4.72 - 11.43		BASALTIC	PHENOCRYST/MATRIX	DALE & HENDERSON (1972)
	0.86 - 87		ANDESITE - DACITE	PHENOCRYST/MATRIX	EWART ET AL (1973)
	1.2 - 32		ANDESITE - DACITE	RAYLEIGH MODEL	EWART ET AL (1973)
	5.0 - 87	1170-1340C, FO2 = 10E-3.4 TO 10E-12.0	AB-AN-DI	% LEVEL DOPING	LINDSTROM (1976)
	70		ANDESITIC	PHENOCRYST/MATRIX	EWART & TAYLOR 1969
	90		DACITIC	PHENOCRYST/MATRIX	SCHOCK (1977)
	13		BASALTIC	PHENOCRYST/MATRIX	BOUGAULT & HEKINIAN (1974)
	12.98		ALKALI BASALT	PHENOCRYST/MATRIX	LE ROEX (UNPUBL.)
V	0.64 - 12.5		ANDESITE - DACITE	PHENOCRYST/MATRIX	EWART ET AL (1973)

TABLE A2-5 (Cont.)

CALCIC PYROXENE/LIQUID DISTRIBUTION COEFFICIENTS

ELEMENT	D	CONDITIONS	COMPOSITION	TECHNIQUE	REFERENCE
(CONTINUED FROM PREVIOUS PAGE)					
	0.94 - 4.1		ANDESITE - DACITE	RAYLEIGH MODEL	EWART ET AL (1973)
	0.04 - 8.50	1310-1200C, FO2 = 10E-3.4 TO 10E-12.0	AB-AN-DI	% LEVEL DOPING	LINDSTROM (1976)
	0.9,18.0		ANDESITIC	PHENOCRYST/MATRIX	EWART & TAYLOR 1969
	0.74		BASALTIC	PHENOCRYST/MATRIX	BOUGAULT & HEKINIAN (1974)
	1.68		ALKALI BASALT	PHENOCRYST/MATRIX	LE ROEX (UNPUBL.)
	1.5			COMPILATION	FREY ET AL (1978)
ZR	0.03-0.22	1113-1128C, 1 ATM	SYNTHETIC APOLLO 17 MARE BASALT	% LEVEL DOPING	MCCALLUM & CHARETTE (1978)
	0.22		ALKALI BASALT	PHENOCRYST/MATRIX	LE ROEX (UNPUBL.)
	0.1, 0.25, 0.6		BASIC - ACID	COMPILATION	PEARCE & NORRY 1979
NB	0.01 - 0.04				MCCALLUM & CHARETTE (1978)
	0.09		ALKALI BASALT	PHENOCRYST/MATRIX	LE ROEX (UNPUBL.)
	0.1, 0.3, 0.8		BASIC - ACID	COMPILATION	PEARCE & NORRY 1979
Y	0.70, 1.1		ANDESITIC	PHENOCRYST/MATRIX	EWART & TAYLOR 1969
	0.69		ALKALI BASALT	PHENOCRYST/MATRIX	LE ROEX (UNPUBL.)
	0.20			COMPILATION	FREY ET AL (1978)
	0.5, 1.5, 4.0		BASIC - ACID	COMPILATION	PEARCE & NORRY 1979
K	.0014 TO .0026	1100-1200C, 15-30KB	DI50-AB25-AN25	PPM LEVEL DOPING + DIFFERENTIAL DISSOLUTION + ID	SHIMIZU (1974)
	0.014 - 0.078		BASALTIC - DACITIC	PHENOCRYST/MATRIX	PHILPOTTS & SCHNETZLER (1970)
	(0.27)				

(CONTINUED ON NEXT PAGE)

T A B L E A2-5 (Cont.)

CALCIC PYROXENE/LIQUID DISTRIBUTION COEFFICIENTS

ELEMENT	D	CONDITIONS	COMPOSITION	TECHNIQUE	REFERENCE
(CONTINUED FROM PREVIOUS PAGE)					
	0.002 - 0.074		BASALTIC	PHENOCRYST/MATRIX	GOODMAN (1972)
	0.002		ANKARAMITE	PHENOCRYST/MATRIX	HART & BROOKS (1974)
	.001 - .005		ANDESITIC-BASALT	PHENOCRYST/MATRIX	HART & BROOKS (1974)
RB	0.001 TO .0041	1100-1200C,15-30KB	DI50-AB25-AN25	PPM LEVEL DOPING, ID	SHIMIZU (1974)
	0.013 - 0.039		BASALTIC - DACITIC	PHENOCRYST/MATRIX	PHILPOTTS & SCHNETZ-
	(0.284)				LER (1970)
	.004 - 0.08		BASALTIC	PHENOCRYST/MATRIX	GOODMAN (1972)
	0.003 & 0.001		ANKARAMITE	PHENOCRYST/MATRIX	HART & BROOKS (1974)
	.002 - 0.009		ANDESITIC-BASALT	PHENOCRYST/MATRIX	HART & BROOKS (1974)
	0.09		DACITIC	PHENOCRYST/MATRIX	SCHOCK (1977)
	0.05			COMPILATION	FREY ET AL (1978)
CS	.00035-.0023	1000-1200C,15-30KB	DI50-AB25-AN25	PPM LEVEL DOPING, ID	SHIMIZU (1974)
BA	.00078 - .0023	1100-1200C,15-30KB	DI50-AB25-AN25	PPM LEVEL DOPING, ID	SHIMIZU (1974)
	0.30	1200C, 20KB	NATURAL THOLEIITIC BASALT,HATA	HEAVY LIQUID SEPARATION + ID	TANAKA & NISHIZAWA (1975)
	0.0309		ALKALI BASALT	PHENOCRYST/MATRIX	NAGASAWA (1973)
	0.013 - 0.046		BASALTIC - DACITIC	PHENOCRYST/MATRIX	PHILPOTTS & SCHNETZ-
	(0.131, 0.388)				LER (1970)
	.0035 +-.001		BASALT	PHENOCRYST/MATRIX	ONUMA ET AL (1968)
	0.43, 0.12	1125C, 20KB	DI-EN-SIO2-H2O	ID	MASUDA & KUSHIRO (1978)
	0.15, 0.02		ANDESITIC	PHENOCRYST/MATRIX	EWART & TAYLOR 1969
	0.002		ANKARAMITE	PHENOCRYST/MATRIX	HART & BROOKS (1974)
	0.002 & 0.014		ANDESITIC-BASALT	PHENOCRYST/MATRIX	HART & BROOKS (1974)

T A B L E A2-5 (Cont.)

CALCIC PYROXENE/LIQUID DISTRIBUTION COEFFICIENTS

ELEMENT	D	CONDITIONS	COMPOSITION	TECHNIQUE	REFERENCE
	(CONTINUED FROM PREVIOUS PAGE)				
	0.02 - 0.06		DACITIC	PHENOCRYST/MATRIX	SCHOCK (1977)
	0.013		ALKALI BASALT	PHENOCRYST/MATRIX	LE ROEX (UNPUBL.)
SR	.119		ALKALI BASALT	PHENOCRYST/MATRIX	NAGASAWA (1973)
	.068 - 0.15		BASALTIC - DACITIC	PHENOCRYST/MATRIX	PHILPOTTS & SCHNETZ-
	(0.43, 0.52)				PHILPOTTS & SCHNETZ-
	0.109 +-0.01		BASALT	PHENOCRYST/MATRIX	ONUMA ET AL (1968)
	0.054 - 0.081	1100-1200C, 15-30KB	DI50-AB25-AN25	PPM LEVEL DOPING,ID	SHIMIZU (1974)
	EXP(42454/T - 31.37)	1140-1190C, FO2 = 10E-8 TO 10E-14	OCEANIC BASALT	% LEVEL DOPING	SUN ET AL (1974)
	0.07, 0.09		ANDESITIC	PHENOCRYST/MATRIX	EWART & TAYLOR 1969
	0.084 & 0.11		ANKARAMITE	PHENOCRYST/MATRIX	HART & BROOKS (1974)
	0.075 & 0.072		ANDESITIC-BASALT	PHENOCRYST/MATRIX	HART & BROOKS (1974)
	0.11		ALKALI BASALT	PHENOCRYST/MATRIX	LE ROEX (UNPUBL.)
	0.165			COMPILATION	FREY ET AL (1978)
	0.078	1265C, 1 ATM	DI-AN-AB	% LEVEL DOPING	GRUTZECK ET AL 1974
GA	0.30 - 0.58		BASALTIC	PHENOCRYST/MATRIX	GOODMAN (1972)
	0.36, 0.65		ANDESITIC	PHENOCRYST/MATRIX	EWART & TAYLOR 1969
	0.39		ALKALI BASALT	PHENOCRYST/MATRIX	LE ROEX (UNPUBL.)
U	.0016 - .0047	1375-1390C, 20KB	DI50-AB25-AN25 + 15% CA3(PO4)2	FISSION TRACKS	BENJAMIN ET AL 1978
	.0008 - .0025	1100-1200C, 10-25KB	DI50-AB25-AN25	FISSION TRACKS	SEITZ (1974)
	0.017 +-.0007		BASALT	PHENOCRYST/MATRIX	ONUMA ET AL (1968)
TH	.0016 - .0053	1375-1390C, 20KB	DI50-AB25-AN25 +	ALPHA TRACKS	BENJAMIN ET AL 1978

T A B L E A2-5 (Cont.)

CALCIC PYROXENE/LIQUID DISTRIBUTION COEFFICIENTS

ELEMENT	D	CONDITIONS	COMPOSITION	TECHNIQUE	REFERENCE
(CONTINUED FROM PREVIOUS PAGE)					
	.007	1240C,1 ATM	15% CA3(PO4)2 DI50-AB25-AN25	ALPHA TRACKS	SEITZ (1973)
	.006	1150C, 25KB			SEITZ (1973)
	0.013 +-.0005		BASALT	PHENOCRYST/MATRIX	ONUMA ET AL (1968)
	0.14 - 0.25		DACITIC	PHENOCRYST/MATRIX	SCHOCK (1977)
CU	1.5 - 2.4	910-950C, 1 KB	DI-NA2-SI2O5-H2O	1% DOPING	SEWARD (1971)
	0.09 - 1.1		ANDESITE - DACITE	PHENOCRYST/MATRIX	EWART ET AL (1973)
	0.12 - 0.87		ANDESITE - DACITE	RAYLEIGH MODEL	EWART ET AL (1973)
	0.18		BASALTIC	PHENOCRYST/MATRIX	BOUGAULT & HEKINIAN (1974)
	0.23		ALKALI BASALT	PHENOCRYST/MATRIX	LE ROEX (UNPUBL.)
ZN	0.50		BASALTIC	PHENOCRYST/MATRIX	BOUGAULT & HEKINIAN (1974)
	0.47		ALKALI BASALT	PHENOCRYST/MATRIX	LE ROEX (UNPUBL.)
HF	0.20 - 0.55		DACITIC	PHENOCRYST/MATRIX	SCHOCK (1977)
TA	0.10 - 0.30		DACITIC	PHENOCRYST/MATRIX	SCHOCK (1977)

TABLE A2-6

SUBCALCIC PYROXENE/LIQUID DISTRIBUTION COEFFICIENT

ELEMENT	D	CONDITIONS	COMPOSITION	TECHNIQUE	REFERENCE
NI	3.1 +-0.07	1326-1338C, 1 ATM	FO30-AN40-SI-30	% LEVEL DOPING	LINDSTROM (1976)
	3.03 +-0.08	1300C, 1 ATM	SIO2-AL2O3-MGO-CAO	0.5% DOPING	BIRD (1971)
	2.47 +-0.07	1350C, 1 ATM			BIRD (1971)
	1.91 +-0.06	1400C, 1 ATM			BIRD (1971)
	1.10 +-0.05	1025-1075C, 10-20KB	AN25-AB25-FO43-SI7	BETA TRACK	MYSEN(1978A)
	8 - 10	1140C, 1 ATM	FO-SIO2	4% DOPING	IRVINE & KUSHIRO (1976)
	8.6 - 13		ANDESITE - DACITE	PHENOCRYST/MATRIX	EWART ET AL (1973)
	7.3 - 11		ANDESITE - DACITE	RAYLEIGH MODEL	EWART ET AL (1973)
	0.60 - 1.4	1025C, 20KB	FO-AN50AB50-SIO2 -H2O	PPM LEVEL DOPING + BETA TRACK MAPPING	MYSEN (1976)
	4.8 - 6.5		ANDESITIC	PHENOCRYST/MATRIX	EWART & TAYLOR 1969
	5 - 3			COMPILATION	FREY ET AL (1978)
	3.15 - 18.1		BASALTIC	MINERAL SEPARATES	LE ROEX (UNPUBL.)
CO	1.3 +-0.04	1326-1338C, 1 ATM	FO30-AN40-SI30	% LEVEL DOPING	LINDSTROM (1976)
	1.41 +-0.06	1300C, 1 ATM	SIO2-AL2O3-MGO-CAO	% LEVEL DOPING	BIRD (1971)
	1.15 +-0.04	1350C, 1 ATM			BIRD (1971)
	3.3 - 12.5		ANDESITE - DACITE	PHENOCRYST/MATRIX	EWART ET AL (1973)
	3.4 - 9.2		ANDESITE - DACITE	RAYLEIGH MODEL	EWART ET AL (1973)
	2.08 +-0.13		BASALT	PHENOCRYST/MATRIX	ONUMA ET AL (1968)
	3.9 - 12.0		ANDESITIC	PHENOCRYST/MATRIX	EWART & TAYLOR 1969
	11.0 - 19.0		DACITIC	PHENOCRYST/MATRIX	SCHOCK (1977)
	2.0			COMPILATION	FREY ET AL (1978)
	1.61 - 6.43		BASALTIC	MINERAL SEPARATES	LE ROEX (UNPUBL.)
MN	0.70 +-0.04	1320-1326C, 1 ATM	FO30-AN40-SI30	% LEVEL DOPING	LINDSTROM (1976)

TABLE A2-6 (Cont.)

SUBCALCIC PYROXENE/LIQUID DISTRIBUTION COEFFICIENT

ELEMENT	D	CONDITIONS	COMPOSITION	TECHNIQUE	REFERENCE
	(CONTINUED FROM PREVIOUS PAGE)				
	0.80 +-0.09	1300C, 1 ATM	SIO2-AL2O3-MGO-CAO	0.5% DOPING	BIRD (1971)
	0.68 +- 0.08	1350C, 1 ATM			BIRD (1971)
SC	0.53 +-0.03	1320-1326C, 1 ATM	FO30-AN40-SI30	% LEVEL DOPING	LINDSTROM (1976)
	1.4 +-0.1	1195C, 1 ATM	SYNTHETIC LOW-K FRA MARE BASALT	% LEVEL DOPING	MCKAY & WEILL (1977)
	1.2 - 6.2		ANDESITE - DACITE	PHENOCRYST/MATRIX	EWART ET AL (1973)
	1.4 - 4.6		ANDESITE - DACITE	RAYLEIGH MODEL	EWART ET AL (1973)
	1.23 +-0.10		BASALT	PHENOCRYST/MATRIX	ONUMA ET AL (1968)
	14.0 - 28.0		RHYOLITIC	PHENOCRYST/MATRIX	EWART & TAYLOR 1969
	2.7 - 7.5		ANDESITIC	PHENOCRYST/MATRIX	EWART & TAYLOR 1969
	6.0 - 7.7		DACITIC	PHENOCRYST/MATRIX	SCHOCK (1977)
	1.1			COMPILATION	FREY ET AL (1978)
	0.06 - 0.58		BASALTIC	MINERAL SEPARATES	LE ROEX (UNPUBL.)
Y	0.9		RHYOLITIC	PHENOCRYST/MATRIX	EWART & TAYLOR 1969
	0.30 - 0.80		ANDESITIC	PHENOCRYST/MATRIX	EWART & TAYLOR 1969
	0.009			COMPILATION	FREY ET AL (1978)
	.20, .45, 1.0		BASIC - ACID	COMPILATION	PEARCE & NORRY 1979
ZR	.03, .08, 0.2		BASIC - ACID	COMPILATION	PEARCE & NORRY 1979
	.003 - .014		BASALTIC	MINERAL SEPARATES	LE ROEX (UNPUBL.)
NB	.15, .35, .80		BASIC - ACID	COMPILATION	PEARCE & NORRY 1979
	0.04 - 0.11		BASALTIC	MINERAL SEPARATES	LE ROEX (UNPUBL.)
TI	0.1, 0.25, 0.4		BASIC - ACID	COMPILATION	PEARCE & NORRY 1979

(CONTINUED ON NEXT PAGE)

TABLE A2-6 (Cont.)

SUBCALCIC PYROXENE/LIQUID DISTRIBUTION COEFFICIENT

ELEMENT	D	CONDITIONS	COMPOSITION	TECHNIQUE	REFERENCE
(CONTINUED FROM PREVIOUS PAGE)					
V	0.06	1326C, FO2 =10E-3.3			LINDSTROM (1976)
	2.8	1320C, FO2=10E-10.6			LINDSTROM (1976)
	3.4	+-1120C, 1 ATM	SYNTHETIC APOLLO 11 MARE BASALT	0.17% DOPING	RINGWOOD (1970)
	0.32 - 7.1		ANDESITE - DACITE	PHENOCRYST/MATRIX	EWART ET AL (1973)
	0.47 - 2.3		ANDESITE - DACITE	RAYLEIGH MODEL	EWART ET AL (1973)
	10.0 - 4.4		RHYOLITIC	PHENOCRYST/MATRIX	EWART & TAYLOR 1969
	0.58 - 7.2		ANDESITIC	PHENOCRYST/MATRIX	EWART & TAYLOR 1969
	0.30			COMPILATION	FREY ET AL (1978)
	0.01 - 1.23		BASALTIC	MINERAL SEPARATES	LE ROEX (UNPUBL.)
CR	1.0 - 60		ANDESITE - DACITE	PHENOCRYST/MATRIX	EWART ET AL (1973)
	0.65 - 17		ANDESITE - DACITE	RAYLEIGH MODEL	EWART ET AL (1973)
	0.62 - 0.71		RHYOLITIC	PHENOCRYST/MATRIX	EWART & TAYLOR 1969
	7.5 - 10.0		ANDESITIC	PHENOCRYST/MATRIX	EWART & TAYLOR 1969
	2.5		DACITIC	PHENOCRYST/MATRIX	SCHOCK (1977)
CU	0.017 - 1.4		ANDESITE - DACITE	PHENOCRYST/MATRIX	EWART ET AL (1973)
	0.16 - 1.2		ANDESITE - DACITE	RAYLEIGH MODEL	EWART ET AL (1973)
	0.22 - 0.28		BASALTIC	MINERAL SEPARATES	LE ROEX (UNPUBL.)
SR	0.018 +-0.003	1200C, 1 ATM	SYNTHETIC LUNAR BASALT	% LEVEL DOPING	WEILL & MCKAY (1975)
	0.009 +-0.006	1340C, 1 ATM			WEILL & MCKAY (1975)
	.0224 & .046		DACITE LAVA	PHENOCRYST/MATRIX	NAGASAWA & SCHNETZ-LER (1971)
	0.010 & 0.024		ANDESITE	PHENOCRYST/MATRIX	PHILPOTTS & SCHNETZ-

(CONTINUED ON NEXT PAGE)

TABLE A2-6 (Cont.)

SUBCALCIC PYROXENE/LIQUID DISTRIBUTION COEFFICIENT

ELEMENT	D	CONDITIONS	COMPOSITION	TECHNIQUE	REFERENCE
(CONTINUED FROM PREVIOUS PAGE)					
					LER (1970)
	0.03 - 0.04		ANDESITIC	PHENOCRYST/MATRIX	EWART & TAYLOR 1969
	0.016			COMPILATION	FREY ET AL (1978)
BA	0.011 +-0.005	1200C, 1 ATM	SYNTHETIC LUNAR BASALT	% LEVEL DOPING	MCKAY & WEILL (1976)
	.0029 & .0025		DACITE LAVA	PHENOCRYST/MATRIX	NAGASAWA & SCHNETZ-LER (1971)
	0.012 & 0.014		ANDESITE	PHENOCRYST/MATRIX	PHILPOTTS & SCHNETZ-LER (1970)
	0.01 - 0.02		RHYOLITIC	PHENOCRYST/MATRIX	EWART & TAYLOR 1969
	0.03 - 0.06		ANDESITIC	PHENOCRYST/MATRIX	EWART & TAYLOR 1969
	0.03		DACITIC	PHENOCRYST/MATRIX	SCHOCK (1977)
RB	.0027 & .00048		DACITE LAVA	PHENOCRYST/MATRIX	NAGASAWA & SCHNETZ-LER (1971)
	0.029 & 0.015		ANDESITE	PHENOCRYST/MATRIX	PHILPOTTS & SCHNETZ-LER (1970)
	0.02			COMPILATION	FREY ET AL (1978)
K	.0023 & .00055		DACITE LAVA	PHENOCRYST/MATRIX	NAGASAWA & SCHNETZ-LER (1971)
	0.009 & 0.019		ANDESITE	PHENOCRYST/MATRIX	PHILPOTTS & SCHNETZ-LER (1970)
U	0.008 +-0.002	1375C, 10KB	NATURAL PERIDOTITE	FISSION TRACK	SEITZ & SHIMIZU 1972
	0.09		DACITIC	PHENOCRYST/MATRIX	SCHOCK (1977)
ZN	2.1 - 3.6		DACITIC	PHENOCRYST/MATRIX	SCHOCK (1977)
	2.04 - 2.17		BASALTIC	MINERAL SEPARATES	LE ROEX (UNPUBL.)
HF	0.04, 0.20		DACITIC	PHENOCRYST/MATRIX	SCHOCK (1977)

(CONTINUED ON NEXT PAGE)

T A B L E A2-6 (Cont.)

SUBCALCIC PYROXENE/LIQUID DISTRIBUTION COEFFICIENT

ELEMENT	D	CONDITIONS	COMPOSITION	TECHNIQUE	REFERENCE
(CONTINUED FROM PREVIOUS PAGE)					
TA	0.15 - 0.70		DACITIC	PHENOCRYST/MATRIX	SCHOCK (1977)
TH	0.13 - 0.18		DACITIC	PHENOCRYST/MATRIX	SCHOCK (1977)
GA	0.80 - 1.0		RHYOLITIC	PHENOCRYST/MATRIX	EWART & TAYLOR 1969
	0.50 - 0.70		ANDESITIC	PHENOCRYST/MATRIX	EWART & TAYLOR 1969

TABLE A2-7

GARNET/LIQUID DISTRIBUTION COEFFICIENTS

ELEMENT	D	CONDITIONS	COMPOSITION	TECHNIQUE	REFERENCE
SR	0.0154		DACITE	PHENOCRYST/MATRIX	PHILPOTTS & SCHNETZ-LER (1970)
RB	0.009		DACITE	PHENOCRYST/MATRIX	PHILPOTTS & SCHNETZ-LER (1970)
	0.02			COMPILATION	FREY ET AL (1978)
K	0.020		DACITE	PHENOCRYST/MATRIX	PHILPOTTS & SCHNETZ-LER (1970)
BA	0.017		DACITE	PHENOCRYST/MATRIX	PHILPOTTS & SCHNETZ-LER (1970)
HF	0.53	950C, 30KB	NATURAL DACITE + 15% H2O	HEAVY LIQUID SEPARATION + INAA	IRVING & FREY (1976,1977)
Y	1.4			COMPILATION	FREY ET AL (1978)
	2.0, 11.0, 35		BASIC - ACID	COMPILATION	PEARCE & NORRY 1979
	3.28		BASALTIC	MINERAL SEPARATES	LE ROEX (UNPUBL.)
ZR	0.3, 0.5, 1.2		BASIC - ACID	COMPILATION	PEARCE & NORRY 1979
	0.02 - 2.42		BASALTIC	MINERAL SEPARATES	LE ROEX (UNPUBL.)
NB	0.10		BASIC	COMPILATION	PEARCE & NORRY 1979
	0.03 - 0.09		BASALTIC	MINERAL SEPARATES	LE ROEX (UNPUBL.)
TI	0.3, 0.5, 1.2		BASIC - ACID	COMPILATION	PEARCE & NORRY 1979
CO	9.0	950C, 30KB	NATURAL DACITE + 15% H2O	HEAVY LIQUID SEPARATION + INAA	IRVING & FREY (1976,1977)
	2.0			COMPILATION	FREY ET AL (1978)

TABLE A2-7 (Cont.)

GARNET/LIQUID DISTRIBUTION COEFFICIENTS

(CONTINUED FROM PREVIOUS PAGE)

ELEMENT	D	CONDITIONS	COMPOSITION	TECHNIQUE	REFERENCE
SC	27.6	950C, 30KB	NATURAL DACITE + 15% H2O	HEAVY LIQUID SEPARATION + INAA	IRVING & FREY (1976,1977)
	6.5			COMPILATION	FREY ET AL (1978)
	2.61 - 65		BASALTIC	MINERAL SEPARATES	LE ROEX (UNPUBL.)
CR	17.5	950C, 30KB	NATURAL DACITE + 15% H2O	HEAVY LIQUID SEPARATION + INAA	IRVING & FREY (1976,1977)
V	0.27			COMPILATION	FREY ET AL (1978)
	0.01 - 2.64		BASALTIC	MINERAL SEPARATES	LE ROEX (UNPUBL.)
MO	0.42	950C, 30KB	NATURAL DACITE + 15% H2O	HEAVY LIQUID SEPARATION + INAA	IRVING & FREY (1976,1977)
NI	5.1 +-0.3	1025C, 20KB	AN45-AB45-FO7-SI3 + EXCESS H2O	BETA TRACKS	MYSEN (1978A)
	0.80			COMPILATION	FREY ET AL (1978)
	0.17 - 0.96		BASALTIC	MINERAL SEPARATES	LE ROEX (UNPUBL.)
ZN	0.51 - 0.55		BASALTIC	MINERAL SEPARATES	LE ROEX (UNPUBL.)
CU	0.17 - 0.22		BASALTIC	MINERAL SEPARATES	LE ROEX (UNPUBL.)

TABLE A2-8

ILMENITE/LIQUID DISTRIBUTION COEFFICIENTS

ELEMENT	D	CONDITIONS	COMPOSITION	TECHNIQUE	REFERENCE
ZR	0.27	1110-1128C, 1 ATM	SYNTHETIC APOLLO 17 MARE BASALT	% LEVEL DOPING	MCCALLUM & CHARETTE (1978)
	0.19 - 1.38		BASALTIC	MINERAL SEPARATES	LE ROEX (UNPUBL.)
NB	0.81	1110-1128C, 1 ATM	SYNTHETIC APOLLO 17 MARE BASALT	% LEVEL DOPING	MCCALLUM & CHARETTE (1978)
	7.5 - 22.5		BASALTIC	MINERAL SEPARATES	LE ROEX (UNPUBL.)
Y	0.40		BASALTIC	MINERAL SEPARATES	LE ROEX (UNPUBL.)
V	12	1120-1140C, 1 ATM	SYNTHETIC APOLLO 11 BASALT	0.1% DOPING	RINGWOOD (1970)
	0.29 - 61		BASALTIC	MINERAL SEPARITES	LE ROEX (UNPUBL.)
ZN	0.38		BASALTIC	MINERAL SEPARATES	PASTER ET AL (1974)
	2.76 - 2.94		BASALTIC	MINERAL SEPARATES	LE ROEX (UNPUBL.)
SC	1.80		BASALTIC	MINERAL SEPARATES	PASTER ET AL (1974)
	0.62 - 6.43		BASALTIC	MINERAL SEPARITES	LE ROEX (UNPUBL.)
GA	0.14		BASALTIC	MINERAL SEPARATES	PASTER ET AL (1974)
CU	1.46		BASALTIC	MINERAL SEPARATES	PASTER ET AL (1974)
CO	2.20		BASALTIC	MINERAL SEPARATES	PASTER ET AL (1974)
	1.46		BASALTIC	MINERAL SEPARITES	LE ROEX (UNPUBL.)
NI	6.86 - 39.5		BASALTIC	MINERAL SEPARITES	LE ROEX (UNPUBL.)
CR	6	1120-1140C, 1 ATM	SYNTHETIC APOLLO 11 BASALT	0.1% DOPING	RINGWOOD (1970)

TABLE A2-9

MAGNETITE/LIQUID DISTRIBUTION COEFFICIENTS

ELEMENT	D	CONDITIONS	COMPOSITION	TECHNIQUE	REFERENCE
NI	12.2	1300C, 1 ATM	NATURAL PICRITIC THOLEIITE,KILAUEA	1% DOPING	LEEMAN (1974)
	19.4	1252C, 1 ATM			LEEMAN (1974)
	20 - 77	1111-1168C, 1 ATM FO2=10E-4.2,10E-12.9	NATURAL ALKALIC BASALT,OLOLKESALIE	% LEVEL DOPING	LINDSTROM (1976)
	5 - 45		ANDESITE - DACITE	PHENOCRYST/MATRIX	EWART ET AL (1973)
	19		ANDESITE - DACITE	RAYLEIGH MODEL	EWART ET AL (1973)
CO	5.8 - 17	1111-1168C, 1 ATM FO2=10E-4.2,10E-12.9	NATURAL ALKALIC BASALT,OLOLKESALIE	% LEVEL DOPING	LINDSTROM (1976)
	6.1 - 16		ANDESITE - DACITE	PHENOCRYST/MATRIX	EWART ET AL (1973)
	6.2 - 11		ANDESITE - DACITE	RAYLEIGH MODEL	EWART ET AL (1973)
	3.40		BASALTIC	MINERAL SEPARATES	PASTER ET AL (1974)
	19 - 34, 72		DACITIC	PHENOCRYST/MATRIX	SCHOCK (1977)
MN	1.7 - 1.81	1111-1168C, 1 ATM FO2=10E-4.2,10E-12.9	NATURAL ALKALIC BASALT,OLOLKESALIE	% LEVEL DOPING	LINDSTROM (1976)
	1.4 - 5.8		ANDESITE - DACITE	PHENOCRYST/MATRIX	EWART ET AL (1973)
	1.4 - 2.9		ANDESITE - DACITE	RAYLEIGH MODEL	EWART ET AL (1973)
CR	100 - 620	1111-1168C, 1 ATM FO2=10E-4.2,10E-12.9	NATURAL ALKALIC BASALT,OLOLKESALIE	% LEVEL DOPING	LINDSTROM (1976)
	21.1 - 25.5		FERROBASALT - LATITE	MODEL CALCULATION (RAYLEIGH)	LEEMAN ET AL (1978)
	40.9 - 67.6		FERROBASALT - LATITE	MODEL CALCULATION (NERNST)	LEEMAN ET AL (1978)
	37 - >240		ANDESITE - DACITE	PHENOCRYST/MATRIX	EWART ET AL (1973)
	27 - 58		ANDESITE - DACITE	RAYLEIGH MODEL	EWART ET AL (1973)
	5 - 20		DACITIC	PHENOCRYST/MATRIX	SCHOCK (1977)

(CONTINUED ON NEXT PAGE)

T A B L E A2-9 (Cont.)

MAGNETITE/LIQUID DISTRIBUTION COEFFICIENTS

ELEMENT	D	CONDITIONS	COMPOSITION	TECHNIQUE	REFERENCE
(CONTINUED FROM PREVIOUS PAGE)					
SC	0.80 - 3.3	1111-1168C, 1 ATM FO2=10E-4.2,10E-12.9	NATURAL ALKALIC BASALT,OLOLKESALIE	% LEVEL DOPING	LINDSTROM (1976)
	2.9 - 6.0		FERROBASALT - LATITE	MODEL CALCULATION (RAYLEIGH)	LEEMAN ET AL (1978)
	2.7 - 7.4		FERROBASALT - LATITE	MODEL CALCULATION (NERNST)	LEEMAN ET AL (1978)
	1.3 - 3.9		ANDESITE - DACITE	PHENOCRYST/MATRIX	EWART ET AL (1973)
	1.3 - 3.0		ANDESITE - DACITE	RAYLEIGH MODEL	EWART ET AL (1973)
	0.73		BASALTIC	MINERAL SEPARATES	PASTER ET AL (1974)
	3.3-4.5, 14.3		DACITIC	PHENOCRYST/MATRIX	SCHOCK (1977)
V	4.9 - 17.0		FERROBASALT - LATITE	MODEL CALCULATION (RAYLEIGH)	LEEMAN ET AL 1978
	5.0 - 98.7		FERROBASALT - LATITE	MODEL CALCULATION (NERNST)	LEEMAN ET AL (1978)
	23 - 190		ANDESITE - DACITE	PHENOCRYST/MATRIX	EWART ET AL (1973)
	24 - 63		ANDESITE - DACITE	RAYLEIGH MODEL	EWART ET AL (1973)
	0.11 - 67	1111-1168C, 1 ATM FO2=10E-4.2,10E-12.9	NATURAL ALKALIC BASALT,OLOLKESALIE	% LEVEL DOPING	LINDSTROM (1976)
CU	1.7 - 7.1		ANDESITE - DACITE	PHENOCRYST/MATRIX	EWART ET AL (1973)
	1.3 - 2.3		ANDESITE - DACITE	RAYLEIGH MODEL	EWART ET AL (1973)
	0.42		BASALTIC	MINERAL SEPARATES	PASTER ET AL (1974)
ZR	0.24		BENMOREITE	PHENOCRYST/MATRIX	LE ROEX (UNPUBL.)
	0.1, 0.2, 0.8		BASIC - ACID	COMPILATION	PEARCE & NORRY 1979
NB	2.16		BENMOREITE	PHENOCRYST/MATRIX	LE ROEX (UNPUBL.)
	0.4, 1.0, 2.5		BASIC - ACID	COMPILATION	PEARCE & NORRY 1979

T A B L E A2-9 (Cont.)

MAGNETITE/LIQUID DISTRIBUTION COEFFICIENTS

ELEMENT	D	CONDITIONS	COMPOSITION	TECHNIQUE	REFERENCE
(CONTINUED FROM PREVIOUS PAGE)					
Y	0.17		BENMOREITE	PHENOCRYST/MATRIX	LE ROEX (UNPUBL.)
	0.2, 0.5, 2.0		BASIC - ACID	COMPILATION	PEARCE & NORRY 1979
ZN	2.6		BASALTIC	MINERAL SEPARATES	PASTER ET AL (1974)
	9.6 - 16.9		DACITIC	PHENOCRYST/MATRIX	SCHOCK (1977)
BA	0.05 - 0.08		DACITIC	PHENOCRYST/MATRIX	SCHOCK (1977)
HF	0.15 - 0.55		DACITIC	PHENOCRYST/MATRIX	SCHOCK (1977)
TA	0.8-1.8, 3.7		DACITIC	PHENOCRYST/MATRIX	SCHOCK (1977)
TH	0.04 - 0.20		DACITIC	PHENOCRYST/MATRIX	SCHOCK (1977)
U	0.09 - 0.20		DACITIC	PHENOCRYST/MATRIX	SCHOCK (1977)
GA	2.0		BASALTIC	MINERAL SEPARATES	PASTER ET AL (1974)

TABLE A2-10

SPINEL/LIQUID DISTRIBUTION COEFFICIENTS

ELEMENT	D	CONDITIONS	COMPOSITION	TECHNIQUE	REFERENCE
SC	0.048 +-.001	1400C, 1 ATM	MGO-AL2O3-SIO2	PPM LEVEL DOPING + HEAVY LIQUID SEPARATION + INAA	NAGASAWA ET AL 1976
NI	5.9 +-0.02	1350C, 1 ATM	SIO2-AL2O3-MGO-CAO	0.5% DOPING	BIRD (1971)
	5.1	1400C, 1 ATM			BIRD (1971)
	10.7 - 53	1275C, 1 ATM FO2=10E-9,10E-10.5	NATURAL ALLENDE METEORITE	BETA TRACKS	MYSEN & KUSHIRO 1976
CO	2.3 - 2.8	1350C, 1 ATM	SIO2-AL2O3-MGO-CAO	0.5% DOPING	BIRD (1971)
	1.9 - 2.4	1400C, 1 ATM			BIRD (1971)
CR	104 - 507	1400-1300C, 1 ATM			BIRD (1971)
	147-568	1450-1300C, 1 ATM	FO-AN-ST	0.7% DOPING	SCHREIBER (1976)
	134 - 187	1450-1300C, 1 ATM	FO-AN-DI	0.7% DOPING	SCHREIBER (1976)
	51 - 125	1350-1175C, 1 ATM	SYNTHETIC FE-TI-AL PYROXENE	1% DOPING	AKELLA ET AL (1976)
	102 - 155	1275C, 1 ATM	NATURAL ALLENDE METEORITE	MICROPROBE	MYSEN & KUSHIRO (1976)
	77	+- 1140C, 1 ATM	SYNTHETIC APOLLO 11 MARE BASALT	0.5% DOPING	RINGWOOD (1970)
V	38	+- 1140C, 1 ATM	SYNTHETIC A11 BASALT	0.5% DOPING	RINGWOOD (1970)

TABLE A2-11

AMPHIBOLE/LIQUID DISTRIBUTION COEFFICIENTS

ELEMENT	D	CONDITIONS	COMPOSITION	TECHNIQUE	REFERENCE
BA	0.044 & 0.054		DACITE-HORNBLENDE	PHENOCRYST/MATRIX	NAGASAWA & SCHNETZ-LER (1971)
	0.316		PHONOLITE-KAERSUTITE	PHENOCRYST/MATRIX	SUN & HANSON (1976)
	0.417 & 0.731		CAMPTONITE - HBL	PHENOCRYST/MATRIX	PHILPOTTS & SCHNETZ-LER (1970)
	0.099		ANDESITE-HBL	PHENOCRYST/MATRIX	PHILPOTTS & SCHNETZ-LER (1970)
	0.05 - 0.14		RHY - AND	PHENOCRYST/MATRIX	EWART & TAYLOR 1969
	0.04		DACITIC	PHENOCRYST/MATRIX	SCHOCK (1977)
SR	.0224 & 0.094		DACITE-HORNBLENDE	PHENOCRYST/MATRIX	NAGASAWA & SCHNETZ-LER (1971)
	0.548 & 0.672		CAMPTONITE - HBL	PHENOCRYST/MATRIX	PHILPOTTS & SCHNETZ-LER (1970)
	0.188		ANDESITE-HBL	PHENOCRYST/MATRIX	PHILPOTTS & SCHNETZ-LER (1970)
	0.54 - 0.26		RHY - AND	PHENOCRYST/MATRIX	EWART & TAYLOR 1969
RB	0.014 & .0077		DACITE-HORNBLENDE	PHENOCRYST/MATRIX	NAGASAWA & SCHNETZ-LER (1971)
	0.411 & 0.427		CAMPTONITE - HBL	PHENOCRYST/MATRIX	PHILPOTTS & SCHNETZ-LER (1970)
	0.0448		ANDESITE-HBL	PHENOCRYST/MATRIX	PHILPOTTS & SCHNETZ-LER (1970)
K	0.081 & 0.065		DACITE-HORNBLENDE	PHENOCRYST/MATRIX	NAGASAWA & SCHNETZ-LER (1971)
GA	0.80 - 1.0		RHY - AND	PHENOCRYST/MATRIX	EWART & TAYLOR 1969
CR	0.52 - 23.0		RHY - AND	PHENOCRYST/MATRIX	EWART & TAYLOR 1969
V	18.0 - 92.0		RHY - AND	PHENOCRYST/MATRIX	EWART & TAYLOR 1969

T A B L E A2-11 (Cont.)

AMPHIBOLE/LIQUID DISTRIBUTION COEFFICIENTS

ELEMENT	D	CONDITIONS	COMPOSITION	TECHNIQUE	REFERENCE
(CONTINUED FROM PREVIOUS PAGE)					
NI	1.5 - 7.2		RHY - AND	PHENOCRYST/MATRIX	EWART & TAYLOR 1969
CO	7.5		ANDESITIC	PHENOCRYST/MATRIX	EWART & TAYLOR 1969
	45		DACITIC	PHENOCRYST/MATRIX	SCHOCK (1977)
SC	260 - 12.5		RHY - AND	PHENOCRYST/MATRIX	EWART & TAYLOR 1969
	20.5		DACITIC	PHENOCRYST/MATRIX	SCHOCK (1977)
ZN	6.8		DACITIC	PHENOCRYST/MATRIX	SCHOCK (1977)
HF	6.0		DACITIC	PHENOCRYST/MATRIX	SCHOCK (1977)
TA	0.30		DACITIC	PHENOCRYST/MATRIX	SCHOCK (1977)
TH	0.22		DACITIC	PHENOCRYST/MATRIX	SCHOCK (1977)
U	0.40		DACITIC	PHENOCRYST/MATRIX	SCHOCK (1977)
Y	10.0 - 3.1		RHY - AND	PHENOCRYST/MATRIX	EWART & TAYLOR 1969
	1.0, 2.5, 6.0		BASIC - ACID	COMPILATION	PEARCE & NORRY 1979
ZR	0.5, 1.4, 4.0		BASIC - ACID	COMPILATION	PEARCE & NORRY 1979
NB	0.8, 1.3, 4.0		BASIC - ACID	COMPILATION	PEARCE & NORRY 1979
TI	1.5, 3.0, 7.0		BASIC - ACID	COMPILATION	PEARCE & NORRY 1979

TABLE A2-12

APATITE/LIQUID DISTRIBUTION COEFFICIENTS

ELEMENT	D	CONDITIONS	COMPOSITION	TECHNIQUE	REFERENCE
SC	0.22		BASALTIC	MINERAL SEPARATES	PASTER ET AL(1974)
CU	0.28		BASALTIC	MINERAL SEPARATES	PASTER ET AL (1974)
CO	0.20		BASALTIC	COMPILATION	BAKER ET AL (1977)
CR	0.20		BASALTIC	COMPILATION	BAKER ET AL (1977)
NI	0.20		BASALTIC	COMPILATION	BAKER ET AL (1977)
SR	2,3,5		BASALTIC,BENMOREITIC TRACHYTIC	COMPILATION	BAKER ET AL (1977)
BA	0.10		BASALTIC	COMPILATION	BAKER ET AL (1977)
TI	0.10		ACID	COMPILATION	PEARCE & NORRY 1979
ZR	0.10		ACID	COMPILATION	PEARCE & NORRY 1979
Y	20, 40		BASIC - ACID	COMPILATION	PEARCE & NORRY 1979
NB	0.10		ACID	COMPILATION	PEARCE & NORRY 1979

TABLE A2-13

MICA/LIQUID DISTRIBUTION COEFFICIENTS

ELEMENT	D	CONDITIONS	COMPOSITION	TECHNIQUE	REFERENCE
TI	0.9		PHLOGOPITE/BASIC	COMPILATION	PEARCE & NORRY 1979
	1.5, 2.5		BIOTITE/INT. - ACID	COMPILATION	PEARCE & NORRY 1979
ZR	0.6		PHLOGOPITE/BASIC	COMPILATION	PEARCE & NORRY 1979
	1.2, 2.0		BIOTITE/INT. - ACID	COMPILATION	PEARCE & NORRY 1979
	0.01 - 0.11		PHLOGOPITE/BASIC	MINERAL SEPARATES	LE ROEX (UNPUBL.)
Y	0.03		PHLOGOPITE/BASIC	COMPILATION	PEARCE & NORRY 1979
	1.2, 2.0		BIOTITE/INT. - ACID	COMPILATION	PEARCE & NORRY 1979
	0.18		PHLOGOPITE/BASIC	MINERAL SEPARATES	LE ROEX (UNPUBL.)
NB	1.0		PHLOGOPITE/BASIC	COMPILATION	PEARCE & NORRY 1979
	1.8, 3.0		BIOTITE/INT. - ACID	COMPILATION	PEARCE & NORRY 1979
	0.09 - 0.26		PHLOGOPITE/BASIC	MINERAL SEPARATES	LE ROEX (UNPUBL.)
SC	0.06 - 0.61		PHLOGOPITE/BASIC	MINERAL SEPARATES	LE ROEX (UNPUBL.)
CO	3.83		PHLOGOPITE/BASIC	MINERAL SEPARATES	LE ROEX (UNPUBL.)
NI	6.04 - 34.8		PHLOGOPITE/BASIC	MINERAL SEPARATES	LE ROEX (UNPUBL.)
V	0.77		PHLOGOPITE/BASIC	MINERAL SEPARATES	LE ROEX (UNPUBL.)
ZN	0.94 - 1.00		PHLOGOPITE/BASIC	MINERAL SEPARATES	LE ROEX (UNPUBL.)
CU	0.30 - 0.38		PHLOGOPITE/BASIC	MINERAL SEPARATES	LE ROEX (UNPUBL.)